Doctoral Dissertation
Doctoral Program in Energetics (29th cycle)

Optimisation of opaque building envelope components with Phase Change Materials

By

Ylenia Cascone
******

Supervisor(s):
Prof. M. Perino
Prof. A. Capozzoli

Doctoral Examination Committee:
Prof. A. Gasparella, Referee, Università di Bolzano
Prof. B. Olesen, Referee, Technical University of Denmark (DTU)
Prof. C. Buratti, Università degli Studi di Perugia
Prof. F. Causone, Politecnico di Milano
Prof. E. Fabrizio, Politecnico di Torino

Politecnico di Torino
2017

Declaration

I hereby declare that, the contents and organization of this dissertation constitute my own original work and does not compromise in any way the rights of third parties, including those relating to the security of personal data.

Ylenia Cascone
2017

Abstract

The objective of the present thesis is to provide a methodological approach for the design of responsive building envelope components through the application of optimisation analyses. In detail, this approach was applied to opaque building envelope components with Phase Change Materials (PCMs). Since multi-objective optimisation problems generally result in a series of trade-off solutions called Pareto-front, the main focus was to investigate which values assumed by the optimisation variables led to the optimal set of solutions. In this way, the optimisation analysis was used as a tool to gain knowledge on specific problems.

After an overview on PCMs and on the application of optimisation analyses to the building envelope for improving the energy efficiency of buildings, three levels of analysis were explored; material level, component level and building level.

At the material level, the optimisation approach was applied to estimate the temperature-dependent specific heat curve of PCMs through best-fit of experimental data. Given the measured surface temperatures of a sample as boundary conditions and the known thermo-physical properties of the materials to a numerical model, the curve which minimised the difference between measured and simulated heat fluxes on both faces of the sample was found.

At the component level, "equivalent" parameters for the dynamic thermal characterisation of opaque building envelope components with PCM were proposed. Starting from the definition of the traditional dynamic thermal properties according to ISO 13786:2007, a monthly equivalent periodic thermal transmittance and the corresponding time shift were defined by imposing steady-periodic conditions with monthly average external air temperature and solar irradiance profiles while keeping a constant air temperature on the internal side. Then, the monthly equivalent values were synthesised in a unique yearly value by means of a simple average. A parametric model was subsequently developed to describe PCM-enhanced multi-layer walls with simultaneous use of at most two PCMs, and an optimisation analysis was carried out for three locations (Palermo, Torino and Oslo) to find wall layout and PCMs' thermo-physical properties (melting temperature, melting temperature range, latent heat of fusion and thermal conductivity) which minimise yearly equivalent periodic thermal transmittance, overall PCM thickness and thickness of the wall.

At the building level, the investigations focused on the application of optimisation analyses for the energy retrofit of office buildings. Three retrofit options on the opaque envelope components were considered in the aforementioned locations; intervention either on the external side of the wall, on the internal side of the wall, or on both sides of the wall. Moreover, either the same retrofit solution for all the walls or a different wall solution for each orientation were considered. In both cases, a maximum of two PCM materials could be selected by the optimisation algorithm. With regard to the objective functions, the problem was faced under two points of view. On one side, optimisations were run with three objectives to minimise the building energy need for heating, cooling and the investment cost. On the other side, the optimisations were performed with two objectives to minimise primary energy consumption and global cost. Only for the climate of Oslo, where heating is mostly electric and no cooling system was adopted, the minimisation objectives were primary energy consumption, global cost and thermal discomfort.

Even though a proper optimisation of the thermo-physical properties of PCMs was found to be especially advisable when the operation of the HVAC system implies a non-trivial solution, the results of these analyses allowed to propose a few design guidelines for PCM selection and application. However, for the analysed case studies, PCM prices need to be reduced in order to become a cost-effective retrofit option.

Contents

List of Figures

List of Tables

Nomenclature

Roman Symbols

A	area	m^2
C	cost	€
c	specific heat capacity	$\text{J/(kg\,K)}$
E_P	primary energy	J
g	g-value (adim.) or gravitational acceleration	m/s^2
h	specific enthalpy	J/kg
h_c	convective heat transfer coefficient	$\text{W/(m}^2\,\text{K)}$
h_e	external heat transfer coefficient	$\text{W/(m}^2\,\text{K)}$
I	solar irradiance	W/m^2
k	thermal conductivity	$\text{W/(m\,K)}$
L	latent heat	J/kg
m	mass	kg
N_{gen}	number of generations	
N_{iter}	number of iterations	
N_{pop}	population size	
p	pressure	Pa
Q	thermal energy	J
q	heat flux	W/m^2
Q_E	electricity	J

R	thermal resistance	$\mathrm{m^2\,K/W}$
r	radius	m
T	temperature	°C
t	time	s
T_p	peak melting temperature	°C
t_x	thickness (when a subscript x is specified)	m
U	thermal transmittance (U-value)	$\mathrm{W/(m^2\,K)}$
u	velocity	m/s
V	volume	$\mathrm{m^3}$
w	width parameter of $c(T)$ curve	
Y_{mn}	periodic thermal transmittance	$\mathrm{W/(m^2\,K)}$

Greek Symbols

α	solar absorption coefficient (adim.) or thermal diffusivity	$\mathrm{m^2/s}$
ΔT	melting temperature range	°C
Δt_{mn}	time shift	h
ϵ	emissivity	
η	efficiency	
μ	dynamic viscosity	$\mathrm{kg/(m\,s)}$
ρ	density	$\mathrm{kg/m^3}$
ρ_l	visible reflection coefficient at normal incidence	
ρ_s	solar reflection coefficient at normal incidence	
τ_l	visible transmission coefficient at normal incidence	
θ	temperature	°C

Superscripts

$*$	equivalent	

Subscripts

a	air
C	cooling
f	frame
G	global
g	glazing
H	heating
I	investment
l	liquid
m	melting, maximum (if referred to specific heat)
nd	need
p	constant pressure
s	solid
sa	sol-air
se	external surface
si	internal surface
w	window
avg	average
op	operative

Acronyms / Abbreviations

ANOVA	Analysis of Variance
Bi	Biot number
CD	Crowding Distance
CDD	Cooling Degree-Day
CFD	Computational Fluid Dynamics
COP	Coefficient Of Performance

CV   Coefficient of Variation

DGU   Double Glazing Unit

dof   Degrees of freedom

DSC   Differential Scanning Calorimetry

EER   Energy Efficiency Ratio

EER   Energy Efficiency Ratio

EPBD   Energy Performance of Buildings Directive

ES   Evolution Strategy

EU   European Union

Fo   Fourier number

GA   Genetic Algorithm

HDD   Heating Degree-Day

HVAC   Heating, Ventilation and Air Conditioning

IEQ   Indoor Environmental Quality

IQR   Interquartile Range

IWEC   International Weather for Energy Calculations

LCA   Life Cycle Assessment

LD   Likelihood of Dissatisfied

LPD   Long-term Percentage of Dissatisfied

MOGA   Multi-Objective Genetic Algorithm

NDS   Non-Dominated Sorting

NSGA   Non-dominated Sorting Genetic Algorithm

NSGA-II   Non-dominated-and-crowding Sorting Genetic Algorithm II

nZEB   Nearly Zero-Energy Building

PCM   Phase Change Material

PCMTS   PCM thermal shield

PF   Pareto front

PSO   Particle Swarm Optimisation

RC   Resistor–Capacitor

SBX   Simulated Binary Crossover

SHGC   Solar Heat Gain Coefficient (g-value)

Ste   Stefan number

TGU   Triple Glazing Unit

WWR   Window-to-Wall Ratio

Chapter 1

Introduction

The European Union (EU) has set five ambitious objectives—on employment, innovation, education, social inclusion and climate/energy—to be reached by 2020. The targets in the climate change and energy sustainability sector aim at a 20% reduction of the greenhouse gas emissions compared to the levels in 1990, a 20% increase of the share of renewable energy sources and a 20% increase in energy efficiency [1].

Considering that commercial and residential buildings in Europe consume approximately 40% of primary energy and are responsible for 24% of greenhouse gas emissions [2], improving the energy performance of buildings could be regarded as an important opportunity in this energy challenge. For this purpose, the European Commission launched the Energy Performance of Buildings Directive (EPBD) (2002/91/EC and recast 2010/31/EU). According to the EPBD recast, all new and existing buildings that are subject to major renovation in the European Union after 2020 (2018 in the case of public buildings) should be "Nearly Zero-Energy Buildings" (nZEB). nZEBs are defined as buildings which have "a very high energy performance, and the nearly zero or very low amount of energy required should be covered to a very significant extent by energy from renewable sources, including energy from renewable sources produced on-site or nearby" [3]. In addition, the Member States are bound to set minimum requirements for the energy performance of buildings and building elements, which should be set "with a view to achieving the cost-optimal balance between the investments involved and the energy costs saved throughout the lifecycle of the building" [3].

With the increasing complexity of the technologies needed to successfully design such high-performance buildings, the nZEB target becomes extremely difficult to achieve through a common "trial and error" design approach. According to the expertise of the designer, a variety of candidate options can be analysed. Unfortunately, given the great number of variables and their relative range of variation, it is practically impossible to evaluate all the possible design solutions and identify the most effective one. A wiser and more effective design strategy should focus

on the application of optimisation algorithms to select the design variables which lead to trade-off solutions between contrasting objectives. Moreover, the design process is even less trivial when responsive envelope components—i.e. "design solutions that react to changes in external or internal conditions and to occupant intervention in order to maintain a balance between optimum interior conditions and environmental performance" [4]—are considered.

In this framework, the objective of the present thesis is to provide a methodological approach for the design of responsive building envelope components through the application of optimisation analyses. In detail, this approach was applied to opaque building envelope components with Phase Change Materials (PCMs).

First, a literature overview on PCMs and on the application of optimisation analyses to the building envelope in order to improve the energy efficiency of buildings was provided. Then, three levels of analysis were explored; material level, component level and building level. Although the common theme, there is no continuity among them.

At the *material level*, the optimisation approach was applied to estimate the thermo-physical properties (specific heat-temperature curve) of PCMs through best-fit of experimental results. Given the measured surface temperatures of a sample as boundary conditions and the known thermo-physical properties of the materials to a numerical model, the specific heat vs temperature curve of the PCM which minimised the difference between measured and simulated heat fluxes on both faces of the sample was found. Three sets of variables were tested to identify the best trade-off between accuracy and computational time.

At the *component level*, "equivalent" parameters for the dynamic thermal characterisation of opaque building envelope components with PCM were proposed. Due to the non-linear behaviour of PCMs, evaluating and comparing the dynamic thermal performance of these components is a challenging task. Starting from the definition of the traditional dynamic thermal properties according to ISO 13786:2007 [5], a monthly equivalent periodic thermal transmittance and the corresponding time shift were defined by imposing steady-periodic conditions with monthly average external air temperature and solar irradiance profiles while keeping a constant air temperature on the internal side. Then, the monthly equivalent values were synthesised in a unique yearly value by means of a simple average.

The influence of the PCM's thermo-physical properties on these equivalent parameters was then analysed by means of a parametric analysis. This analysis was carried out on a set of six wall configurations characterised by a different order of the layers (mass, insulation and PCM) for three locations (Palermo, Torino, and Oslo) and four wall orientations (south, east, north, and west). Given a constant latent heat, wall configuration and the PCM's melting temperature resulted to have the greatest influence on the dynamic thermal performance. Moreover, a potential improvement in the yearly equivalent periodic thermal transmittance was expected

by a seasonal change in the PCM melting temperature. Therefore, subsequent analyses at the component level focused on the investigation of the optimal wall configuration (order of the layers) with the adoption of PCMs with at most two melting temperatures.

A parametric model was developed to describe PCM-enhanced multi-layer walls, and an optimisation analysis was carried out in the aforementioned locations to find wall layout and PCMs' thermo-physical properties (melting temperature, melting temperature range, latent heat of fusion and thermal conductivity) which minimised yearly equivalent periodic thermal transmittance, overall PCM thickness and overall thickness of the wall. The PCM's thickness was selected as a preliminary cost metric, since the amount of PCM was expected to reasonably have the major influence on the cost of the wall. The wall thickness was chosen to be able to explore the effect of PCM in relation with that of traditional thermal mass. From the results of these analyses, the PCM seemed to show its greatest potential in warm climates where low values of yearly equivalent periodic thermal transmittance could be obtained while reducing the wall thickness. This can be expected to be especially useful for retrofit applications.

At the *building level*, the investigations focused on the application of optimisation analyses for the energy retrofit of office buildings. An archetype office building realised in Italy during the period 1946-1970 was chosen as a case study. The same building geometry was adopted for all the investigated locations (Palermo, Torino and Oslo), whereas the envelope properties were differentiated by country. Moreover, differences in the building envelope were highlighted in Oslo between buildings pre-1955 and post-1955. Since this difference regarded not only the insulation level of the buildings but also the wall typology—i.e. massive or lightweight walls—both cases were considered worth of investigation.

The optimisation analyses were performed considering three retrofit options on the opaque envelope components; intervention either on the external side of the wall, on the internal side of the wall, or on both sides of the wall. Intervention on the external side of the wall was considered when interrupting or relocating the office activities during the renovation works was not possible. Intervention on the internal side of the wall was considered for buildings subjected to laws on the conservation of historical buildings (in Italy, buildings older than 50 year). Intervention on both sides of the wall was considered because, according to the literature for traditional walls and the results of the component-level analyses, its dynamic thermal performance was expected to improve. Moreover, either the same intervention for all the façades (i.e. same retrofitted wall regardless of the wall orientation) or differentiated by façade (i.e. a different wall configuration for each wall orientation) were considered. In both cases, a maximum of two PCM materials could be selected by the optimisation algorithm.

With regard to the optimisation objectives, the problem was faced under two points of view. On one side, optimisations were run with three objectives to mini-

mise the building energy need for heating and cooling and the investment cost. On the other side, the optimisations were performed with two objectives to minimise primary energy consumption and global cost. Only for the climate of Oslo, where heating is mostly electric and no cooling system was considered, the minimisation objectives were primary energy consumption, global cost, and thermal discomfort.

Since multi-objective optimisations do not generally have a single solution, but result in a series of trade-off solutions called Pareto-front, special attention was given to the post-optimisation analyses of the results. Rather than emphasising the objectives' values that could be reached by means of the optimisation procedure, the main focus was given to the variables' values which led to the optimal solutions. Therefore, rules were searched for the solutions to belong to the Pareto-front. For this purpose, a series of graphical and numerical analyses were carried out, such as box plots, frequency analyses and variables' mapping of the Pareto front solutions, analysis of the extreme solutions for each objective, and innovization (*innov*ation through optim*ization*) analyses [6–8]. In this way, the multi-objective optimisation analysis was used as a tool to gain knowledge on specific problems, and some design guidelines for the early design stage could be identified. Therefore, the objective was not e.g. to find *what* is the best energy performance that can be obtained, but rather *how* can it be obtained?

Overall, the following research questions were addressed:

- Given the challenges in accurately measuring the thermo-physical properties of PCMs, how can their enthalpy-temperature curve be estimated with sufficient accuracy for simulation purposes?

- How can PCM-enhanced building envelope components be characterised for a synthetic evaluation of their dynamic thermal performance in order to allow for comparison among design solutions?

- How should PCMs be used to enhance the dynamic thermal performance of opaque building envelope components? What are the optimal wall configurations and the corresponding PCM's thermo-physical properties?

- How should PCMs be used to be an effective mean for improving the energy efficiency of existing office buildings? What are the optimal retrofit solutions and the corresponding PCM's thermo-physical properties? How do the PCM-based optimal solutions change according to the climatic conditions?

- How do the thermo-physical properties of PCMs interact when searching for the optimal solutions with respect to energy performance related objectives?

- How should the optimisation objectives be chosen to extract valuable information from the results of the search process, and how can such information be retrieved?

- How can the Pareto solutions be explored to search for common characteristic

to drive the design process?

Eventually, the contents of the present thesis are organised as follows:

- *Chapter 2 – Literature overview.* A literature overview on the main topics addressed in the present work, i.e. Phase Change Materials and optimisation analyses, is presented with the aim of providing the basic theoretical bases on these subjects as well as background information on the context of the research activity. For both topics, general information is reported together with an overview of their use and potentialities in building application.

- *Chapter 3 – Methods.* This chapter is completely theoretical and provides an in-depth description of the adopted numerical methods. Specifically, the finite difference model used to simulate the PCM-enhanced walls at the material and component levels, the optimisation algorithms and the post-optimisation analyses are extensively described and validated.

- *Chapter 4 – Methodology.* In this chapter the actual research activity is explained. First, the PCM modelling shared by all the analyses is described. Then, the methodology applied at each level is detailed. At the material level, the experimental setup and the optimisation procedure are reported. At the component level, the proposed dynamic thermal characterisation of opaque building envelope components with PCM is explained, and the subsequent parametric analysis is described. Then, the parametric model of the PCM-enhanced wall used to carry out the optimisation analyses is described together with the details of the optimisation procedure (i.e. objective functions, optimisation variables, inputs to the optimisation algorithm and constraints). Eventually, at the building level, the case study and the retrofit interventions taken into account are described. Then, the optimisation procedure is explained, and details on the evaluation of each objective function are provided.

- *Chapter 5 – Results.* For each level of investigation, the results are extensively reported together with a first discussion. For all the multi-objective optimisation analyses, the Pareto frontiers and the post-optimisation analyses are illustrated in order to identify the characteristics of the non-dominated sets.

- *Chapter 6 – Discussion.* An overall discussion on the building-level results is provided. Additional analyses were especially performed to investigate the reason behind some of the choices—or lack of choices—of the optimisation algorithm.

- *Chapter 7 – Conclusion.* Aim, methodology and the main results for each level of investigation are summarised, and the conclusions are drawn.

Chapter 2

Literature overview

In this chapter, a literature overview on the main topics addressed in the present thesis—i.e. Phase Change Materials and optimisation analyses—is presented. For both topics, general information is provided together with an overview of their use and potentialities in building application.

2.1   Phase change materials

Phase Change Materials are substances which undergo a phase transition (in general solid-liquid) at their utilisation temperature. They can store (during melting) and release (during solidification) large amounts of energy at an almost constant temperature by exploiting their latent heat of fusion. PCMs in buildings can hence be used to increase the heat storage capacity or to have a stabilising effect on temperature swings [9, 10]. Due to the presence of a liquid phase, some sort of containment is needed for the practical application of PCMs.

2.1.1   Classification and general features

2.1.1.1   Phase change in ideal binary solutions

When a pure substance undergoes a phase transition, its temperature does not change until the phase transition is complete. For mixtures, the phase change occurs over a temperature range—called *mushy zone*—between the solidus and liquidus lines of the phase diagram.

A phase diagram of a binary system in equilibrium characterised by complete miscibility both in solid and liquid states is reported in Fig. 2.1a. For all the possible weight compositions of the system, liquid (L) and solid (S) single-phase fields are

(a) Equilibrium phase diagram.

(b) Non-equilibrium phase diagram.
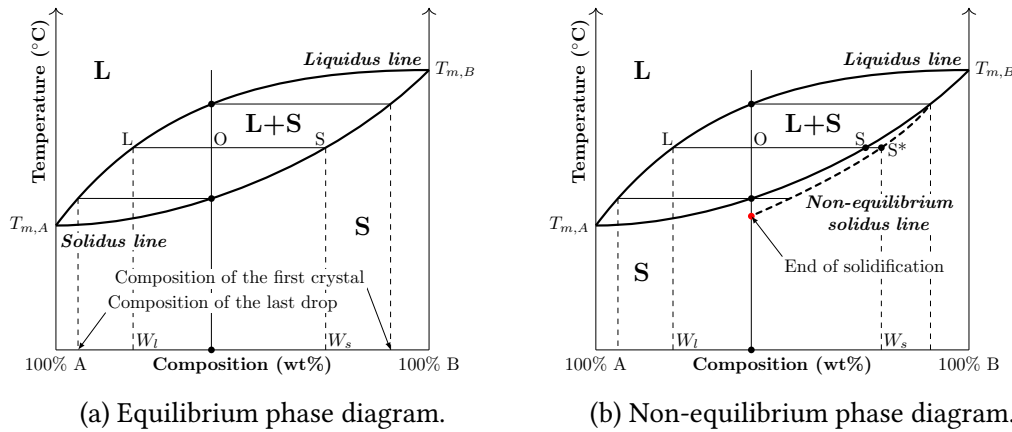
Fig. 2.1 Phase diagram of a completely miscible binary system.

present, together with a biphasic field with co-presence of solid and liquid. The liquidus line represents the temperatures at which the mixtures begin to solidify or end to melt. The solidus line represents the temperatures at which the mixtures begin to melt or end to solidify [11].

Considering the solidification of the mixture in Fig. 2.1a, at the temperature of point O the composition of the liquid and solid phases is respectively given by W_l and W_s, and their relative fraction is respectively equal to $\overline{OS}/\overline{LS}$ and $\overline{OL}/\overline{LS}$ (lever rule). Therefore, the composition of the solid and liquid phases is not constant. If the solidification process is sufficiently slow, diffusion takes place homogenising the composition during the process [12]. Otherwise, non-equilibrium solidification occurs (see § 2.1.1.4.1).

2.1.1.2   Desired properties of PCMs

PCMs should be characterised by a series of properties of thermo-physical, chemical, kinetic and economic nature [13, 14, 9, 10].

The phase change temperature should be chosen in order to suit to the application where the PCM is used. For the best heat storage capability, a high latent heat of fusion and high specific heat are desirable [9]. Moreover, the higher the density, the higher the heat storage per unit volume is. A small density variation (hence volume change) between solid and liquid phases allows to increase the amount of PCM that the container can hold [15].

PCMs should have long-term stability and be compatible with the container's material, which should not be corroded to avoid leakage of the PCM when in liquid state. In addition, vapour pressure at operational temperature should be as low as possible (< 1 bar) to avoid extra costs or risk of rupture of the encapsulating material [15].

The thermo-physical properties of the PCM should remain constant regardless of the number of melting-solidification cycles. Possible sources of poor stability are phase segregation (see § 2.1.1.4.1) and supercooling (see § 2.1.1.4.3), which may result in a decreased ability to store latent heat, or in a difference in the phase change temperature [9]. For safety, the material should be non-toxic, non-flammable and should not be harmful to the environment [16].

Eventually, for a widespread application of PCMs, abundant and cost-effective materials should be used.

2.1.1.3   Classification of PCMs

PCMs can be classified as organic, inorganic or eutectic mixtures (Fig. 2.2). Organic PCMs are generally divided into paraffins and non-paraffins. Salt hydrates and metals belong to the category of inorganic PCMs, whereas eutectic mixtures can be formed by two components with a precise ratio so that the resulting material undergoes a congruent melting at a lower temperature than that of each single component [13, 9, 17].
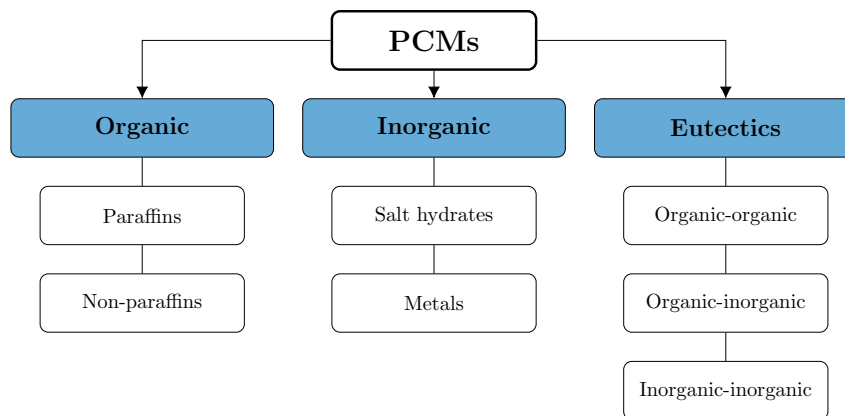
Fig. 2.2 Classification of PCMs.

Extensive information on the thermo-physical properties of organic PCMs and salt hydrates can be respectively found in [18] and [19]. A list of properties of commercial PCMs for potential application in buildings is reported in Table 2.1.

2.1.1.3.1   **Organic PCMs**   Organic PCMs can be either paraffins or non-paraffins.

Paraffins are alkanes (hydrocarbons), whose general formula is C_nH_{2n+2}. The more the number of carbon atoms in the molecular chain, the more the melting temperature increases [17]. The molecular structure of paraffins is

$$CH_3 - (CH_2)_n - CH_3$$

Pure paraffins are very expensive, therefore commercial materials are usually mixed with other hydrocarbons. This causes their phase change to occur in a temperature range (see § 2.1.1.1).

Among the *non-paraffin* PCMs are fatty acids, esters and glycols. The molecular structure of fatty acids is

$$CH_3 - (CH_2)_n - COOH$$
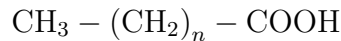
Generally, organic PCMs are chemically stable [20], present no phase segregation and have a high latent heat of fusion, although their density is low compared to inorganic PCMs. They are characterised by a high nucleation rate so that solidification occurs with little or no supercooling [21, 10]. As a drawback, depending on the encapsulation they can be flammable [22], have a low thermal conductivity (around 0.2 W/(m K)), a high volume variation, are not compatible with plastic containers [9, 17], are not stable at high temperatures due to covalent bonds [23], and are more expensive than salt hydrates [10]. Compared to paraffins, non-paraffins are more expensive and can be corrosive [17].

2.1.1.3.2 Inorganic PCMs

Inorganic PCMs can be either metals or salt hydrates; however, metals do not find application in the building sector.

Salt hydrates are inorganic salts which retain a definite number of water molecules within their crystal structure. Their general formula is $AB \cdot nH_2O$, where AB is a salt and *n* is the number of water molecules trapped within the crystal. The phase change in salt hydrates consists in the hydration or dehydration reaction—either total or partial—of the salt.

Hydration (solidification) – exothermic reaction:

$$AB + nH_2O \rightarrow AB \cdot nH_2O + Q$$
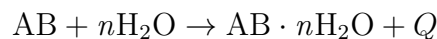
Dehydration (melting) – endothermic reaction:

$$AB \cdot nH_2O + Q \rightarrow AB + nH_2O$$
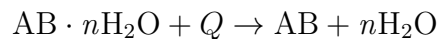
Inorganic PCMs are generally less expensive than other PCMs and are non-flammable. They have a relatively high latent heat of fusion and thermal conductivity (around 0.5 W/(m K)) [17]. However, salt hydrates present some disadvantages such as a high volume change during phase transition [22], supercooling, phase separation, and are corrosive towards metals. Moreover, they are not adequate for impregnation into porous building materials (see § 2.1.1.6.2) [10].
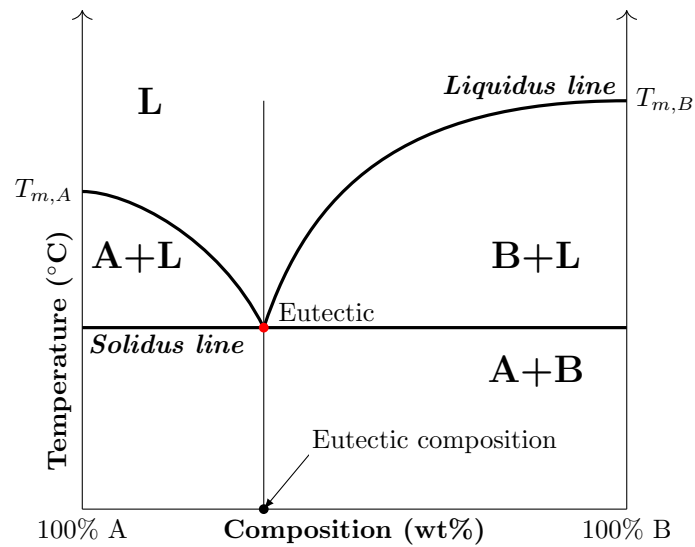
Fig. 2.3 Binary eutectic phase diagram; complete miscibility in liquid state and complete immiscibility in solid state.

2.1.1.3.3 Eutectics Eutectics are mixtures of two (or more) components which do not usually chemically interact to form a new compound but, if mixed with certain ratios, undergo a congruent melting (i.e. insensitive of the cooling rate) with the simultaneous formation of two separate solid phases (Fig. 2.3). Therefore, when melting an eutectic composition, there is direct transition from liquid to solid A+B, without the formation a single phase with only A or B. The melting temperature of the eutectic compound is lower than both its components [12].

Eutectics have a sharp melting point similar to pure substances, but only limited data on their thermo-physical properties are available [9].

2.1.1.4 Typical problems of PCMs

Usually, a PCM does not satisfy all the requirements described in § 2.1.1.2. Moreover, according to the type of PCM, problems such as phase segregation, phase separation, hysteresis and supercooling may arise.

2.1.1.4.1 Phase segregation When solidification occurs at a fast cooling rate for incongruent transformations, diffusion is not sufficient to homogenise the composition, and non-equilibrium solidification takes place. Diffusion in the solid state is very slow, and this causes the formation of layered grains. The new layers that form on top of the existing grains have the equilibrium composition at the corresponding temperature, but once they are solid their composition remains unchanged. Therefore, the grain's core is richer in the high-melting element (B),

Table 2.1 Thermo-physical properties of commercial PCMs.

Product name	L	$T_{p,s}$	$T_{p,m}$	k_s	k_l	ρ_s	ρ_l	c_s	c_l	ΔT
	[kJ/kg]	[°C]		[W/(m K)]		[kg/m³]		[J/(kg K)]		[°C]
Organic										
PureTemp 15	182	N/A	15	0.25	0.15	950	860	2250	2560	9*
PureTemp 18	192	N/A	19.1	0.25	0.15	950	860	1470	1740	9*
PureTemp 20	171	N/A	19.9	0.23	0.14	950	860	2070	2150	10*
PureTemp 23	227	N/A	23.4	0.25	0.15	910	830	1840	1990	9*
PureTemp 25	187	N/A	25.2	0.25	0.15	950	860	1990	2290	8*
PureTemp 27	202	N/A	27	0.25	0.15	950	860	2460	2630	5*
PureTemp 28	190	N/A	28.1	0.25	0.15	950	860	2340	2540	6*
PureTemp 29	202	N/A	28.6	0.25	0.15	940	850	1770	1940	4*
PureTemp 37	210	N/A	38.1	0.25	0.15	920	840	2210	2630	5*
A15	130		15	0.18		790		2260		N/A
A16	213		16	0.18		760		2370		N/A
A17	150		17	0.18		785		2220		N/A
A22	145		22	0.18		785		2220		N/A
A22H	216		22	0.18		820		2850		N/A
A23	145		23	0.18		785		2220		N/A
A24	145		24	0.18		790		2220		N/A
A25	150		25	0.18		785		2260		N/A
A25H	226		25	0.18		810		2150		N/A
A26	150		26	0.21		790		2220		N/A
A28	155		28	0.21		789		2220		N/A
A29	226		29	0.18		810		2150		N/A
A32	130		32	0.21		845		2200		N/A
A36	217		36	0.18		790		2370		N/A
A37	235		37	0.18		810		2850		N/A
X25	110		25	0.36		1055		1630		N/A
X30	105		30	0.36		1050		1650		N/A
RT 15	125*	20*	17*	0.2	0.2	880	770	N/A*	2000*	11.5*
RT 18 HC	230*	18*	18*	0.2	0.2	880	770	3000*	2500*	4*
RT 21	130*	22*	22*	0.2	0.2	880	770	N/A*	2500*	8.5*
RT 21 HC	155*	21*	21*	0.6	0.6	880	770	5500*	2500*	7*
RT 22 HC	170*	22*	22*	0.2	0.2	760	700	4500*	2000*	8.5*
RT 24	125*	24*	23*	0.2	0.2	880	770	N/A*	2000*	9*
RT 25	140*	25*	25*	0.2	0.2	880	760	N/A*	2000*	7*
RT 25 HC	190*	25*	25*	0.2	0.2	880	770	N/A*	2500*	7.5*

Entropy Solutions *(left margin label for PureTemp rows)*

PCM Products *(left margin label for A/X rows)*

Rubitherm *(left margin label for RT rows)*

Continued on next page

	Product name	L [kJ/kg]	$T_{p,s}$	$T_{p,m}$ [°C]	k_s	k_l [W/(m K)]	ρ_s	ρ_l [kg/m³]	c_s	c_l [J/(kg K)]	ΔT [°C]
Rubitherm	RT 26	155*	26*	26*	0.6	0.6	1650	1700	N/A*	2000*	6*
	RT 28 HC	225*	28*	28*	0.2	0.2	880	770	1500*	2500*	5*
	RT 31	150*	31*	31*	0.2	0.2	880	760	N/A*	3500*	8*
	RT 35	150*	32*	33*	0.2	0.2	860	770	N/A*	2000*	10*
	RT 35 HC	215*	35*	35*	0.2	0.2	880	770	4000*	2500*	5.5*
	PX 15	65*	16*	16*	0.2	0.2	650	650	N/A*	1000*	12*
	PX 25	75*	24*	24*	0.1	0.1	650	650	N/A*	1000*	10*
Inorganic											
Climator	ClimSel C21	134	21	26	0.93	0.75	1400		N/A		N/A
	ClimSel C24	140	24	27	0.74	0.93	1400		N/A		N/A
	ClimSel C28	170	27	31	0.98	0.72	1400		N/A		N/A
PCM Energy P. Ltd	Latest™18T	175		18	1.00		1500		2000		N/A
	Latest™20T	175		20	1.00		1500		2000		N/A
	Latest™22T	175		22	1.00		1500		2000		N/A
	Latest™25T	175		25	1.00		1500		2000		N/A
	Latest™29T	175	28	29	1.00		1500		2000		N/A
	Latest™32S	220		32	0.60		1450		2000		N/A
	Latest™34S	230		34	0.60		1450		2000		N/A
	Latest™36S	220		36	0.60		1450		2000		N/A
PCM Products	S15	160		15	0.43		1510		1900		N/A
	S17	160		17	0.43		1525		1900		N/A
	S19	160		19	0.43		1520		1900		N/A
	S21	170		22	0.54		1530		2200		N/A
	S23	175		23	0.54		1530		2000		N/A
	S25	180		25	0.54		1530		2200		N/A
	S27	183		27	0.54		1530		2200		N/A
	S30	190		30	0.48		1304		1900		N/A
	S32	200		32	0.51		1460		1910		N/A
	S34	155		34	0.52		2100		2100		N/A
Rubitherm	SP 21 EK	130*	21*	23*	0.6	0.6	1500	1400	3500*	2500*	8.0*
	SP 24 E	195*	22*	24*	0.6	0.6	1500	1400	1500*	2500*	4.5*
	SP 25 E2	155*	23*	25*	0.6	0.6	1500	1400	3500*	2500*	8.0*
	SP 26 E	170*	25*	26*	0.6	0.6	1500	1400	3500*	2500*	5.0*
	SP 29 Eu	155*	27*	29*	0.6	0.6	1550	1500	2500*	2000*	4.5*
	SP 31	180*	30*	32*	N/A	N/A	1350	1300	4000*	5500*	5.0*

* Estimated from DSC measurement.

while the grain's boundary is richer in the low-melting element (A) (Fig. 2.1b). As a consequence, the average composition of the grain is somewhere between the composition of the core and that of the boundary (S*), which is not the equilibrium composition (S). The solidus line becomes shifted, and solidification completes at a lower temperature, once the average composition of the solid matches that of the original mixture [12].

Non-equilibrium solidification causes the melting temperature to lower; upon heating, the grain boundaries will melt first.

2.1.1.4.2 Phase separation   Phase separation is the conversion from a single-phase to a multi-phase system. When a pure substance melts or solidifies, its composition remains unchanged whether it is in solid or liquid state. However, when a substance is formed by two or more components, according to its composition it may separate in two different phases.

Phase separation occurs mainly in salt hydrates. When in liquid state, there is simultaneous presence of water and salt, which may sink due to gravitation when its density is greater than water's. This leads to a biphasic system with co-presence of water and a solution with a higher salt concentration than initially (Fig. 2.4). Therefore, the melting/solidification temperature of the two phases varies due to the change in concentration.

To solve phase separation, a few options are viable. Mechanical mixing can be used in storages, but it would not be a solution at the material level. As an alternative, additional water can be added to the salt hydrate for a faster homogenisation for diffusion; however, the heat storage capability is reduced and the melting range is broadened. Another option is the adoption of gelling additives, which form a three-dimensional network capable of holding the PCM together at a microscopic scale. Another solution is the addition of thickening additives which increase the viscosity of the PCM. The last but more complex option is to add other materials until congruent melting is achieved [23].
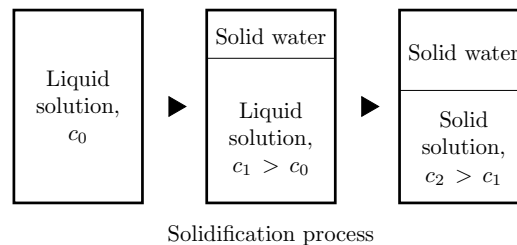
Fig. 2.4 Phase separation; salt concentration increases from c_0 to c_2.

2.1.1.4.3 Supercooling Supercooling is the phenomenon for which a material remains liquid below its solidification temperature (Fig. 2.5).

In order for the solidification process to begin, nucleation—i.e. the formation of initial crystals (nuclei)—has to occur. The capability to produce nuclei when the temperature decreases below the solidification temperature is called nucleation rate. If nucleation does not happen or the nucleation rate is too low, the material can remain liquid even when its temperature becomes lower than the solidification temperature [22]. Only when nuclei with a sufficiently large radius are present, solidification can start.

During supercooling only sensible heat is involved. If the latent heat is larger than the sensible heat lost due to supercooling, the temperature suddenly rises to the phase change temperature and remains there until the phase change process is complete. However, if the loss of sensible heat during supercooling is greater than the latent heat, the temperature does not rise again to the phase change temperature [23].

To solve or reduce the problem of supercooling, solid PCM particles can be added to the supercooled liquid (homogeneous nucleation), or additives can be added to act as nucleators (heterogeneous nucleation). Nucleators should have a similar crystal structure to the solid PCM and a higher melting temperature. However, a similar crystal structure involves a similar melting temperature, therefore many nucleators are stable only up to 10 ℃ to 20 ℃ above the PCM's melting temperature [23].
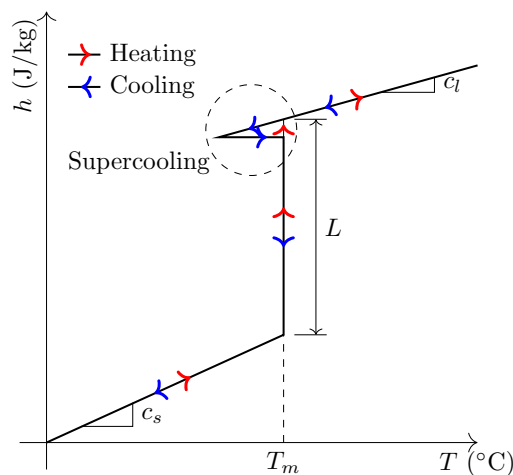
Fig. 2.5 Effect of supercooling on the enthalpy-temperature curve.

2.1.1.4.4 Hysteresis Hysteresis occurs when a material behaves differently upon heating and cooling. Possible causes of hysteresis can be a low rate of crystal formation upon solidification, a slow diffusion in the solid phase, or the formation

of a different solid phase with respect to the beginning of the melting process. Supercooling is also a local form of hysteresis [23].

However, hysteresis can also be apparent, i.e. it is an effect caused by the measurement procedure and not a material property. Apparent hysteresis is caused by non-isothermal conditions in the sample during the measurement [23].

2.1.1.5 Methods for thermal analysis

The content of this section was partly published in [24] and [25].

The determination of the heat storage capability of PCMs as a function of temperature is of great importance to accurately predict the in-situ behaviour of the material [26–28]. The dependency of the storage capacity on temperature can be described in terms of specific heat capacity, $c_p(T)$, or in terms of enthalpy variation, $h(T)$. The relationship between these two quantities is

$$h(T) = \int_{T_1}^{T_2} c_p(T)\,\mathrm{d}T \qquad \text{and} \qquad c_p = \frac{\mathrm{d}h(T)}{\mathrm{d}T}. \tag{2.1}$$

Several test procedures can be performed to measure the $c_p(T)$ or $h(T)$ curve of a PCM, such as Differential Scanning Calorimetry (DSC), T-history method, direct [11] or inverse approaches [29, 30], and others [31].

2.1.1.5.1 DSC The Differential Scanning Calorimetry is a common experimental measurement of the heat absorbed or released by a body during a chemical or physical process. Through a DSC test, qualitative and quantitative information on the phase transitions of a sample, its enthalpy, specific heat and latent heat can be obtained [32].

The working principle of the DSC is to measure the difference between the heat fluxes exchanged with the sample under investigation and a reference while they are both subjected to a controlled temperature program. Two operation modes are possible; a dynamic mode, where the temperature varies with a constant heating or cooling rate, and an isothermal step mode, where the temperature is increased step-wise, and each time is kept constant until the sample reaches thermal equilibrium [33]. The outcomes of the tests are a heat flux vs temperature curve when the DSC is operated in dynamic mode, and a heat flux vs time curve when operated in isothermal step mode. These curves can be used to evaluate the enthalpy-temperature relationship of the material.

There are two main types of DSC apparatuses; the power compensation DSC and the heat-flux DSC [32]. In the power compensation DSC, a crucible containing

the sample (S) and an empty reference crucible (R) are placed in two independent furnaces with their own heating element and temperature sensor. They are separately heated in order to maintain their temperature equal to the program's value (hence their temperature difference is equal to zero). In the heat-flux DSC, the crucibles S and R are placed in the same furnace on a plate with known thermal resistance and an integrated temperature sensor. Due to their different heat capacities, a temperature difference between S and R occurs, which is measured to determine the heat flow to supply (or remove) to maintain the temperature program.

Since the DSC is a relative measure, the instrument needs to be calibrated with known standards to identify both the temperature scale and to quantify the exchanged heat flux [32].

For typical PCM applications, the enthalpy-temperature curve of PCMs should be known with a temperature uncertainty lower than 1 ℃ [34]. With regard to the accuracy of DSC measurements in dynamic mode, they are highly reproducible for one measurement configuration, but a change in the configuration affects the test results [35]. The equivalent heat capacity evaluated through DSC is strongly influenced by the sample mass (which is a few milligrams), heating (or cooling) rate [36, 27] and PCM geometry within the crucible [27], as well as by the measurement procedure, the DSC apparatus itself and its calibration, the preparation of the sample, the crucibles, and the data evaluation [35, 37]. Following the German RAL standard [38] and further improvements which include proper calibration and baseline measurement, a methodology to avoid these influences for DSC in heating mode was proposed by Lazaro et al. [37]. Moreover, supercooling in small samples is often stronger than in large samples, therefore the maximum supercooling determined by DSC is not representative of real applications [21]. A DSC operated in isothermal step mode is much less sensitive to a variation in the sample's mass, and its accuracy can be considered satisfactory for homogeneous materials [33]. However, measurements in isothermal step mode are still unsuitable for materials with strong supercooling [34]. In addition, correct sampling of inhomogeneous materials might be impossible due to the extremely low sample size [34].

The direct use of the curves measured though DSC analysis is not physically correct, because the heat flux exchanged with the sample depends not only on the thermo-physical properties of the material but also on the heat transfer [26, 22]. Especially for dynamic measurements with constant heating and cooling rate, a slow rate is needed for PCMs unlikely the typical standards used in DSC analysis for other materials [33, 34]. In fact, the faster the heating rate, the later the melting appears to end, even though the area beneath the peak remains constant [27, 11]. However, through an appropriate evaluation of the heat transfer processes within the sample and between sample and DSC apparatus, the resulting thermograms can be corrected [39, 26].

2.1.1.5.2   T-history   The T-history method [40] is widely adopted to investigate the thermal behaviour of large PCM samples. Specific heat capacity in solid and liquid state, melting temperature and latent heat of fusion of several PCM samples can be simultaneously measured. Moreover, supercooling can be well characterised [35]. T-history can also be used to evaluate the thermal conductivity of PCMs whose phase change occurs with a clear interface between the two phases. However, thermal conductivity and specific heat cannot be simultaneously determined [40].

To perform a T-history test, at least two tubes are required. One or more tubes are filled with the material under investigation and one is filled with a reference material. The reference should be a substance with well-known thermal properties, such as distilled water. Since the T-history method is based on the lumped capacitance model, the characteristics of the tubes should guarantee a sufficiently small Biot number (below 0.1) in order to ensure a small temperature gradient within the test material (eq. 2.2).

$$\text{Bi} = \frac{h_c\, r}{2k} < 0.1 \tag{2.2}$$

The tubes are preheated above the PCM melting temperature and are subsequently cooled by exposing them to air at ambient temperature. During the cooling process, the curves of temperature versus time are recorded. The thermal properties can be determined by comparing these curves for the PCM and the reference material. To improve the measurement accuracy, a horizontal setup should be preferred over a vertical setup since the effect of buoyancy might be non-negligible [35]. A horizontal setup was also found to reduce the discrepancies between freezing and melting enthalpy-temperature curves [35].

The original T-history method from Zhang et al. [40] is highly suitable for pure materials or eutectics. Several contributions were proposed to improve its mathematical model [41, 42], its measuring process [43, 44] or both [45]. For materials whose phase change occurs in a temperature range, the T-History method as improved by Marín et al. [41] is more suitable. In this method, the thermal balance of the tube with PCM and that of the tube with distilled water are written (eq. 2.3). The subscripts w, PCM and t refer respectively to the water-filled tube, to the PCM-filled tube, and to the tube itself.

$$\begin{cases} m_{\text{PCM}} \cdot \Delta h_{\text{PCM}} + m_t c_t \cdot (T_i - T_{i+1}) = h_c A_t \int_{t_i}^{t_{i+1}} (T - T_a)\, \mathrm{d}t \\ (m_w c_w + m_t c_t) \cdot (T_i - T_{i+1}) = h_c A_t \int_{t_i'}^{t_{i+1}'} (T - T_a)\, \mathrm{d}t \end{cases} \tag{2.3}$$

Under the hypothesis of equal convection heat transfer coefficient for both tubes,

the enthalpy variation within the PCM is determined as follows:

$$\Delta h_{\text{PCM}}(T_i) = \frac{m_w c_w(T_i) + m_t c_t(T_i)}{m_{\text{PCM}}} \cdot \frac{I_i}{I_i'} \cdot \Delta T_i - \frac{m_t}{m_{\text{PCM}}} \cdot c_t(T_i) \cdot \Delta T_i$$

where

$$I_i = \int_{t_i}^{t_{i+1}} (T - T_a)\, \mathrm{d}t,$$

$$I_i' = \int_{t_i'}^{t_{i+1}'} (T - T_a)\, \mathrm{d}t,$$

$$\Delta T_i = T_i - T_{i+1}.$$

Additional information on the T-history method with regard to experimental setup, mathematical model and presentation of the results can be found in [46].

2.1.1.5.3 Inverse methods Inverse methods allow to identify the thermo-physical properties of materials through a matching between experimental and theoretical data [26]. Inverse problems can be dealt with by means of exhaustive search method or can be formulated as optimisation problems (see § 2.2.1.2). In this case, the objective is to minimise the discrepancy between measured values (e.g. of temperature or heat flux) and calculated values based on the estimated properties. However, inverse problems are ill-posed; under small changes of the input, data existence, uniqueness and stability of the solution are not satisfied [47].

With regard to inverse methods applied to PCMs, Lachheb et al. [48] proposed a method for estimating thermal conductivity, specific heat and thermal diffusivity of paraffin/graphite PCM composites from laboratory tests under controlled boundary conditions, but material properties were evaluated at room temperature and their dependency on temperature was hence not investigated.

Thermal conductivity and specific heat as a function of temperature of PCM-concrete bricks subjected to controlled boundary conditions were estimated by Cheng et al. [49] and Pomianowski et al. [50]. The temperature dependency was evaluated through the temperature segment method, which has the advantage of not requiring any a-priori knowledge on the specific heat function. Moreover, the low heating rate was representative of the heat transfer in buildings. However, the number of segments directly determines the number of variables in the optimisation problem.

Temperature-dependent thermal conductivity, heat capacity and thermal diffusivity were simultaneously estimated by Cui et al. [51], who proposed an approach based on the measurement of the temperature distribution within the material and subjected either to Dirichlet or Neumann boundary conditions. Prior information

on the functional form of the thermal properties was not necessary.

Franquet et al. [26] proposed a method for evaluating the enthalpy-temperature curve of either pure substances or binary solutions by fitting experimental DSC curves. They supposed an a priori formulation of the enthalpy based on thermodynamic principles.

The enthalpy-temperature curve of a PCM composite material was retrieved by Tittelein et al. [30, 52] from laboratory tests under controlled boundary conditions (heating and cooling ramps with constant rate) by means of an enthalpy model based on the assumption of binary mixture. In this way, the unknowns estimated by the inverse model were the latent heat of fusion, the melting temperature of the mixture and that of the main component.

2.1.1.6 Incorporation methods

When the PCM is in liquid state, the need for a container arises. Several incorporation methods are viable for applying PCMs in the building envelope, such as direct incorporation, encapsulation (micro and macro), immersion in porous materials and shape stabilisation.

2.1.1.6.1   Direct incorporation   The simplest and cheapest method to apply PCMs in buildings consists in directly mixing liquid or powdered PCM into porous materials such as gypsum, concrete or plaster during their production. However, serious problems of leakage and degradation of the mechanical resistance of the container due to material interaction may occur [22, 53, 54]. Incorporation of microencapsulated PCMs (see § 2.1.1.6.4) can avoid these drawbacks [55–57].

2.1.1.6.2   Immersion   In the immersion method, a porous matrix (such as gypsum board, brick or concrete block) is immersed in a high-temperature liquid PCM, which is absorbed by capillarity [58, 53]. Once the matrix is removed from the PCM and cools down, the PCM solidifies within the matrix pores. The process is cheap, but stability problems due to evaporation of the PCM or material interaction may arise [53]. Products which absorb microencapsulated PCMs (see § 2.1.1.6.4) can avoid this problem, although the production costs increase [59].

2.1.1.6.3   Macroencapsulation   Macroencapsulation is the process of packing loose PCM in big size containers, usually larger than 1 cm [59]. According to the type of application, these containers can have various shapes, such as panels, pouches, spheres or tubes [58, 9]. A small density variation between solid and liquid state is especially desirable.

The container should be optimised to enhance the heat transfer rate during the phase change processes. Even though the melting process is faster than in microencapsulated materials due to convection flow within the liquid, the poor thermal conductivity of many PCMs might cause the material to solidify on the container's wall, slowing down the heat transfer process [53]. This problem can be however mitigated by the use of additives, such as metal foams or expanded graphite, to increase the PCM's thermal conductivity [58, 60].

Encapsulation can help to overcome the flammability problems of some PCMs [53]; however, the size of the macrocapsules imply the need of protection against perforation [54, 9].

2.1.1.6.4 Microencapsulation Microencapsulation is the process of packing solid particles or liquid droplets of a material (core) by surrounding them with a coating of another substance (shell). The resulting microcapsules have a diameter that ranges approximately from $0.05\,\mu m$ to $5000\,\mu m$ [61].

The purpose of microencapsulation is to protect PCMs from harmful interaction with the environment, provide structural stability, make active materials easier and/or safer to handle, and to improve thermal properties by increasing the heat transfer surface [53, 61]. The advantage of this containment is that the PCM-filled microcapsules can be mixed with other materials, providing a significant increase in their thermal capacity with a relatively small decrease in the overall mechanical properties [61]. Moreover, the bulk density of the material does not change between solid and liquid states [9]. However, a disadvantage of microencapsulation is the low thermal conductivity of most materials used to form the microcapsules' shells, usually polymeric films or silica [13, 9]. Moreover, the mass fraction of PCM—and hence the total heat storage capacity—is limited by the shell's thickness, which has to provide mechanical strength to avoid rupture of the capsules [61].

Microencapsulation can be obtained by means either of physical or chemical processes. Reviews on the microencapsulation methods can be found in [61–63].

2.1.1.6.5 Shape-stabilised PCMs Shape-stabilised PCMs are compounds prepared by mixing melted PCM and support material. After cooling, the solidified support material provides structural rigidity, maintaining the shape unchanged whether the PCM is in liquid or solid state [22, 64, 65].

Shape-stabilised PCMs can be formed with several types of PCMs, such as paraffins [66, 67], bio-based PCMs [68], or salt hydrates [69]. The support material, which can be either organic or inorganic (such as high density polyethylene, styrene-butadiene-styrene copolymer, etc.), is characterised by a multi-pore structure with adsorption ability. The porous network absorbs the liquid PCM avoiding

leakage [65]. To increase the thermal conductivity of the material, exfoliated graphite or carbon fibres can be added [70, 67].

Shape-stabilised PCMs look like homogeneous materials. The percentage of PCM can be up to 80%, so the amount of energy that can be stored is comparable to that of traditional PCMs [66].

Reviews on shape-stabilised and composite PCMs can be found in [71, 65, 72].

2.1.1.7   Numerical modelling of PCMs

The heat transfer analysis during the phase change process of pure substances involves the solution of moving boundary problems. Melting and solidification in pure substances occur at a single temperature, hence a clear solid-liquid interface can be identified. This boundary moves according to the speed at which the latent heat is absorbed or released, so the position of the boundary is not known a priori and is part of the solution [20].

The governing heat transfer equations in the solid and liquid phases are respectively given by

$$\rho c_s \frac{\partial T_s}{\partial t} = \nabla \left(k_s \nabla T \right) \quad \text{and} \quad \rho c_l \frac{\partial T_l}{\partial t} = \nabla \left(k_l \nabla T \right).$$

The heat balance at the solid-liquid interface, defined by $F(x, y, z, t) = 0$, is enforced by the Stefan condition. For conduction-dominated heat transfer,

$$k_s \frac{\partial T_s}{\partial n} - k_l \frac{\partial T_l}{\partial n} = \rho L u_n \quad \text{at} \quad F(x, y, z, t) = 0, \tag{2.4}$$

where n is the normal direction vector on the interface pointing towards the liquid region, and u_n is the interface velocity in the normal direction. The densities of the solid and liquid phases are here assumed to be the same. Moreover, to ensure continuity of the temperatures at the interface,

$$T_s(x, y, z, t) = T_l(x, y, z, t) = T_m \quad \text{at} \quad F(x, y, z, t) = 0.$$

If convection in the liquid phase is the dominant mode of heat transfer near the interface, eq. (2.4) becomes

$$k_s \frac{\partial T_s}{\partial n} - h_c \left(T_\infty - T_m \right) = \rho L u_n \quad \text{at} \quad F(x, y, z, t) = 0,$$

where h_c is the heat transfer coefficient at the liquid interface, T_∞ is the bulk temperature of the liquid phase, and T_m is the interface temperature (equal to the melting temperature) [73].

A few analytical solutions of the moving boundary problem are available, mainly for one-dimensional cases of infinite or semi-infinite regions with constant thermal properties and simple boundary conditions [73, 74]. For more complex geometries and boundary conditions, several numerical methods can be applied. The numerical approaches can involve fixed grid methods, variable grid methods, and hybrid methods. In fixed grid methods, the boundary is tracked within a fixed space grid by the use of an auxiliary function. In variable grid methods, the space grid deforms as the solution develops; the interface is explicitly tracked and the grid nodes move along with the moving boundary layer. In hybrid methods, a front tracking scheme follows the movement of the boundary within a fixed background grid [75]. The heat transfer during the phase change process can be simulated by using several mathematical models, such as the enthalpy method, the heat capacity method and the heat source method [76], which can be solved for a variety of geometries [74].

These approaches generally consider a conduction-dominated heat transfer. Even though convective flow within the liquid phase can be neglected for microencapsulated and shape-stabilised PCMs, it may have a significant influence in macroencapsulated PCMs, affecting the melting/solidification rate as well as structure and distribution of the solutes within the liquid phase of multicomponent systems [77]. To quantitatively determine convection in a Newtonian fluid, the continuity equation (mass conservation),

$$\frac{\partial \rho}{\partial t} + \nabla \left(\rho \vec{u} \right) = 0 \tag{2.5}$$

and the Navier-Stokes equation (momentum conservation),

$$\rho \frac{\mathrm{D} \vec{u}}{\mathrm{D} t} = -\nabla p + \mu \nabla^2 \vec{u} + \rho \vec{g} \tag{2.6}$$

need to be solved. Among the approaches that can be adopted to numerically solve equations (2.5) and (2.6) are methods such as the stream-function–vorticity formulation and the primitive variable formulation [77]. As an alternative, convection in the liquid phase can be considered through an effective thermal conductivity [20].

2.1.1.7.1 Enthalpy method In the enthalpy method, sensible and latent heat are accounted for by an enthalpy term [75, 76]. This is especially useful in mixtures, where the phase change occurs over a range of temperatures. For conduction-dominated heat transfer, the enthalpy equation is given by

$$\rho \frac{\partial h(T)}{\partial t} = \nabla \left(k \nabla T \right),$$

whose solution requires the knowledge of the functional form of the enthalpy-temperature curve, as well as the dependency of the thermal conductivity on temperature [20]. The advantages of this approach are that a single governing equation can be applied to all phases, both sharp and gradual phase change can be dealt with, and the position of the solid-liquid boundary does not need to be evaluated, even though it can be easily retrieved. However, the temperature may oscillate with time and supercooling problems are not easy to handle [75]. Nevertheless, a model based on the enthalpy approach which takes into account hysteresis and supercooling was developed in [78].

2.1.1.7.2   Heat capacity method   In the heat capacity method, both sensible and latent heat are accounted for by a heat capacity term, which increases during the phase change process imitating the effect of enthalpy [75, 76]. The heat capacity can be approximated in two ways, which respectively result in an apparent and an effective heat capacity method.

The governing equation in the apparent heat capacity approach is

$$\rho c_{\mathrm{app}}(T) \frac{\partial T}{\partial t} = \nabla \left(k \nabla T \right),$$ (2.7)

where $c_{\mathrm{app}}(T)$ is the apparent heat capacity, which is determined according to the nodal temperature. The advantage of this method is that it can be easily programmed, since the temperature is the only variable that needs to be solved [75]. However, it lacks computational efficiency because a small time step and fine grids are required for accuracy. Moreover, an artificial phase change temperature range must be used when modelling pure materials to avoid making equation (2.7) undefined [77].

The effective heat capacity method is more accurate than the apparent method, but it is very troublesome to implement [77]. In this approach a temperature profile is assumed between the nodes, and an effective heat capacity, $c_{\mathrm{eff}}(T)$, is calculated through the integration over the control volume, V.

$$c_{\mathrm{eff}}(T) = \frac{1}{V} \int_V c_{\mathrm{app}}(T) \, \mathrm{d}V$$

2.1.1.7.3   Heat source method   In the heat source method, the latent heat is treated as a source term [75, 76]. The governing equation is written as

$$\rho c_{\mathrm{avg}} \frac{\partial T}{\partial t} = \nabla \left(k \nabla T \right) - \rho L \frac{\partial f_l}{\partial t},$$

where the solid-liquid interface is tracked through evaluation of a nodal liquid fraction, f_l, given by

$$f_l = \begin{cases} 0 & \text{if } T < T_s \\ \dfrac{T - T_s}{T_l - T_s} & \text{if } T_s \leq T \leq T_l \\ 1 & \text{if } T > T_l. \end{cases}$$

The advantage of this method is that it can deal both with sharp and gradual phase change. However, it lacks computational efficiency and round off errors arise when melting occurs over temperature range [75].

2.1.2   Application of PCMs in the building envelope

PCM application in buildings can provide several advantages, such as reducing building energy use, diminishing peak heating and cooling loads, and improving thermal comfort [9]. PCMs can be applied both as passive strategies, when integrated within the building structure, and as active strategies, when integrated within the HVAC system. In any case, according to the intended application and to the building location, an effective use of PCM in buildings requires an appropriate selection of PCM's thermo-physical properties, quantity and position. Therefore, to guarantee a good functioning of the PCM and ensure economic feasibility, optimisation of the PCM use can be advisable.

Since the focus of the present research is on the application of PCMs in the building envelope, an overview on the use of PCMs in active systems will not be provided. Moreover, active applications are justified only if the benefits deriving from the use of PCM are greater than the system costs [79]. Extensive information on the subject can be found in [10, 14, 80].

2.1.2.1   Passive application strategies

Passive utilisation of PCM in buildings is based on charging (melting during the day) and discharging (solidification during the night) cycles [81]. During summer, this helps avoiding or reducing overheating during the day, and in winter it may help reducing heating during the night [9]. The feasibility of passive utilisation of PCMs depends on the effectiveness of the PCM's thermal cycles, which can be guaranteed by the diurnal temperature variability of the building site [81]. If the PCM does not completely solidify during the night, the effectiveness of the system may be significantly reduced [9]. Room orientation, ventilation, glazing type and size, and shading devices are therefore fundamental elements to consider when

designing passive PCM applications [81].

For cooling applications, the use of night ventilation together with PCMs is a very powerful strategy to enhance the effectiveness of the PCMs' thermal cycles [82]. Night ventilation differs from free cooling in that night ventilation uses the building as a thermal storage, whereas free cooling requires a storage medium, such as a PCM storage unit [83], and the air exchange takes place mechanically [14, 80]. When night cooling ventilation is adopted to discharge the PCM, the ventilation rate should be carefully selected to avoid that the energy used for operating the fans is greater than the energy savings [84]. However, there are some drawbacks in the use of night cooling ventilation, such as a limited heat transfer surface between PCM and air, a low convective heat transfer coefficient which prevents the use of great amounts of PCM, and a low utilisation factor due to the large time shift between discharging and charging times [82].

For winter applications, PCM integration in passive buildings was proposed especially within the floor, since the sunlit floor surface can store solar energy during the day and release it during the night [85, 86].

2.1.2.1.1 Energy demand and load reduction   The latent heat storage ability of PCMs during phase transition can provide potential benefits in reducing the heat transfer in buildings, hence diminishing cooling/heating energy demand and peak loads. According to the climate, the saving in peak loads may be more pronounced than the annual energy savings [87].

For cooling load reduction in a tropical climate, in absence of night cooling PCMs were found to have a better performance when placed on the external surfaces of the walls; the optimal phase change temperature was the lowest temperature allowing a full thermal cycle of the entire PCM layer. However, the melting temperature range and the shape of the enthalpy-temperature curve were found to influence the optimum phase change temperature. A large melting temperature range could improve the adaptability of PCMs to the temperature variations, but the best achievable energy performance may be compromised. Moreover, thin PCM layers showed higher efficiency and cost benefits than thicker layers, even though the latter were capable of reducing the heat gains through the building envelope to a greater extent [88]. When night cooling ventilation is adopted, PCMs should be applied in interior building elements with priority on south, west and east walls, ceiling and north wall [84].

2.1.2.1.2 Peak load shifting   Peak load shifting is the process of shifting the energy demand from on-peak periods (i.e. the hours characterised by a high energy price) to off-peak periods (i.e. the hours characterised by a low energy price). Even though this strategy can be used both for cooling and heating, it is mostly applied

for cooling purposes [17].

For cooling applications, the process takes place by discharging (from a thermo-dynamic point of view) either the thermal mass of the building or a thermal energy storage during off-peak hours by the use of air conditioning or night ventilation [89]. The charging takes place during daytime through the effect of environmental and internal loads. For heating applications, HVAC systems are operated during night-time for the charging process; the stored heat is then released during the day allowing to reduce the operation time of the heating system [90].
Peak load shifting with PCM for cooling application can be achieved by means of PCM-air heat exchangers as well as through passive design strategies with the PCM integrated in the building [9]. For heating application, peak load shifting with PCM is generally provided by means of a PCM underfloor heating system [91–93]. However, PCM application in gypsum wallboards was also found to be effective [94].

By shifting the peak load far from the peak hours of electricity demand, a lower pressure is put on the electrical grid. Moreover, HVAC systems could be dimensioned for smaller heating or cooling loads [9]. Even with no or simple control strategies, PCM application for peak load shifting allow for significant peak cooling load reductions, especially in lightweight buildings. However, the potential of these systems could be further improved through the adoption of more sophisticated load shifting control strategies [89]. For example, peak load shifting in passive cooling PCM design can be improved by means of a price-based method for discharging the PCM during the off peak period by use of the air conditioning [95] or night ventilation [83]. The application of weather forecast data can allow for further energy savings, even though accurate forecasts are necessary to avoid the risk of a higher energy consumption in PCM-enhanced buildings [96].

2.1.2.1.3   Thermal comfort enhancement   PCMs in buildings may be used to improve thermal comfort by reducing both peak temperature and temperature swings within the indoor environment [9]. Moreover, surface and air temperatures can become more uniform, reducing the risk of local discomfort for radiant asymmetry [97, 9].

For improving thermal comfort, PCM can be integrated in buildings both in opaque [97–100] and transparent components [101]. Climate, PCM location and melting temperature have a strong impact on PCM's performance. Moreover, the effectiveness of PCMs in reducing peak zone temperatures is affected by the occupants' behaviour [102, 100].

When applied on existing office buildings with low thermal inertia, thermal comfort in summer can be effectively enhanced if the temperature variations are in the phase change temperature range of the PCM [97], but the energy consumption may increase during the heating period [103]. In residential buildings and mild

climates, PCMs were however found to be more effective in reducing heating energy consumption than in improving thermal comfort [99]. The effect of PCM in reducing cooling loads and improving thermal comfort may become especially beneficial as the impact of the climate change gets more significant [104].

2.1.2.2 PCM integration in the building envelope

Integration of PCM in buildings can occur both in opaque and transparent components [9, 17], as well as in shutters [105] or even in furniture [106]. In the following sections, the focus will however be on the application in the building envelope.

2.1.2.2.1 PCM in opaque components PCMs have been proven, by means of both experimental and numerical studies, to be beneficial especially in lightweight buildings; they contribute to significantly increase the thermal storage capacity of the building, improving thermal comfort and reducing energy consumption [9]. Moreover, the power needed for the HVAC system operation is reduced; however, the energy demand may not be reduced in buildings with a high thermal mass [107].

PCMs can be easily integrated into other building materials, so that the construction process does not need to significantly change compared to traditional buildings [9]. Several experimental tests were carried out, both at laboratory and building scale, to investigate the effect of PCMs integrated in building walls. PCM incorporation can occur through macroencapsulation (such as inside masonry blocks [108, 109] or sealed in thin polymeric pouches [110, 111]), or by means of shape-stabilised panels [64, 97]. Moreover, PCM can be embedded through various techniques in traditional construction materials, such as plasters [112–114], gypsum boards [115–117], or even in composite shape-stabilised PCM-mortar bricks [118, 119]. Some authors also performed numerical and experimental studies on the potential application of PCMs in ventilated façades. Diarce et al. [120] investigated the thermal behaviour of a ventilated façade with PCM integrated in the external layer. De Gracia et al. [121] assessed the potential benefits of a ventilated façade with PCM integrated in the internal layer, exploring different operating principles. Other authors investigated also the potential application of PCM-enhanced thermal insulations. Kosny et al. [122, 123] numerically investigated the effects of a fibre insulation containing microencapsulated PCM. Biswas et al. [124] assessed the thermal behaviour of a PCM-enhanced cellulose insulation both numerically and experimentally. El Omari et al. [125] numerically analysed the effectiveness of an insulating polymer matrix with micro-dispersed PCM on a yearly basis, concluding that a careful design optimisation would be needed.

However, integration of PCMs in buildings occurs most commonly by installing PCM-enhanced wallboards (such as PCM-gypsum composite plates or even better shape-stabilised PCM panels [126]) on the interior side of the building envelope [9].

The thermal performance of PCM wallboards is strongly dependent on the convective heat transfer taking place with the indoor air [127]. Therefore, a correct knowledge of the convective heat transfer coefficient is important [22]. Since the convective heat transfer coefficient was found to be higher for a PCM wall than for an ordinary wall, calculating its value using the equations for ordinary walls can lead its underestimation [128]. Heat transfer of PCM wallboards under natural convection is nevertheless considered too low for an adequate exploitation of the PCM's potential [98]. A possible solution to enhance the heat transfer was numerically investigated by Evola et al. [129], who proposed to leave a narrow cavity between wall and PCM wallboard, where outdoor air could circulate during the night. Moreover, together with ventilation, occupancy patterns should be also taken into account when investigating the effects of PCMs in buildings. The occupancy patters should especially be considered when selecting the PCM's melting temperature [130].

According to the climate, optimal PCM melting temperatures can differ in winter and summer season [9, 131]. PCMs that perform well during the heating period may have only a marginal effect—if any—during the cooling period, and vice versa [79]. Therefore, the application of two different PCMs may be beneficial to improve the energy efficiency of buildings during the whole year [132].
The simultaneous application of two or more PCM layers was investigated by a few authors [133–137]. Pasupathy and Velraj [133] recommended the use of a double PCM layer with two different melting temperatures in a roof application to reduce the air temperature swings throughout the year. Kheradmand et al. [135] proposed the simultaneous incorporation of three different phase change materials in plaster mortars. They found that this hybrid material was able to significantly reduce heating and cooling energy demand of a laboratory scale prototype when compared both to normal plasters and to plasters with a single type of PCM. Zhou et al. [134, 138, 139] presented numerical studies on the application of two layers of shape-stabilised PCM for buildings located in climates requiring both heating and cooling. Their analysis was carried out for the south facing wall of an office building case study. The wall was characterised by an external PCM layer which was active during the cooling season, and by an internal PCM layer which was active during the heating season. The optimal thickness of the PCM layers was identified between 30 mm and 60 mm. Thickness and melting temperature were found to influence each other when searching for the minimum annual energy demand or peak load for heating and cooling [138]. Ascione et al. [137] numerically investigated the simultaneous application a two PCM layers on the inner ad outer sides of the wall of a residential building, and found that the application of a PCM layer with a high melting temperature on the external side and a melting temperature of 25 ℃ on the internal side could maximise the cooling energy saving.

Application of PCMs in roofs has received less attention than in walls [9].

Addition of PCM in roofs was however found to have a positive effect in improving thermal comfort and in reducing cooling loads and, to a lesser extent, also heating loads [140]. For cooling applications, flat roofs which integrated PCM within the concrete slab in holes characterised by conical frustum [141] and cylindrical [142] geometries were investigated. With an appropriate selection of PCM and geometry (the best results were obtained with a conical shape of the holes [141]), the entering heat flux could be significantly reduced. With regard to sloped roofs, the influence on the thermal behaviour due to solar radiation, roof slope, PCM's phase change temperature and latent heat of fusion, thickness of the PCM, and solar absorption coefficient of the external surface was investigated in [143]. Roof slope, PCM's thickness and solar absorption coefficient resulted to have a stronger influence on temperatures and heat fluxes than phase change temperature and latent heat of fusion of the PCM.

For further improving the performance of PCMs for cooling applications, some authors investigated wall and roof systems which coupled PCMs with cool coatings [144, 145]. PCMs and cool coatings rely on different mechanisms to reduce heat gains, therefore they are complementary passive cooling strategies. The cool paint reflects a great amount of solar radiation while the PCM stores the energy that is nevertheless transferred through conduction [144]. This combination was experimentally proven to reduce surface and air temperatures more than when adopting each single strategy (i.e. either PCM or cool paint alone) and to guarantee important monthly and annual energy savings in the climate of Singapore. Moreover, the PCM could be maintained nearby the phase change temperature for a longer period of time [144]. This application is especially promising in tropical climates; however, the performance of this solution in different climatic regions still needs to be evaluated [145]. Combined application of PCM and cool coatings was also proposed as an urban heat island mitigation strategy [146–148].

2.1.2.2.2 PCM in transparent components PCMs integrated in glazing components interact with the impinging solar radiation acting both as a solar shading device and as a heat storage medium. PCMs in glazing systems sensibly increase their inertial behaviour, smoothing the indoor surface temperature and providing peak load shifting. They are expected to improve thermal comfort, as well as to reduce heat gains and losses compared to standard glazing systems.

Several experimental [101, 149–151] and numerical [152–157] studies investigated the performance of PCM-enhanced glazing components. Numerical models were specifically developed to take the interaction with solar radiation into account [158, 159]. Optical properties of PCM play an important role in the thermal performance of PCM-filled glazing units [153, 156], therefore solar and visible properties are also needed for a complete and accurate analysis of the behaviour of such components [160–162]. To further improve this kind of technology, the simultaneous

use of a thermotropic layer can provide a better control on the charging phase of the PCM [163].

A review on PCM technologies developed for transparent and translucent building envelope components, such as windows, shutters and other shading devices can be found in [105].

2.1.2.3   Retrofit applications

The application of PCMs can be beneficial in the retrofit of existing buildings with a low thermal inertia. If the temperature variations within the building are around the phase change temperature range, the thermal comfort of the occupants can be effectively enhanced [97].

PCM wallboards [81] are often used in retrofit applications due to their low thickness and ease of installation; they can either replace the existing interior finishing or can be placed over it [81]. Diurnal thermal variability of the building location [81, 131], peak melting temperature of the PCM [164, 131], PCM's thickness [131], PCM's position within the room and rate of night ventilation [164, 100] have a strong impact on the effectiveness of PCM in improving thermal comfort in existing buildings. PCM can help reducing both peak and daily swings of the internal air temperature, and can be useful also when the windows' size needs to be increased; the excessive solar gains may be absorbed by the PCM, and the thermal comfort can still be enhanced with respect to the pre-retrofit building [81].

2.1.2.4   Economic feasibility

Economic feasibility of PCMs is strongly affected by both PCM and energy prices [36]. Several authors investigated the economic impact of PCMs in buildings; contrasting results were found according to input prices, PCM's thermo-physical properties and building location [53].

Among the studies who found some benefits in the application of PCMs are [165, 166] and [103]. Sun et al. [165] investigated the potential savings for space cooling deriving from the application of PCMs in five cities in China. Considering a PCM cost (purchase and installation) of 2 USD/m^2 for 1 cm of thickness and an electricity price ranging between 0.1181 USD/kWh and 0.1741 USD/kWh according to the location, they found an acceptable simple payback period (below ten years) when the phase change temperature was 3 ℃ higher than mean outdoor air temperature. Mi et al. [166] investigated the potential savings for a typical multi-storey office building in the same locations as in [165], by means of both static and dynamic payback periods and considering different discount rates. With PCM and energy prices equal to those reported in [165] and a PCM melting temperature of 27 ℃,

they found a higher economic value of the investment in the locations characterised by a cold winter. No economic benefit was found in the warmest cities. Saffari et al. [103] analysed the economic performance of PCMs when applied together with a thermostat control based on Fanger's comfort model. Different scenarios were investigated for the location of Madrid, which included HVAC operation schedules for office and residential buildings, PCMs with different melting temperatures and thickness, and variable clothing of the occupants. Considering a PCM cost of 0.62 EUR/kg (5.46 EUR/m^2 for 1 cm of thickness) plus 4.36 EUR/m^2 for its installation, and energy prices for natural gas and electricity in accordance with the Spanish national rates, they found that the PCM with the highest melting temperature ensured the best payback period for the analysed location. Due to the very low cost of the PCM, extremely short payback periods were found, especially for the 24-hours HVAC operation scenario ($<$ 2 years) and the residential one ($<$ 3 years). About 6 years of payback period were instead found for the office schedule because the remarkable energy savings during the cooling seasons were counterbalanced by an increase in the energy consumption during the heating period.

Among the studies who found PCM not to be economically beneficial are [167] and [132]. Baniassadi et al. [167] investigated the potential savings for residential buildings deriving from the application of a bio-based PCM in six cities in Iran. Considering a PCM cost (purchase, transport and installation) of 22.53 USD/m^2 for 2.01 cm of thickness and an electricity price ranging between 0.0130 USD/kWh and 0.0801 USD/kWh according to the monthly consumption range, they searched for the PCM thickness which minimised a total cost function. With a null optimum PCM thickness, they found that PCM was always infeasible. Buonamano et al. [132] investigated the potential savings deriving from the use of innovative technologies in a non-residential nZEB located in Naples (Mediterranean climate). Considering an overall PCM cost of 46.4 k€ for the whole building, they found that the initial material cost was too high for achieving an acceptable payback period.

2.1.2.5   Energy simulation

To correctly evaluate the potential energy savings and economic feasibility of PCM-enhanced buildings, a reliable evaluation of their dynamic thermal performance is necessary. On one hand, numerical models capable of predicting the real life performance of PCMs added to buildings and validated in an exhaustive way are needed; on the other hand, the overall thermal behaviour of PCMs needs to be accurately known [168].

Many building energy simulation tools capable of assessing the energy performance of buildings with PCM-enhanced components are available, such as EnergyPlus, ESP-r and TRNSYS [53].

EnergyPlus is an open source program whose modules work with a simulation

core based on fundamental heat balance principles [169]. To model PCMs, a modified version of the enthalpy method is applied with a conduction finite difference algorithm, which was validated by Tabares-Velasco et al. [170]. They recommended to use a time step equal to 3 minutes and space discretisation constant equal to 1.

ESP-r is an open source building energy simulation tool based on a finite volume approach, where the problem is transformed into a set of conservation equations which are integrated in response to climate, occupants, and control system influences [171]. PCMs are modelled in ESP-r through the effective heat capacity method with an iterative correction scheme [172].

TRNSYS is a modular program whose components—called *Types*—can be linked together so that the output of one Type can provide the input to another [173]. TRNSYS is especially flexible because it allows to call external programs such as MATLAB or FLUENT [87]. Several authors contributed to develop and validate TRNSYS Types for simulation of PCMs in buildings [174, 175, 87].

The importance of a correct evaluation of the enthalpy-temperature curve of PCMs for simulation purposes was recently underlined by Kuznik et al. [28]. They found that, for a free-running residential case study, the enthalpy curves deduced directly from DSC measurements were not able to correctly predict the thermal behaviour of the building and the thermal comfort. In particular, the higher the DSC heating rate, the higher the discrepancy was. As a consequence, inaccurate predictions of the thermal behaviour of PCMs leads to an incorrect design and to a wrong estimation of their efficiency.

2.1.2.6   Environmental impact

The content of this section was partly published in [176].

The environmental impact associated to all the stages of a product's life can be evaluated through the Life Cycle Assessment (LCA) [177]. Both embodied energy—i.e. the overall energy required to realise a product (extraction of raw materials, transports, plant processes of manufacturing and packaging, etc.)—and operational energy—i.e. the energy required during the expected lifetime of the product—are evaluated; in this way, different solutions can be compared in order to identify those characterised by the lowest overall energy use.

Application of PCM in buildings was found to generally have a positive environmental impact, even though results of the impact assessment are strongly dependent on the goal and scope definition of LCAs [16]. The use of PCM is more favourable in locations with similar weather conditions throughout the year and with a suitable optimisation of the PCM type, properties, quantity and position, and through a proper integration between building envelope and building services. The decrease in building energy consumption during operation may not

otherwise be sufficient to reduce the global impact throughout the lifetime of the building [178, 176]. Esters [179] and salt hydrates [178, 180] should be preferred over paraffins due to their lower embodied energy.

2.1.2.7 Performance assessment indicators

Due to the non-linear behaviour of PCMs, evaluating and comparing the dynamic thermal performance of building envelope components with PCM is a challenging task. A series of metrics have been proposed in the literature which can be applied either at the component level or mostly at the building level.

With regard to component level indicators, Zhang et al. [181] proposed the following two parameters, respectively meant for PCM applied to external and internal side fo a wall, to analyse the thermal storage of PCM wallboards:

- *Modifying factor of the inner surface heat flux*, α, defined as the ratio of the real inner surface heat flux on the heat flux which would occur if the heat capacity of the wall could be neglected;

- *Ratio of the thermal storage*, b, defined as the ratio of the charged (or discharged) heat on the total thermal capacity of the wall per unit area.

However, this formulation neglects the presence of solar radiation. Zhou et al. [182] proposed to consider the sol-air temperature rather than the outdoor air temperature to evaluate the wallboard's behaviour. Similarly to the case of traditional wall materials, assuming a sinusoidal variation of the sol-air temperature on the outer side and a constant air temperature on the inner side of the PCM wallboard, they analysed

- *Decrement factor*, f, defined as the ratio of the amplitude of the inner surface temperature wave on that of the outdoor temperature wave;

- *Time lag*, φ, defined as the time delay between the minimum values of outdoor and indoor surface temperature waves.

With regard to building-level indicators, the performance of the PCM can be evaluated in terms of improvement of indoor thermal comfort [98, 183], by assessing the latent heat usage of the PCM during diurnal cycles [98, 183, 184], or in terms of building energy performance improvement [88, 86]. It should be noted that not all the indicators are suitable to buildings with HVAC systems.

Evola et al. [98] proposed the following four metrics to evaluate the effectiveness of PCMs for improving thermal comfort in buildings and the latent heat usage:

- *Intensity of thermal discomfort* (ITD), defined as the time integral over the

occupancy period of the positive difference between the operative tempera-
ture and the upper comfort's threshold;

- *Frequency of thermal comfort* (FTC), defined as the percentage of time within
  the occupancy period when the indoor thermal comfort conditions are met;

- *Frequency of Activation* (FA), defined as the percentage of time, within a given
  period, during which the PCM is undergoing phase change;

- *Storage efficiency* (η_{PCM}), defined as the ratio of the thermal energy stored
  by the PCM on its latent heat.

However, experimental validation by Castell and Farid [185] of the metrics
proposed by Evola et al. revealed that, for buildings with significant heat gains,
limited insulation or low thermal inertia, the ITD was the most relevant indicator
among the four, but it failed in presenting the benefits of PCM for buildings with
high thermal inertia, heavy insulation, and with no solar gains. Moreover, they
suggested to separately evaluate both the discomfort time above the upper and
below the lower comfort thresholds (T_{upper} and T_{lower}, respectively), and to later
group them into a single indicator. Therefore,

$$ITD = \int_P \Delta T^+ (\tau) \, d\tau,$$

with

$$\Delta T^+ (\tau) = \begin{cases} |T_{op} (\tau) - T_{upper}| & \text{if } T_{op} (\tau) > T_{upper} \\ |T_{op} (\tau) - T_{lower}| & \text{if } T_{op} (\tau) < T_{lower}, \end{cases}$$

where P is the occupancy period and T_{op} is the operative temperature.

They additionally suggested the potential application of the *Fluctuation of
thermal discomfort* (FD) defined by Sicurella et al. [186] to PCM-enhanced buildings.

To evaluate PCM effectiveness in enhancing indoor thermal comfort, rather
than considering the time outside the comfort range, Ramakrishnan et al. [183]
proposed an *Effectiveness coefficient* (e), defined as the percentage of time during
which the operative temperature falls within a predefined comfort range during
the occupancy period (P):

$$e = \frac{\sum_{t=1}^P TC_t}{P},$$

where

$$TC = \begin{cases} 1 & \text{if } |T_{comf} - T_{op}| < 3.5 \\ 0 & \text{if } |T_{comf} - T_{op}| \geq 3.5. \end{cases}$$

T_{comf} and T_{op} are respectively the optimal comfort temperature and the indoor
perative temperature, evaluated according to the ASHRAE adaptive model:

$$T_{comf} = 0.31 \cdot T_{mae} + 17.8,$$

$$T_{op} = (T_{ai} + T_{mr})/2,$$

where T_{mae} is the mean monthly outdoor air temperature, T_{ai} is the indoor air emperature, and T_{mr} is the mean radiant temperature.

In addition, Ramakrishnan et al. [183] proposed the following two indices to evaluate the efficiency of PCM operation during a diurnal cycle, which combine the effect of storage capacity and activation period in unique indicators:

- *Cooling efficiency coefficient* (CE), which measures how efficiently PCM works during charging:

$$CE = \sqrt{L_C \cdot T_C},$$

  where L_C is the ratio of diurnal latent charge on latent heat capacity, and T_C is the ratio of charging duration (expressed in minutes) on daytime duration (720 minutes).

- *Heating efficiency coefficient* (HE), which measures how efficiently PCM works during discharging, and defined as

$$HE = \sqrt{L_{DC} \cdot T_{DC}},$$

  where L_{DC} is the ratio of diurnal latent discharge on latent heat capacity, and T_{DC} is the ratio of discharging duration (expressed in minutes) on night-time duration (720 minutes).

On a practical point of view, L_C and L_{DC} are determined as the difference between maximum and minimum effective latent storage, η, respectively during day and night. The effective latent storage is evaluated as

$$\eta = \frac{\sum_{i=1}^{N}[H(T_i) - H(T_0)]}{\Delta H},$$

where ΔH, $H(T_i)$ and $H(T_0)$ are respectively the PCM's latent enthalpy, the specific enthalpy at the i$^{\text{th}}$ node, and specific enthalpy corresponding to the onset melting temperature.

Another indicator to assess the performance of PCMs in terms of charging and discharging ability during a diurnal thermal cycle was proposed by Royon et al. [184], who defined a *Mean activity of PCM* during the thermal cycle, $\bar{a}$, as

$$\bar{a} = \frac{1}{t_c} \int_{t_0}^{t_0+t_c} a \, dt,$$

where t_0 and t_c are respectively the temperatures at the beginning and at the end of a cycle, and a is the percentage of "active" PCM, evaluated as the PCM volume within the melting temperature range.

To assess the effect on the energy performance of buildings of PCMs incorporated into the building envelope, Lei et al. [88] proposed the following two indicators:

- *Total envelope heat gains*, Q (MJ/m^2), defined as the overall heat gains through the building envelope during the entire simulation period;

- *Envelope heat gain reduction rate*, η, defined as the percentage reduction of the heat gains through the envelope due to the addition of a PCM layer:

$$\eta = \left(1 - \frac{Q_{PCM}}{Q_{No\_PCM}} \right) \cdot 100\%,$$

  where Q_{PCM} and Q_{No_PCM} are the envelope heat gains of the building with and without the addition of the PCM layer, respectively.

To evaluate the effect of PCMs in passive buildings, Ye et al. [86] proposed the following two indices to evaluate the hypothetical energy saving deriving from the adoption of PCMs (as well as from other materials or components):

- *Energy saving equivalent* (ESE), (J), defined as the hypothetical energy that should be supplied or removed to maintain a passive room at the same temperature as when a particular material or component is used. In summer, $ESE = \left(Q_C - Q_H \right) / EER$, whereas in winter $ESE = \left(Q_H - Q_C \right) / COP$;

- *Energy saving index* (ESI), defined as the amount of energy saved (or wasted) when a particular material or component is used, with respect to an ideal material or component capable of maintaining a passive room's indoor temperature at a constant comfortable level (e.g. 23 ℃). Therefore, $ESI = ESE / ESE_{\max}$.

2.2   Optimisation analyses

The content of this section was partly published in [187].

Optimisation is the procedure of finding the minimum or maximum of a function (called either *cost* or *fitness* or *objective* function) by choosing, within a certain domain, the values to assign to its independent variables. However, there is often the need to optimise more than a single function. When the optimisation problem needs to be addressed by considering multiple objectives, which are usually contrasting (i.e. minimising one function leads to maximise the other), the process of simultaneously addressing multiple optimisation functions is called *multi-objective optimisation*.

The easiest option to deal with multiple objectives is to apply a weighted sum of the objective functions in order to reduce the multi-optimisation problem to a single optimisation problem. However, a proper choice of the weight factors is not
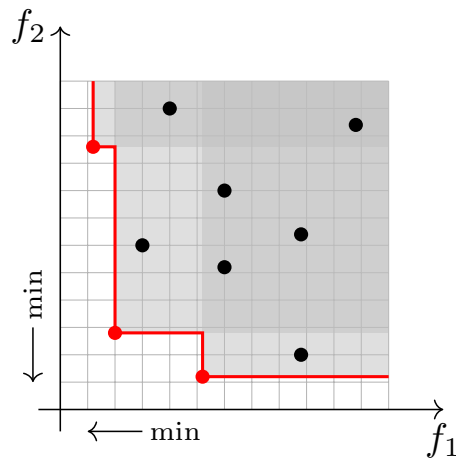
Fig. 2.6 Example of Pareto front for the minimisation of two objective functions.

an easy task, and information on how the different objectives interfere with each other cannot be extracted [188]. An alternative approach is to study the relationship between the solutions through the concept of *dominance* [189]. When comparing two solutions and determining which one is best (for example solutions A and B), if the objective functions are contrasting it may not be the case that solution A outperforms B in all functions, as it may be the case that A outperforms B in one function but B outperforms A in another. Hence:

- If solution A outperforms solution B in at least one function and outperforms or equals solution B in all the other functions, then solution A dominates solution B;

- If solution A outperforms solution B in one or more functions and at the same time solution B outperforms solution A in one or more functions, then solutions A and B do not dominate each other.

The *Pareto front*, also called trade-off set or non-dominated set, is the set of all non-dominated solutions in a given group. They represent the set of solutions where one cannot be said to be better than another if all objective functions are considered in the problem (red dots in Fig. 2.6).

The shape of the Pareto front gives indications on the degree of contrast between objectives; convex, linear or concave shapes respectively denote low, linear and high contrasts. Pareto fronts resulting in a single solution denote instead non-contrasting objectives [188].

2.2.1 Classification and general features

2.2.1.1 Search space and objective space

Multi-objective search problems are often analysed in terms of search space and objective space [188]. The *search space* is the domain space. A representation of the proposed solutions in the search space is described by the values of their variables. In this way, differences and similarities between solutions are highlighted under the design point of view. The dimension of the search space equals the number of problem variables. The *objective space* is the codomain space, hence a representation of the solutions with respect to the values of their objective functions. In this way, differences and similarities between solutions are highlighted under the performance point of view. The dimension of the objective space equals the number of objective functions.

2.2.1.2 Search methods

To investigate the search space and find optimal or near-optimal solutions of a given problem, there are only few situations where an analytical solution can be obtained; due to the non-linear or discontinuous nature of some problems, as well as to their complex mathematical formulation, this possibility cannot always be pursued. Alternative approaches such as parametric analyses, enumerative methods and optimisation techniques can be adopted to overcome these limitations [190].

All non-analytical search algorithms need to transform continuous search spaces into discrete ones. In this way, only a finite number of candidate solutions is studied.

Enumerative methods are exhaustive search processes which evaluate all the solutions in a discrete space and choose the best one. However, using a brute force technique to evaluate all possible solutions is computationally expensive and is generally not a feasible process.

Parametric analyses have been widely used as a basic form of optimisation. Parametric studies usually explore the search space by varying one or more parameters in a certain range and with a predefined step, while keeping the other parameters fixed at a constant value. Even though this kind of procedure does not lead to globally optimal solutions, it finds local optima among the investigated options. An advantage of parametric studies is that no expertise in optimisation is actually required. However, when the search space is wide, the computational effort is still outperformed by that of proper optimisation strategies. In the field of building energy simulation, the jEplus [191, 192] tool allows to easily perform parametric analyses with the EnergyPlus simulation engine.

(a) Unimodal problem.

(b) Multimodal problem.
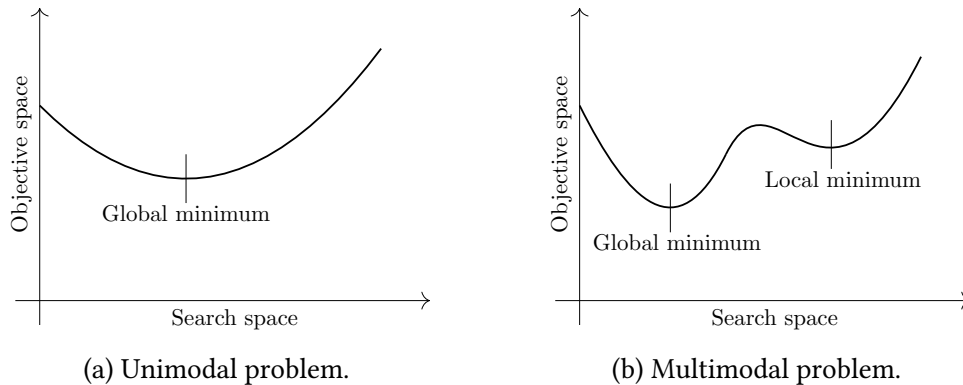
Fig. 2.7 Unimodal vs multimodal problems.

2.2.1.3 Exploration and exploitation

When dealing with optimisation techniques, a great variety of optimisation algorithms can be applied. The selection of the optimisation algorithm is related to the problem that needs to be solved, since not all the optimisation algorithms are suitable for solving all the search problems. In any search method, the processes of exploration and exploitation are involved [188]. *Exploration* is the process responsible for covering the entire search space, in order to include the majority of solutions in the search and to guarantee diversity between them. *Exploitation* is the process responsible for identifying the best performing solutions, in order to direct the search process towards promising areas and generally reduce the search space and time. Exploration and exploitation can hence be considered as opposite processes, and the performance of an optimisation algorithm depends on the trade-off between them.

2.2.1.4 Unimodal and multimodal problems

Optimisation problems can be divided in unimodal and multimodal problems [193] (Fig. 2.7). The *unimodal* problems are characterised by a single minimum value. *Multimodal* problems are instead characterised by multiple minima, where some are local minima and one (or sometimes more) is the global minimum. The distinction between unimodal and multimodal problems also apply to problems with more than one objective function. Multimodality represents a challenge for search algorithms, since they may converge to local minima rather than to the global minimum.

2.2.1.5 Classification of search algorithms

Optimisation algorithms can be classified as deterministic or stochastic [193]. Their main characteristics and differences are summarised in Table 2.2.

Table 2.2 Comparison between deterministic and stochastic algorithms.

Deterministic algorithms	Stochastic algorithms
Every time they are used on the same problem and from the same starting point, the same result is obtained.	Due to the random nature of some operations, different results are obtained from multiple runs of the same problem.
They consider a single candidate solution, whose position is modified according to the information obtained by studying only this solution.	They simultaneously analyse many candidate solutions, which are progressively modified according to the information gathered by studying all of them.
In multimodal problems, they find the global minimum only if the starting point is in the basin of the global minimum and not in that of a local minimum.	Since they consider many starting points, in multimodal problems they have a greater chance of finding the global optima when compared to deterministic algorithms.
The convergence towards a minimum is less time consuming when compared to stochastic algorithms.	The convergence towards a minimum is more time consuming when compared to deterministic algorithms.

Deterministic algorithms generally search for the optimal solution by climbing or descending (respectively for maximisation or minimisation problems) the objective function in the direction of the highest gradient (although some gradient-free algorithms do exist [194]). Deterministic algorithms can be further classified into zeroth-order methods, which evaluate only the objective function, first-order methods, which evaluate also the first derivative, and second-order methods, which evaluate also the second derivative (Hessian matrix). Algorithms in this category include Newton's method (a second order method), Quasi-Newton method (a first order method), Pattern Search (a zeroth order method), and Gradient Descent. These algorithms focus on exploitation rather than exploration, and tend to quickly converge towards a minimum without exploring other possibilities. Since the quality of the result depends on the starting point, preliminary knowledge on the shape of the objective function would be required.

On the other hand, *stochastic algorithms* are characterised by the use of random operations during their search process in order to improve exploration of the search space. An important reason for their success is that they do not require preliminary information on the problem to solve, such as the shape or complexity of the objective space. Algorithms in this category include Simulated Annealing, Particle Swarm Optimisation, Ant Colony Algorithms, Evolutionary Strategies, Genetic Algorithms and Artificial Immune System. Most of these algorithms have their inspiration in natural phenomena and animal behaviour (for example evolutionary competition, cooperation among individuals or defence of a living body). Exploration is an important part of stochastic algorithms, which consider many candidate solutions—called individuals—to investigate the entire search space. This group of solutions is often called *population*, and these algorithms are sometimes referred to as *population*

based algorithms. It should be noted that the true optimal solutions are not ensured to be found. The number of individuals in the population and the number of generations for which the search process is repeated needs to be accurately chosen according to the dimension of the search space.

A brief overview on the formulation of stochastic algorithms is presented for evolutionary and genetic algorithms. Each individual in the population is characterised by a set of input data within the search space domain, and the corresponding value in the objective function represents its fitness to survive. For each generation, only some individuals among the population are selected—according to specific rules—to reproduce and generate new offspring through crossover and mutation operators. Among this class of stochastic algorithms, the NSGA-II variant is considered the most efficient multi objective genetic algorithm [194].

A comprehensive review on algorithms for optimisation of building design can be found in [195].

2.2.1.6 Constraint handling

When formulating an optimisation problem, constraints may be necessary to ensure feasibility of the solutions. They can be either equality or inequality constraints, which are generally imposed in addition to the objective functions [193]. Moreover, they can be either *hard constraints*, i.e. constraints that must be satisfied, or *soft constraints*, i.e. constraints that should be preferably satisfied, but a limited violation can be acceptable (e.g. when this implies an improvement of the fitness, or there is no other choice not to violate hard constraints).

Constrained optimisation problems can be solved by adopting a variety of constraint-handling techniques. Rejecting infeasible individuals (*death penalty*) is probably the easiest way to deal with constraints. It has the advantage of being easy to implement and computationally efficient, but its drawback is that, especially in non-convex feasible search spaces, stagnation may occur as information that could be gained from infeasible individuals is discarded [193, 196, 197].

As an alternative, the most common approach, especially when dealing with inequality constraints, is to adopt *penalty functions*, which imply worsening the fitness of infeasible solutions in order to favour feasible ones. If the exploration starts from a feasible region, an interior method is used. In interior methods, a solutions far from the boundaries is characterised by a small penalty, whereas a penalty tending to infinity is applied when approaching the constraint boundaries. Otherwise, if the exploration starts from an infeasible region to move towards a feasible one, an exterior penalty approach is used. In this case, the relationship between an infeasible individual and the feasible region can be defined in several ways; a penalisation can be applied regardless of the distance from the feasible region, or—better—the amount of constraint violation could be measured to determine the

corresponding penalty, or else "repair" of the individual could be considered [196].

Repair algorithms, which imply changing an infeasible individual into a feasible one, are especially efficient as a constraint handling method in combinatorial optimisation problems. The repaired individual can be used to evaluate its fitness either with a *never replacing* approach (i.e. the repaired individual is not returned to the population), with an *always replacing* approach (i.e. the repaired individual replaces the original individual in the population), or else the repaired version can be returned to the population only in some cases according to a certain probability. Repairing algorithms have to be specifically designed for each problem, and care should be taken not to introduce a strong bias in the search when transforming infeasible solutions into feasible ones [196, 197].

Another approach to constraint-handling is through *separation of objectives and constraints*; constraints are dealt with without modifying the fitness value as the penalty methods do. As an example, the penalty-parameter-less approach [198] takes constraints into account through comparison between individuals in such a way that 1) any feasible solution is preferred over an infeasible solution; 2) among two feasible solutions, the solution with better fitness is preferred; 3) among two infeasible solutions, the solution with smaller constraint violation is preferred. To avoid any sort of bias towards a constraint due to incommensurable units, they are normalised.

A variety of hybrid methods also exist. For additional information, comprehensive reviews on constraint handling techniques can be found in [196] and [197].

2.2.2 Search algorithms for building envelope design

2.2.2.1 Evolutionary and genetic algorithms

To address the optimisation problem in building design, where the objective space is often complex and discontinuous, evolutionary algorithms are among the most popular choices. The optimum seeking process of these algorithms simulates the principles of organic evolution; they are based on the competition among individuals in a population. Each individual is a vector of input data whose value in the objective function represents its fitness to survive.

A popular evolutionary algorithm is the genetic algorithm (GA). First proposed by John Holland in the mid 1970s in the University of Michigan [199], genetic algorithms are a family of population-based search algorithms based on natural selection in the evolution of the species [200]. Due to their efficiency in handling non-linear problems with discontinuities and many local minima, they have been successfully employed in many fields of study, including the energy efficiency of buildings and their components [194].

Many variations of the GA were developed to address specific problems. After a

first non-elitist Multi-Objective GA (MOGA), NSGA-II was developed by Kalyanmoy Deb and his students in 2000 as an elitist[1] version of NSGA (Non-dominated Sorting Genetic Algorithm) [188]. Being a genetic algorithm, NSGA-II shares the same overall GA dynamic. There is a main loop that iterates generation by generation, there is fitness evaluation and there are selection, crossover and mutation operators. However, these operators are especially designed to work with multi-objective problems [190]. In comparison with the normal GA, NSGA-II has a series of modifications to its operators, most importantly its selection operator. NSGA-II does not directly use the fitness values to select the best individuals and, consequently, the individuals who will be used for reproduction. As its name suggests, NSGA-II uses a Non-dominated Sorting (NDS) algorithm to asses the position of all solutions in the objective space and to sort them according to Pareto fronts. Additionally, NSGA-II uses a special diversity preservation algorithm called Crowding Distance (CD). NSGA-II selects its best individuals according to a combination of the values obtained with the NDS and CD algorithms. According to Attia et al., NSGA-II is the most efficient MOGA [194].

2.2.2.2   Performance of the optimisation methods

When performing optimisation analyses, an important issue is the time that is required to carry out the whole process, both in terms of programming and computational efforts. Optimisation methods coupled with whole-building simulation programs require a lot of processing resources. Considering that an optimisation analysis can require up to several thousand evaluations to get a near-optimal solution, and that the computation time required to run an annual building simulation can last from a few seconds to several hours, the total processing time can vary from some minutes to several days. Hence, selecting the appropriate algorithm and applying specific time-saving techniques can significantly decrease the simulation runtime.

In the literature, investigations of the performance of some optimisation algorithms applied to the building energy sector can be found. Tuhus-Dubrow and Krarti [201] compared the performance of genetic algorithms, sequential search technique and particle swarm optimisation (PSO), in terms of robustness (i.e. their ability to minimise the objective function) and efficiency (i.e. the number of simulation needed to reach the optimum). They found that, for a small search space, the sequential search technique slightly outperformed the genetic algorithm in terms of robustness. However, in terms of efficiency, for wide search spaces the genetic algorithm outperformed the other methods. In a later work, Bichiou and Krarti [202] compared the robustness and the effectiveness of the same three algorithms for the optimisation of Lyfe Cycle Cost and utility cost reduction of a

---

[1]The best candidate solutions survive to the next generation.

residential case study. They found that the computational efforts for the sequential search technique tended to be significantly higher than both PSO and GA.

To reduce computational efforts, preliminary sensitivity and uncertainty analyses can be carried out to identify the most influential parameters for the optimisation. Mechri et al. [203] and Heiselberg et al. [204] respectively applied the analysis of variance (ANOVA) approach and the Morris method to identify the design variables which have the greatest impact on the energy performance of an office building. They concluded that a sensitivity analysis can give important information about the design parameters on which to focus in the early stages of the design process, and that it can be very useful in an optimisation of building performance. Jin and Overend [205] performed a sensitivity analysis in terms of energy demand, occupant comfort, and economic cost on a generic cellular office room and a generic open-plan office floor in order to provide sensitivity coefficient charts of a comprehensive list of early-stage design variables and façade performance indicators. Comparing cellular office and open-plan office floor, they found that the cellular office room resulted to be more sensitive to the HVAC parameters, whereas the open-plan office floor was more sensitive to the façade parameters.

Another popular approach is to use more than one optimisation algorithm in a hybrid operation. The typical procedure is to use a global search algorithm to find a near optimal solution, and then use the result as a starting point for a local optimiser in order to refine the final outcome [195].

2.2.2.3   Optimisation tools

The optimisation procedure in building performance studies requires to couple an optimisation algorithm with one or more building simulation programs (Fig. 2.8). Ideal optimisation tools should provide a graphical user interface, should have a satisfactory performance and allow parallel computing, and should have the ability to estimate multiple solutions characterised by a similar performance.

According to Machairas et al. [195], the optimisation tools used for building design can be grouped in three categories; custom programmed algorithms, general optimisation packages and special optimisation tools for building design.

The advantage in adopting *custom programmed algorithms* is their flexibility, although advanced programming skills are required. Examples of this approach can be found in [206, 187].

Among the *general optimisation packages* are modeFRONTIER, MATLAB and GenOpt. ModeFRONTIER [207] is an integration platform for multi-objective and multi-disciplinary optimisation which provides an easy coupling with third party engineering tools. MATLAB [208] is a programming language for technical computing which includes several packages; the user can either take advantage
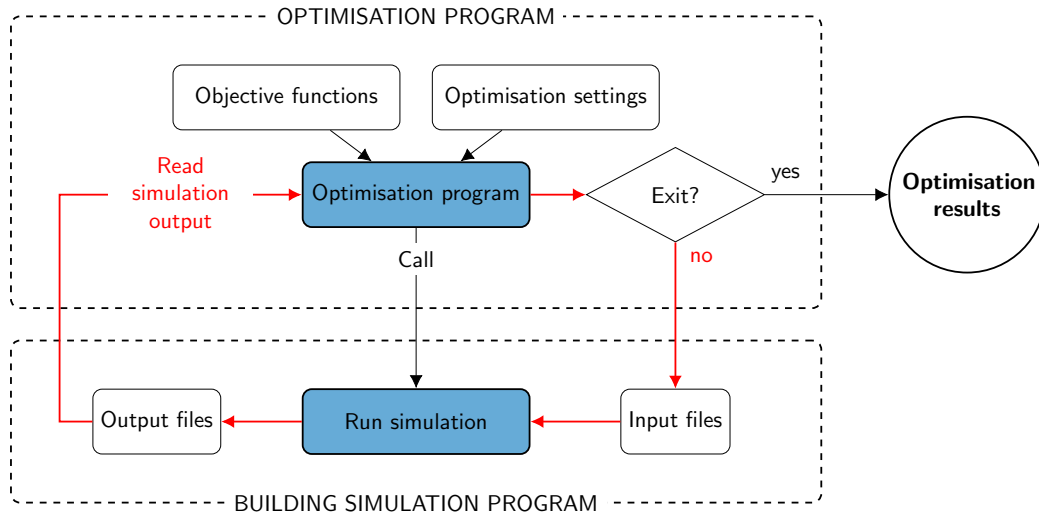
Fig. 2.8 Optimisation procedure in building performance studies (adapted from [214]).

of the features of MATLAB's Optimization Toolbox [209] or can build his custom algorithms. GenOpt [210] is a generic optimisation program for the minimisation of a single objective function that is evaluated by an external simulation program that both reads its inputs and writes its outputs on text files.

Several *special optimisation tools* for building design were developed by many authors; the majority of them include a GA implementation coupled with a whole building simulation program. Some examples of these tools are MultiOpt, ParaGen and BEopt. MultiOpt is a multicriteria tool for optimisation of buildings in the context of renovation operations, developed by Chantrelle et al. [211]. MultiOpt couples the NSGA-II algorithm with TRNSYS together with financial and environmental databases. ParaGen, developed by Turrin et al. [212], is an approach which combines parametric modelling, performance simulation software and a GA to explore design alternatives. BEopt [213] is a software tool that couples the sequential search method with EnergyPlus as simulation engine. The ability of identifying multiple near-optimal solutions is an important feature of this tool.

A full review of current building performance optimisation tools for net zero energy building design was presented by Attia et al. [194].

2.2.2.4   Building performance evaluation

To evaluate the energy performance of buildings in optimisation analyses, three kinds of models can be adopted [195]; analytical models, surrogate models and detailed models.

The application of *analytical models* to evaluate the building energy performance

can be chosen only for sufficiently simple problems. Although the mathematical description of the problem is not an easy task, the advantage of this approach is that the true optimum can be found more easily. An example of an analytical model to minimise seasonal cost for heating and construction cost of a building with an oval base can be found in [206].

Surrogate models (also called meta-models) are statistical models which approximate complex problems in order to obtain numerical tools that run faster than the original model [215]. Surrogate models are created through a machine learning approach, such as artificial neural networks, genetic programming, Bayesian networks or support vector machines.
In general, a surrogate model is created by running the detailed model (e.g. a building energy simulation model) for many cases in order to generate a database of results, which are subsequently used to train and test the meta-model. The advantage of this approach is that running the meta-model allows for much faster fitness evaluation while still providing for a good approximation of the non-linear behaviour of the fitness function. However, it should be noted that the use of surrogate models increases the uncertainty in the optimisation process [214].
An example of surrogate models coupled with a genetic algorithm to optimise retrofit cost, energy savings and thermal comfort of a school building can be found in [216].

Detailed models allow for accurate fitness evaluations by means of building performance simulation tools. The most commonly used software for evaluating the building energy performance in optimisation analyses of residential buildings is TRNSYS, followed by EnergyPlus and DOE-2 [217]. Among other software tools which have been adopted in optimisation analyses of the building's performance can be mentioned Radiance, Ecotect, and CFD tools.
Care should be taken when selecting the optimisation algorithm to couple with these kind of models; the adoption of optimisation algorithms that require smoothness of the objective function should be avoided because these simulation programs usually contain code features that may cause discontinuities [218].

2.2.3   Optimisation strategies for building design

The content of this section was partly published in [187].

Several articles and reviews detailing the use of various search and optimisation algorithms for design support in the building sector have been published. Nguyen et al. [214] and Evins [219] reviewed simulation-based optimisation methods applied to building performance analysis and sustainable building design problems. Stevanović [220] reviewed optimisation of passive solar design strategies, and

provided a summary with regard to building form, opaque envelope components, glazing and shading elements and whole building passive solar design optimisation. Huang and Niu [221] reviewed optimal design of building envelope. De Boeck et al. [217] provided an overview on the literature dealing with optimisation analyses to improve the energy efficiency of residential buildings. They distinguished the five following areas to which optimisation strategies are applied: measures concerning the whole building, building envelope (walls, roof, ceiling and floor), windows and shading devices, HVAC systems, appliances and lighting. However, the number of papers adopting optimisation methods in the building envelope design is still small in comparison with the amount of papers which deal with the optimisation of the building's control [195].

Several performance objectives can be addressed and many design variables can be optimised to improve objectives such as energy demand, system loads, construction and operating cost, thermal comfort, life cycle cost, life cycle environmental impact and CO_2 emissions [187]. The objectives that are most commonly investigated when performing building energy performance analyses are reported in Table 2.3. Statistical analyses reveal that energy consumption (counted together with life cycle cost) is so far the most investigated objective [221].

With regard to the building envelope, some authors optimised the insulation thickness [222–227] or the thermo-physical properties of the opaque envelope's materials [228, 229]. Several researches studied optimal Window-to-Wall Ratio (WWR) configurations [230–232] or combined an optimisation of WWR and thermo-physical properties [233, 234, 202, 235–237]. Other researches focused on the optimisation of shading devices [238, 239] or the combination of shading device and window area [240]. Building shape was investigated as part of the envelope optimisation in [201]. Building layout and shape for the initial design stage of a building with given envelope properties were respectively optimised in [241] and [242, 243]. Curtain wall façade components were studied in terms of carbon emissions during the entire building operation in [244]. Glare and illuminance of several fenestration configurations were studied and optimised in [245]. A sensitivity analysis of the WWR, which has a major role in the energy efficiency of buildings [203], was studied in [246]. The impact upon heating and cooling energy need of additional building envelope design factors in different climate zones was analysed in [247], and a detailed review on energy efficient design criteria is provided in [248]. Building operation [249] and optimal scheduling strategies [250] were also investigated.

Given the great variety of optimisation problems that can be analysed with respect to the energy performance of buildings, the focus will be on reviewing researches on building envelope, analysing it both at the component level and at the building scale.

Table 2.3 Common objectives for building energy performance analyses.

Category	Objective function
Energy performance	Heating energy demand
	Cooling energy demand
	Lighting energy demand
	Energy demand
	Energy fuel consumption
	Energy savings after retrofit
Thermal comfort	PMV's absolute value
	Cumulative sum of discomfort hours
Visual Comfort	Illumination level
	Illumination uniformity
	Daylight factor
	Daylight autonomy
	Useful daylight illuminance
	Daylight glare probability index
Environmental impact	Lifecycle environmental impact
	CO_2 emissions
Economical aspects	Construction cost
	Operational cost
	Lifecycle cost
	Lifecycle energy savings
	Net present value
	Payback rate
	Retrofit cost

2.2.3.1   Component level

Several papers investigate the performance of opaque and transparent building envelope components at the component level. For what concerns the opaque building envelope, position and distribution of the layers within the walls are analysed. The optimisations are generally performed in terms of dynamic thermal properties, such as periodic thermal transmittance, decrement factor, time shift, areal heat capacity, and thermal admittance. The boundary conditions which are adopted are either sinusoidal, in accordance with the methodology reported in ISO 13786:2007 [5], or are representative of a specific location and wall orientation. Position and distribution of the layers within the walls are analysed by focusing on the insulation (with regard to traditional building components and materials) or to PCMs (with regard to innovative and responsive materials).

With regard to the transparent envelope, the selection of optimal glazings is a more complex task due to the contrast between energy performance, thermal and visual comfort. For this reason, optimisation analyses of the transparent envelope do not neglect the interactions with the building.

2.2.3.1.1 Opaque components Optimisation analyses of opaque building envelope components with traditional materials deal mainly with finding the optimal insulation thickness (generally under an economic point of view) or on finding the best distribution of the materials within the wall.

Kontoleon and Eumorfopoulou [251] investigated the influence of solar absorptivity and wall orientation on time lag and decrement factor under non-sinusoidal steady periodic conditions for a Mediterranean climate. They considered a set of six walls characterised by constant R-value and different position and number (up to two) of the layers (masonry and insulation, plus external coating). Regardless of the orientation, they found that placing two layers of insulation led to a greater time lag and a reduced decrement factor compared to a single layer. The maximum time lag was achieved with insulation placed as external and mid-position layers. They additionally found that solar absorptivity had a significant effect on the thermal behaviour of the wall, with an optimum value equal to 0.2 for east and south oriented walls (highest time lag).

Al-Sanea and Zedan [252] optimised the distribution of the insulation within a wall characterised by constant R-value and thermal mass. They first optimised the total insulation thickness under steady periodic conditions according to an economic criterion (initial cost and running cost over the building's lifetime). Since peak load, time lag and decrement factor are greatly affected by the insulation's position, they subsequently searched which distribution of the insulation layer lead to the best dynamic performance of the wall. The best solutions they found were a wall with three layers of insulation equally thick, placed at inside, middle and outside, closely followed by a wall with two insulation layers equally thick, placed in the middle and outside (as it was found by Kontoleon and Eumorfopoulou [251], who did not investigate walls with three layers of insulation). Comparing the performance of the best wall with that of a wall with only one layer of insulation placed on the inside, they found an increase in the time lag from 6 h to 12 h, a 10-fold decrease in decrement factor, a 20% decrease in both peak cooling and heating transmission loads.

Cheng et al. [253] performed an analytical optimisation, by means of the electric analogy (RC model), to find the optimal material distribution corresponding to the minimal space heating or cooling load due to the building envelope. By adopting one capacitive and two resistive layers, they found that placing a concrete material in the middle and evenly distributing the insulating materials on the outermost layers could maximise the module of the thermal impedance for the given conditions.

Ozel [227] investigated, under steady periodic conditions, the effect of the position of the insulation layer on cooling and heating transmission loads, time lag and decrement factor of a south-facing wall. Subsequently, the insulation thickness was optimised by minimising the total lifetime cost over a period of 20 years. In accordance with the results from Al-Sanea and Zedan [252], the insulation's location resulted to have a significant effect on the yearly averaged time lag and decrement factor. However, yearly transmission loads (and, consequently, optimum insulation thickness) were not affected by the insulation's position. Both in summer and winter the maximum temperature swings and peak loads occurred with the insulation placed in the middle, whereas the smallest fluctuations occurred when the insulation was placed towards outside.

Bond et al. [254] analysed magnitude ratio and phase of the frequency response (evaluated at the frequency corresponding to a period of one day) of thirty-three multilayer walls with fixed R-value and thermal mass, by means of an RC model. Although they did not carry out a proper optimisation, they found that a number of layers for which the thermal properties are optimised seem to exist (so that the magnitude ratio is maximised), and that optimal results occurred when both the insulation and thermal mass were distributed evenly within the wall. The best insulating performance was achieved when the insulation was positioned as close as possible to the inside and outside layers of the wall.

Baglivo et al. [255] performed a multi-objective analysis to obtain several types of highly energy efficient external multilayer walls for ZEBs in the Mediterranean climate. They optimised U-value, periodic thermal transmittance, decrement factor, time shift, areal heat capacity, thermal admittance, surface mass and thickness of walls having a maximum of five layers (excluding the plaster), chosen among a database of existing materials with commercially available thicknesses, and a maximum thickness of the wall of 430 mm. They found that the superficial mass was important to obtain the best performance in a warm climate, and that high performance in summer could be also achieved by lighter and thinner walls.

In a later work, Baglivo and Congedo [256] investigated the dynamic thermal performance of precast multilayer walls for buildings located in warm climates, focusing on eco-friendly materials. In addition to the objective functions they adopted in [255], they considered also eco-sustainability score, weight and cost. They found that the best sequences of layers where characterised by high surface mass for the innermost layer, followed by eco-friendly insulating materials for the middle layer and by common insulating materials for the outer layer.

Zhang et al. [257] evaluated the ideal constant thermo-physical properties of an external wall for free cooling or heating of buildings by assessing the integrated discomfort degree for indoor temperature. They investigated walls characterised by a thermal conductivity in the range of 0.05-5.0 W/(m K) and a ρc in the range of 0.1-200 MJ/(m^3 K). They found the existence of critical values of the thermo-physical properties beyond which no additional improvement could be obtained. Results

showed that external walls should be characterised by high ρc and a small thermal conductivity, whereas internal walls should have high values of both ρc and thermal conductivity. For a case study located in Beijing, they found 50 MJ/(m³ K) to be the critical value for external walls and 100 MJ/(m³ K) to be the critical value for internal walls. However, it should be mentioned that ordinary building materials have ρc values of up to 4 MJ/(m³ K).

In a later work, Zhang et al. [258] optimised the ideal thermo-physical properties of an external wall as a function of temperature, in terms of entransy dissipation. They found that to effectively reduce the cooling or heating load in summer or winter, the ideal heat capacity $\rho c(T)$ of the wall should be a δ function, whereas the ideal thermal conductivity $k(T)$ approached a staircase function in summer and maintained the available minimum value in winter.

Under a practical point of view, materials whose heat capacity varies greatly as a function of temperature are phase change materials. By adopting an existing PCM, the problem of the ideal wall can be turned into identifying the best position of the PCM layer (given a certain thickness) [259]. Several articles analyse this problem by means of experimental investigations.

Jin et al. [260] experimentally investigated the optimal location of a PCM layer incorporated in a building wall through encapsulation in polyethylene flat bubbles and sandwiched between two layers of protective aluminium foil. The thermal performance of the walls with and without these "PCM thermal shields" (PCMTSs) was evaluated using a dynamic wall simulator (a cubic box having size of 1.19 m × 1.19 m). The walls were composed by five foam insulating layers comprised between a gypsum wallboard (internal side) and an oriented strand board (external side). The PCM thermal shields were placed within the wall insulation at varying distances from the wallboards. Heating sources were placed on the external side of the walls and reproduced the temperature profiles of exterior surfaces of west-facing building walls. The PCM used in the experiments was a hydrated salt having heat of fusion of approximately 140 kJ/kg and melting temperature range between 24 ℃ and 34 ℃. The experimental results showed that, for the system under study, the optimal location of the PCMTS was at a distance of $1/5L$ from the internal surface of the wallboard, where L was the total thickness of the insulation. In this location, the average reduction of the peak heat flux was approximately 41% compared to the walls without PCM. The load shifting time was about two hours. The reason why $1/5L$ was the optimal location was investigated in [261]. It was found that the PCM placed at $1/5L$ was in the partially-melted state before cooling (unlikely in the other locations where it was fully melted) and was able to quickly release latent heat during the cooling processes.

However, it should be noted that the optimal position of the PCMTS, the reduction of the peak heat flux and the load shifting time depend on the type of PCM. Jin et al. [110] performed additional experimental analyses to identify the optimal location of a PCMTS containing n-octadecane as PCM, which is an organic

paraffin having heat of fusion of 179 kJ/kg and melting temperature of 26-28 ℃. Compared to a wall without a PCMTS, in this new set of experiments they achieved a 11% reduction of the peak heat fluxes when the thermal shield was placed next to external face of the innermost layer of the wall. Only small effects on the peak heat fluxes were instead recorded when the PCMTS was placed halfway between the enclosing surfaces of the wall and almost no effect when it was placed next to the internal face of the outermost layer of the wall.

Further experiments on the optimal location of PCMTSs were performed by Lee et al. [111], who analysed the thermal performance of PCMTSs in south and west facing walls of two identical test houses during two cooling seasons. The investigated PCM was characterised by a melting temperature range of 18-38 ℃, a peak melting temperature of 31.36 ℃ and a latent heat of fusion of 149.9 kJ/kg. The wall structure and the PCMTS's positions were the same as in [260, 110]. The analysed locations were numbered from 1 to 5; their distances from the wallboard were respectively 0 cm, 1.27 cm, 2.54 cm, 3.81 cm and 5.08 cm. Results showed that the optimal positions of the PCMTS were location 3 in the south wall and location 2 in the west wall.

When the position of the PCM is fixed, the investigation deals either with finding the optimum thickness given the PCM's thermo-physical properties, or vice versa. However, investigations simultaneously dealing with the ideal position and thermo-physical properties of PCMs were also performed.

Kuznik et al. [262] performed a numerical optimisation of the thickness of a PCM wallboard in terms of stored energy. The analysed material was DuPont Energain, which is a shape-stabilised PCM composed of 60% of micro-encapsulated paraffin and characterised by a melting temperature of about 22 ℃. The Energain panel was placed within a lightweight multilayer wall, where it was sandwiched between the insulation layer and the internal plaster. Results showed that the optimal PCM's thickness was a function of the amplitude of the internal temperature swing; an optimal thickness of 1 cm was found for the analysed case study. Moreover, the optimal thickness resulted not to be influenced by the insulation's thickness.

Bastani et al. [263] studied how the dimensionless Bi, Ste, and Fo numbers of a PCM wallboard correlate to the time required by the PCM to fully charge. Their main concern was to identify the best design parameters of the PCM wallboard in order to efficiently accomplish peak load shifting. They consequently developed a design tool that relates the PCM thickness and its thermo-physical properties to the charging time. This tool can be used either to select the appropriate thickness of the PCM wallboard given its thermo-physical properties, or to modify its thermo-physical properties given its thickness. However, it should be noted that the PCM wallboard was assumed to be mounted as the innermost layer of a wall. Hence, the room temperature was the boundary condition on one side, while the other side was assumed to be adiabatic (perfectly insulated wall, or partitioning wall where the adjacent room is conditioned at a similar air temperature). In a later work, Bastani

and Haghighat [264] expanded their analysis and created a number of charts which can be considered as the expansion of the Heisler chart from conventional materials to PCMs.

Parametric analyses which simultaneously dealt with ideal position and thermo-physical properties of PCMs were also performed. Zhang et al. [181] parametrically investigated the effect of PCM's latent heat of fusion, melting temperature and thermal conductivity on the thermal performance of a PCM wallboard applied either on the internal or external side of a wall. When the PCM was installed on the external side of the wall, they found the highest energy saving potential with a proper choice of the melting temperature, a high latent heat of fusion and a low thermal conductivity. When the PCM was installed on the internal side of the wall, the best results were obtained with a proper selection of melting temperature and thermal conductivity and a high latent heat of fusion. The internal position was identified as the most efficient one for applying the PCM.

Given a base wall design, El Mankibi et al. [265] numerically investigated the wall's performance in terms of peak heating load, annual heating load, peak cooling load and annual cooling load, by inserting a PCM layer either towards the inside, middle or outside position. The PCM's thermo-physical properties that were varied were latent heat of fusion, melting temperature and melting temperature range. The analyses were performed for the location of Golden (CO, USA) and considering the wall exposed towards the four cardinal directions. Results showed that the maximum savings in annual and peak cooling loads were achieved when the PCM was placed towards the interior and the PCM's melting temperature was close to the cooling setpoint with a narrow melting temperature range. An optimal melting temperature equal to the heating setpoint was required for maximum savings in annual heating load but a lower temperature was needed to achieve maximum savings in peak heating loads. The savings in the peak heating load were much more pronounced than the savings in annual heating loads. The lowest savings were found when the PCM was placed towards the exterior. In this case, the lowest peak heating load was obtained with a PCM characterised by a melting temperature of 10-15 ℃ and a wide melting range of 8-12 ℃. For what concerns the impact of the orientation, due to the high thermal resistance of the investigated wall, it resulted to be insignificant when the PCM was placed towards the inside. In addition, since a better performance in reducing the cooling load was found for the investigated location, a ventilated cavity wall consisting of the main multi-layer wall, a cavity and a double glazing was designed to enhance the PCM's thermal performance in winter. When the cavity was introduced in the south wall, the maximum savings in annual heating loads with the best configuration reached above 95%, with a 65% contribution due to the cavity and more than 30% due to the PCM layer (compared to 3% with no cavity). For what concerns the other wall orientations, a 20% improvement was found for east and west facing walls, whereas no performance improvement was achieved for a north facing wall.

2.2.3.1.2   Transparent components   The selection of appropriate glazing systems in relation with the climate is crucial for improving the energy performance of buildings. However, selecting a window glazing is a complex task when concurrently considering energy saving, thermal comfort and daylighting aspects, due to their conflicting contribution towards energy use [266]. For this reason, optimisation analyses of the transparent building envelope deal with investigations at a building level. Both static and dynamic glazing have advantages and disadvantages, and optimisation process are important for both glazing types. However, designing windows with static glazing usually needs more careful considerations [267].

The majority of authors performed parametric analyses to investigate optimal window configurations of static glazing components.

Grynning et al. [268] performed a parametric analysis to investigate the energy performance for heating and cooling of several windows' configurations by varying U-value in connection with Solar Heat Gain Coefficient (SHGC). The energy performance was assessed with three different rating methods for an office building situated in Oslo and complying with the Norwegian passive house standard. The building was characterised by a WWR of 55%. Results for the first rating method highlighted an optimum SHGC of 0.4 for windows with U-values lower than 0.8 W/(m^{2}K). On the other hand, the other methods suggested that a low U-value combined with SHGC around 0.4 would be desirable. Moreover, the introduction of dynamic solar shading systems resulted to be fundamental to further reduce the energy demand.

Thalfeldt et al. [269] performed a parametric analysis to derive optimal design strategies for an open plan office nZEB in a cold climate alternatively in terms of total energy performance and cost effectiveness. They varied WWR, U-value, SHGC, visible transmittance and solar shading. Cost-optimal insulation thickness of the external walls was used with each glazing variant. The resulting windows based on the most energy efficient solutions were characterised by five panes and a WWR of 60% for all façade orientations, and the presence of external shading for east and west facing windows. The resulting windows based on the cost optimal performance level were instead characterised for all the orientations by three panes with no external shading, and a WWR of 23.9% with the exception of the north-exposed façade which presented a higher WWR of 37.5%.

Vanhoutteghem et al. [270] investigated the relationship between size (glazing-to-floor ratio), orientation and glazing properties of windows in terms of energy consumption, thermal indoor environment and daylighting (under a standardised overcast sky) for different side-lit room geometries in residential nZEBs in Copenhagen. The simulations were carried out with EnergyPlus and DAYSIM, and the results were presented in the form of charts representing combinations of design parameters with minimum space heating demand and defined targets for daylighting and thermal comfort. Results showed that there is more architectural freedom in window design when adopting a low U-value of the glazings. In south-

oriented rooms when the glazing's U-values range between 0.3-0.5 W/(m^2 K), the use of high g-values and large glazing areas did not contribute to reducing space heating demand, but window size should be carefully selected in order to reach the daylight target without overheating. In north-oriented rooms, high g-values were instead recommended for reducing space heating demand. Since the risk of overheating would be small, the combination of g-value and glazing-to-floor ratio allowed for flexibility to fulfil the daylighting target. In addition, in deep or narrow south-oriented rooms, either thermal comfort or daylighting was found to be compromised with the use of permanent solar shading.

A proper optimisation analysis of a transparent building envelope component was performed by Joe et al. [271], who minimised the overall energy consumption for heating and cooling of a building in Seoul (Korea) equipped with a naturally ventilated double skin façade by selecting the type of glazings of the DSF and the thickness of the air cavity. The optimisation was carried out with GenOpt and adopting the PSO algorithm. The simulation software was EnergyPlus 6.0. Before performing the optimisation, a parametric analysis highlighted that the variable having the greatest impact on the building energy consumption was the type of glazing of the external pane of the internal skin.

Optimisation analyses were also performed to investigate the ideal properties of adaptive window technologies.

Dussault et al. [272] optimised the hourly solar absorption rate of an idealised broadband filter placed on surface 2 of a double glazed smart window, in order to minimise the energy consumption for heating, cooling and lighting of a low thermal mass office building. The optimisation process was performed with MATLAB using "fmincon" to minimise the constrained functions. Results showed that the best trade-off between performance and investment cost was achieved by installing the smart window filter on south and west façades.

Favoino et al. [273] minimised the total primary energy use of an office room by investigating the adaptive glazing properties of windows which responded to changing boundary conditions on a monthly or daily basis. The analysed case study was located in three temperate climates and exposed to the four cardinal orientations. Results highlighted that high energy savings could be achieved, and that a unique optimised technology capable of varying its thermo-optical properties between a limited number of states could be effective in different climates and orientations.

2.2.3.2   Building level

An increasing amount of literature on optimisation analyses for improving the energy performance of buildings has been published in the latest years [194, 195, 217]. Even though the majority of studies focused on building design, optimisation

approaches are not limited to new constructions. Retrofitting of existing buildings can significantly reduce global energy consumption and greenhouse gas emissions, and optimisation strategies can be successfully applied to identify the most cost-effective retrofit measures.

2.2.3.2.1   New constructions   Among the great amount of papers dealing with optimisation analyses of the building envelope in new constructions, a first distinction is between investigations with fixed and variable building shape. The first category considers a fixed geometry and improves thermo-physical properties of the building materials and systems. The second category investigates also the building shape, such as in terms of building's aerial projection or of optimal window area.

Among the researches on buildings with fixed geometry, some authors focused on improving energy performance or life cycle cost, whereas some others addressed comfort issues.

Alaidroos and Krarti [274] minimised life cycle cost and energy savings for a residential case study placed in five Arabian cities, by searching for the optimal wall and roof insulation, window area and glazing type, shading (provided by overhangs) and thermal mass. A sensitivity analysis on their results revealed that the cost of energy had a greater influence than the initial costs of the energy efficiency measures on the optimal energy savings and life cycle costs.

Karmellos et al. [275] minimised total primary energy consumption and investment cost of a new building (and an existing building under retrofit actions) in the climates of Edinburgh and Athens. The investigated decision variables regarded the building envelope, the building's energy and lighting systems, and the electrical appliances. The calculations of the primary energy consumption were performed with a steady-state approach. The results showed that increasing the initial investment cost lowered the primary energy consumption.

Carlucci et al. [276] minimised the long-term thermal and visual discomfort in a nearly zero-energy house located in the Mediterranean climate. The optimisation variables were the thermal properties of the enclosure (walls, roof and floor) in terms of U-value and time lag, the glazing type of each façade (in terms of U-value and g-value), the control strategy for closing the solar shading devices and the windows' opening during summer night-time.
Four objective functions were addressed; the Long-term percentage of dissatisfied was used for quantifying the predicted thermal discomfort over a calculation period, the Likelihood of dissatisfied was used for estimating the severity of the deviations from a theoretical thermal comfort objective, the Useful daylight illuminance was used for assessing the amount of available light, and the Discomfort glare index was used for assessing the risk of discomfort glare of the occupants. Results of the optimisation procedure highlighted that the two thermal comfort criteria were not

in contrast, so that the 4D-optimisation problem could be reduced to a 3D one. On the contrary, the maximisation of useful daylight was in contrast with glare risk.

In the group of investigations searching for the optimal window area, the majority of papers analysed the Window-To-Wall ratio.

Leskovar and Premrov [236] performed a parametric analysis on the WWR for the cardinal orientations and six types of lightweight prefabricated timber-frame walls of a residential building. They evaluated the energy demand for heating and cooling by means of the PHPP software in order to obtain the optimal WWR as a function of the U-value of the walls. They found a linear correlation between the energy need and the U-value of the walls as a function of the WWR.

Goia et al. [231] performed a parametric analysis to investigate the optimal WWR of a low energy office building located in Frankfurt (Germany), in order to minimise the energy demand for heating, cooling and lighting. Optimal WWRs were found in the range 35-45% regardless of the orientation.

Koo et al. [233] performed also a parametric analysis to investigate the effect of window type, movable shading devices, WWR and orientation on the heating and cooling energy in the early design phase of a multi-family housing unit. They used a four-node-based Lagrangian shape function in quadrilateral coordinates to solve the non-linearity between inputs (orientation and WWR) and output (heating and cooling energy demand) and extracted an interpolation function.

Azari et al. [277] performed a multi-objective optimisation analysis to minimise building energy use and life cycle environmental impact in a low-rise office building located in Seattle (USA) by varying WWR of south and north facing façades, window type and frame material, thermal resistance of the wall and insulation material. They found optimal WWRs to be about 60% towards south and 10% towards north when adopting fiberglass-framed triple-glazed windows.

A different approach in the search of the optimal window area, which did not directly study the WWR, was performed by Méndez Echenagucia et al. [187], who minimised the energy need for heating, cooling and lighting of an open space office building located in four European climates, by varying number, position, shape and type of windows and the thickness of the masonry walls. Both the cases of absence and presence of an urban context were considered. They found optimal envelope configurations characterised by low WWR values in east, west and north exposed façades. On the other hand, the area of the south facing windows was higher and characterised by a higher variability within the Pareto front solutions.

Another way to search for the optimal WWR while taking the window shape into account was proposed by Harmathy et al. [232], who searched for efficient WWR and window geometry through a multi-criterion optimisation, in order to improve indoor illumination quality and building energy performance.

When investigating optimal building envelope design, several authors simultaneously focused on envelope and HVAC systems. However, a sequential optimisation

approach resulted to provide acceptable results.

Hamdy et al. [278] performed a multi-objective optimisation analysis to mini-mise the carbon dioxide equivalent (CO_2-eq) emissions and the investment cost for a two-storey house in Helsinki. Six building envelope parameters, heating/cooling energy source and heat recovery type were considered as design variables. Results highlighted that the influence of the insulation thickness of the envelope compo-nents on the energy consumption and thermal comfort could be reduced into an overall building U-value. Moreover, the type of heating energy source had a marked influence on the optimal solutions.

A comprehensive optimisation of both envelope and HVAC systems was perfor-med by Bichiou and Krarti [202]. They investigated the performance of a residential case study in five US locations in terms of life cycle cost with and without budget constraints. Even though a combined optimisation of envelope and HVAC systems was found to be preferable to a sequential approach where the HVAC systems are optimised after the envelope, only slightly better results were obtained at the expense of a considerable increase of the computational run time.

Several investigations of building envelope components integrating PCM ma-terials were performed addressing either energy performance or thermal comfort related objectives.

Soares et al. [279] analysed the effect on the yearly energy saving for heating and cooling of substituting the internal gypsum boards of a south-exposed living room with PCM-drywalls. Position and thickness of the PCM-drywalls, as well as the thermo-physical properties of the PCM (enthalpy-temperature and thermal conductivity-temperature functions) and solar absorptance of the inner surfaces were investigated. The optimal melting temperature was found to be higher in warmer climates, whereas the solar absorptance was found to be higher in colder climates. The energy saving effect was more evident for the warmer climates.

Al-Saadi et al. [87] parametrically searched for the optimal thermal properties of PCMs in order to minimise heating and cooling energy demand and peak loads in lightweight buildings under several climates. They found that maximum energy sa-vings for heating (or cooling) were obtained with a melting temperature of the PCM either equal or a degree lower than the heating (or cooling) set-point temperature. A narrow melting temperature range was generally beneficial, although a slightly wider melting range provided better results in mild summer climates. Maximum savings in peak heating load were obtained with a PCM's melting temperature from 1 ℃ to 3 ℃ below the heating set-point, according to latent heat and climate, and a narrow melting temperature range, between 0.1 ℃ and 1 ℃. Eventually, maximum savings in peak cooling load were obtained with a PCM melting temperature of 24-26 ℃ in mild summer climates and 26-27 ℃ in sever summer climates, and a melting temperature range between 0.1 ℃ and 2 ℃. As in [279], energy savings for cooling resulted to be more pronounced.

Kuznik et al. [280] presented a methodology to design PCM composite solutions

for reducing the heating energy consumption, which they applied to a residential case study located in Chambéry (France). The methodology was based on a polinomial meta-model; the simulations were carried out with TRNSYS. The investigated PCM's parameters were peak melting temperature, thickness, latent heat, density and thermal conductivity. The location of the PCM layer was on the internal side of the existing walls, followed by a layer of plasterboard. For each parameter—with the exception of thermal conductivity, which showed an asymptotic behaviour—values that maximised the reduction of heating energy consumption were found. However, the interaction terms between parameters presented a different behaviour. Results of the overall optimisation highlighted a maximisation of storage capacity and thermal conductivity, with an annual heating energy reduction of about 23%.

El Mankibi et al. [265] minimised heating energy consumption and thermal discomfort risk of a building whose south façade was equipped with a multi-layer wall characterised by an external air cavity and a PCM layer, in order to optimise thickness, density and conductivity of the three layers and the melting temperature range and latent heat of the PCM. Two ventilation configurations were considered (with and without ventilation). The optimisation was performed for the first week of January under the climatic conditions of Colorado (USA). The properties of walls and windows were chosen in order to investigate configurations with high and low inertia, and large and small glazing area. The results were compared to reference cases characterised by buildings whose south façades were classical walls as those of the other orientations. Results showed that, in the optimal wall configurations, the thickness of the PCM varied from 1 cm to 4 cm depending on the whole building inertia, whereas that of the other materials depended also on the ventilation configuration. The optimal materials of the external and internal layers were conductive and with a high thermal inertia. The multi-layer wall without cavity ventilation resulted to be thermally more efficient but entailed a higher risk of thermal discomfort. With respect to the reference buildings, results for the optimised configurations showed a 28% decrease in the energy consumption for the configuration with low thermal inertia, and up to 38% for the configuration with high inertia.

Buonomano et al. [132] investigated, by means of a parametric analysis, the application of innovative building integrated technologies such as PCMs, Building Integrated PhotoVoltaic (BIPV) panels and hybrid BIPV/Thermal plants to a non-residential nZEB case study in Mediterranean climate. They found that the adoption of PCM wallboards could lead to the minimum energy requirement when the PCM panels were placed in the interior layer of the perimeter walls and in the exterior layer of the roof. However, the initial cost was too high to achieve acceptable payback periods.

Zwanzig et al. [281] performed a numerical analysis to investigate the optimal position of a PCM composite wallboard in terms of seasonal peak load shifting, seasonal peak load reduction, and total annual cooling and heating load reduction.

The wallboard (which consisted in a gypsum plasterboard 0.0127 m thick that incorporated 25% of paraffin with a temperature range of 25 ℃ to 27.5 ℃) was placed within walls and roof of a typical residential case study located in three US climate zones. Results showed that the optimal location depended on the resistance between the PCM layer and the exterior boundary conditions. During both heating and cooling seasons, the PCM composite wallboard placed in the central location performed better than in the external and internal locations (contrary to the results from [265] and [132]).

Ascione et al. [137] performed a multi-objective optimisation analysis to mini-mise winter and summer energy demand in a residential nZEB in four Mediterra-nean climates with a special attention to thermal comfort, which was considered as a constraint. The optimisation variables were WWR, type of glazing, presence and type of fixed and movable shading devices, type of wall, solar reflectance and infrared emissivity of the roof. To minimise the overall energy demand, they found that walls should be characterised by an areal mass greater than 250 kg/m^2, roofs should have an external cool coating, and triple glazing windows with selective coating and external shading should be installed. In addition, they performed a parametric analysis to investigate the integration of PCM as finishing layer of the walls. They found that a PCM layer with a melting temperature of 25 ℃ on the inner side reduced the cooling energy demand, and that the application of an additional PCM layer with a high melting temperature on the external side could maximise the cooling energy saving.

An analytical optimisation of melting temperature and latent heat of fusion of PCM panels placed in the innermost layer of walls, floor and ceiling of a direct-gain solar room was performed by Xiao et al. [282] and Jiang et al. [283]. Xiao et al. found that the optimal phase change temperature depended on the average indoor air temperature and the amount of solar radiation that was absorbed by the PCM panels. Moreover, an inverse correlation between the amplitude of the temperature oscillations and the product of the area of the PCM panels and the surface heat transfer coefficient was observed. Jiang et al. found that the optimal phase change temperature depended also on the lower limit of the indoor thermal comfort. For the passive solar rooms under investigation in the climatic regions of China, the optimal phase change temperature was 1.1-3.3 ℃ higher than the lower limit of thermal comfort range.

Jiang et al. [229] later extended their analysis and analytically optimised the specific heat of the internal envelope of a direct-gain solar room in order to use the minimal enthalpy to improve indoor thermal comfort the most. They concluded that the optimal specific heat was characterised by a δ function which approached to the effective heat capacity form of phase change materials. This result was also found by Zhang et al. [258].

2.2.3.2.2　Retrofit applications　Retrofit analyses can be translated into multi-objective optimisation problems subjected to many constraints and limitations. Although the building shape is not included in the search process, the specific characteristics of the building need careful consideration. The optimal solution needs to be a trade-off between both energy and non-energy related aspects, such as economical and technical factors. A summary of ranges and relative importance of parameters for energy simulation for the retrofit of residential buildings is reported by Ochoa and Capeluto [284]. A comprehensive review of the state-of-the-art of existing buildings' retrofit can be found in [285].

Huang et al. [286] performed an optimisation of the thermal properties of the envelope in energy-saving renovation of existing public buildings. They investigated the effect of the insulation thickness and type of windows on the energy savings for heating and on the renovation cost, by exploring different window-to-wall ratios and orientations. They found that the performance parameters for the renovation of existing buildings should be determined for each orientation.

Asadi et al. [287] proposed a multi-objective optimisation methodology based on a combination of TRNSYS, GenOpt and a Tchebycheff optimisation technique developed in MATLAB, which they applied to optimise retrofit cost, energy savings and thermal comfort (percentage of discomfort hours) of a residential case study. The decision variables they adopted were insulation material and thickness of the external insulation of walls and roof, window type, solar collector area and its generation efficiency. In a later work [216], they assessed the technological choices in the retrofit of a school building by proposing a methodology based on genetic algorithms and artificial neural networks. They found that the non-dominated solutions could be classified mainly according to the type of windows, HVAC system or solar collector. For achieving the best indoor thermal comfort, investing in expensive HVAC system resulted to be better than investing in additional insulation and other low energy measures.

Shao et al. [288] developed a multi-criteria decision strategy for ranking the Pareto optimal solutions according to the stakeholders' concerns and needs. They applied the proposed methodology for the retrofit of an office building, for which they optimised investment cost, annual heating energy consumption and global warming potential.

Penna et al. [289] investigated the relationship between the initial characteristics of residential buildings and the definition of optimal traditional retrofit solutions. They searched for the optimal retrofit measures of twelve building typologies—three S/V ratios, two orientations (windows only faced either south or east), and two types of pre-retrofit envelopes—by maximising the economic performance and minimising energy consumption and thermal discomfort. They found that the zero energy target could be approached maintaining the economical convenience, but improving the energy efficiency of the buildings led to a significant worsening of the thermal comfort. They obtained cost optimal solutions which were mainly

characterised by large insulation thickness and substitution of the glazing systems with double glazings with a high SHGC. On the other hand, in the comfort optimal solution the insulation level of the opaque envelope resulted not to be very important, but the substitution of the single glazings with low-SHGC ones and the introduction of a mechanical ventilation system seemed to be crucial.

Wu et al. [290] performed a multi-objective energy hub optimisation for the retrofit of building envelope and energy systems of typical residential buildings in Switzerland, minimising life cycle cost and greenhouse gas emissions. To achieve optimal results, they found that the building retrofit should be coordinated with a change in the heating systems.

A study for the retrofit of an office building by adding a PCM plasterboard on the inner side of its exterior envelope was carried out by Ascione et al. [131]. By fixing the phase change enthalpy, they performed a parametric analysis to find the optimal PCM's temperature of fusion, thickness and placement for five Mediterranean climates, both in conditioned and unconditioned buildings. They found that a refurbishment by means of PCM wallboards seemed to be more appropriate for a semi-arid climate.

A parametric optimisation for retrofitting a typical Australian residential building by installing mats of bio-PCM in the ceiling was performed by Ramakrishnan et al. [183]. Through assessment of performance indicators (see § 2.1.2.7), they searched for phase transition temperature, thickness of the PCM layer and night ventilation rate which guaranteed the best indoor thermal comfort, evaluated with the ASHRAE adaptive model. They found that, according to the climatic condition, the optimal phase change temperature was about 3 °C to 5 °C higher than the average outdoor air temperature. However, it was also found that PCM in these conditions might not have the best efficiency. Proper thickness selection and night ventilation resulted to be important to maximise PCM efficiency and minimise cost.

Chapter 3

Methods

In this chapter, the numerical methods applied in the present thesis are presented. Specifically, the finite difference model used to simulate the PCM-enhanced walls, the adopted optimisation algorithms and the post-optimisation analyses are described and validated.

3.1 Numerical model of multilayer walls with PCM

To perform the material and component level analyses, a numerical model to simulate the heat transfer process in multi-layer walls with the inclusion of PCMs was written in MATLAB language [208]. Writing a custom code allowed for a high flexibility in modelling the PCM, in imposing the boundary conditions, and in setting the exchange of information between software.

The phase change process was modelled with the apparent heat capacity method [75] and constant thermal conductivity. The one-dimensional transient heat conduction equation (3.1) was solved through the application of the finite difference method with Crank-Nicolson scheme and Gauss-Seidel overrelaxation [73, 291]. Uniform time step and mesh size were considered.

For materials with constant thermo-physical properties, the model was validated against the set of experimental measurements reported in [292], achieving equal or better results. The phase change was validated against the exact solution of the melting in a half-space problem [73].

3.1.1   Model description

The basic idea of the finite difference method is to approximate differential equations through substitution of each derivative with a difference quotient. In this way, whichever differential equation can be solved by numerical means. However, with the finite difference methods, the solution to the problem is found only for a finite number of points, called nodes, which are defined by the discretisation (with fixed or variable step) of the equation's domain [73, 291].

In the analysed problem, the one-dimensional transient heat conduction equation (Fourier equation) with no heat generation and constant thermal conductivity is considered,

$$\frac{\partial^2 T}{\partial x^2} = \frac{1}{\alpha} \frac{\partial T}{\partial t},$$
(3.1)

where T is the temperature, x and t are respectively the spatial and temporal coordinates, and α is the diffusivity of the material, defined in eq. (3.2).

$$\alpha = \frac{k}{\rho c}$$
(3.2)

Eq. (3.1) is elliptic with respect to the spatial variables and parabolic with respect to time. Under a physical point of view, the ellipticity implies that the temperature in each point is influenced by spatial changes in all directions (both forward and backward). The parabolicity implies that the temperature in each moment is influenced only by the previous conditions [73].

Eq. (3.1) was solved by means of a combined scheme,

$$\theta \cdot \frac{T_{i-1}^{m+1} - 2T_i^{m+1} + T_{i+1}^{m+1}}{\Delta x^2} + (1 - \theta) \cdot \frac{T_{i-1}^m - 2T_i^m + T_{i+1}^m}{\Delta x^2} = \frac{1}{\alpha} \frac{T_i^{m+1} - T_i^m}{\Delta t}.$$
(3.3)

where the subscript i and the superscript m respectively refer to the spatial and temporal coordinates. According to the value assigned to the weight θ, different accuracies can be obtained. When $\theta = 1/2$, the Crank-Nicolson scheme is obtained, which is unconditionally stable [291].

Eq. (3.3) was rearranged as

$$a_1 \, T_{i-1}^m + a_2 \, T_{i-1}^{m+1} + a_3 \, T_i^m + a_4 \, T_i^{m+1} + a_5 \, T_{i+1}^m + a_6 \, T_{i+1}^{m+1} = 0,$$
(3.4)

where the coefficient of the temperature terms are reported in Table 3.1, and Fo is the Fourier number, which is given by

$$Fo = \frac{\alpha \Delta t}{\Delta x^2}.$$

Table 3.1 Coefficients of T.

$\boldsymbol{a_1}$	$\boldsymbol{a_2}$	$\boldsymbol{a_3}$	$\boldsymbol{a_4}$	$\boldsymbol{a_5}$	$\boldsymbol{a_6}$
$Fo \cdot (1-\theta)$	$Fo \cdot \theta$	$1-2Fo\cdot(1-\theta)$	$-(1+2Fo\cdot\theta)$	$Fo \cdot (1-\theta)$	$Fo \cdot \theta$

3.1.1.1 Boundary conditions

The boundary conditions were imposed by writing the energy balance of the boundary nodes [291].

Dirichlet conditions   The Dirichlet (or first-type) boundary conditions are imposed by prescribing the temperature along the boundaries of the domain. Considering node 1 facing the external environment, whose temperature is T_{ae}, and node N facing the internal environment, whose temperature is T_{ai}, we respectively have

$$T(0,t) = T_{ae}(t) \quad \text{and} \quad T(L,t) = T_{ai}(t),$$

which can be expressed as

$$T_1^{m+1} = T_{ae}^{m+1} \quad \text{and} \quad T_N^{m+1} = T_{ai}^{m+1}.$$

Neumann conditions   The Neumann (or second-type) boundary conditions are imposed by prescribing the heat flux along the boundaries of the domain. This condition was applied to determine the temperature of boundary nodes between materials (Fig. 3.1). The heat flux between adjacent materials—L on the left and R on the right—was prescribed to assume the same value, according to eq. (3.5).

$$-k_L A \frac{\partial T}{\partial x}\bigg|_L = -k_R A \frac{\partial T}{\partial x}\bigg|_R \tag{3.5}$$

By replacing the derivative terms in eq. (3.5) with the corresponding backward and forward finite difference schemes, and simplifying the heat transfer surface which is unvaried, we obtain

$$-k_L \frac{T_{i-2}^{m+1} - 4T_{i-1}^{m+1} + 3T_i^{m+1}}{2\Delta x} = -k_R \frac{-3T_i^{m+1} + 4T_{i+1}^{m+1} - T_{i+2}^{m+1}}{2\Delta x}$$

which can be rearranged as

$$a_L \left(4T_{i-1}^{m+1} - T_{i-2}^{m+1}\right) - 3\left(a_L + a_R\right) T_i^{m+1} + a_R \left(4T_{i+1}^{m+1} - T_{i+2}^{m+1}\right) = 0, \tag{3.6}$$
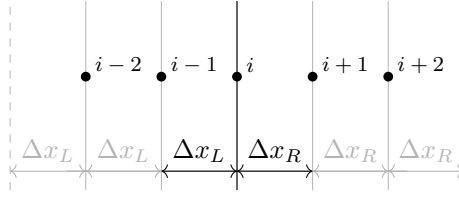
Fig. 3.1 Boundary node between two materials.

where

$$a_L = \frac{k_L}{2\Delta x_L} \qquad \text{and} \qquad a_R = \frac{k_R}{2\Delta x_R}.$$

Rewriting eq. (3.6) with a combined scheme, we obtain

$$\theta \cdot \left[a_L \left(4T_{i-1}^{m+1} - T_{i-2}^{m+1} \right) - 3 \left(a_L + a_R \right) T_i^{m+1} + a_R \left(4T_{i+1}^{m+1} - T_{i+2}^{m+1} \right) \right] +$$
$$+ (1-\theta) \cdot \left[a_L \left(4T_{i-1}^{m} - T_{i-2}^{m} \right) - 3 \left(a_L + a_R \right) T_i^{m} + a_R \left(4T_{i+1}^{m} - T_{i+2}^{m} \right) \right] = 0.$$
$$\tag{3.7}$$

Mixed conditions For the first node, which faced the external environment, the mixed (or third-type) boundary conditions were imposed by prescribing the convective heat transfer and the impinging solar radiation,

$$-kA\frac{\partial T}{\partial x} = h_{ce}A \left[T_{ae}(t) - T(0,t) \right] + \alpha_s I(t) A, \tag{3.8}$$

where h_{ce} is the convective heat transfer coefficient towards the external environment, α_s is the solar absorption coefficient, and I is the solar irradiance. By expressing eq. (3.8) with a central difference scheme, we obtain

$$-k\frac{T_{i+1}^m - T_{i-1}^m}{2\Delta x} = h_{ce} \left(T_{ae}^m - T_i^m \right) + \alpha_s I^m, \tag{3.9}$$

where T_{i-1}^m is a fictitious node. By solving eq. (3.9) for T_{i-1}^m, we find

$$T_{i-1}^m = \frac{2\Delta x}{k} \left[h_{ce} \left(T_{ae}^m - T_i^m \right) + \alpha_s I^m \right] + T_{i+1}^m.$$

Similarly, the fictitious node T_{i-1}^{m+1} is given by

$$T_{i-1}^{m+1} = \frac{2\Delta x}{k} \left[h_{ce} \left(T_{ae}^{m+1} - T_i^{m+1} \right) + \alpha_s I^{m+1} \right] + T_{i+1}^{m+1}.$$

By replacing the fictitious nodes in eq. (3.4), we obtain

$$
\begin{aligned}
\left(a_3 + a_1 c_e\right) T_i^m + \left(a_4 + a_2 c_e\right) T_i^{m+1} + \left(a_1 + a_5\right) T_{i+1}^m + \left(a_2 + a_6\right) T_{i+1}^{m+1} + \\
+ c_e \left(a_1 T_{ae}^m + a_2 T_{ae}^{m+1}\right) + c_e \frac{\alpha_s}{h_{ce}} \left(a_1 I^m + a_2 I^{m+1}\right) = 0,
\end{aligned} \tag{3.10}
$$

where

$$
c_e = h_{ce} \frac{2\Delta x}{k}.
$$

For the last node, which faced the internal environment, the mixed boundary conditions were imposed by prescribing the convective heat transfer,

$$
- kA \frac{\partial T}{\partial x} = h_{ci} A \left[T(L,t) - T_{ai}(t)\right], \tag{3.11}
$$

where h_{ci} is the convective heat transfer coefficient towards the internal environment. By expressing eq. (3.11) with a central difference scheme, we obtain

$$
- k \frac{T_{i+1}^m - T_{i-1}^m}{2\Delta x} = h_{ci} \left(T_i^m - T_{ai}^m\right), \tag{3.12}
$$

where T_{i+1}^m is a fictitious node. By solving eq. (3.12) for T_{i+1}^m, we find

$$
T_{i+1}^m = -h_{ci} \frac{2\Delta x}{k} \left(T_i^m - T_{ai}^m\right) + T_{i-1}^m.
$$

Similarly, the fictitious node T_{i+1}^{m+1} is given by

$$
T_{i+1}^{m+1} = -h_{ci} \frac{2\Delta x}{k} \left(T_i^{m+1} - T_{ai}^{m+1}\right) + T_{i-1}^{m+1}.
$$

By replacing the fictitious nodes in eq. (3.4), we obtain

$$
\begin{aligned}
\left(a_1 + a_5\right) T_{i-1}^m + \left(a_2 + a_6\right) T_{i-1}^{m+1} + \left(a_3 + a_5 c_i\right) T_i^m + \left(a_4 + a_6 c_i\right) T_i^{m+1} - \\
- c_i \left(a_5 T_{ai}^m - a_6 T_{ai}^{m+1}\right) = 0,
\end{aligned} \tag{3.13}
$$

where

$$
c_i = -h_{ci} \frac{2\Delta x}{k}.
$$

3.1.1.2 Gauss-Seidel iteration and overrelaxation

The Gauss-Seidel iteration is a procedure to solve implicit schemes. It requires a first guess of the nodal temperatures, which are used to calculate an approximation of the unknown. Iteration by iteration, the unknowns are substituted by the results

of the previous iteration. The procedure continues until a convergence criterion is met [291].

Solving eq. (3.4) for T_i^{m+1}, we obtain eq. (3.14), where the terms T_{i-1}^{m+1} and T_{i+1}^{m+1} are also unknown.

$$T_i^{m+1} = -\frac{1}{a_4} \left(a_1 \, T_{i-1}^m + a_2 \, T_{i-1}^{m+1} + a_3 \, T_i^m + a_5 \, T_{i+1}^m + a_6 \, T_{i-1}^{m+1} \right). \qquad (3.14)$$

To be able to solve the equation, initial values need to be assigned to T_{i-1}^{m+1} and T_{i+1}^{m+1}. In the first iteration, we have

$$T_i^{m+1} = -\frac{1}{a_4} \left[a_1 \, T_{i-1}^m + a_2 \, T_{i-1}^{m+1}(0) + a_3 \, T_i^m + a_5 \, T_{i+1}^m + a_6 \, T_{i-1}^{m+1}(0) \right],$$

where the values in the brackets denote the iteration number, and zero stands for the first guess. In the second iteration, T_i^{m+1} is evaluated substituting the results of the first iteration to T_{i-1}^{m+1} and T_{i+1}^{m+1}. Generalising for the kth iteration, eq. (3.14) becomes

$$T_i^{m+1}(k+1) = -\frac{1}{a_4} \left[a_1 \, T_{i-1}^m + a_2 \, T_{i-1}^{m+1}(k) + a_3 \, T_i^m + a_5 \, T_{i+1}^m + a_6 \, T_{i-1}^{m+1}(k) \right].$$

The iteration comes to an end when a convergence criterion is met. When the values of the current iteration differ from those of the previous iteration less than a constant K, the process stops. The convergence criterion can hence be expressed as

$$\left| T_i^{m+1}(k+1) - T_i^{m+1}(k+1) \right| < K. \qquad (3.15)$$

To increase the convergence speed, the term $T_i^{m+1}(k) - T_i^{m+1}(k) = 0$ can be added to the right hand side of eq. (3.15).

$$T_i^{m+1}(k+1) = T_i^{m+1}(k) - \left\{ \frac{1}{a_4} \left[a_1 \, T_{i-1}^m + a_2 \, T_{i-1}^{m+1}(k) + \right.\right.$$
$$\left.\left. + a_3 \, T_i^m + a_4 \, T_i^{m+1}(k) + a_5 \, T_{i+1}^m + a_6 \, T_{i-1}^{m+1}(k) \right] \right\}.$$

When the convergence gets close to the exact solution, the quantity in curly brackets approaches zero. This quantity can therefore be seen as a correction term of $T_i^{m+1}(k)$ for each iteration; if multiplied by a term ω—called overrelaxation coefficient—we obtain

$$T_i^{m+1}(k+1) = T_i^{m+1}(k) - \frac{\omega}{a_4} \left[a_1 \, T_{i-1}^m + a_2 \, T_{i-1}^{m+1}(k) + a_3 \, T_i^m + \right.$$
$$\left. + a_4 \, T_i^{m+1}(k) + a_5 \, T_{i+1}^m + a_6 \, T_{i-1}^{m+1}(k) \right].$$

For the convergence to be guaranteed, $0 < \omega < 2$. When $0 < \omega < 1$ we have underrelaxation, for $\omega = 1$ we have the Gauss-Seidel iteration, whereas for $1 < \omega < 2$ we have overrelaxation. A proper choice of ω can dramatically reduce the calculation time.

By applying the same procedure to equations (3.7), (3.10) and (3.13), we respectively obtain

$$
\begin{aligned}
T_i^{m+1}(k+1) = T_i^{m+1}(k) + &\frac{\omega}{3\left(a_L + a_R\right) \cdot \theta} \cdot \\
\cdot \Big\{ a_L &\left[\theta\left(4T_{i-1}^{m+1}(k) - T_{i-2}^{m+1}(k)\right) + (1-\theta)\left(4T_{i-1}^m - T_{i-2}^m\right)\right] + \\
+ a_R &\left[\theta\left(4T_{i+1}^{m+1}(k) - T_{i+2}^{m+1}(k)\right) + (1-\theta)\left(4T_{i+1}^m - T_{i+2}^m\right)\right] - \\
- 3(a_L &+ a_R)\left[\theta T_i^{m+1}(k) + (1-\theta)T_i^m\right]\Big\},
\end{aligned}
$$

$$
\begin{aligned}
T_i^{m+1}(k+1) = T_i^{m+1}(k) - &\frac{\omega}{\left(a_4 + a_2 c_e\right)} \cdot \Big[\left(a_3 + a_1 c_e\right)T_i^m + \\
+ \left(a_4 + a_2 c_e\right)&T_i^{m+1}(k) + \left(a_1 + a_5\right)T_{i+1}^m + \left(a_2 + a_6\right)T_{i+1}^{m+1}(k) + \\
+ c_e&\left(a_1 T_{ae}^m + a_2 T_{ae}^{m+1}\right) + c_e\frac{\alpha_s}{h_e}\left(a_1 I^m + a_2 I^{m+1}\right)\Big],
\end{aligned}
$$

$$
\begin{aligned}
T_i^{m+1}(k+1) = T_i^{m+1}(k) - &\frac{\omega}{\left(a_4 + a_6 c_i\right)} \cdot \\
\cdot \Big[\left(a_1 + a_5\right)&T_{i-1}^m + \left(a_2 + a_6\right)T_{i-1}^{m+1}(k) + \left(a_3 + a_5 c_i\right)T_i^m + \\
+ \left(a_4 + a_6 c_i\right)&T_i^{m+1}(k) - c_i\left(a_5 T_{ai}^m + a_6 T_{ae}^{m+1}\right)\Big].
\end{aligned}
$$

An overrelaxation coefficient of 1.3 was adopted in the calculations. The convergence was considered to be reached for $K = 10^{-6}$.

3.1.2   Model validation

The goodness of fit of the model was evaluated by means of the following metrics:

- Mean Bias Error (MBE) and Mean Percentage Error (MPE)
- Mean Absolute Error (MAE) and Mean Absolute Percentage Error (MAPE)
- Root Mean Squared Error (RMSE) and Percentage Root Mean Squared Error (PRMSE)
- Coefficient of determination (R^2).

A model has a good performance if these metrics have values as close to zero as possible, with the exception of R^2 which should be as close to 1 as possible.

The MBE measures the tendency of a model to overestimate (if positive) or underestimate (if negative) the observed values. It has the same unit of measurement as the estimated quantity. MBE and MPE are given by

$$MBE = \frac{\sum (\hat{y} - y)}{N} \quad \text{and} \quad MPE = \frac{100}{N} \sum \frac{\hat{y} - y}{y}.$$

where y and $\hat{y}$ respectively denote the observed and estimated quantities, and N is the total number of data.

The MAE is a positive metric which avoids the compensation between positive and negative residuals which occurs in the evaluation of the MBE. It has the same unit of measurement as the estimated quantity. MAE and MAPE are given by

$$MAE = \frac{\sum |\hat{y} - y|}{N} \quad \text{and} \quad MAPE = \frac{100}{N} \sum \frac{|\hat{y} - y|}{y}.$$

The RMSE is a positive metric which incorporates both the variance and the square of the bias of an estimator; it penalises high errors more than MAE. It has the same unit of measurement as the estimated quantity. RMSE and PRMSE are given by

$$RMSE = \sqrt{\frac{\sum (\hat{y} - y)^2}{N}} \quad \text{and} \quad PRMSE = 100 \sqrt{\frac{1}{N} \sum \left(\frac{\hat{y} - y}{y}\right)^2}.$$

The coefficient of determination, R^2, is a number comprised between 0 and 1 where $R^2 = 1$ means a prefect correspondence between observed and modelled values, and $R^2 = 0$ means that the model does not provide an estimate of the data better than their average. It si given by

$$R^2 = 1 - \frac{\sum (\hat{y} - y)^2}{\sum (y - \bar{y})^2},$$

where $\bar{y}$ represents the mean of the observed values.

3.1.2.1   Phase change validation

The phase change was validated against the exact solution of the melting in a half-space problem [73]. The theoretical solution was evaluated for Glauber Salt (Table 3.2) with $k = k_l$ at 5 cm, 10 cm and 15 cm from the interface. The initial temperature of the half-space was 25 ℃. The temperature of the boundary was fixed at 90 ℃.

Table 3.2 Thermo-physical properties of the Glauber Salt.

T_m	ρ	c_l	c_s	k_l	k_s	L
[℃]	$[\text{kg/m}^3]$	[kJ/(kg K)]	[kJ/(kg K)]	[W/(m K)]	[W/(m K)]	[kJ/kg]
32	1460	3.31	1.76	0.59	2.16	251.21

In the numerical model, the half-space was approximated to 1 m of PCM. A melting temperature range of 0.5 ℃ was considered. Selecting a smaller range led to great inaccuracies.

The goodness of fit of the model was evaluated considering a mesh size of 2 mm with both 60 s and 180 s as time step. The temperature profiles with the corresponding residual plots for the two time steps are respectively illustrated in Fig. 3.2 and Fig. 3.3, whereas the metrics are respectively reported in Table 3.3 and Table 3.4.

A very good fit was obtained with a time step of 60 s, with a MAPE below 0.65% (MAE below 0.29 ℃) and a PRMSE below 1.6% (RMSE below 0.58 ℃). A tendency of the model to overestimate the exact solution was observed at 5 cm and 10 cm from the interface, whereas a slight tendency to underestimate it occurred at 15 cm. As it could be expected, the model showed a worse performance when increasing the time step, with a MAPE below 0.6% (MAE below 0.79 ℃) and a PRMSE below 3.3% (RMSE below 1.3 ℃).

Table 3.3 Performance metrics with a time step of 60 s.

Position	MBE	MPE	MAE	MAPE	RMSE	PRMSE	R^2
	[℃]	[%]	[℃]	[%]	[℃]	[%]	[−]
5 cm	0.25	0.59	0.29	0.65	0.58	1.6	0.998
10 cm	0.11	0.36	0.21	0.53	0.28	0.80	0.999
15 cm	-0.023	0.027	0.16	0.42	0.17	0.47	0.999

Table 3.4 Performance metrics with a time step of 180 s.

Position	MBE	MPE	MAE	MAPE	RMSE	PRMSE	R^2
	[℃]	[%]	[℃]	[%]	[℃]	[%]	[−]
5 cm	0.79	1.6	0.79	1.6	1.3	3.3	0.988
10 cm	0.72	1.8	0.72	1.8	1.0	2.7	0.992
15 cm	0.36	1.0	0.36	1.0	0.44	1.3	0.997
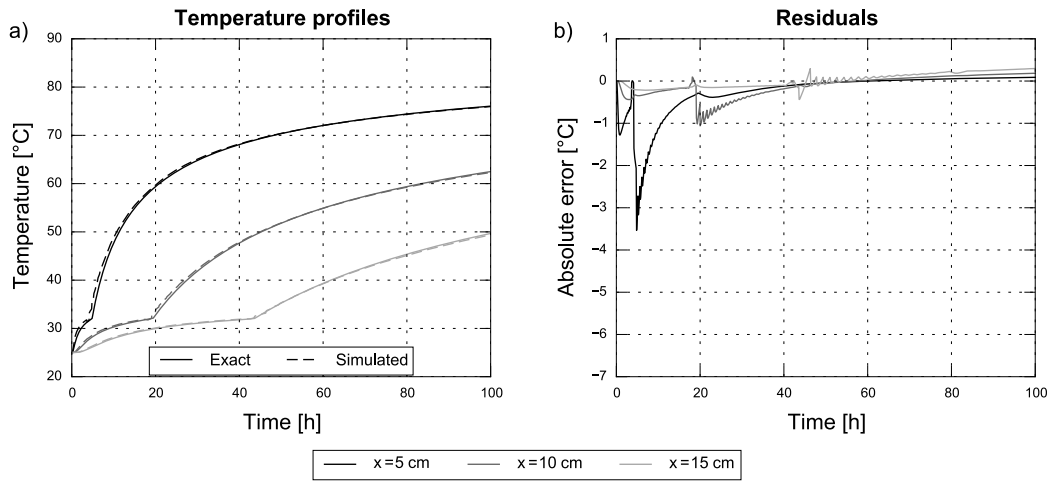
Fig. 3.2 Temperature profiles and residuals with a time step of 60 s.
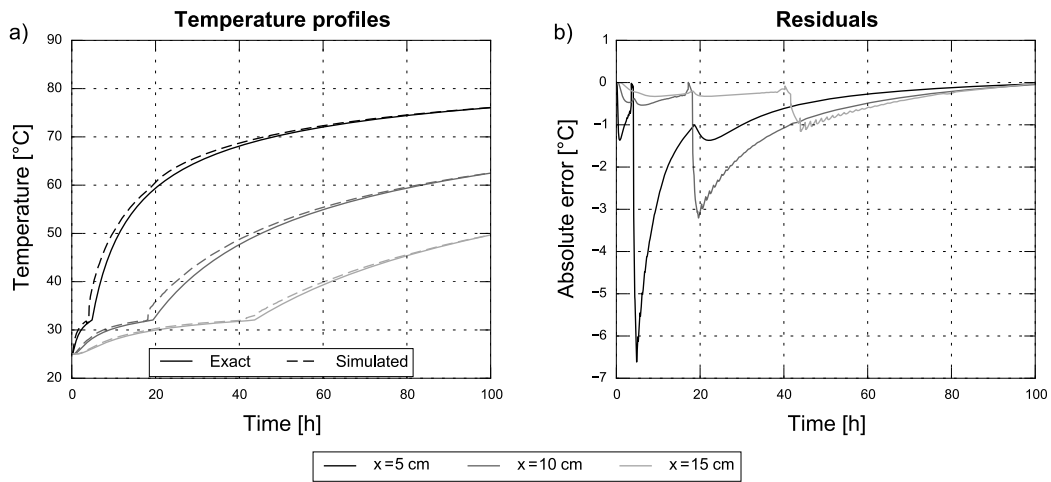
Fig. 3.3 Temperature profiles and residuals with a time step of 180 s.

In general, the model showed a tendency to anticipate the end of the phase change, which was more pronounced with a higher time step. In both cases, the worst fit was obtained on the interface closest to the boundary (5 cm).

3.2 Optimisation algorithms

Two algorithms were selected to perform the optimisation analyses. When dealing with single-objective optimisations, a MATLAB implementation of the $(\lambda + \mu)$ Evolution Strategy (ES) algorithm was specifically written and adopted. Multi-objective optimisations were instead carried out by means of a Python implementation of the Non-dominated-and-crowding Sorting Genetic Algorithm II (NSGA-II) (see § 2.2.2.1). The Python implementation of NSGA-II was written by Méndez Echenagucia [190].

Material level analyses implied single-objective optimisation, whereas the more complex component and building level analyses required multi-objective searches.

3.2.1 Evolution Strategy

The content of this section was partly published in [24].

The $(\lambda + \mu)$ Evolution Strategy technique [293, 294] is a stochastic optimisation algorithm belonging to the category of the Evolutionary algorithms, which are based on the competition among individuals in a population. Each individual is a vector of input data whose value in the objective function represents its fitness to survive. Only μ individuals with the best fitness (lowest or highest values according to the type of optimisation problem, i.e. minimisation or maximisation) among the population are allowed to reproduce and generate new offspring through crossover and mutation algorithms. The $(\lambda + \mu)$ ES is an elitist version of the (λ, μ) ES; in optimisation, *elitism* is the preservation of a fraction of the best individuals in the population, which would otherwise be lost when the offspring have a worse fitness than their parents. Therefore, in the $(\lambda + \mu)$ ES individuals can survive for more than one generation; both parents and offspring are considered for ranking and crossover. The fitness of the new born individuals is evaluated, and the rate of success —i.e. the rate of fitness improvement compared to the previous generation— is used to influence the subsequent mutations. The process continues until a stop criterion is met. The individual with the best fitness represents the final result of the optimisation process.

3.2.1.1 Description of the ES algorithm

The single-objective optimisation problem is structured by deciding the fitness function, which can either be minimised or maximised, and the number of optimisation parameters, n_p (i.e. the input variables, or degrees of freedom).

Among a population of λ individuals (i.e. vectors whose elements contain the

(a) Crossover.
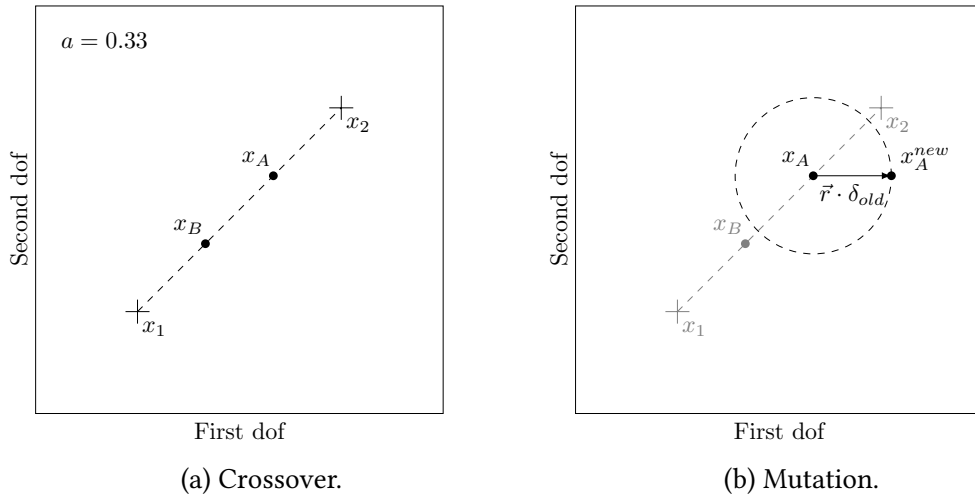
(b) Mutation.

Fig. 3.4 Crossover and mutation operators of the ES algorithm.

input variables of the problem, which are defined within a lower and an upper bound which determine the domain of the fitness function), only the best μ individuals are selected to be parents and recombine into λ offspring which will form the next generation. This operation is called *crossover*. In the ES, the crossover operation consists in a linear combination between the two parents (eq. 3.16), where the parameter a is selected at the beginning of the iteration process (Fig. 3.4a).

$$\begin{cases} X_A = (1 - a) \cdot x_1 + a \cdot x_2 \\ X_B = a \cdot x_1 + (1 - a) \cdot x_2 \end{cases} \tag{3.16}$$

Before the crossover operation, the application of a clustering algorithm to the parent vectors in the search space would be advisable to promote their recombination within clusters rather than between clusters [295].

To improve exploration, *mutation* is carried out after the crossover by adding a vector of normally distributed components to the unmutated descendants (Fig. 3.4b). This allows the offspring to perform a "jump" in the search space that is equally likely to happen in any direction (eq. 3.17). The stepwidth of the jump, δ_{old}, is determined at the beginning of each generation as a function of the rate of success and of a parameter α (usually comprised between 1.1 and 1.3 [296]), which is chosen at the beginning of the iteration process. If the rate of success is high (i.e. the rate of fitness improvement compared to the previous generation), δ_{old} is increased, otherwise it is decreased. This process takes place by either multiplying or dividing δ_{old} by α. In this way, bigger jumps are allowed along steep slopes, whereas only smaller mutations are allowed once the surroundings of the local or global minimum

(or maximum) are reached.

$$X_A^{new} = X_A + \vec{r} \cdot \delta_{old} \tag{3.17}$$

After performing the mutation operator, a check should verify whether the individuals are still within the domain of the problem, and place them again within the boundaries in case they jumped out. The fitness of the offspring can then be evaluated and the best μ individuals among both offspring and parents can be selected to become the new parents.

To decide when to stop the iteration process, a total number of generations can be decided a-priori, or a stopping criterion can be introduced. In the latter case, the quadratic norm, q_n, can be evaluated with respect to the mean value of the population (eq. 3.18), and compared to a limit value.

$$q_n = \frac{1}{\lambda n_p} \sum_{j=1}^{n_p} \sum_{i=1}^{\lambda} \left(\frac{x_{i,j} - \bar{x}_j}{\bar{x}_j} \right)^2 \tag{3.18}$$

The whole process can be summarised with the pseudocode reported in Algorithm 1.

Algorithm 1 $(\lambda + \mu)$ ES algorithm

  1: Generate a random initial population
  2: Evaluate fitness of the initial population
  3: Select the best μ individuals to become parents
  4: **for** $i \leftarrow 1, N_{gen}$ **do**
  5:       Run crossover operator
  6:       Run mutation operator
  7:       Check if mutated descendants are still within the boundaries
  8:       Evaluate fitness
  9:       Evaluate the best μ individuals to become the new parents
10:       Compute the rate of success
11:       Compute δ_{old}
12:       Compute q_n
13:       **if** $q_n < q_{n,lim}$ **then**
14:           Exit ES
15:       **else**
16:           Continue to the next Generation
17:       **end if**
18: **end for**

3.2.1.2 Validation of the ES algorithm

The MATLAB implementation of the $(\lambda + \mu)$ Evolution Strategy (ES) technique was validated against the Rosenbrock function [297]. Due to the difficulty to converge to its global minimum, the Rosenbrock function is often used to test the performance of optimisation algorithms.

In a bidimensional space, the Rosenbrock function is defined as

$$f(x,y) = (a-x)^2 + b \cdot (y-x^2)^2, \tag{3.19}$$

whose global minimum is 0 in (a, a^2). Let $a = 1$ and $b = 100$, then the global minimum is in the point (1,1).

The N-dimensional generalisation of the Rosenbrock function can be expressed as

$$f(x_1, x_2, \ldots, x_N) = \sum_{i=1}^{N-1} 100 \cdot (x_{i+1} - x_i^2)^2 + (1 - x_i)^2.$$

A first set of optimisation test runs were performed minimising eq. (3.19) in the domain $[-2,\ 2]$ for both degrees of freedom (dof) with the following settings of the ES algorithm:

$$\begin{cases} \mu = 20\% \text{ of the population} \\ a = 0.3 \\ \alpha = 1.1. \end{cases}$$

The evolution of the optimisation process is reported in Fig. 3.5 for test runs over 10 generations (N_{gen}) with a population size (N_{pop}) of 100 and 1000 individuals. The convergence towards the minimum of the function is clear.

An analysis on the effect of population size and number of generations with fixed number of iterations (product of the population size and the number of generations) was additionally performed (Fig. 3.6). With a limited number of simulation runs (1000) the convergence was faster and more effective with a high number of individuals and just a few generations (best results with N_{pop} $100 - N_{gen}$ 10). On the other hand, when more iteration runs were available (10000), a high number of generations was preferred over a growing population size (best results with N_{pop} $100 - N_{gen}$ 100).

More comprehensive tests were carried out to evaluate the performance of the algorithm with growing number of degrees of freedom and number of iterations (Table 3.5). Given the stochastic nature of the algorithm, for each case the test were performed over 100 independent runs. The fitness of the best and worst best fits values resulting from these 100 runs are reported in Fig. 3.7.
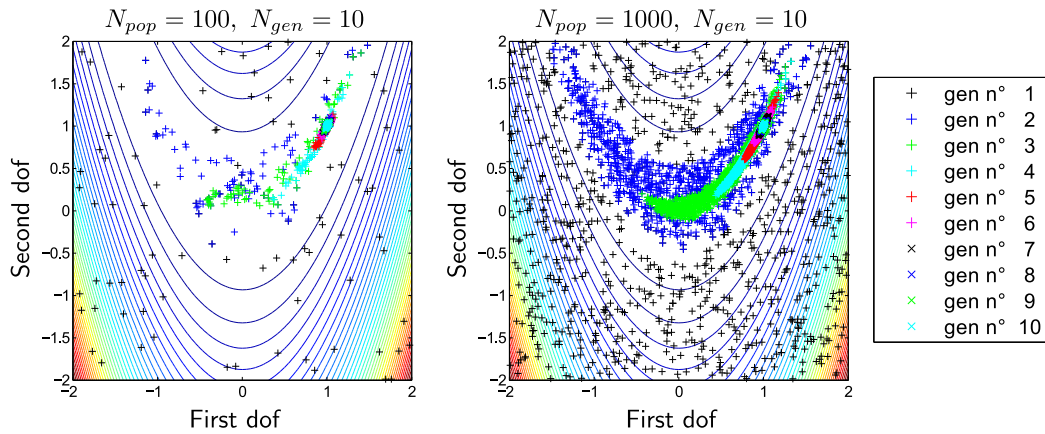
Fig. 3.5 Comparison between the evolution of test runs with 100 and 1000 individuals.
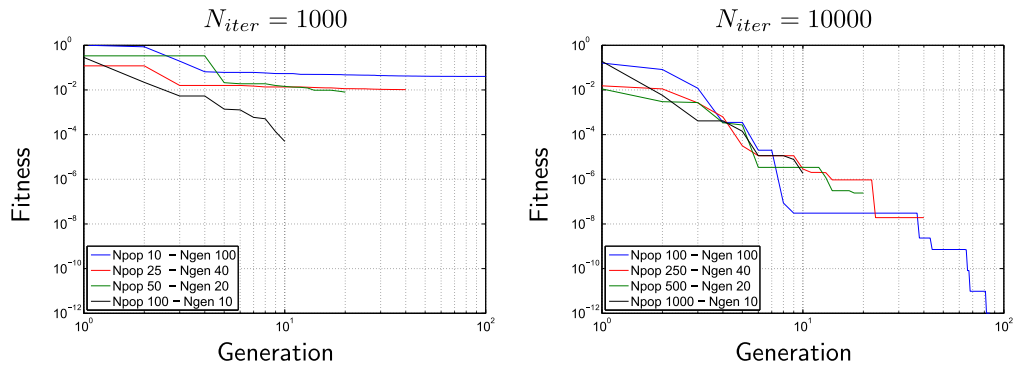
Fig. 3.6 Effect of population size on the evolution of the best fitness.

The more the degrees of freedom, the higher the best fit value that is found. With two degrees of freedom and 10000 iterations the convergence to the solution can be considered always guaranteed (fitness < 0.5). Within five degrees of freedom, in the best case convergence is reached with at least 1000 iteration. As the degrees of freedom grow, 500 iterations are the minimum not to find disproportionately large results (at least N_{pop} 100 regardless of the number of dof). Beyond 50000 no significant improvements are obtained (N_{pop} 1000).

Performance evaluation of ES $(\lambda + \mu)$

Fitness of best values

No. of degrees of freedom

Fitness of worst values

No. of degrees of freedom
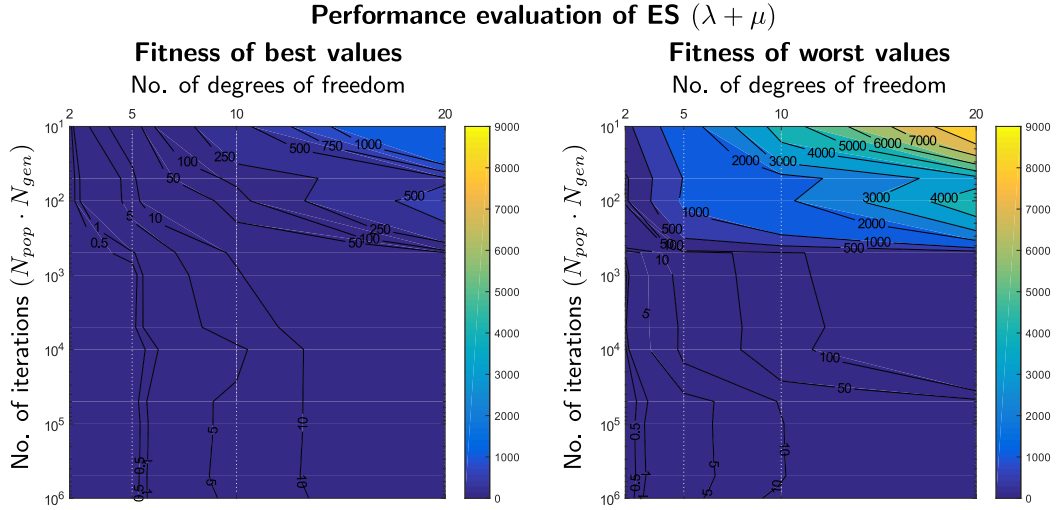
Fig. 3.7 Performance evaluation of the $(\lambda + \mu)$ ES. Fitness of best and worst values.

Table 3.5 Results of the extensive test runs.

N_{pop}	N_{gen}	N_{iter}	Best best-fits				Worst best-fits			
			Degrees of freedom				Degrees of freedom			
			2	5	10	20	2	5	10	20
5	2	10	6.5e-04	16	408	1716	374	1421	4450	8975
10	5	50	1.5e-03	6.1	116	458	46	1021	1572	3590
10	10	10^2	8.0e-05	6.0	62	637	52	1085	1800	4711
100	5	$5\ 10^2$	1.3e-06	0.74	11	47	1.1	15	85	210
100	10	10^3	5.8e-09	7.5e-02	9.1	39	0.26	12	83	198
100	50	$5\ 10^3$	1.5e-13	0.27	7.3	21	0.85	11	76	182
100	100	10^4	4.4e-19	1.3e-04	4.0	23	0.34	11	78	218
1000	50	$5\ 10^4$	4.5e-16	0.12	6.4	18	1.9e-09	2.6	10	35
1000	100	10^5	1.2e-18	7.2e-03	6.5	18	1.4e-13	3.0	9.7	30
1000	500	$5\ 10^5$	0	5.1e-02	6.7	17	0	2.8	9.6	28
1000	1000	10^6	0	0.14	6.1	17	0	3.3	12	30

3.2.2   NSGA-II

NSGA-II is a genetic algorithm designed to work with multi-objective optimisation problems. It was developed by Kalyanmoy Deb and his students as an elitist multi-objective optimisation algorithm [298]. As for all GAs, there is a main loop which iterates for each generation the processes of fitness evaluation, selection, crossover and mutation. However, these operators are especially designed to be used with multiple fitness functions. In addition, NSGA-II has two special operators which are the Non-Dominated Sorting (NDS) and the Crowding Distance (CD) algorithms. These operators allow the outcome of the search process to be a set of evenly distributed solutions along the Pareto front.

To provide elitism, NSGA-II works with a non-constant population size. If an initial population of size N_{pop} is selected, in the main loop it will be doubled to $2N_{pop}$ in order to consider both a Parent population and a Current population.

A graphical scheme of how NSGA-II works is reported in Fig. 3.8. The dashed line encloses the main loop. The variations in the population size are stated in red, whereas the main differences from a single-objective GA are highlighted in blue. A pseudocode of the NSGA-II algorithm is also provided (Algorithm 2).

Although the operating principles of the NSGA-II algorithm will be herewith discussed, for details on the Python implementation and code validation please refer to [190].

Generation of the initial population   To generate the initial population, a number n of binary digits needs to be defined to discretise the domain of each variable. Since a binary code that is n digits long contains 2^n numbers, each domain is divided in 2^n points. The length of each discretised element is therefore given by $(D_{\max} - D_{\min}) / (2^n - 1)$, where $D_{\max}$ and $D_{\min}$ are respectively the upper and lower bounds of the variable's domain. Summing up the number of binary digits of each variable, the length of the chromosome for each individual (i.e. the total number of binary digits) is obtained. The initial population is then generated by assigning random binary values to each digit.

It is important to notice that the complexity of the search problem is a function of both the number of variables and their discretisation; the higher the total number of possible solutions, the less trivial the optimisation process is.

Decoding and scaling of the initial population   To be able to evaluate the fitness of the initial population, the binary codes need to be decoded and scaled. First, the chromosomes are split according to the number of binary digits assigned to each variable. Then, the binary codes of each variable are decoded into decimal numbers, which are eventually scaled in the variables' domains. Let x_d be the
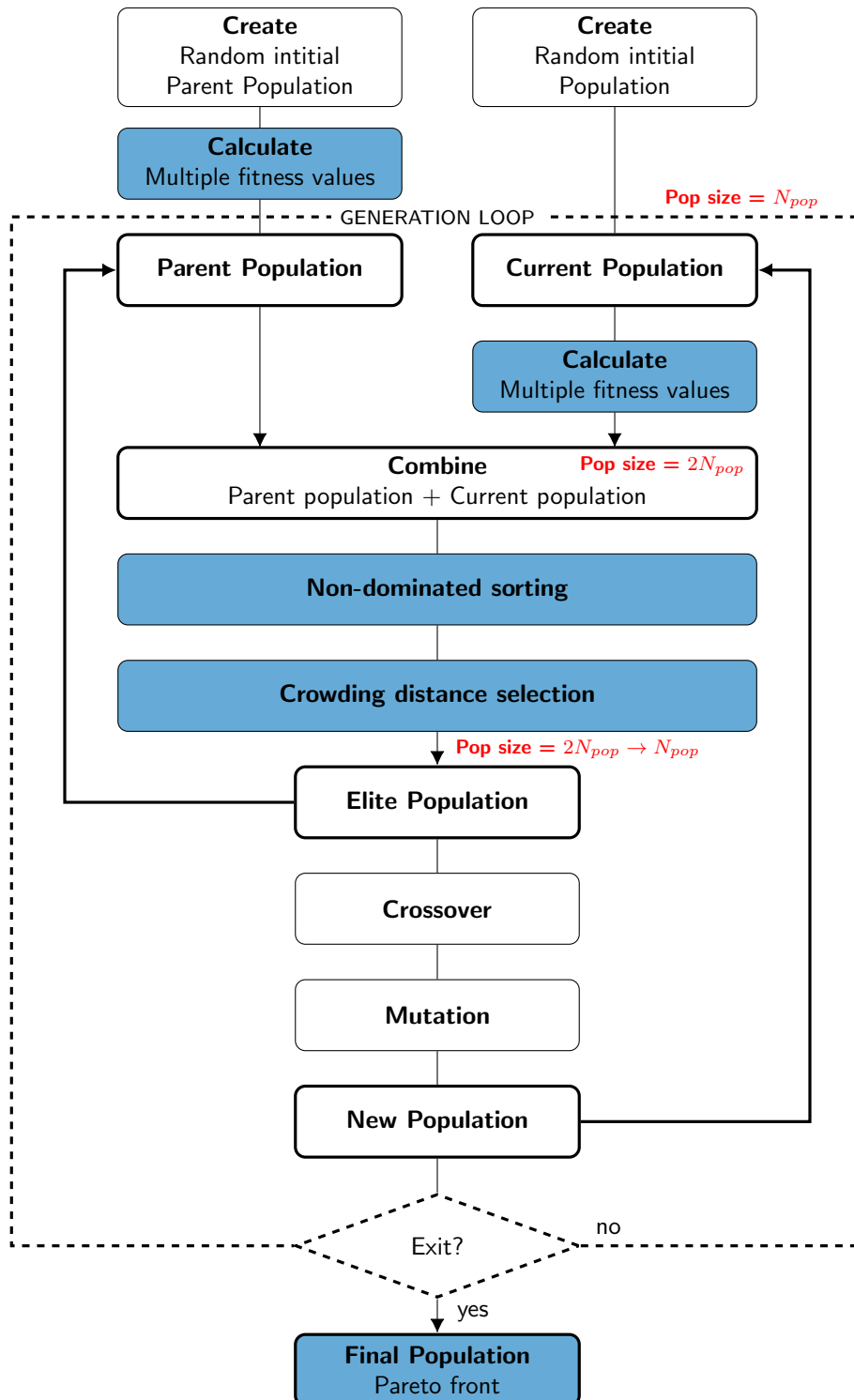
Fig. 3.8 Flow-chart of the NSGA-II algorithm (adapted from [190]).

Algorithm 2 NSGA-II [190]

1: Generate a random and coded *Initial* population with N_{pop} individuals
2: Decode and Scale the *Initial* population
3: Calculate fitness values for the *Initial* population
4: Copy the resulting fitness values to the *Parent* population vector
5: Generate a random and coded *Current* population with N_{pop} individuals
6: **for** $i \leftarrow 1, N_{gen}$ **do**
7: $\quad$ Decode and Scale the *Current* population
8: $\quad$ Calculate fitness values for the *Current* population
9: $\quad$ Combine *Parent* and *Current* populations creating a vector of size $2N_{pop}$
10: $\quad$ Run Non-Dominated Sorting algorithm for the combined population
11: $\quad$ Run Crowding Distance algorithm for the combined population
12: $\quad$ Replace *Parent* population with the first N_{pop} individuals from the combined population according to the NDS and CD results
13: $\quad$ Run Tournament Selection operator
14: $\quad$ Run crossover operator
15: $\quad$ Run mutation operator
16: $\quad$ Replace the *Current* population with the resulting population
17: $\quad$ Perform Exit condition test
18: $\quad$ **if** Exit condition test == True **then**
19: $\quad\quad$ Exit NSGA-II
20: $\quad$ **else**
21: $\quad\quad$ Continue to the next Generation
22: $\quad$ **end if**
23: **end for**

---

decoded variable and x_s the scaled one. The conversion is given by

$$x_s = D_{\min} + \frac{D_{\max} - D_{\min}}{2^n - 1} \cdot x_d.$$

For example, if there are two variables having respectively 6 and 4 binary digits in the domains $[0, \ 1]$ and $[3, \ 5]$, the decoding and scaling processes could take place as follows:

Chromosome	0110011001
Variables	011001, 1001
Decoding	$011001 = 0 \cdot 2^5 + 1 \cdot 2^4 + 1 \cdot 2^3 + 0 \cdot 2^2 + 0 \cdot 2^1 + 1 \cdot 2^0 = 25$
	$1001 = 1 \cdot 2^3 + 0 \cdot 2^2 + 0 \cdot 2^1 + 1 \cdot 2^0 = 9$
Scaling	$0 + (1 - 0) / (2^6 - 1) \cdot 25 = 0.397$
	$3 + (5 - 3) / (2^4 - 1) \cdot 9 = 4.2$

(a) Dominance for point 3.

(b) Sequential Pareto fronts (PF).
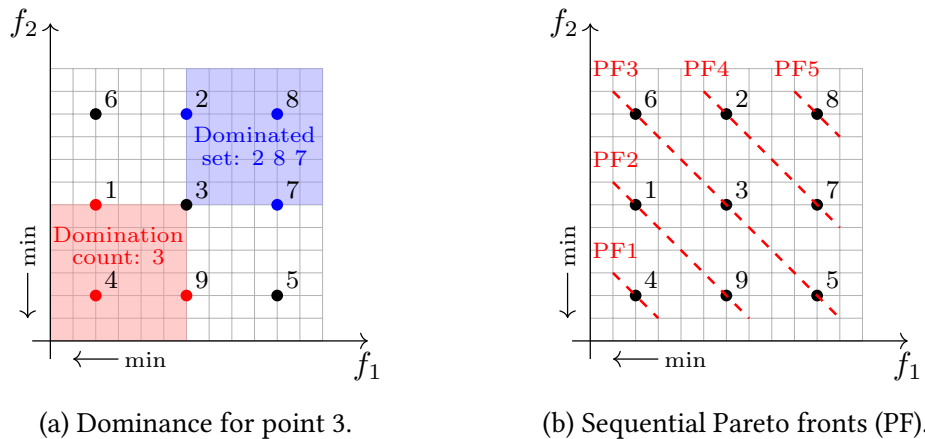
Fig. 3.9 Example of non-dominated sorting.

Fitness evaluation of the initial population   Once the decoded and scaled initial population is obtained, the fitness of all the individuals in the population can be evaluated. While in single-objective optimisation problems there is only one fitness value for each individual in the population, in multi-objective problems a matrix of fitness values is obtained.

Since there is not yet a Parent population before entering the main loop, the fitness values of the initial population are copied to the Parent population vector. A Current population also needs to be randomly created.

Once the main loop starts, the fitness values of the Current population are evaluated. The Current population is then combined with the Parent population; in this way, the number of individuals in the population becomes $2N_{pop}$.

The combined population is subsequently studied by the non-dominated sorting and crowding distance operators. These operators are needed by multi-objective optimisation algorithms to select the individuals which will be processed by the selection operator.

Non-Dominated Sorting operator   The non-dominated sorting algorithm is used to asses the position of the solutions in the objective space by comparing their fitness values.

For a fast evaluation, two entities are calculated for each individual; the *domination count* is the number of dominating individuals, whereas the *dominated set* is a list of dominated individuals (the concept of dominance was explained in § 2.2). The domination count of the solutions in the first non-dominated frontier is zero. Then, the domination count of the elements in the dominated set of each individual in the first front is reduced by one. Those individuals whose domination count becomes zero belong to the second non-dominated front. The procedure is repeated until

all the frontiers are identified. In this way, the population is sorted into sequential Pareto fronts which will be used by the selection operator together with the results of the crowding distance algorithm.

For example, for the individuals in Fig. 3.9 subjected to the minimisation of two objective functions, the non-dominated sorting process would take place as follows:

Individuals	1 2 3 4 5 6 7 8 9
Domination count	1 5 3 0 2 2 5 8 1
Dominated set	62837　8　287　62813795　87　28　8　∅　28375
Pareto front individuals	4, 1 9, 3 5 6, 2 7, 8

		1	2	3	4	5	6	7	8	9	
		1	**2**	**3**	**4**	**5**	**6**	**7**	**8**	**9**	◁ Individuals
		1	5	3	0	2	2	5	8	1	◁ Domination count
PF1	④	-1	-1	-1		-1	-1	-1	-1	-1	◁ Dominated set ind. 4: 62813795
		0	4	2		1	1	4	7	0	◁ Domination count update
PF2	①		-1	-1			-1	-1	-1		◁ Dominated set ind. 1: 62837
	⑨		-1	-1		-1		-1	-1		◁ Dominated set ind. 9: 28375
			2	0		0	0	2	5		◁ Domination count update
	③		-1					-1	-1		◁ Dominated set ind. 3: 287
PF3	⑤							-1	-1		◁ Dominated set ind. 5: 87
	⑥		-1						-1		◁ Dominated set ind. 6: 28
			0					0	2		◁ Domination count update
PF4	②								-1		◁ Dominated set ind. 2: 8
	⑦								-1		◁ Dominated set ind. 7: 8
									0		◁ Domination count update
PF5	⑧										◁ Dominated set ind. 8: ∅

Crowding Distance operator   The crowding distance operator is a diversity preservation algorithm which evaluates the similarity between solutions and ensures their distribution along the Pareto front.

The *crowding distance* of a point, $d_{I_i^m}$, can be defined as a measure of the surrounding objective space which is not occupied by any other individual in
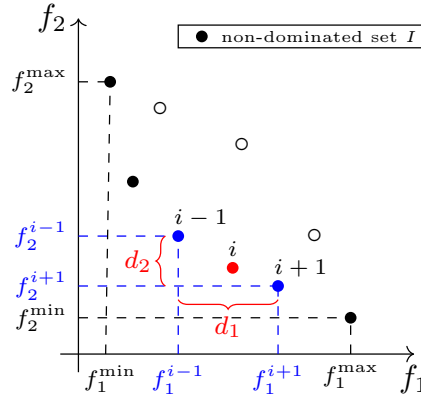
Fig. 3.10 Example of the Crowding Distance concept.

the population. Its computation requires the population to be sorted according to each objective function. Extreme solutions are especially preserved, for they mark the boundary of the Pareto front (they are given infinite $d_{I_i^m}$), whereas the intermediate solutions are assigned a distance equal to the absolute normalised fitness difference of their two adjacent solutions. The calculation can be performed according to eq. (3.20), where I_i^m represents the mth objective function's value of the ith individual in the non-dominated set I, while $f_m^{\max}$ and $f_m^{\min}$ are respectively the maximum and minimum values of the mth objective function.

$$d_{I_i^m} = \frac{f_m^{(I_{i+1}^m)} - f_m^{(I_{i-1}^m)}}{f_m^{\max} - f_m^{\min}} \tag{3.20}$$

The calculation is performed for all the objective functions, and the overall crowding distance of each individual is given by the sum of the distances evaluated for each objective. Individuals with a large crowding distance lay in sparsely covered regions, whereas small $d_{I_i^m}$ values indicate dense portions of space.

The crowding distance can be graphically seen as an estimate of the semi-perimeter of the cuboid formed by the vertices of the nearest neighbours of the individual in the objective space. A representation of the concept is illustrated in Fig. 3.10, where the crowding distance of the ith solution in its Pareto frontier (marked with solid circles) is given by the sum of the distances marked in red after being normalised.

Selection operator   The selection operator is applied to identify which individuals will be used for reproduction. The group of selected individuals is called the *mating pool*.

Due to the presence of many objective functions, selection cannot be simply

done by choosing the individuals with the best fitness; the non-dominated and best distributed individuals are preferred over the others.

To begin with, the Parent population is replaced with the best individuals from the combined population, sorted by the NDS algorithm according to Pareto fronts. The non-dominated fronts fill the new Parent population one at a time, up to the last Pareto that can be completely accommodated (we are passing from a $2N_{pop}$ to a N_{pop} population size). At this point, some individuals of the subsequent Pareto need to be discarded. The points of the last front which could not be fully accommodated are sorted in the descending order of their crowding distance values, and the individuals from the top of the ordered list are chosen (solutions located in lesser crowded regions are hence preferred). In this way, the population size is back to N_{pop}, and the elite individuals are prevented from being lost in the subsequent operations (Fig. 3.11).
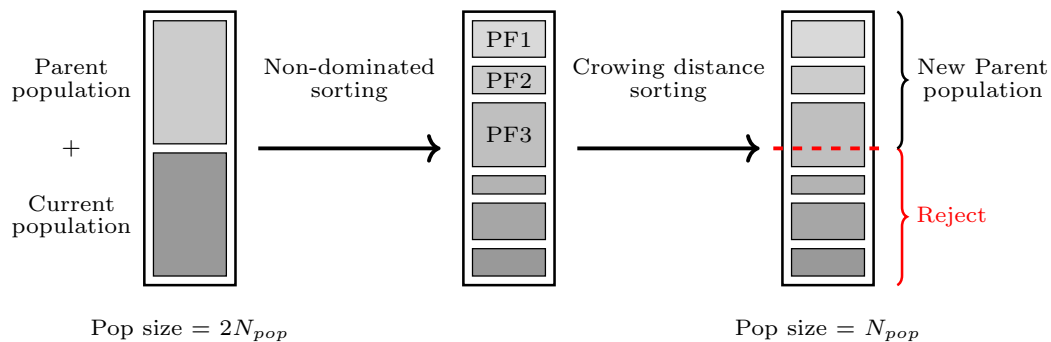
Fig. 3.11 Variations in the population size.

The selection operator has a significant impact on the success of the GA for it can imply both exploitation and exploration. Among the possible selection operators, Tournament Selection is adopted. The Tournament Selection operator randomly selects pairs of individuals to compete for entering in the mating pool. Every individual is selected for two competitions; the winning criterion is based on non-domination level and crowding distance.

This process improves exploitation, for it ensures that good performing individuals have a higher probability to be selected for reproduction. However, if the best performing individuals compete with each other, the ones that get discarded leave place for low performing individuals. This process increases exploration by ensuring a certain degree of diversity in the mating pool.

Crossover operator   A simple crossover operator is adopted to generate the chromosomes of the new population by copying part of the genes from one parent and the other part from the second parent, which are selected from the mating pool (the first half of the mating pool assigns the first parent, while the second half

assigns the second one). A crossover point—i.e. the point of split which determines how many digits are copied from each parent—is selected randomly; its position does not need to be in between variables. For example, if the 6th gene is randomly selected to be the crossover point, a crossover process could take place as follows:

Parent A	011001 | 1001
Parent B	110011 | 0011
Crossover	011001 1001 110011 0011
Offspring AB	011001 | 0011
Offspring BA	110011 | 1001

The crossover operator entails both exploration and exploitation. Since the recombination of genes can imply big changes in the position of the individuals in the search space, exploration is involved. However, exploitation is also at work since the recombination of good performing individuals is expected to yield even better results.

Mutation operator   The mutation operator is a diversity preservation operator whose role is to enhance local exploration by slightly altering a few genes of the chromosomes. The amount of altered genes is determined by the mutation probability, p_m, which is selected as a GA input. A random value $r \in [0, 1]$ is generated for each gene; when r is lower than the mutation probability, the corresponding gene is modified. For example, if a mutation probability of 0.2 is considered, a mutation process could take place as follows:

Chromosome	0	1	1	0	0	1	1	0	0	1
Random value r	0.58	0.32	0.67	0.15	0.46	0.88	0.54	0.23	0.49	0.25
$r < p_m$?	×	×	×	✓	×	×	×	×	×	×
Mutation	0	1	1	1	0	1	1	0	0	1

End condition   Depending on the problem, knowing when an optimal result has been reached is generally impossible. As there are no universal rules of the thumb to estimate population size and mutation probability, deciding when to stop a GA is also a choice. Several types of end conditions can be selected; they can be fitness related end conditions, a limit on the number of calculations, or a limit on calculation time. However, fitness related end conditions (the algorithm stops when an acceptable fitness value is reached) are not a good solution in multi-objective optimisation problems, because the Pareto front might still be sparse. Setting a maximum number of generations or a maximum calculation time is therefore more

common. A maximum number of stagnant generations could also be used to end the optimisation once it stops to evolve properly. However, this is less likely to happen when the are several fitness functions, and even in cases of stagnant Pareto frontiers the algorithm could still work to better populate them.

3.3   Post-optimisation analyses

Other than emphasising the objectives' values that could be reached by means of the optimisation procedure, the main focus was given to the variables' values which led to the optimal solutions. One of the most important differences between single-objective and multi-objective optimisation is that the former finds a single solution, whereas the latter provides multiple solutions corresponding to a trade-off between objectives [299]. Since these solutions are all near optimal, they can be analysed to search for common properties, which can be seen as rules for the solutions to belong to the Pareto-front. Relationships among optimal solutions can therefore provide useful design principles applicable to the problem under investigation.

For carrying out this process of knowledge extraction, a series of graphical, statistical and numerical analyses were performed, which can be globally refereed to as innovization (*innov*ation through optim*ization*) analyses [6–8]. In detail, the statistical variation of the values assumed by the input variables in all the non-dominated solutions was investigated by means of box plots, frequency analyses and variables' mapping of the Pareto-front solutions, analysis of the extreme solutions for each objective, and automated innovization [7]. The main purpose of each type of analysis is briefly detailed in Table 3.6.

Table 3.6 Purpose of post-optimisation analyses in brief.

Analysis	Purpose
Box plots	Identify constant variable values at a glance.
Frequency analyses	Identify the distribution trends of the values assumed by each variable.
Variables' mapping	Identify qualitative relationships between each variable and the objective functions.
Automated innovization*	Quantitatively identify mutual relationships among variables and between variables and objectives.
Extreme solutions	Identify the optimal solution for each single objective.

* Automated innovization was applied only to building-level analyses.

3.3.1 Box plots of the Pareto solutions

The content of this section was partly published in [187].

In descriptive statistics, box plots are concise tools for displaying the degree of dispersion in a dataset without providing information on the underlying statistical distribution. The spacing between the different parts of the plot indicate the degree of dispersion in the data. The boxes delimit the interquartile range (IQR) between the first and the third quartiles, whereas the lines within the boxes represent the median of the distributions. The lines that extend from the boxes, called whiskers, give information on the variability outside the IQR. In Tukey's box plots [300], the whiskers extend up to 1.5 IQR beyond the lower and upper quartiles. Data outside the whiskers are considered to be outliers, and they are plotted as individual points. Outliers can provide important information on the dataset and may represent the key to the phenomenon under study.

The aim of this analysis was twofold. On one hand, the objective was to obtain information on the relative importance of the input variables within the set of the Pareto front solutions. On the other hand, information on the opportunity of reducing the number of input variables could be inferred. Variables characterised by a very low spread represent those inputs for which there is a low degree of freedom in the selection of their value. Since these variables should be almost constant for the solution to belong to the Pareto front, they could be disregarded as input variables in the optimisation process, obtaining in this way a faster convergence to the Pareto front. On the other hand, variables which have a great variability within the Pareto front solutions influence the results in a complex way. Wide-span variables may be the most important to optimise, for the interaction between variables has often a greater effect than single variables.

3.3.2 Frequency analyses of the Pareto solutions

Additional information on the non-dominated solutions was obtained by means of frequency analyses. Where the box plots reveal the degree of variability of a variable within the Pareto front, frequency analyses can provide its underlying distribution. A clear trend may be observed towards a target value, or a tendency of a variable to be minimised or maximised can be more easily identified. If a uniform distribution is found, the variable may be expected to have only a marginal influence, as no preferable value is highlighted. However, no indication on the mutual interactions between variables nor their influence on the objectives' values can be obtained.

3.3.3 Variables' mapping on the Pareto front

To explore how the search space variables affected the results in the objective space, the values assumed by each variable were mapped on the Pareto front. This mapping was obtained by superimposing on the Pareto front a colour-scale representation of the values assumed by each variable, one at a time. This representation allows to qualitatively identify simple relationships between variable and objectives. When constant values are assumed by a variable, the Pareto front is represented by a single colour. A chromatic scale can identify direct or inverse relationships between variable and objectives. Variables mapped by random colours next to each other may signify that they have a little influence on the objective functions. Moreover, clusters in the Pareto front are likely to be identified when categorical variables are involved.

3.3.4 Extreme solutions

The extreme solutions in the Pareto front are especially interesting because they represent the optimal solution for a single objective. If the objectives are contrasted, it is likely that the best solution for one objective corresponds to the worst solution for another. Two extremes of a Pareto front can be generally expected to be far apart in the search space. However, since there is not always continuity between search and objective space, even individuals that are next to each other in the Pareto front may be distant in the search space. A uniform distribution of the Pareto solutions is therefore especially important to retrieve more comprehensive information on the diversity among non-dominated solutions.

3.3.5 Automated innovization

Automated innovization is a systematic procedure to decipher hidden properties which characterise the set of optimal solutions of a given problem [7]. After the proposal of manual innovization approaches [6], an automated GA-based clustering procedure was devised by Bandaru and Deb [7].

Starting from a multi-dimensional variable-objective-constraint $(x\text{-}f(x)\text{-}g(x))$ dataset of near-optimal Pareto solutions, statistically significant parametric relationships—either common to all or to a subset of the Pareto front solutions—are searched through an optimisation approach. The innovized principles of many engineering problems were found to fit into the following generic form [6]:

$$\psi_i \equiv \prod_{j=1}^{N} \phi_j(x)^{b_{ij}} = c_i, \tag{3.21}$$

where ψ_i is the ith parametric relationship object of identification, ϕ_j is the jth basis function, N is the number of basis functions involved in the ith relationship, b_{ij} is the power of the jth basis function of the ith relationship, and c_i is the constant parameter of the ith relationship (later referred to as c-value).

In a knowledge extraction task, it may happen that a relationship is valid for the entire dataset, but may be applicable only to a part of it (i.e. the same left-hand side of eq. (3.21) is valid for several c-values in different parts of the Pareto front). This situation requires the application of clustering techniques prior to the knowledge extraction process. A generic grid-based clustering technique was applied in [7]. If a mono-dimensional dataset of m data points is considered and its domain is divided into d blocks, a block is a sub-cluster if it contains more than the average number of points per block, i.e. m/d, otherwise the points are considered as unclustered. All the adjacent sub-clusters are then merged to form clusters. Simultaneously minimising the number of clusters and unclustered points, the optimal division is obtained. The advantages of this kind of clustering technique is that the number of clusters does not need to be known a-priori, noise and outliers can be easily handled, and clusters of irregular shape can be identified [301]. Adding a constraint requiring no unclustered points should ensure the best possible accuracy of the estimated b_{ij} values [7]. However, in presence of outliers this constraint was found to prevent convergence, and it was therefore discarded.

To avoid multiple solutions, the b_{ij} values need to be normalised. Dividing them by the maximum absolute value in the set, they were bound in the range $[-1, 1]$.

$$b_{ij} = b_{ij} \Big/ \max_{j \in [1, N]} |b_{ij}|, \quad \forall\, j \tag{3.22}$$

Moreover, convergence to the trivial solution $\prod_{j=1}^{N} \phi_j(x)^0 = 1$ should be avoided. Hence, it should be ensured that $|b_{ij}| \geq b_{ij,lim}$, where $b_{ij,lim}$ is an arbitrary threshold. This threshold was set equal to 0.1 for the relationship in eq. (3.21).

To estimate the significance of a relationship, the percentage of data for which the relationship is valid is compared to a threshold value (S_t). This threshold depends on the accuracy of the solutions in the Pareto front, i.e. how distant the dataset is from the true Pareto front. A low threshold may result in artificial relationships, whereas a high threshold may lead to an incomplete knowledge extraction. The percentage coefficient of variation (CV), defined as the ratio of the standard deviation on the mean of the c-values, was adopted as a measure of the significance of a relationship [7],

$$CV = \frac{\sigma}{\mu} \cdot 100\%.$$

Given these premises, to solve the innovization problem the optimisation algorithm would have to simultaneously minimise the number of clusters and of

unclustered points, as well as the percentage coefficient of variation within each cluster. This would be a three-objective optimisation problem. However, since the aim is to find relationships that are equally good with respect to all the objective functions, a weighted sum approach is applied to convert the multi-objective optimisation into a single-objective optimisation problem [7]. The automated innovization problem is therefore defined as

$$
\begin{aligned}
\text{Minimise} \quad & \left(\text{no. clusters} + \text{no. unclustered points} + \sum_{\text{clusters}} CV \right) \\
\text{Subject to} \quad & 1 \leq d_i \leq m, \\
& -1 \leq b_{ij} \leq 1 \quad \forall\, j, \\
& |b_{ij}| \geq b_{ij,lim} \quad \forall\, j, \\
& d_i \in \mathbb{N},\ b_{ij} \in \mathbb{R}.
\end{aligned}
$$

where d_i and b_{ij} are the optimisation variables, and their optimal values for the ith relationship (respectively denoted as d_i^* and b_{ij}^*) are found by means of a genetic algorithm. Binary crossover and bit-wise mutation are used to handle the integer variable (d_i), whereas simulated binary crossover (SBX) [302, 303] and polynomial mutation are used to handle the real-valued variables (b_{ij}).

The constraints are handled with a penalty-parameter-less approach [198]. In this constraint-handling method, constraints are taken into account in the tournament selection operator, so that 1) any feasible solution is preferred over an infeasible solution; 2) among two feasible solutions, the solution with better fitness is preferred; 3) among two infeasible solutions, the solution with smaller constraint violation is preferred. The degree of constraint violation was evaluated by summing for each constraint the outer distance of the d_i and b_{ij} values from their respective bounds and the number of unclustered points. Once the convergence to a set of b_{ij} values is reached, an additional computation is performed for identifying as meaningful sub-clusters those which contain more than $\lfloor (m/d^*) \rfloor + \epsilon$ points, where ϵ is a small integer value. Then, the representative c-value of each cluster, which is a narrow distribution, is set equal to the average c-value within that cluster [7].

To improve the efficiency of the original automated innovization algorithm described in [7], a certain degree of elitism was introduced. The best αN_{pop} individuals among parents and offspring were stored (except the first generation, where only parents are considered). Individuals were ranked according to the penalty-parameter-less conditions. In this way, a small portion of individuals with the best fitness and no or small constraint violation was stored generation by generation. This elite population subsequently replaced the worst individuals (highest degree of constraint violation and lowest fitness) so that the elite could be taken into account for selection, crossover and mutation.

Moreover, due to the nature of the investigated problems, the following linear

relationship was considered in addition to the generic form of the parametric relationship in eq. (3.21):

$$\psi_i \equiv \sum_{j=1}^{N} \phi_j(x) \cdot b_{ij} = c_i. \tag{3.23}$$

To avoid multiple solutions, the b_{ij} values were normalised according to eq. (3.22) and $c_i > 0$. Moreover, to avoid convergence to the trivial solution $\sum_{j=1}^{N} \phi_j(x) \cdot 0 = 0$, $b_{ij,lim}$ was set equal to 0.001.

The description of the automated innovization algorithm can be summarised with the pseudocode reported in Algorithm 3. Since each extraction step can retrieve a single relationship, the index i was removed. The blue lines represent the main differences from the original algorithm due to the introduction of elitism. The algorithm referred to the parametric relationships in eq. (3.23) was not described as the relationship can be simply substituted to eq. (3.21). The input parameters to the automated innovization process are reported in Table 3.7.

Due to the stochastic nature of the optimisation algorithm implied in the automated innovization process, several innovization runs should be performed to search for the optimal result.

Table 3.7 Parameters for the automated innovization.

Parameter	Value
Population size (N_{pop})	100
Number of generations (N_{gen})	100
Crossover probability (p_c)	1
Mutation probability (p_m)	0.2
SBX distribution index (η_c)	2
Polynomial mutation index (η_m)	50
Sub-cluster redefinition parameter (ϵ)	3
Percentage of elitism (α)	0.05
Significance threshold (S_t)	70%

With regard to the application process, parametric relationships should be searched by sequentially increasing the number of basis functions. The cluster analysis for individual variables is performed first. Then, relationships with two or more basis functions are retrieved among the remaining variables. This is especially important in problems with discrete variables, where the Pareto front is often fragmented. If discrete-valued variables are present in the dataset, relationships with a number of clusters equal to the Pareto front fragments can be expected to be of particular interest [7].

Algorithm 3 Automated innovization, elitist version (modified from [7])

Require: Dataset $(x\text{-}f(x)\text{-}g(x))$ (m data points)
Ensure: Relationship having the structure $\prod_{j=1}^{N} \phi_j(x)^{b_j} = c$

1: Choose N
2: Choose $\phi_j(x) \; \forall \; j$ from $(x\text{-}f(x)\text{-}g(x))$
3: Choose GA parameters, N_{pop} and N_{gen}
4: Initialise $d, b_j \; \forall \; j$ for N_{pop} members   ▷ First population
5: $gen \leftarrow 1$
6: **while** $gen < N_{gen}$ **do**
7:      **for** $k \leftarrow 1, N_{pop}$ **do**
8:          **for** $j \leftarrow 1, N$ **do**
9:              $b_j^{(k)} \leftarrow \dfrac{b_j^{(k)}}{\max\limits_{j \in [1,N]} \left| b_j^{(k)} \right|}$
10:         **end for**
11:         **for** $l \leftarrow 1, m$ **do**
12:             Evaluate $c^{(l)} = \prod_{j=1}^{N} \phi_j(x^{(l)})^{b_j^{(k)}}$
13:         **end for**
14:         Sort all $c^{(l)}$
15:         Cluster all $c^{(l)}$ using $d^{(k)}$ divisions ▷ Sub-cluster criterion: $\left\lfloor \left(m/d^{(k)} \right) \right\rfloor$
16:         Evaluate fitness for k^{th} population member
17:         Evaluate constraint violation
18:         Store Elite population
19:         **if** $gen > 1$ **then**
20:             Update Parent population
21:         **end if**
22:     **end for**
23:     Perform GA selection   ▷ Penalty-parameter-less constraint handling
24:     Perform GA crossover
25:     Perform GA mutation   ▷ Offspring population is defined
26:     Store d and b_j population   ▷ Parent population is stored
27:     Update d and b_j population   ▷ Offspring population is saved
28:     $gen \leftarrow gen + 1$
29: **end while**
30: **for** $l \leftarrow 1, m$ **do**   ▷ Re-define clusters for best performing individual
31:     Evaluate $c^{(l)} = \prod_{j=1}^{N} \phi_j(x^{(l)})^{b_j^*}$
32: **end for**
33: Sort all $c^{(l)}$
34: Re-cluster all $c^{(l)}$ using d^* subdivisions ▷ Sub-cluster criterion: $\left\lfloor (m/d^*) \right\rfloor + \epsilon$
35: Evaluate CV
36: Evaluate significance of the relationship

3.3.5.1 Code validation

The automated innovization code was implemented in Python language. For code validation, a series of runs were performed to extract the parametric relationships of predefined datasets. These datasets were implemented both in exact form and with the addition of noise and outliers. Two basis functions were considered for ease of representation.

For the sake of conciseness, in the present section the parametric relationship in eq. (3.21) will be referred to as product relationship, whereas the parametric relationship in eq. (3.23) will be referred to as linear relationship.

From the validation tests, the degree of noise resulted to strongly affect the results. The product relationship was more sensitive to noise than the linear one.

Dataset 1: product relationship Dataset 1 consisted of 100 points divided in two clusters; 25% of the dataset was assigned to cluster 1, whereas 75% of the dataset was assigned to cluster 2. The predefined product relationship was in the form

$$\psi \equiv \begin{cases} x_1^{-1} \cdot x_2^{0.5} = 0.3 & \text{for } x_1 \in [5, 15] \,, \\ x_1^{-1} \cdot x_2^{0.5} = 0.8 & \text{for } x_1 \in [20, 40] \,. \end{cases}$$

Therefore, $b_j = \{-1, 0.5\}$ and $c = \{0.3, 0.5\}$.

Innovization results with clean dataset

Best fitness: 2.08
Optimisation variables: $b_j = \{1.000, -0.499\}$ and $d = 63$

No. of clusters: 2
No. of clustered points: 100
No. of unclustered points: 0

Cluster 1: $x_1^{1.000} \cdot x_2^{-0.499} = 1.256$ (25 points)
  significance: 0.25, CV: 0.030%

Cluster 2: $x_1^{1.000} \cdot x_2^{-0.499} = 3.339$ (75 points)
  significance: 0.75, CV: 0.049%

A significant relationship was found to apply to 100.0% of the data (Fig. 3.12).

Although the apparent difference in the b_j and c-values obtained by the innovization algorithm, the results are simply the inverse of the original dataset formulation, as

$$x_1^{-1} \cdot x_2^{0.5} = 0.3 \quad \equiv \quad x_1 \cdot x_2^{-0.5} = 3.\bar{3},$$
$$x_1^{-1} \cdot x_2^{0.5} = 0.8 \quad \equiv \quad x_1 \cdot x_2^{-0.5} = 1.25.$$

(a) Cluster plot.   (b) Dataset vs fit.
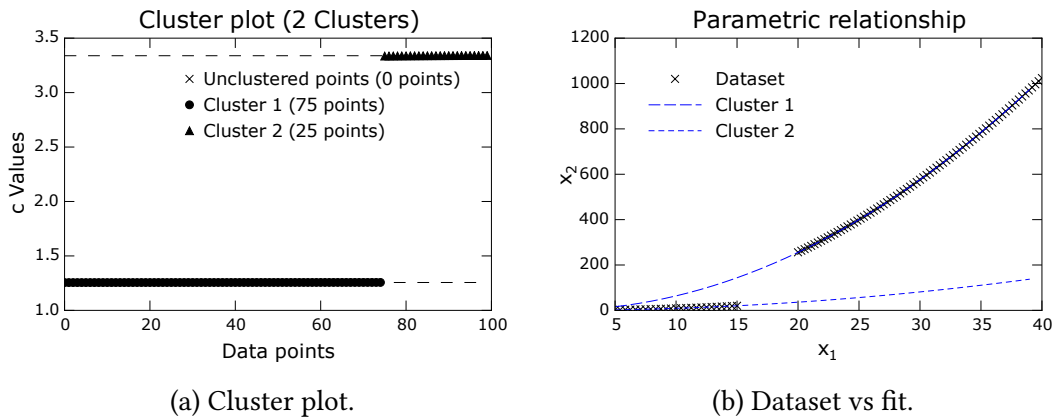
Fig. 3.12 Two-cluster product relationship with clean data.

Innovization results with noisy dataset

Best fitness: 19.3
Optimisation variables: $b_j = \{1.000, -0.506\}$ and $d = 52$

No. of clusters: 2
No. of clustered points: 82
No. of unclustered points: 18

Cluster 1: $x_1^{1.000} \cdot x_2^{-0.506} = 1.205$ (75 points)
    significance: 0.75, CV: 0.66%

Cluster 2: $x_1^{1.000} \cdot x_2^{-0.506} = 3.104$ (7 points)
    significance: 0.07, CV: 0.77%

A significant relationship was found to apply to 82.0% of the data (Fig. 3.13).

(a) Cluster plot.   (b) Dataset vs fit.
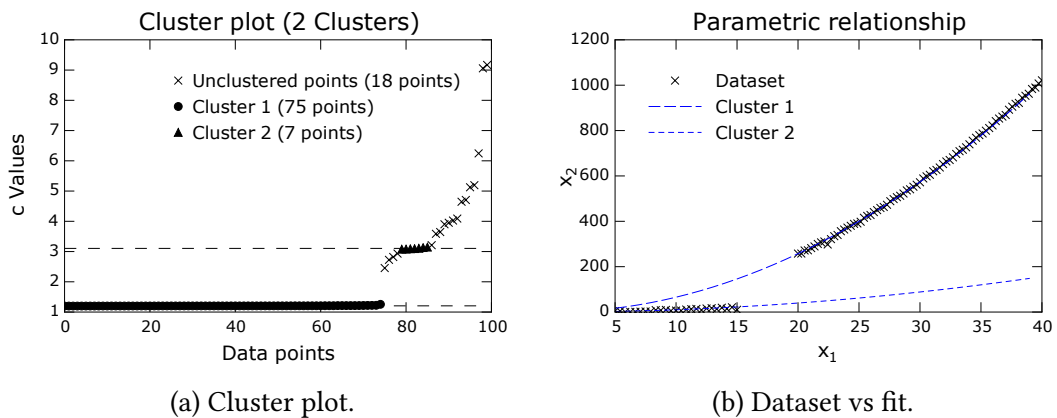
Fig. 3.13 Two-cluster product relationship with noisy data.

Innovization results with noisy dataset and outliers

Best fitness: 19.3
Optimisation variables: $b_j = \{1.000, -0.495\}$ and $d = 53$

No. of clusters: 2
No. of clustered points: 76
No. of unclustered points: 24

Cluster 1: $x_1^{1.000} \cdot x_2^{-0.495} = 1.292$ (71 points)
    significance: 0.71, CV: 0.24%

Cluster 2: $x_1^{1.000} \cdot x_2^{--0.495} = 3.340$ (5 points)
    significance: 0.05, CV: 0.54%

A significant relationship was found to apply to 76.0% of the data (Fig. 3.14).

(a) Cluster plot.   (b) Dataset vs fit.
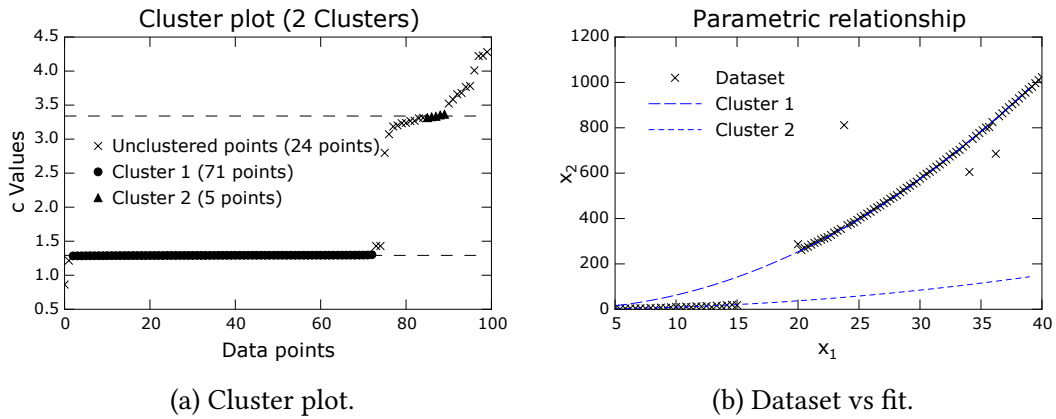
Fig. 3.14 Two-cluster product relationship with noisy data and outliers.

Dataset 2: linear relationship with two clusters   Dataset 2 consisted of 100 points divided in two clusters; 25% of the dataset was assigned to cluster 1, whereas 75% of the dataset was assigned to cluster 2. The predefined linear relationship was in the form

$$\psi \equiv \begin{cases} -x_1 + 0.5\, x_2 = 3 & \text{for } x_1 \in [5, 15]\,, \\ -x_1 + 0.5\, x_2 = 8 & \text{for } x_1 \in [20, 40]\,. \end{cases}$$

Therefore, $b_j = \{-1, 0.5\}$ and $c = \{3, 8\}$.

Innovization results with clean dataset

Best fitness: 2.05
Optimisation variables: $b_j = \{-1.000, 0.500\}$ and $d = 52$

No. of clusters: 2

No. of clustered points: 100
No. of unclustered points: 0

Cluster 1: $-1.000 \cdot x_1 + 0.500 \cdot x_2 = 3.004$ (25 points)
significance: 0.25, CV: 0.030%

Cluster 2: $-1.000 \cdot x_1 + 0.500 \cdot x_2 = 8.011$ (75 points)
significance: 0.75, CV: 0.022%

A significant relationship was found to apply to 100.0% of the data (Fig. 3.16).

(a) Cluster plot.   (b) Dataset vs fit.
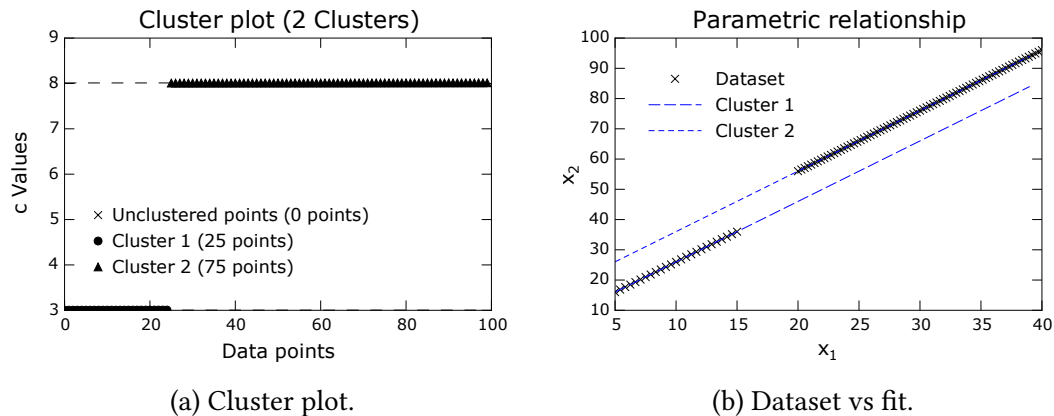
Fig. 3.15 Two-cluster linear relationship with clean data.

Innovization results with noisy dataset

Best fitness: 13.0
Optimisation variables: $b_j = \{-1.000, 0.504\}$ and $d = 6$

No. of clusters: 2
No. of clustered points: 100
No. of unclustered points: 0

Cluster 1: $-1.000 \cdot x_1 + 0.504 \cdot x_2 = 3.087$ (25 points)
significance: 0.25, c_v: 7.9%

Cluster 2: $-1.000 \cdot x_1 + 0.504 \cdot x_2 = 8.327$ (75 points)
significance: 0.75, c_v: 3.1%

A significant relationship was found to apply to 100.0% of the data (Fig. 3.16).

Innovization results with noisy dataset and outliers

Best fitness: 17.6
Optimisation variables: $b_j = \{-1.000, 0.514\}$ and $d = 88$

(a) Cluster plot.

(b) Dataset vs fit.
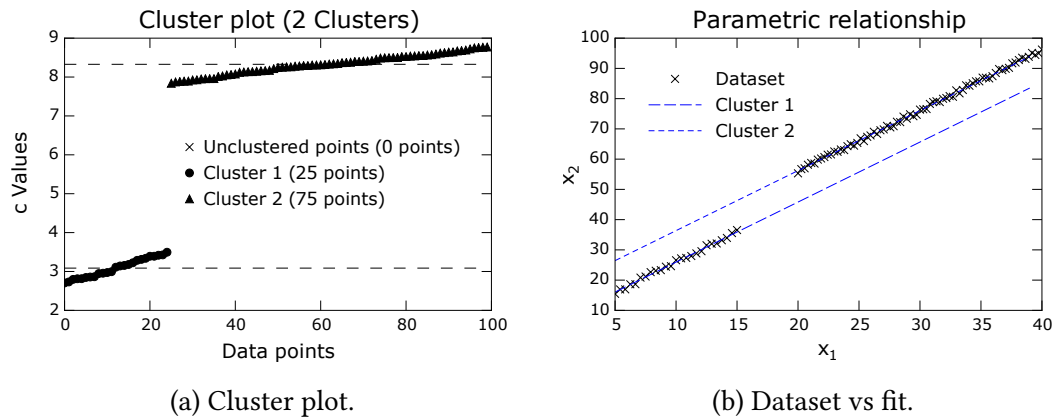
Fig. 3.16 Two-cluster linear relationship with noisy data.

No. of clusters: 2
No. of clustered points: 96
No. of unclustered points: 4

Cluster 1: $-1.000 \cdot x_1 + 0.514 \cdot x_2 = 3.366$ (24 points)
  significance: 0.24, c_v: 8.3%

Cluster 2: $-1.000 \cdot x_1 + 0.514 \cdot x_2 = 9.057$ (72 points)
  significance: 0.72, c_v: 3.7%

A significant relationship was found to apply to 96.0% of the data (Fig. 3.17).

(a) Cluster plot.

(b) Dataset vs fit.
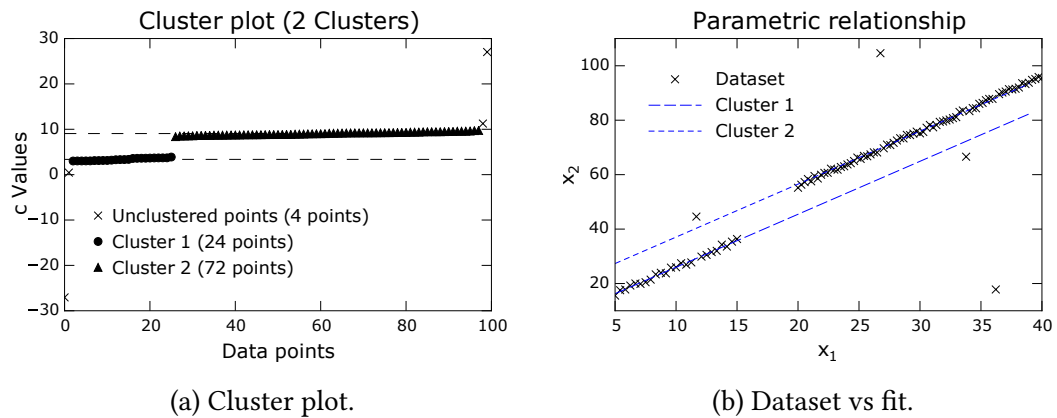
Fig. 3.17 Two-cluster linear relationship with noisy data and outliers.

Chapter 4

Methodology

In this chapter, the methodology applied in the present thesis is presented. First, the PCM modelling procedure shared by all the analyses is described. Then, the analyses carried out at material, component and building level are detailed.

4.1 PCM modelling

For all the analyses, the specific heat-temperature curve of the PCM was described by two half-Gaussian curves, according to eq. (4.1) [304]. Since the shape of the enthalpy-temperature curve was found to influence the optimum phase change temperature [88], a non-linear function was chosen due to its higher representativeness of practical PCMs with a phase change that occurs in a temperature range.

$$c(T) = \begin{cases} c_s + (c_m - c_s) \cdot \mathrm{e}^{-\left(\frac{T_p - T}{w_s}\right)^2} & \text{if } T \leq T_p \\ c_l + (c_m - c_l) \cdot \mathrm{e}^{-\left(\frac{T_p - T}{w_l}\right)^2} & \text{if } T > T_p \end{cases} \quad (4.1)$$

To fully describe the curve (Fig. 4.1), the following variables are needed:

- peak melting temperature, T_p
- specific heat in solid state, c_s
- specific heat in liquid state, c_l
- specific heat at peak melting temperature, c_m
- curve width in solid state, w_s
- curve width in liquid state, w_l.
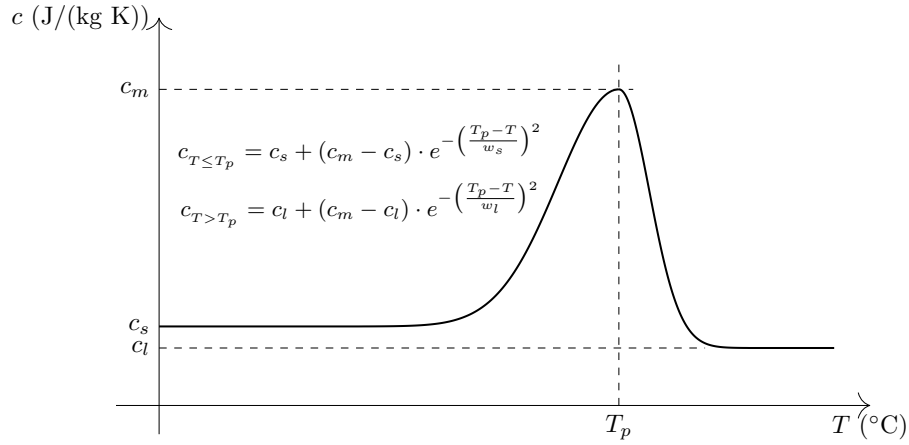
Fig. 4.1 Functional form adopted to describe the specific heat.

4.1.1 Evaluation of the latent heat of fusion

The latent heat of fusion of a PCM is represented by the area beneath the peak of the $c(T)$ curve (A_{ABC} in Fig. 4.2), which can be decomposed in

$$A_s + A_l + A_0 - A_{ADB}. \tag{4.2}$$

The first two terms of eq. (4.2), A_s and A_l, can be evaluated remembering the Gaussian integral,

$$\int_{-\infty}^{+\infty} e^{-x^2} dx = \sqrt{\pi},$$

which can be generalised as

$$\int_{-\infty}^{+\infty} e^{-\alpha x^2} dx = \sqrt{\frac{\pi}{\alpha}}.$$

Eq. (4.1) can be simplified to evaluate A_s and A_l by translating the origin of the axes respectively in O' and O''. Thus,

$$A_s = \int_{-\infty}^{0} (c_m - c_s) e^{-(T/w_s)^2} dx = (c_m - c_s) \frac{w_s \sqrt{\pi}}{2}, \tag{4.3}$$

$$A_l = \int_{0}^{\infty} (c_m - c_l) e^{-(T/w_l)^2} dx = (c_m - c_l) \frac{w_l \sqrt{\pi}}{2}. \tag{4.4}$$
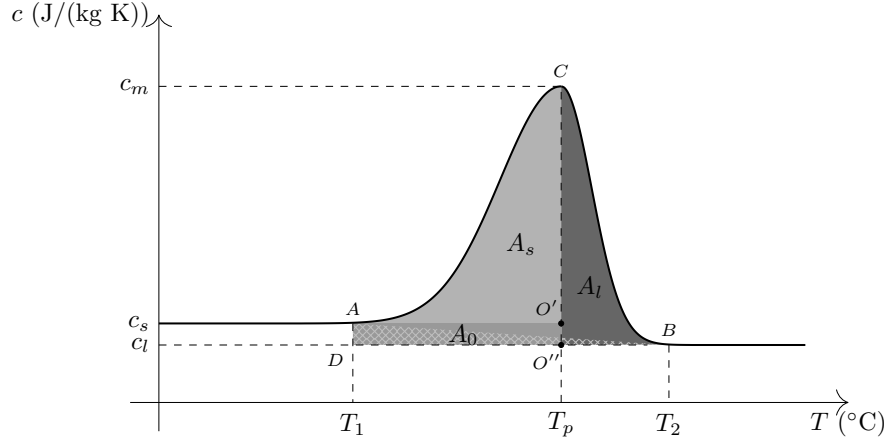
Fig. 4.2 Construction of the latent heat.

The last two terms of eq. (4.2), A_0 and A_{ADB}, are given by

$$A_0 = \begin{cases} (c_s - c_l)(T_p - T_1) & \text{if } c_s \geq c_l \\ (c_l - c_s)(T_2 - T_p) & \text{if } c_s < c_l, \end{cases} \tag{4.5}$$

$$A_{ADB} = \frac{1}{2}(T_2 - T_1)|c_s - c_l|. \tag{4.6}$$

However, considering the exact solution of the latent heat, the melting temperature range is $(-\infty, +\infty)$. To be able to identify a finite melting temperature range, the intersection between the $c(T)$ curve and a constant value can be considered. The distance between c_s (or c_l) and this arbitrary value will be defined as Δc (Fig. 4.3).

Therefore, intersecting eq. (4.1) and the arbitrary constant, we get

$$\begin{cases} c = c_s + (c_m - c_s) \cdot e^{-\left(\frac{T_p - T}{w_s}\right)^2} & \text{if } T \leq T_p \\ c = c_s + \Delta c, \end{cases}$$

whose solution gives the lower bound of the melting temperature range:

$$T_1 = T_p - w_s \sqrt{\ln \frac{c_m - c_s}{\Delta c}}. \tag{4.7}$$

Similarly, the upper bound of the melting temperature range is

$$T_2 = T_p + w_l \sqrt{\ln \frac{c_m - c_l}{\Delta c}}. \tag{4.8}$$
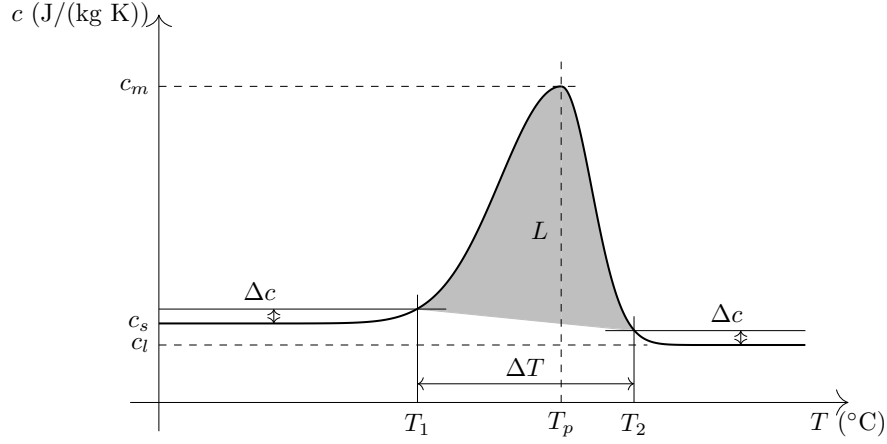
Fig. 4.3 Definition of a finite melting temperature range.

Summing eq. (4.7) and (4.8), the melting temperature range is obtained:

$$\Delta T = w_s \sqrt{\ln \frac{c_m - c_s}{\Delta c}} + w_l \sqrt{\ln \frac{c_m - c_l}{\Delta c}}.$$

Now, substituting eq. (4.7) and (4.8) in (4.5),

$$A_0 = \begin{cases} w_s \, |c_s - c_l| \, \sqrt{\ln \frac{c_m - c_s}{\Delta c}} & \text{if } c_s \geq c_l \\ w_l \, |c_s - c_l| \, \sqrt{\ln \frac{c_m - c_l}{\Delta c}} & \text{if } c_s < c_l. \end{cases} \tag{4.9}$$

Substituting equations (4.7) and (4.8) in eq. (4.6),

$$A_{ADB} = \frac{1}{2} \, |c_s - c_l| \left(w_l \sqrt{\ln \frac{c_m - c_l}{\Delta c}} + w_s \sqrt{\ln \frac{c_m - c_s}{\Delta c}} \right). \tag{4.10}$$

Eventually, substituting equations (4.3), (4.4), (4.9) and (4.10) in eq. (4.2), the latent heat can be evaluated as a function of the variables describing the $c(T)$ curve.

4.1.2 Simplified PCM model

To perform the component and building level optimisation analyses, not all the parameters introduced in section 4.1 were selected as optimisation variables. The problem was simplified by searching

- peak melting temperature, T_p
- melting temperature range, ΔT
- latent heat of fusion, L.

To find the relationship between the new optimisation variables and the original parameters, the following simplification was considered: $c_s = c_l$ (later referred to as c). In this way, the formulation of L becomes

$$L = \frac{\sqrt{\pi}}{2} (c_m - c)(w_s + w_l).$$
(4.11)

Solving eq. (4.11) for c_m, we find that

$$c_m = c + \frac{2L}{\sqrt{\pi}(w_s + w_l)},$$
(4.12)

whose solution can be retrieved by means of an iterative procedure. Given $\Delta T_2 = T_2 - T_p$ and $r = \Delta T_2 / \Delta T$, w_s and w_l can be defined as

$$w_l = \frac{r \cdot \Delta T}{\sqrt{\ln \frac{c_m - c}{\Delta c}}} \qquad \text{and} \qquad w_s = \frac{(1 - r) \cdot \Delta T}{\sqrt{\ln \frac{c_m - c}{\Delta c}}},$$
(4.13)

which are themselves expressed as a function of c_m.

With this formulation, r should be regarded as a new variable. However, since r can be expected to have less influence on the results of the optimisation than the other PCM variables, a fixed r of 0.25 was chosen as a reasonable value [88]. The specific heats in solid and liquid states were assumed fixed to 2000 J/(kg K). They were not included among the search variables because the optimisation algorithm could be expected to converge to the upper bound. Moreover, finding a PCM which respects all the six optimised parameters might be impossible. Eventually, a Δc equal to 0.1 kJ/(kg K) was considered.

4.1.2.1   Constraints

Small melting temperature ranges occur in pure materials, whose latent heat of fusion is higher than non-pure PCMs. Therefore, not all the combinations of melting temperature range and latent heat of fusion could be feasible within their domains.

The relation between melting temperature range and latent heat of fusion was analysed for paraffin-based PCMs, for which detailed data were available (Table 2.1). According to Fig. 4.4, the following linear constraint was added:

$$\Delta T \leq (300 - L)/15,$$

with L in kJ/kg.
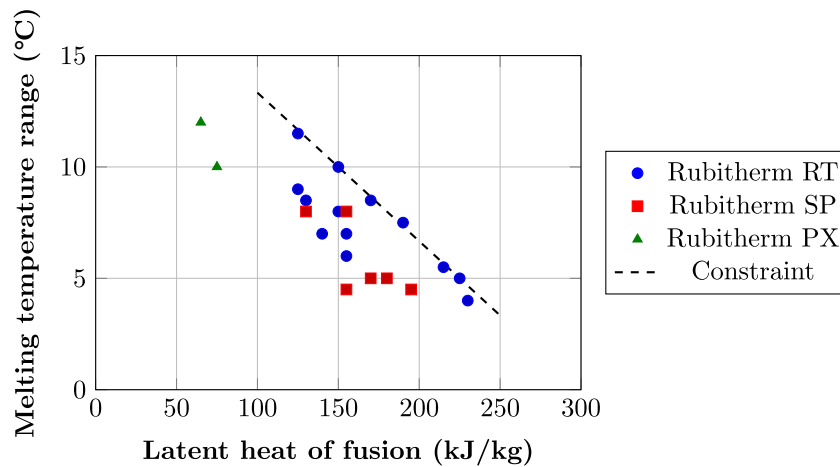
Fig. 4.4 Constraint on the melting temperature range.

4.2 Material-level investigations

The content of this section was partly published in [24].

Even though the use of Phase Change Materials is promising to improve the energy efficiency of buildings, their application in the building sector is still very limited. One of the obstacles to the diffusion of PCMs is the lack of information regarding their thermo-physical properties. Many manufacturers do not provide data on the enthalpy-temperature curve of their products, or these data are not suitable for application in a building energy simulation tool [13, 54]. In addition, the capabilities of building simulation tools may not be totally appropriate to simulate every kind of material. For example, EnergyPlus allows for a single enthalpy-temperature curve as input for each PCM and cannot take the hysteresis phenomenon into account. In this case, the evaluation of a single curve which can still simulate the material behaviour in an acceptable way would prove useful.

A method for estimating the specific heat-temperature curve of a PCM through inverse modelling is herewith presented. This method combined experimental data with a numerical tool able to simulate multilayer walls with the inclusion of PCM materials. Starting from heat flux measurements of a PCM sample subjected to controlled temperature variations on its surfaces, an optimisation algorithm was applied to search for the specific heat-temperature curve of the PCM which guaranteed the best fit between measured and simulated data.

A first experimental campaign was performed and its results were validated against tests on different samples and discussed in comparison with a low-speed (0.05 ℃/min [305]) DSC measurement [24]. However, since the peak melting tempe-
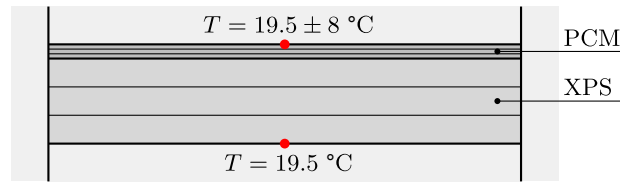
Fig. 4.5 Schematic view of the tested sample.

rature of the PCM did not match with the manufacturer's indications, new tests were needed to gather data within a wider temperature range. Only the measurement procedure and results of the new tests are herewith reported.

4.2.1 Experimental setup

The tested sample was a multilayer board composed by 15 mm of a shape-stabilised PCM (DuPont™ Energain©, whose nominal melting temperature is 21.7 ℃) and 90 mm of XPS. Details on the thermo-physical properties of the sample materials are reported in Table 4.1. Material properties where either measured (thermal conductivity), retrieved by the manufacturer datasheets (density) or found in literature (specific heat).

Table 4.1 Thermo-physical properties of the sample's materials.

Material	k [W/(m K)]	ρ $\left[\text{kg/m}^3\right]$	c [J/(kg K)]
PCM	0.14	950.57	-
XPS	0.0333	36.14	1700

The sample was placed in a LASERCOMP FOX 600 guarded hot plate and heat flow meter apparatus, which was modified by the manufacturer to allow for sinusoidal temperature variations on its plates with a period of 24 hours and a pre-settable amplitude. The stability on the temperature control was ± 0.03 ℃, whereas the measurement accuracy of the heat flux was about 2% [306]. To cover the material phase-change range, the upper plate was subjected to a sinusoidal temperature variation with average temperature of 19.5 ℃ and amplitude of 8 ℃ while the lower plate was kept at a constant temperature of 19.5 ℃ (Fig. 4.5). The test duration was 48 hours.

Although the presence of another material introduced additional uncertainties, the reason not to perform the measurements on a PCM only sample was that, given its low thermal resistance, the deviation of the heat flux response from a sinusoidal curve would have been too small for the optimisation algorithm to work properly.
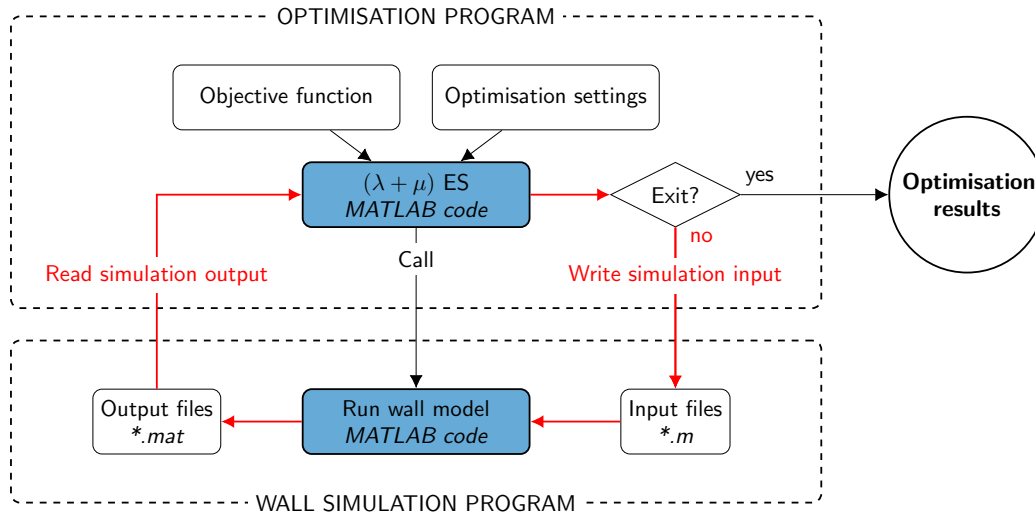
Fig. 4.6 Material-level optimisation procedure.

4.2.2 Optimisation procedure

The numerical simulation of the heat transfer process was carried out with the model described in section 3.1. Given the measured surface temperatures of the sample as boundary conditions and the known thermo-physical properties of the materials to the model, the specific heat vs temperature curve of the PCM which minimised the difference between measured and simulated heat fluxes on both faces of the sample was found through the ES optimisation algorithm described in § 3.2.1 (Fig. 4.6). The dependency of the specific heat on temperature was modelled according to eq. (4.1) [304]. Even though a-priori knowledge of the functional form of the specific heat was not strictly necessary, this approach was chosen to reduce the number of search variables.

The time required to perform a single optimisation run with 10000 iterations was approximately 70 minutes on a computer equipped with an Intel Core i5-3470 processor at 3.20 GHz and 8 Gb of RAM.

4.2.2.1 Objective function

The objective function was formulated as maximisation of the coefficient of determination R^2, simultaneously evaluated for the heat fluxes exchanged with both plates. When evaluating the fitness accuracy, the first 10 hours were disregarded to exclude the influence of the initial conditions.
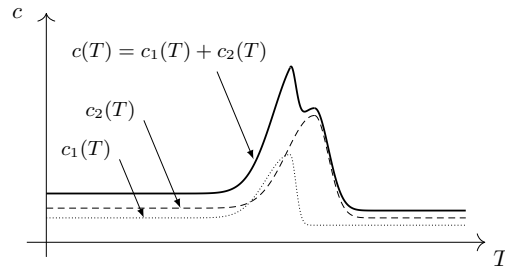
Fig. 4.7 Double peak $c(T)$ curve for non-pure PCMs.

4.2.2.2   Optimisation variables

A series of optimisation tests were carried out which differed in the set of input variables.

- First, the six variables describing the $c(T)$ curve according to eq. (4.1) were considered (six variables).
- Secondly, the contact resistances with the plates were added to the problem (eight variables).
- Lastly, in order to consider a more complex shape of $c(T)$ where a double peak could occur, the dependency of the specific heat on temperature was modelled as the sum of two curves (Fig. 4.7); the contact resistances with the plates were also considered (fourteen variables).

The fit without and with contact resistances with a single $c(T)$ curve were respectively denoted as V1 and VR. The fit with two $c(T)$ curves plus contact resistances was denoted as VR2C.

Given the temperature range of the experimental test (19.5 ± 8 ℃), the validity range of the estimated $c(T)$ curves is [11.5 ℃, 27.5 ℃].

4.2.2.3   ES inputs

V1   The fitness function for the V1 case can be explained as

$$
\text{Case study} \begin{cases} \text{Maximise} & f_1(x) = R^2 \\ \text{subject to} & 1500 \leq c_s \leq 4000 \\ & 0 \leq w_s \leq 20 \\ & 15 \leq T_p \leq 25 \\ & 12000 \leq c_m \leq 18000 \\ & 1500 \leq c_l \leq 3000 \\ & 0 \leq w_l \leq 20 \end{cases}
$$

The list of genetic inputs is reported in Table 4.2. For all simulations, $(\lambda + \mu)$ ES explored 10 generations with 1000 individuals in each generation. Ten independent optimisation runs were performed for each case.

Table 4.2 ES inputs (V1 case).

Population Size	1000	
Number of Variables	6	
Variable Domains	$x_{c_s} \in [1500, 4000]$	$x_{c_l} \in [1500, 3000]$
	$x_{w_s} \in [0, 20]$	$x_{w_l} \in [0, 20]$
	$x_{c_m} \in [12000, 18000]$	$x_{T_p} \in [15, 25]$
$\boldsymbol{\mu}$	20% of the population	
$\boldsymbol{a}$	0.3	
$\boldsymbol{\alpha}$	1.1	
End Condition	End after 10 generations	

VR The fitness function for the VR case can be explained as

$$
\text{Case study} \begin{cases}
\text{Maximise} & f_1(x) = R^2 \\
\text{subject to} & 1500 \le c_s \le 4000 \\
& 0 \le w_s \le 20 \\
& 15 \le T_p \le 25 \\
& 12000 \le c_m \le 18000 \\
& 1500 \le c_l \le 3000 \\
& 0 \le w_l \le 20 \\
& 1e\text{-}10 \le R_{si} \le 0.25 \\
& 1e\text{-}10 \le R_{se} \le 0.25
\end{cases}
$$

The list of genetic inputs is reported in Table 4.3. For all simulations, $(\lambda + \mu)$ ES explored 10 generations with 1000 individuals in each generation. Ten independent optimisation runs were performed for each case.

Table 4.3 ES inputs (VR case).

Population Size	1000
Number of Variables	8
Variable Domains	$x_{c_s} \in [1500, 4000]$ $x_{c_l} \in [1500, 3000]$
	$x_{w_s} \in [0, 20]$ $x_{w_l} \in [0, 20]$
	$x_{c_m} \in [12000, 18000]$ $x_{T_p} \in [15, 25]$
	$x_{R_{si}} \in [1e\text{-}10, 0.25]$ $x_{R_{se}} \in [1e\text{-}10, 0.25]$
μ	20% of the population
a	0.3
α	1.1
End Condition	End after 10 generations

VR2C   The fitness function for the VR2C case can be explained as

$$
\text{Case study} \begin{cases}
\text{Maximise} & f_1(x) = R^2 \\
\text{subject to} & 500 \leq c_{s,1} \leq 3000 \\
& 500 \leq c_{s,2} \leq 3000 \\
& 0 \leq w_{s,1} \leq 10 \\
& 0 \leq w_{s,2} \leq 10 \\
& 15 \leq T_{p,1} \leq 25 \\
& 15 \leq T_{p,2} \leq 25 \\
& 5000 \leq c_{m,1} \leq 18000 \\
& 5000 \leq c_{m,2} \leq 18000 \\
& 500 \leq c_{l,1} \leq 3000 \\
& 500 \leq c_{l,2} \leq 3000 \\
& 0 \leq w_{l,1} \leq 10 \\
& 0 \leq w_{l,2} \leq 10 \\
& 1e\text{-}10 \leq R_{si} \leq 0.25 \\
& 1e\text{-}10 \leq R_{se} \leq 0.25
\end{cases}
$$

The list of genetic inputs is reported in Table 4.4. For all simulations, $(\lambda + \mu)$ ES explored 30 generations with 2500 individuals in each generation. Ten independent optimisation runs were performed for each case.

Table 4.4 ES inputs (VR2C case).

Population Size	2500	
Number of Variables	14	
Variable Domains	$x_{c_s,1} \in [500, 3000]$	$x_{c_s,2} \in [500, 3000]$
	$x_{w_s,1} \in [0, 10]$	$x_{w_s,2} \in [0, 10]$
	$x_{T_p,1} \in [15, 25]$	$x_{T_p,2} \in [15, 25]$
	$x_{c_m,1} \in [5000, 18000]$	$x_{c_m,2} \in [5000, 18000]$
	$x_{c_l,1} \in [500, 3000]$	$x_{c_l,2} \in [500, 3000]$
	$x_{w_l,1} \in [0, 10]$	$x_{w_l,2} \in [0, 10]$
	$x_{R_{si}} \in [1e\text{-}10, 0.25]$	$x_{R_{se}} \in [1e\text{-}10, 0.25]$
μ	20% of the population	
a	0.3	
α	1.1	
End Condition	End after 30 generations	

4.2.2.4   Settings for the numerical model

The time discretisation constant of the numerical model was set equal to 60 s. The spatial discretisation was set according to each material. A node thickness of 2.6 mm and 1 cm were respectively considered for PCM and XPS.

4.3   Component-level investigations

Due to the non-linear behaviour of PCMs, evaluating and comparing the dynamic thermal performance of opaque building envelope components with PCM is a challenging task. A series of metrics have been proposed in the literature, which can be applied mostly at the building-level, where the performance of PCMs is generally evaluated in terms of improvement of indoor thermal comfort or of building energy performance, or by assessing the latent heat usage of the PCM during diurnal cycles (see § 2.1.2.7).

The reason for the complexity in finding a metric to characterise the dynamic thermal properties of opaque building envelopes with PCM at a component level lies in the dependency of the PCM's behaviour on the temperature. On one side, traditional metrics defined according to ISO 13786:2007 [5] can be evaluated only when the thermo-physical properties of the materials are constant. On the other side, the response of a PCM-enhanced component undergoing phase change varies according to mean temperature, amplitude and shape of the stimulus itself. There-

fore, the choice of the boundary conditions has a strong impact on the component's response, which can be significantly different according to the location and period of the year.

To find a possible solution to the thermal characterisation of opaque building envelope components with PCM, a novel approach was proposed by introducing "equivalent" parameters related to the traditional dynamic thermal properties evaluated according to ISO 13786:2007. To consider boundary conditions representative of real building applications, a monthly equivalent periodic thermal transmittance and the corresponding time shift were defined by imposing steady-periodic conditions with monthly average external air temperature and solar irradiance profiles while keeping a constant air temperature on the internal side. Eventually, the monthly equivalent values can be synthesised in a unique yearly value by means of a simple average. In this way, the characterisation is strictly related to the installation context, so the "equivalent" parameters provide information that can be effectively used to compare solutions for a specific application.

Once a metric was defined for evaluating the dynamic thermal properties of opaque building envelope components with PCMs, investigations were carried out to identify how to effectively apply PCMs in the building envelope. Preliminary parametric investigations highlighted that, given a constant latent heat, wall configuration and PCM melting temperature resulted to have the greatest influence on the dynamic thermal performance. Moreover, a potential improvement in the yearly equivalent periodic thermal transmittance was expected by a seasonal change in the PCM melting temperature. Therefore, the analyses focused on the investigation of the best wall configuration (order of the layers) with the adoption of PCMs with at most two melting temperatures (lower or greater than 23 ℃).

A parametric model was developed to describe PCM-enhanced multi-layer walls and, given a constant U-value, an optimisation analysis was carried out in the climates of Palermo, Torino and Oslo to find wall layout and PCMs' thermo-physical properties (melting temperature, melting temperature range, latent heat of fusion and thermal conductivity) which minimised yearly equivalent periodic thermal transmittance, overall PCM thickness and overall thickness of the wall. Post-Pareto analyses were then performed to identify general rules and trends of the optimised solutions.

Other than application of the proposed equivalent periodic thermal transmittance for evaluating the thermal performance of opaque building envelope components with the inclusion of PCM, the novelty of such optimisation approach is that, to the best of the author's knowledge, no investigation on layer distribution and repetition within a wall with the inclusion of phase change materials has been previously proposed, even less with the simultaneous presence of two PCMs with different thermo-physical properties.

4.3.1 Dynamic thermal characterisation of opaque building envelope components with PCM

Starting from the definition of the dynamic thermal properties of opaque building envelope components according to ISO 13786:2007 [5], "equivalent" parameters for the dynamic thermal characterisation of opaque components with PCM are herewith proposed. A monthly equivalent periodic thermal transmittance and the corresponding time shift were defined by imposing steady-periodic conditions with monthly average external air temperature and solar irradiance profiles while keeping a constant air temperature on the internal side.

According to [5], a component which separates zone m and zone n is considered, where the temperature of zone n is subjected to a periodic variation and the temperature of zone m is constant. Under steady-periodic regime, the *periodic thermal transmittance*, Y_{mn}, can be defined as the ratio of the complex amplitude of the heat flux density through the surface of the component adjacent to zone m on the complex amplitude of the temperature in zone n (Fig. 4.8). Therefore,

$$Y_{mn} = -\frac{\hat{q}_m}{\hat{\theta}_n},$$

which is a complex quantity characterised by modulus and phase[1]. The phase is strictly related to the time shift, Δt_{mn}, which is the period of time between the maximum amplitude of the periodic temperature variation on the component adjacent to zone n (cause), and the maximum amplitude of the heat flux density on the component adjacent to zone m (effect).

Similarly, ISO 13786:2007 defines the *thermal admittance*, Y_{mm}, as the ratio of the complex amplitude of the heat flux density through the surface of the component adjacent to zone m on the complex amplitude of the temperature in the same zone, when the temperature of zone m is subjected to a periodic variation, and temperature on the other side is kept constant (Fig. 4.9). Therefore,

$$Y_{mm} = \frac{\hat{q}_m}{\hat{\theta}_m}.$$

As in the previous case, its phase is related to the time shift, Δt_{mm}, which is the time period between the maximum amplitude of the periodic temperature variation on the component adjacent to zone m (cause), and the maximum amplitude of the heat flux density on the component adjacent to the same zone (effect).
In the same way, thermal admittance and time shift on the side n of wall can also be evaluated (respectively, Y_{nn} and Δt_{nn}).

---

[1]The sign convention considers positive heat fluxes when entering the component.
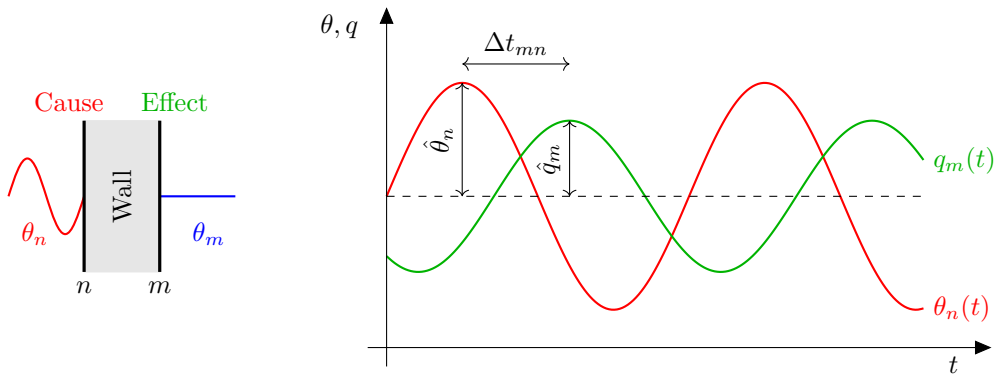
Fig. 4.8 Schematic representation of Y_{mn}.
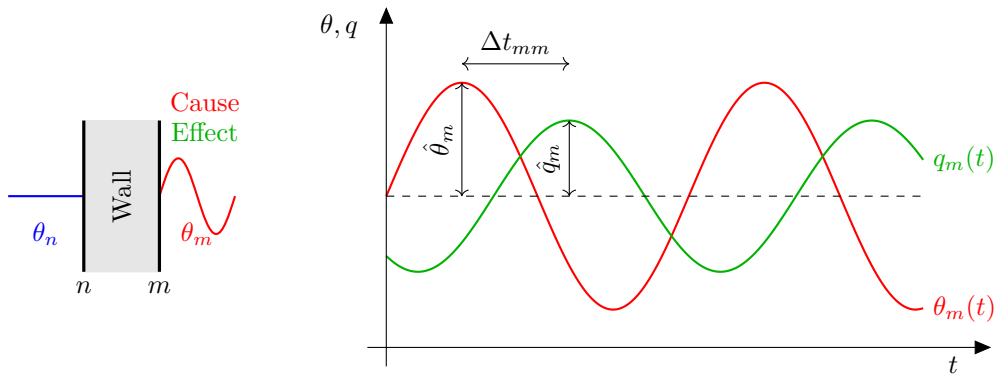
Fig. 4.9 Schematic representation of Y_{mm}.

Moreover, ISO 13786:2007 defines the *decrement factor*, f_a, as the ratio of the modulus of the periodic thermal transmittance on the steady-state thermal transmittance (i.e. the U-value). This quantity can be expressed as

$$f_a = \frac{|Y_{mn}|}{U},$$

and it represents the ratio of the amplitude of the effect on that of the cause,

$$f_a = \frac{A_{\text{effect}}}{A_{\text{cause}}}.$$

When an opaque building component with PCM is considered, the evaluation of the dynamic thermal properties according to [5] cannot be performed due to the strong dependency of the specific heat of PCMs on temperature. On one side, to obtain the exact solution of Y_{mn} and Y_{mm}, heat transfer functions are used by ISO 13786:2007, but the thermo-physical properties of the materials need to be constant. On the other side, even if Y_{mn} and Y_{mm} were retrieved by other means

(e.g. through application of the conduction finite differences), other problems arise. When subjected to sinusoidal temperature variations, the component's response in terms of heat flux density is no more a sinus, and varies both with the average and the amplitude of the temperature stimulus.

Given the impossibility of defining the periodic thermal properties according to ISO 13786:2007 for PCM components, equivalent parameters are proposed. To consider boundary conditions representative of real building applications, the stimulus of zone n (here considered as the external environment) is defined on a monthly basis as the combination of average external air temperature and solar irradiance daily profiles for a given location. The temperature of zone m (here considered as the internal environment) is a constant value representative of the set-point temperature of the month under investigation.
When a component subjected to the aforementioned boundary conditions is in steady-periodic regime, the monthly equivalent periodic thermal transmittance, Y^*_{mn}, can be evaluated as

$$Y^*_{mn} = \frac{\Delta q_{si}}{\Delta \theta_{sa}},$$ (4.14)

where Δq_{si} is the difference between maximum and minimum value of the heat flux density through the surface of the component adjacent to the internal environment, and $\Delta \theta_{sa}$ is the difference between maximum and minimum value of the sol-air temperature (as a reminder, the sol-air temperature is defined as $\theta_{sa} = \theta_{se} + \alpha \cdot I / h_e$). The corresponding time shift, Δt^*_{mn}, can be defined as the time difference between the maximum heat flux density through the surface of the component adjacent to the internal environment and the maximum value of the sol-air temperature.

It should be mentioned that such a definition of the equivalent periodic thermal transmittance requires the specification not only of the location where the component is mounted, but also its orientation and solar absorptance. Moreover, for a complete thermal analysis, when the average temperature of the surrounding surfaces and the sky radiant temperature is different from the air temperature, the radiation heat transfer should also be taken into account [307]. However, since the radiation heat transfer would be dependent on the urban context of the building, in the definition of the equivalent periodic thermal transmittance, which was meant to be a component scale parameter, it was neglected.

Moreover, due to the non-linear behaviour of PCMs, different time shifts are indeed obtained whether they are evaluated as a difference between maximum wave values or minimum wave values. For completeness, both values should be provided. However, since the dynamic thermal characterisation parameters have greater importance and effectiveness in describing the thermal behaviour of components under summer conditions and in hot climates[2], in the present work only the time

---

[2]Italian standards require $Y_{mn} < 0.10$ W/(m^{2}K) for vertical walls (except those facing NW-N-NW) in locations were the average horizontal global irradiance is greater than 290 W/m^2 during

shift between the maximum wave values was considered.

With regard to the definition of an equivalent thermal admittance, the problem is more complex. On one hand, a constant temperature of the external environment would not be a realistic boundary condition, on the other hand, the oscillation of the internal air temperature is a consequence of the interaction between the behaviour of the whole building and its systems. The proposal of an equivalent thermal admittance for building envelope components with PCM was therefore not ventured.

With regard to the decrement factor, this parameter was evaluated by Zhou et al. for a PCM wallboard subject either to temperature or heat flux variations [182, 309] (see § 2.1.2.7). Given a PCM wallboard subject to a sinusoidal sol-air temperature on one side (outside) and constant air temperature on the other side (inside), the decrement factor was defined as the ratio of the inner surface temperature wave amplitude on the outdoor temperature wave amplitude [182]. For a PCM wallboard subject to a sinusoidal heat flux wave on one side (outside) and constant air temperature on the other side (inside), the decrement factor was defined as the ratio of the inner surface's heat flux wave amplitude on that of the outer surface [309]. In both cases, due to the non-sinusoidal response on the inner face, the amplitude was evaluated as the difference between maximum and minimum wave values.

In the framework of a thermal characterisation of envelope components with PCMs under representative boundary conditions, the definition of decrement factor by Zhou et al. in [182] can be applied on a monthly basis considering the sol-air temperature profile for the location and orientation under investigation.

Eventually, the monthly equivalent values can be synthesised in a unique yearly value by means of a simple average. This allows to easily compare solutions under an overall point of view. However, separate monthly values provide information to better understand the behaviour of a component throughout the year.

4.3.2   Parametric analyses

To start investigating the effectiveness of the proposed metrics for evaluating the dynamic thermal properties of opaque envelope components with PCM, parametric analyses on a set of six wall configurations characterised by a different order of the layers (mass, insulation and PCM) were carried out for three locations (Palermo, Torino, and Oslo, see § 4.3.2.1) and four wall orientations (south, east, north, and west). The analysed wall configurations are reported in Fig. 4.10.

For each wall configuration, the following parametrisation variables (represented by the checked items) were considered:

---

the month with highest solar irradiance [308].
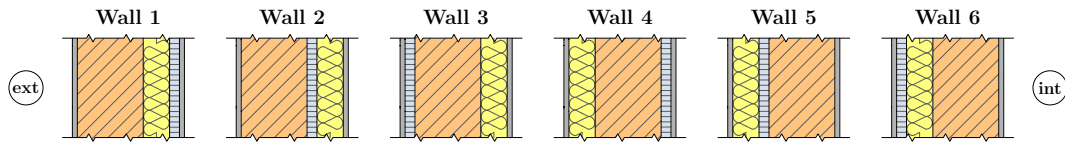
Fig. 4.10 Wall configurations for the parametric analyses.

- PCM properties
  - ✓ melting temperature, T_p (18 ℃, 20 ℃, 22 ℃, 24 ℃, 26 ℃, 28 ℃)
  - ✓ thermal conductivity, k (0.2 W/(m K), 0.6 W/(m K), 1.0 W/(m K))
  - ✓ thickness, t_{PCM} (1 cm, 2 cm, 3 cm)
- ✓ solar absorption coefficient, α (0.3, 0.6, 0.9)

The cooling enthalpy-temperature curve of Rubitherm RT26, characterised by a latent heat of fusion of 155 kJ/kg (Table 2.1), was adopted and adapted to all melting temperatures by shifting it. The thickness and thermo-physical properties of each material are reported in Table 4.5. A constant U-value of 0.33 W/(m²K) was considered, and the insulation thickness (t_{ins}) was evaluated accordingly with eq. (4.15), where U_{unins} is the U-value of the wall without insulation.

$$t_{\text{ins}} = k_{\text{ins}} \cdot \left(\frac{1}{U} - \frac{1}{U_{\text{unins}}} \right) \tag{4.15}$$

The results of these analyses are reported in § 5.2.1. They provide the reason behind some of the modelling choices of the subsequent optimisation analyses.

Table 4.5 Material properties and thickness.

Material	Thickness	k	ρ	c
	[m]	[W/(m K)]	$\left[\text{kg/m}^3\right]$	[J/(kg K)]
Plaster/Render	0.015	0.9	1800	840
Insulation	*variable*	0.04	36	1030
Mass	0.20	0.30	800	840
PCM	*variable*	*variable*	1650	*variable*

4.3.2.1 Climatic data

The climate data for the component-level investigations were retrieved from the statistics file of the EnergyPlus weather data (*.stat* files) [310]. The selected data source was the International Weather for Energy Calculations (IWEC) [311].
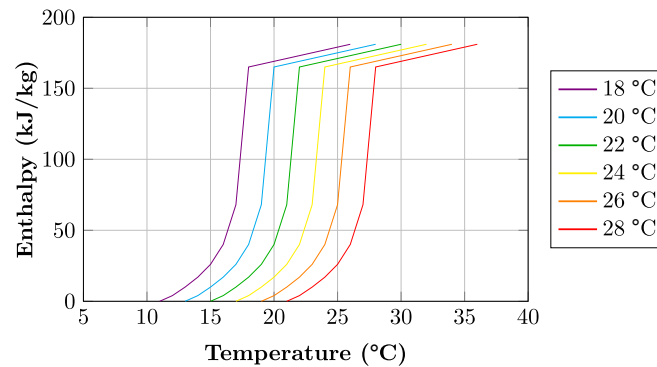
Fig. 4.11 Enthalpy-temperature curves of the PCMs adopted for the parametric analyses.

Position, climate type according to the Köppen classification [312], and annual heating (HDD) and cooling (CDD) degree days (18 ℃ baseline) of the selected locations (Paermo and Torino, Italy, and Oslo, Norway) are briefly summarised in Table 4.6. Average monthly dry bulb temperature with corresponding daily excursion and average global horizontal irradiation for the three locations are reported in Fig. 4.12.

Table 4.6 Position and climate information of the analysed locations.

Location	Climate type	Coordinates	HDD	CDD
Palermo	*Csa* (hot-summer Mediterranean climate)	38.11° N - 13.33° E	724	1022
Torino	*Cfa* (humid subtropical climate)	45.07° N - 7.67° E	2506	381
Oslo	*Dfb* (warm-summer humid continental climate)	59.91° N - 10.75° E	4171	33

4.3.2.2 Boundary conditions

For each location, the monthly average external air temperature profiles were set equal to the *Average Hourly Statistics for Dry Bulb Temperatures* reported in the corresponding *.stat* file (see § 4.3.2.1). The solar radiation impinging on the walls was calculated for each location and orientation from the *Average Hourly Statistics for Direct Normal Solar Radiation* and *Average Hourly Statistics for Diffuse Horizontal Solar Radiation*. Sun position and solar irradiance on a vertical surface were evaluated according to the equations reported in the ASHRAE Handbook of Fundamentals 2009 [313, Chapter 14].

A constant air temperature was set on the internal side. Temperatures of 20 ℃, 23 ℃ and 26 ℃ were respectively considered during winter, mid-season and summer months. In Palermo, winter conditions were considered from December to March and summer conditions from May to October. In Torino, winter and summer periods
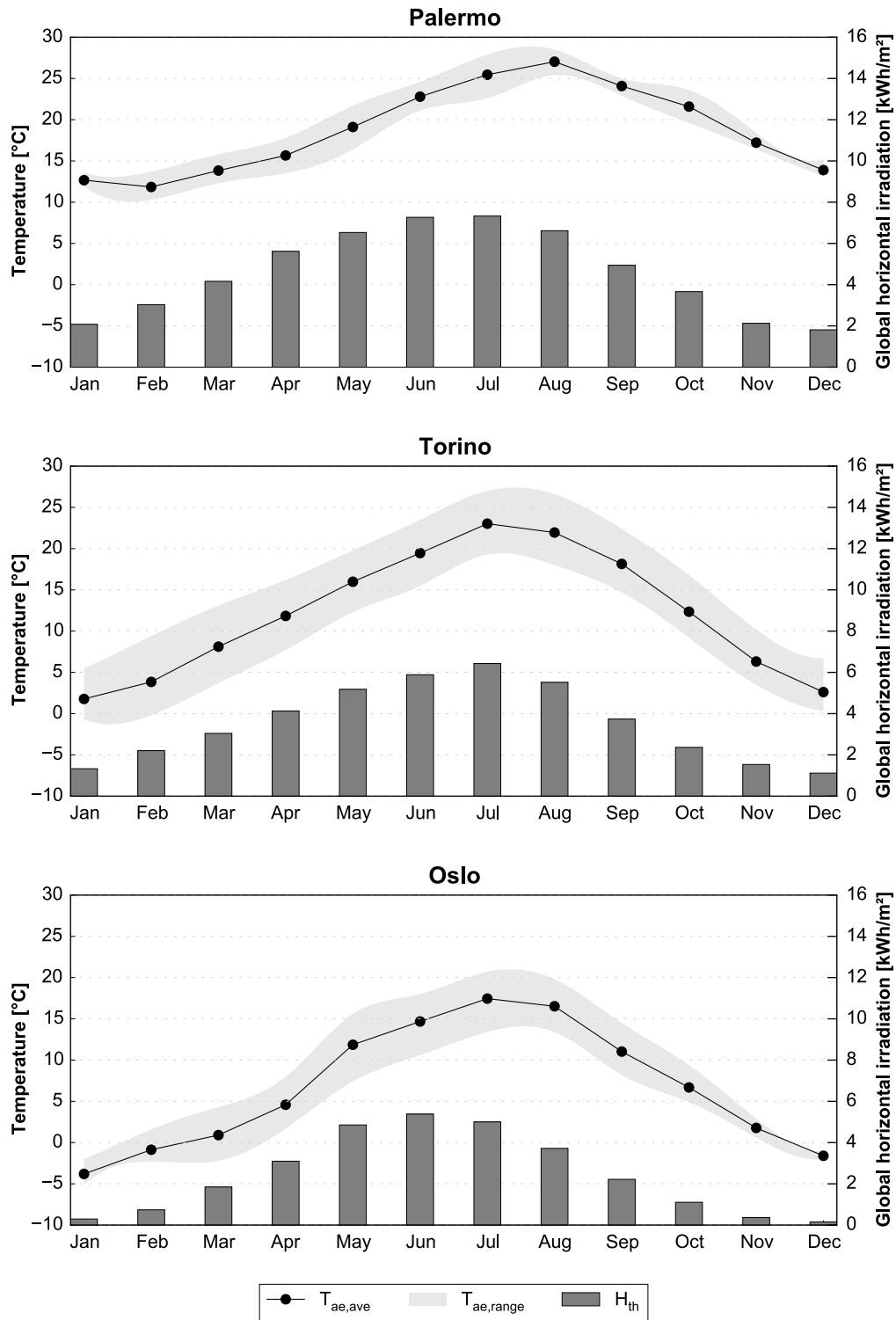
Fig. 4.12 Monthly climatic data of the analysed locations.

were respectively considered from October to April and from June to August. In Oslo, winter conditions were considered for the whole year except July and August, whose temperatures were considered as mid-season.

Eventually, internal and external surface resistances were respectively set equal to 0.04 m^{2}K/W and 0.17 m^{2}K/W [314].

4.3.2.3   Settings for the numerical model

A series of tests were performed in order to select appropriate trade-off parameters which could guarantee a good precision of the numerical model with reasonable computation run-times. The time discretisation constant was set equal to 180 s. The spatial discretisation was set according to each material. A maximum node thickness of 2 mm was considered for PCM layers, whereas a maximum thickness of 2 cm and 4 cm was respectively considered for mass and insulation. These values guaranteed a maximum error of 0.5% on the evaluation of Y_{mn}^* when traditional materials were involved (the results of the numerical analyses were compared to the exact solution from ISO 13786:2007). With regard to the PCM, the "exact" solution adopted for comparison involved a time discretisation of 60 s and a space discretisation of 0.5 mm. A maximum error of 3.7% was guaranteed in the worst condition when a sole layer of PCM undergoing phase change was analysed.

The steady-periodic conditions were considered to be reached when the heat flux wave on the inner face differed no more than 0.05% from the previous iteration.

4.3.3   Parametric model

To perform the optimisation analyses, a parametric model was developed to describe multi-layer walls. To be combined with the genetic algorithm, the parametric model needed to satisfy the following requirements:

- Fixed number of variables;
- Selection lists composed by 2^n items;
- Discretisation of continuous domains in 2^n values.

According to the findings reported in § 2.2.3.1.1, the optimised distribution of layers within a traditional wall requires an even distribution of massive and insulating layers [252, 253, 227, 254]. For this reason, the same material was allowed to be placed in several positions within the wall. Moreover, the U-value was kept constant to evaluate the effects given only by PCM, thermal mass, and layout of the wall.

With regard to the description of PCM materials, two options are viable. Hypothetical PCMs can be defined by selecting a set of thermo-physical properties accor-

ding to a predefined $c(T)$ shape (the shape itself cannot be a variable, for the same number of parameters should be able to describe all the shape functions and should be characterised by the same domain); otherwise, a list of real materials can be provided. However, since the reliability and the completeness of the data provided by manufacturers is questionable, the first option was chosen. Results deriving the from optimisation of hypothetical PCM materials can be used to provide guidelines for product development.

Given these premises, the details of the model can be discussed. Prior to the actual optimisation process, the U-value of the wall and a number of "slot-layers" are chosen. Slot-layers are units which can host a material. If adjacent slot-layers host the same material, they can be compacted into a single layer. Therefore, the number of layers is not fixed, but it cannot exceed the number of slot-layers. Once the U-value of the wall and the number of slot-layers are chosen, the optimisation process can take place. First, a material is assigned to each slot-layer; internal plaster and external render are then added. For each material, with the exception of the insulation, a total thickness is selected. The overall thickness of the insulation is calculated according to eq. (4.15) to obtain the desired U-value. The thickness of each slot-layer is equally split according to the number of slot-layers made of the same material. For example, if there are three slot-layers hosting Material A, and the total thickness assigned to Material A is 15 cm, the thickness of each slot-layer of Material A is 15/3=5 cm. Adjacent slot-layers of the same material are then compacted into a single layer. In this way, layers of the same material with different thicknesses can be obtained, although their thickness would be a multiple of that of the slot-layer's for the same material. Then, the PCM is modelled considering a constant thermal conductivity, k, and the specific heat-temperature curve described by eq. (4.1). However, to simplify the optimisation problem, the variables describing the PCM's $c(T)$ curve were reduced to the peak melting temperature, T_p, the melting temperature range, ΔT, and the latent heat of fusion, L. The conversion from these optimisation variables to the parameters in input to eq. (4.1) was carried out through equations (4.12) and (4.13) according to the procedure reported in § 4.1.

Overall, the parametric wall is described by the following variables:

1. Wall configuration
   - ✓ A material for each slot-layer
   - ✓ A thickness for each material, except the insulation

2. PCM properties (for each PCM)
   - ✓ Peak melting temperature, T_p
   - ✓ Melting temperature range, ΔT
   - ✓ Latent heat of fusion, L
   - ✓ Thermal conductivity, k.

Preliminary steps
- Definition of a list of materials
- Definition of the number of slot-layers
- Definition of the U-value

Selection of wall configuration
- Choice of the material for each slot-layer (the same material can be in different positions)
- Selection of the overall thickness for each material. The thickness will be equally distributed among all slot-layers characterised by the same material
- Evaluation of the overall thickness of insulation, according to the insulating material and the desired U-value
- Selection of a set of thermo-physical properties for one or more PCMs

---

Fig. 4.13 Main steps to describe the parametric wall.

A summary of the main steps which describe the parametric model is provided in Fig. 4.13.

Additionally, the parametric model could be expanded to provide a wider range of material choices. By the use of sub-choice levels, material groups could be defined, as well as the lists of materials belonging to each material group (e.g. Insulation $\rightarrow$ Type of insulation). A summary of the main steps which describe this extended version of the parametric model is provided in Fig. 4.14.

4.3.4 Optimisation procedure

The parametric model described according to the procedure in Fig. 4.13 was adopted to perform component-level optimisation analyses of walls with the inclusion of PCM. The analyses were carried out by coupling the Python implementation of the NSGA-II optimisation algorithm (see § 3.2.2) with the numerical model developed in MATLAB of the transient heat transfer in opaque envelopes with PCMs (see § 3.1) (Fig. 4.15).

The investigated walls faced south, east, north and west, and were subjected to the climatic conditions of Palermo, Torino and Oslo (see § 4.3.2.1). The optimisations' objective was the minimisation of the yearly equivalent periodic thermal transmittance, overall PCM thickness and the overall thickness of the wall. The PCM's thickness was selected as a preliminary cost metric, since the amount of PCM reasonably has the major influence on the cost of the wall. The wall thickness was chosen to be able to explore the effect of PCM in relation with that of traditional thermal mass.

Preliminary steps
- Definition of a list of material groups
- Definition of a list of materials for each group
- Definition of the number of slot-layers
- Definition of the U-value

Selection of wall configuration
- Choice of the material group for each slot-layer (the same material can be in different positions)
- Choice of the type of material for each material group
- Selection of the overall thickness for each material. The thickness will be equally distributed among all slot-layers characterised by the same material
- Evaluation of the overall thickness of insulation, according to the insulating material and the desired U-value
- Selection of a set of thermo-physical properties for one or more PCMs

---

Fig. 4.14 Main steps to describe the extended version of the parametric wall.

The following list of materials, whose thermo-physical properties are reported in Table 4.7, was considered for the construction of the walls:

1. Masonry;

2. Insulation;

3. PCM1 (melting temperature below 23 ℃);

4. PCM2 (melting temperature above 23 ℃).

The reason for choosing two PCMs was to investigate the potential benefits deriving from their application during both cold and warm season (see § 5.2.1). PCM1 was especially fit for the winter season since it was characterised by a melting temperature below 23 ℃, while PCM2 was apt for the summer season.

Table 4.7 Material properties.

Material	k [W/(m K)]	ρ $\left[\text{kg/m}^3\right]$	c [J/(kg K)]
Masonry	0.59	1600	840
Insulation	0.04	36	1030
PCM	*variable*	1000	*variable*
External render (1.5 cm)	0.9	1800	840
Internal plaster (1.5 cm)	0.7	1400	1010

The U-value of the walls was chosen according to the climate in order to comply with the local standards. A U-value of 0.45 W/(m^{2}K) was selected in Palermo [308],
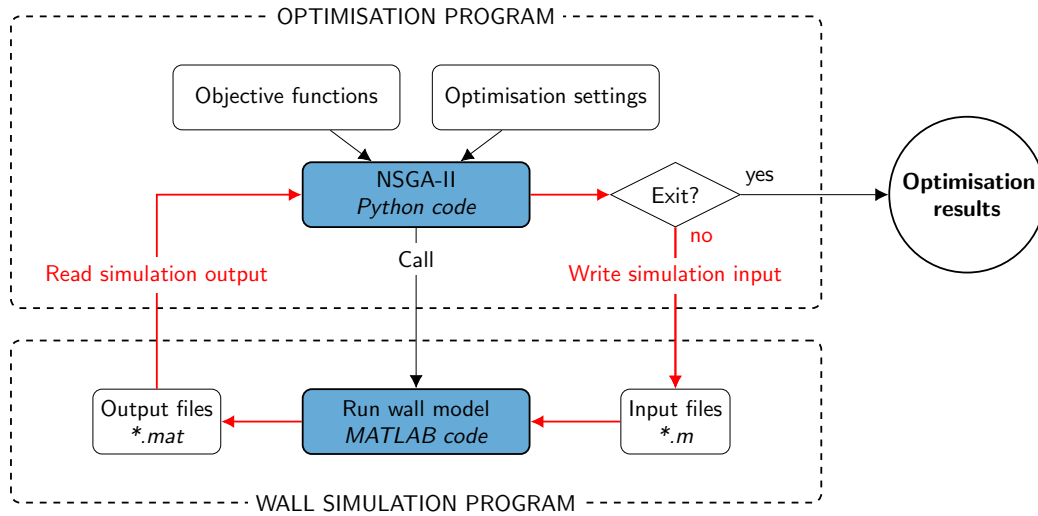
Fig. 4.15 Component-level optimisation procedure.

whereas 0.30 W/(m²K) and 0.22 W/(m²K) were respectively selected in Torino [308] and Oslo [315]. For all the case studies, the overall masonry thickness was allowed to vary between 10 cm and 25 cm, whereas each PCM's thickness could vary in the range 5 mm to 4 cm. Further details on the variables' domains and discretisation are reported in § 4.3.4.3. Moreover, a fixed solar absorption coefficient of 0.6 was considered. Boundary conditions and general settings of the numerical model were the same as those adopted for the parametric analyses (see § 4.3.2.2 and § 4.3.2.3).

A graphical representation of the parametric model as applied to the investigated case studies is reported in Fig. 4.16. In the figure, masonry is generically referred to as "Mass". Italic texts denote the optimisation variables.

The total time required to perform a single optimisation run was approximately three days on a computer equipped with an Intel Core i7-3770 processor at 3.40 GHz and 16 Gb of RAM, in presence of a serious RAM failure. Three MATLAB instances were run in parallel, one for each location, whereas the optimisation runs on the orientations were run in series.

4.3.4.1 Objective functions

To summarise, the objective for all the component-level investigations was the minimisation of the following functions:

1. Equivalent periodic thermal transmittance, Y_{mn}^*;
2. Total thickness of the PCM layers, t_{PCM};
3. Overall thickness of the wall, t_{Wall}.

Material's choice
for each slot-layer

Thicknesses' choice

PCM's properties

TOT Mass thick.: 15.0 cm
TOT PCM1 thick.: 3.0 cm
TOT PCM2 thick.: 1.0 cm
TOT Ins thick.: x cm

Slot-layer Mass: $15/3 = 5$ cm
Slot-layer PCM1: $3/2 = 1.5$ cm
Slot-layer PCM2: $1/1 = 1$ cm
Slot-layer Ins: $x/2 = x/2$ cm

PCM 1
Peak melting temp., $T_{p,1} \leq 23$ °C
Melting temp. range, ΔT_1
Latent heat of fusion, L_1
Thermal conductivity, k_1

PCM 2
Peak melting temp., $T_{p,2} > 23$ °C
Melting temp. range, ΔT_2
Latent heat of fusion, L_2
Thermal conductivity, k_2

No. of slot-layers: 8

No. of layers: 6 (+ plaster)

Fig. 4.16 Description of the parametric model with an application example.

4.3.4.2   Optimisation variables

The optimisation variables (represented by the checked items) of the component level investigations can be summarised as follows:

- ✓ Material for each slot-layer (either mass, insulation, PCM1 or PCM2)
- • Overall thickness of each material (except the insulation):
    - ✓ Mass thickness [m]
    - ✓ PCM1 thickness [m]
    - ✓ PCM2 thickness [m]
- • Thermo-physical properties of each PCM:
    - ✓ Peak melting temperature [°C]
    - ✓ Melting temperature range [°C]
    - ✓ Latent heat of fusion [J/(kgK)]
    - ✓ Thermal conductivity [W/(mK)]

Considering eight slot-layers, three variable thicknesses, and four thermo-physical properties for two PCMs, the total number of variables of the optimisation problem was 19.

4.3.4.3   GA inputs

The inputs to the genetic algorithm for all the component-level case studies are reported in Table 4.8. The fitness functions can be explained by the following expression:

$$\text{Case study} \begin{cases} \text{Minimise} & f_1(x) = Y_{mn}^* \\ \text{Minimise} & f_2(x) = t_{PCM} \\ \text{Minimise} & f_3(x) = t_{wall} \\ \\ \text{subject to} & 0 \leq x_{material} \leq 3 \qquad \times 8 \text{ slot-layers} \\ & 0.10 \leq x_{MassThick} \leq 0.25 \\ & 0.005 \leq x_{PCMthick} \leq 0.04 \quad \times 2 \text{ PCM} \\ & 0.15 \leq x_{k_{PCM}} \leq 0.9 \qquad \times 2 \text{ PCM} \\ & 80000 \leq x_{L_{PCM}} \leq 230000 \quad \times 2 \text{ PCM} \\ & 0.5 \leq x_{\Delta T_{PCM}} \leq 8 \qquad \times 2 \text{ PCM} \\ & 15.5 \leq x_{T_{p,PCM1}} \leq 23 \\ & 23.5 \leq x_{T_{p,PCM2}} \leq 39 \end{cases}$$

where "$\times 8$ slot-layers" means that the variable is repeated as many times as the number of slot-layers, and "$\times 2$ PCM" means that the variable is double (one value for each PCM).

Table 4.8 Genetic inputs.

Population Size	100	
Number of Variables	19	
Number of binary digits	2 for Material type	4 for Mass thickness
	3 for PCM thickness	4 for k_{PCM}
	4 for L_{PCM}	4 for ΔT_{PCM}
	4 for $T_{p,PCM1}$	5 for $T_{p,PCM2}$
Variable Domains	$x_{materialType} \in [0,3]$	$x_{MassThick} \in [0.10, 0.25]$
	$x_{PCMthick} \in [0.005, 0.04]$	$x_{k_{PCM}} \in [0.15, 0.9]$
	$x_{L_{PCM}} \in [80000, 230000]$	$x_{\Delta T_{PCM}} \in [0.5, 8]$
	$x_{T_{p,PCM1}} \in [15.5, 23]$	$x_{T_{p,PCM2}} \in [23.5, 39]$
Mutation Probability	0.2	
End Condition	End after 100 generations	

For all simulations, NSGA-II explored 100 generations with 100 individuals in each generation.

4.3.4.4   Constraints

To guarantee coherence and feasibility of all the potential solutions, some constraints were needed. Due to the combinatorial nature of the optimisation problem, constraints were handled with repair algorithms which introduced modifications on non-complying individuals (see § 2.2.1.6). An *always replacing* approach was chosen in order not to discard any potential solution and hence obtaining a well-populated Pareto front. In this way, post-optimisation analyses on a statistically significant dataset of Pareto solutions could be carried out.

1. To avoid solutions with unreasonably small thickness of one or more layers, a constraint on the minimum layer thickness was set. If, after joining the adjacent slot-layers made of the same material, the thickness of a single layer was below the threshold set for that material, the thickness of that layer was set equal to the threshold value. This threshold was set equal to 5 mm for PCM and 3 cm for both insulation and mass.

2. To avoid solutions without insulation, which would not comply with the U-value requirement, if missing, an additional layer of insulation was added just after the external render[3].

3. To avoid solutions without thermal mass, if missing, an additional layer of thermal mass was added just before the internal plaster. The thickness of this thermal mass layer was set equal to the middle value of the variable's domain.

Eventually, a check was performed to make sure that each material's thickness and the maximum number of layers were still within their respective domains.

The additional constraint on the PCM properties reported in § 4.1.2.1 was also considered.

4.3.5   Effect of the number of layers

For a systematic evaluation of the effect of the number of layers on the dynamic thermal performance of traditional walls, the relationship between monthly equivalent periodic thermal transmittance and corresponding time shift for a variety of mutual positions of mass and insulation layers evenly distributed within the wall was evaluated (Fig. 4.17). These wall configurations were characterised by the same amount of insulation (evaluated for each location according the wall's U-value) and mass (equal to the upper bound, i.e. 25 cm), and no PCM. Periodic thermal transmittance and time shift of these wall configurations were evaluated both in terms of monthly equivalent values and traditional values according to

---

[3]The layer sequence is referred to from the outside to the inside.
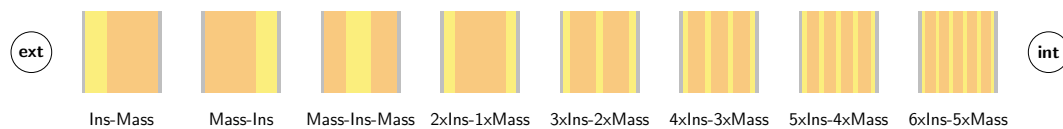
Fig. 4.17 Wall stratigraphies selected for comparing the Y_{mn}^* values.

ISO 13786:2007 [5]. This analysis allowed to identify how Y_{mn}^* and Δt_{mn}^* differ from the traditional values in relation to the boundary conditions for the various locations and orientations. Moreover, these values were used as a reference to compare the performance of solutions of the optimisation problem.

4.4 Building-level investigations

As commercial and residential buildings in Europe consume approximately 40% of primary energy and are responsible for 24% of greenhouse emissions [2], improving the energy performance of buildings is considered to be an important opportunity in the energy challenge set by the European Union by 2020 [1]. Due to the low replacement rate (around 1.0-3.0% per year) of existing buildings by new ones, energy retrofit of the existing building stock is of outermost importance to reach the EU targets and promote energy efficiency and environmental sustainability [285].

In this framework, the application of PCM in the context of building refurbishment was studied. Building-level investigations focused on the application of optimisation analyses for the energy retrofit of office buildings. An archetype office building realised in Italy during the period 1946-1970 was chosen as a case study. In this epoch, office buildings were characterised by a low WWR. The application of PCM could hence be more effective than on post-1970 highly glazed office buildings.

The analyses were carried out in the climates of Palermo, Torino and Oslo. The same building geometry was adopted for all locations, whereas the envelope properties were differentiated by country. Moreover, differences in the building envelope were highlighted in Oslo between buildings pre-1955 and post-1955. Since this difference regarded not only the insulation level of the buildings, but also the wall typology—i.e. massive or lightweight walls—both cases were considered worth of investigation.

The following retrofit strategies were considered on envelope and systems:

- Retrofit of the external walls with the addition of insulation and PCM (up to two layers with a different melting temperature);
- Replacement of the existing windows;
- Substitution of internal movable shading devices with external ones (with the exception of the windows on the north façade);

- Installation of a mechanical ventilation system;

- Revamping of heating and cooling[4] systems;

- Installation of dimming lighting control.

Moreover, the optimisation analyses were performed considering the following three retrofit options on the opaque envelope components:

1. Intervention on the external side of the wall. This option can be adopted when interruption or relocation of the office activities is not possible during the renovation works.

2. Intervention on the internal side of the wall. According to the Italian laws on the conservation of historical buildings, this option is necessary for buildings which are older than 50 years (ante-1966).

3. Intervention on both sides of the wall. According to the literature for traditional walls—for which the periodic thermal transmittance is improved with a symmetrical layout and the insulation on the outermost layers (§ 2.2.3.1.1)—and according to the results from the component-level analyses—for which the equivalent periodic thermal transmittance of the wall was generally improved with an outer insulation layer and an inner PCM layer (§ 5.2.3)—this option was also taken into account.

Moreover, either the same intervention for all the façades (i.e. same retrofit solution for all the walls) or differentiated by façade (i.e. different wall solution for each orientation) were considered (investigations from the literature suggest that performance parameters for the renovation of existing buildings should be determined for each orientation [286]). In both cases, a maximum of two PCM materials could be selected by the optimisation algorithm.

With regard to the optimisation objectives, the problem was faced under two points of view. On one side, optimisations were run with three objectives to minimise the building energy need for heating and cooling and the investment cost. On the other side, the optimisations were performed with two objectives to minimise primary energy consumption and global cost. Only for the climate of Oslo, where no cooling system was considered, the minimisation of the cooling energy need was substituted by the minimisation of thermal discomfort. Moreover, since the most common energy vector for space heating in Norway is electricity, minimisation of primary energy was directly considered instead of building energy need for heating.

Post-Pareto analyses were then performed to identify general rules and trends of the optimised solutions.

To the best of the author's knowledge, no similar investigation on layer distri-

---

[4]Except in Oslo.

bution within a wall of either new or existing building with the inclusion of phase change materials has been previously proposed, even less with the simultaneous presence of two PCMs with different thermo-physical properties. In the existing literature, investigations of the optimal application of PCMs for new and retrofitted buildings mostly involved simple parametric analyses [281, 131, 183]; when true optimisation processes were adopted, they involved either analytical optimisation for specific applications (e.g. direct gain solar rooms [282, 283]), single-objective analyses [279], or simulations explored only a short time window (e.g. a week [265]). Moreover, the comparison between several retrofit strategies and optimisation results according to the selected objective functions introduces an additional novelty to the present work. However, the main focus is on the methodological approach rather than on the optimisation problem itself.

4.4.1   Description of the case study

The building-level analyses were carried out considering the energy retrofit of an archetype office building realised during the period 1946-1970.

According to the researches of Margiotta [316] and Rollino [317], until the 1970 the representative office building in Italy is considered to have a cellular plan with a moderate amount of glazing (Fig. 4.18), to have no more than six floors, and to be located in urban areas where it is surrounded by shorter buildings. No geometrical data was found for archetype office buildings in Norway. Hence, the same building geometry was adopted for the case study of Oslo.

For the optimisation analyses, the building was considered to have five floors and to be surrounded by buildings four floors tall at a distance of 14 m. Only the third floor was modelled.

For Torino and Palermo, the external wall of the archetype building was selected in accordance with the national technical report UNI/TR 11552:2014 [318], which provides a list of typical opaque building envelopes in existing Italian buildings. The masonry cavity wall denoted as MCV04 was chosen (U-value of 1.30 W/(m^{2}K), 30 cm of thickness). This type of wall is considered to be a typical wall in buildings from 1930 to 1975 in the Piedmont region, where Turin is located. Since no region-specific information is provided in [318] for the Sicily region, the same kind of wall was considered also for Palermo. Details on the layers and thermo-physical properties of the selected wall are reported in Table 4.9. Also the floor slabs were selected according to UNI/TR 11552:2014. The slab denoted as SOL02 was chosen (U-value of 1.56 W/(m^{2}K), 37.5 cm of thickness). Details on the layers and thermo-physical properties of the selected floor slab are reported in Table 4.10.

For the transparent envelope, a single glazing with uninsulated metal frame (U-value of 5.7 W/(m^{2}K), g-value of 0.85) was selected according to the "National
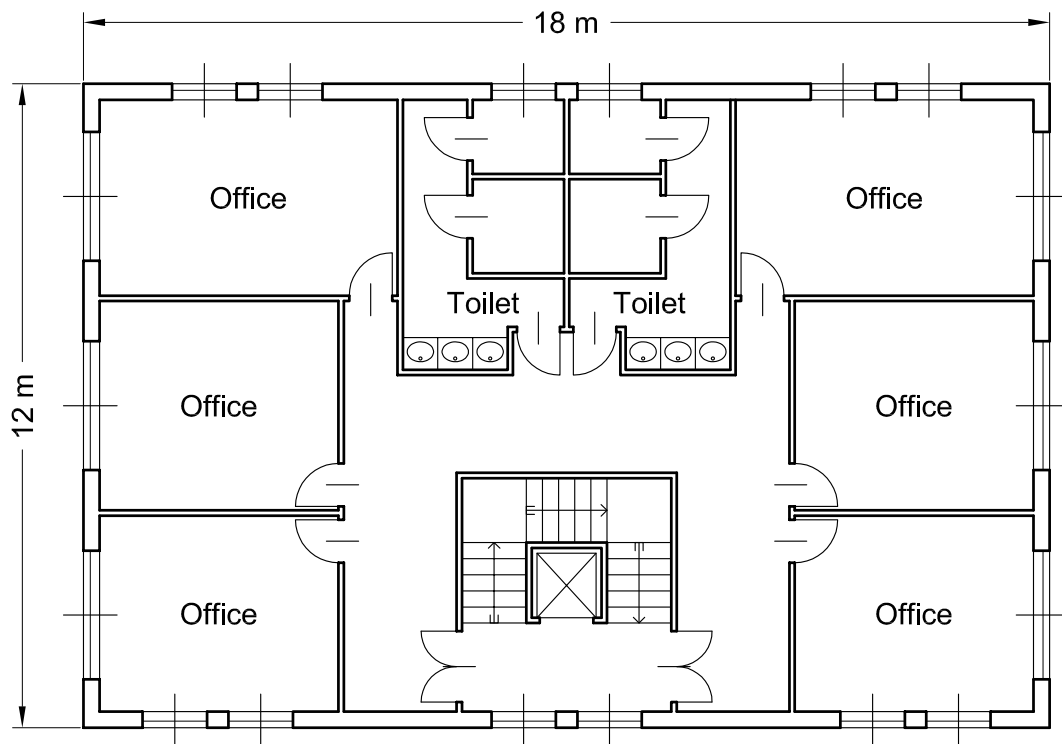
Fig. 4.18 Plan of the archetype office building.

scientific report on the TABULA activities in Italy" [319].

With regard to the systems, no data typical for office buildings was found. Data for residential buildings were therefore used. Considering the efficiencies for emission, regulation, distribution and generation reported in [319], a seasonal efficiency of the heating systems of 0.63 was evaluated according to UNI/TS 11300-2 [320]. Since no data was found for cooling systems (as they were not typically used in residential buildings), a seasonal energy efficiency ratio of 2.5 was hypothesised.

No information on the characteristics of opaque envelope components was found for office buildings in Norway. Data referring to residential multifamily buildings were therefore adopted. These data were retrieved from the report of the Norwegian EPISCOPE project [321, 322], which highlighted a difference between buildings pre-1955 and post-1955. Since this difference regarded not only the insulation level of the buildings, but also the wall typology—i.e. massive or lightweight walls—both cases were considered worth of investigation. U-values of 0.96 W/(m^{2}K) and 0.35 W/(m^{2}K) were hence chosen respectively for the periods pre-1955 and post-1955 [321, 322] (these values are in accordance with the Norwegian legislation set in 1949 [323], which required masonry buildings (or made with other fire-resistant materials) in Oslo with a floor area greater than 200 m^2 to have a maximum U-value of 0.9 kcal/(m^2 h °C)—i.e. 1.0465 W/(m^{2}K)). The selected U-values were obtained by adapting the wall examples for apartment blocks reported in the

Norwegian EPISCOPE Building Typology Brochure [324] (Table 4.9). The floor slab was taken from the same examples (Table 4.10).

With regard to the transparent envelope, buildings with a ratio of glazed surface on net floor area greater than 1/8 were enforced to install double glazing [323]. Given a ratio of glazed surface on net floor area of 0.167 (> 1/8), an air-filled double glazing with a U-value of 2.60 W/(m²K) was considered [321, 322].

With regard to the systems, most of the archetype buildings for the service sector in Norway use electricity directly as the energy carrier for space heating [325].

Given a floor size of 18×12 m (external dimensions) and a floor height of 3 m, in Torino and Palermo the net floor area before the retrofit is 198.36 m² and the net volume is 595.08 m³. In Oslo, the net floor area before the retrofit is 201.25 m² and 207.09 m², respectively for the periods pre-1955 and post-1955, and the net volume is 603.75 m³ and 621.27 m³, respectively.

Table 4.9 Description of the external walls of the archetype building.

Material	Thickness	ρ	c	k	R
	[m]	$\left[\text{kg/m}^3\right]$	[J/(kg K)]	[W/(m K)]	$\left[\text{m}^2\text{K/W}\right]$
Palermo and Torino					
External render	0.02	1800	1000	0.90	-
Bricks	0.12	1800	1000	0.72	-
Air cavity	0.06	-	-	-	0.18
Hollow bricks	0.08	800	1000	-	0.20
Internal plaster	0.02	1400	1000	0.70	-
U-value: 1.30 W/(m²K), thickness: 30 cm					
Oslo, pre-1955					
External render	0.02	1800	1000	0.90	-
Bricks	0.12	1800	1000	0.72	-
Autoclaved aerated concrete	0.10	400	1000	0.15	-
Internal plaster	0.01	1400	1000	0.70	-
U-value: 0.96 W/(m²K), thickness: 25 cm					
Oslo, post-1955					
External plasterboard	0.025	1150	840	0.35	-
Mineral wool	0.10	55	1030	0.04	-
Internal plasterboard	0.025	745	840	0.25	-
U-value: 0.35 W/(m²K), thickness: 15 cm					

Table 4.10 Description of the floor slabs of the archetype building.

Material	Thickness [m]	ρ [kg/m³]	c [J/(kg K)]	k [W/(m K)]	R [m²K/W]
Palermo and Torino					
Floor tiles	0.015	1700	1000	1.47	-
Cement mortar	0.02	2000	1000	1.4	-
Lightened screed	0.06	900	1000	0.58	-
Cement mortar	0.02	2000	1000	-	0.35
Slab	0.24	900	1000	-	
Internal plaster	0.02	1400	1000	0.70	-
U-value: 1.56 W/(m²K), thickness: 37.5 cm					
Oslo, pre-1955 and post-1955					
Floor tiles	0.015	1700	1000	1.47	-
Cement mortar	0.02	2000	1000	1.4	-
Lightened slab	0.25	1600	1000	0.54	-
Internal plaster	0.01	1400	1000	0.70	-
U-value: 1.56 W/(m²K), thickness: 29.5 cm					

4.4.2 Parametric model

The parametric model was realised in order to consider three possible retrofit options (intervention either on the external side, on the internal side, or both sides of the wall), and to consider either the same intervention for all the façades (i.e. same retrofit solution for all the walls) or differentiated by façade (i.e. different wall solution for each orientation). Both in case of same intervention on all the façades (referred to as NF1) or differentiated by façade (referred to as NF4), a maximum of two PCM materials could be selected by the optimisation algorithm.

4.4.2.1 Opaque envelope

The retrofitted walls were described by the following variables (the marked items represent the actual optimisation variables):

- Wall configuration
- ✓ U-value of the wall
- ✓ Insulation material
- ✓ Internal lining material

Wall configuration   According to the retrofit type—i.e. on the external side of the wall, on the internal side, or on both sides—three sets of wall configurations were selected. The retrofit configurations were chosen in order to test all the combinations of layer positions having no more than one layer of the same PCM, and no more than one insulation layer on the same side of the original wall. These wall configurations were mathematically described by:

✓ PCM use (none, only PCM1, only PCM2, both PCMs)

• Layers' position:

   ✓ PCM position 1 (0/1)
   ✓ PCM position 2 (0/1)
   ✓ PCM position 3 (0/1)
   ✓ PCM position 4 (0/1) – *Only for retrofit on both sides*
   ✓ PCM position 5 (0/1) – *Only for retrofit on both sides*

These variables acted as switches for the selection of the wall configuration. The full list of possibilities is reported in Fig. 4.19 for retrofit on the external side (referred to as RT0), in Fig. 4.20 for retrofit on the internal side (referred to as RT1), and in Figs. 4.21, 4.22 and 4.23 for retrofit on both sides of the wall (referred to as RT2). The same colour legend as in Fig. 4.16 was considered; the grey area additionally refers to the existing wall.

It is important to mention that the wall configurations are not always described by all the position variables. For example in Fig. 4.19, if PCMuse is 0 (no PCM), the wall will be "ext0000" regardless of the values of the PCM position variables. In the same way, if PCMuse is either 1 or 2 (only PCM1 or only PCM2), only PCMpos1 will affect the selection of the wall regardless of the values assumed by PCMpos2 and PCMpos3. This lack of uniqueness in the search space—i.e. more sets of variables can generate equivalent solutions with the same fitness—introduces a certain degree of epistasis in the problem. The higher the epistasis, the more difficult the problem is to solve [193].

U-value of the wall   The U-value of the new wall was chosen in order to comply with the standards. The maximum U-value for walls is 0.45 W/(m^{2}K) in Palermo [308], 0.30 W/(m^{2}K) in Torino [308] and 0.22 W/(m^{2}K) in Oslo [315]. The lower bound for the U-value was set equal to 0.15 W/(m^{2}K), which is the upper limit for Passive Houses [326].

In case of intervention differentiated by façade, the U-value was selected for each wall orientation.

Insulation material   The insulation material could be chosen among a set of eight options, whose thermo-physical properties are reported in Table 4.11. The
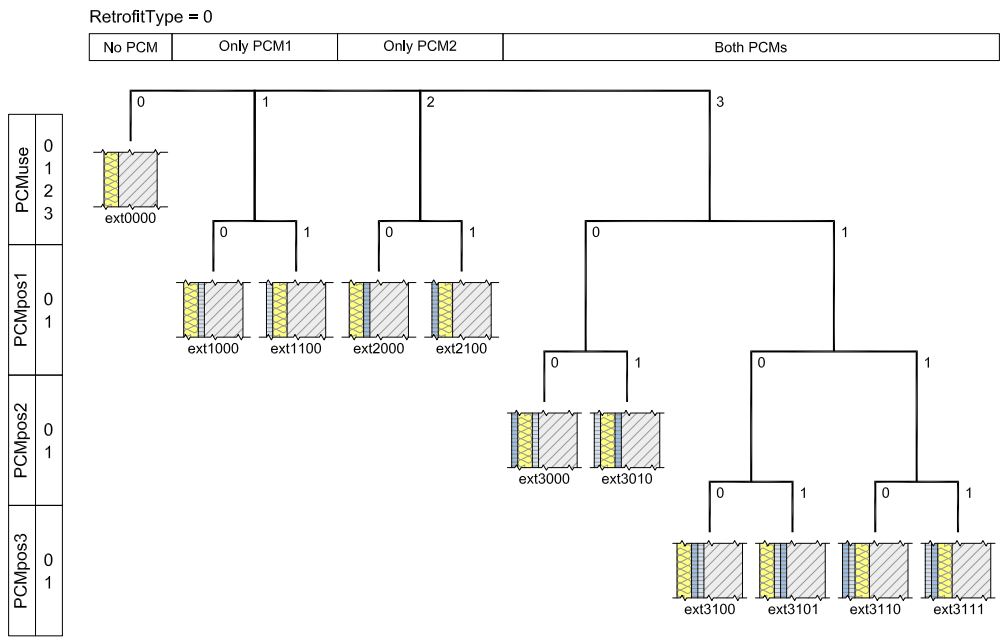
Fig. 4.19 Wall configurations for retrofit on the external side.
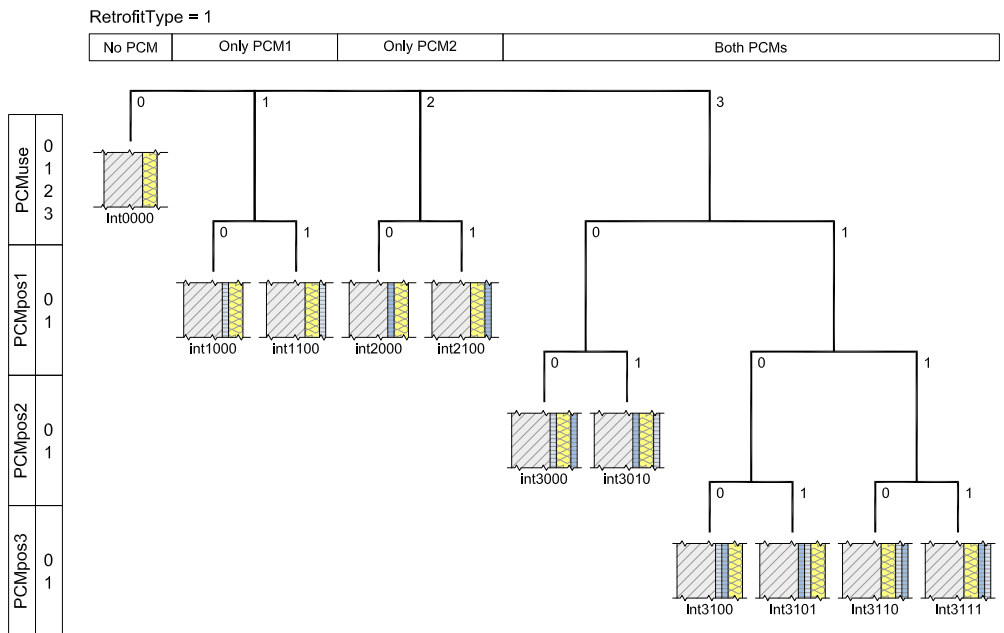
Fig. 4.20 Wall configurations for retrofit on the internal side.
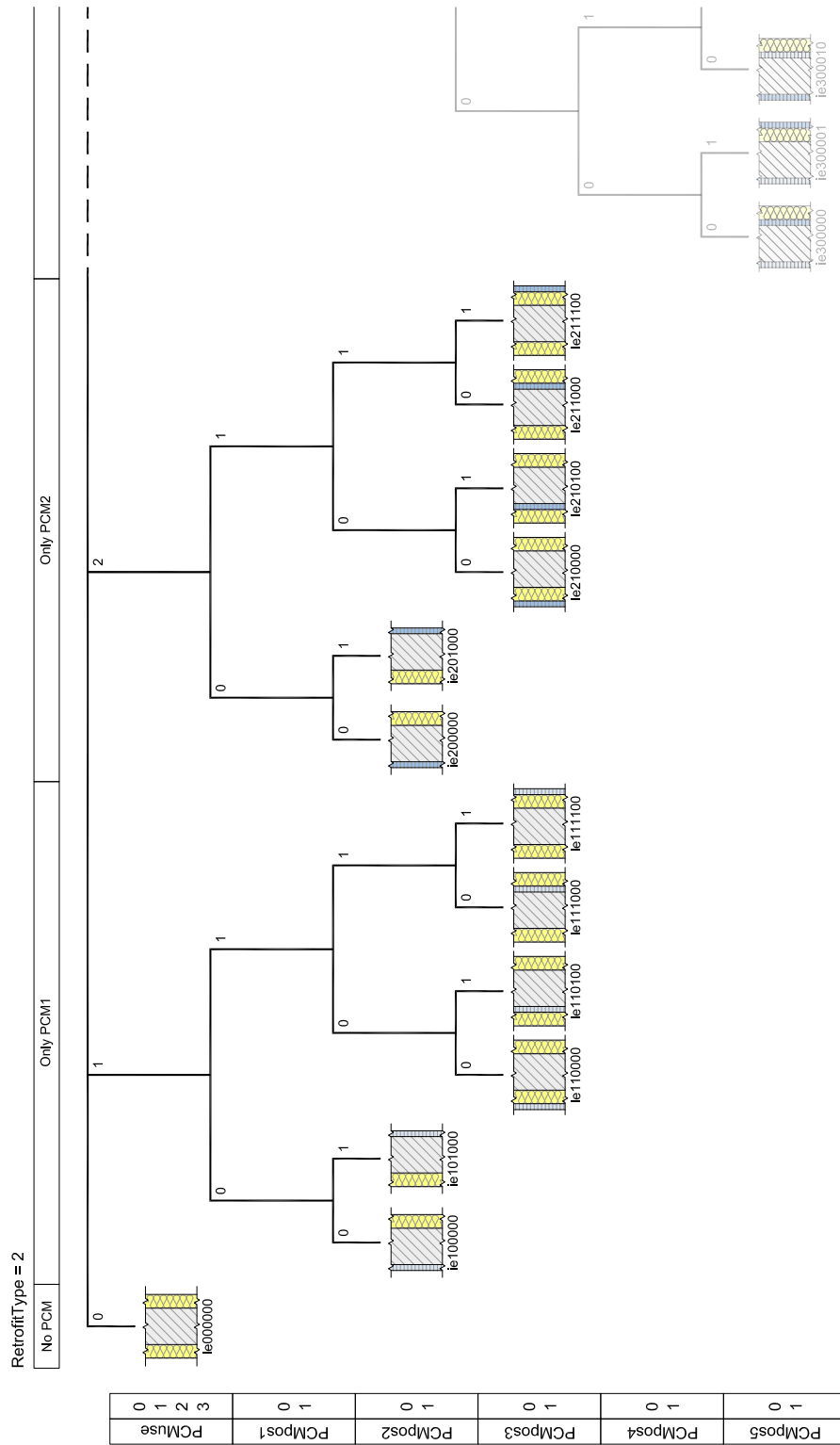
Fig. 4.21 Wall configurations for retrofit on both sides (a).
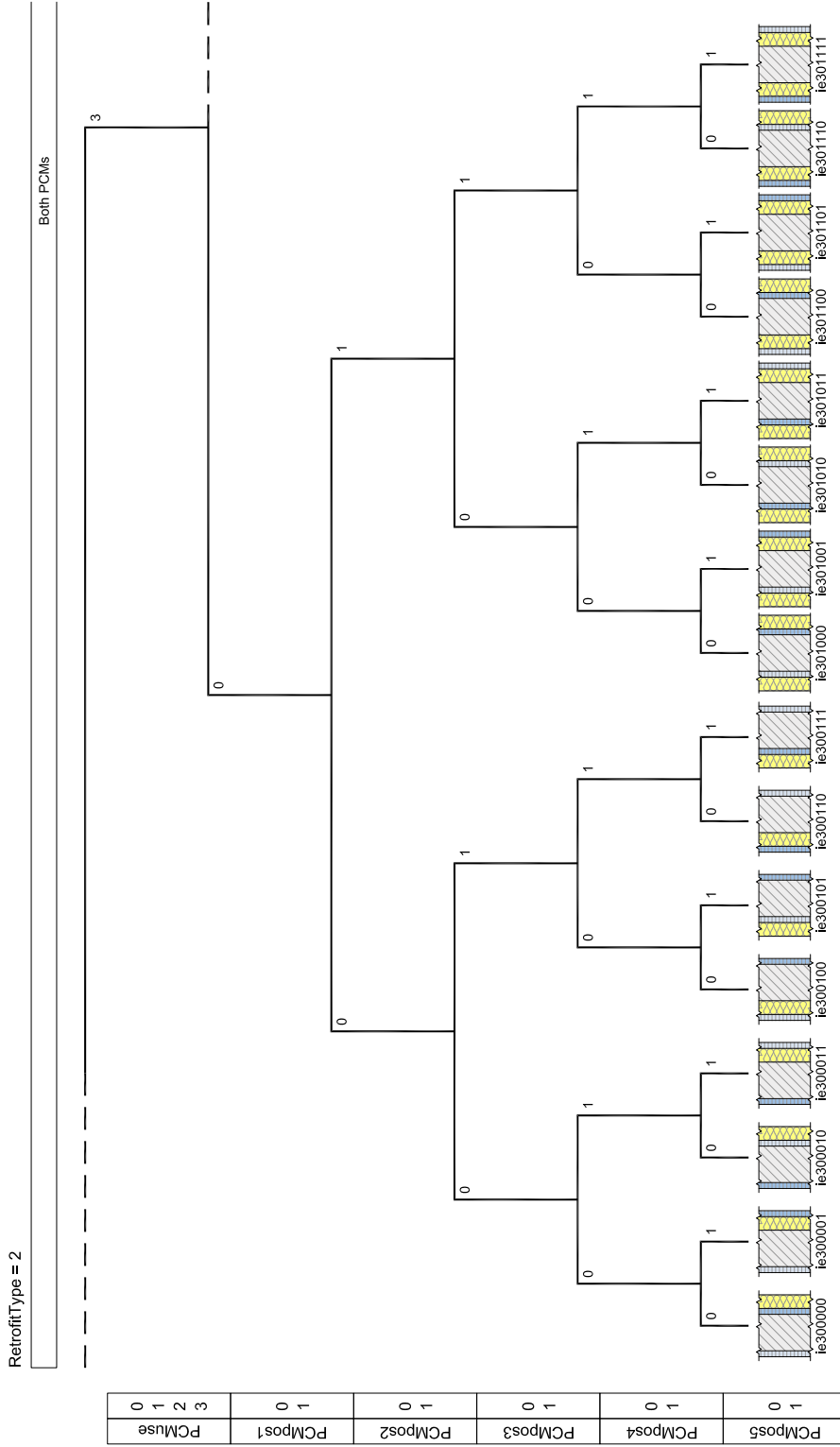
Fig. 4.22 Wall configurations for retrofit on both sides (b).
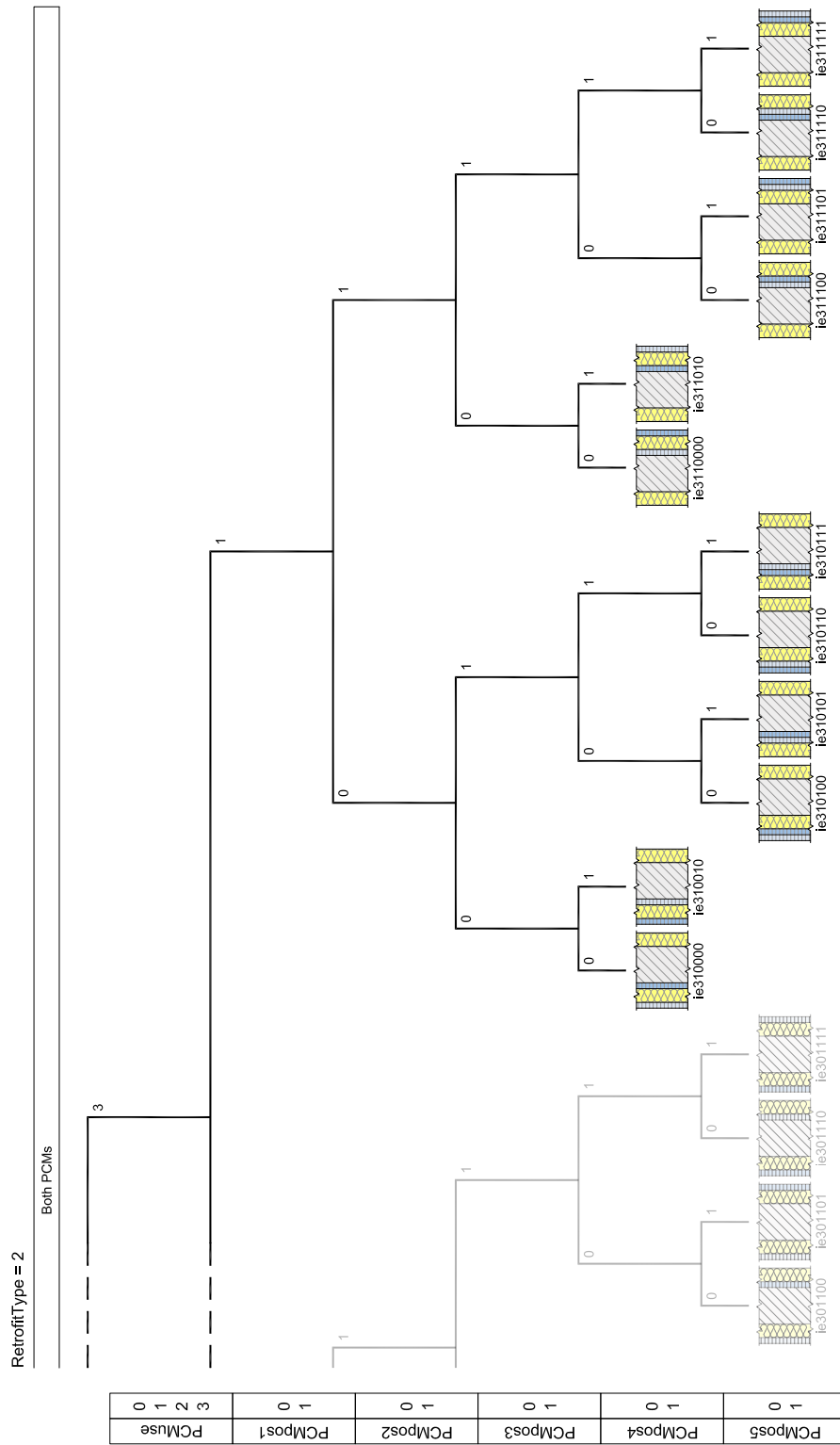
Fig. 4.23 Wall configurations for retrofit on both sides (c).

Table 4.11 Thermo-physical properties of the insulation materials.

ID	Material	k	ρ	c
		[W/(m K)]	$[\mathrm{kg/m^3}]$	[J/(kg K)]
0	EPS	0.042	13	1250
1	Rock wool	0.040	36	1030
2	XPS	0.033	35	1250
3	Sheep wool	0.037	20	1720
4	Cork	0.044	130	850
5	Wood-fiber board	0.038	160	2100
6	Cellulose fiber panels	0.039	40	2150
7	Aerogel mats	0.0135	150	1000

insulation thickness was calculated in order to obtain the U-value selected each time by the optimisation algorithm. A single insulation material was selected both in case of NF1 and NF4.

Internal lining material   In case of retrofit on the inner side of the wall, the material of the internal lining was also selected. The reason for choosing the plaster type is the effect it has on the internal areal heat capacity. The internal areal heat capacity, κ_m, defined by ISO 13786:2007 [5], is a measure of the ability of the wall to accumulate heat on the inner side. Especially in rooms with high internal loads, such as offices, high κ_m values contribute to reduce the internal surface temperatures and hence the operative temperature in summer [327]. Increasing κ_m can also have an influence in reducing the energy demand [328].

The thermo-physical properties and the thickness of the selected internal lining materials (four options) are reported in Table 4.12. A single internal lining material was selected both in case of NF1 and NF4.

Table 4.12 Thermo-physical properties and thickness of internal lining materials.

ID	Material	Thickness	k	ρ	c
		[m]	[W/(m K)]	$[\mathrm{kg/m^3}]$	[J/(kg K)]
0	Lime and gypsum plaster	0.02	0.70	1400	1010
1	Clay plaster	0.02	0.90	1800	2100
2	Mineralised wooden board	0.04	0.26	1800	2100
3	Thermo-plaster	0.05	0.091	400	1000

Additional notes   In case of retrofit on the external side or on both sides of the wall (RT0 or RT2) in Palermo and Torino, the existing render on the external side

of the wall was considered to have deteriorated and was hence removed. In this way, in case of RT2, the maximum limit of 10 layers in an EnergyPlus *Construction* could always be respected. Moreover, when the retrofit intervention required to operate on the internal side of the walls, a vapour barrier was considered to prevent interstitial condensation. In addition, thermal bridges were supposed to be solved by turning up the insulation [187].

4.4.2.1.1 PCM properties A maximum of two PCMs was considered both in case of same intervention on all the façades (NF1) or differentiated by façade (NF4).

The PCM properties were modelled in the same way as for the component level investigations, as described in section 4.3.3. Therefore, the variables describing each PCM were the peak melting temperature, the melting temperature range, the latent heat of fusion, and the thermal conductivity.

4.4.2.2 Transparent envelope

The windows were replaced to comply with the standards. The complete list of the new glazing types is reported in Table 4.13. U-values, g-values and visible transmission coefficients were evaluated with the software WINDOW 7.4 [329].

For each location, the optimisation algorithm could choose among four windows, with a maximum U-value of 3.2 W/(m^{2}K) in Palermo [308] (ID from 0 to 3), 1.9 W/(m^{2}K) in Torino [308] (ID from 4 to 7), and 1.2 W/(m^{2}K) in Oslo [315] (ID from 7 to 10). A single type of window was selected whether the intervention was differentiated by façade or not.

The U-values of glazing, frame and windows are summarised for each orientation in Table 4.14.

4.4.2.2.1 Shading devices In order to comply with the Italian standard [308] which requires g_{gl+sh} (i.e. SHGC when the shading device is in use) to be lower than 0.35 for windows with expositions from west to south to east, external shading devices were installed on all windows with the exception of those placed on the north-facing façade. Technical details of the selected shading devices are reported in Table 4.15.

Table 4.13 Glazing specifications.

ID	Type	Coating	Gap	U_g $[W/(m^2K)]$	g $[-]$	τ_l $[-]$
0	4/12/4	None	Air	2.84	0.75	0.81
1	4/12/4	Low-e (3)	Air	1.61	0.58	0.80
2	4/12/4	Low-e (2)	Air	1.61	0.40	0.71
3	6/16/4	Selective (2)	Ar 90%	1.07	0.26	0.61
4	4/12/4	Low-e (3)	Ar 90%	1.28	0.58	0.80
5	4/12/4	Low-e (2)	Ar 90%	1.28	0.40	0.71
6	4/12/4/12/4	Low-e (3,5)	Air	0.94	0.49	0.71
7	4/12/4/12/4	Low-e (3,5)	Ar 90%	0.72	0.49	0.71
8	4/12/4/12/4	Low-e (2,5)	Ar 90%	0.75	0.54	0.71
9	4/15/4/15/4	Low-e (3,5)	Ar 90%	0.61	0.49	0.71
10	4/12/4/12/4	Low-e (3,5)	Kr 95%	0.48	0.50	0.71

Table 4.14 U-values of glazing, frame and windows.

ID	U_g	U_f	U_w (S-N)	U_w (E-W)	Used in Torino	Palermo	Oslo
0	2.84	2.0	2.77	2.72	✓		
1	1.61	2.0	1.93	1.81	✓		
2	1.61	2.0	1.93	1.81	✓		
3	1.07	2.0	1.54	1.39	✓		
4	1.28	1.8	1.64	1.51		✓	
5	1.28	1.8	1.64	1.51		✓	
6	0.94	1.2	1.23	1.11		✓	
7	0.72	1.2	1.07	0.94		✓	✓
8	0.75	0.8	0.98	0.87			✓
9	0.61	0.8	0.88	0.76			✓
10	0.48	0.8	0.79	0.67			✓

Table 4.15 Properties of shading devices.

Slat geometry			Thermo-physical properties			
Width [mm]	Separation [mm]	Thickness [mm]	k $[-]$	ρ_s $[-]$	ρ_l $[-]$	ϵ $[-]$
25	18.8	1.5	0.9	0.7	0.7	0.9
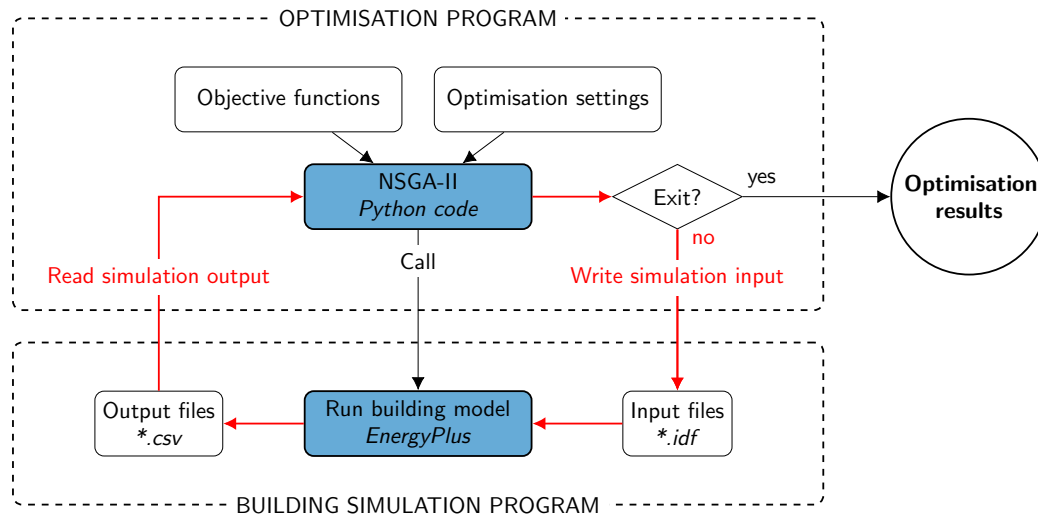
Fig. 4.24 Building-level optimisation procedure.

4.4.3 Optimisation procedure

The parametric model described according to the procedure in § 4.4.2 was adopted to perform the building-level optimisation analyses. These analyses were carried out by coupling the Python implementation of the NSGA-II optimisation algorithm (see § 3.2.2) with the building energy model of the archetype office building developed in EnergyPlus (see § 4.4.4) (Fig. 4.24).

For each optimisation problem, separate optimisation runs were performed to consider the three possible retrofit options (intervention either on the external side, on the internal side, or both sides of the wall), and to consider either the same intervention for all the façades or differentiated by façade (Fig. 4.25). Therefore, six runs were performed for each set of objective functions and location (Fig. 4.26).

The total time required to perform a single optimisation run was approximately eight days on computers with at least 8 Gb of RAM. Each optimisation run could be launched in parallel, with a limit given by the maximum number of simultaneous EnergyPlus instances that each computer could handle. Three and six instances were launched on computers respectively equipped with an Intel Core i5-3470 processor at 3.20 GHz with 8 Gb of RAM and an Intel Core i7-4790 processor at 3.60 GHz with 32 Gb of RAM.

4.4.3.1 Objective functions

The building level investigations in Italy were analysed under two points of view. On one side, the focus was the reduction, with minimum cost, of the building energy
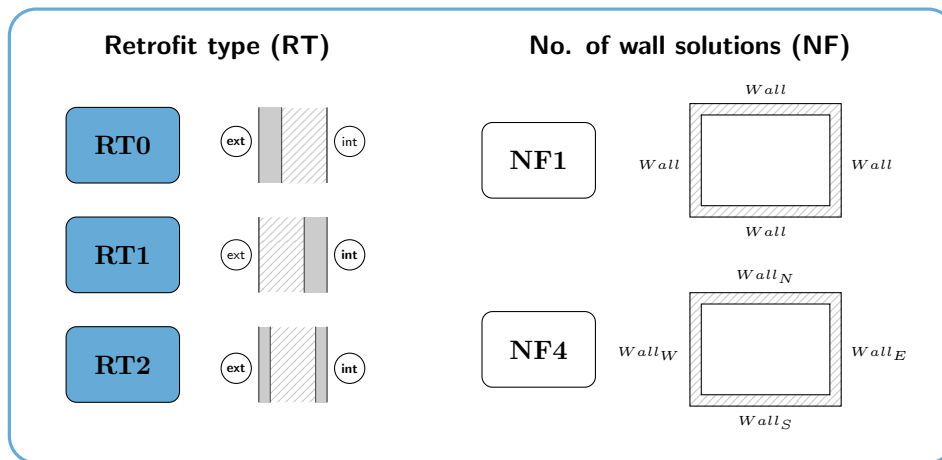
Fig. 4.25 Summary of the retrofit interventions.
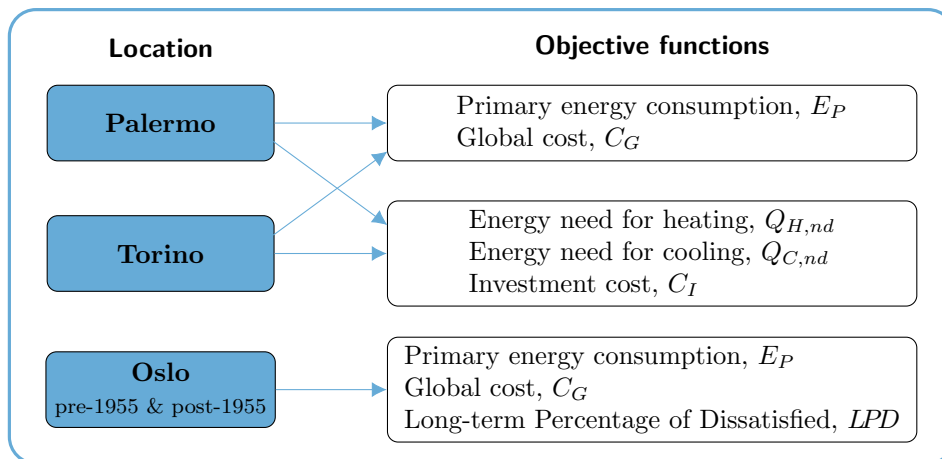
Fig. 4.26 Summary of locations and objective functions.

need. The optimisations were therefore run to minimise the following functions:

1. Building energy need for heating, $Q_{H,nd}$ (see § 4.4.4);

2. Building energy need for cooling, $Q_{C,nd}$ (see § 4.4.4);

3. Investment cost, C_I (see § 4.4.6.1).

From these results, subsequent analyses can be carried out to estimate the best solution in terms of primary energy consumption or global cost by selecting various system options. On the other side, heating and cooling systems were defined and the optimisations were performed to directly minimise

1. Primary energy consumption, E_P (see § 4.4.5);

2. Global cost, C_G (see § 4.4.6).

For the climate of Oslo, where no cooling system was considered and the prevalent heating energy vector is electricity, the objective was the minimisation of the following functions:

1. Primary energy consumption, E_P (see § 4.4.5);

2. Long-term Percentage of Dissatisfied, LPD (see § 4.4.7);

3. Global cost, C_G (see § 4.4.6).

4.4.3.2   Optimisation variables

The optimisation variables (represented by the checked items) of the building level investigations can be summarised as follows:

✓ Window type

✓ Insulation material

✓ Internal lining material – *Except for retrofit on the external side*

✓ U-value of the wall $[\mathrm{W/(m^2 K)}]$

- Wall configuration:

  ✓ PCM use (none, only PCM1, only PCM2, both PCMs)
  ✓ PCM position 1
  ✓ PCM position 2
  ✓ PCM position 3
  ✓ PCM position 4 – *Only for retrofit on both sides*
  ✓ PCM position 5 – *Only for retrofit on both sides*

✓ Thickness of each PCM

- Thermo-physical properties of each PCM:

  ✓ Peak melting temperature $[°\mathrm{C}]$
  ✓ Melting temperature range $[°\mathrm{C}]$
  ✓ Latent heat of fusion $[\mathrm{J/(kg\ K)}]$
  ✓ Thermal conductivity $[\mathrm{W/(m\ K)}]$

The number of variables for each optimisation problem is reported in Table 4.16.

Table 4.16 Number of variables.

	RT0	RT1	RT2		RT0	RT1	RT2
NF1	17	18	20	**NF4**	38	39	47

4.4.3.3   GA inputs

The inputs to the genetic algorithm for all the building-level case studies are reported in Tables 4.17, 4.18 and 4.19 respectively for Palermo, Torino, and Olso.

For all simulations, NSGA-II explored 100 generations with 100 individuals in each generation. Considering that the number of variables for retrofit intervention differentiated by façade (NF4) is more than double than in the case of same intervention for all the façades (NF1), the exploration level achieved for the NF1 optimisation runs was higher.

Palermo   The fitness functions for the building-level investigations in Palermo can be explained by the following expression:

$$
\text{Case study}
\begin{cases}
\begin{array}{ll}
\left.\begin{array}{ll}
\text{Minimise} & f_1(x) = Q_{H,nd} \\
\text{Minimise} & f_2(x) = Q_{C,nd} \\
\text{Minimise} & f_3(x) = C_I
\end{array}\right\} \quad \text{or} \quad
\left.\begin{array}{ll}
\text{Minimise} & f_1(x) = E_P \\
\text{Minimise} & f_2(x) = C_G
\end{array}\right\} \\[2em]
\begin{array}{lll}
\text{subject to} & 0 \le x_{winType} \le 3 & \\
& 0.15 \le x_{U-value} \le 0.45 & \times \text{NF} \\
& 0.005 \le x_{PCMthick} \le 0.04 & \times 2\,\text{PCM} \\
& 0.15 \le x_{k_{PCM}} \le 0.9 & \times 2\,\text{PCM} \\
& 80000 \le x_{L_{PCM}} \le 230000 & \times 2\,\text{PCM} \\
& 0.5 \le x_{\Delta T_{PCM}} \le 8 & \times 2\,\text{PCM} \\
& 15.5 \le x_{T_{p,PCM1}} \le 23 & \\
& 23.5 \le x_{T_{p,PCM2}} \le 39 & \\
& 0 \le x_{PCMuse} \le 3 & \times \text{NF} \\
& 0 \le x_{PCMpos1} \le 1 & \times \text{NF} \\
& 0 \le x_{PCMpos2} \le 1 & \times \text{NF} \\
& 0 \le x_{PCMpos3} \le 1 & \times \text{NF} \\
& 0 \le x_{PCMpos4} \le 1 \ (\text{RT2 only}) & \times \text{NF} \\
& 0 \le x_{PCMpos5} \le 1 \ (\text{RT2 only}) & \times \text{NF} \\
& 0 \le x_{InsulationType} \le 7 & \\
& 0 \le x_{PlasterType} \le 3 &
\end{array}
\end{array}
\end{cases}
$$

where $\times$NF means that the variable is repeated as many times as the number of different façades (i.e. one value for NF1 and 4 values for NF4), and $\times 2$ PCM means that the variable is double (one value for each PCM).

The list of genetic inputs is reported in Table 4.17.

Table 4.17 Genetic inputs, Palermo.

Population Size	100	
Number of Variables	17 for RT0-NF1	38 for RT0-NF4
	18 for RT1-NF1	39 for RT1-NF4
	20 for RT2-NF1	47 for RT2-NF4
Number of binary digits	2 for win Type	4 for U-value
	3 for PCM thickness	4 for k_{PCM}
	4 for L_{PCM}	4 for ΔT_{PCM}
	4 for $T_{p,PCM1}$	5 for $T_{p,PCM2}$
	2 for PCMuse	1 for PCMpos
	3 for Ins Type	2 for Plaster Type
Variable Domains	$x_{winType} \in [0,3]$	$x_{U-value} \in [0.15, 0.45]$
	$x_{PCMthick} \in [0.005, 0.04]$	$x_{k_{PCM}} \in [0.15, 0.9]$
	$x_{L_{PCM}} \in [80000, 230000]$	$x_{\Delta T_{PCM}} \in [0.5, 8]$
	$x_{T_{p,PCM1}} \in [15.5, 23]$	$x_{T_{p,PCM2}} \in [23.5, 39]$
	$x_{PCMuse} \in [0,3]$	$x_{PCMpos} \in [0,1]$
	$x_{InsulationType} \in [0,7]$	$x_{PlasterType} \in [0,3]$
Mutation Probability	0.2	
End Condition	End after 100 generations	

Torino   The fitness functions for the building-level investigations in Torino can be explained by the following expression:

$$
\text{Case study}
\begin{cases}
\begin{array}{ll}
\text{Minimise} & f_1(x) = Q_{H,nd} \\
\text{Minimise} & f_2(x) = Q_{C,nd} \\
\text{Minimise} & f_3(x) = C_I
\end{array}
\Bigg\} \quad \text{or} \quad
\begin{array}{ll}
\text{Minimise} & f_1(x) = E_P \\
\text{Minimise} & f_2(x) = C_G
\end{array}
\Bigg\} \\[2em]
\begin{array}{lll}
\text{subject to} & 4 \leq x_{winType} \leq 7 & \\
& 0.15 \leq x_{U-value} \leq 0.30 & \times \text{NF} \\
& 0.005 \leq x_{PCMthick} \leq 0.04 & \times 2\,\text{PCM} \\
& 0.15 \leq x_{k_{PCM}} \leq 0.9 & \times 2\,\text{PCM} \\
& 80000 \leq x_{L_{PCM}} \leq 230000 & \times 2\,\text{PCM} \\
& 0.5 \leq x_{\Delta T_{PCM}} \leq 8 & \times 2\,\text{PCM} \\
& 15.5 \leq x_{T_{p,PCM1}} \leq 23 & \\
& 23.5 \leq x_{T_{p,PCM2}} \leq 39 & \\
& 0 \leq x_{PCMuse} \leq 3 & \times \text{NF} \\
& 0 \leq x_{PCMpos1} \leq 1 & \times \text{NF} \\
& 0 \leq x_{PCMpos2} \leq 1 & \times \text{NF} \\
& 0 \leq x_{PCMpos3} \leq 1 & \times \text{NF} \\
& 0 \leq x_{PCMpos4} \leq 1 \;(\text{RT2 only}) & \times \text{NF} \\
& 0 \leq x_{PCMpos5} \leq 1 \;(\text{RT2 only}) & \times \text{NF} \\
& 0 \leq x_{InsulationType} \leq 7 & \\
& 0 \leq x_{PlasterType} \leq 3 &
\end{array}
\end{cases}
$$

The list of genetic inputs is reported in Table 4.18.

Table 4.18 Genetic inputs, Torino.

Population Size	100	
Number of Variables	17 for RT0-NF1	38 for RT0-NF4
	18 for RT1-NF1	39 for RT1-NF4
	20 for RT2-NF1	47 for RT2-NF4
Number of binary digits	2 for win Type	4 for U-value
	3 for PCM thickness	4 for k_{PCM}
	4 for L_{PCM}	4 for ΔT_{PCM}
	4 for $T_{p,PCM1}$	5 for $T_{p,PCM2}$
	2 for PCMuse	1 for PCMpos
	3 for Ins Type	2 for Plaster Type
Variable Domains	$x_{winType} \in [4,7]$	$x_{U-value} \in [0.15, 0.30]$
	$x_{PCMthick} \in [0.005, 0.04]$	$x_{k_{PCM}} \in [0.15, 0.9]$
	$x_{L_{PCM}} \in [80000, 230000]$	$x_{\Delta T_{PCM}} \in [0.5, 8]$
	$x_{T_{p,PCM1}} \in [15.5, 23]$	$x_{T_{p,PCM2}} \in [23.5, 39]$
	$x_{PCMuse} \in [0,3]$	$x_{PCMpos} \in [0,1]$
	$x_{InsulationType} \in [0,7]$	$x_{PlasterType} \in [0,3]$
Mutation Probability	0.2	
End Condition	End after 100 generations	

Oslo The fitness functions for the building-level investigations in Oslo can be explained by the following expression:

$$
\text{Case study}
\begin{cases}
\begin{aligned}
&\text{Minimise} && f_1(x) = E_P \\
&\text{Minimise} && f_2(x) = LPD \\
&\text{Minimise} && f_3(x) = C_G \\[6pt]
&\text{subject to} && 7 \le x_{winType} \le 10 \\
&&& 0.15 \le x_{U-value} \le 0.22 && \times \text{NF} \\
&&& 0.005 \le x_{PCMthick} \le 0.04 && \times 2\,\text{PCM} \\
&&& 0.15 \le x_{k_{PCM}} \le 0.9 && \times 2\,\text{PCM} \\
&&& 80000 \le x_{L_{PCM}} \le 230000 && \times 2\,\text{PCM} \\
&&& 0.5 \le x_{\Delta T_{PCM}} \le 8 && \times 2\,\text{PCM} \\
&&& 15.5 \le x_{T_{p,PCM1}} \le 23 \\
&&& 23.5 \le x_{T_{p,PCM2}} \le 39 \\
&&& 0 \le x_{PCMuse} \le 3 && \times \text{NF} \\
&&& 0 \le x_{PCMpos1} \le 1 && \times \text{NF} \\
&&& 0 \le x_{PCMpos2} \le 1 && \times \text{NF} \\
&&& 0 \le x_{PCMpos3} \le 1 && \times \text{NF} \\
&&& 0 \le x_{PCMpos4} \le 1 \ (\text{RT2 only}) && \times \text{NF} \\
&&& 0 \le x_{PCMpos5} \le 1 \ (\text{RT2 only}) && \times \text{NF} \\
&&& 0 \le x_{InsulationType} \le 7 \\
&&& 0 \le x_{PlasterType} \le 3
\end{aligned}
\end{cases}
$$

The list of genetic inputs is reported in Table 4.19.

Table 4.19 Genetic inputs, Oslo.

Population Size	100	
Number of Variables	17 for RT0-NF1	38 for RT0-NF4
	18 for RT1-NF1	39 for RT1-NF4
	20 for RT2-NF1	47 for RT2-NF4
Number of binary digits	2 for win Type	3 for U-value
	3 for PCM thickness	4 for k_{PCM}
	4 for L_{PCM}	4 for ΔT_{PCM}
	4 for $T_{p,PCM1}$	5 for $T_{p,PCM2}$
	2 for PCMuse	1 for PCMpos
	3 for Ins Type	2 for Plaster Type
Variable Domains	$x_{winType} \in [7,10]$	$x_{U-value} \in [0.15, 0.22]$
	$x_{PCMthick} \in [0.005, 0.04]$	$x_{k_{PCM}} \in [0.15, 0.9]$
	$x_{L_{PCM}} \in [80000, 230000]$	$x_{\Delta T_{PCM}} \in [0.5, 8]$
	$x_{T_{p,PCM1}} \in [15.5, 23]$	$x_{T_{p,PCM2}} \in [23.5, 39]$
	$x_{PCMuse} \in [0, 3]$	$x_{PCMpos} \in [0, 1]$
	$x_{InsulationType} \in [0, 7]$	$x_{PlasterType} \in [0, 3]$
Mutation Probability	0.2	
End Condition	End after 100 generations	

4.4.3.4   Constraints

The constraint on the PCM properties reported in § 4.1.2.1 was considered.

4.4.4   Energy building model

The energy analyses to evaluate the heating and cooling energy needs were performed with EnergyPlus 8.0.0 [169].

Considering the high number of simulation runs required for the optimisation process, to reduce the calculation run time the space was treated as a single thermal zone. In Torino and Palermo, set-point air temperatures were set to 20 ℃ for heating and 26 ℃ for cooling (according to the Italian regulation [330]). The systems were active from 7.00 AM to 6.00 PM during weekdays only. In Oslo, the heating set-point operative temperature was set to 21 ℃ with a nocturnal set-back of 19 ℃ (according to the Norwegian regulation [331]). To retrieve the building energy need for heating and cooling, the system was modelled as *IdealLoadsAirSystem* with infinite heating and cooling capacity.

Exterior surfaces were modelled using the outside dimensions of walls. The correct values of internal volume and floor area of the building were specified as inputs to EnergyPlus for each simulation. Windows were placed in their correct spatial position with respect to the outer dimension of walls. In this way, EnergyPlus automatically accounted for the shading deriving from the reveals [169]. External shading devices were operated when the solar irradiance on the window was higher than 300 W/m^2. A fixed slat angle of 45° was considered.

A fixed ground reflectance value of 0.15 was assumed [332].

Details on material properties and opaque constructions of the pre-retrofit walls are reported in Tables 4.9 and 4.10. Details on the material properties added during the retrofit intervention (except the PCMs) are reported in Tables 4.11 and 4.12. The solar absorption coefficient of the external opaque surfaces was set to 0.6 (medium colour). The glazing characteristics of the windows are reported in Table 4.13, whereas the U-value of the frame is reported in Table 4.14. Internal partition walls were taken into account as internal mass.

To model the PCM, the indications from Tabares-Velasco et al. [170] were followed, i.e. timestep equal to 3 minutes and space discretisation constant set equal to 1. The *ConductionFiniteDifference* algorithm was selected to model walls with PCM, whereas the *ConductionTransferFunction* model was used in absence of PCM in order to reduce the calculation run time. The enthalphy-temperature curve of the PCMs was obtained by integration of the $c(T)$ curve according to eq. (2.1). A maximum of 16 points were chosen as input values due to the intrinsic limitation of EnergyPlus. The selection was performed in order to guarantee the smallest

discrepancy from the analytical curve.

Schedules were set according to ISO 13790:2008 [333], which assumes 20 W/m^2 for internal gains deriving from people activity and electric equipment during daytime in the office rooms, and 2 W/m^2 during night-time. In the other spaces, 8 W/m^2 are assumed during occupied hours and 1 W/m^2 during unoccupied hours. Since a single zone was modelled, the following average values with respect to the floor area were given as input to EnergyPlus:

- 7.5 W/m^2 for internal gains deriving from people activity during daytime,

- 8.3 W/m^2 for internal gains deriving from electric equipment during daytime and 1.7 W/m^2 during night-time.

In Oslo, occupancy time was considered from 7.00 AM to 5.00 PM during weekdays according to ISO 13790:2008, whereas in Palermo and Torino a realistic occupancy was considered to be from 8.00 AM to 6.00 PM.

Daylighting control was performed with dimming option. Two control points were placed along the longitudinal axis of the building in the middle of the office rooms. The illuminance setpoint was set to 500 lx. The maximum lighting level was set to 10 W/m^2 per zone floor area. The lighting schedule was set equal to the occupancy one.

Mechanical ventilation strategy was adopted with sensible heat recovery having 70% efficiency. According to UNI 10339:1995 [334], the ventilation rate was set to 0.792 air changes per hour during the occupation time, i.e. during weekdays from 8.00 AM to 6.00 PM. During the rest of the day and during weekends, the ventilation rate was set to 0.25 h^{-1} [335].

During the summer season, night-time ventilation was allowed from 11.00 PM to 7.00 AM [333, 336] when the internal temperature was above 24 ℃ and the difference between internal and external air temperature was higher than 2 ℃. The night cooling air change rate was set to 6 h^{-1}. A fan pressure rise of 75 Pa and fan total efficiency of 0.5 were selected (EnergyPlus default values) with balanced ventilation type.

The outcomes of the energy simulation process were building heating and cooling thermal energy need ($Q_{H,nd}$ and $Q_{C,nd}$, respectively) and electric energy consumption for artificial lighting and fans, Q_E (see § 4.4.5). When the thermal comfort was among the objective functions, mean radiant temperature and occupancy profile were additional simulation outputs (see § 4.4.7).

4.4.5   Primary energy

For evaluating of the primary energy consumption, energy vectors and system efficiencies needed to be defined.

In Italy, natural gas was assumed as the energy vector for heating; the system was considered to have a seasonal efficiency, η_H, of 0.8. Cooling was considered to be provided by means of a chiller with seasonal energy efficiency ratio (EER) of 3.0.

In Norway, 71.7% of the archetype buildings for the service sector use electricity directly as the energy carrier for space heating, followed by a 15.4% which use oil, 6.5% district heating, 5.5% heat from heat pump, 0.9% natural gas, and 0.1% wood [325]. Therefore, electricity was considered as the sole energy carrier for the case study of Oslo ($\eta_H = 1$). Moreover, according to TEK 10 and amendments, the installation of heating systems based on fossil fuels is not allowed [315].

The primary energy is given by [320]

$$E_P = f_{P,tot,gas} \cdot \frac{Q_{H,nd}}{\eta_H} + f_{P,tot,el} \cdot \left(\frac{Q_{C,nd}}{\text{EER}} + Q_E \right),$$

where $Q_{H,nd}$ and $Q_{C,nd}$ represent the building energy need respectively for heating and cooling; Q_E is the total electricity use, which comprises lighting, equipment, and the energy required for operating the fans of the ventilation system; $f_{P,tot,gas}$ and $f_{P,tot,el}$ are the primary energy conversion factors respectively for natural gas and electricity.

Primary energy factors (PEF) of 1.05 and 2.42 were respectively adopted for natural gas and electricity in Italy, according to the values reported in the decree D.M 26 giugno 2015 [308]. This PEF value for electricity includes both renewable and non-renewable shares. A primary energy factor of 1.54, evaluated according to EN 15603:2008 [337], was adopted for electricity in Norway [338].

4.4.6   Cost analyses

The cost analyses were performed according to EN 15459:2007 [339]. In [339], the global cost is defined as the sum of the initial investment cost and the annual costs for every component or system minus their value at the end of the calculation period. Therefore,

$$C_G(\tau) = C_I + \sum_j \left\{ \sum_{i=1}^{\tau} \left[C_{a,i}(j) \cdot R_d(i) \right] - V_{f,\tau}(j) \right\}, \qquad (4.16)$$

where $C_G(\tau)$ is the global cost, which is a function of the calculation period, τ; C_I is the investment cost; $C_{a,i}(j)$ are the annual costs for year i of the component j;

$R_d(i)$ is the discount rate for year i; and $V_{f,\tau}(j)$ is the final value of component j at the end of the calculation period.

The initial investment costs generally include design, purchase of systems and components, connections to suppliers, installation and commissioning process. For its calculation, the procedure and input data reported in § 4.4.6.1 were adopted.

The annual costs, which are given by eq. (4.17), include running costs, C_r, and periodic or replacement costs, $C_{R,i}(j)$. According to eq. (4.18), the running costs comprise energy costs, C_e, operational costs, C_o, maintenance costs, C_m, and added costs, C_{ad}. However, only the energy costs were considered in the analysis; the other components of the running costs were neglected since their value could be assumed to be the same for all the candidate solutions. The procedure for evaluating the energy costs is reported in section 4.4.6.2.

$$C_{a,i}(j) = C_r + C_{R,i}(j) \tag{4.17}$$

$$C_r = C_e + C_o + C_m + C_{ad} \tag{4.18}$$

The replacement costs were evaluated according to eq. (4.19), where $V_0(j)$ is the initial value of component j at the beginning of the calculation period, τ_0; and R_p is the rate of development of the price for products (a value of 0.02 was assumed [339]).

$$C_{R,i}(j) = V_0(j) \cdot (1 + R_p)^i \tag{4.19}$$

The discount rate was calculated according to eq. (4.20), where R_R is the real interest rate as in eq. (4.21), R is the market interest rate, and R_i is the inflation rate. Values of 0.045 and 0.02 were respectively assumed for R and R_i [339].

$$R_d(i) = \left(\frac{1}{1 + R_R}\right)^i \tag{4.20}$$

$$R_R = \frac{R - R_i}{1 + R_i} \tag{4.21}$$

Eventually, the final value of each component was evaluated considering a straight-line depreciation—either of the initial investment or the last replacement cost—until the end of the calculation period, and referred to the beginning of the calculation period. Therefore,

$$V_{f,\tau}(j) = V_0 \cdot (1 + R_p)^{n_\tau(j) \cdot \tau_n(j)} \cdot \frac{[n_\tau(j) + 1] \cdot \tau_n(j) - \tau}{\tau_n(j)} \cdot R_d(\tau),$$

where $\tau_n(j)$ is the lifespan of component j, and $n_\tau(j)$ is the total number of replacements of component j during the calculation period. A lifetime of the building

of 50 years after renovation and a calculation period of 30 years were assumed. The lifespan of the opaque envelope was considered equal to the lifetime of the building, whereas lifespans of 30 and 25 years were respectively considered for the transparent envelope and the shading devices [339].

4.4.6.1 Investment cost

The initial investment cost was calculated considering only material and installation costs related to the building envelope. The installation cost of the systems—as well as the costs for design, etc.—were not considered since their value was assumed to be the same for all the candidate solutions in the same location.

With the exception of the PCM, the data source for evaluating the investment cost was the official price list for public works of Regione Piemonte [340]. Although prices change with the location, material and installation costs were assumed to be the same regardless of the case study. The highest accuracy of the investment cost was hence obtained for the analyses performed in Torino.

4.4.6.1.1 Opaque envelope The unit costs of insulation and internal lining materials that could be chosen for the retrofit intervention (Tables 4.11 and 4.12) are reported in Table 4.20.

The costs of the insulation are raw material costs, which in [340] are given in $\text{\euro}/\text{m}^2$ for predefined thicknesses. However, a linear regression was found to describe the relationship between cost and thickness, with a coefficient of determination greater than 0.9999 for all the materials with the exception of the wood-fiber board (R^2=0.9766). Therefore, insulation prices in $\text{\euro}/\text{m}^2/\text{cm}$ were estimated and used in the calculations. Installation costs of 42.47 $\text{\euro}/\text{m}^2$ and 51.65 $\text{\euro}/\text{m}^2$ were respectively considered for insulation installed on the external or internal side of the wall.

The costs of the internal lining materials include both raw material and installation. According to [340], the reference surface for the cost calculation was the total area of the wall regardless of the presence of windows; when the wall has openings smaller than 4 m^2, the area of the openings is not removed to account for the extra work and material needed for realising the openings' sides.

Table 4.20 Costs of insulation and internal lining materials.

ID	0	1	2	3	4	5	6	7
Insulation $\left[\text{\euro}/\text{m}^2/\text{cm}\right]$	0.34	0.58	1.02	1.77	2.01	2.15	2.22	65.28
Internal lining $\left[\text{\euro}/\text{m}^2\right]$	18.05	19.50	31.31	48.78				

When the retrofit intervention required to operate on the external side of the walls, the cost for removing the existing render was set to 6.31 €/m². Morover, an additional cost of 9.31 €/m² was considered for the scaffolding, plus 1.59 €/m² for each month after the first one. Two months of installation of the scaffolding were estimated. When the retrofit intervention required to operate on the internal side of the walls, a vapour barrier was added to prevent interstitial condensation, with a cost of 17.04 €/m² for both raw material and installation.

4.4.6.1.2 Transparent envelope The costs of glazing, frame and installation are reported in Table 4.21, together with the total window cost. The costs of glazing are raw-material costs, whereas the frame costs include the frame material's cost (PVC for windows from 0 to 3, wood/aluminium for windows from 4 to 7, PVC/wood/aluminium for windows from 8 to 10) and the cost for installing the window. Two values are reported for frame/installation costs due to the different sizes of the windows; $1.92\,\mathrm{m}^2 (< 2\,\mathrm{m}^2)$ along the south and north façades, and $3.84\,\mathrm{m}^2 (> 3.5\,\mathrm{m}^2)$ on the east and west façades.

In addition, the cost for removing the existing windows was set equal to 12.14 €/m². The cost of the shading devices was set equal to 59.10 €/m².

Table 4.21 Cost of the windows.

| ID | Glazing | Frame/Installation | | Window | |
| | | (S-N) | (E-W) | (S-N) | (E-W) |
	$[\text{€}/\mathrm{m}^2]$	$[\text{€}/\mathrm{m}^2]$	$[\text{€}/\mathrm{m}^2]$	$[\text{€}/\mathrm{m}^2]$	$[\text{€}/\mathrm{m}^2]$
0	37.55	154.38	138.72	191.93	176.27
1	38.77	154.38	138.72	193.15	177.49
2	38.77	154.38	138.72	193.15	177.49
3	70.08	154.38	138.72	224.46	208.80
4	44.67	278.93	271.53	323.60	316.20
5	44.67	278.93	271.53	323.60	316.20
6	74.33	306.82	298.68	381.15	373.01
7	81.48	306.82	298.68	388.30	380.16
8	81.48	308.51	300.06	389.99	381.54
9	81.48	308.51	300.06	389.99	381.54
10	110.07	308.51	300.06	418.58	410.13

4.4.6.1.3 PCM The cost of PCMs varies widely according to their type, melting temperature and purity (which affects melting temperature range and latent heat of fusion) [341]. Unfortunately, it is impossible to take all of these factors into account to accurately estimate the cost of PCM. An average cost was thus estimated

Table 4.22 PCM costs (1 \$ = 0.9033 €).

PCM type	\$/kg	€/kg	€/m²/cm	Ref.
Organic, paraffins				
Paraffin wax	1.94	1.75	13.32	[341]
Eicosan, Laboratory-grade (>99%)	53.90	48.69	428.45	[341]
Eicosan, Technical-grade (90%-95%)	7.04	6.36	55.96	[341]
PCM Products	-	6.00	52.80	[342]
Rubitherm RT20	16.32	14.74	110.56	[343]
Rubitherm RT (23 - 25 - 27 ℃) in CSM	-	0.62	5.46	[103]
Rubitherm RT27	-	5.00	38.00	*
Rubitherm RT28HC	-	8.25	63.53	*
Organic, fatty acids				
Oleic acid	1.72	1.55	13.79	[341]
Biodiesel crude glicerine	0.26	0.23	2.88	[341]
PureTemp (min)	1.65	1.49	12.82	[341]
PureTemp (max)	5.50	4.97	42.73	[341]
PureTemp (max)	11.02	9.96	85.63	[344]
BioPCM	1.30	1.18	10.13	[167]
Inorganic, salt hydrates				
PCM Energy P. Ltd (min)	3.08	2.78	41.73	[341]
PCM Energy P. Ltd (max)	4.95	4.47	67.07	[341]

* Personal communication with Rubitherm (2012).

from values reported in the literature (Table 4.22). Costs for commercial amounts (> 500 kg) were considered whenever known.

From the costs reported in Table 4.22, an average cost (with the exclusion of the laboratory-grade PCM) of about 40 €/m²/cm was chosen for the raw material. An additional 20% was considered for macroencapsulation [341]. The total estimated cost of PCM was hence 48 €/m²/cm, plus 4.36 €/m² for installation [103].

4.4.6.2 Energy costs

The energy costs were evaluated including taxes, levies and VAT, considering the energy vectors and system efficiencies defined in § 4.4.5.

In Italy, according to the "Autorità per l'energia elettrica il gas e il sistema idrico" (AEEGSI) [345], the cost of electricity is given by the sum of three amounts; a fixed share (C_{PDP}, in €/y), a power share (C_{kW}, in €/kW/y), and an energy share (C_{kWh}, in €/kWh). The electricity prices for non-domestic users with a power request of 10 kW are reported in Table 4.23 (prices for the 3rd trimester 2016). These prices

include taxes and levies but exclude VAT.

According to AEEGSI, the price of natural gas in Italy is given by the sum of two amounts; a fixed share (C_{PDR}, in €/y), and an energy share (C_{smc}, in €/smc). The price of the energy share is given in € per standard cubic metre, i.e. the amount of gas in 1 m^3 when it has a temperature of 15 ℃ and pressure of 101325 Pa. The conversion from smc to m^3 is obtained through a multiplier C, whose value is 1.015284 in Palermo and 1.017505 in Torino. The two cities are also subjected to a different taxation. To evaluate the amount of gas needed to satisfy the heating energy requirement, a lower calorific value of 9.6 kWh/m^3 was used. A consumption below 120 smc/year and a nominal flow rate between 4 m^3/h and 6 m^3/h was considered to evaluate the shares of the cost for natural gas in Palermo, whereas a consumption between 481 smc/year and 1560 smc/year and a nominal flow rate between 10 m^3/h and 40 m^3/h was considered in Torino. The final prices are reported in Table 4.23 (prices for July 2016). These prices include taxes and levies but exclude VAT.

In Norway, for non-domestic end-users with an annual energy consumption below 20 MWh, an electricity price of 0.0856 €/kWh was adopted, according to the data provided by Eurostat [2]. This price refers to the year 2015; it includes taxes and levies but excludes VAT.

Table 4.23 Costs of electricity and natural gas.

Location	Electricity				Natural gas		
	C_{PDP} [€/PDP]	C_{kW} [€/kW]	C_{kWh} [€/kWh]	VAT [%]	C_{PDR} [€/PDR]	C_{smc} [€/smc]	VAT [%]
Palermo					119.25	0.267597	10%
Torino	286.3201	31.7675	0.174168	22%	399.45	0.586447	22%
Oslo	-	-	0.0856	25%	-	-	-

4.4.7 Thermal comfort

The *Long-term Percentage of Dissatisfied* (LPD) index introduced by Carlucci [346] was adopted to quantify thermal comfort. The LPD is defined as

$$LPD = \frac{\sum_{t=1}^{T} \sum_{z=1}^{Z} (p_{z,t} \cdot LD_{z,t} \cdot h_t)}{\sum_{t=1}^{T} \sum_{z=1}^{Z} (p_{z,t} \cdot h_t)},$$

where T is the calculation period; Z is the number of thermal zones; $p_{z,t}$ is the occupation rate of zone z at the time step t; $LD_{z,t}$ is the *Likelihood of Dissatisfied* inside zone z at the time step t; and h_t is the duration of a calculation time step.

As reported in [346], the Likelihood of Dissatisfied (LD) is an estimate of the deviation of the thermal comfort conditions from a theoretical objective; its value depends on the comfort model. For the EN 15251:2008 adaptive thermal comfort model [347], the LD index is given by the *Overheating risk* [348], which is defined as

$$LD_{Adaptive}^{EN} = \frac{e^{0.4743\ \Delta\theta_{op}-2.067}}{1 + e^{0.4743\ \Delta\theta_{op}-2.067}},$$

where $\Delta\theta_{op}$ is the absolute value of the difference between the indoor operative temperature and the optimal comfort temperature. Since a comfort category II was considered [347], LD was evaluated as deviation from the category bounds.

Chapter 5

Results

In this chapter, the results and a first discussion are reported for each level of investigation. For all the multi-objective optimisation analyses, the Pareto frontiers and the post-optimisation analyses are illustrated in order to identify the characteristics of the non-dominated sets. Additional discussion on the building-level results will be reported in Chapter 6.

5.1 Material-level analyses

The content of this section was partly published in [24].

The results of the inverse modelling procedure for estimating the enthalpy-temperature curve of a PCM presented in § 4.2 are herewith reported and discussed in comparison with a low-speed (0.05 ℃/min) DSC measurement.

5.1.1 Estimation of the enthalpy-temperature curve of PCMs

The comparisons between measured fluxes both at the dynamic and static plates and the simulated values after solution of the inverse problems are respectively reported in Fig. 5.1a and Fig. 5.2a. The goodness of each fit was evaluated by means of MBE, MAE, RMSE and R^2 as defined in § 3.1.2.1. The respective percentage values were not computed because they would have dramatically increased for heat fluxes close to zero. Their interpretation would have hence been misleading. The fit without and with contact resistances with a single $c(T)$ curve were respectively denoted as V1 and VR. The fit with two $c(T)$ curves plus contact resistances was denoted as VR2C. The resulting values of MBE, MAE, RMSE, R^2 and Adj-R^2 of the
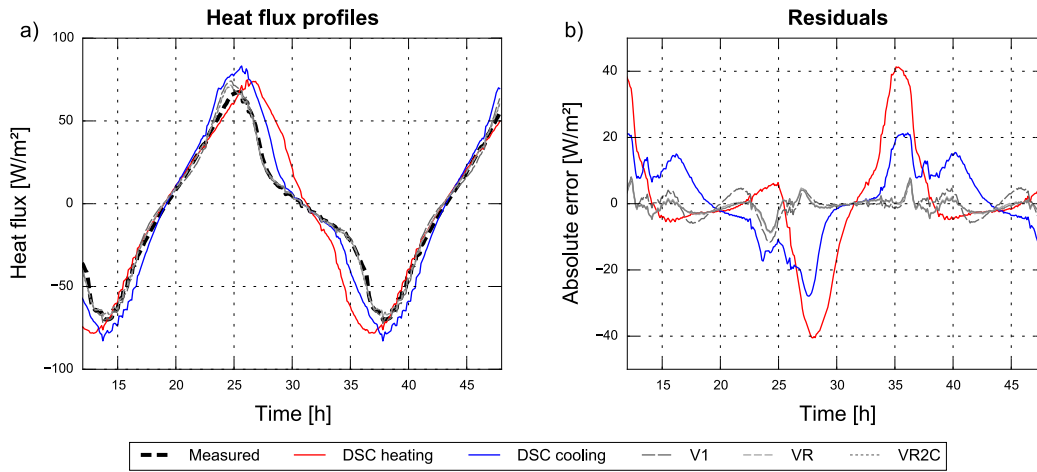
Fig. 5.1 Dynamic plate: a) Measured vs simulated heat flux profiles and b) residuals.
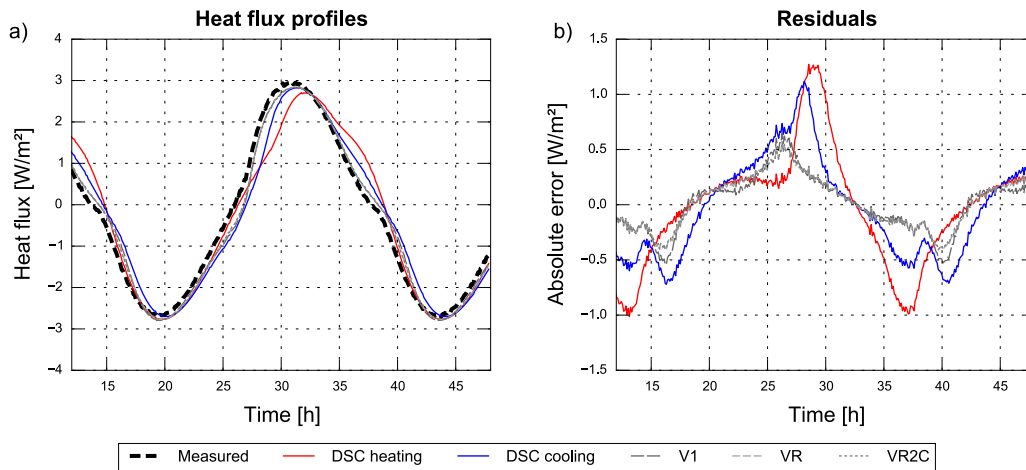
Fig. 5.2 Static plate: a) Measured vs simulated heat flux profiles and b) residuals.

heat flux densities exchanged with the dynamic and static plates are respectively summarised in Tables 5.1 and 5.2.

A very good agreement between measured and simulated data was found. The highest MAE and RMSE for the heat flux density, respectively 2.5 W/m^2 and 3.4 W/m^2 on the dynamic plate and 0.20 W/m^2 and 0.25 W/m^2 on the static plate, were obtained for the V1 estimate. Slight improvements were achieved in terms of MAE and RMSE with the VR case (when estimating the contact resistances with the plates) and the VR2C case (when estimating the contact resistances with the plates and considering the summation of two $c(T)$ curves). However, the VR and VR2C cases were characterised by increased MBE values. For all the estimates, a slight overestimation of the heat flux density was observed on the dynamic plate and underestimation on the static plate. The residuals of the fits are reported in
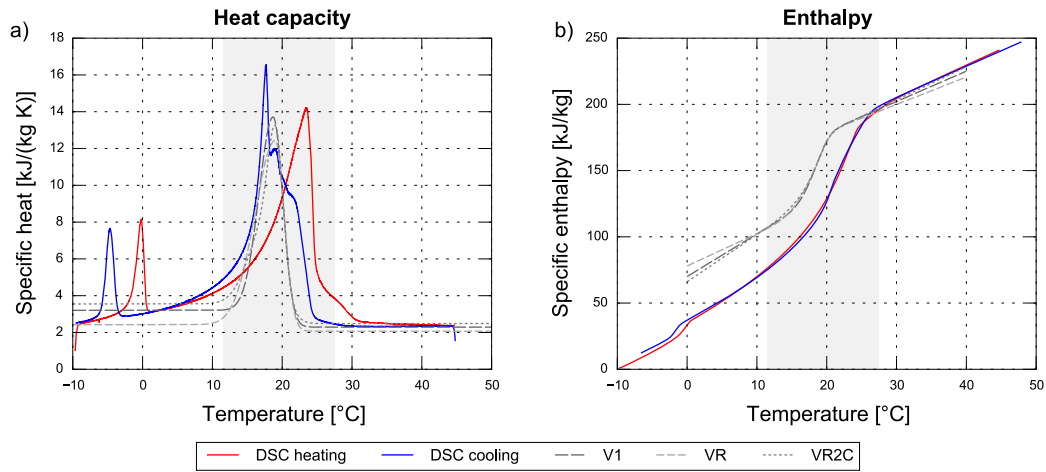
Fig. 5.3 a) Specific heat and b) specific enthalpy from DSC measurements vs inverse model.

Fig. 5.1b and Fig. 5.2b respectively for the dynamic and static plates. As it can be observed, they exhibit a certain degree of autocorrelation. This could be due to the modelling limitations of considering a functional form of the $c(T)$ curve and a constant thermal conductivity. In particular, the optimisation process can be expected to have compensated the effects deriving from the variability of thermal conductivity in solid and liquid states with those due to the dependency of the specific heat on temperature. The implementation of a model with variable thermal conductivity should therefore improve the results by removing a source of error in the estimation of the $c(T)$ curve. Moreover, modelling the melting and solidification processes with the same $c(T)$ curve may also lead to inaccuracies if a certain degree of hysteresis is present. Neglecting hysteresis did however provide satisfactory results; all fits were characterised by R^2 greater than 0.98 (Tables 5.1 and 5.2).

Heating and cooling $c(T)$ and $h(T)$ curves from a dynamic DSC measurement with a rate of 0.05 ℃/min are respectively shown in Fig. 5.3a and 5.3b, and compared with the curves resulting from the inverse problems. The grey portion of the graphics refers to the validity range of the fitted curves (between 11.5 ℃ and 27.5 ℃). The output values of the estimations (specific heat in solid and liquid phase, peak melting temperature, maximum specific heat, amplitude coefficients of the solidification/melting peak, and additionally contact resistances for the VR and VR2C case) are reported in Table 5.3. Moreover, the latent heat of fusion was evaluated according to the procedure reported in § 4.1.1. Additionally, to obtain information on the repeatability associated to the estimated values, mean and standard deviation were evaluated for several simulation runs (Table 5.4).

Although the low speed of the DSC measurement, a significant apparent hysteresis can be observed. A comparison between measured and simulated fluxes with specific heat data from the DSC is also reported in Fig. 5.1a and Fig. 5.2a. Only

Table 5.1 Goodness of fit of the heat flux densities on the dynamic plate.

Test	MBE $[\mathrm{W/m^2}]$	MAE $[\mathrm{W/m^2}]$	RMSE $[\mathrm{W/m^2}]$	R^2 $[-]$	Adj-R^2 $[-]$
DSC heating	-2.3	11.5	17.7	0.7819	
DSC cooling	-1.7	9.2	11.5	0.9069	
V1	0.37	2.5	3.4	0.9919	0.9918
VR	0.60	2.5	3.3	0.9922	0.9921
VR2C	0.57	1.6	2.4	0.9961	0.9959

Table 5.2 Goodness of fit of the heat flux densities on the static plate.

Test	MBE $[\mathrm{W/m^2}]$	MAE $[\mathrm{W/m^2}]$	RMSE $[\mathrm{W/m^2}]$	R^2 $[-]$	Adj-R^2 $[-]$
DSC heating	0.049	0.38	0.50	0.9260	
DSC cooling	0.042	0.37	0.44	0.9442	
V1	-0.0065	0.20	0.25	0.9822	0.9819
VR	-0.011	0.19	0.24	0.9835	0.9831
VR2C	-0.011	0.20	0.23	0.9846	0.9840

some portions of the curves were in agreement with the measured data. With MAE and RMSE on the dynamic plate respectively of 11.5 W/m^2 and 17.7 W/m^2 for simulations with the heating DSC curve, and 9.2 W/m^2 and 11.5 W/m^2 respectively for simulations with the cooling DSC curve, the errors were high. Much lower errors were observed on the heat flux densities exchanged with the lower plate. However, since higher fluxes were exchanged with the dynamic plate which was in direct contact with the PCM, there is less uncertainty on the heat fluxes exchanged with the dynamic plate than with the static plate. Moreover, an inverted bias trend was observed when using data from DSC measurements compared to the results from the inverse modelling (Tables 5.1 and 5.2).

The $c(T)$ from DSC measurements was compared to those resulting from the inverse modelling procedures to obtain qualitative indications on the possible interpretation of the DSC data (Fig. 5.3a). The estimated peak melting temperature was quite in agreement with the DSC solidification curve, whereas the maximum value of the specific heat was quite in agreement with the DSC melting curve. The nominal melting temperature (21.7 ℃) was higher than the estimated value (19.0 ℃ on average). The specific heat in liquid phase was slightly underestimated. It can be inferred that the upper temperature bound of the measurement should have been higher; with more data in full liquid state, the model could have provided a better fit. This is supported by the results reported in [24] from previous tests in the range 18–28 ℃, which were characterised by a specific heat in liquid phase in very good

Table 5.3 Estimated values of the unknowns of the inverse problems.

Test	T_p	c_s	c_l	c_m	w_s	w_l	R_{si}	R_{se}	L
	[℃]	[J/(kg K)]			[$-$]		[m^{2}K/W]		[kJ/kg]
V1	18.7	3203	2291	13725	2.86	1.94	-	-	76.3
VR	19.0	2421	2070	12435	4.13	1.79	0.05	0.25	86.1
VR2C	19.2	1701	1282	7603	1.56	1.36	0.12	0.12	72.1
	18.0	1849	1205	6439	3.71	2.67			

Table 5.4 Mean and standard deviation of the estimated values of the unknowns.

Test	T_p	c_s	c_l	c_m	w_s	w_l	R_{si}	R_{se}	L
	[℃]	[J/(kg K)]			[$-$]		[m^{2}K/W]		[kJ/kg]
Mean	19.0	2969	2268	13538	3.35	1.68	0.15	0.10	78.5
Dev. St.	0.4	379	258	548	0.41	0.25	0.05	0.08	2.7

agreement with the DSC data, but the left side of the peak melting temperature was missed. High discrepancies were observed between the specific heat values in solid phase, but no measurement data was actually available in the full solid state for the model to fit. Experimental tests which cover a wider temperature range should allow for a more comprehensive characterisation of the PCM.

By graphically comparing the results of the three types of fits (Fig. 5.3a and Fig. 5.3b), the $c(T)$ curves practically overlapped on the right side of the peak melting temperature, while a higher discrepancy was observed on the left side of the peak and on the c_m value. Even though this is far more evident in Fig. 5.3a, this discrepancy can be observed also in Fig. 5.3b. The three $h(T)$ curves however resulted to be very similar within the validity range of the fit, while they diverged outside the validity bounds. All the enthalpy-temperature curves obtained with the inverse method resulted to be shifted towards lower temperatures than those from DSC (Fig. 5.3b). This is in line with the results from Kuznik et al. [28]. However, due to the narrow measurement range, the latent heat of fusion retrieved by means of the inverse procedure might be underestimated. As it can be observed in [28], the
in the phase change range.

Moreover, no double peak was highlighted in the shape of the $c(T)$ curve despite the presence of multiple peaks on the apparent specific heat curve from the DSC in cooling mode. Although the VR2C provided the best fist among the three, adopting an increased number of variables resulted not to be worthy since the greater number of simulation runs did not lead to a significant improvement of the fit.

5.2 Component-level analyses

In the present section, the results of the parametric analyses presented in § 4.3.2 to investigate the influence of the PCM's thermo-physical properties on the proposed metrics for evaluating the dynamic thermal properties of opaque building envelope components with PCM (see § 4.3.1) are reported. The influence of wall orientation and configuration, PCM melting temperature, thickness and thermal conductivity and solar absorption coefficient of the external surface of the wall is discussed.

Then, the results of the component-level optimisation analyses presented in § 4.3.4 are reported. First, the Pareto fronts obtained for each location were analysed. Secondly, post-optimisation analyses were performed to investigate the properties of the optimised wall solutions.

5.2.1 Parametric analyses

The results of the parametric analyses described in § 4.3.2 are herewith discussed. For the sake of brevity, only a few representative graphics will be reported. These graphics can be divided in the following two categories: yearly profiles of the monthly Y_{mn}^* and Δt_{mn}^* values (taken as absolute value) and scatter plots of the yearly average values of Y_{mn}^* vs Δt_{mn}^*. The modulus of Y_{mn} and the corresponding time shift evaluated according to ISO 13786:2007 [5] are additionally reported in red in the scatter plots for the sake of comparison. The legend to all the plots in this section can be found in Fig. 5.4.

On one hand, the yearly profiles of the monthly Y_{mn}^* and Δt_{mn}^* values allow for a comprehensive understanding of the walls' behaviour, as the equivalent periodic thermal transmittance decreases and time shift increases during the months when the PCM undergoes phase transition. On the other hand, the scatter plots synthesise
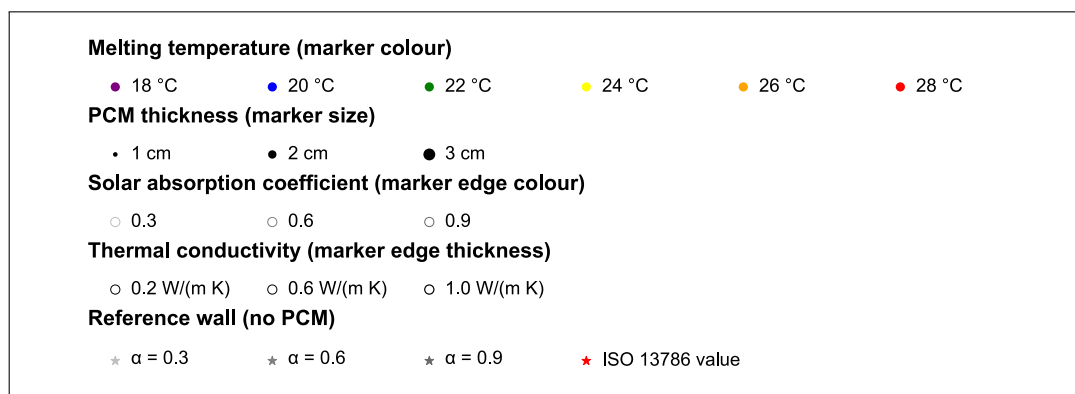
Fig. 5.4 Parametric analyses: legend.
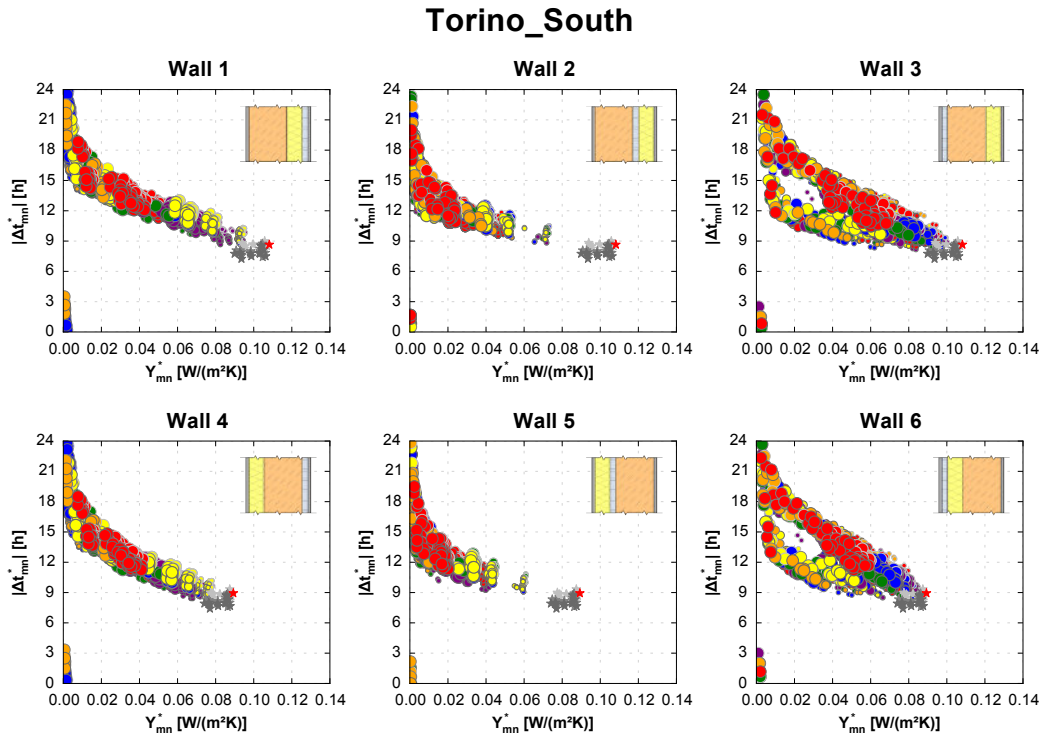
Fig. 5.5 Parametric analyses: monthly Y_{mn}^* vs $|\Delta t_{mn}^*|$. Torino, south.

the previous information on a yearly basis. When investigating the effect of the parametric variables on the yearly Y_{mn}^* and Δt_{mn}^* values, the slope and distance between points provide information on the magnitude of the influence of the selected variable on the equivalent dynamic thermal properties (low and high slopes are respectively associated to a high variation of Y_{mn}^* or Δt_{mn}^*).

A summary plot of the monthly Y_{mn}^* vs Δt_{mn}^* for all the values of the parametric variables is reported in Fig. 5.5 for the case of south-facing walls in Torino. The greatest variability in Y_{mn}^* was observed for PCM placed either towards the internal (Walls 1 to 3) or external (Walls 4 to 6) environment. When the PCM was placed within the wall, lower Y_{mn}^* were obtained even for the worst cases. With regard to the time shift, placing the PCM towards the internal environment tended to provide higher values compared to the other wall configurations. The greatest variability was instead observed when the PCM was placed on the outer side of the wall.

The detailed analysis of the effect of wall orientation and configuration, PCM's melting temperature and thermal conductivity, and eventually solar absorption coefficient is subsequently reported.

Palermo

Torino

Oslo
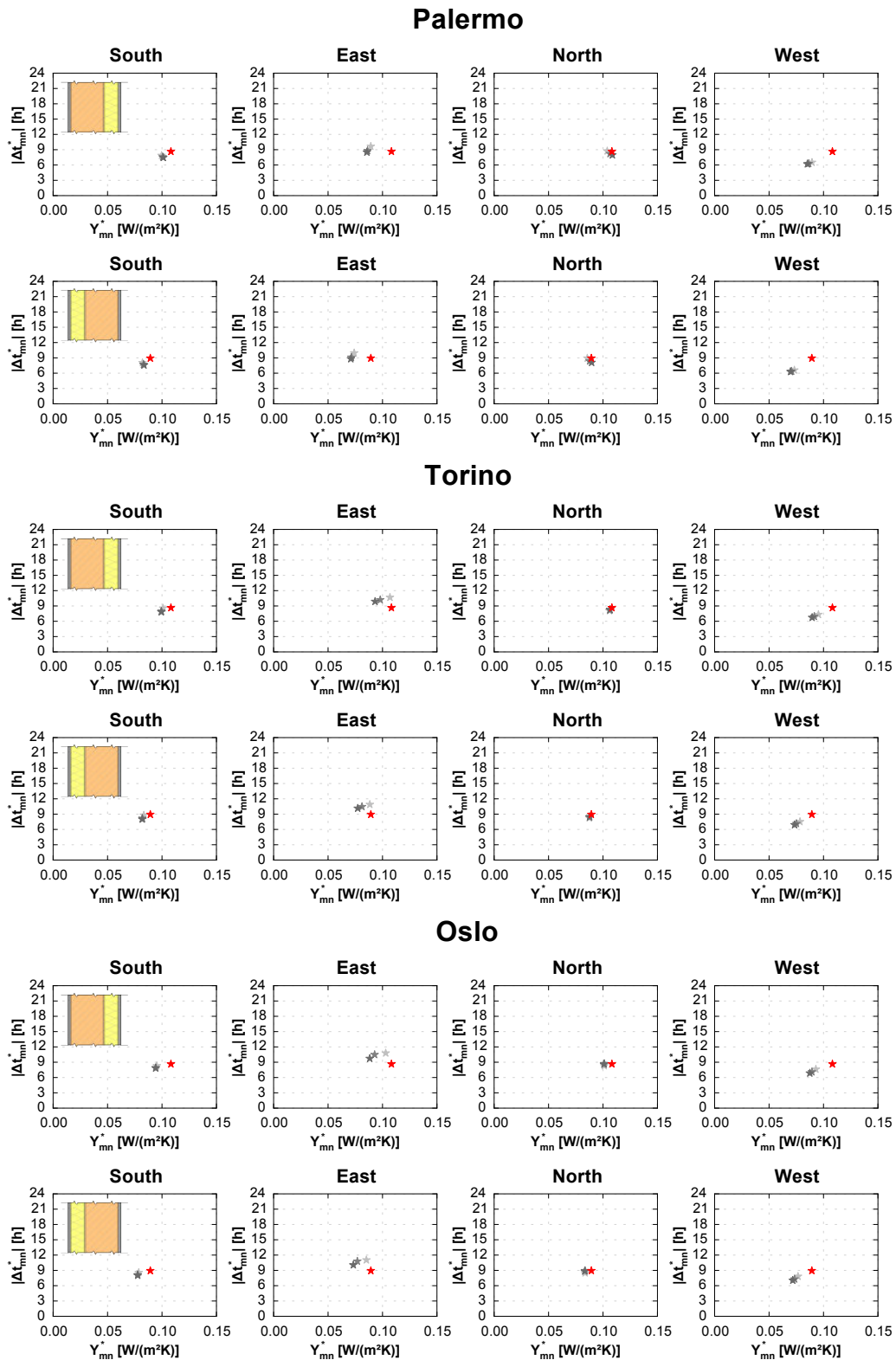
Fig. 5.6 Yearly effect of wall orientation.

5.2.1.1   Effect of wall orientation

The effect of the wall orientation on the equivalent dynamic thermal properties is analysed. In Fig. 5.6 a scatter plot of Y_{mn}^* vs Δt_{mn}^* is reported for reference walls without PCM and same U-value as those in Fig. 4.10. The traditional values of the modulus of Y_{mn} and corresponding time shift evaluated according to ISO 13786:2007 are also reported in red for comparison. The lowest difference with the corresponding equivalent values was observed for the north orientation, where the influence of solar radiation was the least. For all the other orientations, with the exception of the north walls in Palermo with α values of 0.9, the Y_{mn}^* values resulted to be smaller than Y_{mn}, especially for east and west exposition. With regard to the time shift, Δt_{mn}^* resulted to be significantly lower than Δt_{mn} for the west walls, slightly lower for south walls and almost unvaried for north walls, especially in Oslo. The solar absorption coefficient resulted to have the greatest impact on Y_{mn}^* of east facing walls in Torino and Oslo, where Δt_{mn}^* was instead found to be higher than Δt_{mn}, whereas in Palermo it was closer to the standard ISO value. These results are in agreement with the findings in [251, 349, 350].

5.2.1.2   Effect of wall configuration

The effect of the wall configuration on the equivalent dynamic thermal properties is analysed. Results are reported in Fig. 5.7 for the south orientation in Palermo and all the melting temperatures. When the PCM was fully solid, the lowest Y_{mn}^* values were obtained when the PCM was in mid position and the highest when it was placed towards the external environment. For each PCM placement, the lowest Y_{mn}^* was obtained with the external insulation layer. However, if the PCM curves are compared to their respective reference, Y_{mn}^* was reduced to a greater extent with internal insulation. The effect of the wall configuration on the time shift was very limited in absence of phase transition (as for the reference without PCM), whereas during the phase change process it was strongly dependent on PCM melting temperature and boundary conditions. When the PCM was placed towards the internal environment (Walls 1 and 4), as it could be expected a very good performance was obtained when the PCM melting temperature was close to the internal air temperature, whereas the more the PCM was close to the outer side of the wall, the more its performance improved with melting temperatures closer to that of the external environment. For example for the climate of Palermo, a melting temperature of 18 ℃ was effective during winter when the PCM was placed towards the outdoor environment, whereas it was completely melted on the inner side of the wall. A melting temperature of 20 ℃ was effective during winter when the PCM was placed towards the indoor environment because the PCM melting temperature corresponded to the internal set-point temperature. If placed on the outer side of the wall, the same PCM was more effective during mid season. Melting
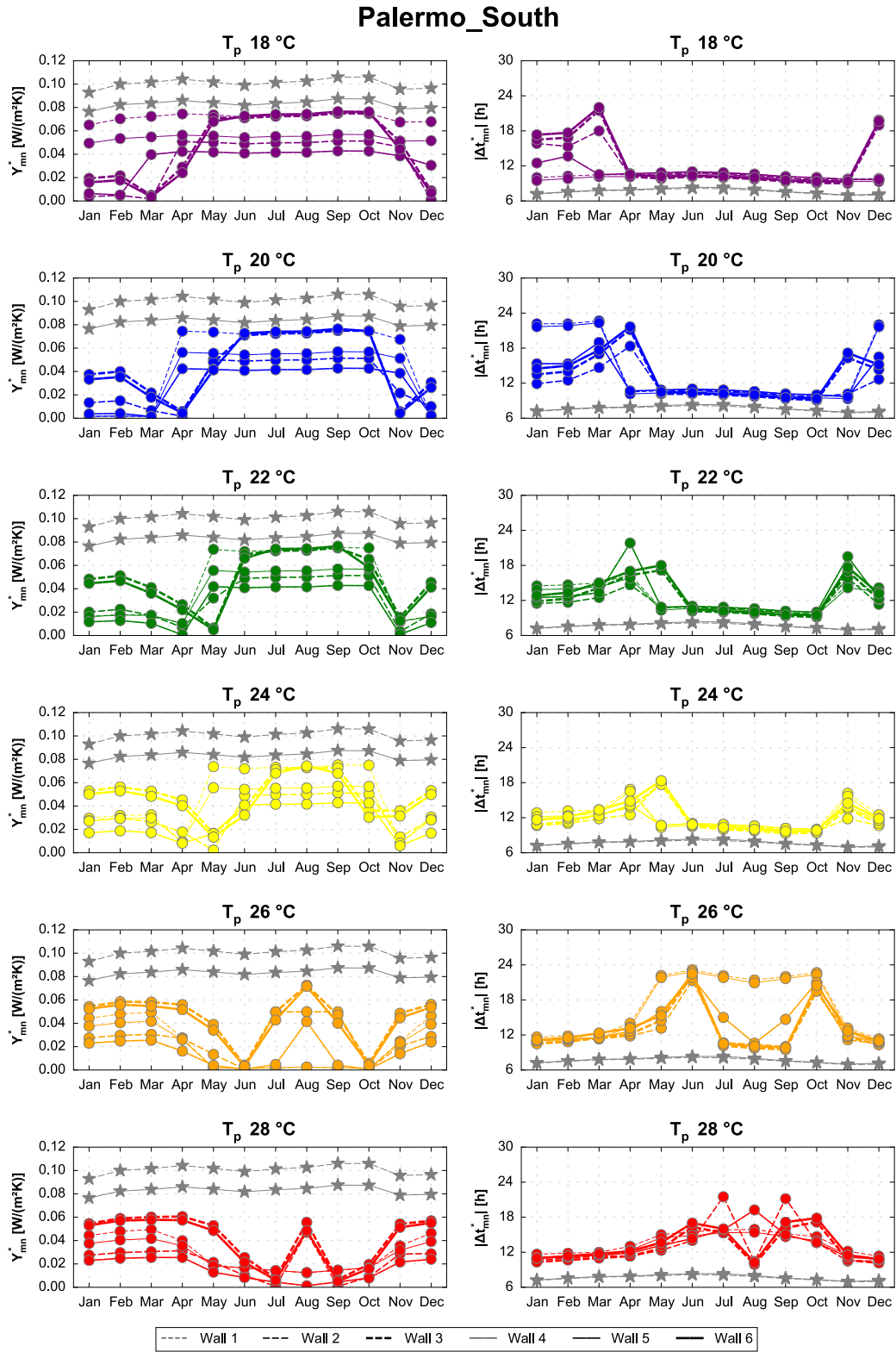
Palermo_South

Fig. 5.7 Effect of wall configuration (t_{PCM}=2 cm, k=0.2 W/(m K), α=0.6). Palermo, south.

temperatures of 22 ℃ and 24 ℃ were effective almost only during mid season, and the best wall configuration changed according to the month. A melting temperature of 26 ℃ was effective during the summer if the PCM was placed towards the indoor environment, when the PCM melting temperature corresponded to the internal set-point temperature. It was also effective during early and late summer for other wall configurations but it was always melted during the hottest months. A melting temperature of 28 ℃ was mostly effective during the summer for PCM in mid position, but only in Wall 5 it did not undergo complete melting in August.

5.2.1.3   Effect of PCM melting temperature

The yearly effect of melting temperature and PCM thickness on the equivalent dynamic thermal properties was analysed. Monthly results are reported for the south orientation in Fig. 5.8, Fig. 5.9 and Fig. 5.10 respectively for the climates of Palermo, Torino and Oslo, while the corresponding yearly plots are respectively reported in Fig. 5.11, Fig. 5.12 and Fig. 5.13. Obviously, climate, location and thickness of the PCM layer influenced the wall performance. The solar absorption coefficient had also a significant effect when the PCM was close to the external environment (see § 5.2.1.5). For a clear understanding of the wall's behaviour throughout the year, the monthly values of Y^*_{mn} and Δt^*_{mn} provide more comprehensive and construable information as described in § 5.2.1.2. However, the yearly average values give concise information to identify the best trade off temperature between winter and summer behaviour. With this regard, if the monthly plots are analysed (especially for Walls 1 and 3 when the PCM was placed on the internal side) a potential improvement in the yearly equivalent periodic thermal transmittance could be expected by a seasonal change in the PCM melting temperature (adoption of two melting temperatures close to the winter and summer set point temperatures).

In general, higher time shifts were obtained when the PCM was placed on the internal side (Walls 1 and 3), whereas the lowest yearly Y^*_{mn} values were obtained for PCM in mid position (Walls 2 and 5). However, the lowest yearly Y^*_{mn} for each wall configuration did not always correspond to the highest time shift. When the combined effect of PCM thickness and melting temperature is analysed, for 1 cm of thickness the melting temperature was found to have a significant influence on both Y^*_{mn} and Δt^*_{mn} when the PCM was placed towards the internal environment, whereas little and negligible influences were observed respectively for PCM in mid and external position. For layers of 2 cm and 3 cm of PCM, when placed on the internal side the melting temperature had a greater effect on the time shift for those PCMs which significantly underwent phase transition. The difference among melting temperatures on the other wall configurations was still limited. The melting temperature which guaranteed the lowest Y^*_{mn} was found to be dependent on the PCM thickness.
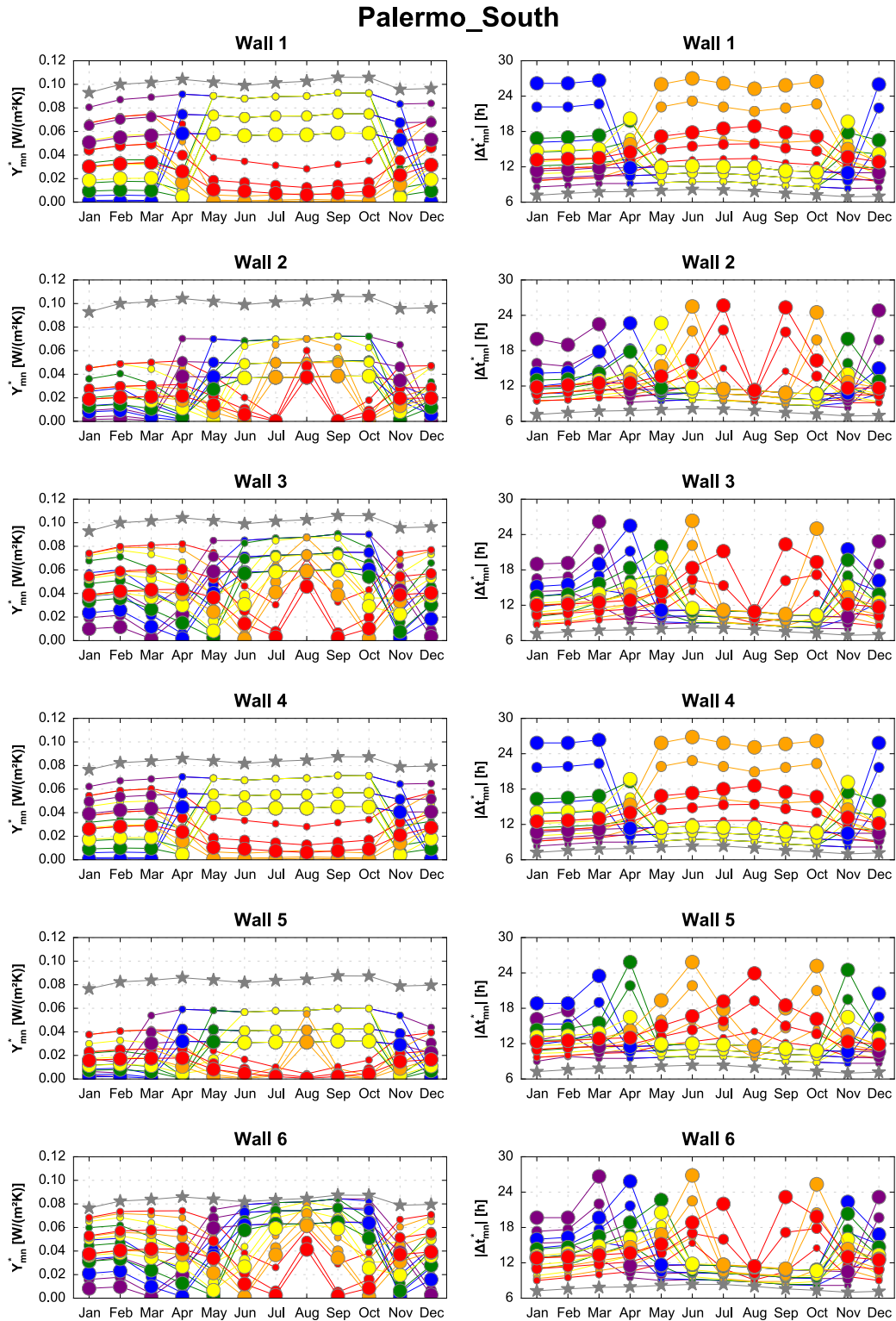
Palermo_South

Fig. 5.8 Monthly effect of T_p and t_{PCM} (k=0.2 W/(m K), α=0.6). Palermo, south.

Fig. 5.9 Monthly effect of T_p and t_{PCM} (k=0.2 W/(m K), α=0.6). Torino, south.
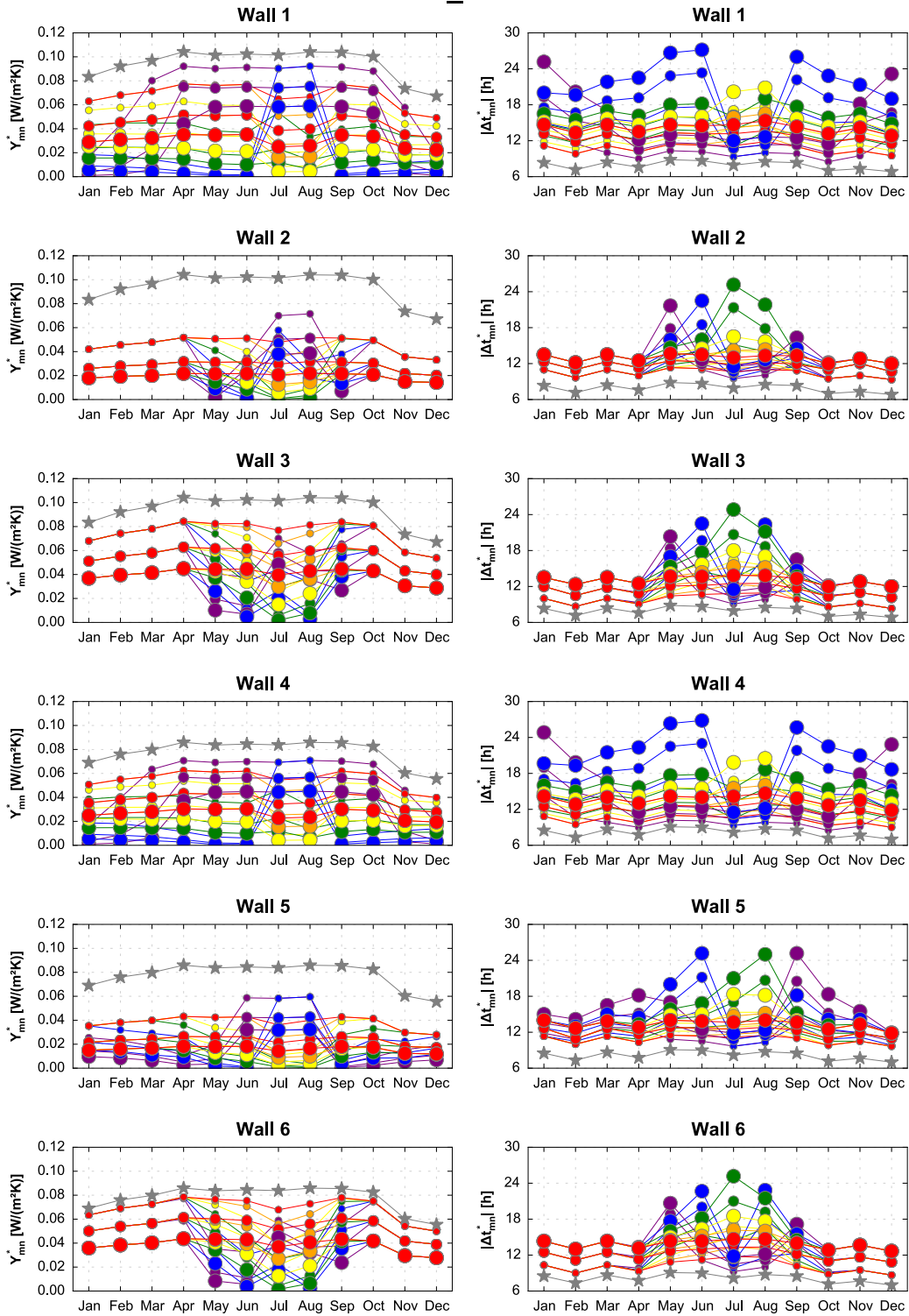
Oslo_South

Fig. 5.10 Monthly effect of T_p and t_{PCM} (k=0.2 W/(m K), α=0.6). Oslo, south.

Palermo_South

Fig. 5.11 Yearly effect of T_p and t_{PCM} (k=0.2 W/(m K), α=0.6). Palermo, south.
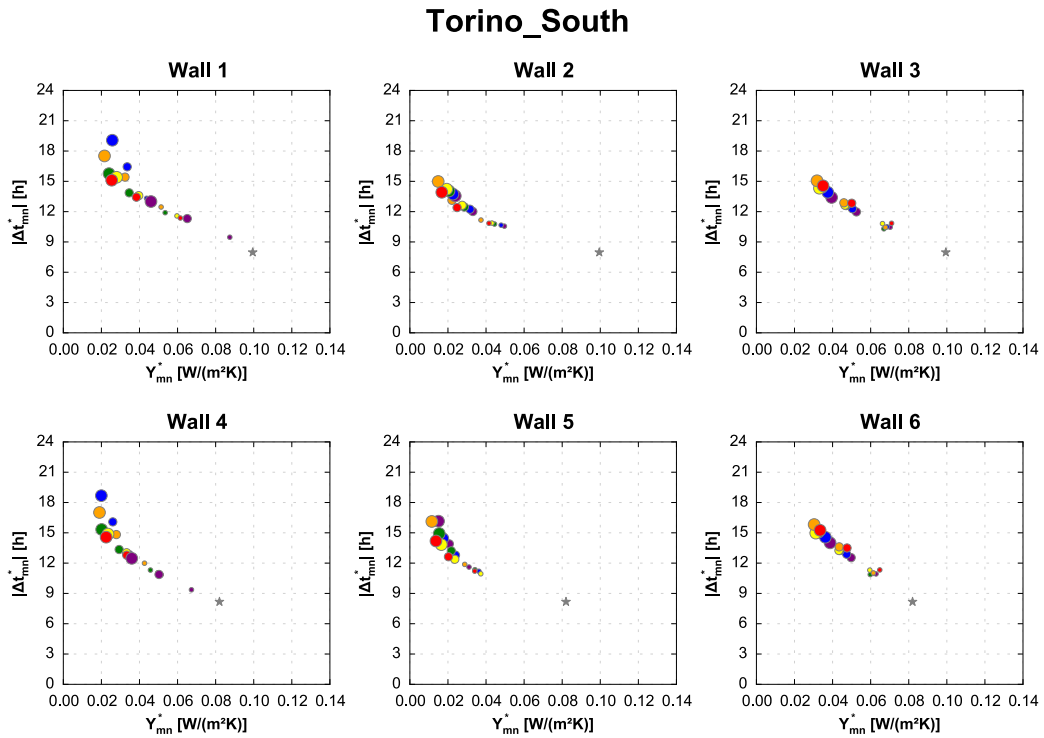
Torino_South

Fig. 5.12 Yearly effect of T_p and t_{PCM} (k=0.2 W/(m K), α=0.6). Torino, south.
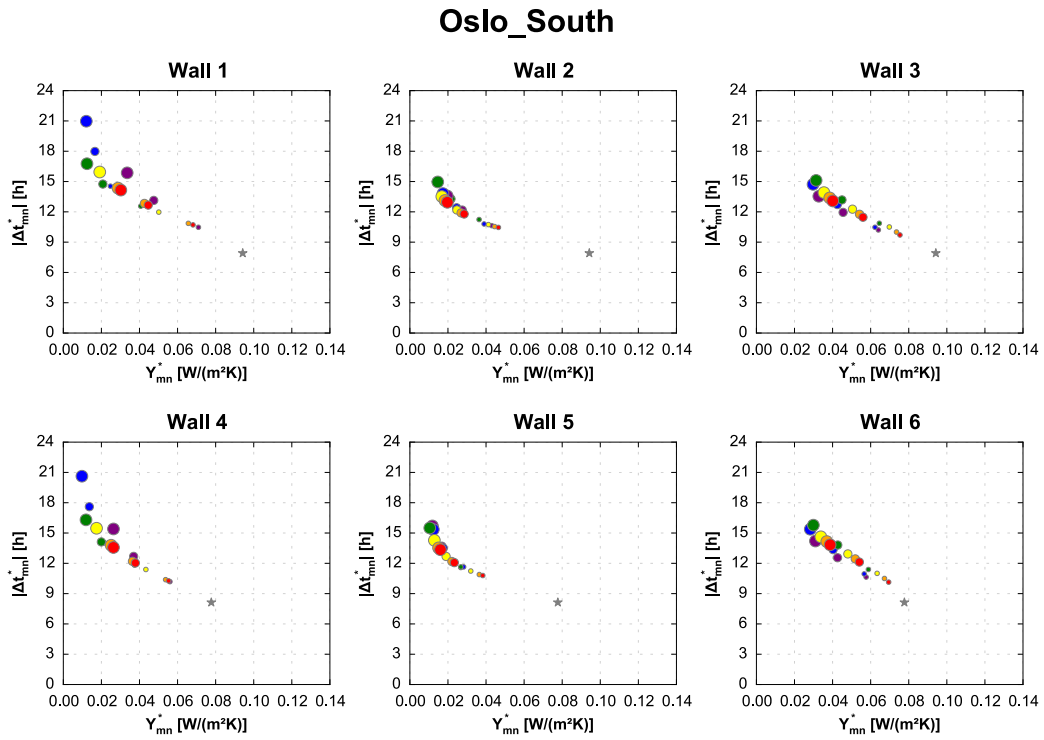
Oslo_South

Fig. 5.13 Yearly effect of T_p and t_{PCM} (k=0.2 W/(m K), α=0.6). Oslo, south.
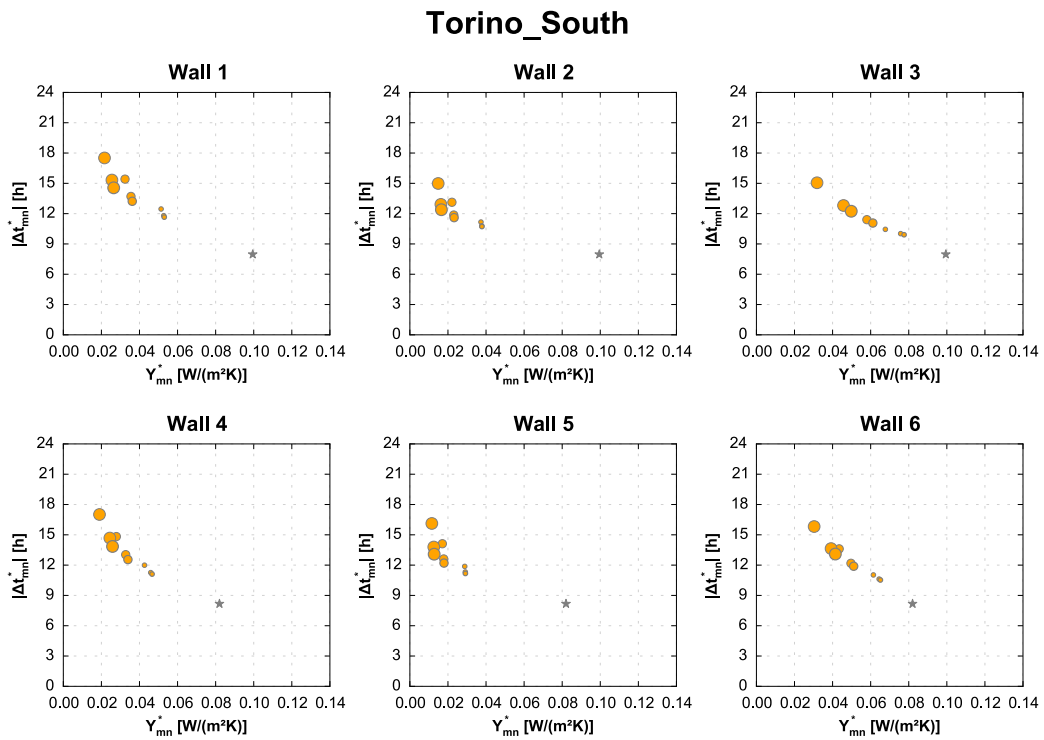
Torino_South

Fig. 5.14 Yearly effect of k and t_{PCM} (T_p=26 ℃, α=0.6). Torino, south.

5.2.1.4 Effect of thermal conductivity

The effect of the thermal conductivity on the equivalent dynamic thermal properties is analysed. Since no significant differences were detected between location and orientation, only Fig. 5.14 and Fig. 5.15 are reported. As the heat transfer is influenced by the thermal resistance of the layers within a wall, the thermal conductivity had a greater influence the thicker the PCM layer (Fig. 5.14). Decreasing the thermal conductivity of the PCM always resulted in a decrease of the equivalent periodic thermal transmittance and an increase in time shift. The influence of the thermal conductivity on Y_{mn}^* was however negligible when the PCM was placed between mass and insulation (Walls 2 and 5), still limited when the PCM was placed towards the indoor environment (Walls 1 and 4) (only k = 0.2 W/(m K) could be clearly distinguished from the other curves), whereas it was more significant when the PCM was placed towards the outdoor environment (Walls 3 and 6) (Fig. 5.14). However, during the months when the PCM underwent phase transition, the influence of thermal conductivity on the time shift was significant for every PCM position. Considering that very high time shifts are not necessarily desirable, optimising the thermal conductivity of thick PCM layers could prove useful.

5.2.1.5 Effect of solar absorption coefficient

The effect of the solar absorption coefficient on the equivalent dynamic thermal properties is analysed. Results are reported in Fig. 5.16 for the south orientation in Palermo and all the melting temperatures. Since solar radiation is concerned, results varied according to the wall orientation. Obviously, the solar absorption coefficient had almost no effect when the PCM was placed towards the indoor environment, but its influence increased as the PCM layer moved towards the exterior. For Walls 2 and 5 the effect on Y_{mn}^* was still quite limited, but a significant increase of time shift was observed when the PCM underwent phase transition. However, on a monthly basis there was not a constant trend, as the effect of the solar absorption coefficient was strongly affected by PCM melting temperature and boundary conditions. According to the month, the same PCM could have been more effective (lower Y_{mn}^* and hence higher Δt_{mn}^*) with a low α (high values would have caused the PCM to remain mostly liquid) or with a high α (low values would have caused the PCM to remain mostly solid). This can be verified e.g. for the melting temperature of 28 ℃ (red dots) in Walls 3 and 6; between June and July the effect of α was inverted. Hence, a direct analysis of the yearly values of Y_{mn}^* and Δt_{mn}^* would be of difficult interpretation. This strong variability on how the solar absorption coefficient affected the equivalent dynamic thermal properties suggests that the more the PCM is placed towards the outdoor environment, the more its melting temperature should be optimised according to the solar absorption coefficient and vice versa. In new buildings, a combined optimisation can be advisable.
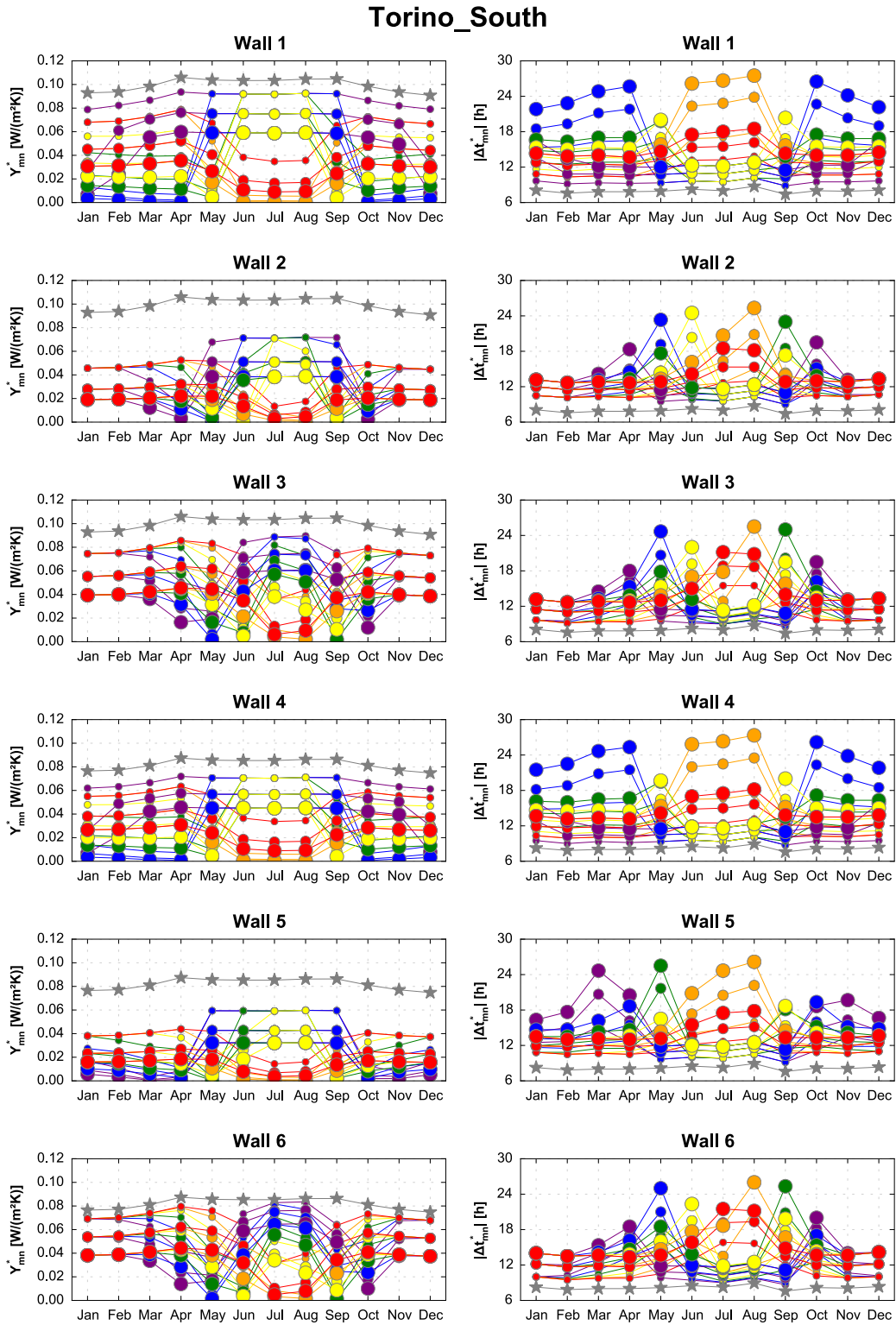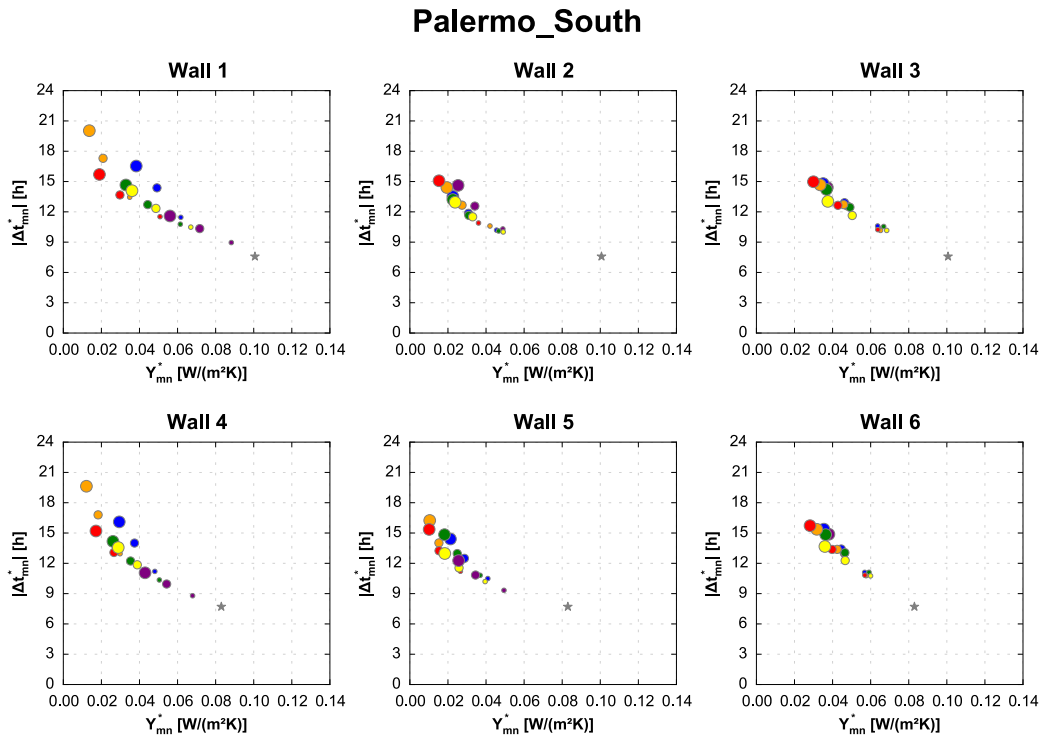
Torino_South
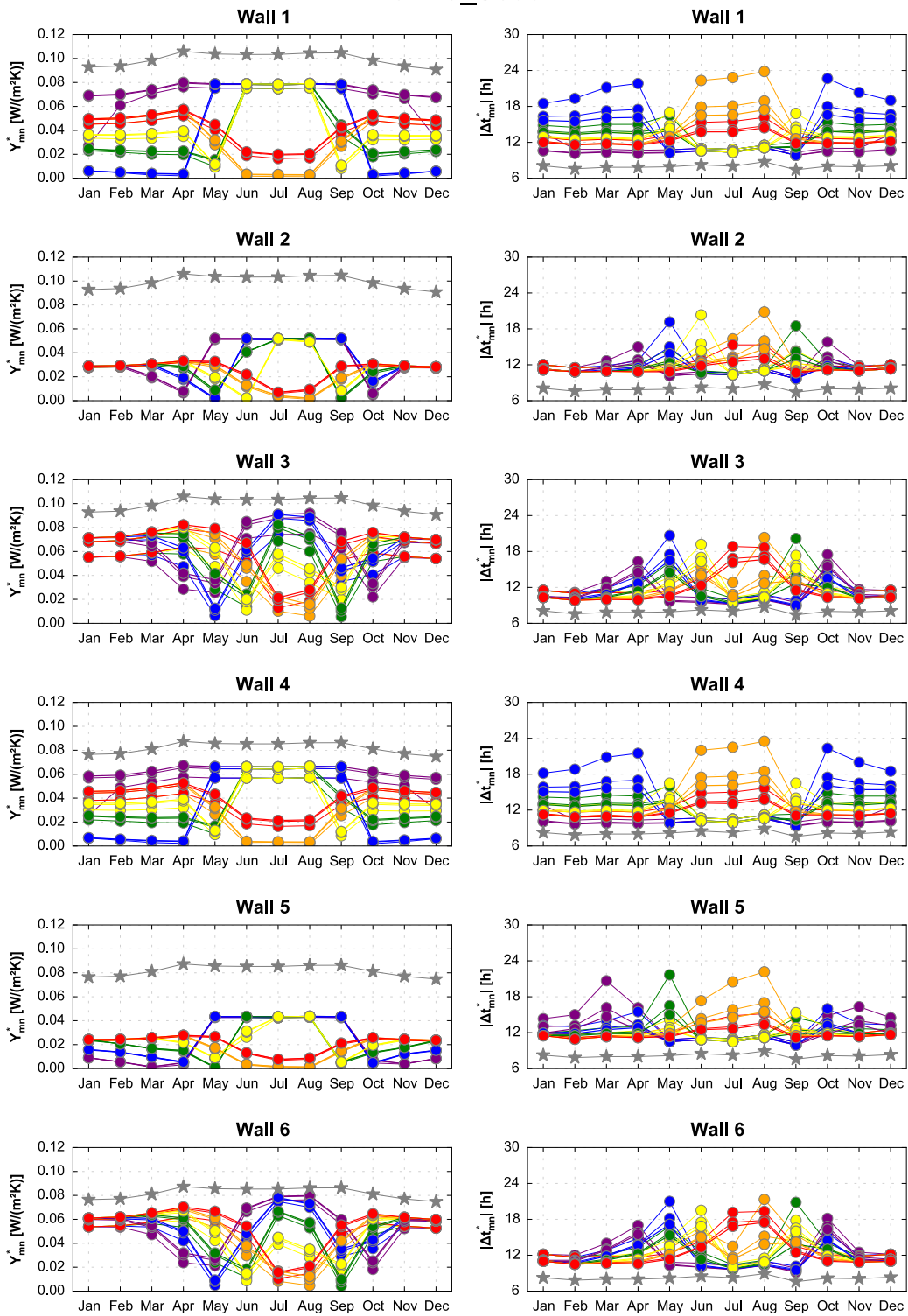
Fig. 5.15 Monthly effect of k and T_p (t_{PCM}=2 cm, α=0.6). Torino, south.
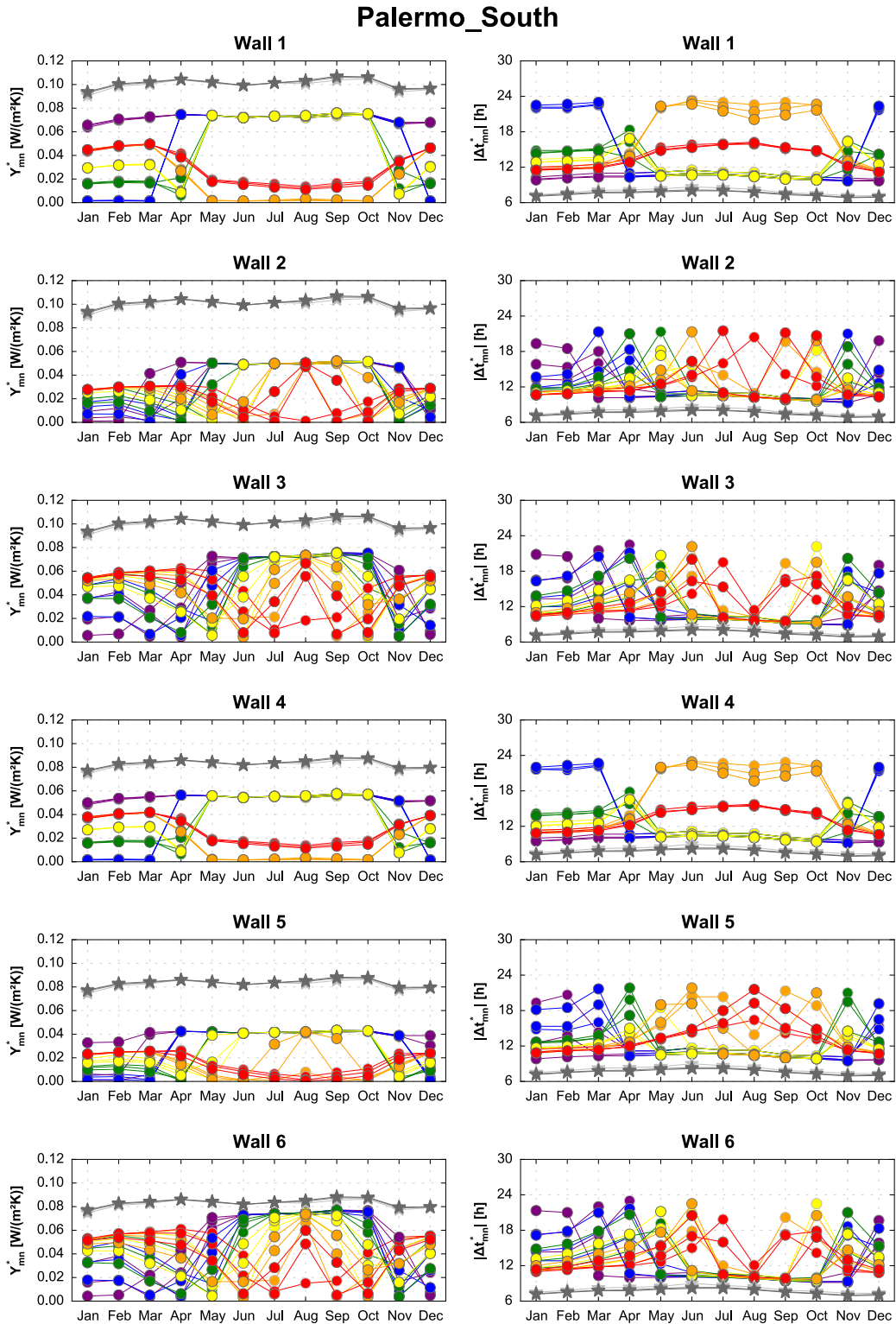
Fig. 5.16 Monthly effect of α and T_p (t_{PCM}=2 cm, k=0.2 W/(m K)). Palermo, south.

5.2.2   Pareto frontiers

The Pareto fronts of the component level investigations are reported in Fig. 5.18, Fig. 5.19 and Fig. 5.20 respectively for the climates of Palermo, Torino and Oslo. The three-dimensional fronts for all the orientations are represented together with the two-dimensional projections on each plane, where the big dots highlight the bi-dimensional Pareto front.

For all the locations, the non-dominated sets for each orientation were extremely similar, almost overlapping. However small, the greatest differences could be observed in Palermo, where the west and east fronts were shifted closer to the zero of Y^*_{mn} than the south and north fronts (this is in line with the results of the parametric analyses in § 5.2.1.1). As it could be expected, a certain degree of contrast was found between Y^*_{mn} and both PCM and wall thickness. No contrast was instead observed between PCM and wall thickness, as only one point belonged to the bi-dimensional Pareto front between these objectives.

The fitnesses of the extreme solutions are reported in Table 5.5, Table 5.6 and Table 5.7 respectively for the climates of Palermo, Torino and Oslo. Solution A is characterised by the lowest equivalent periodic thermal transmittance. Due to the contrast between objectives, it is also the solution with highest PCM and wall thickness. Solution B is characterised by the lowest equivalent periodic thermal transmittance achieved with no PCM, whereas Solution C is the solution with the lowest wall thickness. It is also characterised by the absence of PCM and the highest equivalent periodic thermal transmittance. It can be noted that in Palermo, according to the Italian standards [308], Y_{mn} should be lower than 0.10 W/(m^{2}K) for vertical walls (except those facing NW-N-NW). This value was verified by Y^*_{mn} for all the Pareto front solutions.

Observing the inter-climate differences, it stands out that the variability of Y^*_{mn} within the Pareto front increased for warmer climates, while for cold climates it was almost negligible being already extremely close to zero. Moreover, the zone between the solutions in the group of B's and those in the in the group of A's grew steeper the colder the climate, showing an asymptotic behaviour. The reason for this is that the colder the climate and the lower the U-value, the less significant is the evaluation of dynamic thermal properties, as the component's behaviour is close to steady-state conditions. Moreover, as the heat flux profiles in steady periodic conditions oscillate around the same average value, low Y^*_{mn} values have an implication on the sizing of the systems and on thermal comfort.

For each orientation, the edge of the Pareto front between solutions in the group of C's and those in the group of B's was characterised by an increasing mass thickness from the lower to the upper bound, and it spanned the greatest variation in Y^*_{mn}. Considering the distance between the solutions in the group of C's and those in the group of B's, the importance of massive layers for warm climates was
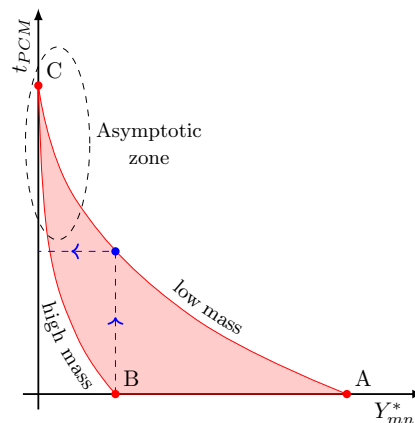
Fig. 5.17 General structure of the Pareto fronts.

highlighted. Given the very low values of Y_{mn}^* already achieved by the solutions in the group of B's, only a small improvement was obtained when adding PCM to such optimised walls, spanning from the solutions in the group of B's and those in the in the group of A's. Within the whole range of variation of Y_{mn}^*, the improvement that could be achieved without PCM was estimated to be about 80% in Palermo, 88% in Torino, and 89% to 92% in Oslo.

The effect of the PCM was much more significant when considering the impact on the overall wall thickness, especially in Palermo. Wall thickness in Torino resulted to have a smaller effect, and it was practically negligible in Oslo. If the Pareto front were cut by a plane passing for solution B and parallel to the thicknesses plane (Fig. 5.17), according to the orientation it could be observed that the same Y_{mn}^* of solution B could approximately be achieved either by 25 cm of mass (upper bound) and no PCM, or by 10 cm of mass (lower bound) plus 3 cm to 4 cm of PCM in Palermo, 5 cm in Torino and 2 cm to 4 cm in Oslo. Moreover, the steepness of the front showed, on one hand, that the more the PCM, the less the influence of the traditional massive layers, as very similar Y_{mn}^* values could be achieved almost regardless of the mass thickness. On the other hand, a limit on the PCM thickness beyond which no significant improvement could be obtained was highlighted. Overall, whether the wall was massive or lightweight, limits of approximately 6 cm, 4.5 cm and 2 cm were respectively identified in Palermo, Torino and Oslo.

To summarise, the PCM seemed to show its greatest potential in warm climates where low values of Y_{mn}^* could be obtained while reducing the wall thickness. This could be especially useful for retrofit applications. However, these results need to be confirmed at a higher scale. These component-level analyses have the limitation of considering steady-periodic boundary conditions and of not taking the interactions between orientations and other building elements or occupants into account.
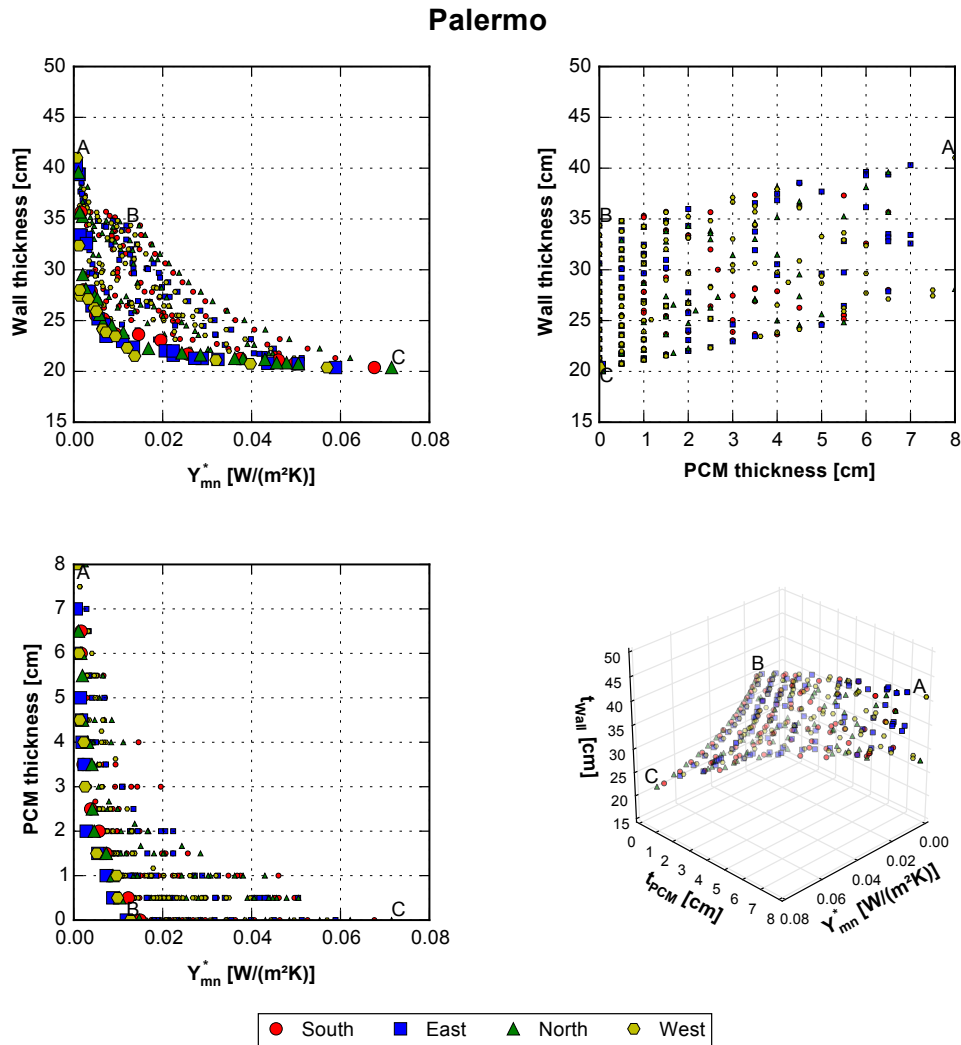
Palermo

Fig. 5.18 Pareto fronts: Palermo.

Table 5.5 Fitness of the extreme solutions: Palermo.

Solution	Y^*_{mn} [W/(m²K)]	t_{PCM} [cm]	t_{Wall} [cm]	Y^*_{mn} [W/(m²K)]	t_{PCM} [cm]	t_{Wall} [cm]
		South			**East**	
Solution A	0.00164	6.5	35.7	0.000564	7.0	40.3
Solution B	0.0149	0	34.4	0.0118	0	34.4
Solution C	0.0676	0	20.4	0.0589	0	20.4
		North			**West**	
Solution A	0.00105	6.5	39.6	0.000658	8.0	41.0
Solution B	0.0147	0	34.4	0.0128	0	34.4
Solution C	0.0715	0	20.4	0.0570	0	20.4
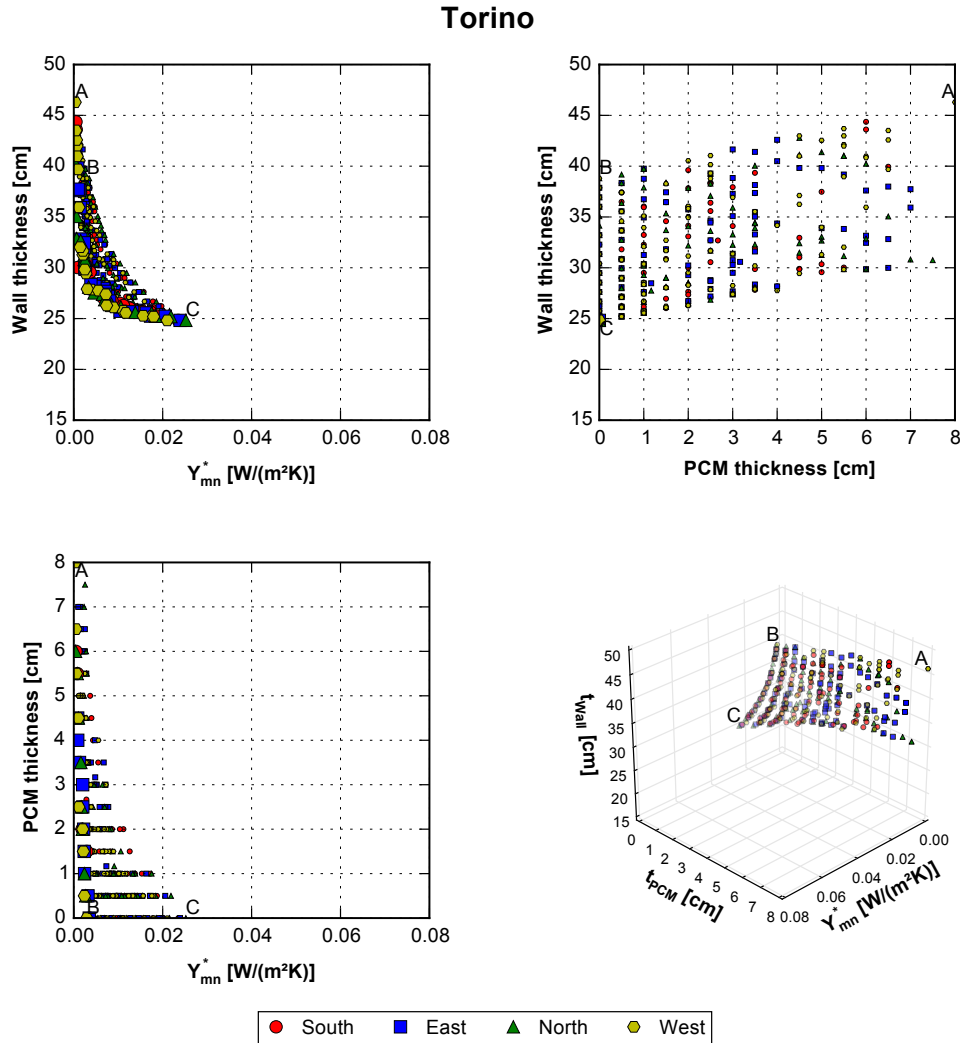
Torino

Fig. 5.19 Pareto fronts: Torino.

Table 5.6 Fitness of the extreme solutions: Torino.

Solution	Y^*_{mn} $[\mathrm{W/(m^2K)}]$	t_{PCM} [cm]	t_{Wall} [cm]	Y^*_{mn} $[\mathrm{W/(m^2K)}]$	t_{PCM} [cm]	t_{Wall} [cm]
	South			**East**		
Solution A	0.000497	6.0	44.4	0.000878	4.5	39.8
Solution B	0.00355	0	37.9	0.00347	0	37.9
Solution C	0.0235	0	20.8	0.0239	0	24.8
	North			**West**		
Solution A	0.000403	6.0	40.2	0.000300	8.0	46.3
Solution B	0.00346	0	38.8	0.00293	0	38.8
Solution C	0.0252	0	24.8	0.0210	0	24.8
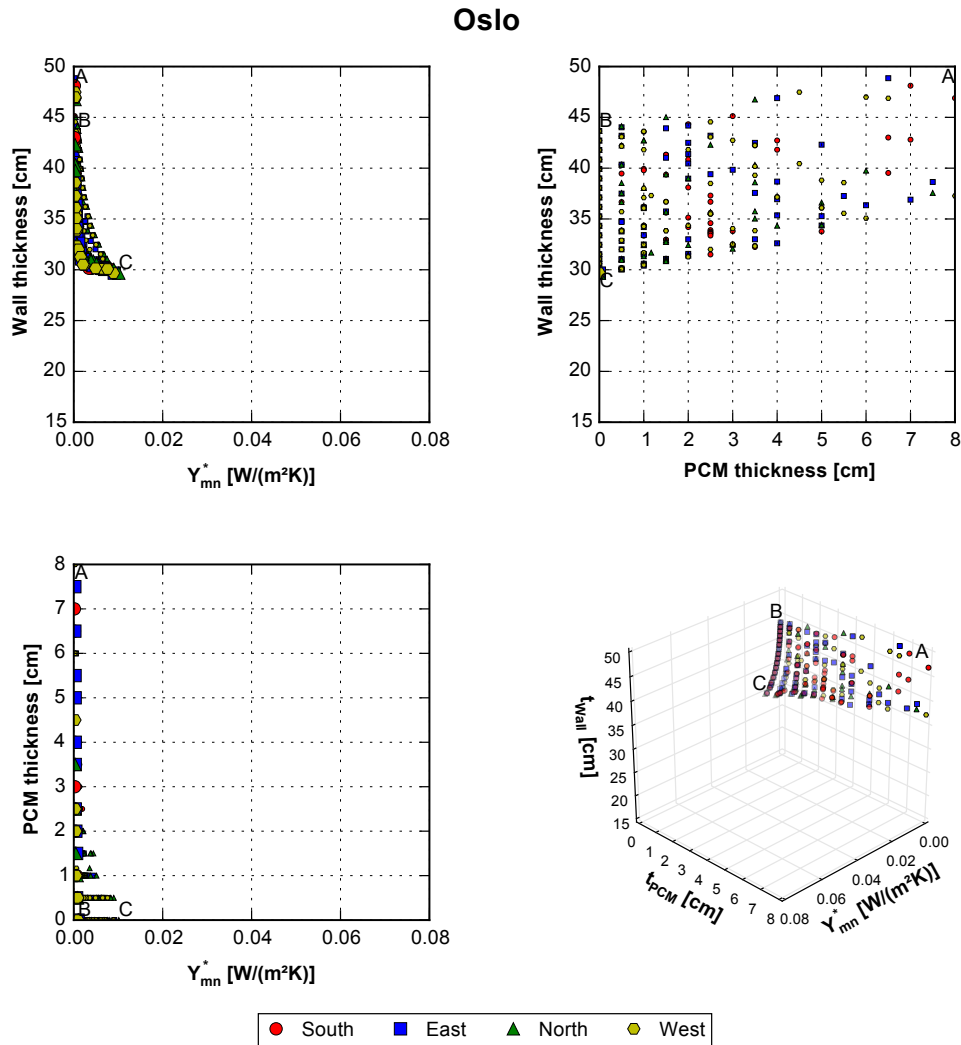
Oslo

Fig. 5.20 Pareto fronts: Oslo.

Table 5.7 Fitness of the extreme solutions: Oslo.

Solution	Y^*_{mn} $[\mathrm{W/(m^2K)}]$	t_{PCM} [cm]	t_{Wall} [cm]	Y^*_{mn} $[\mathrm{W/(m^2K)}]$	t_{PCM} [cm]	t_{Wall} [cm]
		South			**East**	
Solution A	0.000127	7.0	48.1	0.000231	7.5	38.6
Solution B	0.00113	0	42.7	0.000951	0	43.7
Solution C	0.00905	0	29.7	0.00910	0	29.7
		North			**West**	
Solution A	0.000276	3.5	46.8	0.000253	4.5	47.5
Solution B	0.00109	0	43.7	0.000953	0	43.7
Solution C	0.0101	0	29.7	0.00895	0	29.7

5.2.3   Post-optimisation analyses

As the analysis of the Pareto fronts focused on the results in the objective space, the post-optimisation analyses (see § 3.3) focused on the results in the search space. These analyses were meant to investigate which combination of variables lead to the optimal solutions, in order to find design principles and common trends among the various case studies.

For this purpose, a series of graphical analyses were carried out. Frequency analyses of the number of layers within the Pareto front solutions, as well as of the number of layers chosen for each material, were performed. The layers' distribution within the walls was also investigated. Box plots and frequency analyses of the variables belonging to the non-dominated sets were represented to find their range of variability and possible constant values.

Moreover, the values assumed by each variable were mapped on the Pareto front, in order to explore how the search space variables affected the results in the objective space. Due to the vast amount of graphs, the variables' mapping on the Pareto front are reported in Appendix B.

The extreme solutions of the Pareto front reported in § 5.2.2 were also depicted. Wall layouts were represented with the external environment on their left and the internal environment on their right. Even though the GA is likely to have failed in finding the true optimal solutions for each objective, the information retrieved from the analyses of the Pareto solutions allow to devise the properties of further improved solutions.

Eventually, the relationship between monthly equivalent periodic thermal transmittance and corresponding time shift (taken as absolute value) of the extreme solutions was concisely illustrated. Additional values representing a variety of mutual positions of mass and insulation layers evenly distributed within the wall was also reported for the sake of comparison (Fig. 4.17). These wall configurations were characterised by the same amount of insulation and mass (equal to the upper bound), and no PCM (see § 4.3.5). Periodic thermal transmittance and time shift of these wall configurations were reported both in terms of monthly equivalent values and traditional values according to ISO 13786:2007.

5.2.3.1   Palermo

The optimal solutions in Palermo will be herewith discussed.

Frequency analyses of the number of layers within the Pareto front solutions are reported for each orientation in Fig. 5.21. Almost 40% of solutions were characterised by seven layers (computed with the exception of external render and internal plaster) except in the east façade, where six layers were mostly adopted. The number of

layers selected for each material is detailed in Fig. 5.22. A clear preference over three layers of insulation was highlighted for all the orientations, and especially in the south and west façades (almost 80% of solutions). In the east and north walls, and to a good extent also in the south wall, the probability of finding three layers of insulation was practically equal to that of finding two layers of mass. The reason for this will soon be evident. With regard to the PCM, being Palermo a cooling-dominated climate, PCM2 was generally preferred over PCM1. More often than not, at least one layer of PCM2 was added in all the orientations, whereas PCM1 was generally preferred not to be used except on the west façade, where one layer was more often selected. Considering that seven layers were mostly chosen, two of which being mass and three being insulation, it could be inferred that two layers of PCM were often selected, regardless of the PCM type.

Details on the layers' distribution within the walls with 5 to 8 layers are shown in Fig. 5.23 and Fig. 5.24. When 5 layers were chosen (approximately 15% to 20% of the Pareto front), three layers of insulation alternated with two layers of mass were selected for almost all the solutions in all the orientations. This is in agreement with the findings of Al-Sanea and Zedan [252], which optimised the distribution of the insulation within a wall characterised by constant R-value and thermal mass. When 6 or more layers were chosen, PCM started to be used to a much larger extent. In the south exposition, PCM2 was mostly placed as the innermost layer or just before. PCM1 was used more scarcely and placed mostly after the external insulation layer (layer 2) or in intermediate positions. The reason for this will be detailed in the analysis of the extreme solutions. In the east exposition with a large number of layers, a much clearer preference for PCM1 in position 2 was observed. With growing number of layers, it was often used also in the last three layers towards the internal environment, while PCM2 was often used also in intermediate positions. In the north exposition, the outermost layer was always insulation, followed mostly by mass or by PCM1. As for the other expositions, a clear preference for PCM in the innermost layers was observed. In the west exposition, PCM1 was used mostly in intermediate positions, while PCM2 was again preferred in the innermost layers. In general, as the PCM was placed in the inner layers, the mass was placed more towards the external environment just after the outermost insulation. The alternating trend between insulating and massive/PCM layers was always present.

To have an overview of the values assumed by the continuous variables within the Pareto front, box plots are reported in Fig. 5.25. Although it was not an optimisation variable, the insulation thickness was also included in the analyses. As it can be inferred from its very small interquartile range, all the solutions in all the orientations were characterised almost by the same peak melting temperature of PCM2. A median value of 27 ℃ was observed for all the orientation with the exception of the north-facing walls, where 26.5 ℃ was found. Even though the peak
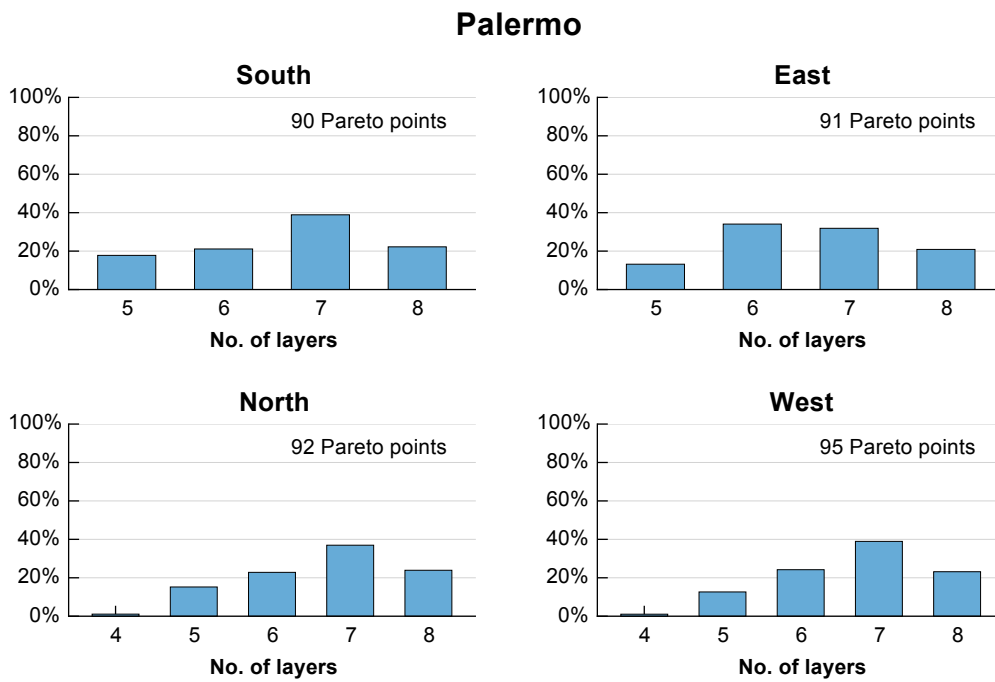
Palermo

Fig. 5.21 No. of layers within the Pareto front solutions: Palermo.
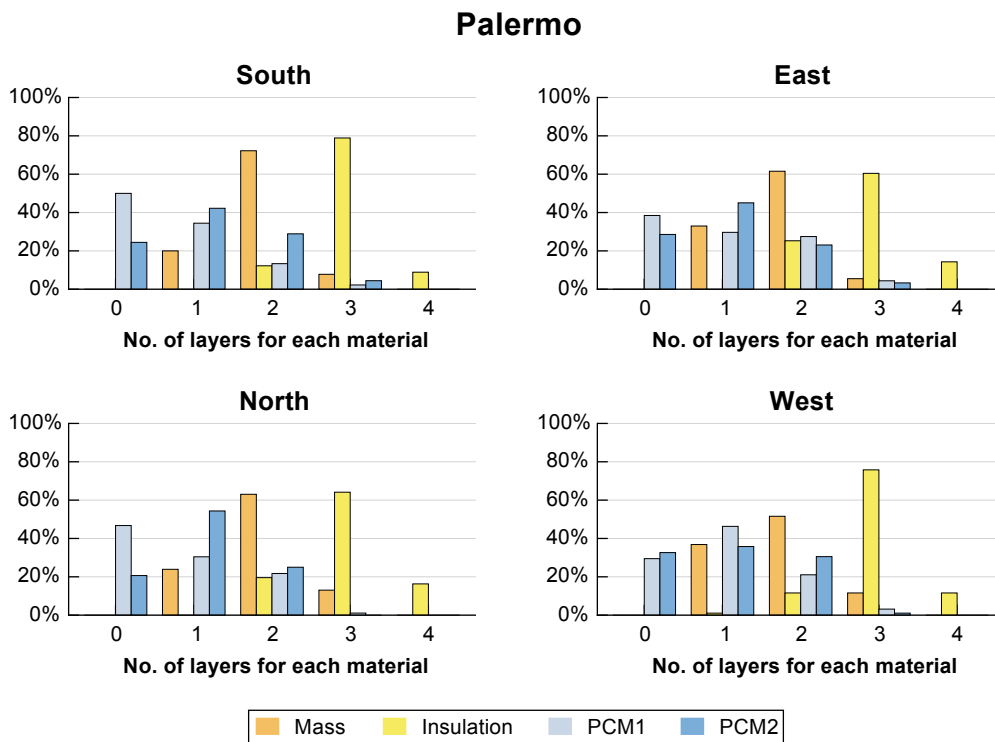
Palermo

Fig. 5.22 No. of layers for each material within the Pareto front solutions: Palermo.
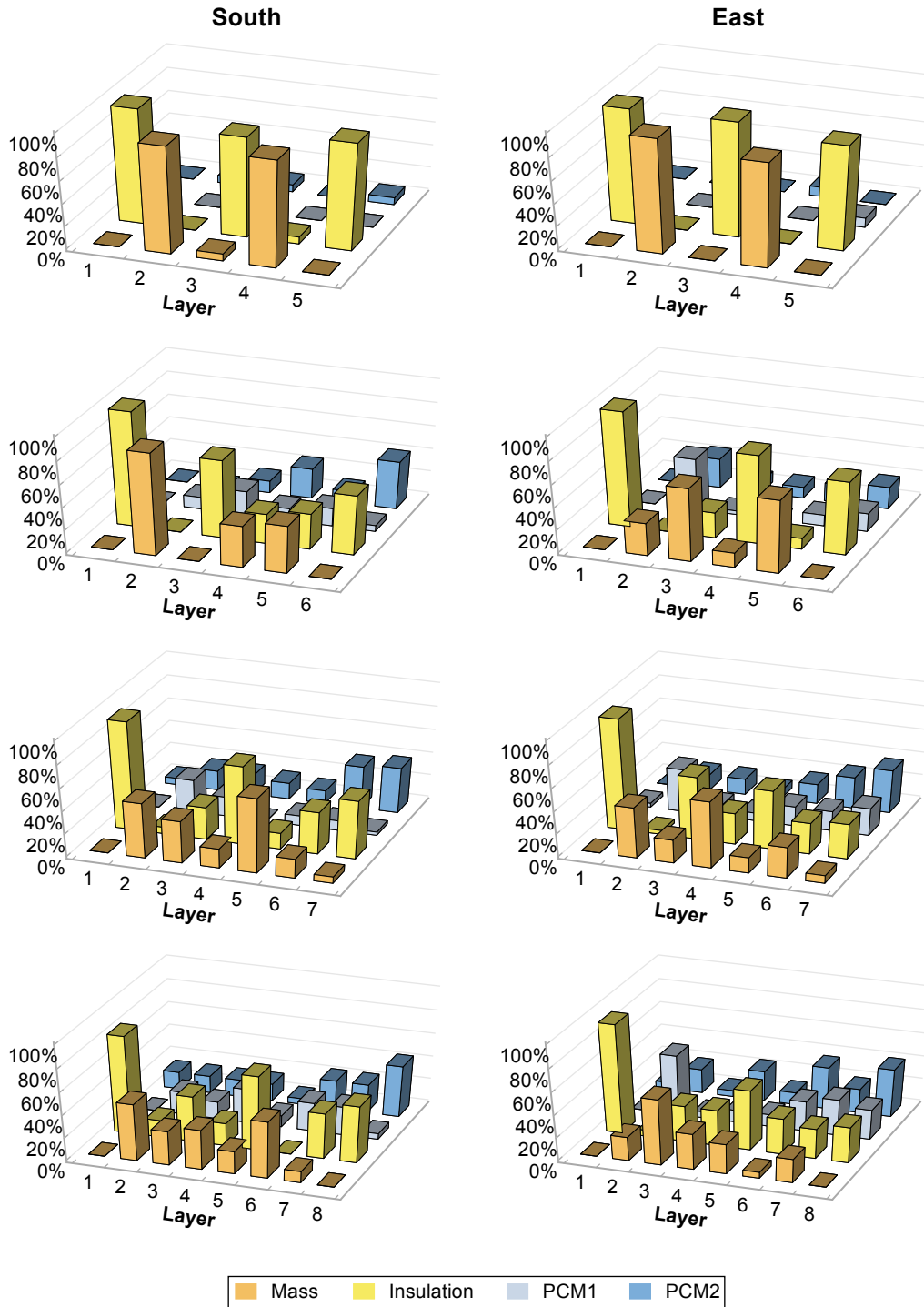
Fig. 5.23 Frequency analysis of the layers' position: Palermo, south and east façades.
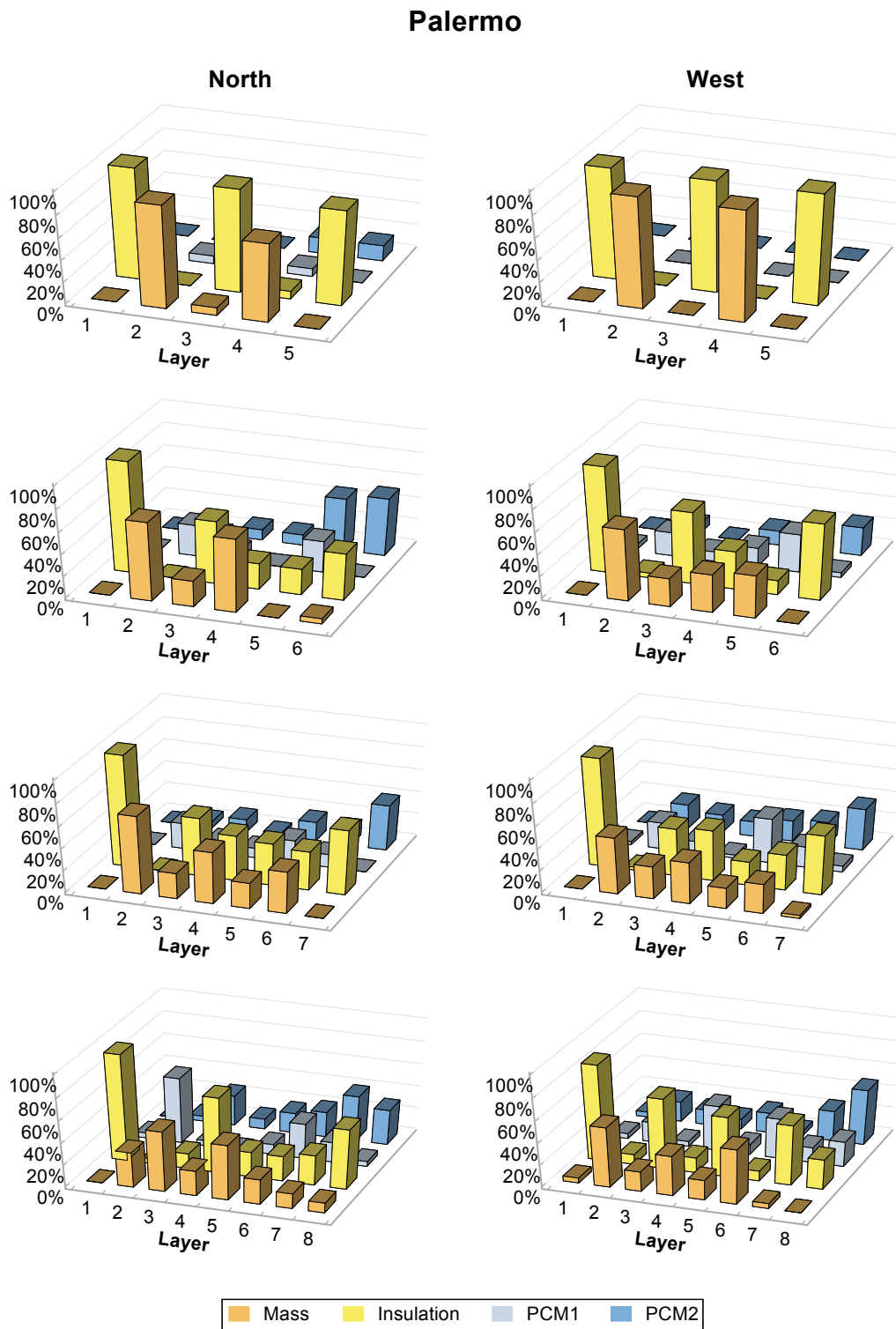
Fig. 5.24 Frequency analysis of the layers' position: Palermo, north and west façades.
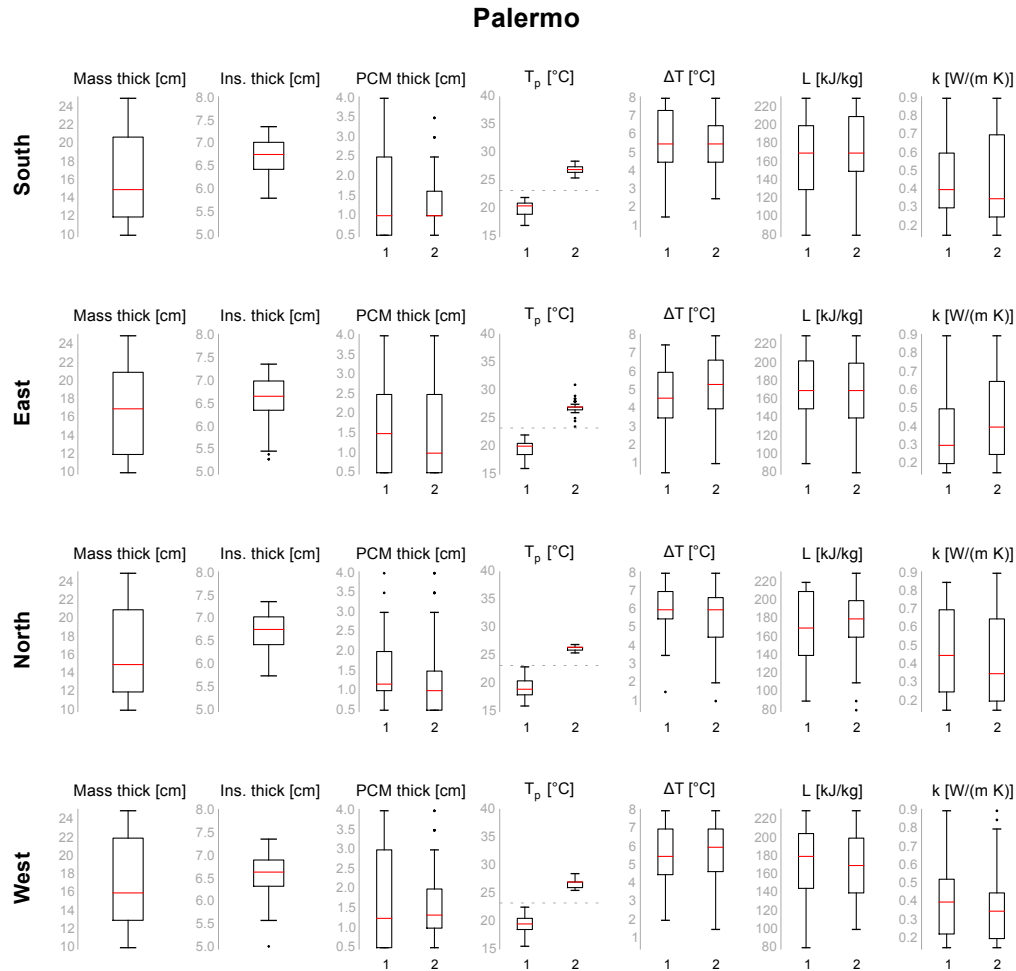
Palermo

Fig. 5.25 Box plots: Palermo.

melting temperature of PCM1 appears to vary in a quite small range, it actually varied greatly within its bounds. Melting temperature range and latent heat of fusion tended to assume high values for both PCMs in all the orientations. If no constraint was added, they would have led to unrealistic solutions where both properties were simultaneously maximised. A high latent heat of fusion is beneficial to store a greater amount of energy and reduce temperature oscillations. A high melting temperature range improves the adaptivity of the PCM when subject to variable conditions, such as when placed towards the external environment, although it may compromise the energy performance [88]. Low thermal conductivities seemed to be preferred for both PCMs. This is in line with the results of Zhang et al. [181] for PCM placed on the external side of the wall. Eventually, low values were mostly selected for PCM and mass thickness; this is in line with the objectives of the search process.
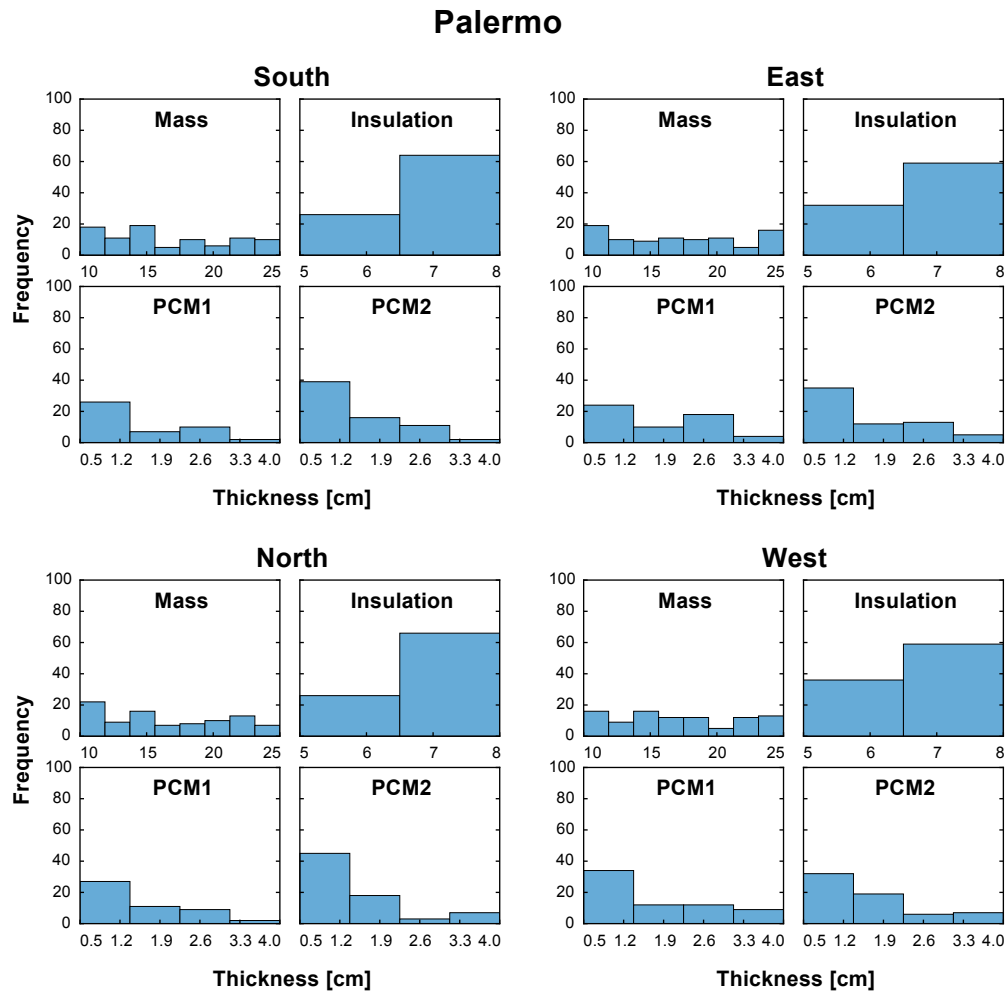
Fig. 5.26 Frequency analyses of the materials' thickness: Palermo.

Since box plots do not provide information on the underlying distributions, further details are shown in Fig. 5.26, Fig. 5.27 and Fig. 5.28, where frequency analyses of the materials' overall thickness and thermo-physical properties of PCM1 and PCM2 are respectively reported. With regard to the materials' thickness, a tendency for low values was confirmed for the PCMs, whereas the massive layer did not apparently exhibit any trend. With regard to the thermo-physical properties of PCM1, a mild peak of the distribution could be observed for the peak melting temperature, where 21 ℃ were mostly preferred for the south and east expositions and about 19 ℃ in the north and west façades. A melting temperature range of about 5.5/6 ℃ or higher was chosen for the north wall, whereas it ranged more over the domain in the other expositions. Low thermal conductivities were mostly preferred in the east and west expositions, whereas no trend could be observed for the north walls. The latent heat of fusion did not exhibit any clear trend other than in the west exposition, where PCM1 was used the most, and high values tended to
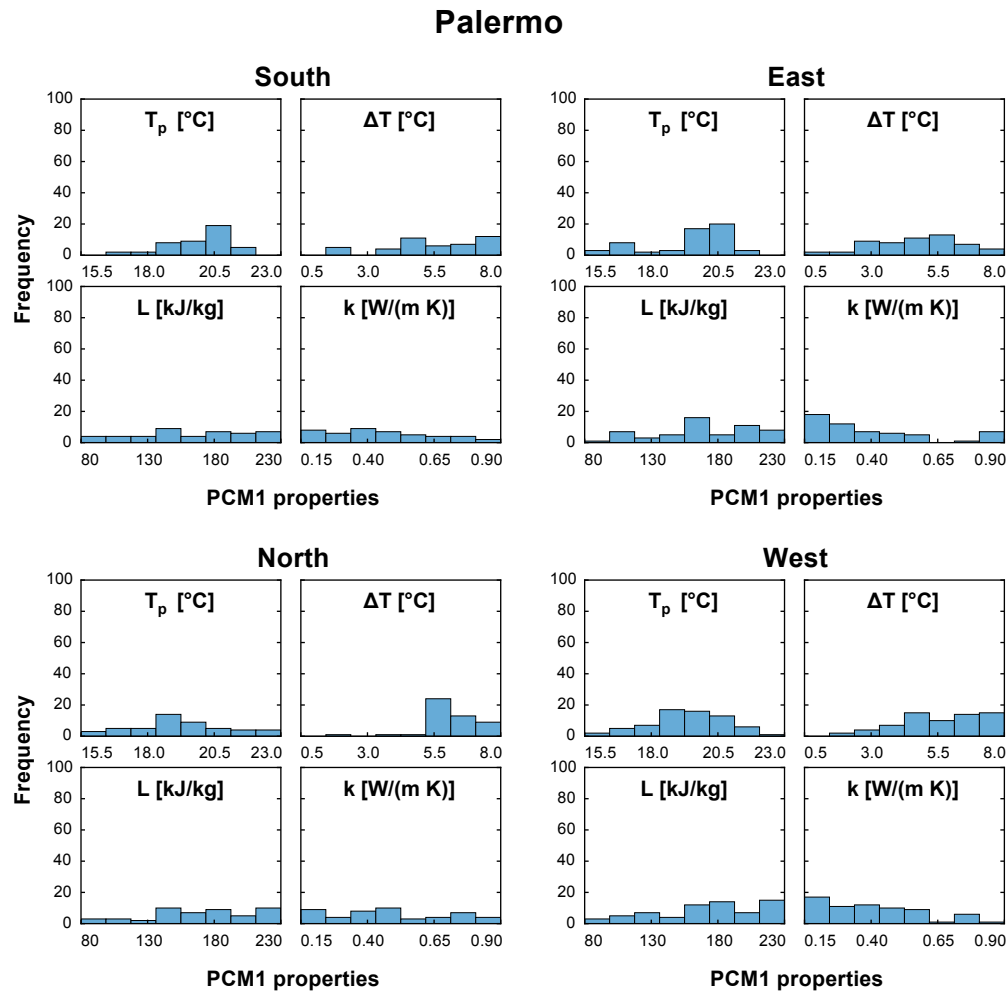
Palermo

Fig. 5.27 Frequency analyses of the PCM1's properties: Palermo.

be preferred.

Much more evident trends could be observed for the properties of PCM2. As it was already highlighted by the box plots, all the solutions shared almost the same peak melting temperature; this preference being more evident in the north façade, where clear trends could be devised for all the properties. Medium/high melting temperature ranges were selected for all the expositions. It could be inferred that the constraint had an evident effect in the north façade, the peak of melting temperature range being not in the upper bound and the same for the latent heat of fusion. The thermal conductivity tended to low values in all the expositions (in accordance with the results of the parametric analyses in § 5.2.1.4) and the latent heat of fusion to high values, although the generally spanned along their whole domains.

To explore how the search space variables affected the results in the objective
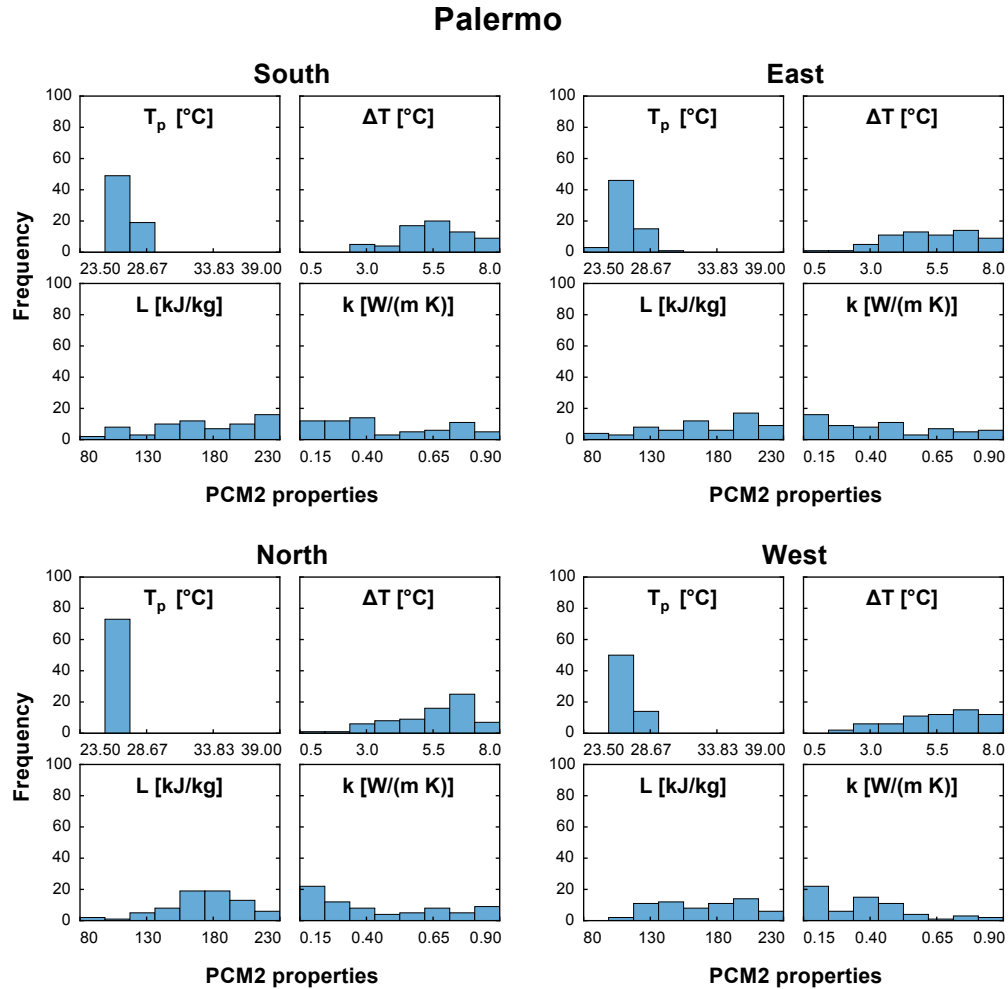
Fig. 5.28 Frequency analyses of the PCM2's properties: Palermo.

space, the values assumed by each variable were mapped on the Pareto front. Maps for materials' thickness plus number of layers and for PCM properties in the south-facing walls are respectively reported in Fig. B.1 and Fig. B.2. As it could be expected, the mass thickness increased with the wall thickness, and the thickness of the two PCMs increased along the PCM thickness axis; however, values below 1.5 cm were mostly selected, as confirmed by the frequency analysis in Fig. 5.26. The increasing trend of the mass characterised also the sequence of the non-dominated sets between Y^*_{mn} and PCM thickness. To keep a constant U-value, the insulation thickness obviously decreased with wall and PCM thicknesses. As it was highlighted by Fig.5.22, the majority of solutions presented three layers of insulation. Two layers of mass were mostly selected when the total PCM thickness was below or equal to 2 cm. For increasing PCM thickness, a single layer was preferred with the exception of many solutions belonging to the non-dominated front between Y^*_{mn} and t_{PCM}. A couple of solutions with no PCM and high mass

thickness were characterised by three layers of mass and fours layers of insulation. This trend will be more evident in other expositions. Solutions with PCM were mostly characterised by a single layer. PCM1 occurred to be placed twice within the wall only when the overall thickness was at least 2 cm. Unexpectedly, almost all solutions with 1 cm of PCM were characterised by 2 layers of PCM2. This behaviour was probably caused by the constraint on the minimum PCM thickness in each slot-layer, for which single thicknesses lower than 0.5 cm were increased up to this value. With regard to the PCM properties, other than the almost constant peak melting temperature of PCM2 and a peak melting temperature of PCM1 that exhibited mostly values around 21 ℃ no trends between property and fitness were detected.

Maps for materials' thickness plus number of layers and for PCM properties in the east-facing walls are respectively reported in Fig. B.3 and Fig. B.4. No significant differences from the south façade were observed. Also in this case, two layers of mass were mostly selected when the total PCM thickness was below or equal to 2 cm. For increasing PCM thickness, a single layer was preferred. Some solutions with no PCM and high mass thickness were characterised by three layers of mass and fours layers of insulation. Solutions with PCM1 were mostly characterised by a single layer up to 2 cm of overall PCM thickness; then, two layers were often selected. With regard to the PCM properties, other than the almost constant peak melting temperature of PCM2 and a peak melting temperature of PCM1 that exhibited mostly values around 21 ℃ no trend between property and fitness were detected. Higher thicknesses of PCM2 were used on the extreme area of the Pareto front around solution A and beneath. The asymptotic portion of Pareto was moreover characterised by a quite homogeneous peak melting temperature of PCM1 around 20 ℃. Compared to the south exposition, lower thermal conductivities were mostly selected for both PCM1 and PCM2.

Maps for materials' thickness plus number of layers and for PCM properties in the north-facing walls are respectively reported in Fig. B.5 and Fig. B.6. The same considerations about the materials' thickness applied also in this case. With regard to the number of layers for each material, two layers of mass were mostly selected within the whole Pareto front. Solutions with no PCM and thickness approximately higher than 29 cm were all characterised by three layers of mass and four layers of insulation. With regard to the PCM properties, other than the constant peak melting temperature of PCM2, the melting temperature range of both PCMs assumed high values. Apart for a few outliers, the melting temperature range of PCM1 especially varied from 5 cm to 8 cm. Although low thermal conductivities were mostly selected for both PCMs, high values were chosen for PCM2 in the portion of Pareto front around solution A.

Maps for materials' thickness plus number of layers and for PCM properties in the west-facing walls are respectively reported in Fig. B.7 and Fig. B.8. Unlikely

Palermo - Solution A

South

PCM1 properties
Peak melting temperature: 19.5 °C
Melting temperature range: 8.0 °C
Latent heat of fusion: 170 kJ/kg
Thermal conductivity: 0.40 W/(m K)

PCM2 properties
Peak melting temperature: 26.5 °C
Melting temperature range: 5.0 °C
Latent heat of fusion: 150 kJ/kg
Thermal conductivity: 0.80 W/(m K)

East

PCM1 properties
Peak melting temperature: 20.0 °C
Melting temperature range: 3.5 °C
Latent heat of fusion: 170 kJ/kg
Thermal conductivity: 0.20 W/(m K)

PCM2 properties
Peak melting temperature: 26.5 °C
Melting temperature range: 3.5 °C
Latent heat of fusion: 200 kJ/kg
Thermal conductivity: 0.45 W/(m K)

North

PCM1 properties
Peak melting temperature: 20.0 °C
Melting temperature range: 5.5 °C
Latent heat of fusion: 180 kJ/kg
Thermal conductivity: 0.75 W/(m K)

PCM2 properties
Peak melting temperature: 27.0 °C
Melting temperature range: 5.3 °C
Latent heat of fusion: 220 kJ/kg
Thermal conductivity: 0.85 W/(m K)

West

PCM1 properties
Peak melting temperature: 20.0 °C
Melting temperature range: 4.5 °C
Latent heat of fusion: 230 kJ/kg
Thermal conductivity: 0.60 W/(m K)

PCM2 properties
Peak melting temperature: 27.5 °C
Melting temperature range: 4.7 °C
Latent heat of fusion: 230 kJ/kg
Thermal conductivity: 0.15 W/(m K)

Mass   Insulation   PCM1   PCM2

Fig. 5.29 Solutions in the group of A's, Palermo.

the previous orientations, where PCM1 was not as used, higher thicknesses were selected in the extreme portion of the Pareto front. With regards to the PCM properties, the considerations drawn from the frequency analyses were confirmed. As for the other orientations, no trends were highlighted.

The extreme solutions of the Pareto front are reported in Fig. 5.29, Fig. 5.30 and Fig. 5.31. Solution C (worst performance in terms of Y_{mn}^*, no PCM and minimum mass) was the same for all the orientations; it was characterised by three layers of insulation alternated with two layers of mass. Solution B (best performance in terms of Y_{mn}^* with no PCM and maximum mass) was characterised by the same wall configurations of solution C for the south exposition, whereas four layers of insulation and three layers of mass were adopted for the other façades. These solutions are in line with the findings from [252] and [254]. Solution A for the south-facing walls was characterised by a configuration very similar to that of
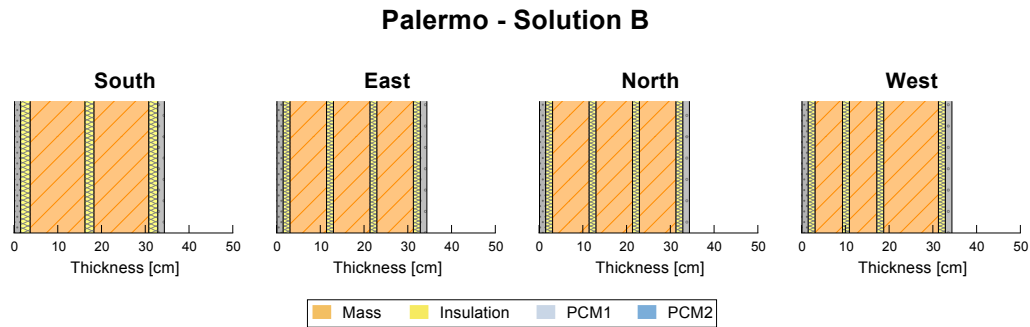
Palermo - Solution B

Fig. 5.30 Solutions in the group of B's, Palermo.
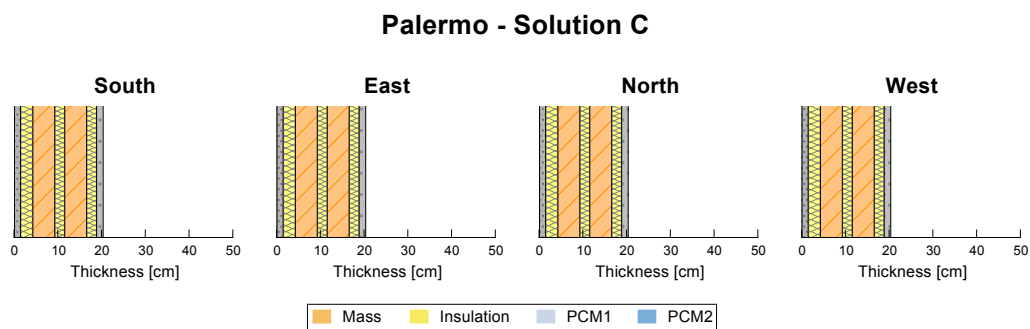
Palermo - Solution C

Fig. 5.31 Solutions in the group of C's, Palermo.

solutions B and C. One layer of PCM1 was placed just after the external insulation, while a layer of PCM2 was placed in the innermost position (excluding the internal plaster). In all the orientations, at least one layer of PCM1 was placed in position 2, and either PCM1 or PCM2 faced the internal environment. The reason for placing PCM1 on the outer side of the wall just after the insulation can be explained by observing Fig. 5.8; the optimised solutions are somewhat similar to Wall 5, where PCM with a melting temperature of 20 ℃ was found to be effective during the winter months. It was additionally verified that, given the $c(T)$ curves of PCM1, it underwent phase transition during mid season and also during winter when the melting temperature range was sufficiently wide. As it can be seen in Fig. 5.32, the temperatures within the layer with PCM1 (light blue area) fall within the peak of the corresponding $c(T)$ curve.

East, north and west walls were characterised by quite similar layouts. Only two layers of insulation and one big central layer of mass were selected, plus at least one layer of PCM2 and PCM1 in a sequence facing the internal environment. They all had two layers of PCM1, one of which placed as innermost layer only in the east façade. The north and west walls presented a single thick layer of PCM2. Unlikely the other exposition, the second insulation layer in the west façade was placed in position 3. The overall thickness was almost the same for all the expositions with the exception of the south wall which was thinner. With
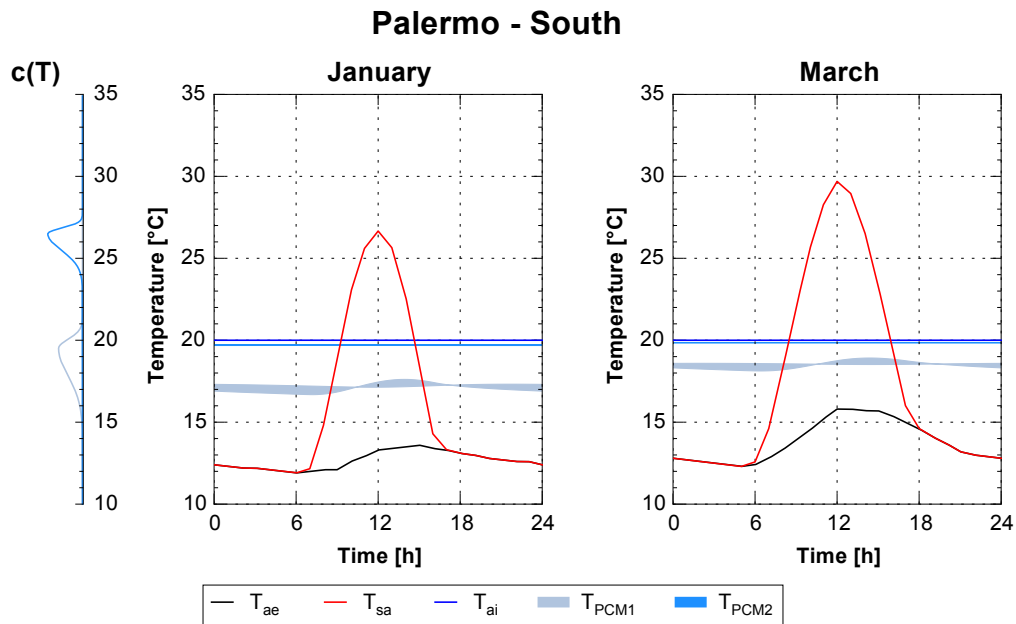
Fig. 5.32 Temperature profiles within the PCM layers in Palermo (Solution A, south).

regard to the thermo-physical properties of the PCMs, the melting temperature differed of at most 1 ℃ among the solutions of all the orientations. The highest melting temperature range was chosen for PCM1 in the south wall, whereas the lowest selected value of 3.5 ℃ was assumed by both PCMs for the east wall. In all the other cases, the melting temperature range varied between 4.5 ℃ and 5.5 ℃. The lowest latent heat of fusion of 150 kJ/(kg K) was chosen for PCM2 in the south wall. High values were selected for PCM2 in the other expositions. Especially for the west-facing solution, the latent heat of fusion of both PCMs reached the upper bound. The choice of the thermal conductivity appeared to be quite random. High values were especially selected in the north wall. According to the results of the parametric analyses in § 5.2.1.4, low values were expected. However, since the PCM was mostly placed towards the indoor environment, the thermal conductivity was found not to have a strong influence on Y_{mn}^*.

The relationship between monthly equivalent periodic thermal transmittance and corresponding time shift is concisely reported in Fig. 5.33. Among the extreme solutions of the Pareto front, the most evident differences between each group of solutions was an increase of the time shift as the equivalent periodic thermal transmittance decreased. Moreover, the time shift of the solutions in the group of A's, which were characterised by the presence of PCM, showed a much greater monthly variability, reaching about and even over 24 h during some months. Generally, such a time shift would not be beneficial as the maximum of the temperature wave would overlap to the maximum of the heat flux wave of the previous day. However, in steady-periodic conditions the entity of the equivalent periodic thermal
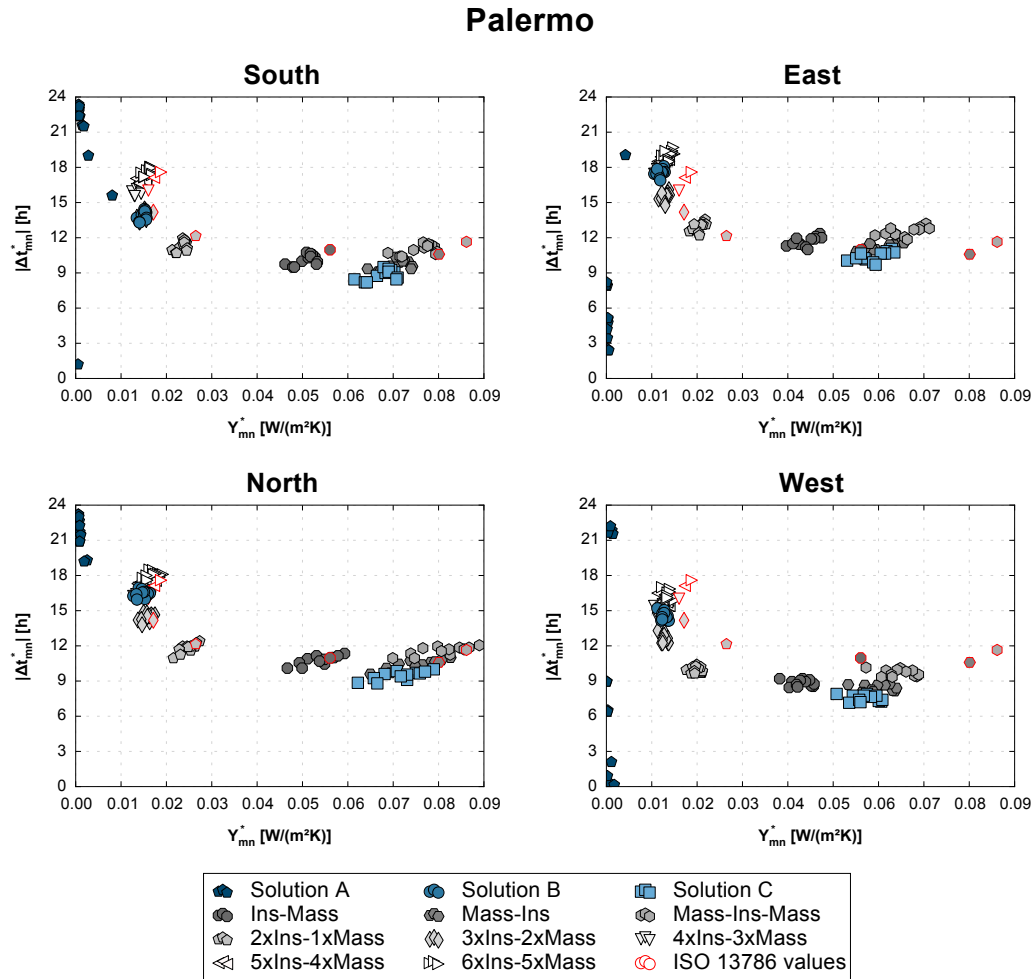
Palermo

Fig. 5.33 Monthly Y_{mn}^* vs Δt_{mn}^*, Palermo.

transmittance was such that the heat flux wave was almost flat, and this potential drawback could hence be ignored.

For the sake of comparison, additional values representing a variety of wall configurations characterised by the same amount of insulation and mass (equal to the upper bound) is reported. These wall configurations differed only in the number of mass and insulation layers and their mutual position within the wall. The overall thickness of mass and insulation was unvaried (Fig. 4.17). On average, the worst performance in terms of Y_{mn}^* was obtained by the configuration where all the insulation was in the middle of the wall and the mass was evenly distributed on the sides. Although the greater amount of mass, this configuration and that characterised by a single layer of mass and the insulation in the innermost position were slightly outperformed by solution C. Therefore, a correct distribution of the layers (especially placing the insulation in the outermost position) can be more

important than having a greater amount of mass.

Overall, this set of configurations exhibits an interesting behaviour. As the number of layers increased, the absolute value of the time shift always increased but the equivalent periodic thermal transmittance did not continue to decrease. A minimum value (corresponding to the configuration with three layers of mass and four layers of insulation) was found beyond which Y^*_{mn} started to increase again. The minimum overlapped with the solutions in the group of B's (except towards south, where it could already be inferred that the true minimum was not found). This could be expected since this group of solutions was characterised by the greatest amount of mass within their domain and optimal layers' distribution. However, this finding seems to confirm the results from Bond et al. [254], which suggested that a number of layers for which the dynamic thermal properties are optimised could exist.

5.2.3.2 Torino

The optimal solutions in Torino will be herewith discussed.

Frequency analyses of the number of layers within the Pareto front solutions are reported for each orientation in Fig. 5.34. About 40% of solutions were characterised either by seven or eight layers (computed with the exception of external render and internal plaster) except in the west façade, where the preference for seven layers was slightly more evident. The number of layers selected for each material is detailed in Fig. 5.35. A clear preference over three layers of insulation was highlighted for all the orientations although, unlikely in Palermo, there were less solutions with two layers and many more with four. In the same way, more solutions where characterised by three layers of mass. As in Palermo, the probability of finding three layers of insulation was almost equal to that of finding two layers of mass. With regard to the PCM, being Torino a heating-dominated climate, PCM1 was generally preferred over PCM2. More often than not, at least one layer of PCM1 was added in all the orientations. Apart in the east façade, the probability of occurrence of one layer of PCM2 was only slightly less than the probability of lacking it.

Details on the layers' distribution within the walls with 5 to 8 layers are shown in Fig. 5.36 and Fig. 5.37. Similarly to Palermo, when 5 layers were chosen, three layers of insulation alternated with two layers of mass were always selected in all the orientations except east. When 6 or more layers were present, PCM started to be used. The trends were however inverted with respect to Palermo. In the south and east expositions, PCM1 was mostly placed in the last three layers, close to the internal environment. PCM2 was used more scarcely and placed mostly in intermediate positions. Differently from Palermo, the innermost layer was more likely to be insulation than PCM. Compared to south and east, in the north and west expositions a higher probability of PCM1 being selected as the innermost
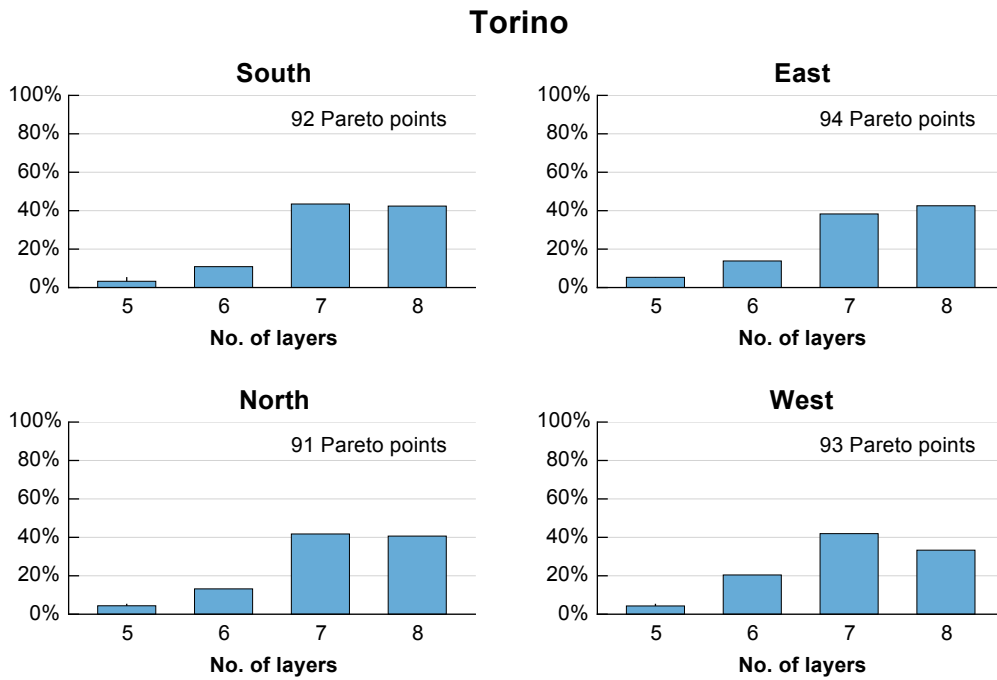
Fig. 5.34 No. of layers within the Pareto front solutions: Torino.
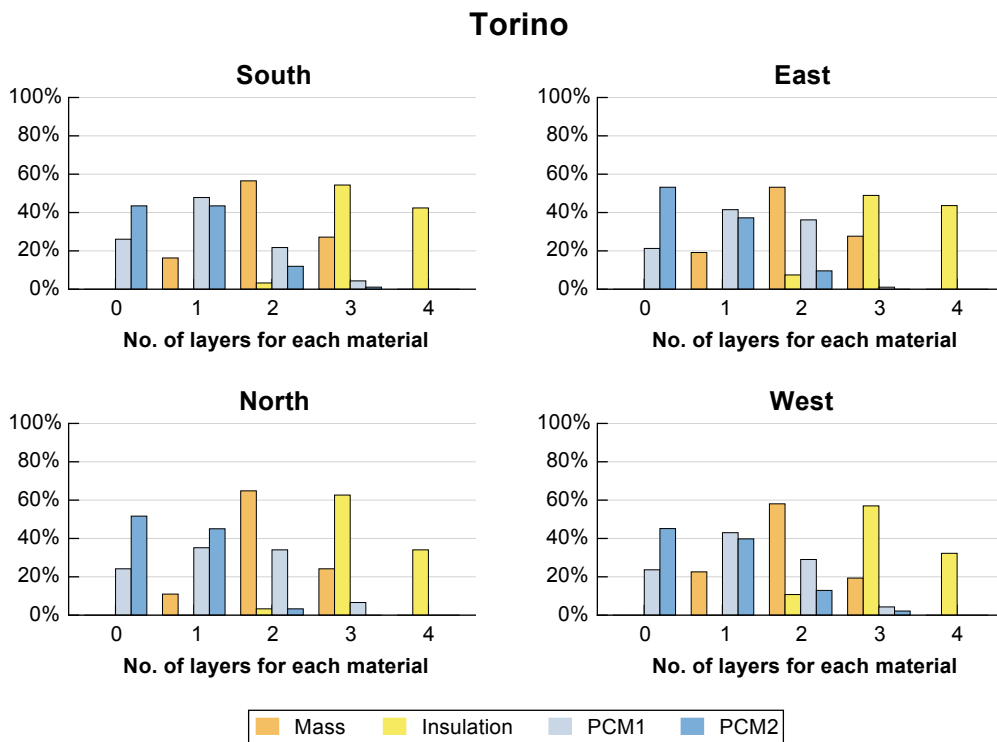
Fig. 5.35 No. of layers for each material within the Pareto front solutions: Torino.

Torino

South East
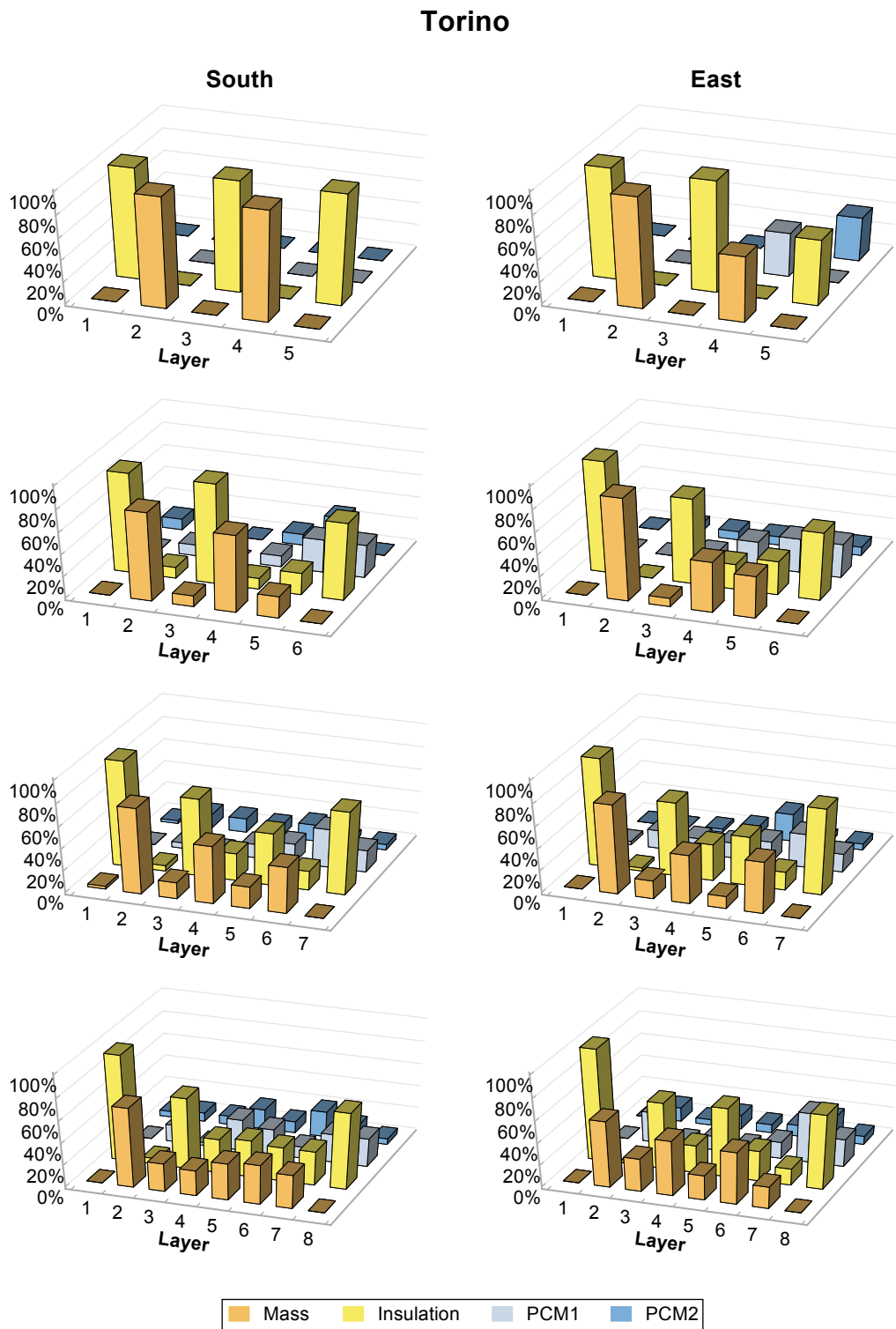
Fig. 5.36 Frequency analysis of the layers' position: Torino, south and east façades.

Torino
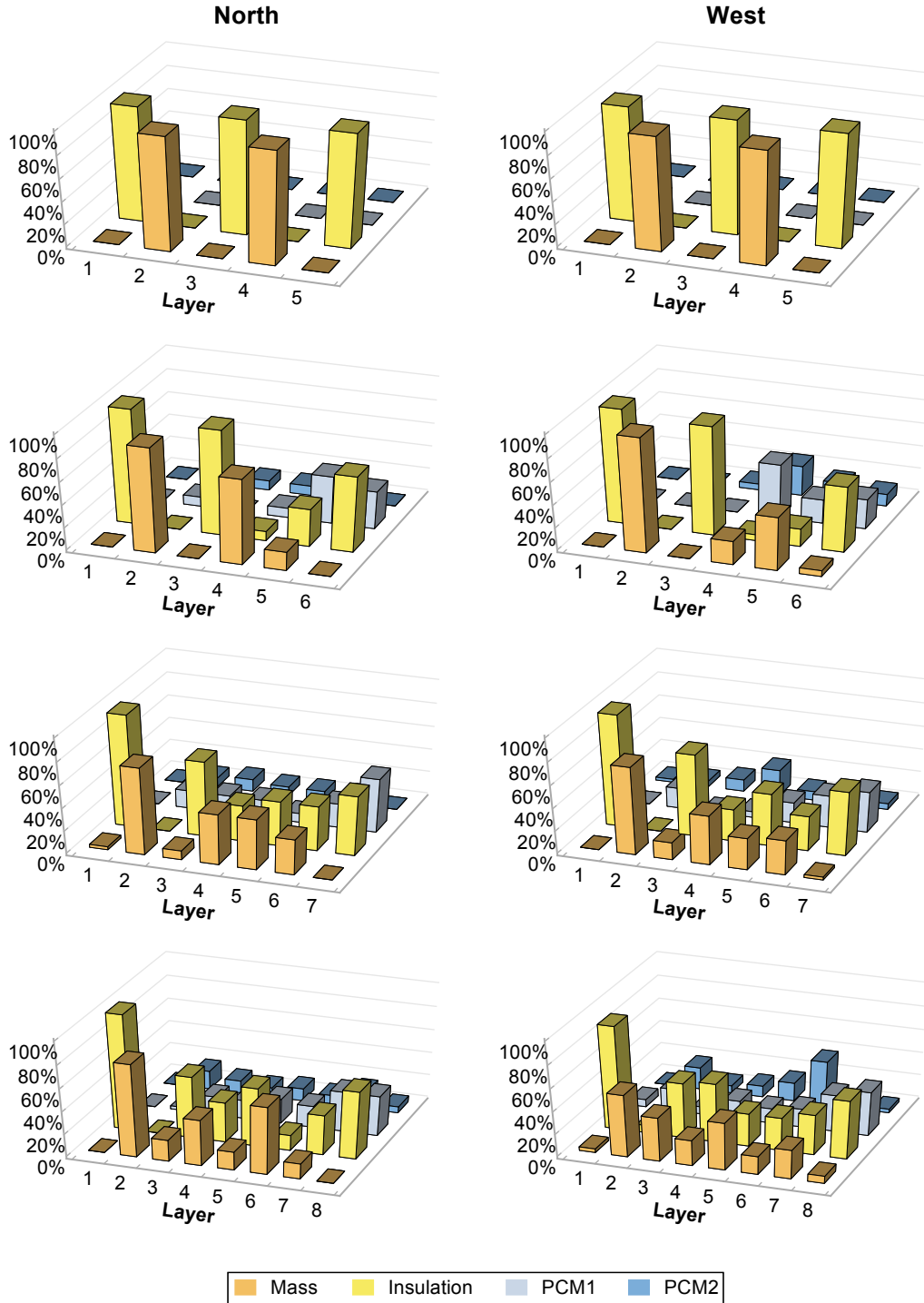
North

West

Fig. 5.37 Frequency analysis of the layers' position: Torino, north and west façades.
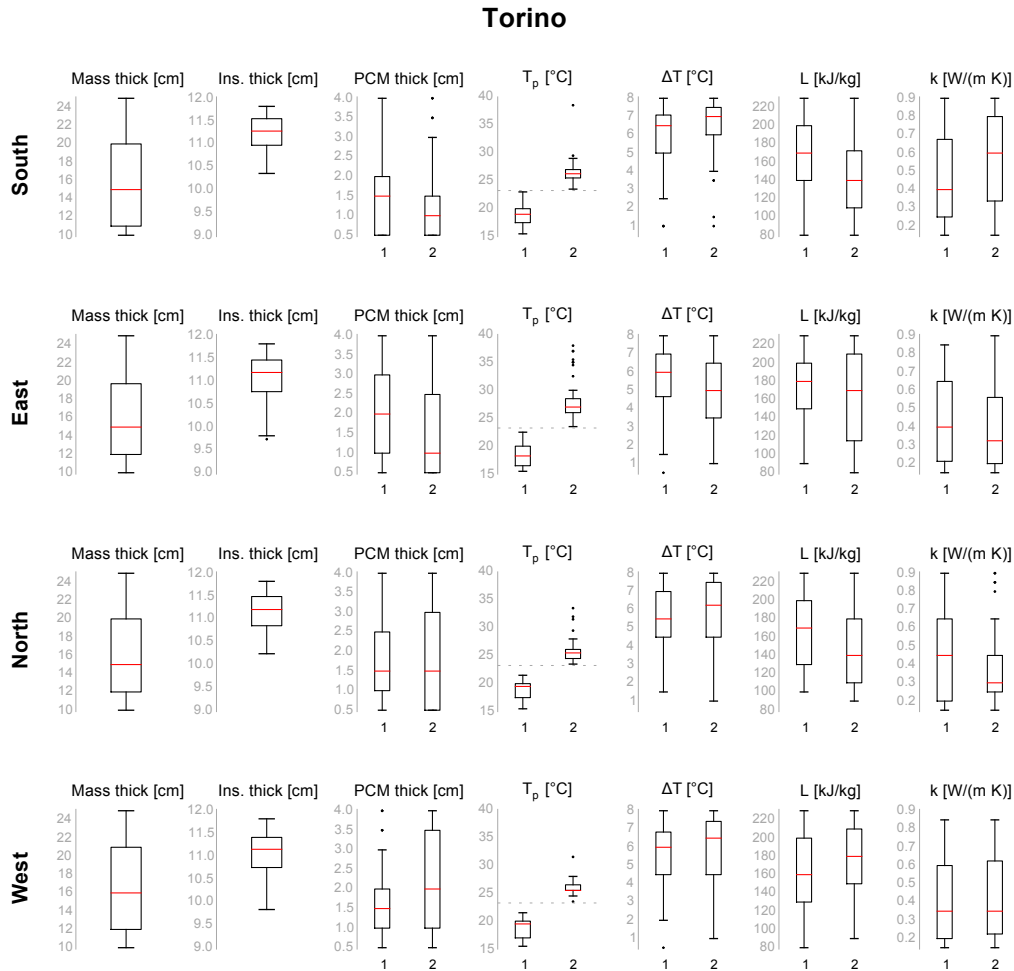
Fig. 5.38 Box plots: Torino.

layer occurred. Towards west, PCM2 could likely be assigned to the third to last position. In general, the outermost layer was always insulation, followed mostly by mass. The alternating trend between insulating and massive/PCM layers was always present. When 7 or 8 layers were selected, four layers of insulation were generally used. Unlikely in Palermo, PCM was seldom assigned to position 2.

To have an overview of the values assumed by the continuous variables within the Pareto front, box plots are reported in Fig. 5.38. All the solutions in all the orientations were characterised almost by the same peak melting temperature of PCM2, even though the interquartile range was not as narrow as in Palermo. A median value of 25.5 ℃ was observed for north and west-facing walls, 26.25 ℃ in the south façade and 27 ℃ towards east. The peak melting temperature of PCM1 appears to vary a bit less than in Palermo. Melting temperature range and latent heat of fusion tended to assume high values for both PCMs in all the orientations,
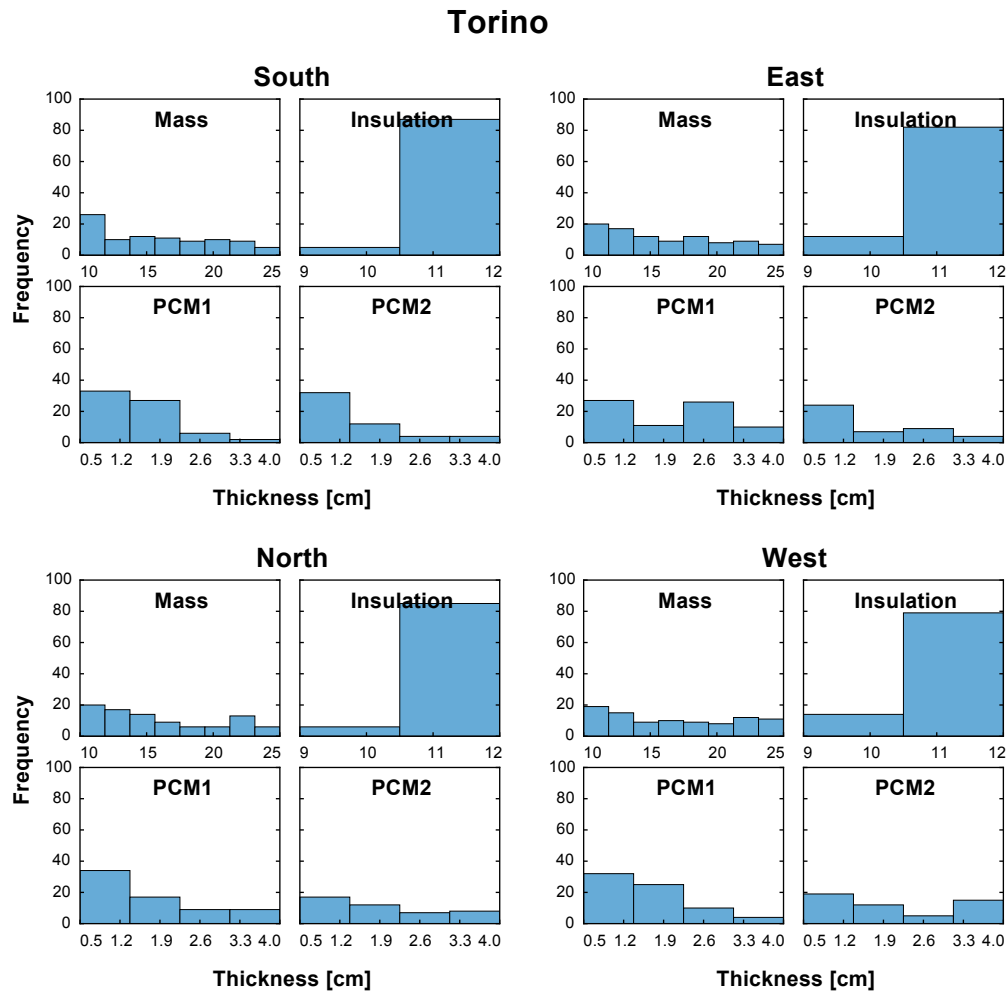
Fig. 5.39 Frequency analyses of the materials' thickness: Torino.

with the exception of the latent heat of PCM2 in the south and north façades. Low thermal conductivities seemed to be preferred for both PCMs, except PCM2 towards south. With regard to the mass thickness, low values were mostly selected. Except for the east façades, the medians were the same as in Palermo, but the interquartile ranges were shifted slightly lower. Due to the lower U-value, higher thicknesses of insulation were necessary. Eventually, low thicknesses of PCM1 were mostly selected. Towards south and east, low values were generally selected also for PCM2.

Since box plots do not provide information on the underlying distributions, further details are shown in Fig. 5.39, Fig. 5.40 and Fig. 5.41, where frequency analyses of the materials' overall thickness and thermo-physical properties of PCM1 and PCM2 are respectively reported. With regard to the materials' thickness, a tendency for low values was confirmed for the PCMs, with the exception of PCM2 towards north and especially west, where high values were almost as likely to
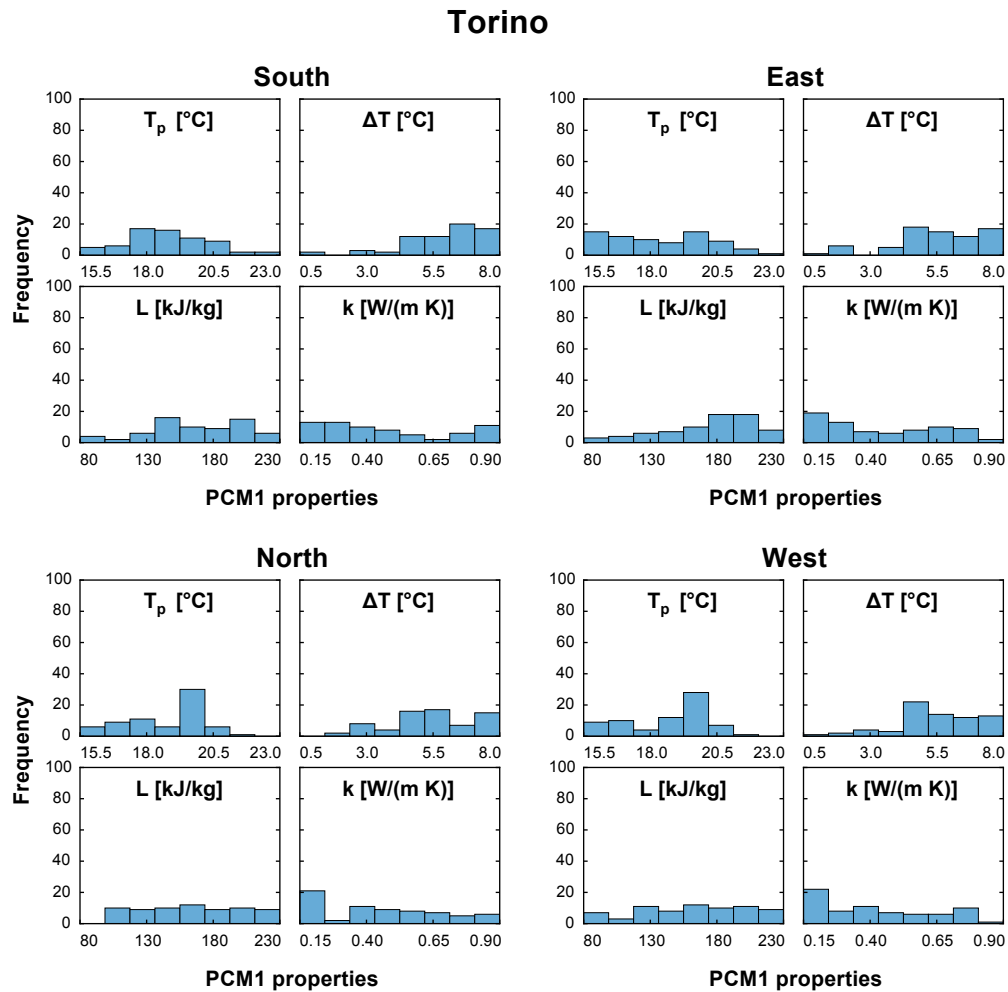
Fig. 5.40 Frequency analyses of the PCM1's properties: Torino.

occur. Unlikely in Palermo, a mild trend for low mass was observed. With regard to the thermo-physical properties of PCM1, a mild peak of the distribution could be observed for the peak melting temperature towards south and east, whereas a clear preference for 19.5/20 ℃ was observed for the north and west façades. A melting temperature range of about 4.5/5 ℃ or higher was chosen for the west wall, whereas it ranged more over the domain in the other expositions. Low thermal conductivities were mostly preferred in all the expositions. The latent heat of fusion did not exhibit any clear trend other than in the east exposition and high values tended to be preferred. More evident trends could be observed for the peak melting temperature of PCM2. As it was already highlighted by the box plots, the peak melting temperature varied within a very small interval. Medium/high melting temperature ranges were selected especially for the south-facing walls. The thermal conductivity tended to low values in all the expositions except south. The latent heat of fusion did not show any clear trend.
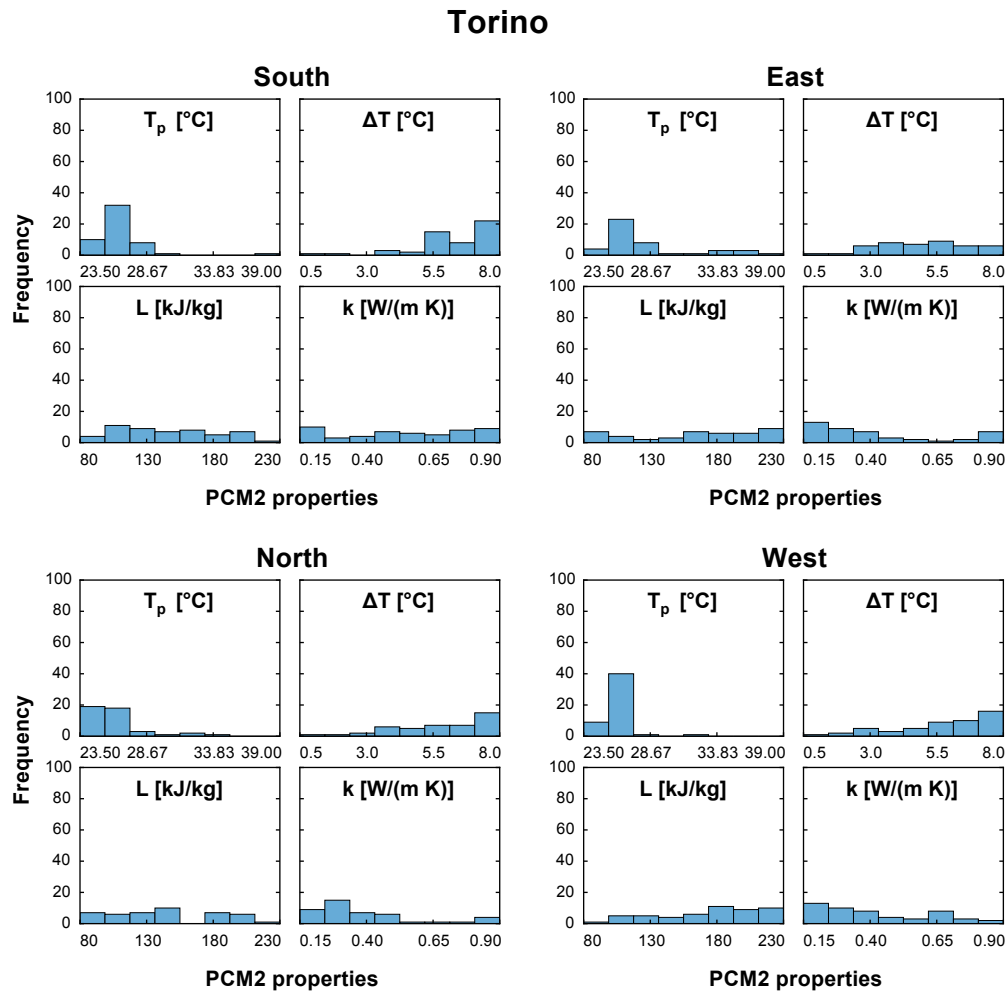
Fig. 5.41 Frequency analyses of the PCM2's properties: Torino.

To explore how the search space variables affected the results in the objective space, the values assumed by each variable were mapped on the Pareto front. Maps for materials' thickness plus number of layers and for PCM properties in the south-facing walls are respectively reported in Fig. B.9 and Fig. B.10. Contrary to Palermo, PCM2 reached higher thicknesses than PCM1. Similarly to Palermo, solutions with no PCM were characterised by increasing number of insulation/mass layers for growing mass thickness. However, the switch occurred earlier, so that solutions thicker than 27 cm were characterised by four layers of insulation and three layers of mass. In general, solutions with three layers of mass were only selected when the total PCM thickness was below or equal to 1.5 cm. For increasing PCM thickness, either one or two layers were preferred. Solutions with PCM were mostly characterised by a single layer. Both PCMs occurred to be placed twice within the wall only when the overall thickness was at least 1.5 cm. As in Palermo, three layers were seldom selected. With regard to the PCM properties, other than the

almost constant peak melting temperature of PCM2, the peak melting temperature of PCM1 exhibited mostly values around 18/20 ℃, and the melting temperature range of both PCMs was mostly characterised by values greater than 5 ℃.

Maps for materials' thickness plus number of layers and for PCM properties in the east-facing walls are respectively reported in Fig. B.11 and Fig. B.12. No significant differences from the south façade were observed, except higher thicknesses of PCM1 towards the extreme portion of the Pareto front. With regard to the PCM properties, compared to the south façade, a greater variability for the peak melting temperatures and generally higher latent heats of fusion were observed. Moreover, lower melting temperature ranges and thermal conductivities were often selected for PCM2.

Maps for materials' thickness plus number of layers and for PCM properties in the north-facing walls are respectively reported in Fig. B.13 and Fig. B.14. The same considerations about the materials' thickness applied also in this case. With regard to the number of layers for each material, two layers of mass were mostly selected within the whole Pareto front. Solutions with no PCM and wall thickness approximately higher than 29 cm were all characterised by three layers of mass and four layers of insulation. Apart from very few exceptions, solutions with PCM2 were characterised by a single layer. With regard to the PCM properties, the peak melting temperature of PCM1 varied less than for the other expositions. Low thermal conductivities for PCM2 were mainly selected. Considering also its low latent heat of fusion, it could be inferred that PCM2 did not have a significant effect and was mostly used like a traditional material.

Maps for materials' thickness plus number of layers and for PCM properties in the west-facing walls are respectively reported in Fig. B.15 and Fig. B.16. Compared to the other expositions, lower thicknesses of PCM1 were used. Its peak melting temperature was characterised by a quite narrow range of variation as it was observed for the north façade, and that of PCM2 varied less than in the other orientations.

Eventually, the extreme solutions of the Pareto front are reported in Fig. 5.42, Fig. 5.43 and Fig. 5.44. Solution C (worst performance in terms of Y^*_{mn}, no PCM and minimum mass) was extremely similar for all the orientations; as in Palermo it was characterised by three layers of insulation alternated with two layers of mass. Solution B (best performance in terms of Y^*_{mn} with no PCM and maximum mass) was characterised by four layers of insulation and three layers of mass in all the façades. Solution A was characterised by four layers of insulation in the south and east façades, three layers towards north, and only two in the west-facing wall. As all the solutions embedded both PCMs, no more than two layers of mass were selected (south and east façades only). The PCM was placed mostly close to the internal environment. Only in the east wall insulation was selected as the innermost material. The melting temperature of PCM1 was coherently lower than in the other

Torino - Solution A

South

PCM1 properties
Peak melting temperature: 21.0 °C
Melting temperature range: 6.5 °C
Latent heat of fusion: 90 kJ/kg
Thermal conductivity: 0.35 W/(m K)

PCM2 properties
Peak melting temperature: 26.0 °C
Melting temperature range: 6.5 °C
Latent heat of fusion: 110 kJ/kg
Thermal conductivity: 0.75 W/(m K)

East

PCM1 properties
Peak melting temperature: 17.5 °C
Melting temperature range: 5.3 °C
Latent heat of fusion: 220 kJ/kg
Thermal conductivity: 0.65 W/(m K)

PCM2 properties
Peak melting temperature: 27.0 °C
Melting temperature range: 5.5 °C
Latent heat of fusion: 80 kJ/kg
Thermal conductivity: 0.15 W/(m K)

North

PCM1 properties
Peak melting temperature: 20.0 °C
Melting temperature range: 4.0 °C
Latent heat of fusion: 230 kJ/kg
Thermal conductivity: 0.50 W/(m K)

PCM2 properties
Peak melting temperature: 26.5 °C
Melting temperature range: 8.0 °C
Latent heat of fusion: 150 kJ/kg
Thermal conductivity: 0.20 W/(m K)

West

PCM1 properties
Peak melting temperature: 19.0 °C
Melting temperature range: 6.0 °C
Latent heat of fusion: 210 kJ/kg
Thermal conductivity: 0.60 W/(m K)

PCM2 properties
Peak melting temperature: 25.5 °C
Melting temperature range: 7.3 °C
Latent heat of fusion: 190 kJ/kg
Thermal conductivity: 0.65 W/(m K)

Mass   Insulation   PCM1   PCM2

Fig. 5.42 Solutions in the group of A's, Torino.

orientations. Unlikely in Palermo, a layer of PCM1 was placed in position 2 only in the north façade, where it underwent phase transition only during May and September, but its effect was however not very significant. Only south and east façades were characterised by a single layer for each PCM. Two layers of PCM1 were selected in the north wall, whereas two layers of PCM2 were placed in the west orientation. The overall thickness was minimum in the east and north façades and maximum towards west. With regard to the thermo-physical properties of the PCMs, the melting temperature differed no more than 2 ℃ among the solutions of all the orientations except a low value for PCM1 in the east façade. In all the cases, the melting temperature range was greater than 4.0 ℃. The highest value, equal to the upper bound, was chosen for PCM2 in the north wall. A very low latent heat of fusion was chosen for PCM2 in the north wall and PCM1 in the south wall (respectively 80 kJ/(kg K) and 90 kJ/(kg K)); selecting higher values would have yielded to a better wall performance. High values were selected for PCM1 in all
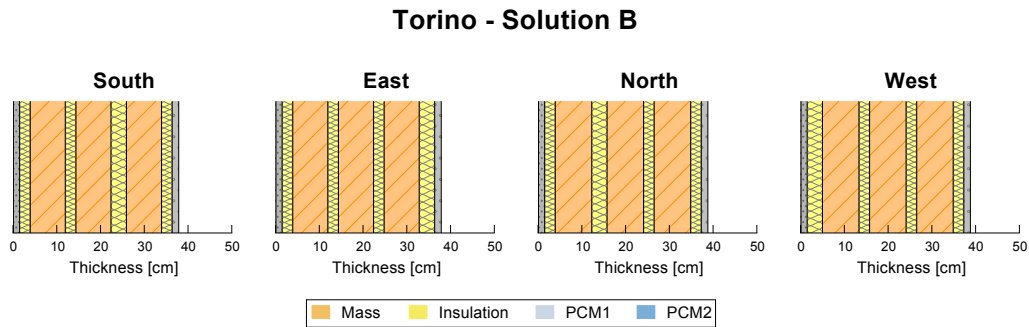
Torino - Solution B

Fig. 5.43 Solutions in the group of B's, Torino.
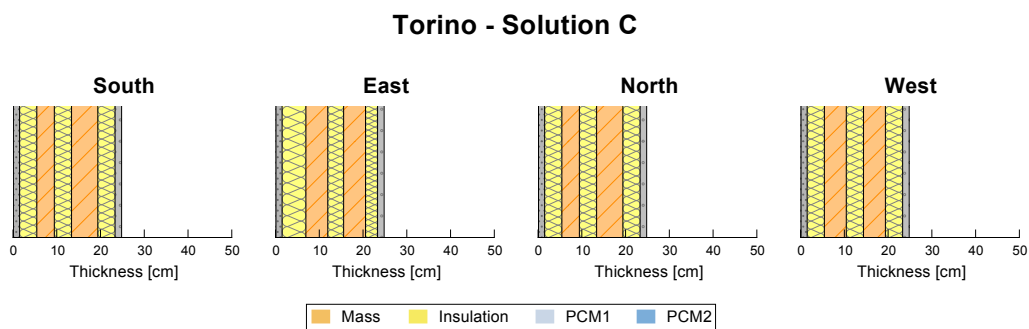
Torino - Solution C

Fig. 5.44 Solutions in the group of C's, Torino.

the expositions other than south. The highest latent heat of fusion of PCM2 was observed for the west-facing solution. As in Palermo, the choice of the thermal conductivity appeared to be quite random. High values were especially selected in the west wall.

The relationship between monthly equivalent periodic thermal transmittance and corresponding time shift is concisely reported in Fig. 5.45. As in the case of Palermo, the most evident differences between each group of the extreme solutions of the Pareto front was an increase of the time shift as the equivalent periodic thermal transmittance decreased. The time shift of the solutions in the group of A's showed again a much greater monthly variability. For all the groups of solutions, the time shifts were higher than in Palermo.

With regard to the additional wall configurations introduced for comparison, some differences compared to the climate of Palermo were observed. First, in terms of Y^*_{mn} solution C outperformed also the configuration with outermost insulation and single layers. Moreover, unlikely in Palermo, the absolute value of the time shift of the solutions in the group of C's was comparable to that of the outperformed configurations, with the only exception of the case with insulation in the middle of the wall. Secondly, when increasing the number of layers, a limit value of Y^*_{mn} was observed beyond which no further improvement—nor worsening—was obtained.
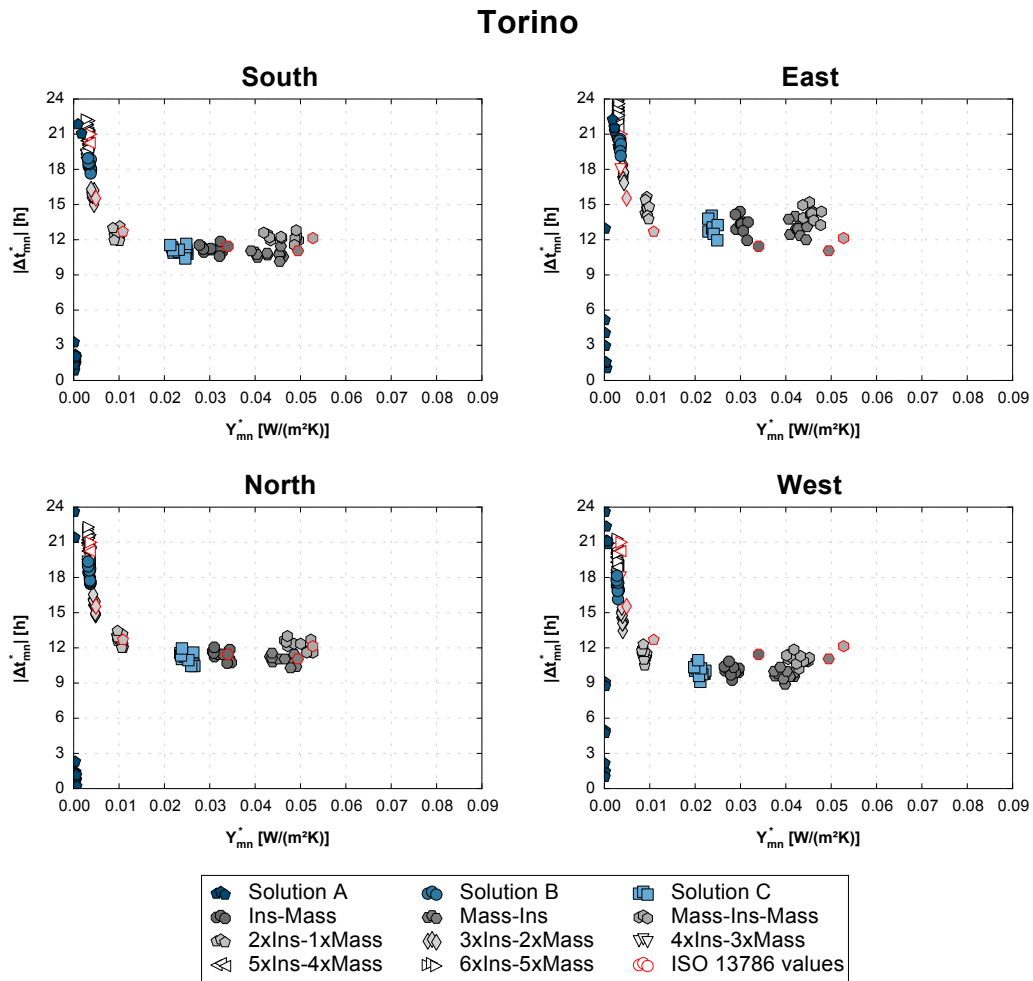
Torino

Fig. 5.45 Monthly Y_{mn}^* vs Δt_{mn}^*, Torino.

However, as in Palermo, the time shift continued to increase. Indeed, although less evident than in Palermo, a minimum value of the traditional Y_{mn} was found for the configuration with four layers of mass and five layers of insulation. It is therefore likely that a minimum Y_{mn}^* would have been found if the optimisation algorithm had been allowed to select more layers.

5.2.3.3 Oslo

The optimal solutions in Oslo will be herewith discussed.

Frequency analyses of the number of layers within the Pareto front solutions are reported for each orientation in Fig. 5.46. Compared to the other locations, less individuals belonged to the Pareto fronts. In all the orientations, at least 40% of solutions were characterised by seven layers (computed with the exception of external render and internal plaster), and more than another 40% of solutions had eight layers in the east and west façades. The number of layers selected for each material is detailed in Fig. 5.47. Unlikely the other locations, a slight preference over three layers of insulation was highlighted only for the south and west orientations. A clear preference between three and four layers was observed towards north, whereas four layers were mostly selected in the east façade. The same trends were observed for the mass, but shifted counting one layer less. Due to the heating-dominated climate of Oslo, PCM2 was used no more than in 25% of the solutions, and mostly in the west and east façades. PCM1 was used especially in the south and north expositions. Two layers were most often selected in the north and west façades, whereas no strong preference between one or two layers was observed towards east and south.

Details on the layers' distribution within the walls with 5 to 8 layers are shown in Fig. 5.48 and Fig. 5.49. Similarly to Torino, three layers of insulation alternated with mass were generally selected in the solutions with five or six layers, whereas four layers of insulation were mostly chosen in solutions with seven or eight layers. In the south, north and west façades, PCM1 was almost always placed in the innermost position. When eight layers were selected in the south and west expositions, another layer of PCM1 was sometimes added in position 2. A greater variability in the position of the potential second layer of PCM1 within the wall was observed in the other orientations. PCM2 was used scarcely.

To have an overview of the values assumed by the continuous variables within the Pareto front, box plots are reported in Fig. 5.50. Grey box plots indicate that less than 20 values were used to draw them. Unlikely the other locations, all the solutions in all the orientations were characterised by almost the same peak melting temperature of PCM1, approximately 20 ℃, which was the imposed boundary condition of the internal air temperature for the majority of the months throughout the year. For the peak melting temperature of PCM2, a narrow range of values was selected only in the south façade. The latent heat of fusion of PCM1 tended to assume high values, as well as the melting temperature range, although to a lesser extent. It can be inferred that the constraint over the melting temperature range prevented it from consistently reaching the upper bound (the narrower the interquartile range of the latent heat of fusion, the lower the melting temperature range). In the opposite way, a high melting temperature range for PCM2 in the
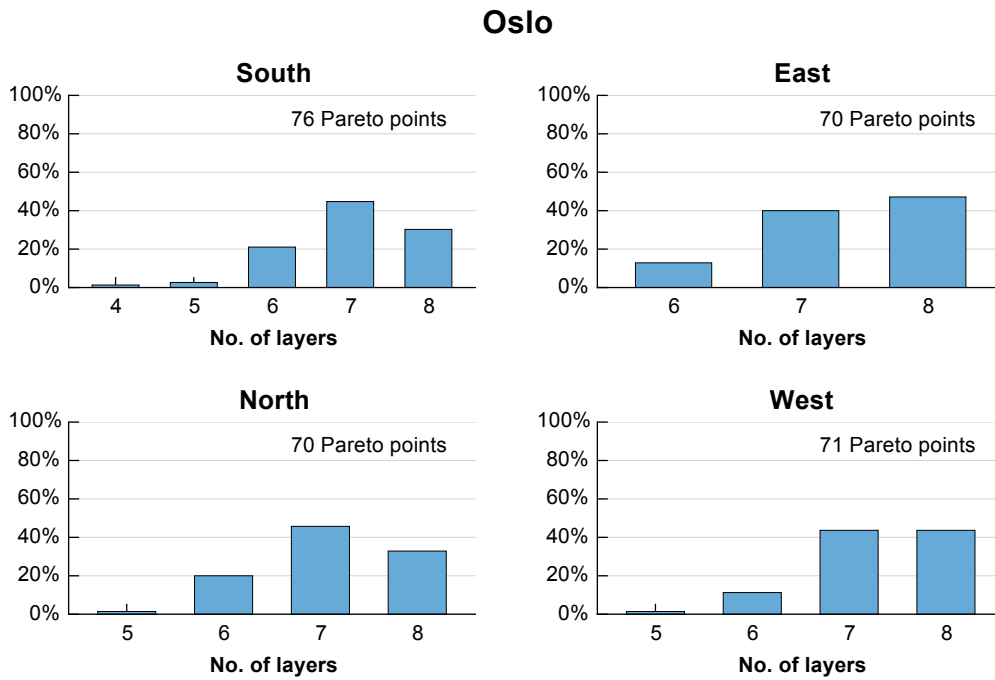
Oslo

Fig. 5.46 No. of layers within the Pareto front solutions: Oslo.
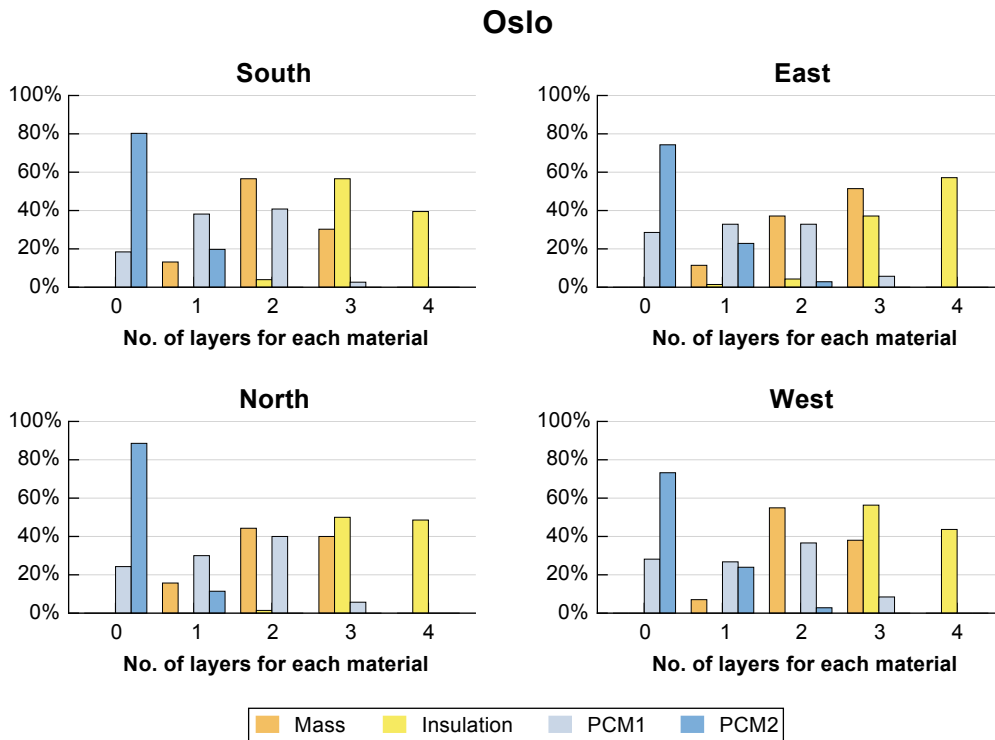
Oslo

Fig. 5.47 No. of layers for each material within the Pareto front solutions: Oslo.
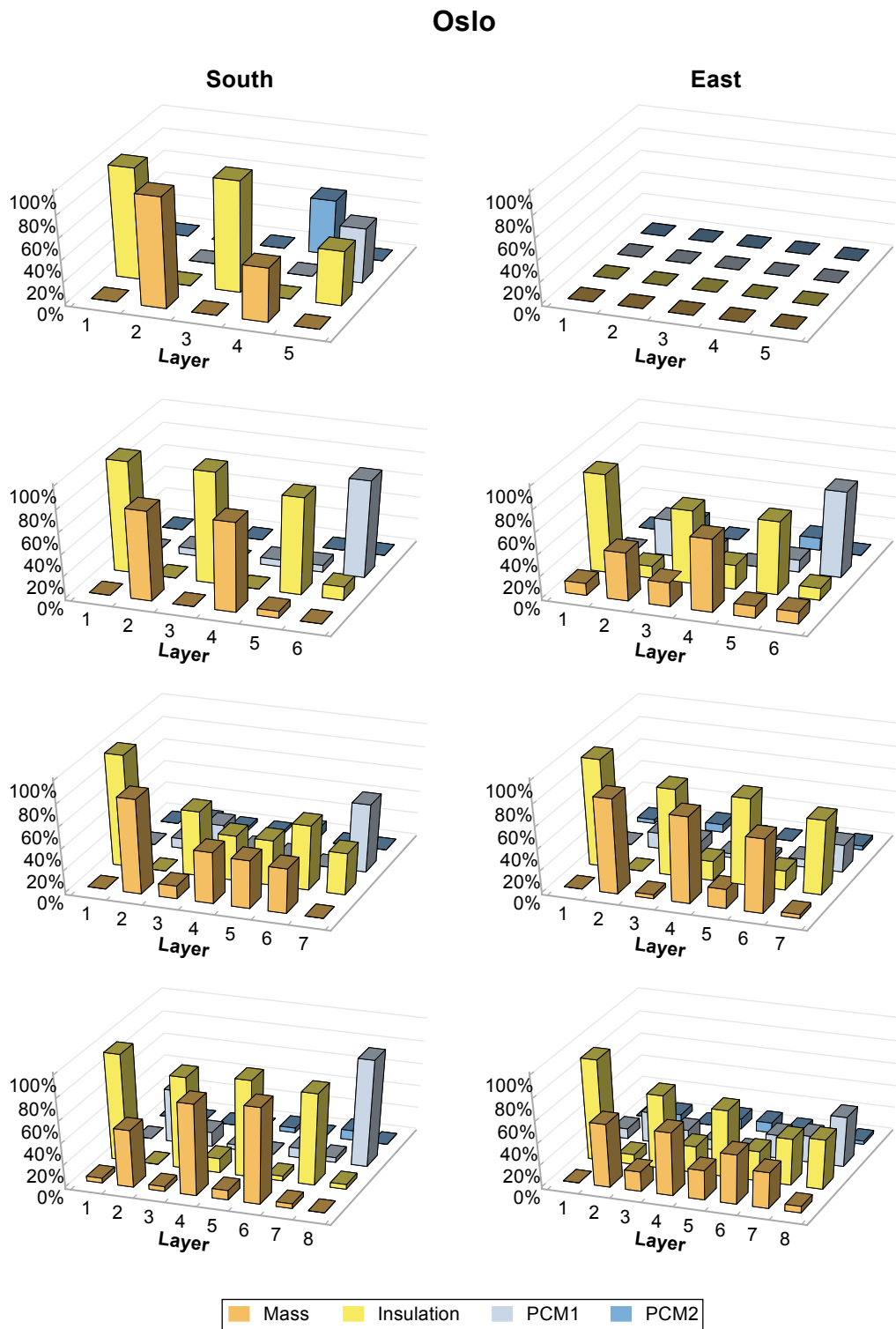
Fig. 5.48 Frequency analysis of the layers' position: Oslo, south and east façades.

Oslo

North   West
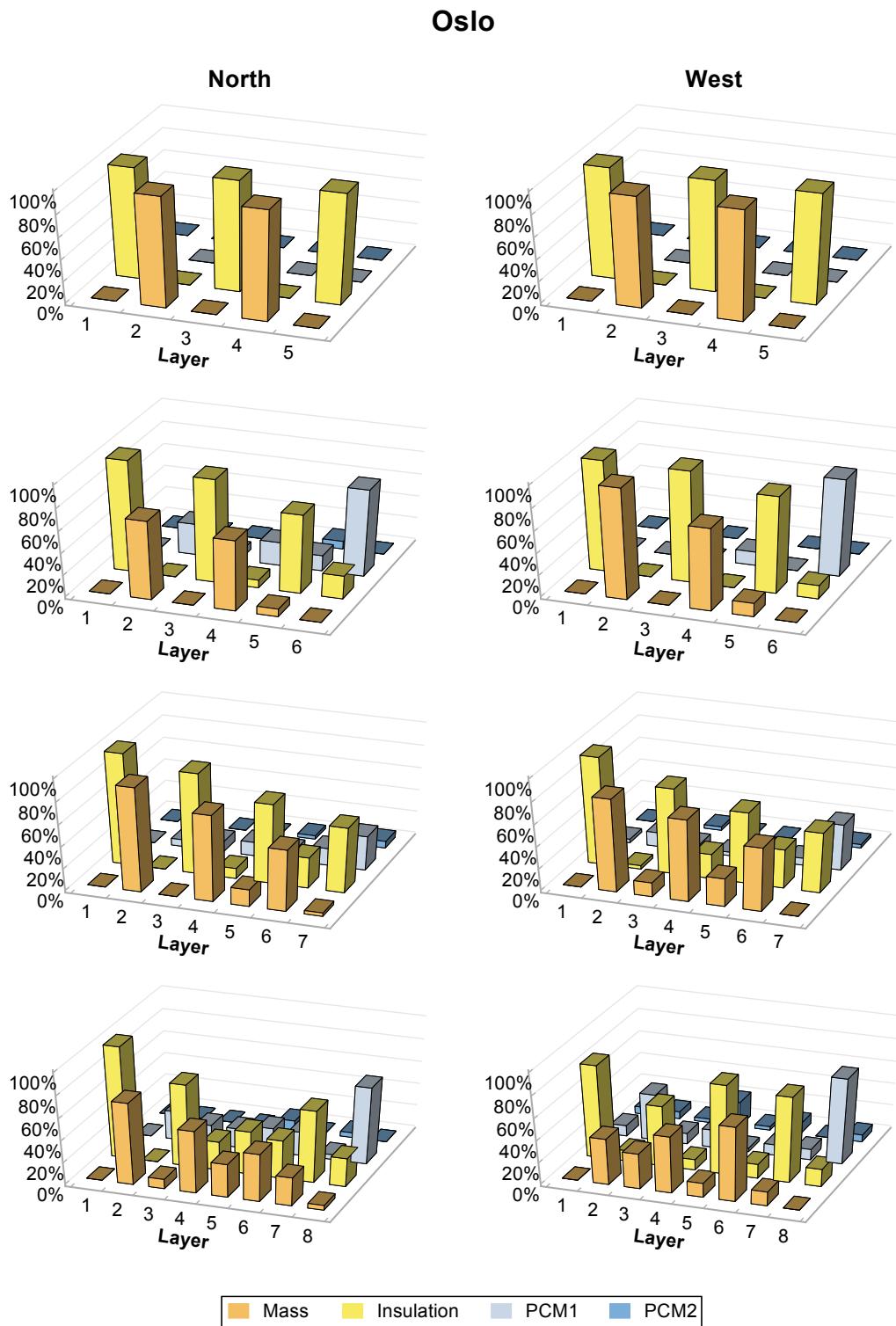
Fig. 5.49 Frequency analysis of the layers' position: Oslo, north and west façades.
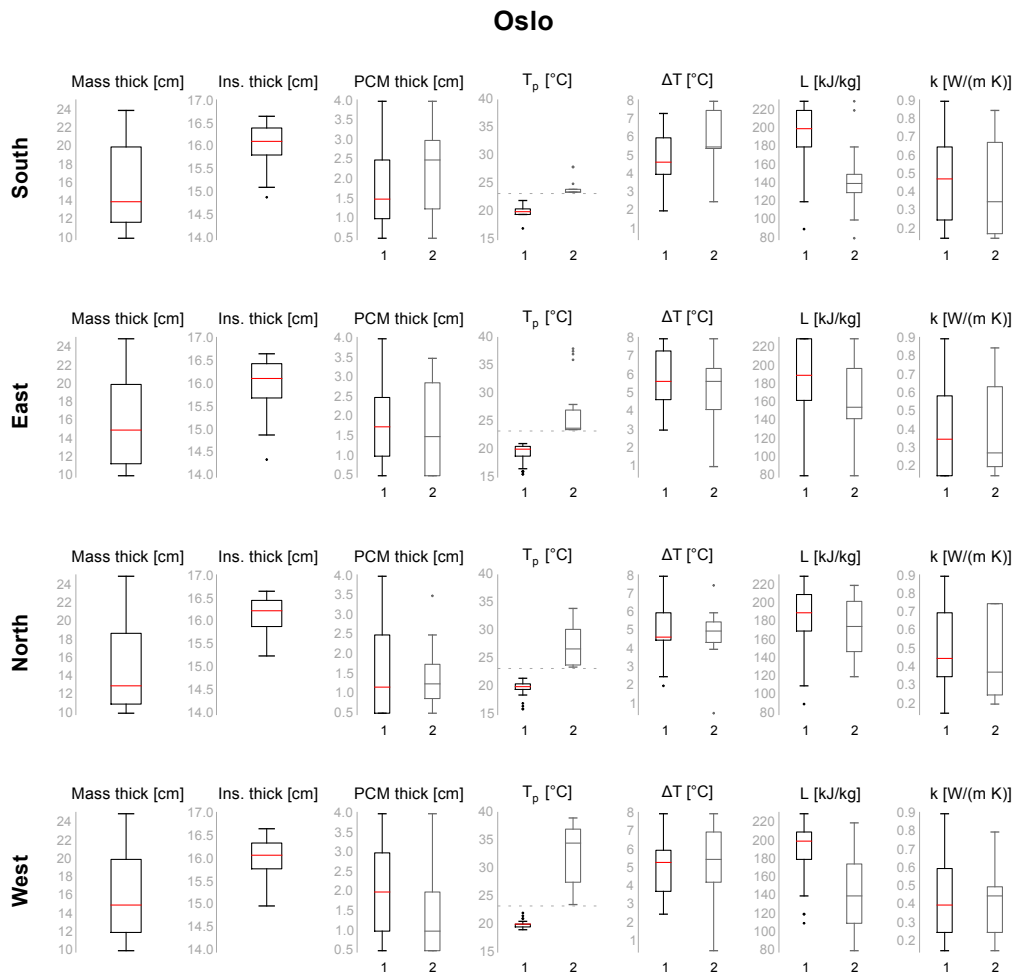
Fig. 5.50 Box plots: Oslo.

south and west façades corresponded to lower latent heats of fusion. With regard to the thermal conductivity, medium/low values seemed to be preferred for both PCMs. Mostly low thicknesses of PCM1 were selected for all the orientations, with higher values on the west façade. Low thicknesses of PCM2 were preferred in the north-facing walls, whereas higher values were selected especially towards south and east.

Since box plots do not provide information on the underlying distributions, further details are shown in Fig. 5.51, Fig. 5.52 and Fig. 5.53, where frequency analyses of the materials' overall thickness and thermo-physical properties of PCM1 and PCM2 are respectively reported. With regard to the materials' thickness, a tendency for low values was confirmed for the PCMs, with the exception of PCM2 towards south, where no clear preference was highlighted. A trend for low mass was observed especially in the north façade. With regard to the thermo-physical
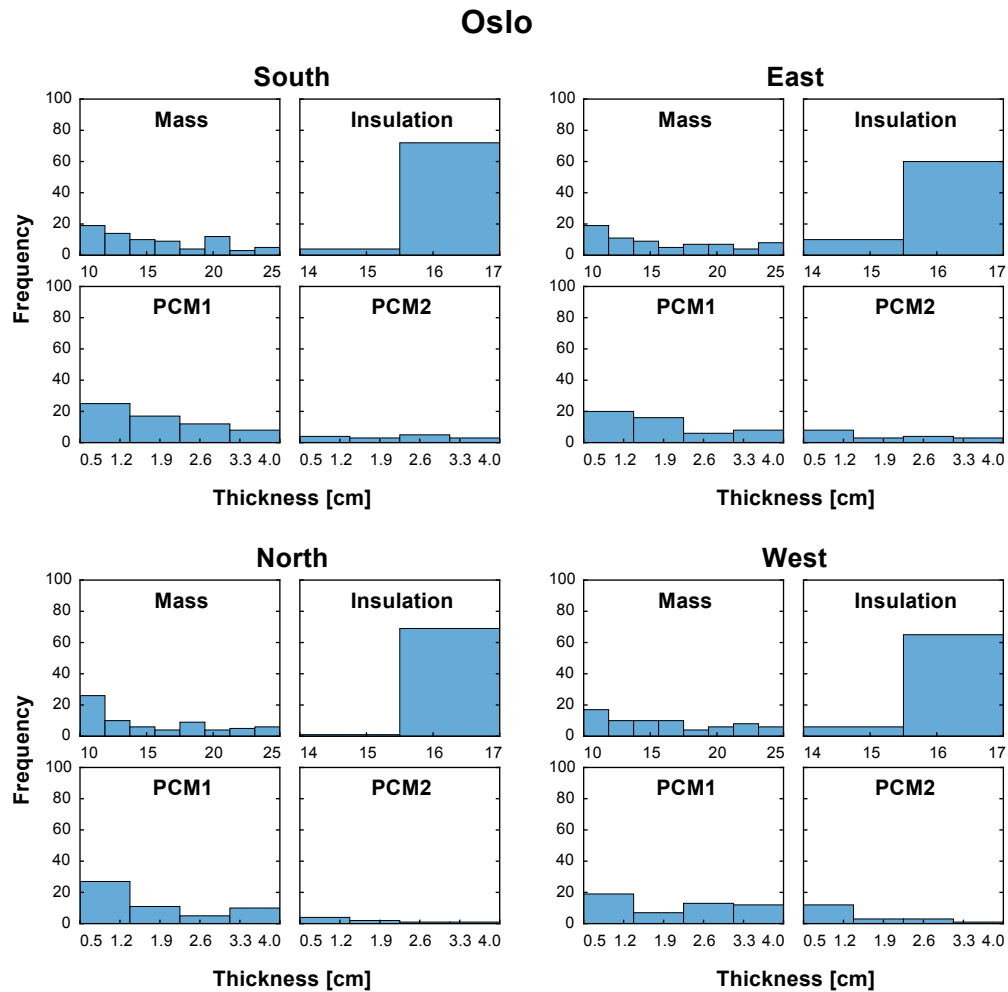
Fig. 5.51 Frequency analyses of the materials' thickness: Oslo.

properties of PCM1, a clear peak of the distribution could be observed for the peak melting temperature especially towards west, south and north. A median value of 20 ℃ was evaluated for all the orientations, with a lower average towards east and north. Medium to high melting temperature ranges were chosen in all the orientations, even though the highest values were selected in the east and west walls. A high latent heat of fusion was generally preferred, whereas no clear trend was observed for the thermal conductivity, except for low modal values towards east. With regard to the PCM2 properties, a modal peak melting temperature of 23.5 ℃ was observed towards south and east. PCM2 was therefore effective during mid-season and summer months when the internal set-point temperature was 23 ℃. Due to the very low number of solutions with PCM2, no other clear trend could be devised.

To explore how the search space variables affected the results in the objective
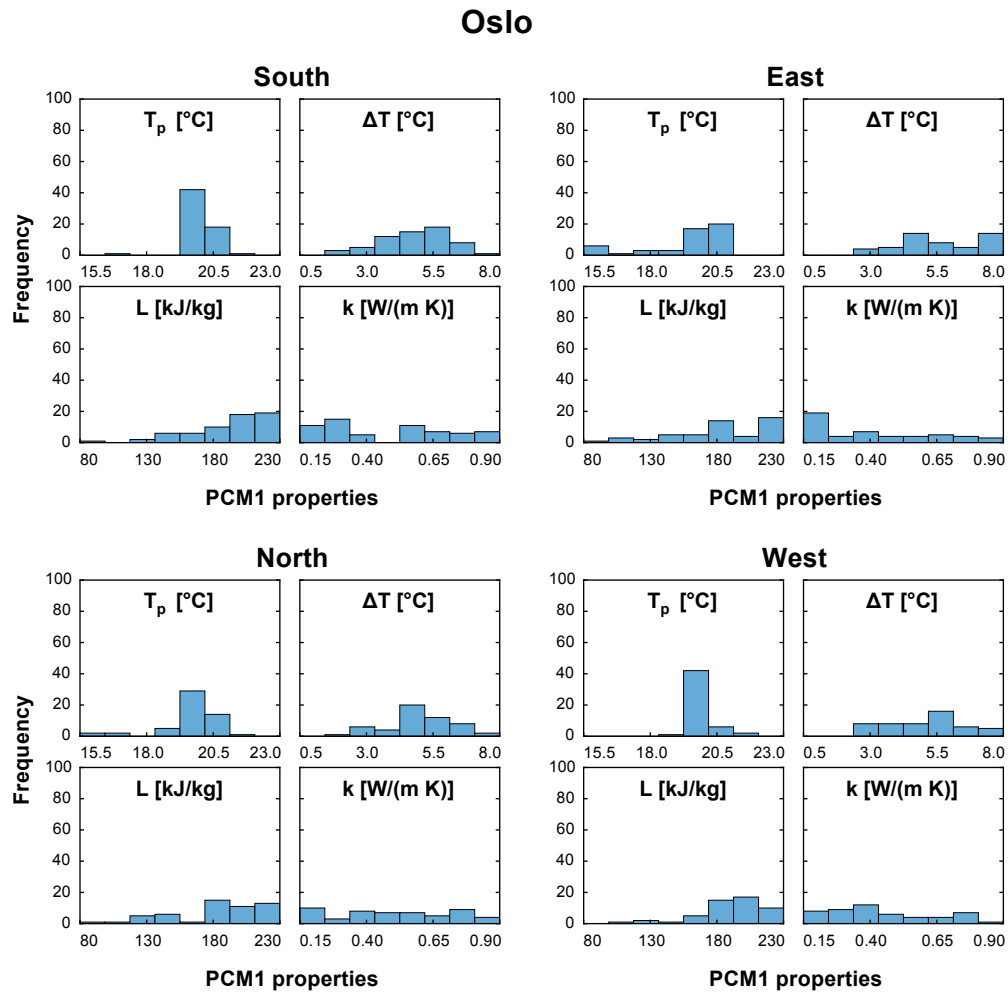
Fig. 5.52 Frequency analyses of the PCM1's properties: Oslo.

space, the values assumed by each variable were mapped on the Pareto front. Maps for materials' thickness plus number of layers and for PCM properties in the south-facing walls are respectively reported in Fig. B.17 and Fig. B.18. Although the low number of solutions with PCM2, its thickness was on average higher than that of PCM1. In Oslo as well, solutions with no PCM were characterised by increasing number of insulation/mass layers for growing mass thickness. However, only solution C was characterised by three layers of insulation except towards east, where all the solutions with no PCM presented four layers of insulation and therefore three layers of mass. Apart from a few exceptions, solutions with PCM1 were mostly characterised by either one or two layers, whereas only one layer was selected for PCM2. With regard to the PCM properties, what emerged from the previous analyses was simply confirmed, i.e. almost constant peak melting temperature of both PCMs and high latent heat of fusion of PCM1.
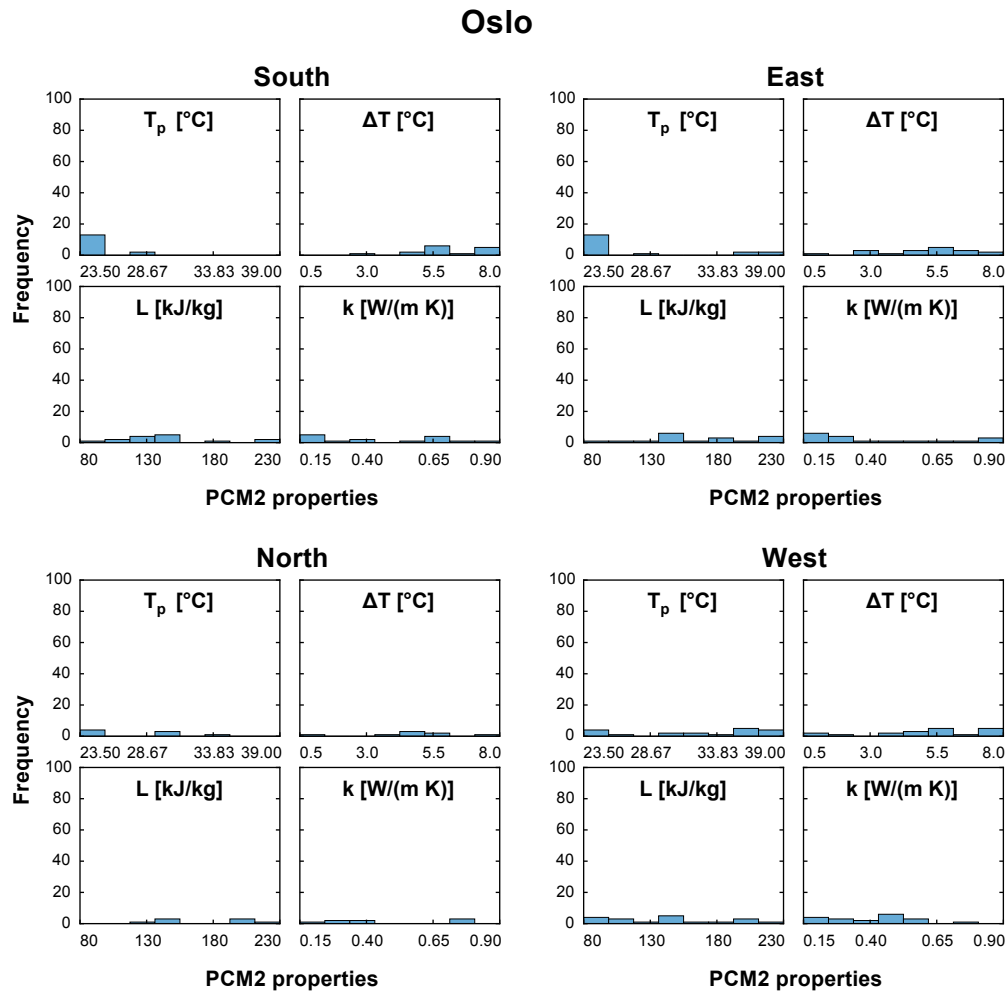
Oslo

Fig. 5.53 Frequency analyses of the PCM2's properties: Oslo.

Maps for materials' thickness plus number of layers and for PCM properties in the east-facing walls are respectively reported in Fig. B.19 and Fig. B.20. No significant differences from the south façade were observed. With regard to the PCM properties, a greater variability for the peak melting temperatures was observed compared to the south façade. Moreover, higher melting temperature ranges and latent heats of fusion were reached for PCM1. No trends were observed for the properties of PCM2.

Maps for materials' thickness plus number of layers and for PCM properties in the north-facing walls are respectively reported in Fig. B.21 and Fig. B.22. With regard to the number of layers for each material, three layers of mass and four layers of insulation were generally preferred with no or low PCM thickness, whereas two layers of mass and three of insulation were mostly preferred when PCM was adopted. Solutions with only one layer of mass were either characterised by a low

Oslo - Solution A

South

PCM1 properties
Peak melting temperature: 19.5 °C
Melting temperature range: 4.5 °C
Latent heat of fusion: 170 kJ/kg
Thermal conductivity: 0.30 W/(m K)

PCM2 properties
Peak melting temperature: 23.5 °C
Melting temperature range: 5.5 °C
Latent heat of fusion: 140 kJ/kg
Thermal conductivity: 0.85 W/(m K)

East

PCM1 properties
Peak melting temperature: 20.0 °C
Melting temperature range: 3.0 °C
Latent heat of fusion: 230 kJ/kg
Thermal conductivity: 0.70 W/(m K)

PCM2 properties
Peak melting temperature: 23.5 °C
Melting temperature range: 6.0 °C
Latent heat of fusion: 130 kJ/kg
Thermal conductivity: 0.85 W/(m K)

North

PCM1 properties
Peak melting temperature: 20.0 °C
Melting temperature range: 4.7 °C
Latent heat of fusion: 230 kJ/kg
Thermal conductivity: 0.35 W/(m K)

PCM2 properties
N/A

West

PCM1 properties
Peak melting temperature: 19.5 °C
Melting temperature range: 5.5 °C
Latent heat of fusion: 210 kJ/kg
Thermal conductivity: 0.25 W/(m K)

PCM2 properties
Peak melting temperature: 29.5 °C
Melting temperature range: 4.5 °C
Latent heat of fusion: 110 kJ/kg
Thermal conductivity: 0.35 W/(m K)

Mass   Insulation   PCM1   PCM2

Fig. 5.54 Solutions in the group of A's, Oslo.

mass thickness or they were in the surroundings of solution A. When thicknesses of PCM1 higher than 1 cm were involved, two layers of PCM1 were mostly selected. Solutions with PCM2 were characterised by a single layer. With regard to the PCM properties, results were quite similar to those for the south façade.

Maps for materials' thickness plus number of layers and for PCM properties in the west-facing walls are respectively reported in Fig. B.23 and Fig. B.24. Compared to the other expositions, where four layers of insulation were selected when at most 3.5/4 cm of PCM were present, in the west façade four layers if insulation were found with up to 5.5 cm of PCM thickness. With regard to the PCM properties, no significant difference was observed compared to the other orientations. Apart from a few outliers, the peak melting temperature of PCM1 was characterised by the narrowest range of variation.

Eventually, the extreme solutions of the Pareto front are reported in Fig. 5.54,
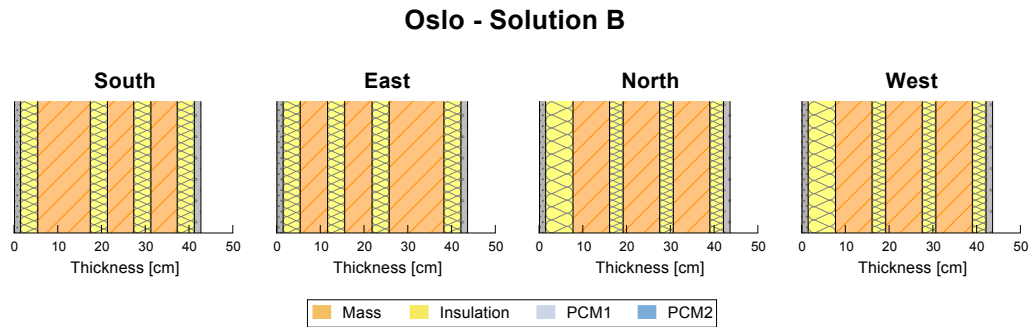
Oslo - Solution B

Fig. 5.55 Solutions in the group of B's, Oslo.
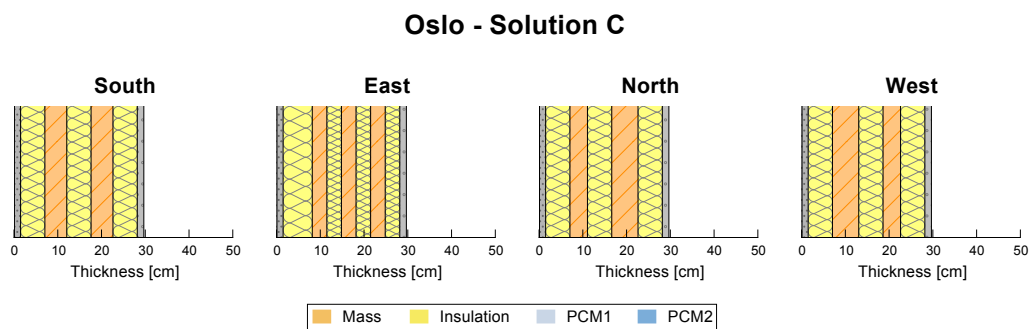
Oslo - Solution C

Fig. 5.56 Solutions in the group of C's, Oslo.

Fig. 5.55 and Fig. 5.56. Solution C (worst performance in terms of Y^*_{mn}, no PCM and minimum mass) was very similar to those of the other orientations. It was characterised by three layers of insulation alternated with two layers of mass in all the orientations except east, where four and three layers were respectively selected for insulation and mass. Similarly to Torino, solution B (best performance in terms of Y^*_{mn} with no PCM and maximum mass) was characterised by four layers of insulation and three layers of mass in all the façades. Solution A was characterised by three layers of insulation in all the expositions, two layers of mass towards south and west, by a single thin mass layer towards east and a thick mass layer in the north facing wall. All the solutions were characterised by at least two thin layers of PCM1 on both sides of the wall; one of which was always placed as the innermost layer. According to its position, the outermost PCM1 layer underwent phase transition mostly during mid-season or summer months (Fig. 5.57). Therefore, the same PCM could be used to enhance both winter and summer performance according to its position within the wall. The peak melting temperature of PCM1 was either 19.5 ℃ or 20.0 ℃, and its latent heat of fusion was either equal or close to the upper bound except towards south. Quite low thermal conductivities were generally preferred except in the east façade. The melting temperature range varied between 3.0 ℃ and 5.5 ℃. A thick layer of PCM2 was embedded in intermediate positions in the south and east walls with a peak melting temperature of 23.5 ℃
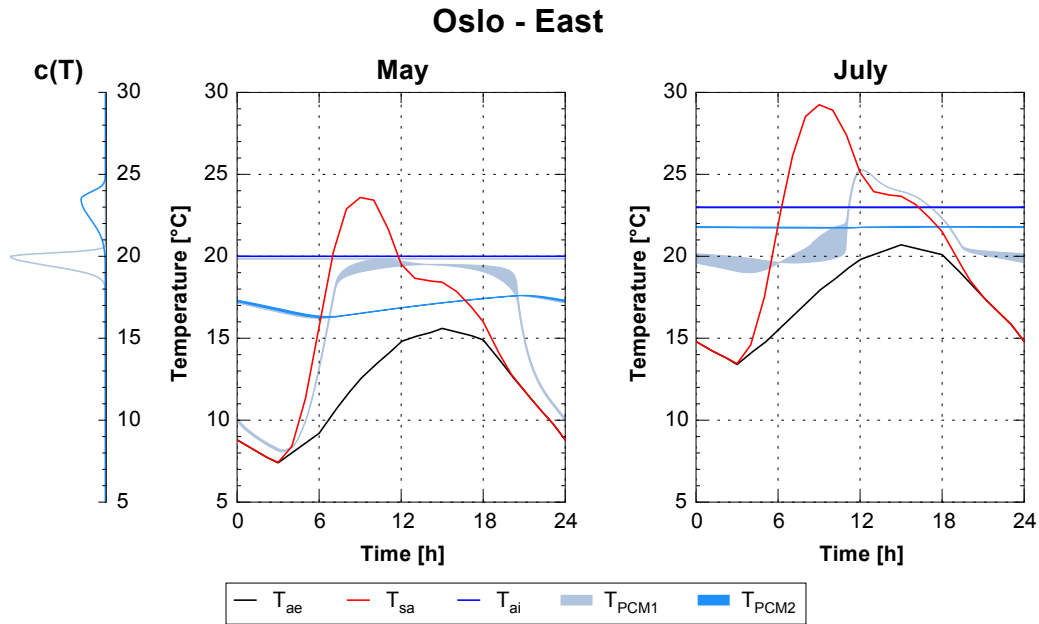
Fig. 5.57 Temperature profiles within the PCM layers in Oslo (Solution A, east).

and a high thermal conductivity. Only a thin layer was added in the outermost position towards west, with a reasonably higher peak melting temperature of 29 ℃. In the north wall, PCM2 was not used. All solutions with PCM2 were characterised by a latent heat of fusion no higher than 140 kJ/(kg K) and a melting temperature range which varied between 4.5 ℃ and 6.0 ℃.

The relationship between monthly equivalent periodic thermal transmittance and corresponding time shift is concisely reported in Fig. 5.58. As in the previous cases, the most evident differences between each group of the extreme solutions of the Pareto front was an increase of the time shift as the equivalent periodic thermal transmittance decreased. Also in this location, the time shift of the solutions in the group of A's showed a greater monthly variability. Although the lower Y_{mn}^* values, the time shifts were only slightly higher than in Torino.

With regard to the additional wall configurations introduced for comparison, results were quite similar to those of Torino. In terms of Y_{mn}^*, solution C outperformed the same configurations as in Torino. However, the absolute value of the time shifts were even more similar between the group of outperformed configurations, and in the east exposition solution C was characterised also by a greater time shift. When increasing the number of layers, a limit value of Y_{mn}^* was observed beyond which no further improvement nor worsening was obtained, as in the case of Torino. However, although even less evident than in Torino, a minimum value of the traditional Y_{mn} was found for the configuration with four layers of mass and five layers of insulation.
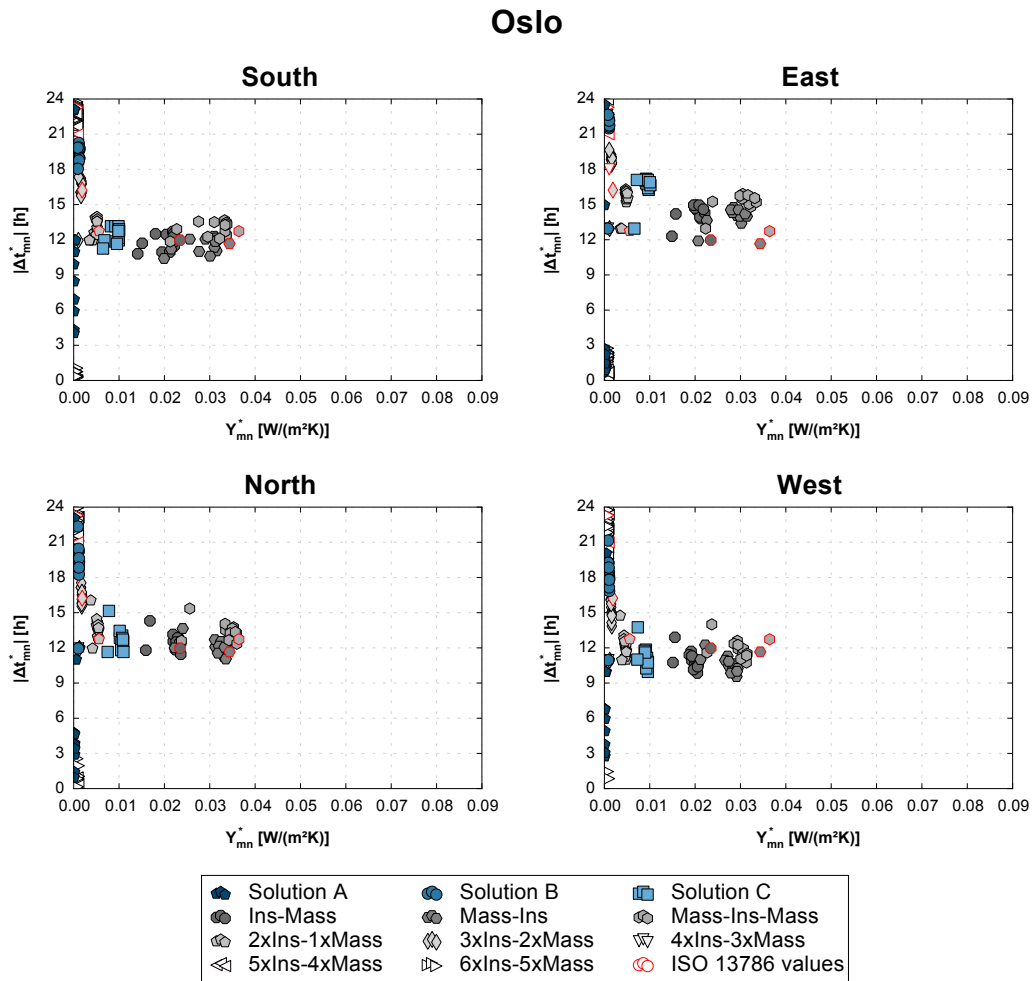
Oslo

Fig. 5.58 Monthly Y_{mn}^* vs Δt_{mn}^*, Oslo.

As it was already highlighted, when comparing the solutions in the group of B's and those in the group of A's, the presence of PCM did not introduce significant improvements in terms of Y_{mn}^*. The difference was mainly in terms of time shift. However, the time shift becomes practically meaningless for Y_{mn}^* values that are so low that the heat flux response can be considered flat.

5.3 Building-level analyses

In the present section, the results of the building-level optimisation analyses presented in § 4.4 are reported. First, the energy performance of the archetype building before the retrofit intervention (baseline) is presented. The Pareto fronts obtained for each case study were subsequently analysed, and post-optimisation analyses were eventually performed to investigate the properties of the optimised solutions for each retrofit option.

5.3.1 Baseline

The energy performance of the archetype building described in § 4.4.1 for each location is summarised in Table 5.8. The building energy need for heating, cooling and electricity (lighting plus equipment), the primary energy consumption and the share of heating, cooling and electricity on the total primary energy consumption are reported.

Table 5.8 Energy performance of the archetype building (pre-retrofit).

Case study	$Q_{H,nd}$	$Q_{C,nd}$	Q_E $[\text{kWh/(m}^2\text{y)}]$	E_P	$E_{P,H}$	$E_{P,C}$ [%]	$E_{P,E}$
Palermo	7.75	32.94	38.15	137.19	9.5%	23.2%	67.3%
Torino	58.13	14.28	39.43	206.63	47.1%	6.7%	46.2%
Oslo, pre-1955	226.63	-	40.04	410.67	85.0%	-	15.0%
Oslo, post-1955	188.02	-	41.41	353.33	82.0%	-	18.0%

As it can be observed in Table 5.8, in Palermo the electricity share accounts for most of the primary energy consumption. In Torino, space heating and electricity account for almost half of the E_P consumption each. In Oslo, the electricity use for space heating is the major contributor to the primary energy consumption.

5.3.2 Pareto frontiers

The Pareto frontiers resulting from all the building level investigations are herewith illustrated and briefly described. All the energy related values are reported in kWh/(m²y), whereas all the cost values are reported in €/m² (both referred to the gross floor area). It should be remembered that the investment costs were evaluated only for the envelope, as the installation costs of the new HVAC systems were assumed to be unvaried among all the solutions for each location (see § 4.4.6.1).
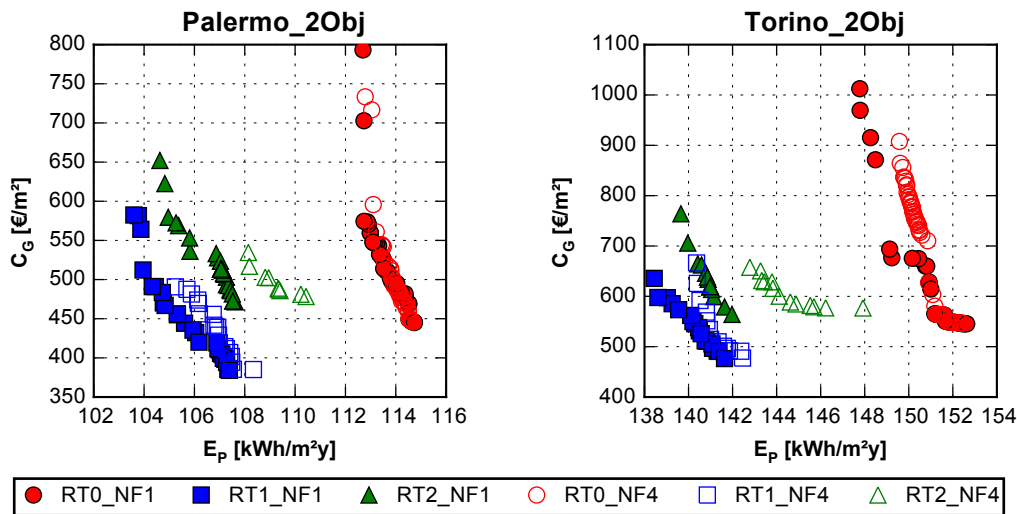
Fig. 5.59 Pareto front: Palermo and Torino, two objectives.

5.3.2.1   Two objectives (Italy)

The Pareto fronts of the two-objective building level investigations, which aimed at minimising primary energy consumption and global cost, are reported in Fig. 5.59. Out of the total population (100 individuals), only few solutions (ranging from 9 to 42 in Palermo and from 13 to 56 in Torino) belonged to the non-dominated sets.

For both locations, the retrofit on the internal side (RT1) allowed to achieve lower energy consumption with a lower global cost. The retrofit on both sides of the wall (RT2) allowed to obtain primary energy consumption approximately in the same range of RT1 but with a higher global cost. The retrofit on the external side (RT0) resulted instead to be the worst option. Also, the RT1 and RT0 cases resulted to be characterised respectively by the lowest and highest contrast between objective functions.

With regard to the differences between the same retrofit solution for all walls (NF1) or a different wall solution for each orientation (NF4), very similar solutions (at least in terms of objective space) were found for the RT0 case. Some of the solutions belonging to the NF4 front dominated part of the NF1 front. For the RT1 and RT2 cases, the NF1 front always dominated the NF4 front. The greatest difference was obtained in case of retrofit on both sides of the wall, probably due to the lower exploration level reached by the optimisation algorithm for such case.

The fitnesses of the extreme solutions are reported in Table 5.9 and Table 5.10 respectively for the climates of Palermo and Torino. Solution A is characterised by the lowest primary energy consumption. Due to the contrast between objectives, it is also the solution with highest global cost. On the contrary, solution B is

Table 5.9 Fitness of the extreme solutions: Palermo, two objectives.

Solution	E_P $[\text{kWh/(m}^2\text{y)}]$	C_G $[\text{€/m}^2]$	E_P $[\text{kWh/(m}^2\text{y)}]$	C_G $[\text{€/m}^2]$
	RT0 – NF1		**RT0 – NF4**	
Solution A	112.7	793.23	112.8	733.33
Solution B	114.7	445.08	114.7	445.95
	RT1 – NF1		**RT1 – NF4**	
Solution A	103.6	582.45	105.2	490.73
Solution B	107.4	384.06	108.3	385.12
	RT2 – NF1		**RT2 – NF4**	
Solution A	104.6	652.06	108.1	534.56
Solution B	107.6	471.51	110.4	478.34

Table 5.10 Fitness of the extreme solutions: Torino, two objectives.

Solution	E_P $[\text{kWh/(m}^2\text{y)}]$	C_G $[\text{€/m}^2]$	E_P $[\text{kWh/(m}^2\text{y)}]$	C_G $[\text{€/m}^2]$
	RT0 – NF1		**RT0 – NF4**	
Solution A	147.8	1012.43	149.6	907.70
Solution B	152.6	545.52	152.4	546.70
	RT1 – NF1		**RT1 – NF4**	
Solution A	138.4	635.66	140.4	666.30
Solution B	141.6	476.41	142.5	477.47
	RT2 – NF1		**RT2 – NF4**	
Solution A	139.7	763.96	142.8	657.67
Solution B	142.0	564.07	147.9	576.84

characterised by the lowest global cost (cost-optimal solution), and therefore by the highest primary energy consumption. However, the variation in primary energy consumption between best and worst solution within each Pareto front was very small, ranging only from 2 kWh/(m²y) to 5 kWh/(m²y). The difference in terms of global cost was much more significant.
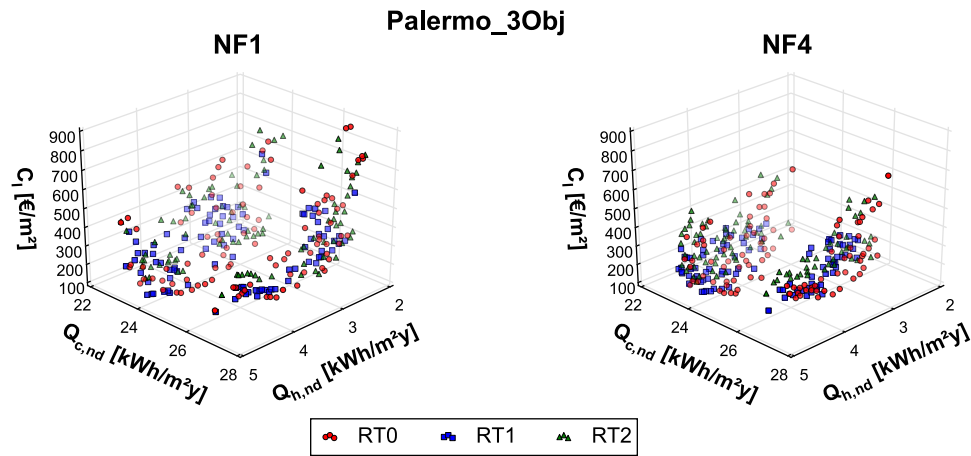
Fig. 5.60 Pareto front 3D: Palermo, three objectives.
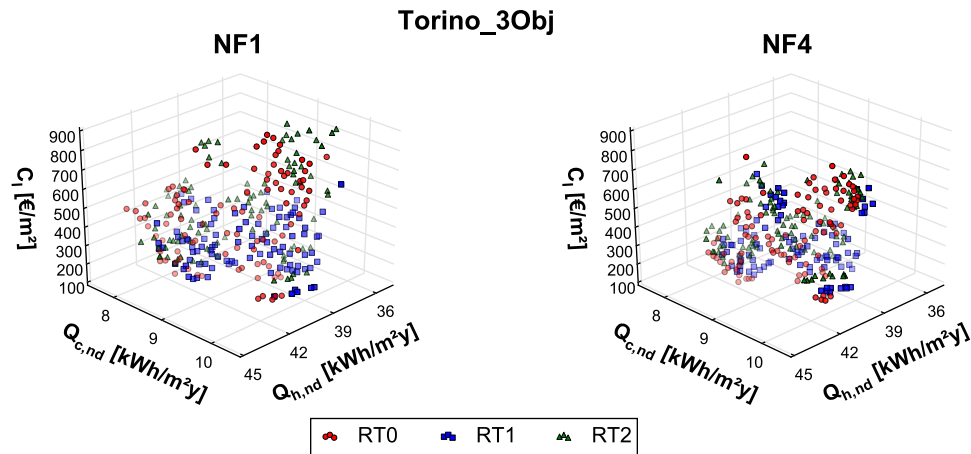
Fig. 5.61 Pareto front 3D: Torino, three objectives.

5.3.2.2   Three objectives (Italy)

The Pareto fronts of the three-objectives investigations, which aimed at minimising building energy need for heating and cooling and investment cost, are reported in Fig. 5.60 and Fig. 5.61 respectively for the cases of Palermo and Torino. The corresponding two-dimensional projections on each plane, where the big dots highlight the bi-dimensional Pareto front, are respectively reported in Fig. 5.65 and Fig. 5.66. In addition, for a better understanding of the mutual position of the Pareto fronts, they were plotted as continuous surfaces in Fig. 5.62 and Fig. 5.63 respectively for the cases of Palermo and Torino. It should however be noted that this is an improper representation, because the Pareto fronts exhibit a discontinuous behaviour.

Both in the case of Palermo and Torino, intervention on the internal side
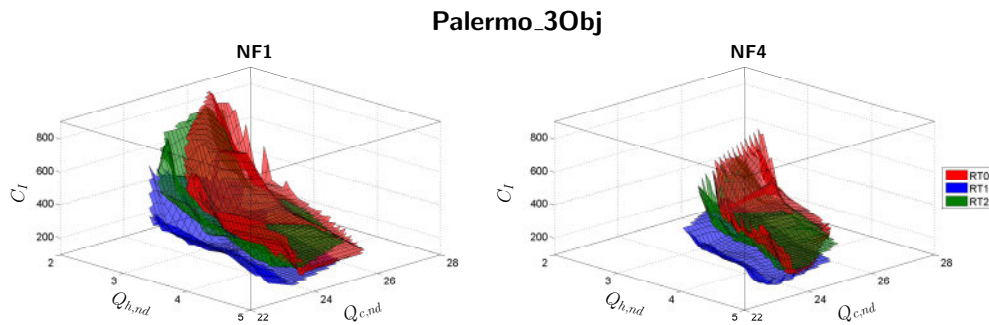
Fig. 5.62 Pareto front 3D surface, Palermo, three objectives.
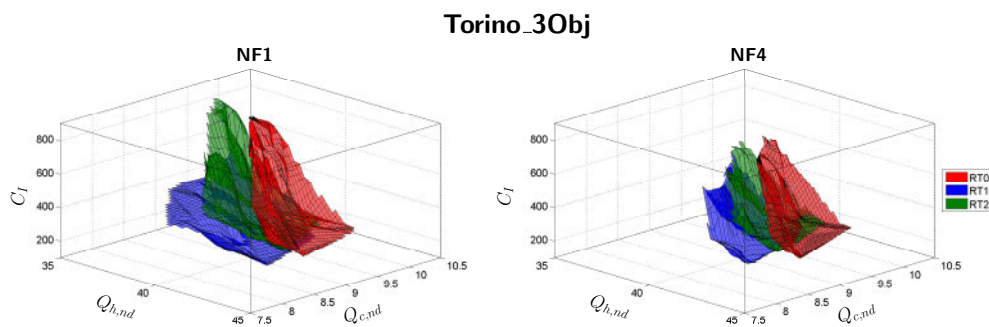
Fig. 5.63 Pareto front 3D surface, Torino, three objectives.

showed an advantage both in terms of energy performance and costs. However, the difference between RT0, RT1 and RT2 fronts in Palermo was less pronounced than in Torino. As it could be expected, a certain degree of contrast was found between all the objective functions. Beyond a limit value (the knee point in the 2D projections of the Pareto fronts), a strong contrast was especially observed between cooling or heating energy need and investment cost in Palermo, and between heating energy need and investment cost in Torino.

All the Pareto fronts in Palermo seemed to be divided in two main clusters, which are especially noticeable from the projection on the $(Q_{h,nd}, Q_{c,nd})$ plane. The reasons behind this characteristic will be evident in § 5.3.3. Even though less pronounced, the Pareto fronts were clustered also in Torino.

With regard to the differences between the same retrofit option for all walls (NF1) or a different wall solution for each orientation (NF4), very similar solutions (at least in terms of objective space) were found for the RT0 and RT1 cases in Palermo and for the RT0 and RT2 cases in Torino. The NF1 front always dominated the NF4 front with the exception of few solutions. Again, this could be due to the lower exploration level reached by the optimisation algorithm for the NF4 cases. Also, the NF1 fronts tended to span along a wider portion of the objective space.

The fitnesses of the extreme solutions are reported in Table 5.11 and Table 5.12 respectively for the climates of Palermo and Torino. Solution A is characterised by the lowest building energy need for heating. In some cases, it also corresponds to the solution with highest investment cost. Solution B is characterised by the lowest building energy need for cooling, whereas Solution C is the solution with the lowest investment cost. Both in Palermo and Torino, the lowest building energy need for heating was obtained with retrofit intervention on both sides of the wall (RT2), whereas the lowest building energy need for cooling together with the lowest investment cost were achieved with intervention on the internal side (RT1). The only exception was the NF4 case in Torino; this was likely due to the lower exploration level reached by GA in that case. However, the solution characterised by the lowest heating energy need in the RT1 case had only a slightly lower performance but a significantly lower investment cost.

The greatest variation between best and worst optimised solution was observed for the investment cost. Only a limited difference was observed for heating energy need in Palermo and cooling energy need in Torino.

A comparison between the Pareto fronts in Palermo and Torino is reported in Fig. 5.64, where the investment cost is colour coded, and the fronts are represented as continuous surfaces just for sake of ease of understanding. For all the cases in Palermo, the lowest investment cost was associated to a high building energy need for heating and cooling, yet not the highest. In Torino the lowest investment cost was instead associated to the highest building energy need for cooling. In both locations, the highest costs were found when simultaneously reducing the building energy need for heating and cooling. However, the greatest impact on investment cost was due to the reduction of building energy need for heating; achieving the lowest building energy need for cooling required only moderate (with respect to the range of variation of the Pareto front) investment costs.

Comparing the NF1 and NF4 cases, NF4 dominated NF1 at least in some regions of the Pareto fronts, especially in case of retrofit on the external side of the wall (RT0). It can therefore be expected that, with an equal exploration level, the NF4 model could have an advantage over the NF1 one within wider portions of Pareto front. However, the computational time required to perform a deeper investigation would be significantly higher.

Table 5.11 Fitness of the extreme solutions: Palermo, three objectives.

Solution	$Q_{h,nd}$ $Q_{c,nd}$ $[\text{kWh}/(\text{m}^2\text{y})]$		C_I $[\text{€}/\text{m}^2]$	$Q_{h,nd}$ $Q_{c,nd}$ $[\text{kWh}/(\text{m}^2\text{y})]$		C_I $[\text{€}/\text{m}^2]$
	RT0 − NF1			**RT0 − NF4**		
Solution A	2.07	26.51	858.18	2.67	27.15	699.22
Solution B	3.81	23.11	549.26	4.80	23.46	409.60
Solution C	4.67	26.35	171.87	4.11	26.41	172.76
	RT1 − NF1			**RT1 − NF4**		
Solution A	2.05	26.72	523.07	2.70	26.12	305.21
Solution B	4.53	22.58	358.47	4.24	22.82	299.53
Solution C	4.87	25.98	116.79	4.43	25.96	117.11
	RT2 − NF1			**RT2 − NF4**		
Solution A	2.04	27.04	736.97	2.65	26.63	559.52
Solution B	4.79	22.82	454.17	4.57	23.08	424.71
Solution C	4.44	26.16	215.90	4.50	26.03	223.57

Table 5.12 Fitness of the extreme solutions: Torino, three objectives.

Solution	$Q_{h,nd}$ $Q_{c,nd}$ $[\text{kWh}/(\text{m}^2\text{y})]$		C_I $[\text{€}/\text{m}^2]$	$Q_{h,nd}$ $Q_{c,nd}$ $[\text{kWh}/(\text{m}^2\text{y})]$		C_I $[\text{€}/\text{m}^2]$
	RT0 − NF1			**RT0 − NF4**		
Solution A	37.19	9.85	769.68	38.72	9.85	642.14
Solution B	44.12	7.98	521.88	43.03	8.46	384.76
Solution C	42.11	9.99	205.44	43.22	8.92	206.82
	RT1 − NF1			**RT1 − NF4**		
Solution A	36.03	9.83	587.83	37.05	9.66	584.08
Solution B	39.73	7.71	431.82	41.85	8.18	307.44
Solution C	41.40	8.76	149.35	41.36	8.66	150.06
	RT2 − NF1			**RT2 − NF4**		
Solution A	35.87	9.66	853.47	37.59	9.66	669.50
Solution B	41.15	7.86	515.99	42.64	8.20	407.40
Solution C	41.82	8.76	248.25	42.30	8.69	259.62
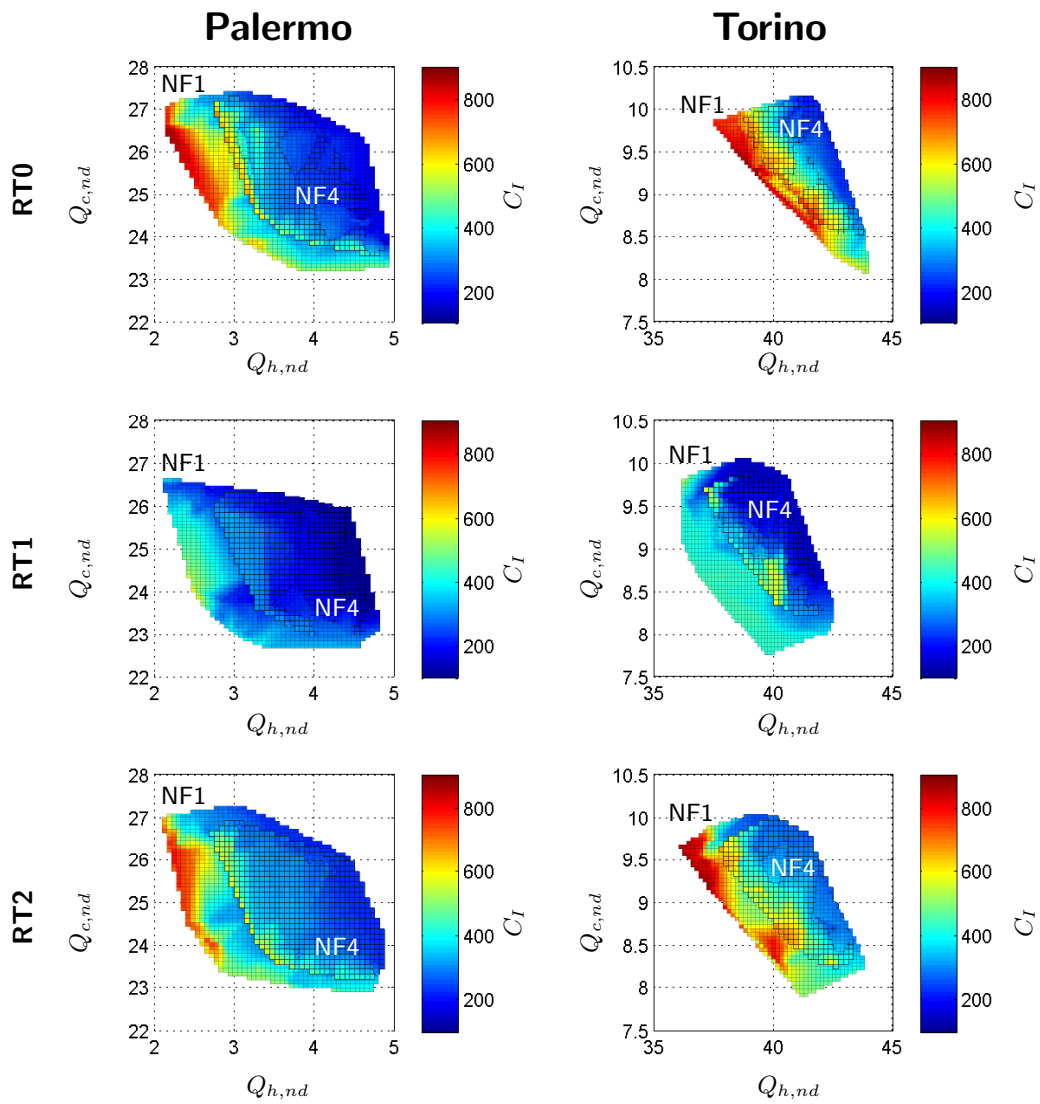
Fig. 5.64 Colour coded Pareto fronts in Palermo and Torino.
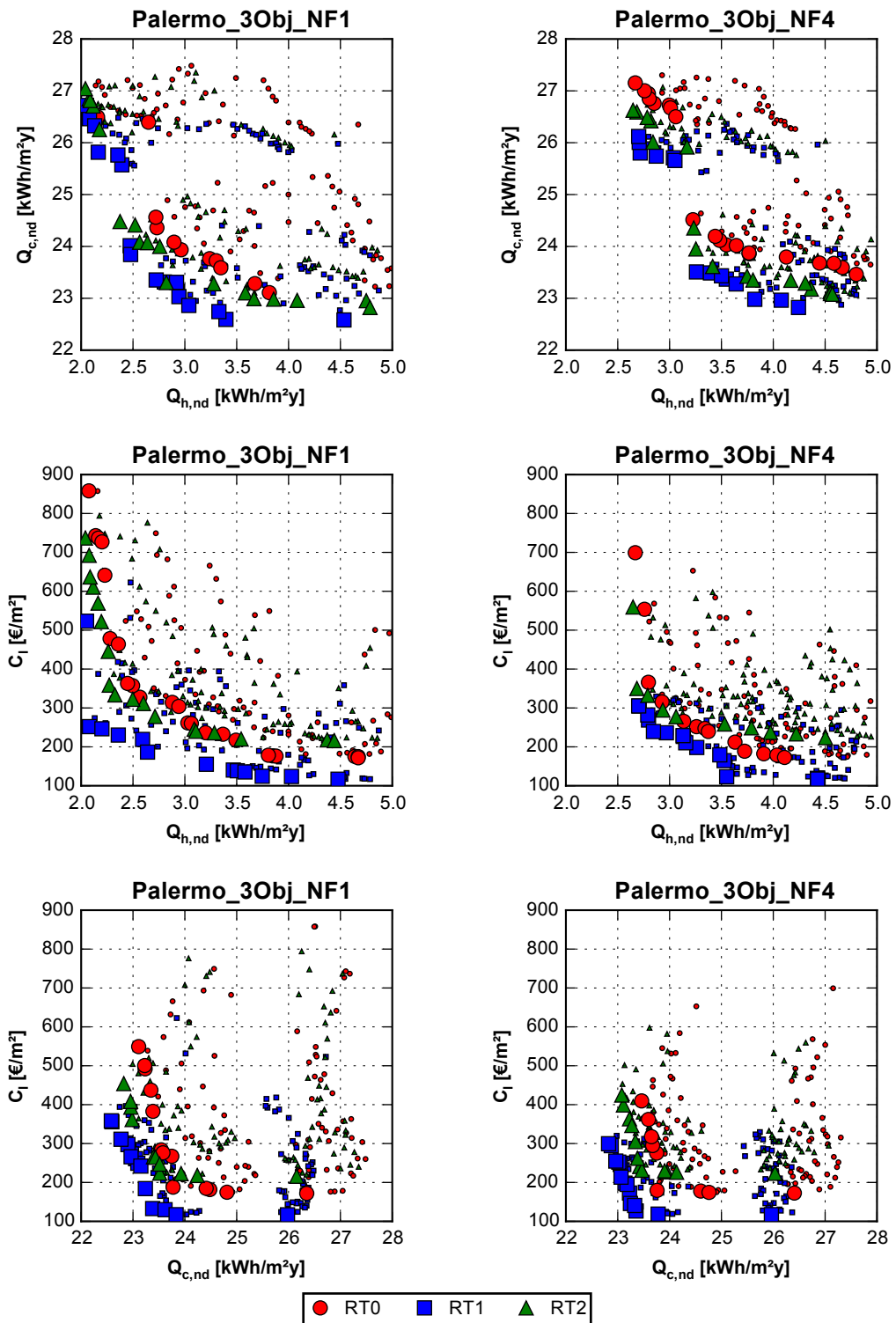
Fig. 5.65 Pareto front: Palermo, three objectives.
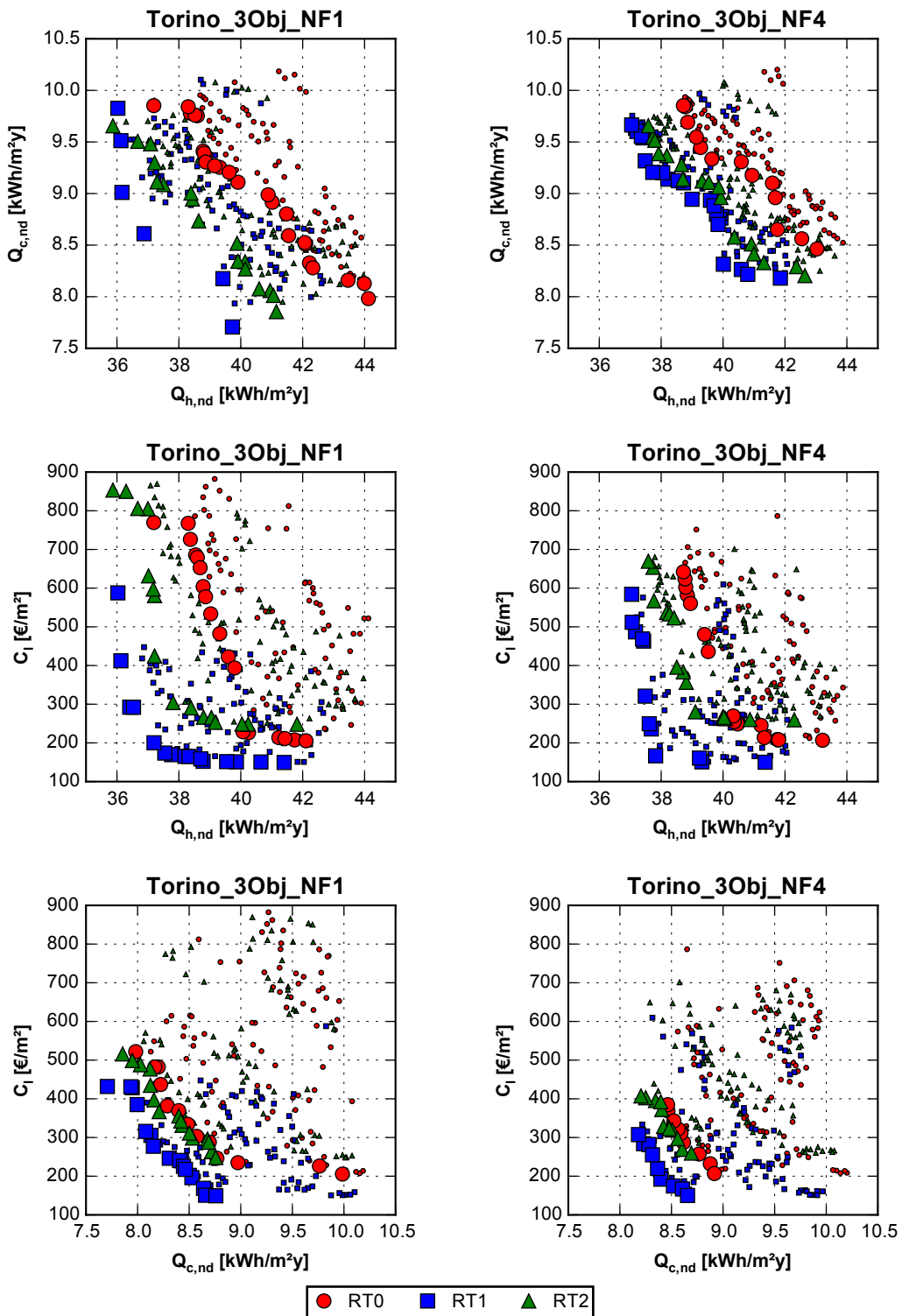
Fig. 5.66 Pareto front: Torino, three objectives.
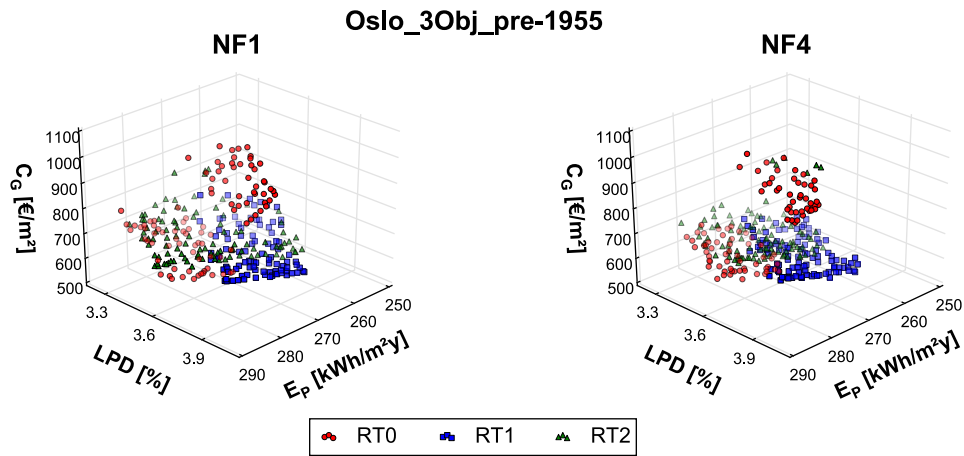
Fig. 5.67 Pareto front 3D: Oslo, pre-1955.
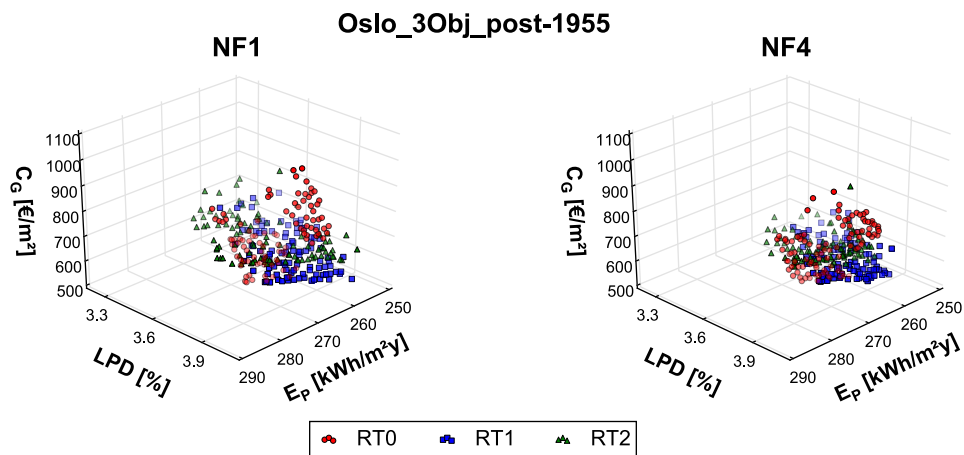
Fig. 5.68 Pareto front 3D: Oslo, post-1955.

5.3.2.3   Three objectives (Oslo)

The Pareto fronts for the case of Oslo, which aimed at minimising primary energy consumption, global cost and Long-term Percentage of Dissatisfied, are reported in Fig. 5.67 and Fig. 5.68 respectively for the retrofit of pre-1955 and post-1955 building. The corresponding two-dimensional projections on each plane, where the big dots highlight the bi-dimensional Pareto front, are respectively reported in Fig. 5.72 and Fig. 5.73. In addition, for a better understanding of the mutual position of the Pareto fronts, they were plotted as continuous surfaces in Fig. 5.69 and Fig. 5.70 respectively for the retrofit of pre-1955 and post-1955 building. It should however be noted that this is an improper representation, because the Pareto fronts exhibit a discontinuous behaviour.

Both in the case of retrofit of the pre-1955 and post-1955 building, intervention
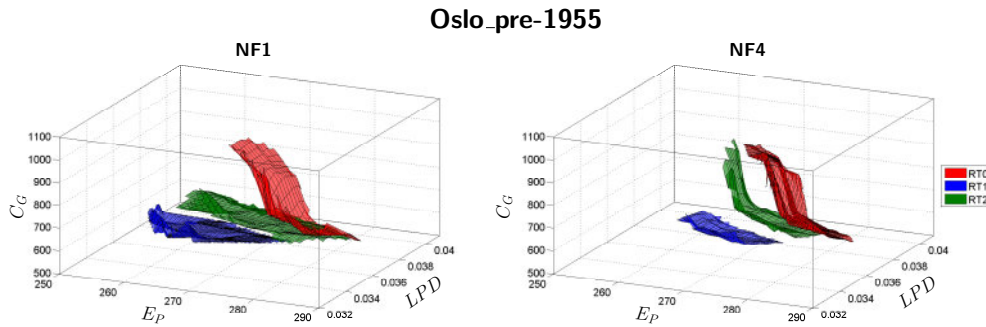
Oslo_pre-1955

Fig. 5.69 Pareto front 3D surface, Oslo, pre-1955.
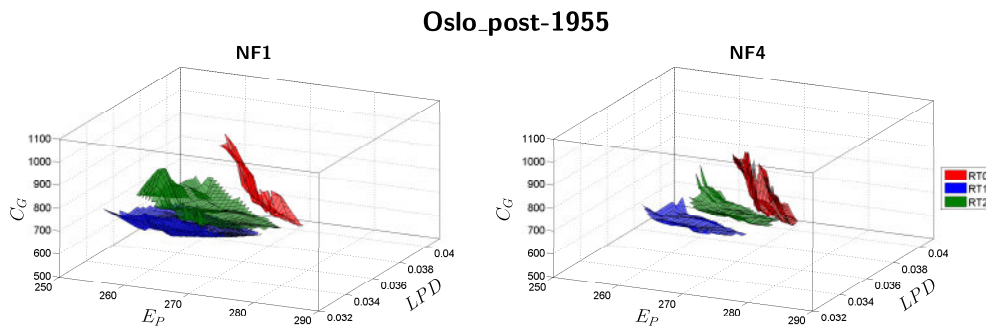
Oslo_post-1955

Fig. 5.70 Pareto front 3D surface, Oslo, post-1955.

on the internal side showed an advantage both in terms of energy performance and global cost. Intervention on both sides of the wall could instead provide the maximum thermal comfort but to the detriment of the other two objectives.

As it could be expected, a certain degree of contrast was found between all the objective functions. Beyond a limit value (the knee point in the 2D projections of the Pareto fronts), a strong contrast was especially observed between primary energy consumption and global cost. A quite linear behaviour was instead observed between LPD and global cost along most of the Pareto fronts.

In case of intervention on the external side of the walls (RT0), the Pareto fronts seemed to be divided in two main clusters. The reasons behind this characteristic will be evident in § 5.3.3. Even though less pronounced, also the RT1 and RT2 Pareto fronts presented small clustered portions.

With regard to the differences between the same retrofit solution for all the walls (NF1) or a different wall solution for each orientation (NF4), very similar solutions (at least in terms of objective space) were found for the RT0 and RT1 cases. The NF1 front always dominated the NF4 front with the exception of few solutions. As for the other locations, this is probably due to the lower exploration level reached by the optimisation algorithm for the NF4 cases. Also, the NF1 fronts

tended to span along a wider portion of the objective space.

The fitnesses of the extreme solutions are reported in Table 5.13 and Table 5.14 respectively for the retrofit of the pre-1955 and post-1955 building. Solution A is characterised by the lowest primary energy consumption. In a couple of cases, it also corresponds to the solution with the highest global cost. Solution B is characterised by the lowest global cost, and it is often also the solution with the highest thermal discomfort. Solution C is the solution with the lowest Long-term Percentage of Dissatisfied, as well as with the highest primary energy consumption.

The greatest variation between best and worst optimised solution was observed for the global cost. The difference in primary energy consumption spanned between $9\,\text{kWh/(m}^2\text{y)}$ and $23\,\text{kWh/(m}^2\text{y)}$, whereas the variation in LPD was almost negligible.

The comparison between pre-1955 and post-1955 Pareto fronts is reported in Fig. 5.71, where the global cost is colour coded, and the fronts are represented as continuous surfaces just for sake of ease of understanding. In case of intervention on the external side of the walls (RT0), lower primary energy consumptions could be achieved with a lower global cost when retrofitting the post-1955 building. Retrofitting the massive pre-1955 building could guarantee a better thermal comfort, but reducing E_P beyond a certain limit (or both E_P and LPD) implied very high costs. The best thermal comfort corresponded to the highest energy consumption and moderate cost, whereas the lowest global cost corresponded to moderate thermal discomfort (referred to the range of variation of the Pareto front) and the highest energy consumption. In case of intervention on the internal side or both sides of the walls (RT1 and RT2, respectively), the difference between the Pareto fronts was much less pronounced. The lowest primary energy consumptions could again be achieved by the post-1955 building and the lowest LPD by the pre-1955 building. In both cases, the lowest costs were associated to the highest discomfort but, at the same time, to a quite low E_P. Reducing the thermal discomfort implied an increase in terms of global cost. Especially in the RT2 case, the highest costs were found towards the Utopia point when reducing both E_P and LPD.

Table 5.13 Fitness of the extreme solutions: Oslo, pre-1955.

Solution	E_P [kWh/(m²y)]	C_G [€/m²]	LPD [%]	E_P [kWh/(m²y)]	C_G [€/m²]	LPD [%]
	RT0 – NF1			**RT0 – NF4**		
Solution A	267.5	1023.00	3.64	269.3	948.31	3.71
Solution B	283.9	620.87	3.69	284.3	621.08	3.69
Solution C	288.2	824.43	3.36	286.9	728.27	3.42
	RT1 – NF1			**RT1 – NF4**		
Solution A	256.4	659.17	3.60	260.3	633.81	3.60
Solution B	264.5	542.98	3.82	266.5	545.37	3.81
Solution C	266.9	752.13	3.34	271.1	695.32	3.39
	RT2 – NF1			**RT2 – NF4**		
Solution A	260.5	739.92	3.68	266.3	966.84	3.75
Solution B	266.0	629.33	3.82	269.1	650.66	3.78
Solution C	283.1	719.18	3.28	284.4	742.06	3.32

Table 5.14 Fitness of the extreme solutions: Oslo, post-1955.

Solution	E_P [kWh/(m²y)]	C_G [€/m²]	LPD [%]	E_P [kWh/(m²y)]	C_G [€/m²]	LPD [%]
	RT0 – NF1			**RT0 – NF4**		
Solution A	260.4	890.08	3.86	261.6	780.13	3.98
Solution B	271.7	589.77	3.85	271.6	589.79	3.85
Solution C	275.5	834.49	3.61	274.9	745.49	3.70
	RT1 – NF1			**RT1 – NF4**		
Solution A	250.8	711.55	3.47	254.1	697.49	3.65
Solution B	258.2	528.87	3.93	260.6	531.99	3.91
Solution C	265.3	725.46	3.43	263.5	662.13	3.52
	RT2 – NF1			**RT2 – NF4**		
Solution A	252.8	714.28	3.62	259.5	632.36	3.93
Solution B	259.8	609.21	3.87	268.6	627.32	3.79
Solution C	269.5	737.53	3.40	268.8	736.98	3.53
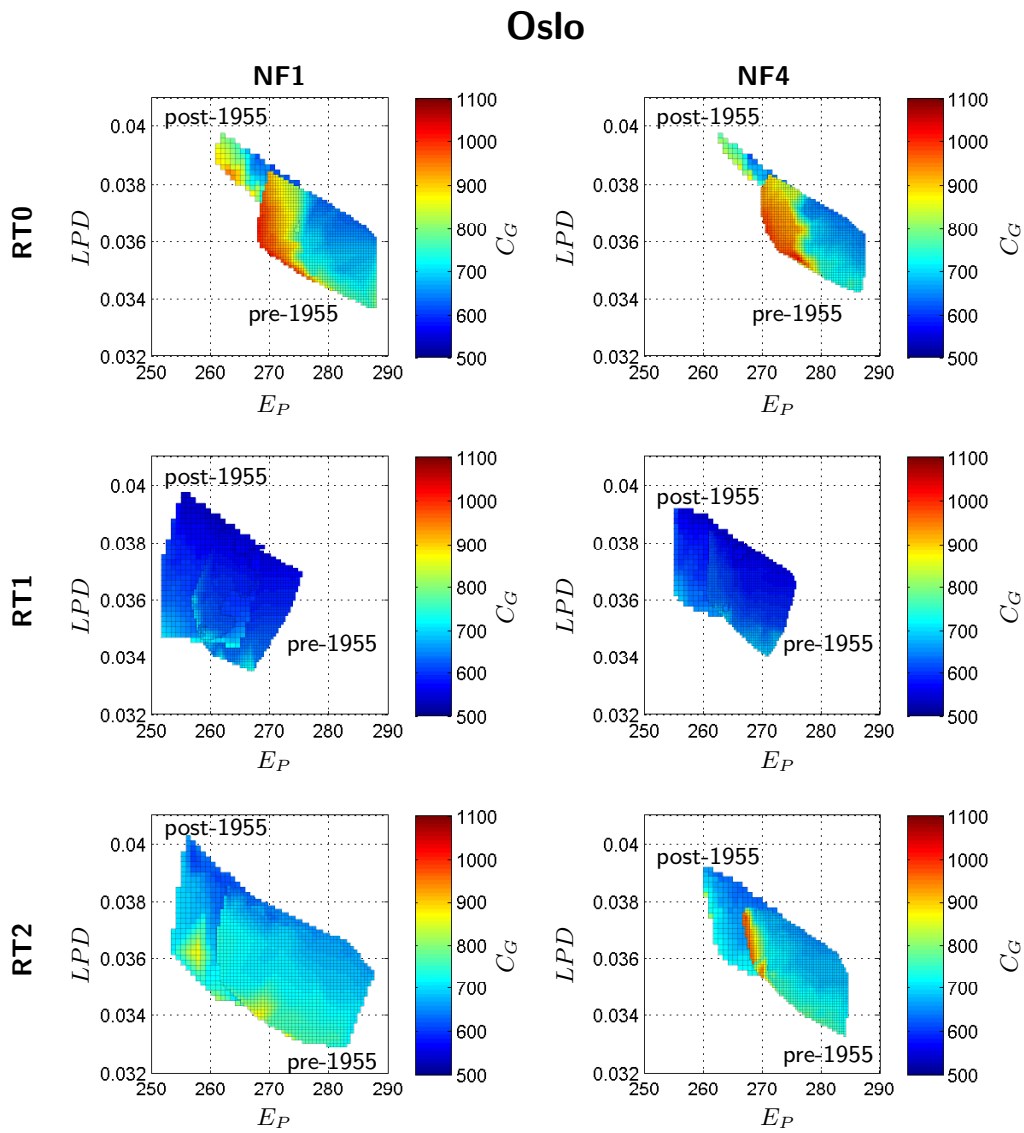
Fig. 5.71 Comparison between pre-1955 and post-1955 Pareto fronts in Oslo.
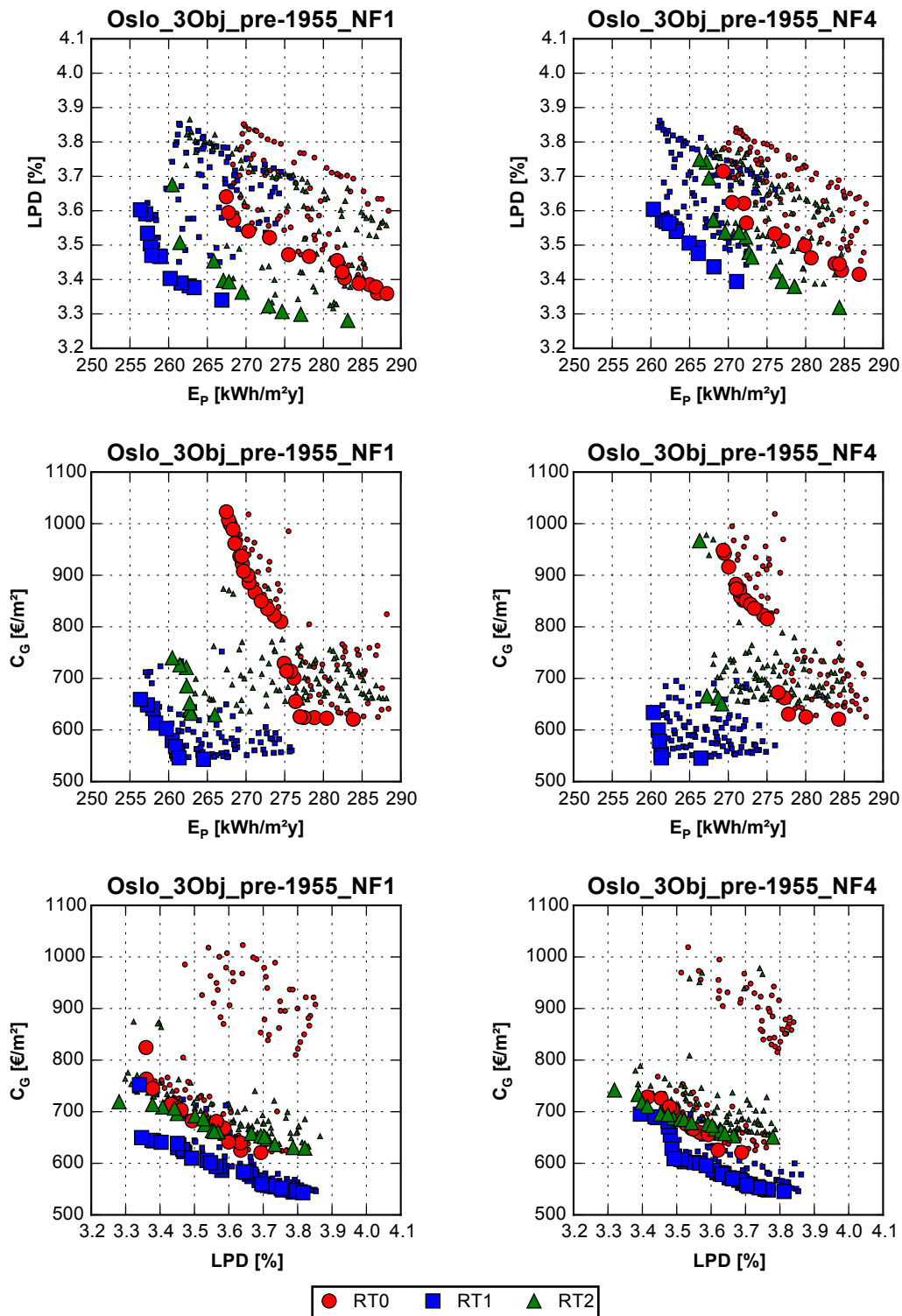
Fig. 5.72 Pareto front: Oslo, pre-1955.
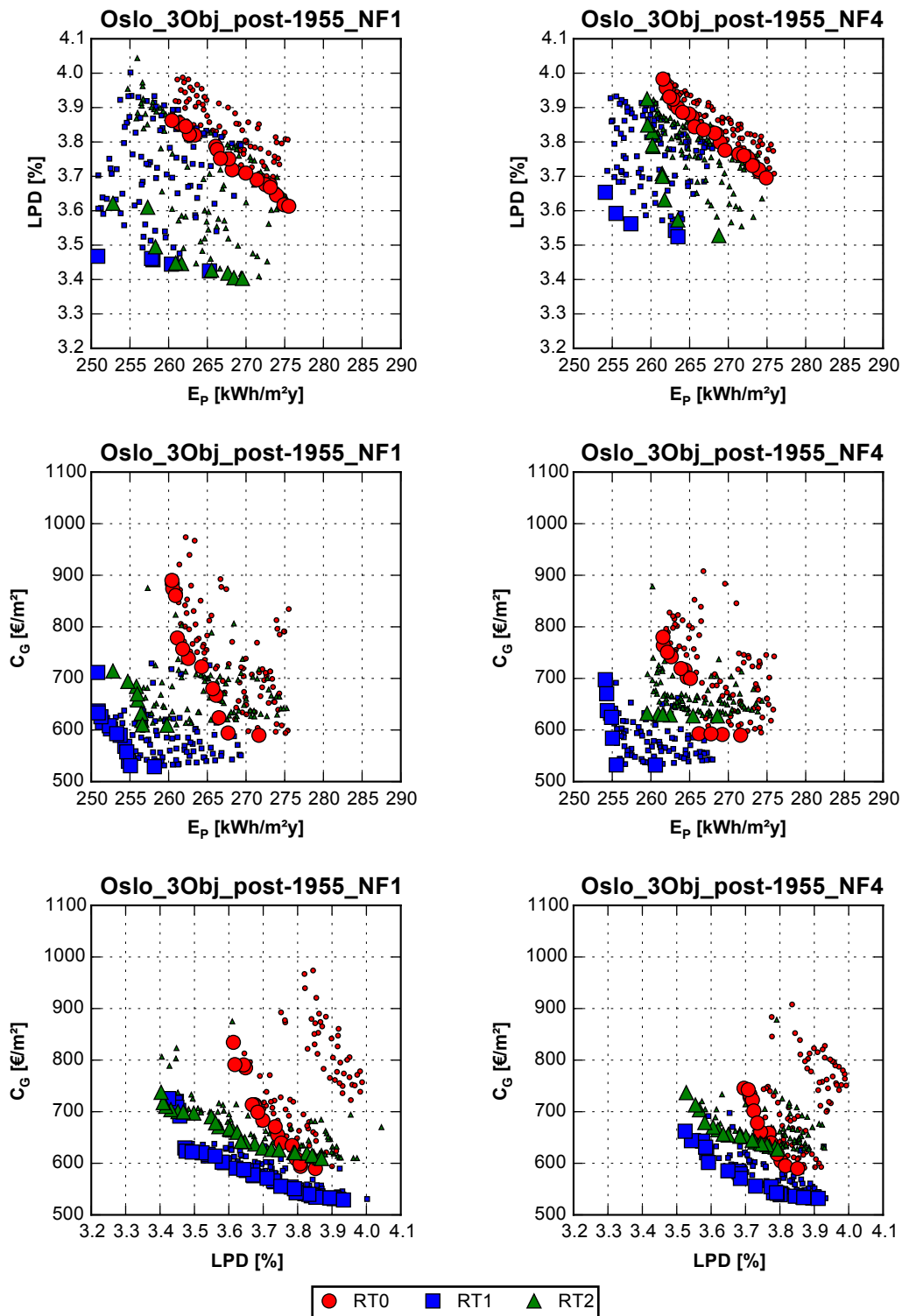
Fig. 5.73 Pareto front: Oslo, post-1955.

5.3.3   Post-optimisation analyses

The solutions belonging to the Pareto fronts were analysed and discussed in order to find design principles and common trends among the various case studies. As the analysis of the Pareto fronts focused on the results in the objective space, the post-optimisation analyses (see § 3.3) focused on the results in the search space.

For this purpose, a series of graphical and numerical analyses were carried out. Box plots of the continuous variables belonging to the non-dominated sets were represented to find their range of variability and possible constant values, and frequency analyses of the variables were plotted and compared among case studies. Box plots and frequency analyses are reported in Appendix A.

Moreover, the values assumed by each variable were mapped on the Pareto front, in order to explore how the search space variables affected the results in the objective space. Due to the vast amount of graphs, the variables' mapping on the Pareto fronts are reported in Appendix B[1]. Automated innovization runs (see § 3.3.5) were additionally performed to find relationships between variables and fitness functions.

An important note to the interpretation of box plots and frequency analyses is that, even though the crowding distance algorithm in NSGA-II is designed to provide variability among solutions, in some cases small portions of the Pareto fronts were found to be populated by a large number of individuals. Therefore, especially for the two-objective optimisations, frequency analyses may be misleading if their interpretation is not supported by the combined analysis of the variables' mappings on the Pareto fronts.

Eventually, the extreme solutions of the Pareto front were depicted, where solutions A, B (and C) were the best performing individuals with respect to each objective function. The extreme solutions are reported in Appendix C. Wall layouts are represented with the external environment on their left and the internal environment on their right. In the same way, wall descriptions are from outside to inside.

In the following sections, the results for each location and set of objective functions will be analysed. For each retrofit type, the characteristics of the Pareto solutions will be described both for the cases of same wall solutions on all the façades (NF1) and different wall solution for each façade (NF4). However, for the sake of brevity, only the graphics related to the NF1 cases will be reported.

Considering that the search space for the NF4 cases—and especially the RT2 – NF4 case—was much wider than the NF1 case studies, the exploration level achieved

---

[1]For the sake of conciseness, the variables' mappings for the three-objective optimisation analyses are reported as three-dimensional representations; however, the corresponding bi-dimensional projections on each plane were analysed for a clear interpretation and understanding.

by the GA was lower. Comparing the performance of the extreme solutions for the NF1 and NF4 cases, it can be inferred that the GA was not as close in finding the best solutions. However, even when the GA failed in finding the true optimal solutions for each objective, the information retrieved from the analyses of the Pareto solutions can allow to devise the properties of the true extreme solutions.

Eventually it should be noted that, out of the total population (100 individuals), only few solutions belonged to the non-dominated sets of the two-objective optimisations, whereas almost all the population belonged to the non-dominated sets of the three-objective analyses. This does not imply that the two-objective optimisation results are less reliable, but only that any information extracted from the post-optimisation analyses was retrieved from smaller datasets.

5.3.3.1   Palermo, two objectives

The two-objective case studies in Palermo aimed at minimising primary energy consumption and global cost.

A first glance at the solutions was obtained by analysing Fig. A.1, where the box plots of all the retrofit options are summarised. The corresponding frequency analyses are reported from Fig. A.7 to Fig. A.13.

Although Palermo is a cooling-dominated climate, very low U-values were selected with the exception of the RT0 case studies (retrofit on the external side of the wall). For the RT1 – NF1 and RT2 – NF1 all the solutions shared a U-value equal to 0.15 W/(m²K), i.e. the lower bound. Although the primary energy consumption for heating was lower than that for cooling (see Table 5.8), it was verified that its reduction deriving from a lower U-value was greater than the consequent increase in primary energy consumption for cooling and night ventilation fans.

With regard to the PCM selection, PCM1 was generally preferred over PCM2. Choosing the low-temperature PCM in a cooling-dominated location may seem unexpected. However, analysing the temperature profiles within the building (see Fig. 6.1 in § 6.2), it can be inferred that PCM1 can have a stabilising effect on the internal temperature for a longer period of time, since the climatic conditions in winter and especially during mid-season are mild. On the other hand, high temperatures in summer tend to be too extreme even for PCM2 to work effectively.

High thicknesses were chosen for PCM1 especially for the RT0 – NF4 case study. However, both the box plot representations and the frequency analyses fail at providing more details, which will be retrieved by analysing the variables' maps on the Pareto fronts.

The most evident piece of information that can be devised from the box plots is that very high latent heats of fusion were selected especially for PCM1 in the RT0

and RT1 – NF1 cases. Medium/low values seemed to suffice for PCM2, which was used to a lesser extent.

The interquartile range of the peak melting temperature of PCM1 was similar for the RT0 and RT1 cases, with a median value generally around 20 ℃ or slightly less. This is in line with the winter set point temperature. On the other hand, the interquartile range of the peak melting temperature of PCM2 was not homogeneous. The median passed from about 24 ℃ for the RT1 – NF1 case (retrofit intervention on the internal side of the wall regardless of the façade)—which can be explained by the night ventilation set point temperature— up to temperatures over 30 ℃, which can be explained by the PCM being positioned towards the external environment.

The melting temperature range of PCM1 generally assumed medium/low values, whereas for PCM2 there was not a clear trend apart from the RT0 – NF4 case, where high values were preferred. When the PCM is on the outer side of the wall it is subject to variable conditions, therefore a high melting temperature range improves the adaptivity of the PCM [88].

High values were often selected for PCM1's thermal conductivity, whereas also medium/low values were sometimes adopted for PCM2. However, no clear trends were generally identified, as it will be more clear from the mapping of the Pareto solutions.

In the detailed comments to each retrofit option, information on the values assumed by the discrete variables (window type, insulation and internal lining materials, PCM use) will be also provided, together with specific trends along the non-dominated set. The extreme solutions of the Pareto front were additionally reported, where solution A was the best performing individual with respect to the primary energy (therefore also the most expensive) whereas solution B was the individual with lowest global cost but highest primary energy consumption.

5.3.3.1.1 Retrofit on the external side (RT0)

Same retrofit solution for all the walls (NF1)

In the case of retrofit intervention on the external side of the wall and same retrofit solution on all the façades, the innovization analyses highlighted the use of either only PCM1 for most of the solutions, or no PCM when minimising the global cost. Only wall types *ext0000* (insulation-existing wall) or *ext1000* (insulation-PCM1-existing wall) were selected by the GA.

The preferred insulation materials were XPS and EPS. The two most expensive solutions adopted aerogel mats (Fig. B.25). No clear trend can be observed in the choice of the U-value; medium values within the allowed range were generally adopted. Only window types 2 (air filled double glazing unit (DGU) with low-e coating on face 2) and 1 (air filled DGU with low-e coating on face 3) were selected;

since they were characterised by the same cost, choosing one instead of the other had an impact only the primary energy consumption. Even though window type 2 (the best option for reducing the cooling energy need) was chosen for both the extreme solutions, it was mainly adopted by the solutions characterised by a low primary energy need.

The Pareto front was characterised by an increasing PCM thickness in order to decrease the primary energy consumption (hence increasing the global cost). The relationship between PCM thickness and E_P can be described by the following equation:

$$E_P = -48.5 \cdot t_1 + 114.67 \quad (\text{R}^2 = 0.967).$$

Moreover, the relationship between PCM thickness and global cost, excluding the two solutions with aerogel insulation, is described by

$$C_G = 3080 \cdot t_1 + 451 \quad (\text{R}^2 = 0.995).$$

The following linear relationship between global cost and investment cost was additionally found:

$$C_G = 0.800 \cdot C_I + 308.1 \quad (\text{R}^2 = 0.999).$$

With regard to the PCM properties, all the solutions shared an almost constant latent heat of fusion, mainly equal to 230 kJ/(kg K) and always higher than 200 kJ/(kg K) (Fig. B.26). The peak melting temperature tended to increase with the PCM thickness according to the following relationship (excluding the solutions with aerogel):

$$T_{p,1} = 35.8 \cdot t_1^{0.15} \quad (\text{R}^2 = 0.814);$$

however, only a narrow range of temperatures around 19.7 ℃ were selected. It could be argued that a relationship between melting temperature and E_P should rather be identified; however, the goodness of fit was significantly lower. This result is however in line with the results of the parametric analysis (see § 5.2.1.3) as well as with the findings of Zhu et al. [138], who found that thickness and melting temperature influenced each other when searching for the minimum annual energy demand or peak load for heating and cooling.
Low melting temperature ranges were mostly preferred. No clear trend can be observed for the PCM's thermal conductivity; mainly high values were selected.

Eventually, the extreme solutions of the Pareto front are reported in Fig. C.2. Solution A (minimum primary energy consumption) was characterised by window type 2 (air filled DGU with low-emissivity coating on face 2), a U-value of 0.21 W/(m^{2}K), aerogel insulation, and 4.0 cm of PCM1 with a melting temperature of 20.5 ℃, melting temperature range of 1.5 ℃, 200 kJ/kg of latent heat of fusion, and a thermal conductivity of 0.75 W/(m K). Although close to the true optimum, this solution was verified to be only sub-optimal, as reducing the U-value to 0.15 W/(m^{2}K)

and increasing both latent heat of fusion and thermal conductivity of the PCM led to a slightly lower E_P.

Solution B (minimum global cost) was characterised by window type 2 (not the cheapest option, but the cost difference was negligible with respect to window type 0 and its energy performance was much better), a U-value of 0.45 W/(m²K), i.e. the maximum value according to the national standard [308], EPS insulation (i.e. the cheapest one) and no PCM.

Different wall solution for each orientation (NF4)

In the case of retrofit intervention on the external side of the wall and different retrofit solution for each façade, the innovization analyses highlighted mainly the use of no PCM or only PCM1. A few cases where both PCMs were adopted occurred only for west and south expositions. All the solutions with no PCM or only PCM1 were respectively characterised by wall types *ext0000* and *ext1000* (insulation-PCM1-existing wall).

The preferred insulation materials were XPS, EPS and rock wool. Aerogel mats were selected only for the two solutions with lowest primary energy consumption. Only window types 1 and 2 were selected, but no clear preference was recognised in any portion of the Pareto front. In the same way, the U-value did not show any trend regardless of the exposition.

With regard to the PCM1 thickness, the majority of solutions facing south were characterised by 3.5 cm, whereas those facing east by 4.0 cm. High thicknesses were selected also for the north and west facing walls. The following relationship was identified between E_P and the global thickness of PCM1:

$$E_P = -10.9 \cdot (t_{1,S} + t_{1,E} + t_{1,N} + t_{1,W}) + 114.57 \quad (\text{R}^2 = 0.948).$$

The following relationship between global and investment cost was also found:

$$C_G = 0.802 \cdot C_I + 308.0 \quad (\text{R}^2 = 0.999).$$

With regard to the PCM1 properties, which were the same regardless of the exposition, all the solutions shared an almost constant peak melting temperature of 20.7 ℃. As for the NF1 case, medium/low melting temperature ranges and latent heat of fusion mainly equal to 230 kJ/(kg K) were found. Lower melting temperatures could be graphically detected for the solutions with higher primary energy consumption, although no clear relationship could be defined. No clear trend was observed for the PCM's thermal conductivity either.

Eventually, the extreme solutions of the Pareto front are very similar to those found for the RT0 − NF1 case. However, comparing their fitness, it can be inferred that, in the current case, the GA failed at finding the extreme A and B solutions due to the broader search space. Identical B solutions could especially be expected.

5.3.3.1.2 Retrofit on the internal side (RT1)

Same retrofit solution for all the walls (NF1)

In the case of retrofit intervention on the internal side of the wall and same retrofit solution on all the façades, the innovization analyses highlighted mainly the use of only PCM1, apart from the solutions towards the extremes of the front; no PCM was used when minimising the global cost and both PCMs when minimising the primary energy consumption. Although hidden in Fig. B.27, two solutions with only PCM2 also occurred; their performance in terms of primary energy consumption was however poor. Almost only wall type *int1100* (existing wall-insulation-PCM1) was chosen by the GA for the PCM1 only solutions, whereas *int0000* (existing wall-insulation) and *int3110* (existing wall-insulation-PCM1-PCM2) were selected for the cases without PCM and with both PCMs, respectively.

The preferred insulation material was EPS (Fig. B.27). Lime and gypsum plaster or mineralised wooden board were mainly selected as internal lining materials. As for the RT0 case, only window types 2 (DGU Air low-e(2)) and 1 (DGU Air low-e(3)) were selected; window type 1 (the best option for reducing the heating energy need) was mainly adopted by the solutions characterised by a high primary energy consumption. All the solutions shared a U-value of 0.15 W/(m^{2}K), i.e. the lowest bound.

Solutions with PCM1 were characterised by increasing thickness when decreasing the primary energy consumption (hence increasing the global cost). Two out of three solutions which had also PCM2 were characterised by the highest allowable thickness of 4 cm. The following relationships between PCM1 thickness, E_P and global cost were identified (PCM1 and EPS only):

$$E_P = -78 \cdot t_1 + 107.4 \quad (\text{R}^2 = 0.947),$$

$$C_G = 2400 \cdot t_1 + 391 \quad (\text{R}^2 = 0.968).$$

The following linear relationship between global cost and investment cost was additionally found:

$$C_G = 0.784 \cdot C_I + 289.7 \quad (\text{R}^2 = 0.999).$$

With regard to the PCM1 properties, all the solutions shared an almost constant peak melting temperature of 19.9 ℃, low melting temperature range and the maximum latent heat of fusion (Fig. B.28). A high thermal conductivity can be generally observed, with the exception of the two solutions with highest global cost. For the few solutions with also PCM2, an almost constant peak melting temperature of 24.6 ℃ can be observed, together with a medium melting temperature range, medium/low latent heat of fusion and low thermal conductivity.

Eventually, the extreme solutions of the Pareto front are reported in Fig. C.4.

Solution A (minimum primary energy consumption) was characterised by window type 2, a U-value of 0.15 W/(m²K), EPS insulation, clay plaster, and 4.0 cm for both PCMs with melting temperatures respectively of 21.5 ℃ and 24.5 ℃.

Solution B (minimum global cost) was characterised by window type 2, a U-value of 0.15 W/(m²K) (i.e. the lowest bound, unlikely the RT0 – NF1 case), EPS insulation, lime and gypsum plaster, and no PCM.

The added thickness, ranging among all solutions between 27 cm and 35 cm, highlights the need of a constraint on the overall wall thickness or floor surface reduction; the lowest the net floor area, the lowest the commercial value of the building generally is.

Different wall solution for each orientation (NF4)

In the case of retrofit intervention on the internal side of the wall and different retrofit solution for each façade, the innovization analyses highlighted mainly the use of no PCM in the north and west expositions, either no PCM or PCM1 for the south wall, and either no PCM, PCM2 or PCM1 for the east wall. Both PCMs were adopted only in a few cases. The Pareto front was sequentially clustered by the PCM use in the east-facing façade.

A variety of wall types was adopted; however, the U-value was almost constant regardless of the exposition, and mainly equal to 0.15 W/(m²K). The preferred insulation types were EPS and cork. Almost all solutions were characterised by window type 1 (DGU Air low-e(3)). Lime and gypsum plaster was mainly selected as internal lining material, although there is no clear preference over thermo-plaster and mineralised wooden board.

With regard to the PCM thicknesses, medium/high values were chosen for both PCM1 and PCM2 in the east facing walls. No clear trends were identified in the other cases. Even though the goodness of fit is not as good as for the RT0 – NF4 case, the following relationship between E_P and the global thickness of PCM (PCM1 plus PCM2) was identified:

$$E_P = -15 \cdot \sum t_{i,j} + 107.5 \quad (\text{R}^2 = 0.880).$$

The following relationship between global and investment cost was also found:

$$C_G = 0.785 \cdot C_I + 290.4 \quad (\text{R}^2 = 0.999).$$

With regard to the PCM properties, an almost constant peak melting temperature of 19.9 ℃ was shared by most of solutions with PCM1. No other clear trend could be deduced.

Eventually, the extreme solutions of the Pareto front are described. Compared to the NF1 case, where solution A was characterised by the adoption of both PCMs which were applied between clay plaster and EPS insulation, in the current case the

adoption of both PCMs occurred only for the east-facing wall. Moreover, cork and mineralised wooden board were respectively selected as insulation and internal lining materials. With regard to the PCM properties, a lower melting temperature for PCM1 and a higher one for PCM2 were selected due to their location within the walls. Moreover, a high thermal conductivity was chosen for both PCMs.

Solution B was almost identical to that of the NF1 case; the only difference is a higher U-value of 0.21 W/(m^{2}K) for the south wall. Even though this implies a lower investment cost, the resulting global cost is slightly higher than that of solution B of the NF1 case.

5.3.3.1.3 Retrofit on both sides (RT2)

Same retrofit solution for all the walls (NF1)

In the case of retrofit intervention on both sides of the wall and same retrofit solution on all the façades, the innovization analyses highlighted the use of either only PCM1 when minimising the global cost or both PCMs when minimising the primary energy consumption. Even though a predominance of individuals with both PCMs may seem to occur, indeed only 14 solutions had PCM2 against 16 with only PCM1. Wall type *ie100000* (PCM1-existing wall-insulation) was always selected for the solutions with only PCM1, whereas *ie300011* (PCM2-existing wall-insulation-PCM1) and a few *ie300010* (PCM2-existing wall-PCM1-insulation) were selected for the solutions with both PCMs (Fig. B.29).

As for the RT0 and RT1 cases, only window types 1 (DGU Air low-e(3)) and 2 (DGU Air low-e(3)) were selected; window type 1 (the best option for reducing the heating energy need) was however generally preferred. The internal lining materials that were chosen the most were thermo-plaster and lime and gypsum plaster. The preferred insulation materials were cork and EPS. Also in this case, all the solutions shared a U-value of 0.15 W/(m^{2}K).

All solutions with only PCM1 were characterised by a constant thickness of 0.5 cm. When PCM2 was additionally introduced, an increasing thickness of PCM1 could be observed for reducing the primary energy consumption, according to the following relationship:

$$E_P = -69 \cdot t_1 + 107.6 \quad (\text{R}^2 = 0.893).$$

The thickness of PCM2 was always 0.5 cm apart from the two solutions with highest global cost. The relationship between the total PCM thickness (PCM1 plus PCM2) and global cost is described by

$$C_G = 2500 \cdot (t_1 + t_2) + 475 \quad (\text{R}^2 = 0.913),$$

whereas the relationship between global cost and investment cost is given by

$$C_G = 0.788 \cdot C_I + 298.8 \quad (\text{R}^2 = 0.999).$$

With regard to the PCM properties, a higher variation for all the properties of PCM1 can be observed in comparison with RT0 and RT1 cases (Fig. B.30). This can be explained by the greater variability in the PCM's position within the wall. As for the RT0 case, the peak melting temperature tended to increase with the PCM1 thickness. However, a clear relationship was not identified.

The solutions with only PCM1 were characterised mainly by a low melting temperature range, a high latent heat of fusion and a high thermal conductivity. No trend was found to describe the properties of PCM2.

Eventually, the extreme solutions of the Pareto front are reported in Fig. C.6. Solution A (minimum primary energy consumption) was characterised by window type 2, a U-value of 0.15 W/(m^{2}K), EPS insulation, thermo-plaster, 4.0 cm of PCM1 and 2.5 cm of PCM2, with a melting temperature respectively of 21.5 ℃ and 33.5 ℃. Compared to solution A of the RT1 case, PCM2 was placed towards the external environment with a comprehensibly higher melting temperature. Similar thermo-physical properties were selected for PCM1. A higher thermal conductivity was preferred for both PCMs.

Solution B (minimum global cost) was extremely similar to that of the RT1 case; the only difference was the presence of 0.5 cm of PCM1 on the outermost layer (except the external render). Since intervening on both sides could not be avoided in the RT2 case, the most similar solution to solutions B of the RT1 case was found.

Different wall solution for each orientation (NF4)

In the case of retrofit intervention on both sides of the wall and different retrofit solution for each façade, only eight solutions belonged to the Pareto front. Therefore, significant conclusions cannot be drawn. The innovization analyses highlighted a preference for PCM2 on the north and west facing walls, whereas PCM1 was generally chosen in the south and east façades. All the solutions with PCM2 and PCM1 were respectively characterised by wall types *ie200000* and *ie100000* (PCM1-existing wall-insulation). Especially for the south and north expositions, low U-values were generally selected.

Both window types 1 and 2 were chosen as glazing options. The preferred insulation materials were EPS and cork, whereas the internal lining material which occurred the most was clay plaster.

Apart from the case of PCM1 on south facing walls, minimal thicknesses of PCM were selected both for PCM1 and PCM2.

With regard to the PCM properties, a melting temperature range of about 5.4 ℃ was mainly found for PCM1. This could be explained by the greater variability in the PCM's position within the wall. No other clear trend could be devised.

The only relationship that could be identified was between global cost and investment cost;
$$C_G = 0.76 \cdot C_I + 309 \quad (\text{R}^2 = 0.998).$$

Eventually, the extreme solutions of the Pareto front are analysed. Solution A was quite different from that of the NF1 case. Although a different insulation choice and a higher U-value of the west facing wall, no PCM was placed towards the internal environment. PCM1 was preferred over PCM2 for the east and north façades, whereas no PCM was selected for the west one.

Solution B was very similar to that of the NF1 case. The main differences are a higher U-value of the walls, the adoption of either PCM1 or PCM2 in the outermost layers, and no PCM in the east wall, which resulted in adding insulation on both sides.

As it was already mentioned when discussing the Pareto frontiers, the exploration level achieved by the RT2 – NF4 case study was significantly lower than the others options. The obtained non-dominated set might still be far from the true Pareto front.

5.3.3.2 Torino, two objectives

The two-objective case studies in Torino aimed at minimising primary energy consumption and global cost.

A first glance at the solutions was obtained by analysing Fig. A.2, where the box plots of all the retrofit options are summarised. The corresponding frequency analyses are reported from Fig. A.14 to Fig. A.20.

The same U-value results obtained for Palermo also applied to Torino. Very low U-values were selected with the exception of the RT0 case studies (retrofit on the external side of the wall). For the RT1 – NF1 and RT2 – NF1 all the solutions shared a U-value equal to 0.15 W/(m^{2}K), i.e. the lower bound. Torino is a heating-dominated climate, so it can be inferred that low U-values were preferred to reduce the heat losses through the opaque envelope in winter. Heating energy consumption was the most important aspect to minimise, and it was indeed effectively reduced (see Table 6.1).

With regard to the PCM selection, PCM1 was generally preferred over PCM2. Since minimising the primary energy consumption in a heating-dominated climate implies mostly reducing the heating energy consumption, this result could be expected.

High thicknesses were chosen for PCM1 especially for the RT0 – NF1 case study and for the south-facing wall in the RT0 – NF4 case. However, both the box plot representations and the frequency analyses fail at providing significant information that can be retrieved by analysing the variables' maps on the Pareto fronts.

As for Palermo, the most evident piece of information that can be devised from the box plots is that very high latent heats of fusion were selected especially for PCM1 in the RT0 and RT1 cases.

The interquartile range of the peak melting temperature of PCM1 was very small especially in the RT1 cases (retrofit on the internal side of the wall), with a median value generally slightly lower than 20 ℃. On the other hand, as in Palermo the range of variation of the peak melting temperature of PCM2 was not homogeneous. It passed from about 24 ℃ for the RT1 − NF1 case (a sample of 2 points is however not significant) up to temperatures over 30 ℃, which can be explained by the PCM being positioned towards the external environment.

Medium/low melting temperature ranges were selected for the RT0 − NF1 and RT1 − NF1 cases, whereas medium/high values were preferred for the RT2 cases. No clear trends were generally identified for the thermal conductivity. High values were selected for the RT1 − NF1 case and low ones for the RT0 − NF1.

In the detailed comments to each retrofit option, information on the values assumed by the discrete variables (window type, insulation and internal lining materials, PCM use) will be also provided, together with specific trends along the non-dominated set. The extreme solutions of the Pareto front were additionally reported, where solution A is the best performing individual with respect to the primary energy (therefore also the most expensive) whereas solution B is the individual with lowest global cost but highest primary energy consumption.

5.3.3.2.1 Retrofit on the external side (RT0)

Same retrofit solution for all the walls (NF1)

In the case of retrofit intervention on the external side of the wall and same retrofit solution on all the façades, the innovization analyses highlighted the use of either no PCM when minimising the global cost, or only PCM1 when minimising the primary energy consumption. As for the case of Palermo, only wall types *ext0000* or *ext1000* (insulation-PCM1-existing wall) were selected by the GA.

Solutions were further clustered according to insulation material and window type, as it can be observed in Fig. B.31. Even though a predominance of individuals with PCM may seem to occur, indeed only 12 solutions had PCM against 28 without. In the same way, 20 solutions were characterised by window type 4 (90%Ar filled double glazing unit (DGU) with low-e coating on face 3)—the cheapest option but with a worse winter performance—and 19 by window type 7 (90%Ar filled triple glazing unit (TGU) with low-e coating on faces 3 and 5)—more expensive but the best option to reduce the heating energy consumption.

The solutions without PCM can be divided in the three groups, for each of which the U-value gradually varied from 0.30 W/(m^{2}K) to 0.21 W/(m^{2}K). From

the highest to the lowest primary energy, these groups of solutions differed by insulation material and window type, as follows:

1. insulation material: EPS, window type: 4;

2. insulation material: XPS, window type: 4;

3. insulation material: XPS, window type: 7.

Apart from a couple of exceptions, the solutions with PCM shared all the same type of glazing—i.e. window type 7— and were characterised either by XPS or aerogel as insulation materials. Their U-value tended to 0.15 W/(m^{2}K), which was the lowest bound. The PCM thickness tended to 4 cm, i.e. the upper bound.

With regard to the PCM properties, all the solutions shared an almost constant peak melting temperature of 16.9 ℃ on average, low melting temperature range and high latent heat of fusion (220/230 kJ/kg) (Fig. B.32). No clear trend can be observed for the PCM's thermal conductivity; unlikely in Palermo, mainly low values were selected. The only relationship that could be identified was between global cost and investment cost;

$$C_G = 0.800 \cdot C_I + 381.3 \quad (\text{R}^2 = 0.999).$$

Eventually, the extreme solutions of the Pareto front are reported in Fig. C.3. Solution A (minimum primary energy consumption) was very similar to that of Palermo. It was characterised by window type 7 (90%Ar filled TGU with low-emissivity coating on faces 3 and 5), a U-value of 0.15 W/(m^{2}K) (unlikely in Palermo, the lowest bound was chosen), aerogel insulation, and 4.0 cm of PCM1. The lower melting temperature of 16.0 ℃ can be explained by Torino's colder climate. As in Palermo, low melting temperature range, high of latent heat of fusion, and high thermal conductivity were selected.

Also solution B (minimum global cost) was extremely similar to that of Palermo. It was characterised by window type 4 (cheapest option), a U-value of 0.30 W/(m^{2}K), i.e. the maximum value for Torino according to the national standard [308], EPS insulation (i.e. the cheapest one) and no PCM.

Different wall solution for each orientation (NF4)

In the case of retrofit intervention on the external side of the wall and different retrofit solution for each façade, the innovization analyses highlighted mainly the use of no PCM, or only PCM1 when minimising the primary energy consumption in each Pareto cluster formed by the insulation type. Only in the east-facing wall PCM2 was preferred to PCM1 in the extreme solutions. Almost only wall types *ext0000* or *ext1000* (insulation-PCM1-existing wall) were chosen by the GA.

Solutions were clustered according to insulation material and partly by window type. The preferred insulation materials were aerogel and XPS. Window type 7 was adopted by almost all the solutions with the exception of the low-cost ones, for

which window type 4 was selected.

The U-value on the south-facing walls assumed generally higher values compared to the others expositions. In the group of solutions clustered by the aerogel, in the north and west facing walls a decreasing trend for the U-value could be clearly recognised as the EP diminished; it was present yet not so strong in the south and east facing walls. However, no clear relationship could be devised. In the group of solutions clustered by XPS and EPS, a weak trend was be observed again for the north and west walls, whereas no clear trend could be seen for the other expositions.

As very few solutions for each exposition adopted PCM, not much can be said with regard to the PCM thickness. Especially for the south and west facing walls, it seemed to tend to 4 cm when decreasing the primary energy consumption.

With regard to the PCM1 properties, which were the same regardless of the exposition, all the solutions shared an almost constant peak melting temperature of 18.1 ℃, medium/low melting temperature range and high latent heat of fusion. No clear trend was observed for the PCM's thermal conductivity.

The only relationship that could be identified was between global cost and investment cost;

$$C_G = 0.8030 \cdot C_I + 381.1 \quad (\text{R}^2 = 1.00).$$

Eventually, the extreme solutions of the Pareto front are described. Solution A was similar to that of Palermo and to Torino's RT0 – NF1 only for the south wall. It was characterised by the adoption of PCM2 for the east wall and PCM1 for the south wall, respectively in external and middle positions. The lowest U-value was selected for the north and west facing walls, where no PCM was used, whereas the highest U-value was selected for the east wall. Given the high number of potential solutions for the NF4 analyses, it is probable that the extreme solution A was not found. It can also be inferred that the extreme solution B was not found by the GA, as it would have been the same as for the RT0 – NF1 case.

5.3.3.2.2   Retrofit on the internal side (RT1)

Same retrofit solution for all the walls (NF1)

In the case of retrofit intervention on the internal side of the wall and same retrofit solution on all the façades, the innovization analyses highlighted the use of either only PCM1 when minimising the primary energy consumption, or no PCM when minimising the global cost. Only the extremal solution with lowest primary energy consumption and highest global cost (solution A in Fig. C.5) adopted both PCMs (Fig. B.33). Almost only wall types *int0000* or *int1100* (existing wall-insulation-PCM1) were chosen by the GA.

The preferred insulation material was EPS. Thermo-plaster and window type 7

were chosen respectively as internal lining material and glazing, with the exception of the cheapest solutions which respectively adopted lime and gypsum plaster and window type 4. All the solutions shared a U-value of 0.15 W/(m²K), i.e. the lowest bound.

Solutions with PCM1 where characterised by an increasing thickness in order to decrease the primary energy consumption (hence increasing the global cost). Only two solutions had also PCM2, but its thickness was minimal. The following relationships between PCM1 thickness, E_P and global cost were identified (EPS and thermo-plaster only):

$$E_P = -61 \cdot t_1 + 141.09 \quad (\text{R}^2 = 0.966),$$

$$C_G = 2900 \cdot t_1 + 504 \quad (\text{R}^2 = 0.954).$$

The following linear relationship between global cost and investment cost was additionally found:

$$C_G = 0.792 \cdot C_I + 357 \quad (\text{R}^2 = 0.999).$$

With regard to the PCM properties, all the solutions shared an almost constant peak melting temperature of 18.5 ℃, low melting temperature range and the maximum latent heat of fusion (Fig. B.34). No clear trend can be observed for the PCM's thermal conductivity; medium to high values were selected.

Eventually, the extreme solutions of the Pareto front are reported in Fig. C.5. Solution A (minimum primary energy consumption) was quite similar to that of Palermo. It was characterised by window type 7, a U-value of 0.15 W/(m²K), EPS insulation and thermo-plaster. The two PCMs' positions were inverted, so that PCM1 was in this case closer to the internal environment and with a lower melting temperature. Moreover, only 1.0 cm was selected for PCM2.

Solution B (minimum global cost) was identical to that of Palermo, apart from the window type which could not be the same.

As for Palermo, the added thickness of 32 cm and 26 cm respectively for solution A and B highlights the need for a constraint on the overall wall thickness or reduction of the available floor surface.

Different wall solution for each orientation (NF4)

In the case of retrofit intervention on the internal side of the wall and different retrofit solution for each façade, the innovization analyses highlighted mainly the use of no PCM in the north and west expositions, and either no PCM or PCM1 for the south and east walls. Both PCMs were adopted for the lowest primary energy solutions for all the expositions with the exception of the east wall. PCM2 was also selected in a few cases. Most of the wall types were either *int0000, int1000,* or *int1100.*

The preferred insulation type was EPS. Window type 7 and thermo-plaster were adopted for the majority of solutions with the exception of the low-cost ones, for which window type 4 and lime and gypsum plaster were selected. The U-value was almost constant regardless of the exposition, and mainly equal to 0.15 W/(m^{2}K).

No clear trend could be detected with regard to the PCM thickness. An increased thickness of PCM2 in south and east facing walls seemed to be associated to lower primary energy consumption.

With regard to the PCM1 properties, all the solutions shared an almost constant peak melting temperature of 19.7 ℃ and a high latent heat of fusion. The solutions with lowest primary energy consumption were also characterised by a high thermal conductivity. No clear trends could be detected for the melting temperature range of PCM1, probably due to the variability in the PCM's position within the wall. No trends were found for the thermo-physical properties of PCM2 either.

The only relationship that could be identified was between global cost and investment cost;

$$C_G = 0.800 \cdot C_I + 357 \quad (\mathrm{R}^2 = 0.999).$$

Eventually, the extreme solutions of the Pareto front are described. Compared to the NF1 case, where only PCM1 was applied between thermo-plaster and EPS insulation, solution A was characterised by the adoption of also PCM2 for all expositions with the exception of the east wall. In the current case, PCM1 was placed mainly in intermediate positions and was therefore characterised by a higher melting temperature range. Similarly to the correspondent solution in Palermo, the selected insulation material was cork.

As for the RT0 – NF4 case, the extreme solution A was likely not found. It can also be inferred that the extreme solution B was not found by the GA, as again it would have been the same of the RT1 – NF1 case.

5.3.3.2.3   Retrofit on both sides (RT2)

Same retrofit solution for all the walls (NF1)

In the case of retrofit intervention on both sides of the wall and same retrofit solution on all the façades, the innovization analyses highlighted the use of either only PCM1 when minimising the global cost or both PCMs when minimising the primary energy consumption. Wall type *ie100000* (PCM1-existing wall-insulation) was always selected for the solutions with only PCM1, whereas *ie300010* (PCM2-existing wall-PCM1-insulation) and *ie300011* (PCM2-existing wall-insulation-PCM1) were selected for the solutions with both PCMs (Fig. B.35).

All the solutions with the exception of solution A were characterised by window type 7 (Fig. C.7). Thermo-plaster was selected as internal lining with the exception of the two cheapest solutions. The preferred insulation materials were cork and

EPS. Also in this case, all the solutions shared a U-value of 0.15 W/(m^{2}K).

As in Palermo, all solutions with only PCM1 were characterised by a constant thickness of 0.5 cm. When PCM2 was additionally introduced, an increasing thickness of PCM1 could be observed for reducing the primary energy consumption, according to the following relationship:

$$E_P = -33 \cdot t_1 + 141.13 \quad (\text{R}^2 = 0.900).$$

The thickness of PCM2 was always 0.5 cm apart from solution B. The relationship between the total PCM thickness and global cost is described by

$$C_G = 2600 \cdot (t_1 + t_2) + 597 \quad (\text{R}^2 = 0.912),$$

whereas the relationship between global cost and investment cost is given by

$$C_G = 0.796 \cdot C_I + 366.1 \quad (\text{R}^2 = 0.999).$$

With regard to the PCM properties, a higher variation for all properties of PCM1 can be observed in comparison with the RT0 and RT1 cases (Fig. B.36). This could be explained by the greater variability of the PCM's position within the wall. The solutions with only PCM1 were characterised by latent heat values which tended to the upper bound. When both PCMs were present, an increasing trend of the latent heat of fusion of PCM1 was graphically detected as the primary energy consumption decreased, although no clear relationship could be defined. No clear trend can be observed for PCM1's thermal conductivity; medium to high values were mainly selected. No trend was found to describe the properties of PCM2.

Eventually, the extreme solutions of the Pareto front are reported in Fig. C.7. Although a different choice for the insulation material, and of course a different window type, solution A (minimum primary energy consumption) was very similar to that of Palermo. Also in this case, PCM2 was placed towards the external environment, whereas PCM1 was placed as the innermost layer after the thermoplaster. PCM2's thermo-physical properties were identical apart from the thermal conductivity. PCM1's properties were very similar as well.

Also solution B (minimum global cost) was similar to that of Palermo apart from PCM1's thermo-physical properties. Since intervening on both sides could not be avoided in the RT2 case, the most similar solution to solution B of the RT1 case was found.

Different wall solution for each orientation (NF4)

In the case of retrofit intervention on both sides of the wall and different retrofit solution for each façade, the innovization analyses highlighted a clear preference for PCM1 on the north facing wall, whereas PCM2 was often chosen in the west and east façades. As for the same case in Palermo, all the solutions with PCM2

and PCM1 were respectively characterised by wall types *ie200000* and *ie100000* (PCM1-existing wall-insulation).

Low U-values were generally selected, especially for the north and south façades. The preferred insulation and internal lining materials were respectively EPS and lime and gypsum plaster. Window type 4 was generally selected; window type 7 was chosen for the solutions with lowest primary energy consumption. Window type 5 (DGU Ar low-e(2)), which was never selected before, was adopted for the extreme solution with worse energy performance.

Low PCM thicknesses were chosen for PCM1 and PCM2 respectively in the north and west facing walls. A medium thickness was selected for PCM1 in the west walls.

With regard to the PCM properties, no clear trend could be recognised. This could be explained by the greater variability in the PCM's position within the wall. However, lower primary energy consumptions seemed to be associated with a lower melting temperature range of PCM1 and partly of PCM2.

The only relationship that could be identified was between global cost and investment cost;

$$C_G = 0.78 \cdot C_I + 375 \quad (\text{R}^2 = 0.997).$$

Eventually, the extreme solutions of the Pareto front are described. Solution A was similar to the correspondent case for Palermo. Unlikely the RT1 − NF1 case, no PCM was placed towards the internal environment. As in Palermo, PCM1 was preferred over PCM2 for the east and north façades.

Solution B was very similar to that of the NF1 case. The main differences are a higher U-value of the walls, the adoption of either PCM1 or PCM2 in the outermost layers, and no PCM in the south wall, which resulted in adding insulation on both sides.

As it was already mentioned, the exploration level achieved by the RT2 − NF4 case study was significantly lower than the others options. The obtained non-dominated set might still be far from the true Pareto front.

5.3.3.3   Palermo, three objectives

The three-objective case studies in Palermo aimed at minimising heating energy need, cooling energy need and investment cost.

A first glance at the solutions was obtained by analysing Fig. A.3, where the box plots of all the retrofit options are summarised. The corresponding frequency analyses are reported from Fig. A.21 to Fig. A.27.

Due to the contrast between the heating and cooling objectives, the Pareto solutions were characterised by a wide range of U-values. However, as it was previously observed, since the heating energy need could be reduced more effectively than the cooling energy need, at least in the NF1 cases (same retrofit type for all the façades) low U-values were mostly preferred. Moreover, the Pareto fronts resulted to be strongly clustered by window type. Unlikely the two-objective analyses, all window types were selected. In particular, window type 0 was used only by the solution characterised by minimum investment cost, whereas window type 3 was chosen when reducing the cooling energy need. In the same way, all insulation and internal lining materials were used.

With regard to the PCM selection, as in the two-objective optimisations, PCM1 was generally preferred over PCM2. However, when reducing the cooling energy need, many solutions were also characterised by the simultaneous presence of both PCMs.

High thicknesses were mostly chosen for PCM1, whereas no uniform trends were obsvered for PCM2 among the various cases. As for the two-objective optimisations, some trends can be retrieved by analysing the variables' maps on the Pareto fronts.

The most evident piece of information that can be devised from the box plots is that very high latent heats of fusion were selected for PCM1. Medium values seemed to suffice for PCM2, except in the RT0 − NF1 case. When the PCM cannot totally melt and freeze, the latent heat of fusion does not need to be increased [181]. Maximisation of the latent heat of fusion can therefore be seen as an indicator of how effectively a PCM undergoes melting and solidification cycles.

The interquartile range of the peak melting temperature of PCM1 was similar among the various cases, with a median value approximately around 20 ℃. However, a much smaller interquartile range was found for the peak melting temperature of PCM2 for the RT0 − NF1 and RT1 − NF1 cases, with median values around 24/25 ℃. For the NF1 case, this is in line with the night ventilation set-point temperature. As for the two-objective optimisations, the melting temperature range of PCM1 generally assumed medium/low values, whereas for PCM2 there was not a clear trend apart from the RT0 − NF1 case, where high values were preferred. With regard to the thermal conductivity, no clear trends could be identified.

In the detailed comments to each retrofit option, more information on the values assumed by the discrete and continuous variables will be also provided, together with specific trends along the non-dominated set. The extreme solutions of the Pareto front were additionally reported, where solution A was the best performing individual with respect to the heating energy need, solution B was the individual with lowest cooling energy need, and solution C was characterised by the lowest investment cost.

5.3.3.3.1   Retrofit on the external side (RT0)

Same retrofit solution for all the walls (NF1)

In the case of retrofit intervention on the external side of the wall and same retrofit solution for all the façades, the innovization analyses highlighted a prevalent use of PCM1. About 25% of the Pareto front was characterised by both PCMs. A few solutions with no PCM were selected when minimising the investment cost. When only PCM1 was chosen, the preferred wall type was *ext1000* (insulation-PCM1-existing wall), whereas *ext3100* and *ext3101* (insulation-PCM1/PCM2-PCM2/PCM1-existing wall) were equally selected when both PCMs were used (Fig. B.37). The solutions with both PCMs were approximately placed on the non-dominated set between heating and cooling energy need. Compared to the best cases without PCM, a greater improvement when adding PCM could be observed for reducing the heating energy need.

The Pareto front was strongly clustered by the window type. Two main clusters can be observed; one formed by window types 0 and 1, and the other formed by window types 2 and 3. Window type 0 (DGU Air) was chosen only for the solution with lowest investment cost (solution C). As it could be expected, the group of solutions which mounted window type 1 (DGU Air low-e(3)) was characterised by the highest cooling energy need, whereas window type 3 (DGU 90%Ar selective(2)) was chosen when reducing the cooling energy need. Although individuals with window type 1 were characterised by a better winter performance, the difference compared to window type 3 can be considered negligible.

The preferred insulation materials were aerogel, which was selected for the most expensive solutions on the non-dominated set of the heating and cooling energy need functions, and XPS. The U-value presented a clear trend within each cluster; high values corresponded to low cooling but high heating energy needs, and vice versa for low U-values. However, only for the points characterised by window type 3 a relationship between U-value, $Q_{H,nd}$ and $Q_{C,nd}$ was found,

$$\text{Uvalue} = 3.6 + 0.058 \, Q_{H,nd} - 0.145 \, Q_{C,nd} \quad (\text{R}^2 = 0.925).$$

The following relationship between U-value, $Q_{C,nd}$ and investment cost was additionally obtained,

$$\text{Uvalue} = 5.2 - 0.204\, Q_{C,nd} - 0.00027\, C_I \quad (\text{R}^2 = 0.938).$$

The Pareto front was characterised by an increasing PCM1 thickness in order to decrease heating and cooling energy needs (hence increasing the investment cost). High values were mostly selected.

With regard to the PCM properties, all the solutions shared an almost constant latent heat of fusion, mainly equal to 230 kJ/(kg K) and always higher than 210 kJ/(kg K) (Fig. B.38). The peak melting temperature of PCM1 exhibited a slight tendency to increase with the layer's thickness. However, only a narrow range of temperatures around 21.0 ℃ were selected. Apart from a few exceptions, the peak melting temperature of PCM2 was about 24.3 ℃. Medium/low melting temperature ranges were mostly preferred for PCM1, whereas medium/high values were chosen for PCM2. No clear trend can be observed for the PCM's thermal conductivity; mainly high values were selected for PCM1 and medium values for PCM2.

Eventually, the extreme solutions of the Pareto front are reported in Fig. C.8. Solution A (minimum heating energy need) was characterised by window type 1 (air filled DGU with low-emissivity coating on face 3), a U-value of 0.15 W/(m^{2}K), aerogel insulation, 4.0 cm of PCM1 and 3.0 cm of PCM2. PCM1 was characterised by a melting temperature of 22.5 ℃, melting temperature range of 1.0 ℃, 220 kJ/kg of latent heat of fusion, and a thermal conductivity of 0.80 W/(m K). PCM2 was characterised by a melting temperature of 24.0 ℃, melting temperature range of 6.5 ℃, 180 kJ/kg of latent heat of fusion, and a thermal conductivity of 0.45 W/(m K). Although close to the true optimum, this solution was verified to be only sub-optimal, as increasing thickness of PCM2, latent heat of fusion and thermal conductivity of both PCMs led to a slightly lower $Q_{H,nd}$.

Solution B (minimum cooling energy need) was characterised by window type 3 (90% Argon filled DGU with selective coating on face 2), a U-value of 0.43 W/(m^{2}K) (almost the upper bound), aerogel insulation, and the same thicknesses for PCM1 and PCM2 as in solution A. Although the relative position of the two PCMs were inverted compared to solution A, the thermo-physical properties of PCM1 were almost identical. The thermo-physical properties of PCM2 were also very similar; lower melting temperature range and thermal conductivity were chosen. Although close to the true optimum, this solution was verified to be only sub-optimal, as increasing the U-value to 0.45 W/(m^{2}K) and increasing thickness of PCM2, latent heat of fusion and thermal conductivity of both PCMs led to a slightly lower $Q_{C,nd}$.

Solution C (minimum investment cost) was characterised by the cheapest materials; window type 0, a U-value of 0.45 W/(m^{2}K), i.e. the maximum allowed value, EPS insulation and no PCM. Except for the window type, this solution is the same as solution B for the corresponding two-objective optimisation, where window performance however prevailed on investment cost.

Different wall solution for each orientation (NF4)

In the case of retrofit intervention on the external side of the wall and different retrofit solution for each façade, the innovization analyses highlighted mainly the use of PCM1 on the south and east façades and mostly no PCM on the north and west-facing walls. A few cases where both PCMs were adopted occurred mostly in the south and north expositions. The majority of solutions on the south and east façades were characterised by wall type *ext1000* (insulation-PCM1-existing wall).

The preferred insulation materials were XPS and aerogel, which was selected for the solutions on the non-dominated set between heating and cooling energy need. Window types 1 and 3 were mostly selected. Two main clusters were observed; one formed by window type 1, and the other formed by window types 2 and 3. In all the façades, but especially on the north-facing wall, high U-values in each cluster corresponded to high heating energy need and low cooling energy need, and vice versa.

With regard to the PCM1 thickness, the majority of solutions of the north-facing wall were characterised by either 4.0 cm or 3.5 cm. High thicknesses were selected also for the south and east facing walls. Due to the lower number of cases, no clear preference could be observed for PCM2. However, low thicknesses seemed to be preferred for the north wall, and high thicknesses for the south wall for the solutions on the non-dominated set between heating and cooling energy need.

With regard to the PCM1 properties, which were the same regardless of the exposition, an average peak melting temperature of 20.8 ℃ was selected. The latent heat of fusion was mostly equal to 230 kJ/(kg K). A medium-low melting temperature range was mostly preferred, whereas no clear trend could be observed for the PCM's thermal conductivity. No clear trend could be observed for the properties of PCM2. Peak melting temperatures over 35 ℃ were mostly selected for the solutions on the non-dominated set between heating and cooling energy need.

Eventually, the extreme solutions of the Pareto front are described. Solution A (minimum heating energy need) was characterised by window type 1 (air filled DGU with low-emissivity coating on face 3) and aerogel insulation. Unlikely the NF1 case, both PCMs were selected only for the south wall. PCM1 was chosen as the only PCM on the north and east façades, whereas no PCM was selected for the west exposition. A U-value of 0.15 W/(m²K) was chosen on the north and east façades and a slightly higher value for the other walls. The thermo-physical properties of PCM1 were very similar to those of the NF1 case. A much higher melting temperature was selected for PCM2, which was placed on the outermost layer just after the external render.

Solution B (minimum cooling energy need) was characterised by window type 3 (90% Argon filled DGU with selective coating on face 2) and aerogel insulation. A U-value of 0.43 W/(m²K) (as for the NF1 case) was selected on the south and east walls, 0.45 W/(m²K) the north façade, and 0.35 W/(m²K) on the west one. Unlikely the NF1 case, only one PCM was selected in each façade. Even though both PCMs

were chosen on the south wall, the thickness of PCM1 compared to that of PCM2 can be considered negligible. A high thickness of PCM2 was selected for the south and north façades, whereas a thickness of 1.5/2 cm was chosen for the east and west façades. The thermo-physical properties of the two PCMs were quite similar to those of the NF1 case, even though the latent heat of fusion of PCM1 was in this case much lower (140 kJ/(kg K)).

Solution C (minimum investment cost) was characterised by window type 1, a U-value of 0.45 W/(m^{2}K) for the south wall and lower for the other façades, EPS insulation and no PCM. It can be inferred that, in the current case, the GA failed at finding the extreme solutions due to the broader search space.

5.3.3.3.2   Retrofit on the internal side (RT1)

Same retrofit solution for all the walls (NF1)

In the case of retrofit intervention on the internal side of the wall and same retrofit solution on all the façades, the innovization analyses highlighted a prevalent use of PCM1 or, to a lesser extent, both PCMs or no PCM. When only PCM1 was chosen, the preferred wall type was *int1100* (existing wall-insulation-PCM1), whereas *int3111* and *int3110* (existing wall-insulation-PCM1/PCM2-PCM2/PCM1) were almost equally selected when both PCMs were used (Fig. B.39). As for the RT0 – NF1 case, the solutions with both PCMs were approximately placed on the non-dominated set between heating and cooling energy need. Compared to the best cases without PCM, a greater improvement when adding PCM could be observed for reducing the heating energy need.

As in the previous case, the Pareto front was strongly clustered by the window type. Window type 0 (DGU Air) was chosen only for the solution with lowest investment cost (solution C). Each of the other window types formed a separate cluster. As it could be expected, the group of solutions which mounted window type 1 (DGU Air low-e(3)) was characterised by the highest cooling energy need, whereas window type 3 (DGU 90%Ar selective(2)) was chosen when reducing the cooling energy need.

The preferred insulation materials were EPS and XPS (Fig. B.39). Thermo-plaster or lime and gypsum plaster were mainly selected as internal lining materials. Thermo-plaster was especially associated to a reduction of the cooling energy need. In each cluster, high U-values were associated to a high heating energy need, but almost no effect on the cooling energy need was observed. No clear relationship was however identified.

The Pareto front was characterised by an increasing PCM1 thickness in order to decrease the heating energy need (hence increasing the investment cost). High values were mostly selected. With regard to the PCM1 properties, all the solutions shared a quite uniform peak melting temperature of about 21.0 ℃, low melting

temperature range and the maximum latent heat of fusion (Fig. B.40). No clear trend could be observed for the thermal conductivity. High values seemed to be mostly associated to a low cooling energy need. PCM2 was characterised by an almost constant peak melting temperature of about 23.9 ℃. No other trend could be detected.

Eventually, the extreme solutions of the Pareto front are reported in Fig. C.10. Solution A (minimum heating energy need) was characterised by window type 1 (air filled DGU with low-emissivity coating on face 3), a U-value of 0.17 W/(m^{2}K), aerogel insulation, lime and gypsum plaster, 4.0 cm of only PCM1 with a melting temperature of 20.5 ℃, melting temperature range of 3.5 ℃, 220 kJ/kg of latent heat of fusion, and a thermal conductivity of 0.50 W/(m K). Although close to the true optimum, this solution was verified to be only sub-optimal, as reducing the U-value to 0.15 W/(m^{2}K) and increasing latent heat of fusion and thermal conductivity of the PCM led to a slightly lower $Q_{H,nd}$.

Solution B (minimum cooling energy need) was characterised by window type 3 (90% Argon filled DGU with selective coating on face 2), a U-value of 0.43 W/(m^{2}K) (as for the RT0 – NF1 case), sheep wool insulation and thermo-plaster. Both PCMs were selected with a thickness of 3.0 cm and 3.5 cm respectively for PCM1 and PCM2. Their peak melting temperatures (23 ℃ and 24 ℃, respectively) and latent heat of fusion were similar; however, a narrow melting temperature range was chosen for PCM1, which was the closest to the internal environment, whereas a higher melting temperature range was selected for PCM2. Although close to the true optimum, this solution was verified to be only sub-optimal, as increasing the U-value to 0.45 W/(m^{2}K) and increasing thickness, latent heat of fusion and thermal conductivity of both PCMs led to a slightly lower $Q_{C,nd}$.

Solution C (minimum investment cost) was characterised by the cheapest materials; window type 0, a U-value of 0.45 W/(m^{2}K), EPS insulation, lime and gypsum plaster and no PCM. As for the RT0 case, this solution is the same as solution B for the corresponding two-objective optimisation except for the window type.

The added thickness, ranging among all solutions between 9 cm and 35 cm, highlights again the usefulness of a constraint on the overall wall thickness or floor surface reduction.

Different wall solution for each orientation (NF4)

In the case of retrofit intervention on the internal side of the wall and different retrofit solution for each façade, the innovization analyses highlighted a general preference for no PCM, with the exception of the south wall where a few more solutions with only PCM1 were chosen. The introduction of PCM1 and then both PCMs had an effect mostly on reducing the heating energy need. However, its effect was not very significant. At least 50% of solutions in each façade were characterised either by wall type *int0000* or *int1100* (existing wall-insulation-PCM1).

Window types 1 and 3 were mostly selected. Two main clusters were observed;

one formed by window type 1, and the other formed by window types 2 and 3. Window type 0 (DGU Air) was chosen only for the solution with lowest investment cost (solution C).

The preferred insulation materials were EPS and XPS. Lime and gypsum plaster or thermo-plaster were mainly selected as internal lining materials. Thermo-plaster was generally associated to a reduction of the cooling energy need.

No clear trend could be detected for the U-values with the exception of the north-facing wall, where high U-values in each cluster corresponded to low cooling energy need. Corresponding high heating energy needs were generally observed in the cluster formed by window type 3, whereas no effect on the heating energy need was observed in the cluster formed by window type 1.

With regard to the PCM1 thickness, most of the solutions of the south-facing wall were characterised by a high thickness, and especially by 4.0 cm when reducing the cooling energy need. High thicknesses were selected also for the north and east facing walls, where high thicknesses seemed to be associated to a low heating energy need. No clear trend could be observed in the west-facing wall. No clear trends could be observed for PCM2. High thicknesses seemed to be preferred for the north and east walls.

With regard to the PCM1 properties, which were the same regardless of the exposition, a peak melting temperature of 19.5℃ was mostly selected. Higher values were generally associated to high $Q_{H,nd}$ and low $Q_{C,nd}$. A latent heat of fusion higher than 200 kJ/(kg K), and mostly equal to 230 kJ/(kg K), was chosen. A medium-low melting temperature range was mostly preferred, whereas no clear trend could be observed for the PCM's thermal conductivity. A median value of peak melting temperature of PCM2 of 25 ℃ was selected for the solutions on the non-dominated set between heating and cooling energy need. No clear trend could be observed for the other properties, apart from a high thermal conductivity associated to solutions with low heating energy need in the cluster characterised by window type 1.

Eventually, the extreme solutions of the Pareto front are described. Solution A (minimum heating energy need) was characterised by window type 1 (air filled DGU with low-emissivity coating on face 3), insulation with cellulose fiber panels and mineralised wooden board as internal lining material. Unlikely the NF1 case, PCM1 only was selected only for the south wall. Both PCMs were selected on the north and east façades, whereas a thin layer of only PCM2 was selected for the west exposition. A U-value of 0.17 W/(m^{2}K) was chosen only for the south façade as for the NF1 case, 0.25 W/(m^{2}K) and 0.23 W/(m^{2}K) were respectively selected for the east and north walls, whereas a U-value of 0.45 W/(m^{2}K) (upper limit) was chosen only for the west façade. The thermo-physical properties of PCM1 were very similar to those of the NF1 case. Given the low latent heat of fusion of PCM2, its presence was not as effective as that of PCM1.

Solution B (minimum cooling energy need) was characterised by window type 3 (90% Argon filled DGU with selective coating on face 2), XPS insulation and thermo-

plaster as internal lining material. A U-value of 0.43 W/(m^{2}K) (as for the NF1 case) was selected on the east and north walls, 0.39 W/(m^{2}K) the west façade, and 0.29 W/(m^{2}K) on the south one. As in solution A, the same layer sequence of the NF1 case was chosen only for the south wall. Thin layers of both PCMs were added in the north and west façades, whereas no PCM was selected for the east-facing wall. The thermo-physical properties of the two PCMs were quite similar to those of the NF1 case.

Solution C (minimum investment cost) was characterised by window type 1, EPS insulation, lime and gypsum plaster, no PCM, and U-values below or equal to 0.43 W/(m^{2}K).

5.3.3.3.3   Retrofit on both sides (RT2)

Same retrofit solution for all the walls (NF1)

In the case of retrofit intervention on both sides of the wall and same retrofit solution on all the façades, the innovization analyses highlighted a prevalent use of PCM1 and both PCMs to a lesser extent. When only PCM1 was chosen, the preferred wall type was *ie101000* (insulation-existing wall-PCM1), whereas *ie311111* (insulation-existing wall-insulation-PCM2-PCM1) was mostly selected when both PCMs were used (Fig. B.41). Unlikely the previous cases, the non-dominated set between heating and cooling energy need was not populated almost exclusively by individuals with both PCMs.

As in the previous cases, the Pareto front was strongly clustered by window type. Window type 0 (DGU Air) was chosen only for the solution with the lowest investment cost (solution C). Two main clusters can be observed; one formed by window types 0 and 1, and the other formed by window types 2 and 3. As it could be expected, the group of solutions which mounted window type 1 (DGU Air low-e(3)) was characterised by the highest cooling energy need, whereas window type 3 (DGU 90%Ar selective(2)) was chosen when reducing the cooling energy need.

The preferred insulation materials were EPS and XPS (Fig. B.41). Lime and gypsum plaster or thermo-plaster were mainly selected as internal lining materials. As in the RT1 – NF1 case, thermo-plaster characterised the solutions with lowest cooling energy need in each cluster.

High U-values corresponded to high heating energy need and low cooling energy need; however, no clear relationship was found.

The Pareto front was characterised by an increasing PCM1 thickness in order to decrease heating and cooling energy needs (hence increasing the investment cost). High values were mostly selected. However, no clear relationship was identified.

With regard to the PCM1 properties, all the solutions shared an almost constant peak melting temperature of about 20.7 ℃, medium/low melting temperature range and the maximum latent heat of fusion (Fig. B.42). No clear trend could be observed

for the thermal conductivity. With regard to the PCM2 properties, no clear trend could be identified.

Eventually, the extreme solutions of the Pareto front are reported in Fig. C.12. Solution A (minimum heating energy need) was characterised by window type 1 (air filled DGU with low-emissivity coating on face 3), a U-value of 0.15 W/(m^{2}K), aerogel insulation on the outer side of the wall, mineralised wooden board as internal lining material, 4.0 cm of only PCM1 on the inner side of the wall with a melting temperature of 21.5 ℃, melting temperature range of 5.3 ℃, 220 kJ/kg of latent heat of fusion, and a thermal conductivity of 0.85 W/(m K).

Solution B (minimum cooling energy need) was characterised by window type 3 (90% Argon filled DGU with selective coating on face 2), a U-value of 0.45 W/(m^{2}K), rock wool insulation and thermo-plaster. Both PCMs were selected, with a thickness of 3.0 cm each. Their peak melting temperatures were 23 ℃ and 26 ℃ respectively for PCM1 and PCM2. They shared the same melting temperature range of 3 ℃. Their latent heat of fusion was similar. A low thermal conductivity was selected for PCM1 whereas a high value was chosen for PCM2.

Solution C (minimum investment cost) was very similar to that of the RT1 – NF1 case. The main difference was the presence of 0.5 cm of PCM1 on the outermost layer (except the external render). Since intervening on both sides could not be avoided in the RT2 case, the most similar solution to RT1's solutions B was selected. However, due to the wider search space for the RT2 case study, the real solution C was not found by the GA; a U-value of 0.41 W/(m^{2}K) was chosen.

Different wall solution for each orientation (NF4)

In the case of retrofit intervention on both sides of the wall and different retrofit solution for each façade, the innovization analyses highlighted a general preference for PCM1 in the south ans north exposed walls, mostly no PCM towards east, and either no PCM or PCM1 on the west façade. The adoption of both PCMs in the south and north façades were mainly associated to a low cooling energy need. Most of solutions in each façade except the east wall were characterised either by wall type *ie000000* or *int101000* (insulation-existing wall-PCM1).

Window types 1 and 3 were mostly selected. Two main clusters eere observed; one formed by window type 1 and the other formed by window types 2 and 3. Window type 0 (DGU Air) was chosen only for the solution with lowest investment cost (solution C).

The preferred insulation materials were EPS, XPS and rock wool. Thermo-plaster or lime and gypsum plaster were mainly selected as internal lining materials. Thermo-plaster was generally associated to a reduction of the cooling energy need.

No clear trend could be detected for the U-values with the exception of the north-facing wall, where high U-values in each cluster corresponded to low cooling energy need and high heating energy need.

With regard to the PCM1 thickness, the majority of solutions of the north and

south-facing walls were characterised by a high thickness. High thicknesses on the south-facing wall were generally associated to solutions in the non-dominated set between heating and cooling energy need. No clear trend could be observed in the east and west-facing walls. No clear trends could be observed for PCM2. High thicknesses seemed to be preferred for the east and north walls to reduce the cooling energy need.

With regard to the PCM1 properties, an average peak melting temperature of 20.1℃ was selected. Higher values were generally associated to high $Q_{H,nd}$ and low $Q_{C,nd}$. A latent heat of fusion higher than 170 kJ/(kg K), and mostly equal to 230 kJ/(kg K), was chosen. A medium-low melting temperature range was mostly preferred, whereas no clear trend could be observed for the PCM's thermal conductivity. A median value of peak melting temperature of PCM2 of 27.75 ℃ was selected, whereas no clear trend could be observed for the other properties.

Eventually, the extreme solutions of the Pareto front are described. Solution A (minimum heating energy need) was characterised by window type 1 (air filled DGU with low-emissivity coating on face 3), aerogel insulation and lime and gypsum plaster. Unlikely the RT0 and RT1 cases, the same wall type as the NF1 case was selected for the north and west façades. Both PCMs were selected on the south façade, whereas no PCM was chosen for the east exposition. A U-value of 0.17 W/(m²K) was chosen for the south façade, 0.29 W/(m²K) and 0.21 W/(m²K) were respectively selected for the east and north walls, whereas a U-value of 0.45 W/(m²K) (upper limit) was chosen only for the west façade. The thermo-physical properties of PCM1 were very similar to those of the NF1 case, with the exception of a lower thermal conductivity. Given the relatively low thickness and latent heat of fusion of PCM2, its presence was not as effective as that of PCM1.

Solution B (minimum cooling energy need), as for the RT1 case, was characterised by window type 3 (90% Argon filled DGU with selective coating on face 2), XPS insulation and thermo-plaster as internal lining material. However, the selected wall types were different from that of the NF1 case. Given the different position within the wall, the PCM properties were quite different as well. A U-value of 0.45 W/(m²K) (as for the NF1 case) was selected on north wall, 0.41 W/(m²K) the east façade, 0.29 W/(m²K) on the west one, and 0.15 W/(m²K) on the south-facing wall.

Solution C (minimum investment cost) was characterised by window type 1, EPS insulation, lime and gypsum plaster, no PCM, and U-values equal to 0.43 W/(m²K), apart from the east façade which was characterised by a lower U-value. A thin layer of either PCM2 or PCM1 was placed as the outermost layer (except the external render) on the south and east-facing walls, whereas insulation on both sides of the wall was chosen for the north and west façades.

Due to the wider search space for the RT2 – NF4 case study, it can be inferred that the real extreme solutions were not found by the GA.

5.3.3.4 Torino, three objectives

The three-objective case studies in Torino aimed at minimising heating energy need, cooling energy need and investment cost.

A first glance at the solutions was obtained by analysing Fig. A.4, where the box plots of all the retrofit options are summarised. The corresponding frequency analyses are reported from Fig. A.28 to Fig. A.34.

Due to the contrast between the heating and cooling objectives, the Pareto solutions were characterised by a wide range of U-values, although low U-values were mostly selected especially for the RT1 − NF1 case. This is in line with the heating-dominated climate of Torino.

As in Palermo, the Pareto fronts resulted to be strongly clustered by window type. Unlikely the two-objective analyses, window type 4 was used only by a small group of solutions characterised by the highest cooling energy need. Window type 5, which was previously almost never selected, was used in the cluster characterised by the lowest cooling energy need and therefore highest heating energy need, and vice versa for window type 7. In the same way, all insulation and internal lining materials were used. As for the two-objective cases, thermo-plaster was often selected.

With regard to the PCM selection, unlikely the two-objective optimisations, solutions characterised by PCM2 or both PCMs were selected more often than solutions with only PCM1. Solutions with both PCMs were especially able to simultaneously minimise both the energy need for heating and cooling. Even though heating energy consumption was the most important aspect to minimise, in Torino PCM2 could work more effectively than in Palermo due to the milder summer conditions.

High thicknesses were mostly chosen for both PCMs, and the trends that could be previously detected by analysing the variables' maps on the Pareto fronts were not as definite.

The most evident piece of information that can be devised from the box plots is a narrow peak melting temperature of PCM2, with median values around 24/25 ℃.

High latent heats of fusion were selected for both PCMs, even though the interquartile ranges were not very narrow. The melting temperature range of PCM2 generally assumed medium/low values, whereas for PCM1 the trend was milder. With regard to the thermal conductivity, no clear trends could be identified.

In the detailed comments to each retrofit option, more information on the values assumed by the discrete and continuous variables will be also provided, together with specific trends along the non-dominated set. The extreme solutions of the Pareto front were additionally reported, where solution A was the best performing

individual with respect to the heating energy need, solution B was the individual with lowest cooling energy need, and solution C was characterised by the lowest investment cost.

5.3.3.4.1   Retrofit on the external side (RT0)

Same retrofit solution for all the walls (NF1)

In the case of retrofit intervention on the external side of the wall and same retrofit solution for all the façades, the innovization analyses highlighted a prevalent use of PCM2. About 25% of the Pareto front was characterised by both PCMs and 20% by only PCM1. Some solutions with no PCM minimised the investment cost, while some others were characterised by a good winter performance but high cooling energy need and high cost. When only PCM2 was chosen, the preferred wall type was always *ext2000* (insulation-PCM2-existing wall), whereas *ext3100* and *ext3101* (insulation-PCM1/PCM2-PCM2/PCM1-existing wall) were equally selected when both PCMs were used (Fig. B.43). The PCM use strategy was less defined than in Palermo. The solutions with both PCMs were approximately placed on the non-dominated set between heating and cooling energy need. Most of the solutions with only PCM2 were associated to low cooling but high heating energy need, and vice versa for PCM1. As in Palermo, when adding PCM to the best cases without PCM, a greater improvement could be observed for reducing the heating energy need.

The Pareto front was strongly clustered by the window type. Window type 4 (DGU 90%Ar low-e(3)) was chosen only for the solutions with intermediate heating energy need but the highest cooling energy need. As it could be expected, the group of solutions which mounted window type 7 (TGU 90%Ar low-e(3,5)) was characterised by low heating energy need, whereas window type 5 (DGU 90%Ar low-e(2)) was chosen when reducing the cooling energy need.

Aerogel insulation was adopted by more than 50% of the solutions, the majority of which were associated to a low heating energy need. However, a cluster of solutions with aerogel was characterised by a low cooling energy need when window type 5 was selected. The reason for choosing aerogel when minimising the heating energy need in case of retrofit on the external side of the wall is that, due to its low thermal conductivity, low U-values can be obtained with a small thickness. This has a strong implication on shading; the less the added thickness, the more the available solar gains. The colder the climate, the more preventing excessive shading was found to be important.

With regard to the U-value, Torino's case was very different from Palermo's. Within each cluster, high U-values were mainly associated to a high heating energy need. However, both high and low U-values could lead to low cooling energy need. No relationship between U-value, $Q_{H,nd}$ and $Q_{C,nd}$ could be devised.

A high thickness of both PCMs was mostly selected, especially for the solutions placed on the non-dominated set between heating and cooling energy need.

With regard to the PCM properties, peak melting temperatures of PCM1 close to 23 ℃ were selected for the solutions with lowest cooling energy need, whereas values around 19 ℃ to 15 ℃ were chosen for the solutions with lowest heating energy need (Fig. B.44). However, the Pareto front exhibited no clear trend. On the other hand, the peak melting temperature of PCM2 was almost constant and on average equal to 25.1 ℃.

All the solutions shared a very high latent heat of fusion for both PCM1 and PCM2. Medium/low melting temperature ranges were mostly selected for both PCMs, whereas no clear trend was observed for the PCM's thermal conductivity.

Eventually, the extreme solutions of the Pareto front are reported in Fig. C.9. Solution A (minimum heating energy need) was quite similar to the corresponding solution in Palermo. The main differences were the selection of window type 7 (90%Ar filled TGU with low-emissivity coating on faces 3 and 5), the absence of PCM2 and a lower peak melting temperature for PCM1. This solution was almost identical to solution A (minimum primary energy consumption) of the corresponding two-objective optimisation.

Solution B (minimum cooling energy need) was characterised by window type 5 (90% Argon filled DGU with low-e coating on face 2), a U-value of 0.29 W/(m²K) (almost the upper bound), rock wool insulation, and both PCM1 and PCM2. As in Palermo, PCM2 was placed in the outermost position with respect to PCM1, and their thermo-physical properties were also quite similar. A peak melting temperature of 23 ℃ was chosen for PCM1 and of 26 ℃ for PCM2. It can be inferred that this solution is close to the true solution B but still slightly sub-optimal.

Solution C (minimum investment cost) was almost identical to that of Palermo. It was characterised by window type 4 (90% Argon filled DGU with low-e coating on face 3) A U-value of 0.30 W/(m²K), i.e. the maximum allowed value, EPS insulation and no PCM. This solution was identical to solution B (minimum global cost) of the corresponding two-objective optimisation.

Different wall solution for each orientation (NF4)

In the case of retrofit intervention on the external side of the wall and different wall solution for each façade, the innovization analyses highlighted mainly the use of no PCM or PCM2 for all the façades, and also both PCMs especially on the south-facing wall. The majority of solutions on all the façades were characterised by wall types *ext0000* and *ext2000* (insulation-PCM2-existing wall). Wall type *ext3010* (PCM1-insulation-PCM2-existing wall) was also mostly selected for the solutions with both PCMs on the south-facing wall.

As for the NF1 case, the Pareto front was strongly clustered by window type. The same comments on window type reported for the NF1 case can be applied.

The preferred insulation materials were aerogel and XPS. Aerogel was especi-

ally selected for the group of solutions characterised by window type 7 and the solutions with the lowest heating energy need in the cluster formed by window type 5. However, all these solutions were associated to installation costs higher than 400 €/m^2.

With regard to the PCM thickness, no clear trend could be observed for PCM1. Mostly high thicknesses were selected for PCM2 on the north and south-facing walls.

With regard to the PCM properties, all the solutions shared a preference for a high latent heat of fusion, especially for PCM2. Medium/low melting temperature ranges were mostly selected for both PCMs, whereas no clear trend was observed for the PCM's thermal conductivity. Apart from a few exceptions, a peak melting temperature of PCM2 around 25.5 ℃ was shared by all the solutions.

Eventually, the extreme solutions of the Pareto front are described. Solution A (minimum heating energy need) was characterised by window type 7 (90%Ar filled TGU with low-emissivity coating on faces 3 and 5) and aerogel insulation. Unlikely the NF1 case, PCM1 was used only on the north and east façades. A U-value of 0.20 W/(m^{2}K) was chosen for the west-facing wall, whereas values close to the lower bound were selected of all the other walls. Apart from the thermal conductivity, the thermo-physical properties of PCM1 were very similar to those of the NF1 case.

Solution B (minimum cooling energy need) was characterised by window type 3 (90% Argon filled DGU with selective coating on face 2) and XPS insulation. Compared to the NF1 case, lower U-values were selected for all the façades. Both PCMs were chosen only for the south and west exposed walls, even though their order within the wall was inverted with respect to the NF1 case. Only PCM2 was chosen for the north and east-facing walls. Apart from the thermal conductivity, the thermo-physical properties of PCM2 were quite similar to those of the NF1 case. A lower peak melting temperature was selected for PCM1, which can be explained by the different position within the walls.

Solution C (minimum investment cost) was characterised by window type 1, a U-value of 0.29 W/(m^{2}K) for the south and west walls (close to the NF1 case) and a lower value for the other façades, EPS insulation and no PCM.

5.3.3.4.2 Retrofit on the internal side (RT1)

Same retrofit solution for all the walls (NF1)

In the case of retrofit intervention on the internal side of the wall and same retrofit solution for all the façades, the innovization analyses highlighted the prevalent use of either PCM2 or both PCMs. solutions with no PCM or only PCM1 were adopted to a lesser extent. When only PCM2 was chosen, the selected wall type was always *int2100* (existing wall-insulation-PCM2), whereas *int3111* (existing wall-insulation-PCM2-PCM1) was mainly chosen when both PCMs were used (Fig. B.45). Solutions

with both PCMs were selected when reducing both heating and cooling energy need.

As for the previous cases, the Pareto front was strongly clustered by window type. Window type 4 (DGU 90%Ar low-e(3)) characterised solutions with the lowest investment cost (yet windows 4 and 5 had the same price), intermediate heating energy need but the highest cooling energy need. As it could be expected, the group of solutions which mounted window type 7 (TGU 90%Ar low-e(3,5)) was characterised by low heating energy need, whereas window type 5 (DGU 90%Ar low-e(2)) was chosen when reducing the cooling energy need.

The preferred insulation materials were EPS and rock wool (Fig. B.45). Thermo-plaster or lime and gypsum plaster were mainly selected as internal lining materials. Thermo-plaster was mostly adopted for the solutions with both PCMs. Low U-values were selected for the majority of solutions, and especially by the trade-off solutions which minimised both heating and cooling energy need.

A high thickness was mostly selected for PCM1, especially for the solutions placed on the non-dominated set between heating and cooling energy need. An increasing thickness of PCM2 can be observed in each cluster in order to decrease the cooling energy need (hence increasing the investment cost). High values were mostly selected.

With regard to the PCM properties, no clear trends could be recognised for the peak melting temperatures of PCM1 (Fig. B.46). An almost constant peak melting temperature of PCM2 could instead be observed, on average equal to 25.1 ℃. High latent heats of fusion were mostly chosen for both PCMs, especially when they were simultaneously selected. Medium/low melting temperature ranges were preferred for PCM2, whereas no clear trend could be observed for PCM1. No clear trend could be observed for the PCM's thermal conductivity. However, high values were mainly selected for the solutions placed on the non-dominated set between heating and cooling energy need with PCM1. A high thermal conductivity of PCM2 was mostly associated to solutions with low cooling energy need.

Eventually, the extreme solutions of the Pareto front are reported in Fig. C.11. Solution A (minimum heating energy need) was very similar to the corresponding case in Palermo. The main differences were the selection of window type 7 (90%Ar filled TGU with low-emissivity coating on faces 3 and 5) and a peak melting temperature of PCM1 of 15.5 ℃. It was verified that selecting a U-value of $0.15/(m^2K)$ and a lower thermal conductivity would slightly reduce the building energy consumption. However, a peak melting temperature of 16.0 ℃ was also found to be preferable. In such case, increasing the thermal conductivity was more beneficial.

Also solution B (minimum cooling energy need) was similar to the corresponding case in Palermo. Even though it was characterised by window type 5 (best summer performance), a U-value of $0.16/(m^2K)$ (almost the lowest value) was selected. As for the RT0 case in Torino, rock wool insulation was chosen. Both PCMs were selected with a thickness of 4.0 cm. However, a narrow melting temperature

range was chosen for PCM2, which was in the furthest position from the internal environment, whereas a higher melting temperature range was selected for PCM1.

Solution C (minimum investment cost) was characterised by the cheapest materials; window type 4, a U-value of 0.30 W/(m²K), EPS insulation, lime and gypsum plaster and no PCM.

As it was previously highlighted, with an added thickness between 13 cm and 35 cm among the Pareto solutions, adding a constraint on the overall wall thickness or reduction of the available floor surface could be useful.

Different wall solution for each orientation (NF4)

In the case of retrofit intervention on the internal side of the wall and different retrofit solution for each façade, the innovization analyses highlighted a prevalent use of no PCM on the east and west façades, PCM2 on the north façade and both PCMs on the south-facing wall. The majority of solutions on all the façades were characterised by wall type *int0000* when no PCM was selected. With PCM, wall type *int3000* (existing wall-PCM1-insulation-PCM2) was mostly preferred on the south façade, *int2100* (existing wall-insulation-PCM2) towards north, *int1100* (existing wall-insulation-PCM1) towards west, and either *int3110* or *ext3111* on the east-facing wall (existing wall-insulation-PCM1/PCM2-PCM2/PCM1).

As for the NF1 case, the Pareto front was strongly clustered by window type. The same comments on window type reported for the NF1 case can be applied.

The most selected insulation materials were ESP and aerogel. Aerogel was especially chosen for the solutions with the lowest heating energy need in the clusters formed by window types 5 and 7. However, these solutions were associated to installation costs higher than 400 €/m². Thermo-plaster and lime and gypsum plaster were mainly selected as internal lining materials. Thermo-plaster was mostly associated to a reduction of the heating energy need within the clusters formed by window types 5 and 7.

With regard to the PCM thickness, no clear trend could be observed for PCM1. Mostly high thicknesses were selected for PCM2 on the south-facing wall.

With regard to the PCM properties, no clear trend could be observed for PCM1. A high latent heat of fusion was observed for PCM2, together with a small range of variation of the peak melting temperature, whose median value was 24.5 ℃. No clear trend could be observed for the PCM's thermal conductivity. Medium values were mostly selected for the melting temperature range.

Eventually, the extreme solutions of the Pareto front are described. Solution A (minimum heating energy need) was characterised by window type 7 (90%Ar filled TGU with low-emissivity coating on faces 3 and 5), aerogel insulation and thermo-plaster. Unlikely the NF1 case where only PCM1 was selected, no PCM was chosen for the south wall, both PCMs for the east and north façades, and a very thin layer of PCM2 towards west. A U-value of 0.15 W/(m²K) was chosen for the south and north-facing walls, whereas 0.17 W/(m²K) was selected for the east and west

façades. Apart from the latent heat of fusion, the thermo-physical properties of PCM1 were quite different to those of the NF1 case.

Solution B (minimum cooling energy need) was characterised by window type 3 (90% Argon filled DGU with selective coating on face 2), EPS insulation and clay plaster. Both PCMs were selected for the south and west façades, and their position was on both sides of the insulation layer. Only PCM2 was selected for the east and north facing walls. A much lower peak melting temperature of PCM1 was selected compared to the NF1 case, whereas the thermo-physical properties of PCM2 were similar, with the exception of the thermal conductivity. A U-value of 0.23 W/(m^{2}K) was chosen for the south and west-facing walls, whereas 0.15 W/(m^{2}K) and 0.19 W/(m^{2}K) were respectively selected for the east and north façades.

Solution C (minimum investment cost) was very similar to that of the NF1 case. Lower U-values were selected likely due to the broader search space.

5.3.3.4.3   Retrofit on both sides (RT2)

Same retrofit solution for all the walls (NF1)

In the case of retrofit intervention on both sides of the wall and same retrofit solution for all the façades, the innovization analyses highlighted a prevalent use of both PCMs (over 50% of the Pareto front). A great variety of wall types was selected (Fig. B.47). Solutions with both PCMs were selected when reducing both heating and cooling energy need.

As for the previous cases, the Pareto front was strongly clustered by the window type. Window type 4 (DGU 90%Ar low-e(3)) characterised solutions with the lowest investment cost (yet windows 4 and 5 had the same price), intermediate heating energy need but the highest cooling energy need. As it could be expected, the group of solutions which mounted window type 7 (TGU 90%Ar low-e(3,5)) was characterised by a low heating energy need, whereas window type 5 (DGU 90%Ar low-e(2)) was chosen when reducing the cooling energy need.

The insulation material which occurred the most was aerogel (Fig. B.47). Due to the aforementioned considerations on this choice with regard to shading, this implies that at least one layer insulation was often placed on the outer side of the wall. Thermo-plaster was the preferred internal lining material, which was mostly adopted for the solutions with both PCMs (as in the RT1 – NF1 case). High U-values were generally associated to a high heating energy need.

The Pareto front was characterised by an increasing thickness of PCM towards the non-dominated set between the energy functions. Increasing thicknesses of PCM1 seemed mainly to lead to a reduction of the heating energy need, whereas increasing thicknesses of PCM2 seemed mainly to lead towards a reduction of cooling energy need.

With regard to the PCM properties, a high latent heat of fusion was selected for

both PCMs (Fig. B.48). In all the solutions PCM2 was characterised by an almost constant peak melting temperature of about 25.3 ℃ and mostly medium/low melting temperature ranges. No other trend could be devised.

Eventually, the extreme solutions of the Pareto front are reported in Fig. C.13. Solution A (minimum heating energy need) was quite dissimilar to that of Palermo. Both PCMs were selected, and two layers of insulation were placed on both sides of the wall. PCM1 was the innermost layer after the thermo-plaster, and a layer of insulation divided it from PCM2. Given the low latent heat of fusion and high melting temperature of PCM2 with respect to its position within the wall, it could be verified that its contribution as a phase change material was negligible.

Solution B (minimum cooling energy need) was quite similar to that of Palermo. The best window type for reducing the cooling energy need was chosen (window type 5) but, in this case, a very low U-value was selected instead of its upper bound. The peak melting temperature of the two PCMs was almost identical to the values adopted in Palermo, but different thermal conductivities were chosen.

Solution C (minimum investment cost) was very similar to that of Palermo. As in the RT0 and RT1 cases, window type 4, a U-value of 0.30 W/(m^{2}K), EPS insulation and lime and gypsum plaster were selected. The thinnest possible layer of PCM1 was placed on the external side of the wall.

Different wall solution for each orientation (NF4)

In the case of retrofit intervention on both sides of the wall and different solution on each façade, the innovization analyses highlighted a prevalent use of no PCM on the east and west façades, PCM2 on the north façade and both PCMs on the south-facing wall. The majority of solutions on all the façades were characterised by wall type *ie000000* when no PCM was selected. With PCM, wall type *ie311000* (insulation-existing wall-PCM1-insulation-PCM2) was mostly preferred on the south façade, *ie111000* (insulation-existing wall-PCM1-insulation) towards east, *ext100000* (PCM1-existing wall-insulation) towards west, and a variety of options on north-facing wall.

As for the other cases, the Pareto front was strongly clustered by the window type. The same comments on window type reported for the NF1 case can be applied.

The most selected insulation materials were aerogel and XPS. Aerogel was especially chosen for the solutions with the lowest heating energy need in the clusters formed by window types 5 and 7. However, these solutions were associated to installation costs higher than 490 €/m^2. Thermo-plaster was selected as internal lining material for the majority of solutions. It was mostly associated to a reduction of the heating energy need within the clusters formed by window types 5 and 7.

With regard to the PCM thickness, no clear trend could be observed, apart from a preference for low values of PCM1 on the west façade, and for high thicknesses of PCM2 on the south-facing wall.

With regard to the PCM properties, a high latent heat of fusion was observed for both PCMs. The peak melting temperature of PCM2 varied within a small range, whose median value was 25.0 ℃. No clear trend could be observed for the PCM's thermal conductivity. Low/medium values were mostly selected for the melting temperature range.

Eventually, the extreme solutions of the Pareto front are described. Solution A (minimum heating energy need) was characterised by window type 7 (90%Ar filled TGU with low-emissivity coating on faces 3 and 5), aerogel insulation and thermo-plaster. Unlikely the NF1 case where both PCMs were selected, no PCM was chosen for the south wall, and only PCM1 for the other façades. However, towards west only a thin layer of PCM1 was added. The thermo-physical properties of the PCM were quite similar to those selected for the NF1 case. U-values equal or close to the lowest bound were selected for all the façades with the exception of the west-facing wall, were a U-value of 0.21 W/(m^{2}K) was chosen.

Solution B (minimum cooling energy need) was characterised by window type 3 (90% Argon filled DGU with selective coating on face 2), XPS insulation and clay plaster. A U-value of 0.18 W/(m^{2}K) was chosen for the south-facing wall, and it increased to 0.20 W/(m^{2}K), 0.24 W/(m^{2}K), 0.26 W/(m^{2}K) respectively for the west, east and north expositions. Unlikely the NF1 case where both PCMs were selected, only PCM2 was chosen towards east, west and practically south (where only 0.5 cm of PCM1 were added). Only the north façade adopted both PCMs. The thermo-physical properties of PCM1 were similar to those chosen for the NF1 case with the exception of the thermal conductivity. A lower peak melting temperature was instead selected for PCM2, probably due to a more inward position within the wall.

Solution C (minimum investment cost) was characterised by the same wall type and U-value selected for the NF1 case only on the north façade. Lower U-values, insulation on both sides of the walls and no PCM were selected for the other expositions. Compared to the NF1 case, different thermo-physical properties were selected for PCM1. However, given its low thickness (0.5 cm), its effect can be considered negligible.

5.3.3.5 Oslo, pre-1955

Oslo's case studies aimed at minimising primary energy consumption, Long-term Percentage of Dissatisfied and global cost.

A first glance at the solutions was obtained by analysing Fig. A.5, where the box plots of all the retrofit options are summarised. The corresponding frequency analyses are reported from Fig. A.35 to Fig. A.41.

Similarly to the previous three-objective optimisations, the Pareto fronts were clustered by window type. Window 8, which was characterised by the highest

U-value among the options available in Oslo, was almost never selected.

Since Oslo is a heating-dominated climate, low U-values were mostly selected. A clear preference for aerogel insulation was observed for the RT0 cases (as in the other locations), whereas the cheapest insulation materials were chosen for the other cases. Unlikely Palermo and Torino, thermo-plaster was almost never used, whereas clay plaster and mineralised wooden board were mostly selected respectively for the RT1 and RT2 cases.

With regard to the PCM selection, PCM1 was clearly preferred over PCM2. Since minimising the primary energy consumption in a heating-dominated climate implies mostly reducing the heating energy consumption, this result could be expected.

Low thicknesses tended to be selected for PCM2, whereas for PCM1 both the box plot representations and the frequency analyses fail at providing significant information that can be retrieved by analysing the variables' maps on the Pareto fronts.

The most evident piece of information that can be devised from the box plots is a very narrow peak melting temperature of PCM1, with median values of 18 ℃ for the RT0 cases and 19.5 ℃ for all the others except RT2 – NF4 where 19.0 ℃ was preferred. The peak melting temperature of the few solutions with PCM2 were also characterised by a narrow peak melting temperature in the RT0 – NF1 and RT1 – NF1 cases.

A high latent heat of fusion and a medium/low melting temperature range were selected for PCM1 (the latter especially for the RT1 – NF1 case), whereas no clear trend could be identified for the thermal conductivity. Due to the very limited amount of solutions with PCM2, no other significant information on its thermo-physical properties can be retrieved.

In the detailed comments to each retrofit option, more information on the values assumed by the discrete and continuous variables will be also provided, together with specific trends along the non-dominated set. The extreme solutions of the Pareto front were additionally reported, where solution A was the best performing individual with respect to the primary energy consumption, solution B was the individual with lowest global cost, and solution C was characterised by the lowest Long-term Percentage of Dissatisfied.

5.3.3.5.1   Retrofit on the external side (RT0)

Same retrofit solution for all the walls (NF1)

In the case of retrofit intervention on the external side of the wall and same retrofit solution on all the façades, the innovization analyses highlighted a prevalent use of

PCM1. Solutions without PCM were located on the edge of the Pareto front with highest LPD and lowest cost. Wall type *ext1000* (insulation-PCM1-existing wall) was selected by the GA for almost all the solutions with PCM and *ext0000* when no PCM was adopted (Fig. B.49).

The Pareto front was strongly clustered by the insulation type. Two main clusters were present; one was the group of solutions with the lowest primary energy consumption but highest global cost, where only aerogel was selected, and the other cluster which grouped all the other insulation materials. Among them, XPS was especially selected for reducing E_P in the second Pareto cluster. As it was previously mentioned, the insulation thickness played a major role, as a low thickness implied less shading and therefore more solar gains [187]. This was especially noticeable is this case; the best energy performance was obtained with aerogel followed by XPS, which were characterised by the lowest thermal conductivities among the available insulation materials.

As for the other locations, also window type had a clustering effect on the Pareto front. Window type 10 (TGU 95%Kr low-e(3,5)) was chosen for the solutions with the lowest primary energy consumption. Window type 9 (TGU 90%Ar low-e(3,5)) was selected for medium energy performance and thermal comfort, whereas window type 7 (TGU 90%Ar low-e(3,5)) with smaller gap size compared to window type 9) characterised the solutions with the worst energy performance but which guaranteed the best thermal comfort.

With regard to the U-value, a trend could by identified within each of the two main clusters, for which the lowest U-values corresponded to the lowest primary energy consumption. The following relationships between U-value and fitness functions could be defined in the cluster with aerogel[2]:

$$\text{Uvalue} = -2.5 - 7.0 \; LPD + 0.011 \; E_P \quad (\text{Adj R}^2 = 0.934),$$

$$\text{Uvalue} = 1.3 - 20 \; LPD - 0.00046 \; C_G \quad (\text{Adj R}^2 = 0.958).$$

A clear trend for the thickness of PCM1 was identified; increasing it allowed to improve thermal comfort. The few solutions which presented also PCM2 were instead characterised by a very low thickness of PCM2 except for two solutions with low LPD (including solution C). The relationship between PCM1 thickness, LPD and E_P can be described by the following equation:

$$t_1 = 1.0 - 14 \; LPD - 0.0018 \; E_P \quad (\text{Adj R}^2 = 0.932).$$

Moreover, a relationship between thickness of PCM1 and global cost was found, which differed for each cluster. For all the solutions without aerogel,

$$t_1 = 0.00031 \cdot C_G - 0.19 \quad (\text{R}^2 = 0.961),$$

---

[2]The only solutions with both PCMs and window type 7 were excluded.

whereas for the solutions with aerogel:

$$t_1 = 0.32 - 11LPD + 0.00013C_G \quad (\text{Adj } R^2 = 0.944).$$

In addition, the following linear relationship between global cost and investment cost was found:

$$C_G = 0.762 \cdot C_I + 445 \quad (R^2 = 0.999).$$

With regard to the PCM properties (Fig. B.50), a quite uniform peak melting temperature of 18.0 ℃ and a very high latent heat of fusion were selected for PCM1. Medium-low values were chosen for the melting temperature range, whereas no clear trend was observed for the thermal conductivity; however, the solutions with lowest LPD were mostly characterised by high values. No definite trend could be devised for the properties of PCM2 due to the limited amount of solutions. However, they shared an almost constant peak melting temperature of about 34.0 ℃. Moreover, a high latent heat of fusion and thermal conductivity were selected for the solutions which guaranteed the best thermal comfort.

Eventually, the extreme solutions of the Pareto front are reported in Fig. C.14. Solution A (minimum primary energy consumption) was characterised by window type 10 (95%Kr filled TGU with low-emissivity coating on faces 3 and 5), a U-value of 0.15 W/(m²K), aerogel insulation, and 4.0 cm of PCM1 with a melting temperature of 19.0 ℃, melting temperature range of 4.7 ℃, 230 kJ/kg of latent heat of fusion and a thermal conductivity of 0.60 W/(m K).

Solution B (minimum global cost) was characterised by window type 9 (not the cheapest option, but the cost difference was negligible with respect to window type 7 and its U-value was lower), a U-value of 0.19 W/(m²K), EPS insulation (i.e. the cheapest one) and no PCM.

Solution C (minimum Long-term Percentage of Dissatisfied) was characterised by window type 7, a U-value of 0.21 W/(m²K) (i.e. almost the upper bound), EPS insulation and both PCMs (4 cm of PCM1 and 2.5 cm of PCM2), which were characterised by a high latent heat of fusion and thermal conductivity. The melting temperature range of PCM1 was also extremely narrow.

Different wall solution for each orientation (NF4)

In the case of retrofit intervention on the external side of the wall and different retrofit solution for each façade, the innovization analyses highlighted mainly the use of PCM1 or no PCM for all the façades except east, where several solutions presented both PCMs when simultaneously minimising primary energy consumption and thermal discomfort. The majority of the solutions on all the façades were characterised by wall types *ext1000* (insulation-PCM1-existing wall) and *ext0000*. In addition, wall type *ext3000* (PCM2-insulation-PCM1-existing wall) was mostly selected for the solutions with both PCMs on the east-facing wall.

As for the NF1 case, the Pareto front was strongly clustered by the insulation

type. The same comments on the effects of insulation material and window type can be applied.

No clear trends could be observed for the U-value. The lowest U-values generally corresponded to the lowest primary energy consumption whereas the highest U-values corresponded to the greatest thermal comfort as well as to the highest E_P.

With regard to the thickness of PCM1, high values tended to be selected in all the orientations except west to reduce LPD. No trends could instead be devised for the thickness of PCM2. The relationship between the overall thickness of PCM1, LPD and E_P can be described by the following equation:

$$\sum t_{1,j} = 1.3 - 14 \; LPD - 0.0027 \; E_P \quad (\text{Adj R}^2 = 0.930).$$

Moreover, the following relationship between overall thickness of PCM1, global cost and LPD was identified:

$$\sum t_{1,j} = 0.32 - 11 LPD + 0.00011 C_G \quad (\text{Adj R}^2 = 0.944).$$

In addition, the following linear relationship between global cost and investment cost was found:

$$C_G = 0.763 \cdot C_I + 456 \quad (\text{R}^2 = 0.999).$$

With regard to the PCM properties, a peak melting temperature of 18.0 ℃ and a very high latent heat of fusion were selected for PCM1 as for the NF1 case. However, the peak melting temperature presented a wider spread. No clear trends could be devised for the melting temperature range. Values around 4.0 ℃ seemed to be mostly selected in each cluster for PCM1 when reducing LPD, whereas mostly high values seemed to be preferred for PCM2 when simultaneously reducing LPD and E_P. No trend was observed for the thermal conductivity.

Eventually, the extreme solutions of the Pareto front are described. Solution A (minimum primary energy consumption) was very similar to that of the NF1 case. The U-value ranged between 0.15 W/(m^{2}K) for the north facing wall to 0.17 W/(m^{2}K) for the east facing one. A layer of PCM1 (wall type *ext1000*) was placed for all the expositions except north (wall type *ext0000*). The PCM properties were extremely similar to those of the NF1 case except for the thermal conductivity.

Solution B (minimum global cost) was identical to that of the NF1 case except for the selection of walls with a U-value of 0.21 W/(m^{2}K) towards north and west.

Unlikely the NF1 case, also solution C (minimum Long-term Percentage of Dissatisfied) was characterised by wall type *ext1000*. Similarly, window type 7, a U-value between 0.16 W/(m^{2}K) and 0.22 W/(m^{2}K) and EPS insulation were selected. Probably due to the lack of PCM2, the thermal properties of PCM1 were quite different.

5.3.3.5.2   Retrofit on the internal side (RT1)

Same retrofit solution for all the walls (NF1)

In the case of retrofit intervention on the internal side of the wall and same retrofit solution on all the façades, the innovization analyses highlighted a prevalent use of PCM1. As for the RT0 case, solutions without PCM were located on the edge of the Pareto front with highest LPD and lowest cost. Wall type *int1100* (existing wall-insulation-PCM1) was selected by the GA for almost all the solutions with PCM and *int0000* when no PCM was adopted (Fig. B.51). The extra thickness applied to the walls ranged between 15 cm and 33 cm.

The Pareto front was clustered by PCM use and window type. In particular, solutions with both PCMs were clearly divided by the rest of the front due to their higher global cost. These solutions belonged the non-dominated set between E_P and LPD. With regard to the window type, as in the RT0 case, window type 10 (TGU 95%Kr low-e(3,5)) was chosen for the solutions with the lowest primary energy consumption, window type 9 (TGU 90%Ar low-e(3,5)) for medium energy performance and thermal comfort, and window type 7 (TGU 90%Ar low-e(3,5)) for the worst energy performance but the best thermal comfort.

The preferred insulation material was EPS. Clay plaster or mineralised wooden board were mainly selected as internal lining materials. Thermo-plaster was selected only for the solution with the lowest primary energy consumption (solution A). Most of the solutions had a low U-value. The solutions with the highest U-values were characterised by window type 7 and were associated to a high energy consumption. A decreasing trend could be detected within each cluster formed by the window type to obtain lower E_P values. The following relationships were identified:

$$\text{Uvalue} = -1.81 - 5.8 \; LPD + 0.0081 \; E_P \quad (\text{Adj R}^2 = 0.992),$$

for the solutions characterised by window type 7, and

$$\text{Uvalue} = -1.5 - 7.1 \; LPD + 0.0072 \; E_P \quad (\text{Adj R}^2 = 0.930),$$

for the solutions characterised by window type 9.

A clear trend for the thickness of PCM1 was identified. High thicknesses were selected when simultaneously decreasing primary energy consumption and LPD. The few solutions with also PCM2 were characterised by medium to high thicknesses, especially for the solutions with low LPD (including solution C). The relationship between PCM1 thickness, LPD and E_P can be described by the following equation:

$$t_1 = 0.65 - 8.9 \; LPD - 0.0012 \; E_P \quad (\text{Adj R}^2 = 0.921).$$

Moreover, the following relationship between thickness of PCM1 and global cost was identified:

$$C_G = 556 + 2230\,t_1 \quad (\text{Adj R}^2 = 0.976).$$

In addition, the following linear relationship between global cost and investment cost was found:

$$C_G = 0.740 \cdot C_I + 426 \quad (\text{R}^2 = 0.985).$$

With regard to the PCM properties (Fig. B.52), all the solutions shared a uniform peak melting temperature of PCM1 of about 19.5 ℃, a very high latent heat of fusion and a narrow melting temperature range. No clear trend was identified for the thermal conductivity. The peak melting temperature of PCM2 was about 25.0 ℃, but no other trend could be devised due to the limited amount of solutions.

Eventually, the extreme solutions of the Pareto front are reported in Fig. C.16. Solution A (minimum primary energy consumption) was characterised by window type 10 (95%Kr filled TGU with low-emissivity coating on faces 3 and 5), a U-value of 0.15 W/(m^{2}K), EPS insulation, thermo-plaster, and 4.0 cm of PCM1 with a melting temperature of 18.0 ℃, melting temperature range of 1.5 ℃, 230 kJ/kg of latent heat of fusion, and a thermal conductivity of 0.20 W/(m K).

Solution B (minimum global cost) was characterised by window type 9 (not the cheapest option, but the cost difference was negligible with respect to window type 7 and its U-value was lower), a U-value of 0.15 W/(m^{2}K) (as it occurred also for Palermo and Torino in the two-objective analyses), EPS insulation, lime and gypsum plaster (i.e. the cheapest material options) and no PCM.

Solution C (minimum Long-term Percentage of Dissatisfied) was characterised by window type 7, a U-value of 0.17 W/(m^{2}K), cork insulation, lime and gypsum plaster and 4 cm of both PCMs (PCM1 was placed closer to the internal environment), which were characterised by a medium latent heat of fusion (160 kJ/kg and 180 kJ/kg respectively for PCM1 and PCM2). Considering the general trend for the latent heat, it is possible that a solution characterised by a higher latent heat of fusion of PCM1 would have resulted in a lower LPD.

Different wall solution for each orientation (NF4)

In the case of retrofit intervention on the internal side of the wall and different retrofit solution for each façade, the innovization analyses highlighted mainly the adoption of no PCM for all the façades except south, where PCM1 was most often selected. Both PCMs were used in the solutions with low LPD. The majority of solutions on all the façades were characterised by wall types *int1100* (existing wall-insulation-PCM1) and *int0000*. The extra thickness applied to the walls ranged approximately between 13 cm and 35 cm; the highest and lowest thicknesses were respectively selected for the north and west walls.

The Pareto front was clustered by window type. The same comments on window type reported for the NF1 case can be applied.

The preferred insulation material was EPS. Clay plaster and, to a lesser extent, lime and gypsum plaster, were selected as internal lining materials. Unlikely the NF1 case, thermo-plaster was never chosen. Most of the solutions had a low U-value, especially towards south. The solutions with highest U-value were associated to a high energy consumption. No definite trend was however identified.

With regard to the thickness of PCM1, high values tended to be selected especially towards south and north to reduce LPD. No trends could instead be devised for the thickness of PCM2. The following relationship between overall PCM thickness and global cost was identified:

$$C_G = 552 + 670 \sum t_{1,j} \quad (\text{Adj R}^2 = 0.948).$$

In addition, the following linear relationship between global cost and investment cost was found:

$$C_G = 0.78 \cdot C_I + 421 \quad (\text{R}^2 = 0.981).$$

With regard to the PCM properties, a uniform peak melting temperature of 19.5 ℃ and a very high latent heat of fusion were selected for PCM1 as for the NF1 case. However, the peak melting temperature presented a lower spread. Low values were generally preferred for the melting temperature range of PCM1 and medium values for that of PCM2 when minimising LPD. Mostly high values were selected for the thermal conductivity of PCM1 and low values for that of PCM2.

Eventually, the extreme solutions of the Pareto front are described. Solution A (minimum primary energy consumption) was very similar to that of the NF1 case. The U-value was equal to 0.15 W/(m²K) except for the north facing wall (0.17 W/(m²K)), and clay plaster was selected. A layer of PCM1 was placed in all the expositions, although towards east it was placed between the existing wall and the insulation layer. The PCM properties were very similar to those of the NF1 case, but a higher thermal conductivity was selected.

Solution B (minimum global cost) was identical to that of the NF1 case except for the selection of walls with a U-value of 0.16 W/(m²K) and 0.18 W/(m²K) towards north.

Solution C (minimum Long-term Percentage of Dissatisfied) was characterised by wall type *int3010* except towards east, were the same wall type of the NF1 case was chosen. The U-value ranged between 0.18 W/(m²K) and 0.21 W/(m²K), and rock wool insulation was selected. The thermal properties of PCM1 were extremely similar to those of the NF1 case, whereas the peak melting temperature of PCM2 was significantly higher.

5.3.3.5.3   Retrofit on both sides (RT2)

Same retrofit solution for all the walls (NF1)

In the case of retrofit intervention on both sides of the wall and same retrofit so-
lution on all the façades, the innovization analyses highlighted a prevalent use of
PCM1 although, unlikely the previous cases, more solutions presented only PCM2
rather than no PCM. When only PCM1 was chosen, the preferred wall type was
ie101000 (insulation-existing wall-PCM1), whereas *ie201000* (insulation-existing
wall-PCM2) was mostly selected when PCM2 was used (Fig. B.53).

The Pareto front was clustered by PCM use and window type (Fig. B.59). In
particular, few solutions with 4 cm PCM2 were clearly divided by the rest of the
front due to their higher global cost. These solutions belonged the non-dominated
set between E_P and LPD. With regard to the window type, a trend similar to the
RT0 and RT1 cases was identified. However, there was not a clear separation bet-
ween clusters as quite low E_P values were achieved also with window type 7 (TGU
90%Ar low-e(3,5)). Two solutions presented window type 8 (TGU 90%Ar low-e(2,5)),
which had not been previously selected.

The preferred insulation material was EPS, followed by rock wool and XPS
(Fig. B.59). Mineralised wooden boeard and clay plaster board were mainly selected
as internal lining materials. Thermo-plaster was selected only for one solution
among those with the lowest primary energy consumption. Low U-values were
mostly selected. Although high U-values were obviously associated to a high energy
consumption, no clear trend could be identified.

The Pareto front was characterised by an increasing PCM1 thickness in order
to decrease LPD (hence increasing the global cost). Low thicknesses were instead
mostly selected for PCM2 (Fig. B.59).

With regard to the PCM1 properties (Fig. B.54), all the solutions except a few
shared an almost constant peak melting temperature of about 19.5 ℃, medium/low
melting temperature range and high latent heat of fusion. No clear trend could be
observed for the thermal conductivity. With regard to the PCM2 properties, no
clear trend could be identified.

The only relationship that could be found was between global cost and invest-
ment cost;

$$C_G = 0.76 \cdot C_I + 448 \quad (\text{R}^2 = 0.958).$$

Eventually, the extreme solutions of the Pareto front are reported in Fig. C.18.
Solution A (minimum primary energy consumption) was characterised by window
type 10 (95%Kr filled TGU with low-emissivity coating on faces 3 and 5), a U-value
of 0.15 W/(m^{2}K), rock wool insulation, mineralised wooden board, 4.0 cm of PCM1
on the inner side of the wall and 5 mm of PCM2 on the outer side of the wall. It
could be inferred that PCM2 was selected only because an outer layer was imposed
by the parametric model. PCM1 and PCM2 were respectively characterised by a

melting temperature of 18.5 ℃ and 26.5 ℃, quite low melting temperature ranges, low thermal conductivities and a medium/low latent heat of fusion. Considering the general trend for the latent heat, it is probable that solutions characterised by higher latent heat of fusions would have resulted in a lower E_P.

Solution B (minimum global cost) was characterised by window type 9 (not the cheapest option, but the cost difference was negligible with respect to window type 7 and its U-value was lower), a U-value of 0.15 W/(m^{2}K), EPS insulation, lime and gypsum plaster (i.e. the cheapest material options) and 0.5 cm of PCM1 on the outer side of the wall. It could be inferred that the PCM was selected only because an outer layer was imposed by the parametric model.

Solution C (minimum Long-term Percentage of Dissatisfied) was characterised by window type 7, a U-value of 0.16 W/(m^{2}K), external EPS insulation in order to provide shading during the summer months, clay plaster and 3 cm of PCM1 on the inner side of the wall, which was characterised by a melting temperature of 19.0 ℃, melting temperature range of 1.5 ℃, 230 kJ/kg of latent heat of fusion, and a thermal conductivity of 0.40 W/(m K). Considering the general trend for the PCM thickness, it is probable that solutions characterised by higher thickness of PCM1 would have resulted in a lower LPD.

Different wall solution for each orientation (NF4)

In the case of retrofit intervention on both sides of the wall and different retrofit solution for each façade, the innovization analyses highlighted mainly the adoption of no PCM towards south and west, and mostly PCM1 towards north and east. Both PCMs were mostly applied in the north façade to the solutions with lowest LPD. The majority of solutions with PCM1 on all the façades were characterised by wall type *ie101000* (insulation-existing wall-PCM1) except towards north, where wall type *ie111100* (insulation-existing wall-insulation-PCM1) was more often selected.

The Pareto front was clustered by insulation material and window type. Similarly to the RT0 case, there was a cluster formed by a small group of solutions with the lowest primary energy consumption but highest global cost, where only aerogel was selected, and a second cluster which grouped all the other insulation materials. Among them, EPS was the preferred insulation material. With regard to the window type, a trend similar to the previous cases was identified. However, as for the NF1 case, there was not a clear separation between clusters.

Mineralised wooden board was mostly selected as internal lining material. A few solutions with thermo-plaster were characterised by the minimum primary energy consumption and corresponded mainly to those with aerogel insulation.

No clear trends could be observed for the U-value. The lowest U-values generally corresponded to the lowest primary energy consumption, whereas the highest U-values corresponded to the greatest thermal comfort as well as to the highest E_P. Low values were generally preferred for the south façade and medium values for the east façade.

With regard to the thickness of PCM1, high values tended to be selected especially towards north and east to reduce LPD. No trends could instead be devised for the thickness of PCM2. Low values were mostly selected towards south.

With regard to the PCM1 properties, all the solutions except a few (those with highest LPD and lowest cost) shared an almost constant peak melting temperature of about 19.0 ℃, medium/low melting temperature range and high latent heat of fusion. No clear trend could be observed for the thermal conductivity. With regard to the PCM2 properties, no clear trend could be identified.

The only relationship that could be found was between global cost and investment cost;

$$C_G = 0.773 \cdot C_I + 445 \quad (\text{R}^2 = 0.993).$$

Eventually, the extreme solutions of the Pareto front are described. Solution A (minimum primary energy consumption) was characterised by window type 10 (95%Kr filled TGU with low-emissivity coating on faces 3 and 5), a U-value ranging from 0.15 W/(m^{2}K) (north) to 0.18 W/(m^{2}K) (east), aerogel insulation, thermo-plaster and a high thickness of PCM1 on the inner side of all the walls except towards south, where it was placed on the outer side. The insulation was placed on the inner and outer side respectively towards south and east, whereas it was placed on both sides towards north and west. PCM1 was characterised by a melting temperature of 19.0 ℃, melting temperature range of 4.5 ℃, 220 kJ/kg of latent heat of fusion, and a thermal conductivity of 0.30 W/(m K).

Solution B (minimum global cost) was characterised by window type 10, a U-value of 0.16 W/(m^{2}K) except towards east (0.22 W/(m^{2}K)), XPS insulation and clay plaster. Insulation was placed on both sides of the wall towards east and west, whereas internal insulation and an external PCM layer was chosen for the other façades. However, due to the low thickness of the PCM (5 mm), it could be inferred that it was selected only because an outer layer was imposed by the parametric model.

Solution C (minimum Long-term Percentage of Dissatisfied) was characterised by window type 7, a U-value of 0.22 W/(m^{2}K) except towards south (0.15 W/(m^{2}K)), external wood-fiber board insulation, lime and gypsum plaster and 3 cm to 4 cm of PCM1 on the inner side of the wall except towards west, where PCM2 was selected (2 cm). PCM1 was characterised by a melting temperature of 19.0 ℃, melting temperature range of 1.5 ℃, 230 kJ/kg of latent heat of fusion, and a thermal conductivity of 0.40 W/(m K). Considering that PCM2, placed on the inner side, was characterised by a melting temperature of 30.0 ℃ and a latent heat of fusion of 90 kJ/kg, it can be inferred that it does not work as a phase change material.

5.3.3.6   Oslo, post-1955

Oslo's case studies aimed at minimising primary energy consumption, Long-term Percentage of Dissatisfied and global cost.

A first glance at the solutions was obtained by analysing Fig. A.6, where the box plots of all the retrofit options are summarised. The corresponding frequency analyses are reported from Fig. A.42 to Fig. A.48.

Similarly to the pre-1955 case, the Pareto fronts were clustered by window type. Window 8, which was characterised by the highest U-value among the options available in Oslo, was never selected.

Compared to the pre-1955 case, lower U-values tended to be selected for the RT0 and RT2 cases. Similar preferences over insulation and internal lining materials were observed.

With regard to the PCM selection, PCM1 was clearly preferred over PCM2, although a few more solutions than the pre-1955 cases were characterised by both PCMs. The solutions with PCM2 tended to have higher thickness except in the RT2 cases, whereas for PCM1 both the box plot representations and the frequency analyses fail at providing significant information that can be retrieved by analysing the variables' maps on the Pareto fronts.

The most evident piece of information that can be devised from the box plots is a very narrow peak melting temperature of PCM1, with median values of 16 ℃ and 17.5 ℃ for the RT0 cases. As in the pre-1955 building, peak melting temperatures of 19.5 ℃ were selected for all the other cases except RT2 – NF4 where 19.0 ℃ was mostly chosen.

A high latent heat of fusion was always selected for PCM1. Medium melting temperature ranges were mostly chosen for the RT0 cases and low values for RT1 and RT2. No clear trend could be identified for the thermal conductivity as well as for the thermo-physical properties of PCM2.

It is worth noting that in the RT1 – NF1 case, all the solutions shared almost constant properties of both PCMs except for the thermal conductivity. However, the amount of solutions with PCM2 was not significant.

In the detailed comments to each retrofit option, more information on the values assumed by the discrete and continuous variables will be also provided, together with specific trends along the non-dominated set. The extreme solutions of the Pareto front were additionally reported, where solution A was the best performing individual with respect to the primary energy consumption, solution B was the individual with lowest global cost, and solution C was characterised by the lowest Long-term Percentage of Dissatisfied.

5.3.3.6.1   Retrofit on the external side (RT0)

Same retrofit solution for all the walls (NF1)

In the case of retrofit intervention on the external side of the wall and different retrofit solution for each façade, the innovization analyses highlighted a prevalent use of PCM1. Solutions without PCM were located on the edge of the Pareto front with highest LPD and lowest cost, whereas solutions with both PCMs were placed on the egde which minimised thermal discomfort. Wall type *ext1000* (insulation-PCM1-existing wall) was selected by the GA for the solutions with PCM1 and *ext0000* when no PCM was adopted (Fig. B.55).

As for the pre-1955 case, the Pareto front was strongly clustered by the insulation type (Fig. B.55). Two main clusters were present; one was the group of solutions with the lowest primary energy consumption but highest global cost, where only aerogel was selected, and the other cluster which grouped all the other insulation materials. Very low U-values were selected for all the solutions except for those simultaneously characterised by the worst energy performance and thermal comfort.

Window type had an additional subclustering effect on the Pareto front within each cluster (Fig. B.55). Window type 10 (TGU 95%Kr low-e(3,5)) was chosen for the solutions with the lowest primary energy consumption. Window type 9 (TGU 90%Ar low-e(3,5)) was selected for medium energy performance and thermal comfort, whereas window type 7 (TGU 90%Ar low-e(3,5))) characterised the solutions with the worst energy performance but which guaranteed the best thermal comfort.

As for the pre-1955 case, thermal discomfort was found to decrease for high thicknesses of PCM1 (Fig. B.55). However, if the Pareto fronts between pre-1955 and post-1955 cases are compared (Fig. 5.71), it is evident that the effect of PCM in improving thermal comfort when placed on the outer side of the wall is much more limited than in the pre-1955 building.

With regard to the PCM properties (Fig. B.56), a quite uniform peak melting temperature of 16.0 ℃ and a very high latent heat of fusion were selected for PCM1. Medium values were chosen for the melting temperature range, whereas no clear trend was observed for the thermal conductivity. No definite trend could be devised for the properties of PCM2 due to the limited amount of solutions.

The only relationship that could be identified was between global cost and investment cost;

$$C_G = 0.771 \cdot C_I + 435 \quad (\text{R}^2 = 0.998).$$

Eventually, the extreme solutions of the Pareto front are reported in Fig. C.15. They were all characterised by the same retrofit intervention as in the pre-1955 case. Solution A (minimum primary energy consumption) was characterised by window type 10, a U-value of 0.15 W/(m^{2}K), aerogel insulation and 4.0 cm of PCM1. A lower melting temperature (17.5 ℃), melting temperature range and thermal conductivity

of PCM1 were observed compared to the pre-1955 case.

Solution B (minimum global cost) was characterised by window type 9 (not the cheapest option, but the cost difference was negligible with respect to window type 7 and its U-value was lower), a U-value of 0.19 W/(m^{2}K), EPS insulation and no PCM.

Solution C (minimum Long-term Percentage of Dissatisfied) was characterised by window type 7, a U-value of 0.15 W/(m^{2}K), EPS insulation and 4 cm of both PCMs, which were characterised by a high latent heat of fusion and low thermal conductivity.

Different wall solution for each orientation (NF4)

In the case of retrofit intervention on the external side of the wall and different retrofit solution for each façade, the innovization analyses highlighted a prevalent use of no PCM or PCM1. Solutions without PCM were located on the edge of the Pareto front with highest LPD and lowest cost, whereas solutions with both PCMs were placed on the egde which minimised thermal discomfort. However, the difference in terms of LPD was negligible. Wall type *ext1000* (insulation-PCM1-existing wall) was mostly selected by the GA for the solutions with PCM1, wall type *ext3000* (PCM2-insulation-PCM1-existing wall) when both PCMs were used and *ext0000* when no PCM was adopted.

As for the NF1 case, the Pareto front was strongly clustered by the insulation type. Two main clusters were present; one was the group of solutions with the lowest primary energy consumption but highest global cost, where only aerogel was selected, and the other cluster which grouped all the other insulation materials. Low U-values tended to be selected for all the solutions, especially towards south and north.

Window type had an additional subclustering effect on the Pareto front within each cluster. The same comments on window type reported for the NF1 case can be applied.

With regard to the thickness of PCM1, high values tended to be selected especially towards south. No trends could instead be devised for the thickness of PCM2.

With regard to the PCM properties, an average peak melting temperature of 17.5 ℃ and a very high latent heat of fusion were selected for PCM1. However, the peak melting temperature was characterised by a wider spread compared to the other cases. Medium values were mostly chosen for the melting temperature range, whereas no clear trend was observed for the thermal conductivity. No definite trend could be devised for the properties of PCM2 due to the limited amount of solutions.

The only relationship that could be identified was between global cost and investment cost;

$$C_G = 0.770 \cdot C_I + 435 \quad (\text{R}^2 = 0.996).$$

Eventually, the extreme solutions of the Pareto front are described. Unlikely the NF1 case, solution A (minimum primary energy consumption) was characterised by the absence of PCM except towards north, where 1 cm of PCM, characterised by a peak melting temperature of 27.0 ℃, a wide melting temperature range of 7.0 ℃, a latent heat of fusion of 150 kJ/kg and a thermal conductivity of 0.75 W/(m K) was used. A U-value of 0.15 W/(m²K) was selected for all the façades except towards west (0.17 W/(m²K)).

Solution B (minimum global cost) was almost identical to that of the RT1 case, except for the U-values which ranged between 0.18 W/(m²K) and 0.20 W/(m²K).

Solution C (minimum Long-term Percentage of Dissatisfied) was characterised by a similar wall to the NF1 case only for the west façade. Both PCMs were selected also for the south and north walls, by they were placed between the external insulation and the existing wall, whereas only PCM1 was selected for the east façade. A U-value of 0.16 W/(m²K) was selected for all the façades except towards north (0.20 W/(m²K)). The thermo-physical properties of both PCMs were similar to those of the NF1 case, except for a low latent heat of fusion of PCM2.

5.3.3.6.2   Retrofit on the internal side (RT1)

Same retrofit solution for all the walls (NF1)

In the case of retrofit intervention on the internal side of the wall and same retrofit solution on all the façades, the innovization analyses highlighted a prevalent use of PCM1. As for the RT0 case, solutions without PCM were located on the edge of the Pareto front with highest LPD and lowest cost. Wall type *int1100* (existing wall-insulation-PCM1) was selected by the GA for all the solutions with PCM, *int0000* when no PCM was adopted, and *int3111* (existing wall-insulation-PCM2-PCM1) when both PCMs were chosen (Fig. B.57). The extra thickness applied to the walls ranged between 9 cm and 26 cm.

The Pareto front was clustered by PCM use and window type (Fig. B.57). In particular, solutions with both PCMs were clearly divided by the rest of the front due to their higher global cost. These solutions belonged the non-dominated set between E_P and LPD. With regard to the window type, as in the RT0 case, window type 10 (TGU 95%Kr low-e(3,5)) was chosen for the solutions with the lowest primary energy consumption, window type 9 (TGU 90%Ar low-e(3,5)) for medium energy performance and thermal comfort, and window type 7 (TGU 90%Ar low-e(3,5)) for the worst energy performance but the best thermal comfort.

The preferred insulation material was EPS (Fig. B.57). Clay plaster or lime and gypsum plaster were mainly selected as internal lining materials. Most of the solutions had a low U-value. The solutions with highest U-value were characterised by window type 7 and were associated to a high energy consumption. A decreasing trend could be identified within each cluster formed by the window type to obtain

lower E_P values. The following relationships were identified:

$$\text{Uvalue} = -1.57 - 8.0\ LPD + 0.0078\ E_P \quad (\text{Adj R}^2 = 0.984),$$

for the solutions characterised by window type 7, and

$$\text{Uvalue} = -1.51 - 9.3\ LPD + 0.0078\ E_P \quad (\text{Adj R}^2 = 0.957),$$

for the solutions characterised by window type 9.

A clear trend for the thickness of PCM1 was identified (Fig. B.57); a positive effect of PCM was found both on primary energy consumption and thermal comfort. The relationship between PCM1 thickness, LPD, E_P and C_G can be described by the following equation:

$$t_1 = 0.18 - 3.6\ LPD - 0.00070\ E_P + 0.00026\ C_G \quad (\text{Adj R}^2 = 0.981).$$

The few solutions with also PCM2 were mostly characterised by high thicknesses.

In addition, the following linear relationship between global cost and investment cost was found:

$$C_G = 0.740 \cdot C_I + 426 \quad (\text{R}^2 = 0.985).$$

With regard to the PCM properties (Fig. B.58), as for the pre-1955 case all the solutions shared a uniform peak melting temperature of PCM1 of about 19.5 ℃, a very high latent heat of fusion and a narrow melting temperature range. No clear trend was identified for the thermal conductivity. The peak melting temperature of PCM2 was about 27.5 ℃ and a high latent heat of fusion was selected.

Eventually, the extreme solutions of the Pareto front are reported in Fig. C.17. Solution A (minimum primary energy consumption) was characterised by window type 10 (95%Kr filled TGU with low-emissivity coating on faces 3 and 5), a U-value of 0.15 W/(m^{2}K), EPS insulation, lime and gypsum plaster and, unlikely the pre-1955 case, by 4.0 cm of both PCMs (where PCM1 was placed closer to the internal environment). The melting temperature of PCM1 and PCM2 was respectively of 19.0 ℃ and 25.5 ℃ and they were both characterised by a latent heat of fusion of 230 kJ/kg. A higher thermal conductivity was selected for PCM1.

Solution B (minimum global cost) was characterised by the same retrofit intervention as in the pre-1955 case (i.e. window type 9, a U-value of 0.15 W/(m^{2}K), EPS insulation, lime and gypsum plaster and no PCM).

Solution C (minimum Long-term Percentage of Dissatisfied) was similar to that of the pre-1955 case. The same wall type of solution A was selected. Solution C was characterised by window type 7, a U-value of 0.22 W/(m^{2}K) (i.e. the upper bound), EPS insulation, lime and gypsum plaster and 4 cm of PCM1 and 3.5 cm of PCM2 (PCM1 was placed closer to the internal environment). The melting temperature of PCM1 and PCM2 was respectively of 19.0 ℃ and 30.0 ℃ (which is significantly higher than in the pre-1955 case) and they were both characterised by a high latent

heat of fusion. A higher thermal conductivity was selected for PCM1.

Different wall solution for each orientation (NF4)

In the case of retrofit intervention on the internal side of the wall and different retrofit solution for each façade, the innovization analyses highlighted a prevalent use of no PCM or PCM1. Solutions without PCM were generally characterised by high LPD and low global cost. Wall type *int1100* (existing wall-insulation-PCM1) was selected by the GA for almost all the solutions with PCM1 and *int0000* when no PCM was adopted. The extra thickness applied to the walls ranged between 8 cm and 26 cm.

The Pareto front was clustered by window type and partly by PCM use. The same comments on window type reported for the NF1 case can be applied.

The preferred insulation material was EPS. Clay plaster was mainly selected as internal lining material. Most of the solutions had a low U-value. Solutions with high U-value in the east and north expositions tended to be associated to a high energy consumption.

With regard to the thickness of PCM1, high values tended to be selected to reduce LPD. No trends could instead be devised for the thickness of PCM2.

With regard to the PCM properties, similarly to the NF1 case most of the solutions shared an almost uniform peak melting temperature of PCM1 of about 19.5 ℃, a very high latent heat of fusion and a low melting temperature range. No clear trend was identified for the thermal conductivity.

The only significant relationships that could be identified were between overall PCM thickness and global cost,

$$C_G = 537 + 630 \sum t_{i,j} (\text{Adj R}^2 = 0.967),$$

and between global cost and investment cost,

$$C_G = 0.758 \cdot C_I + 414 \quad (\text{R}^2 = 0.986).$$

Eventually, the extreme solutions of the Pareto front are described. Solution A (minimum primary energy consumption) was characterised by a similar wall to the NF1 case only for the south and north façades. Towards east and west the PCM was placed between existing wall and internal insulation, and only PCM1 was used on the west façade. Similar thermo-physical properties were chosen for both PCMs, except a lower melting temperature range and latent heat of fusion of PCM2. A U-value of 0.15 W/(m²K) was selected for the south and east façades and 0.16 W/(m²K) for the other ones.

Solution B (minimum global cost) was almost identical to that of the RT1 case, except for the U-values which ranged between 0.15 W/(m²K) and 0.18 W/(m²K).

Solution C (minimum Long-term Percentage of Dissatisfied) was characterised

by a similar wall to the NF1 case only for the south façade. The position of the two PCMs was inverted in the north wall, whereas only PCM1 was selected towards east and west. The U-value ranged between 0.16 W/(m^{2}K) and 0.20 W/(m^{2}K). Similar thermo-physical properties were chosen for PCM1, whereas PCM2 was characterised by a peak melting temperature of 24.5 ℃ a melting temperature range of 3.0 ℃, a latent heat of fusion of only 80 kJ/kg and a thermal conductivity of 0.65 W/(m K).

5.3.3.6.3 Retrofit on both sides (RT2)

Same retrofit solution for all the walls (NF1)

In the case of retrofit intervention on both sides of the wall and same retrofit solution on all the façades, the innovization analyses highlighted a prevalent use of PCM1, although several solutions presented only PCM2 (located on the edge of the Pareto front with highest LPD and lowest cost) or both PCMs, and almost none had no PCM. When only PCM1 was chosen, the preferred wall type was *ie101000* (insulation-existing wall-PCM1). Wall types *ie200000* (PCM2-existing wall-insulation) and *ie201000* (insulation-existing wall-PCM2) were selected when PCM2 was used, whereas wall type *ie300011* (PCM2-existing wall-insulation-PCM1) was preferred when both PCMs were used (Fig. B.59).

The Pareto front was clustered by PCM use and window type (Fig. B.59). In particular, the window type varied within the PCM use clusters with a trend similar to the RT0 and RT1 cases; window type 10 (TGU 95%Kr low-e(3,5)) was chosen for the solutions with the lowest primary energy consumption within each cluster, window type 9 (TGU 90%Ar low-e(3,5)) for medium energy performance and thermal comfort, and window type 7 (TGU 90%Ar low-e(3,5)) for the worst energy performance but the best thermal comfort.

The preferred insulation material was EPS, followed by XPS and rock wool (Fig. B.59). Clay plaster was mainly selected as internal lining material. However, lime and gypsum plaster and mineralised wooden board were also broadly used in solutions respectively with low and high primary energy consumption. Low U-values were mostly selected. Although high U-values were obviously associated to a high energy consumption, no clear trend could be identified.

The Pareto front was characterised by an increasing PCM1 thickness in order to decrease LPD (hence increasing the global cost). Low thicknesses were instead mostly selected for PCM2 (Fig. B.59). The relationship between PCM1 thickness, *LPD* and E_P can be described by the following equation[3]:

$$t_1 = 0.64 - 9.5\ LPD - 0.00105\ E_P \quad (\text{Adj R}^2 = 0.955).$$

---

[3]The solutions with PCM2 were excluded.

In addition, the following linear relationship between global cost and investment cost was found:

$$C_G = 0.78 \cdot C_I + 423 \quad (\text{R}^2 = 0.976).$$

With regard to the PCM1 properties (Fig. B.60), all the solutions except a few shared an almost constant peak melting temperature of about 19.5 ℃, low melting temperature range and high latent heat of fusion. No clear trend could be observed for the thermal conductivity. With regard to the PCM2 properties, no clear trend could be identified.

Eventually, the extreme solutions of the Pareto front are reported in Fig. C.19. Solution A and B were similar to that of the pre-1955 case, whereas solution C was different. Solution A (minimum primary energy consumption) was characterised by window type 10 (95%Kr filled TGU with low-emissivity coating on faces 3 and 5), a U-value of 0.15 W/(m^{2}K), cork insulation, mineralised wooden board as internal lining material, 3.5 cm of PCM1 on the inner side of the wall and 5 mm of PCM2 on the outer side of the wall. It could be inferred that PCM2 was selected only because an outer layer was imposed by the parametric model. PCM1 was characterised by a melting temperature of 19.0 ℃, a narrow melting temperature range and a high latent heat of fusion.

Solution B (minimum global cost) was characterised almost by the same retrofit intervention as in the pre-1955 case. It differed in the internal lining material (clay plaster) and in the thermo-physical properties of PCM1, which was again selected only because an outer layer was imposed by the parametric model.

Solution C (minimum Long-term Percentage of Dissatisfied) was characterised by window type 7, a U-value of 0.22 W/(m^{2}K) (i.e. the upper bound), both external and internal cork insulation, lime and gypsum plaster and 4 cm of PCM1 on the inner side of the wall, which was characterised by a melting temperature of 19.0 ℃, melting temperature range of 2.5 ℃, 230 kJ/kg of latent heat of fusion, and a thermal conductivity of 0.20 W/(m K).

Different wall solution for each orientation (NF4)

In the case of retrofit intervention on both sides of the wall and different retrofit solution for each façade, the innovization analyses highlighted a prevalent use of PCM1 towards south and north and of no PCM towards east and west. Several solutions towards south presented both PCMs when minimising LPD. When only PCM1 was chosen, the preferred wall types were *ie100000* (PCM1-existing wall-insulation) towards south and *ie101000* (insulation-existing wall-PCM1) towards north.

The Pareto front was clustered by window type. The same comments on window type reported for the NF1 case can be applied.

As for the RT1 case, the preferred insulation material was EPS, followed by XPS and rock wool. Clay plaster and mineralised wooden board were mainly selected

as internal lining material. Low U-values were mostly selected for the south and north façades. Although high U-values were obviously associated to a high energy consumption, no clear trend could be identified.

With regard to the thickness of PCM1, high values tended to be selected to reduce LPD. Low thicknesses of PCM2 tended to be selected towards east and north.

With regard to the PCM1 properties, all the solutions except those with the lowest global cost shared an almost constant peak melting temperature of about 19.0 ℃, quite low melting temperature range and high latent heat of fusion. High thermal conductivity values were mostly selected in the clusters characterised by window types 7 and 9. With regard to the PCM2 properties, no clear trend could be identified.

The only relationship that could be found was between global cost and investment cost;

$$C_G = 0.76 \cdot C_I + 434 \quad (\text{R}^2 = 0.981).$$

Eventually, the extreme solutions of the Pareto front are described. They were significantly different from the NF1 case. Considering that the search space for the RT2–NF4 cases was the widest and comparing the performance of the extreme solutions for the NF1 and NF4 cases, it can be inferred that the GA was still far from finding the best solutions. Solution A (minimum primary energy consumption) was characterised by window type 10, sheep wool and clay plaster. The U-value was 0.15 W/(m^{2}K) for all the expositions except east (0.16 W/(m^{2}K)). Internal insulation and outer PCM were selected for all the walls except west, where the insulation was placed on both sides. The thickness of the PCMs was low; it could therefore be inferred that they were selected only because an outer layer was imposed by the parametric model.

Solution B (minimum global cost) was characterised by internal rock wool insulation layer and external very thin PCM layer in the south and east façades, external insulation and internal very thin PCM layer towards north, and insulation placed on both sides towards west. As for solution A, it can be inferred that the PCMs were selected only because an outer layer was imposed by the parametric model.

Solution C (minimum Long-term Percentage of Dissatisfied) was characterised by a wall configuration similar to that of the NF1 case only for the north façade. Insulation was however placed on both sides of all walls except towards south, where an outer position was selected. Only PCM1 was chosen towards east and north, whereas both PCMs were selected for the other expositions. However, the mutual position layers varied greatly. XPS and mineralised wooden board were respectively chosen as insulation and internal lining materials. The thermo-physical properties of PCM1 were nonetheless extremely similar to those of the NF1 case.

Chapter 6

Discussion

In this chapter, an overall discussion on the building-level results is provided. Additional analyses were especially performed to investigate the reason behind some of the choices—or lack of choices—of the optimisation algorithm.

First, the energy performance of the extreme solutions is detailed. Then, the temperature profiles within the building during representative weeks are plotted to provide a better understanding of the differences among solutions and on the effect of PCM. Subsequently, the identified innovization relationships are summarised and discussed. Since the effect of thermal conductivity and melting temperature range of the PCM could not be clearly determined in the previous analyses, the mutual influence of these variables and peak melting temperature was additionally investigated. Then, the selection of the objective functions is discussed, and some overall comments on the results of the component and building level analyses are provided. Eventually, a few design guidelines for the application of PCMs to the energy retrofit of office buildings are proposed.

6.1   Energy performance of the extreme solutions

The best-performing solutions (as they were found by the optimisation algorithm, i.e. even if sub-optimal) among all the cases of the building-level optimisation analyses with respect to each objective function is reported in Table. 6.1. The percentage reduction in energy need and primary energy consumption compared to the pre-retrofit building is additionally reported in Table 6.2. The solutions characterised by minimum heating energy need and investment cost in Oslo were added for completeness but do not necessarily correspond to any extreme solution.

In Palermo, the improvement in $Q_{H,nd}$ spanned from 41% to almost 74% among the reported solutions, whereas the energy need for cooling was reduced up to 31%

Table 6.1 Energy performance of the optimised solutions.

Solution	Case	$Q_{H,nd}$	$Q_{C,nd}$	Q_E	E_P	C_I	C_G	LPD
		$\left[\text{kWh}/(\text{m}^2\text{y})\right]$				$\left[\text{€}/\text{m}^2\right]$		[%]
Palermo								
Baseline		*7.75*	*32.94*	*38.15*	*137.19*	*-*	*-*	*-*
min E_P	RT1 (Sol. A, 2Obj)	2.90	23.89	33.27	103.59	373.06	582.45	-
min C_G	RT1 (Sol. B, 2Obj)	4.28	24.17	34.00	107.39	121.13	384.06	-
min $Q_{H,nd}$	RT2 (Sol. A, 3Obj)	2.04	27.04	35.55	110.52	736.97	897.55	-
min $Q_{C,nd}$	RT1 (Sol. B, 3Obj)	4.53	22.58	35.90	111.04	358.47	583.24	-
min C_I	RT1 (Sol. C, 3Obj)	4.48	25.98	35.43	112.56	116.79	389.77	-
Torino								
Baseline		*58.13*	*14.28*	*39.43*	*206.63*	*-*	*-*	*-*
min E_P	RT1 (Sol. A, 2Obj)	36.62	9.42	34.20	138.44	352.43	635.66	-
min C_G	RT1 (Sol. B, 2Obj)	38.78	10.06	34.14	141.63	152.39	476.41	-
min $Q_{H,nd}$	RT2 (Sol. A, 3Obj)	35.87	9.66	35.89	141.73	853.47	1053.54	-
min $Q_{C,nd}$	RT1 (Sol. B, 3Obj)	39.73	7.71	33.93	140.47	431.82	699.22	-
min C_I	RT1 (Sol. C, 3Obj)	41.40	8.76	35.95	148.41	149.35	485.36	-
Oslo, pre-1955								
Baseline		*226.63*	*-*	*40.04*	*410.67*	*-*	*-*	*3.62*
min E_P	RT1 (Sol. A)	128.13	-	38.33	256.36	322.88	659.17	3.60
min C_G	RT1 (Sol. B)	132.95	-	38.80	264.50	165.61	542.98	3.82
min LPD	RT2 (Sol. C)	142.89	-	40.97	283.15	341.21	719.18	3.28
min $Q_{H,nd}$	RT1 (Sol. A)	128.13	-	38.33	256.36	322.88	659.17	3.60
min C_I	RT1	139.19	-	39.79	275.64	164.59	558.40	3.70
Oslo, post-1955								
Baseline		*188.02*	*-*	*41.41*	*353.33*	*-*	*-*	*4.55*
min E_P	RT1 (Sol. A)	123.60	-	39.28	250.83	398.67	711.55	3.47
min C_G	RT1 (Sol. B)	127.53	-	40.10	258.15	160.41	528.87	3.93
min LPD	RT2 (Sol. C)	134.00	-	41.03	269.54	389.90	737.53	3.40
min $Q_{H,nd}$	RT1	123.09	-	39.83	250.90	305.94	636.85	3.61
min C_I	RT1	133.16	-	40.99	268.19	159.60	542.84	3.80

in the best case, and around 28% by the solution which ensured the lowest E_P. In absolute terms, a higher cooling energy reduction was however obtained. Although the greater electricity demand due to fan operation and the worse lighting performance of the retrofitted windows with external movable shading devices, the

Table 6.2 Variation of energy performance of the optimised solutions.

Solution	$\Delta Q_{H,nd}$	$\Delta Q_{C,nd}$	ΔQ_E	ΔE_P	ΔLPD
Palermo					
min E_P	-62.6%	-27.5%	-12.8%	-24.5%	-
min C_G	-44.8%	-26.6%	-10.9%	-21.7%	-
min $Q_{H,nd}$	-73.7%	-17.9%	-6.8%	-19.4%	-
min $Q_{C,nd}$	-41.5%	-31.4%	-5.9%	-19.1%	-
min C_I	-42.2%	-21.1%	-7.1%	-18.0%	-
Torino					
min E_P	-37.0%	-34.0%	-13.3%	-33.0%	-
min C_G	-33.3%	-29.5%	-13.4%	-31.5%	-
min $Q_{H,nd}$	-38.3%	-32.4%	-9.0%	-31.4%	-
min $Q_{C,nd}$	-31.7%	-46.0%	-14.0%	-32.0%	-
min C_I	-28.8%	-38.7%	-8.8%	-28.2%	-
Oslo, pre-1955					
min E_P	-43.5%	-	-4.3%	-37.6%	-0.5%
min C_G	-41.3%	-	-3.1%	-35.6%	+5.4%
min LPD	-36.9%	-	+2.3%	-31.1%	-9.4%
min $Q_{H,nd}$	-43.5%	-	-4.3%	-37.6%	-0.5%
min C_I	-38.6%	-	-0.6%	-32.9%	+2.2%
Oslo, post-1955					
min E_P	-34.3%	-	-5.1%	-29.0%	-23.7%
min C_G	-32.2%	-	-3.2%	-26.9%	-13.5%
min LPD	-28.7%	-	-0.9%	-23.7%	-25.1%
min $Q_{H,nd}$	-34.5%	-	-3.8%	-29.0%	-20.7%
min C_I	-29.2%	-	-1.0%	-24.1%	-16.5%

electricity demand was still overall reduced by the dimming lighting strategy. The major reduction was obtained by the solutions of the two-objective optimisation analyses. In the best case, the primary energy consumption was reduced up to almost 25%.

In Torino, both cooling and especially heating energy need could be significantly reduced. The solutions which ensured the lowest E_P had a similar energy performance to the solution which ensured the lowest heating energy need, but it was characterised by a significantly lower investment cost. In the best case, the primary energy consumption was reduced up to 33%.

In Oslo, the total heating energy need could be significantly reduced especially in the pre-1955 building, whose envelope performance was the poorest. The reduction in electricity demand was however very limited, and it even increased in the solution characterised by the lowest thermal discomfort in the pre-1955 case. It can be inferred that, due to the latitude of Oslo, the dimming lighting strategy was not as effective as in Palermo and Torino, and it hardly counterbalanced the increased electricity demand due to fan operation. The greatest electricity reduction was obtained by the solutions characterised by the lowest E_P which, in the pre-1955 case, corresponded to the solution characterised also by the lowest heating energy need.

With regard to the thermal comfort, in the pre-1955 case it was almost unvaried, and in the solution characterised by the lowest global cost it even worsened. In the post-1955 case, which was characterised by the best thermal performance but worst thermal comfort conditions before retrofit, thermal discomfort could be reduced to levels similar to the pre-1955 building. The worst performance in terms of comfort was again obtained for the solution characterised by the lowest global cost. Moreover, both in the pre-1955 and post-1955 case, the solutions which ensured the lowest LPD were also characterised by the highest global cost. This is in agreement with the findings in [289].

In general, the solutions characterised by the lowest investment cost were characterised only by a slightly higher global cost compared to the solutions with minimum C_G. However, their performance in terms of primary energy consumption was far lower, with a difference of up to 11 kWh/(m^{2}y) in Oslo for the pre-1955 building.

6.2   Temperature profiles of the extreme solutions

To provide a better understanding of the behaviour of the various solutions and of the reason behind the choices of the optimisation algorithm, the internal air temperature profiles of significant weeks for the extreme solutions of the of the various location are reported in Fig. 6.1, Fig. 6.2, Fig. 6.3 and Fig. 6.4 respectively for the cases of Palermo, Torino, Oslo pre-1955 and Oslo post-1955. Only the extreme solutions of the RT1 cases (i.e. retrofit intervention on the internal side of the wall) are reported.

In Palermo during winter (week A), a significant increase of the night temperatures (when the heating system is turned off) can be observed for all the retrofitted solutions. The highest temperature is reasonably found for solution A of the three-objective analyses, i.e. the solution characterised by the lowest $Q_{H,nd}$. In this way, the lowest amount of energy is needed to bring the indoor air temperature back to the set-point, and less energy is required to maintain it compared to the other solutions. The winter temperature profiles drop following the same ascending order
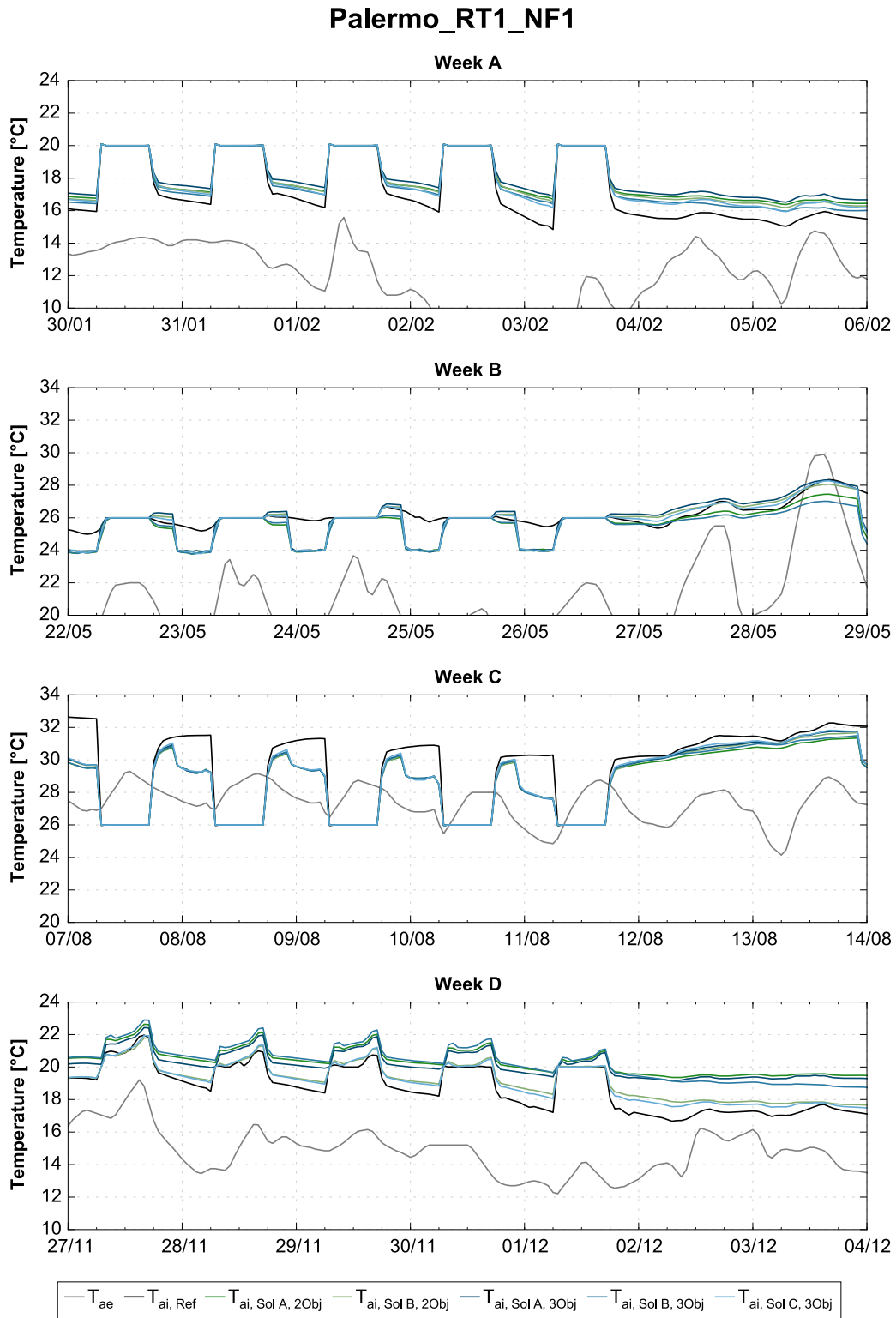
Fig. 6.1 Temperature profiles of the extreme solutions for significant weeks in Palermo.
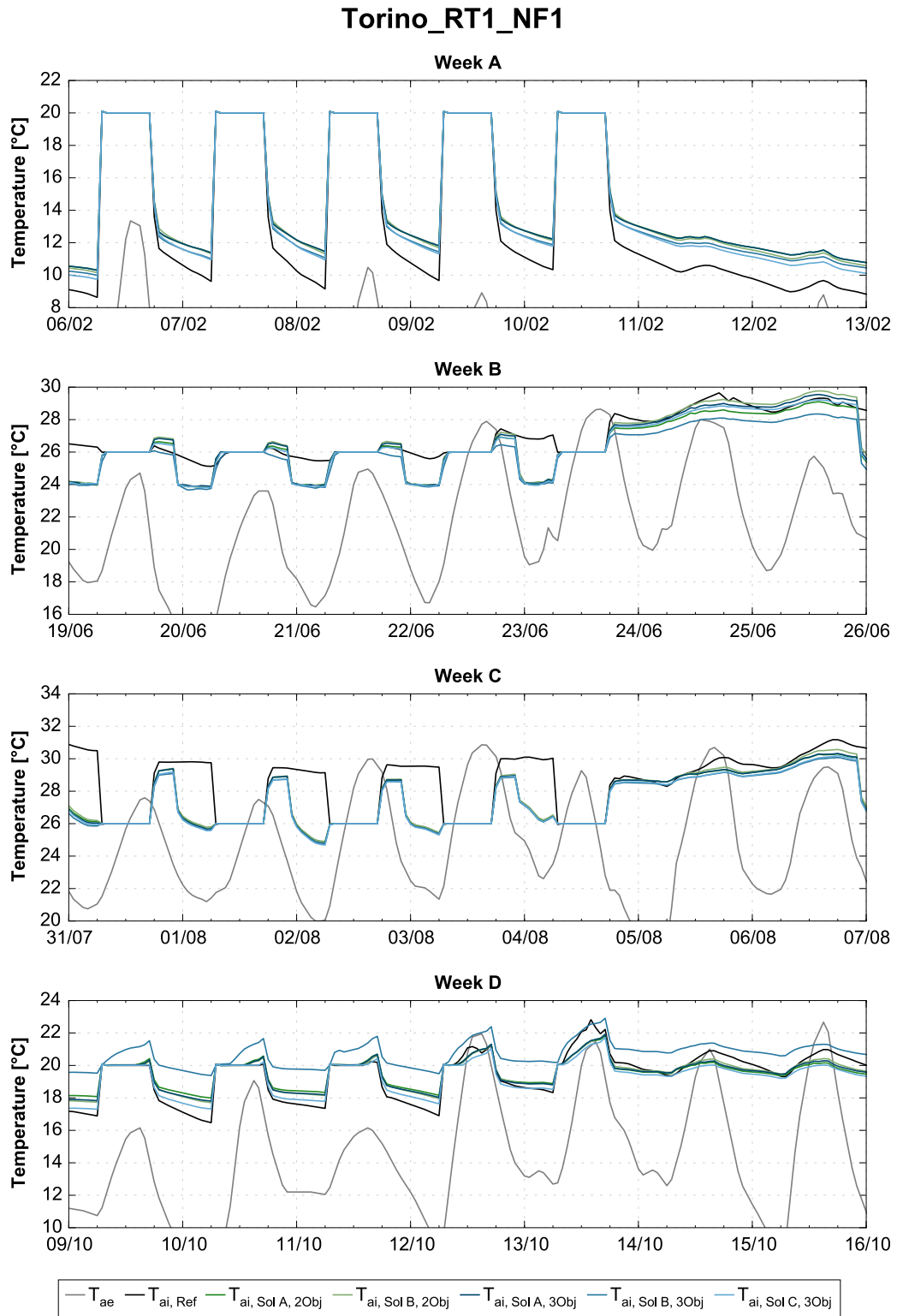
Fig. 6.2 Temperature profiles of the extreme solutions for significant weeks in Torino.
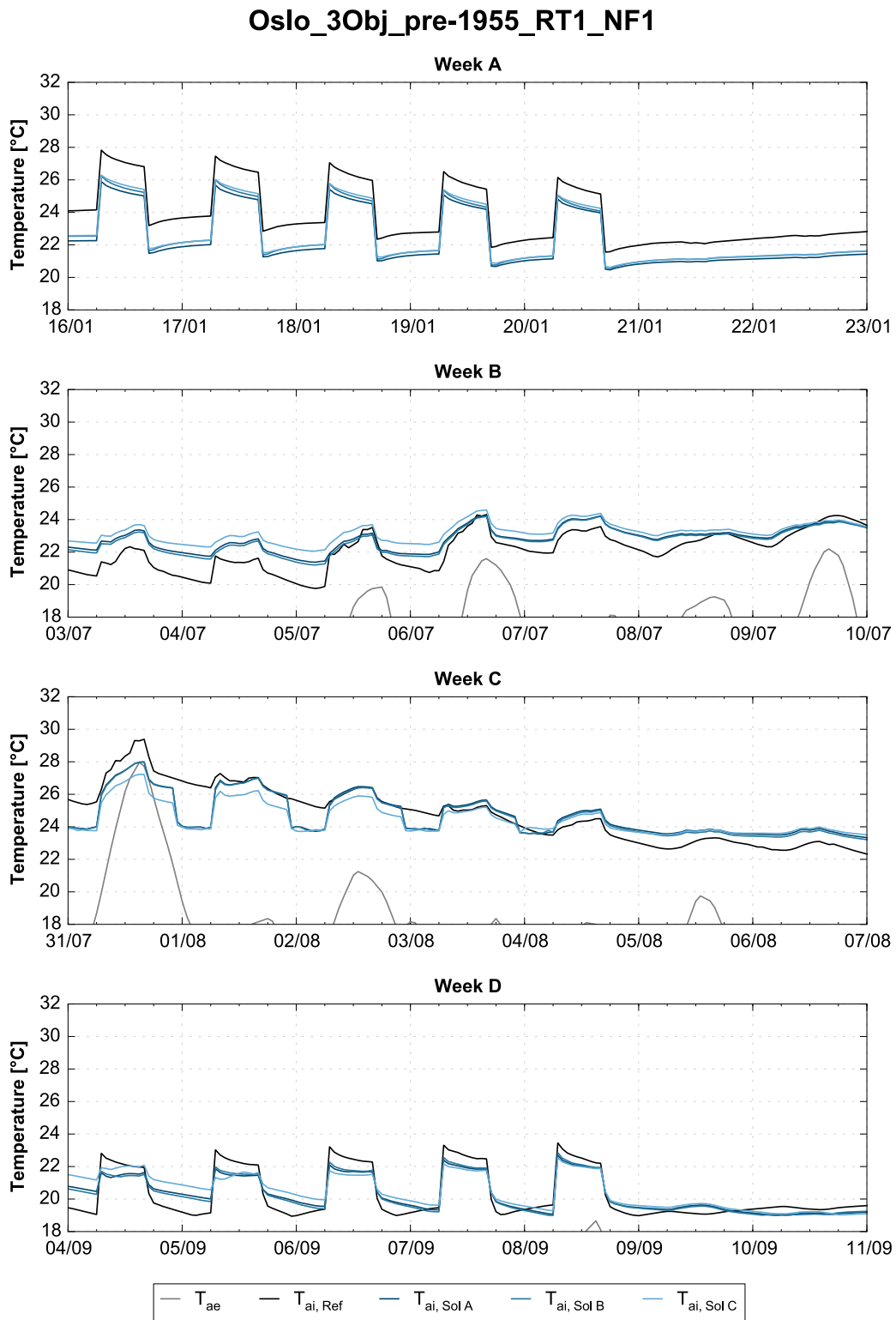
Fig. 6.3 Temperature profiles of the extreme solutions for significant weeks in Oslo, pre-1955.

Oslo_3Obj_post-1955_RT1_NF1
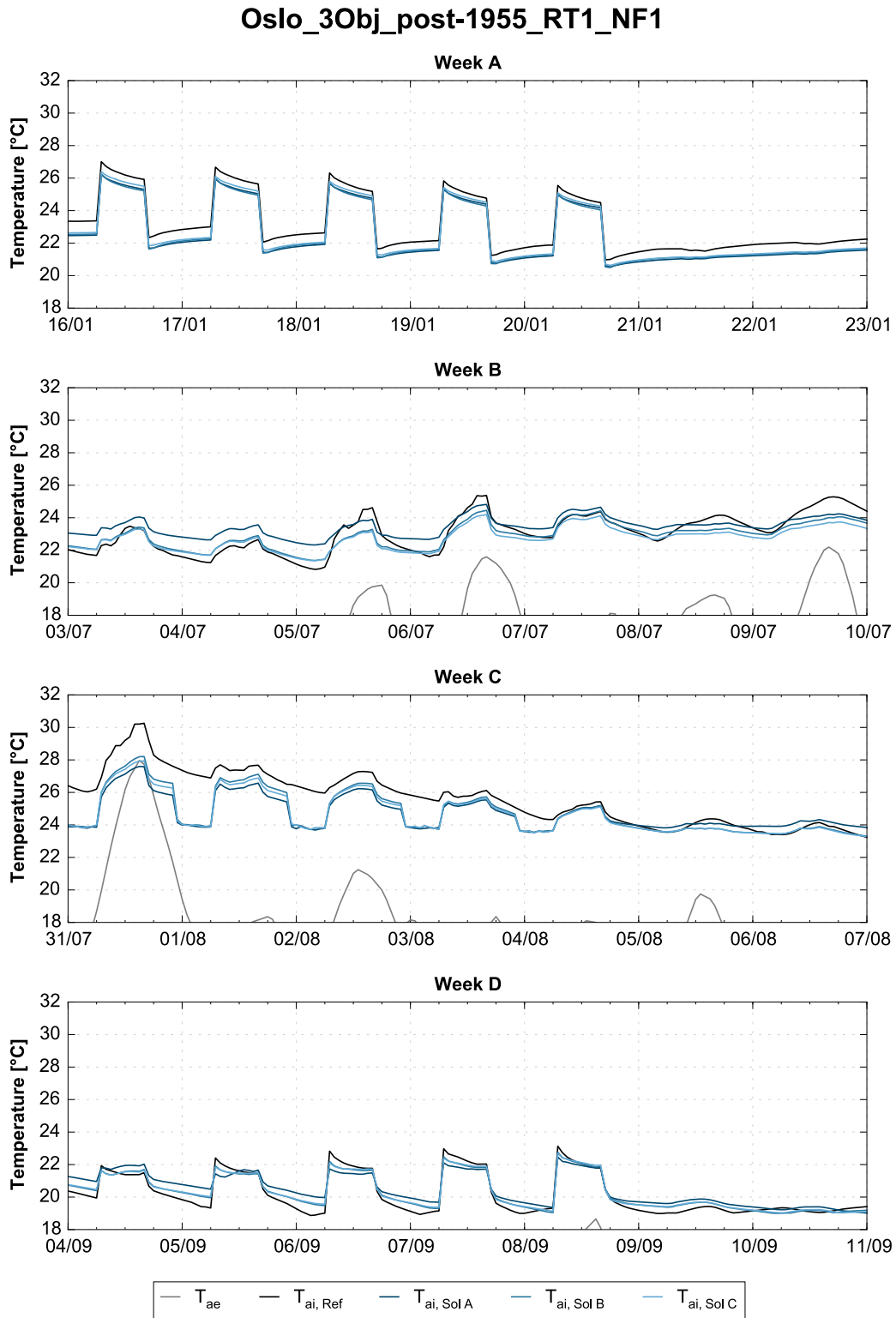
Fig. 6.4 Temperature profiles of the extreme solutions for significant weeks in Oslo, post1955.

of the building energy need for heating highlighted in Table 6.1.

During spring (week B), cooling energy is already needed. When the HVAC system is switched off at night, the internal air temperature of solution A of the two-objective analyses (i.e. minimum E_P) and of solution B of the three-objective analyses (i.e. minimum $Q_{C,nd}$) drop, whereas all the others rise. When night ventilation is activated, all cases drop to the night ventilation set-point temperature, i.e. 24 ℃. After two days of free running during the weekend, the solution characterised by the lowest $Q_{C,nd}$ shows an advantage in terms of cooling, as it remained the lowest curve, followed by the solution characterised by the lowest E_P.

During summer (week C), when the HVAC system is switched off at night, the internal air temperatures dramatically rise. Night ventilation allows to reduce the temperature but the external conditions are such that its efficiency is severely reduced. Except from the night ventilation, the profiles are similar to those of the pre-retrofit building. This implies that the PCM is always liquid and there is practically no difference among solutions.

During autumn (week D), when the pre-retrofit building would have started to need heating, all the solutions clearly show higher temperatures and therefore no or low heating energy need. However, there is a clear difference between the two solutions with lowest investment and global cost, which have no PCM, and all the other solutions, whose temperature is approximately 1 ℃ to 1.5 ℃ higher.

If the solution characterised by the lowest primary energy consumption is compared to those resulting from the three-objective optimisation analyses, it is evident that it provides the best compromise between summer and winter performance. This can also be inferred from the results in Table 6.1, as it is simultaneously characterised by the second best performance for both heating and cooling energy need as well as by the lowest electricity demand.

In Torino during winter (week A), the same considerations for the climate of Palermo apply. Moreover, the curves of the solutions in the group of A's for the two and three objective optimisations overlap.

During late spring (week B), the situation is similar to week B in Palermo, even though only solution B of the three-objective optimisation (i.e. lowest cooling energy need) allows the temperature to either drop or increase the least when the HVAC system is turned off. The worst performance is observed for the solutions characterised by the lowest global cost and heating energy need.

During summer (week C), when the HVAC system is switched off at night, the internal air temperatures rise, although to a lesser extent than in Palermo. Due to the lower external air temperatures, night ventilation is more effective, even though the set-point is not reached. Although the solution characterised by the lowest global cost shows the worst performance, the difference among solutions is almost negligible.

During autumn (week D), when the pre-retrofit building would already need heating, solution B of the three objective analyses (i.e. lowest cooling energy need) is

characterised by the highest temperature profile, with a difference of approximately 2 ℃ from the worst solution. This may seem unexpected; however, this solution is characterised by the presence of PCM1 with a peak melting temperature of 22.5 ℃ and a melting temperature range of 5.3 ℃, therefore it is in the midst of the phase change.

If the solution characterised by the lowest primary energy consumption is compared to those resulting from the three-objective optimisation analyses, its performance tends to be similar to that of the solution characterised by the lowest heating energy need. However, observing the results in Table 6.1, the lowest primary energy consumption is obtained by means of an accurate trade-off between heating, cooling and electricity.

The temperature profiles for the climate of Oslo are significantly different from those in Palermo and Torino due to the different control strategy. The set-point was on the operative temperature, which was set to 21 ℃ with a nocturnal set-back of 19 ℃ (see § 4.4.4). The use of PCM could provide the advantage of requiring to maintain a lower air temperature by guaranteeing higher internal surface temperatures. Therefore, the lower the air temperature, the lower the energy consumption in winter and also the thermal discomfort in summer, since no cooling system was considered.

In Oslo during winter (week A), solution A, i.e. the solution characterised by the lowest primary energy consumption, with a peak melting temperature of PCM1 of 18 ℃ required to maintain the lowest air temperature during both day and night in the pre-1955 building. On the other hand, in the post-1955 building solution A guaranteed the lowest air temperature during the night (longest time duration) whereas solution B (i.e. lowest global cost) required the lowest air temperature during the day.

During early summer (week B), when the building is in free running and night ventilation is not needed, all the retrofitted solutions are within the comfort range.

During summer (week C), night ventilation is activated and the building can be effectively cooled down to 24 ℃. In the pre-1955 building, solution C allows to maintain the temperature below 26 ℃ for the longest amount of time. Solutions A and B were instead characterised by a very similar performance, and the temperature was at times higher than the pre-retrofit building. On the other hand, in the post-1955 building all the solutions guaranteed a better performance compared to the pre-retrofit case. The lowest temperature was however guaranteed by the solution characterised by the lowest primary energy consumption.

During late summer (week D), heating is required again. However, all the retrofitted solutions are capable of maintaining sufficiently high temperatures at night so that set-back heating is not required (as the temperatures decrease, the building is in free running, whereas they increase for the reference, which is heated, to counterbalance the decreasing surface temperatures). Therefore, in this case the highest temperature profile at night is the most beneficial. In the pre-1955 building

the solution characterised by the lowest thermal discomfort (solution C) allows to maintain the highest internal air temperature during free running and the lowest one when the heating system is active, whereas in the post-1955 building the same happens with solution A (lowest primary energy consumption).

6.3   Innovization relationships

A summary of the innovization principles and information on their interpretation are presented. The significance of each fit was verified through the R software [351], and the precision of each coefficient was made sure to be coherent with its uncertainty. In some cases, the presence of relationships could be visually identified from the variables' mappings on the Pareto fronts, but different equations (and not simply different c-values) would apply to each cluster, or the noise in data was too high for the automated innovization algorithm to work properly. In such cases, relationships were manually searched through linear regression in R. All the equations were rewritten in order to provide more clarity in their interpretation. When necessary, the cluster of application was reported in superscript. Moreover, when relationships involved the overall PCM thickness among the four orientations (NF4), the counters i and j respectively refer to the PCM type and the wall orientation.

Overall, significant relationships were found to a greater extent under the following conditions:

- Same retrofit solution for all the façades (NF1);

- Retrofit intervention on a single side of the wall (i.e. RT0 and RT1);

- Main use of only one PCM.

On one hand, this confirms that the non-dominated set needs to be sufficiently close to the true Pareto front to be able to extract valuable knowledge from it [7] (the RT2 and NF4 cases were characterised by the widest search space and the lowest exploration level). On the other hand, the excessive variability of the solutions due to the formulation of the optimisation problem (i.e. the application of two types of PCMs which could be used in different positions within the wall) has likely affected the potential of extracting clear and more extensive information from the non-dominated sets. As it was found during validation (see § 3.3.5.1), the automated innovization procedure was very sensitive to the noise in the data (especially when searching for product relationships), so even when definite trends could be graphically identified, no acceptable equation could be retrieved unless the goodness of fit was sufficiently high.

When searching for constant values, the innovization procedure was found to be sensitive to the discretisation of the variables' domains; highly discretised

variables led to clustering of homogeneous values. In such cases (which occurred especially for the latent heat of fusion), the results were post-processed to provide a unique value. With regard to the summarised values, constants were reported only when the coefficient of variation was lower than 5% and the relationship was valid for at least 70% of the Pareto solutions or, for PCM properties, at least 65% of Pareto solutions and 75% of the total amount of solutions with PCM. Starred values refer to the presence of unclustered points (outliers).

When the innovization process involved more than one basis function, the parametric relationships that were identified were all linear with only one exception. This exception, having the generic form in eq. (3.21), was also the only relationship identified between variables and not between a variable and one or more fitness functions. Unfortunately, under a design perspective, finding more functional relationships among variables would have been far more interesting. As already mentioned, it is likely that the combinatorial nature of the problem reduced this possibility. However, relationships among variables and fitness functions can also be of interest, answering questions like: "What would the primary energy consumption be if x cm of PCM were installed?". It is important to underline that each relationship is not generally valid—e.g. it is not that "increasing PCM thickness will in any case reduce the primary energy consumption of x kWh/(m^{2}y)"—but it is only valid for the optimised set of variables. If, for example, a constant peak melting temperature is found, the same relationship between E_P and PCM thickness will not apply to a different peak melting temperature. Moreover, it is important to remark that, when analysing the meaning of the various relationships, their range of validity (i.e. the domain of each variable and codomain of each fitness function) needs to be kept in mind, for extrapolation is always a hazard that can lead to erroneous conclusions.

The complete sets of equation for the two-objective optimisation analyses in Palermo and Torino are reported in Table 6.3 and Table 6.4 respectively for the NF1 and NF4 cases. All the NF1 solutions shared a constant U-value of 0.15 W/(m^{2}K) in the RT1 and RT2 cases, and the same tended to occur for the corresponding NF4 solutions except on the east walls.

The only relationship of the generic form in eq. (3.21) was found between thickness and melting temperature of PCM1 in the RT0 – NF1 case in Palermo. In the other cases the peak melting temperature varied within a very small range and no such trend could therefore be identified. However, as already mentioned in § 5.3.3.1.1, this finding is in line with the results of the parametric analysis (see § 5.2.1.3) as well as with the findings of other authors [138].

With regard to the relationships between primary energy consumption and thickness of PCM1 (PCM2 was seldom selected), the higher the PCM thickness, the lower the primary energy consumption. For each case, the intercept of the equation corresponds (or is very close) to the primary energy consumption of the corresponding solution B (minimum global cost), where PCM was never used.

Table 6.3 Relationships for the two-objective optimisations, NF1 cases.

Retrofit Type	Relationships	CV	R^2
	Palermo		
RT0	$L_1^* = 226.4$ kJ/kg	2.7%	
	$E_P = -48.5\, t_1 + 114.67$		0.967
	$C_G = 3080\, t_1 + 451$		0.995
	$C_G = 0.800\, C_I + 308.1$		0.999
	$T_{p,1} = 35.8\, t_1^{0.15}$		0.814
RT1	Uvalue $= 0.150$ W/(m^{2}K)	0.0%	
	$E_P = -78\, t_1 + 107.4$		0.947
	$C_G = 2400\, t_1 + 391$		0.968
	$C_G = 0.784\, C_I + 289.7$		0.999
RT2	Uvalue $= 0.150$ W/(m^{2}K)	0.0%	
	$E_P = -69\, t_1 + 107.6$		0.893
	$C_G = 2500\ (t_1 + t_2) + 475$		0.913
	$C_G = 0.788\, C_I + 298.8$		0.999
	Torino		
RT0	$C_G = 0.800\, C_I + 381.3$		0.999
RT1	Uvalue $= 0.150$ W/(m^{2}K)	0.0%	
	$T_{p,1}^* = 18.5$ ℃	2.5%	
	$L_1^* = 230$ kJ/kg	0.0%	
	$E_P = -61\, t_1 + 141.09$		0.966
	$C_G = 2900\, t_1 + 504$		0.954
	$C_G = 0.792\, C_I + 357$		0.999
RT2	Uvalue $= 0.150$ W/(m^{2}K)	0.0%	
	$E_P = -33\, t_1 + 141.13$		0.900
	$C_G = 2600\ (t_1 + t_2) + 597$		0.912
	$C_G = 0.796\, C_I + 366.1$		0.999

Moreover, the greater the absolute value of the slope, the more the use of PCM is an effective energy saving strategy. As it was already observed from the Pareto fronts (see § 5.3.2.1), retrofit intervention on the internal side was confirmed to be the best option both in terms of intercept and slope, whereas retrofit intervention on the external side was less preferable.

As a consequence of the increase of the amount of PCM, relationships between PCM thickness and global cost were also found. Even though the existence of these relationships is trivial, they can still provide some information. The intercepts are close to the minimum global cost (that of solution B), while the other term

Table 6.4 Relationships for the two-objective optimisations, NF4 cases.

Retrofit Type	Relationships	CV	R^2
	Palermo		
RT0	$L_1^* = 230$ kJ/kg	0.0%	
	$E_P = -10.9 \sum t_{1,j} + 114.57$		0.948
	$C_G = 0.802\, C_I + 308.0$		0.999
RT1	$\text{Uvalue}_S{}^* = 0.150$ W/(m^{2}K)	0.0%	
	$\text{Uvalue}_N = 0.150$ W/(m^{2}K)	0.0%	
	$\text{Uvalue}_W{}^* = 0.150$ W/(m^{2}K)	0.0%	
	$E_P = -15 \sum t_{i,j} + 107.5$		0.880
	$C_G = 0.785\, C_I + 290.4$		0.999
RT2	$\text{Uvalue}_S{}^* = 0.153$ W/(m^{2}K)	4.6%	
	$t_{2,N} = 0.5$ cm	0.0%	
	$t_{2,W}^* = 0.5$ cm	0.0%	
	$C_G = 0.76\, C_I + 309$		0.998
	Torino		
RT0	$C_G = 0.8030\, C_I + 381.1$		1.00
RT1	$\text{Uvalue}_S{}^* = 0.153$ W/(m^{2}K)	4.0%	
	$\text{Uvalue}_N{}^* = 0.150$ W/(m^{2}K)	0.0%	
	$\text{Uvalue}_W = 0.155$ W/(m^{2}K)	4.8%	
	$C_G = 0.800\, C_I + 357$		0.999
RT2	$\text{Uvalue}_N{}^* = 0.153$ W/(m^{2}K)	3.0%	
	$C_G = 0.78\, C_I + 375$		0.997

represents the added global cost due to the PCM. The lower the slope, the more cost-effective the PCM is.

With regard to the relationships between global cost and investment cost, the lower the intercept and the lower the slope, the more the retrofit intervention is cost effective. However, a proper interpretation of these equations is not straightforward. Observing eq. (4.16), the global cost is given by the investment cost plus a term that comprises annual costs, replacement costs and final value, which are also dependent on the investment cost. As a whole, this term is given by $q - (1 - m)\, C_I$, where m and q respectively denote slope and intercept of the tabulated equations. It should however be noted that the differences among the slopes is very limited, so that the straight lines are indeed almost parallel. Moreover, the results of the NF1 and corresponding NF4 cases were extremely similar, except for the RT2 – NF4 cases. This is an additional sign that the obtained non-dominated set was not as close to the true Pareto front. Eventually, since the costs for the new HVAC systems

Table 6.5 Relationships for the three-objective optimisations in Italy, NF1 cases.

Retrofit Type	Relationships	CV	Adj R^2
	Palermo		
RT0	$L_1^* = 224.6$ kJ/kg	3.0%	
	$\text{Uvalue}^{win3} = 3.6 + 0.058\,Q_{H,nd} - 0.145\,Q_{C,nd}$		0.925
	$\text{Uvalue}^{win3} = 5.2 - 0.204\,Q_{C,nd} - 0.00027\,C_I$		0.938
RT1	—		
RT2	—		
	Torino		
RT0	$T_{p,2} = 25.1$ °C	4.0%	
RT1	$T_{p,2}^* = 25.1$ °C	3.7%	
RT2	$T_{p,2}^* = 24.9$ °C	3.7%	

Table 6.6 Relationships for the three-objective optimisations in Italy, NF4 cases.

Retrofit Type	Relationships	CV	Adj R^2
	Palermo		
RT0	—		
RT1	—		
RT2	—		
	Torino		
RT0	$T_{p,2} = 25.5$ °C	4.4%	
RT1	—		
RT2	—		

were assumed to be unvaried among all the solutions for each location, and the investment cost was hence evaluated only for the envelope (see § 4.4.6.1), the correct relationships between global cost and investment cost would be characterised by an increased intercept.

The complete sets of equation for the three-objective optimisation analyses in Palermo and Torino are reported in Table 6.5 and Table 6.6 respectively for the NF1 and NF4 cases. Due to the extensive use of both PCMs, very few relationships were identified, and they were mainly of constant nature.

As in the two-objective optimisation analyses, in the RT0 case in Palermo the

Table 6.7 Relationships for the three-objective optimisations in Oslo, NF1 cases.

Retrofit Type	Relationships	CV	Adj R^2
	Oslo, pre-1955		
RT0	$T_{p,1}^* = 17.8\,°C$	4.2%	
	$\text{Uvalue}^{ins7} = -2.5 - 7.0\,LPD + 0.011\,E_P$		0.934
	$\text{Uvalue}^{ins7} = 1.3 - 20\,LPD - 0.00046\,C_G$		0.958
	$t_1 = 1.0 - 14\,LPD - 0.0018\,E_P$		0.932
	$t_1^{ins0-6} = 0.00031\,C_G - 0.19$		0.961
	$t_1^{ins7} = 0.32 - 11\,LPD + 0.00013\,C_G$		0.944
	$C_G = 0.762\,C_I + 445$		0.961
RT1	$T_{p,1}^* = 19.5\,°C$	1.9%	
	$\text{Uvalue}^{win7} = -1.81 - 5.8\,LPD + 0.0081\,E_P$		0.992
	$\text{Uvalue}^{win9} = -1.5 - 7.1\,LPD + 0.0072\,E_P$		0.930
	$t_1 = 0.65 - 8.9\,LPD - 0.0012\,E_P$		0.921
	$C_G = 556 + 2230\,t_1$		0.976
	$C_G = 0.740\,C_I + 426$		0.985
RT2	$T_{p,1}^* = 19.2\,°C$	2.3%	
	$C_G = 0.78\,C_I + 421$		0.958
	Oslo, post-1955		
RT0	$C_G = 0.771\,C_I + 435$		0.998
RT1	$T_{p,1} = 19.4\,°C$	1.7%	
	$\text{Uvalue}^{win7} = -1.57 - 8.0\,LPD + 0.0078\,E_P$		0.984
	$\text{Uvalue}^{win9} = -1.51 - 9.3\,LPD + 0.0078\,E_P$		0.957
	$t_1 = 0.18 - 3.6\,LPD - 0.00070\,E_P + 0.00026\,C_G$		0.981
	$C_G = 0.740\,C_I + 426$		0.985
RT2	$T_{p,1}^* = 19.4\,°C$	2.0%	
	$t_1 = 0.64 - 9.5\,LPD - 0.00105\,E_P$		0.955
	$C_G = 0.76\,C_I + 448$		0.976

latent heat of fusion of PCM1 was maximised. However, as suggested in [280], it could be possible that a latent heat of fusion of 230 kJ/kg would have been optimal even searching within a greater range of variation. For the same case, relationships among U-value, building energy need for heating and cooling and investment cost were additionally found within the cluster characterised by window type 3.

In Torino, only constant values for the peak melting temperature of PCM2 were identified (around 25 ℃ for all the retrofit options in the NF1 cases).

The complete sets of equation for the three-objective optimisation analyses

Table 6.8 Relationships for the three-objective optimisations in Oslo, NF4 cases.

Retrofit Type	Relationships	CV	Adj R^2
	Oslo, pre-1955		
RT0	$\sum t_{1,j} = 1.3 - 14\,LPD - 0.0027\,E_P$		0.930
	$\sum t_{1,j} = 0.32 - 11\,LPD + 0.00011\,C_G$		0.944
	$C_G = 0.763\,C_I + 456$		0.999
RT1	$T^*_{p,1} = 19.5\ ^\circ\text{C}$	0.0%	
	$C_G = 552 + 670\,\sum t_{1,j}$		0.948
	$C_G = 0.78\,C_I + 421$		0.981
RT2	$T^*_{p,1} = 19.0\ ^\circ\text{C}$	0.0%	
	$C_G = 0.773\,C_I + 445$		0.993
	Oslo, post-1955		
RT0	$C_G = 0.770\,C_I + 435$		0.996
RT1	$T^*_{p,1} = 19.4\ ^\circ\text{C}$	2.0%	
	$C_G = 537 + 630\,\sum t_{i,j}$		0.967
	$C_G = 0.758\,C_I + 414$		0.986
RT2	$T^*_{p,1} = 19.1\ ^\circ\text{C}$	3.9%	
	$C_G = 0.76\,C_I + 434$		0.981

in Oslo for both pre-1955 and post-1955 buildings are reported in Table 6.7 and Table 6.8 respectively for the NF1 and NF4 cases.

A constant peak melting temperature of PCM1 of about 19.5℃ was identified especially for the RT1 and RT2 retrofit types, where the PCM was placed mostly close to the internal environment.

Relationships among U-value, primary energy consumption and LPD were found in the NF1 cases. In the RT0 case, only in the pre-1955 building such a relationship was identified within the cluster characterised by aerogel insulation. In the RT1 case, the relationship was instead clustered by window type both in the pre-1955 and post-155 buildings. As it could be expected, for decreasing U-values, the primary energy consumption was found to decrease to the detriment of thermal comfort.

Relationships among thickness of PCM1, primary energy consumption, LPD and global cost were additionally identified in many cases. Increasing PCM thickness was confirmed to have a positive effect both on primary energy consumption and thermal comfort.

Eventually, relationships between global cost and investment cost were also found. However, probably due to the presence of the LPD function, their goodness of fit was not as high as in the two-objective optimisation analyses in Italy.

6.4   Mutual influence of the PCM's thermo-physical properties

Both for the component and building level analyses, no clear information regarding the most suitable thermal conductivity and melting temperature range of the PCMs were derived. The reason behind the general lack of trends in these variables, especially in the three-objective optimisation analyses, may be partly ascribed to the variety of positions of the PCM within the wall. However, analysing the extreme solutions, it was found that the best thermal conductivity varied with the PCM's melting temperature; when sub-optimal, low thermal conductivities could sometimes improve the energy performance of the building (with an optimal value within the variable's range), but when the optimal melting temperature was found, high thermal conductivities seemed to be preferable. Moreover, the sensitivity of the results to a variation of the PCM's thermal conductivity was not constant, as it reasonably tended to decrease close to the optimal value.

To better investigate the effect of thermal conductivity on the optimality of the results and to analyse the mutual influence between thermal conductivity, peak melting temperature and melting temperature range, a few simple parametric analyses were performed. Solutions in the group of A's (minimum heating energy need) for the RT0 and RT1 case studies (retrofit intervention respectively on the external and internal side of the wall) of the three-objective optimisation analyses in Torino were used as a reference. The abovementioned thermo-physical properties of PCM1 (the only PCM used in those solutions) were varied in pairs while keeping all the other properties constant. The resulting values of building energy need for heating and cooling were plotted, and the points corresponding to the minimum energy value for each case were highlighted. The variation in primary energy consumption considering the system efficiencies reported in § 4.4.5 was additionally reported. No information on the influence of the thermo-physical properties of PCM on the electricity demand was provided as it was practically negligible in these analyses. The thermo-physical properties of PCM1 for the two solutions (Fig. C.9 and Fig. C.11) are summarised in Table 6.9.

Table 6.9 Thermo-physical properties of PCM1 in the solutions in the group of A's for the RT0 and RT1 case studies of the three-objective optimisation analyses in Torino.

Property	RT0	RT1
Peak melting temperature [℃]	17.0	15.5
Melting temperature range [℃]	2.0	4.7
Latent heat of fusion [kJ/kg]	230	230
Thermal conductivity [W/(m K)]	0.85	0.55
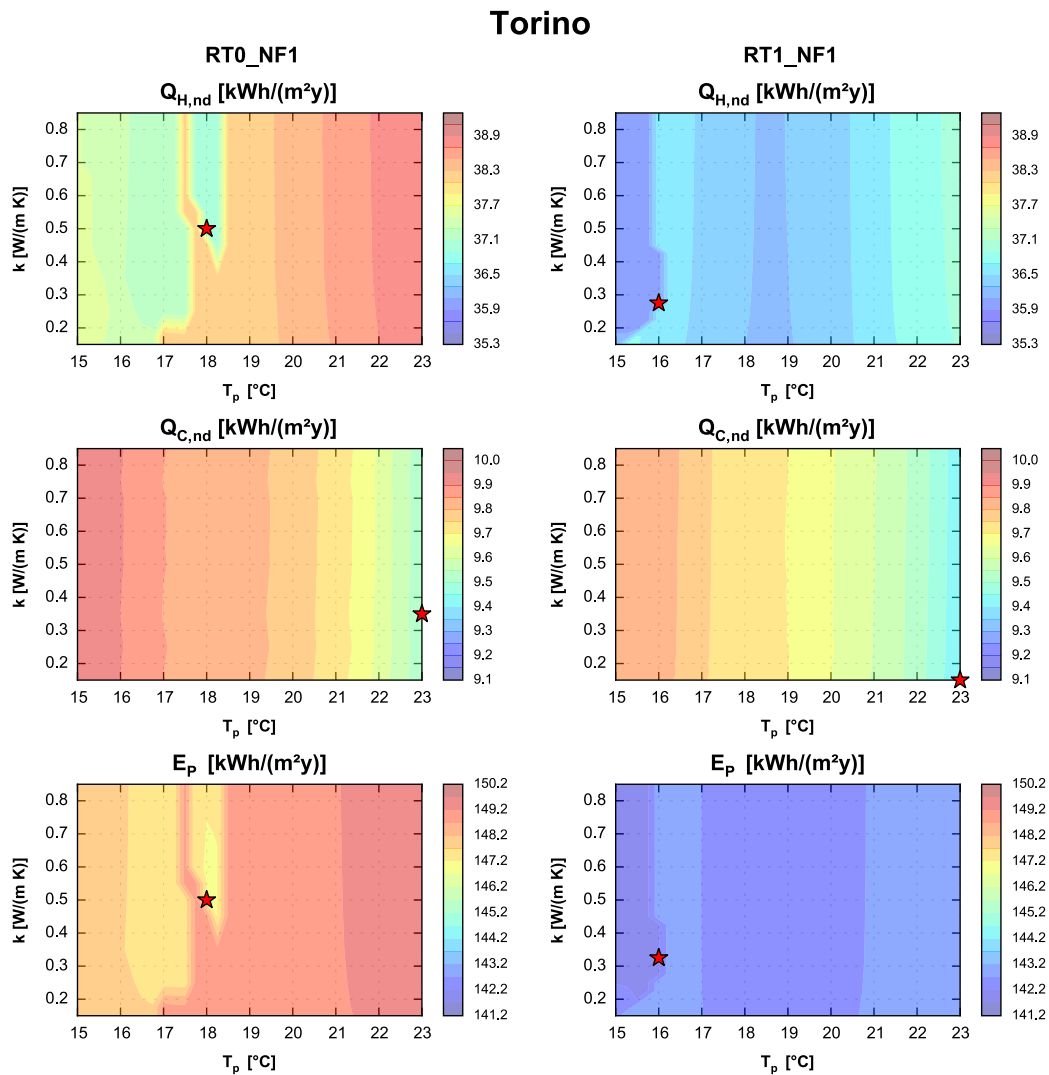
Fig. 6.5 Building energy requirement as a function of peak melting temperature and thermal conductivity of PCM (T_p from 15℃ to 23℃).

The mutual influence of peak melting temperature and thermal conductivity on building energy performance is shown in Fig. 6.5. With regard to the energy need for heating, the thermal conductivity which ensured the minimum energy consumption was found within the exploration range both for the RT0 and RT1 cases. As it was observed when analysing the extreme solutions, the optimal thermal conductivity is dependent on the peak melting temperature. Outside the optimal ranges for the peak melting temperature, thermal conductivities equal to the lower bound ensured a slightly better performance. However, since the variation in $Q_{H,nd}$ for such temperatures was very limited, a randomness in the GA solutions can be expected unless the optimal peak melting temperature is found.

Torino
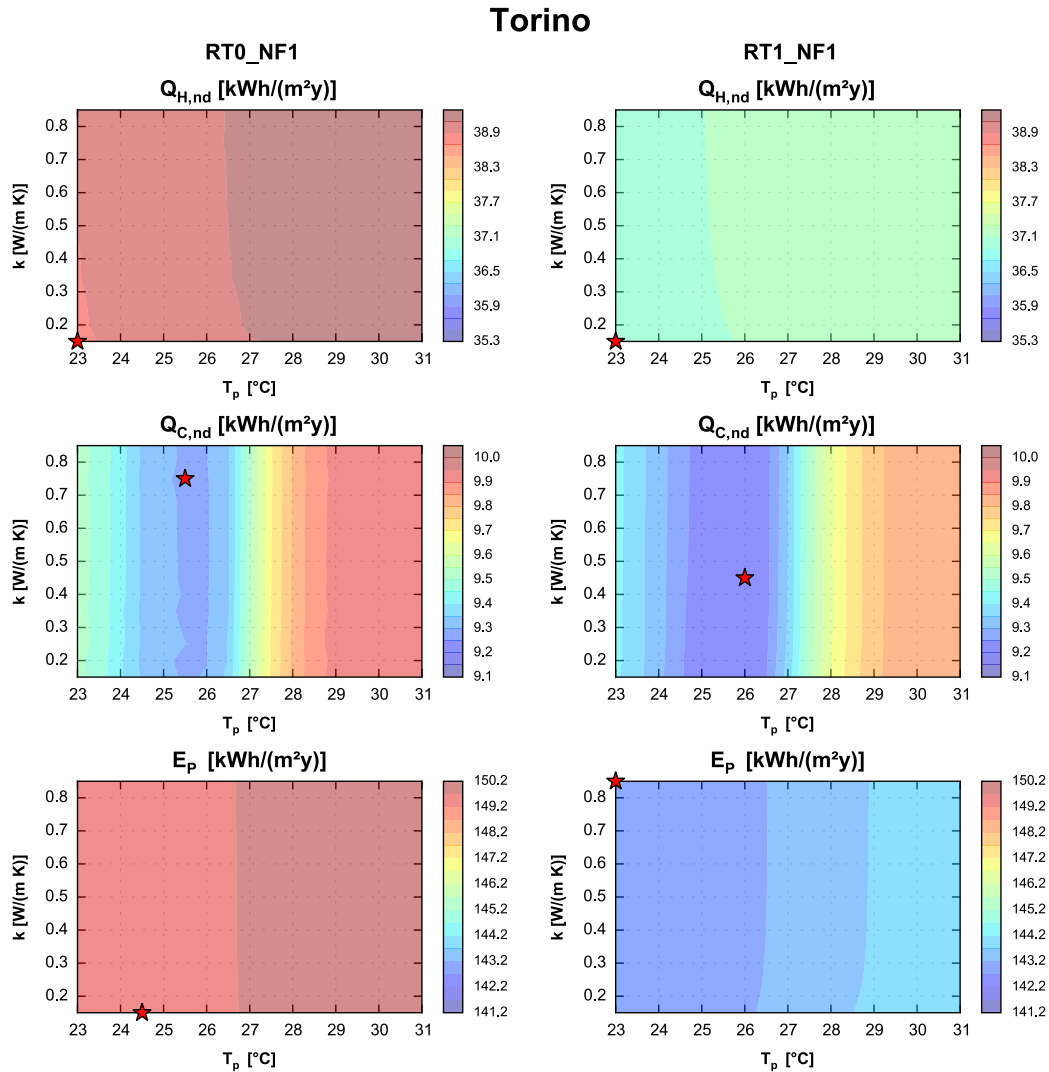
Fig. 6.6 Building energy requirement as a function of peak melting temperature and thermal conductivity of PCM (T_p from 23℃ to 31℃).

With regard to the energy need for cooling, the optimal peak melting temperature within the investigated range was the highest (i.e. 23 ℃). For the sake of completeness, the extension of Fig. 6.5 within the domain of PCM2 is shown in Fig. 6.6. Both in the RT0 and RT1 cases, the best thermal conductivity corresponding to the optimal peak melting temperature did not match with the best value for heating. Moreover, no region where the influence of thermal conductivity was significant with respect to that of peak melting temperature was observed.

With regard to the primary energy consumption, the optimum was a trade-off between the results for heating and cooling energy need. The optimal thermal conductivity was however closer to the optimum value for the heating energy need
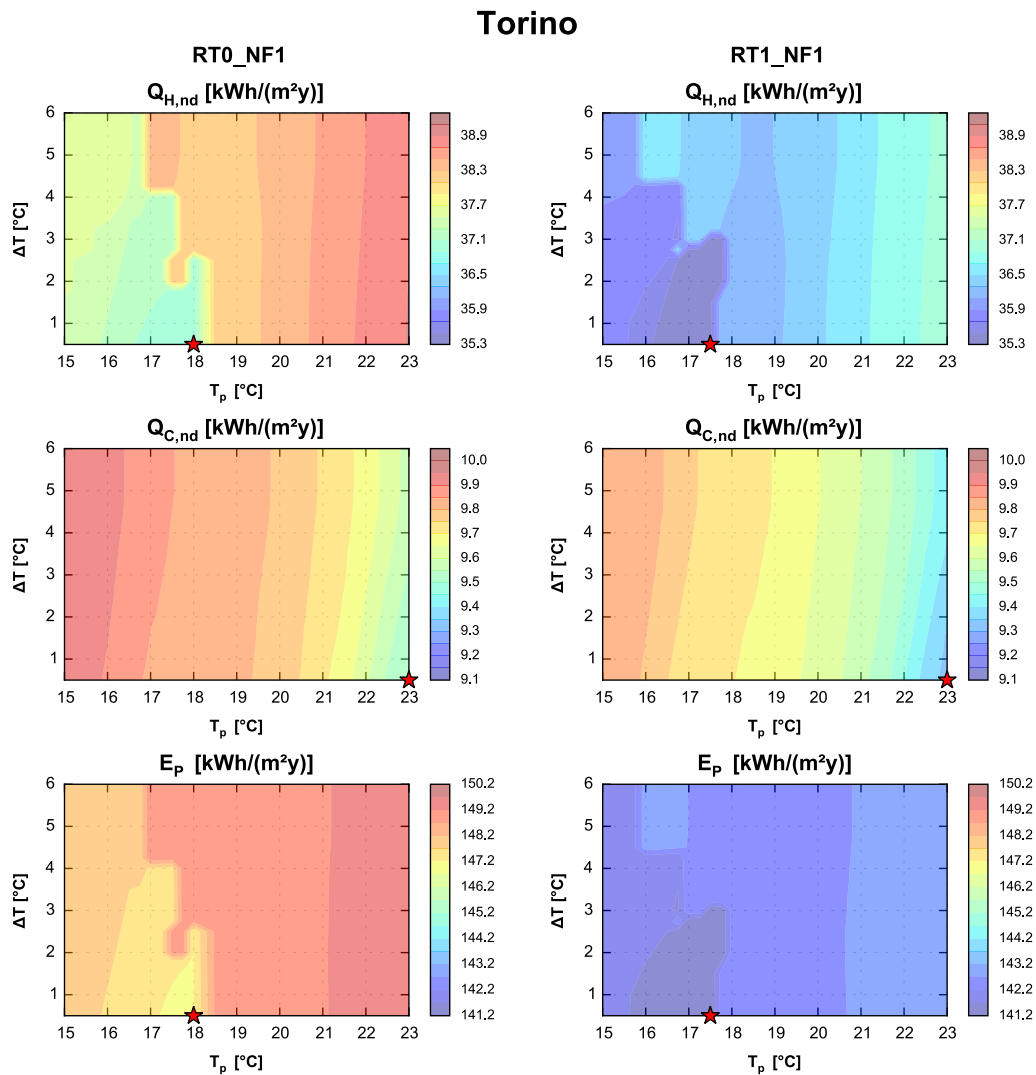
Fig. 6.7 Building energy requirement as a function of peak melting temperature and melting temperature range of PCM (T_p from 15℃ to 23℃).

due to its higher primary energy share.

From these analyses it can be inferred that finding the optimal thermal conductivity is not a trivial task due both to the complex non-linear shape of the objective space and to the need for a trade-off between heating and cooling. However close, it was verified that the GA did not find the true minimum.

The mutual influence of peak melting temperature and melting temperature range on building energy performance is shown in Fig. 6.7. Similar trends were observed for the RT0 and RT1 cases. Moreover, results were found not to change beyond a melting temperature range of 5 ℃. This can explain why the optimisation algorithm almost never selected solutions with melting temperature ranges close
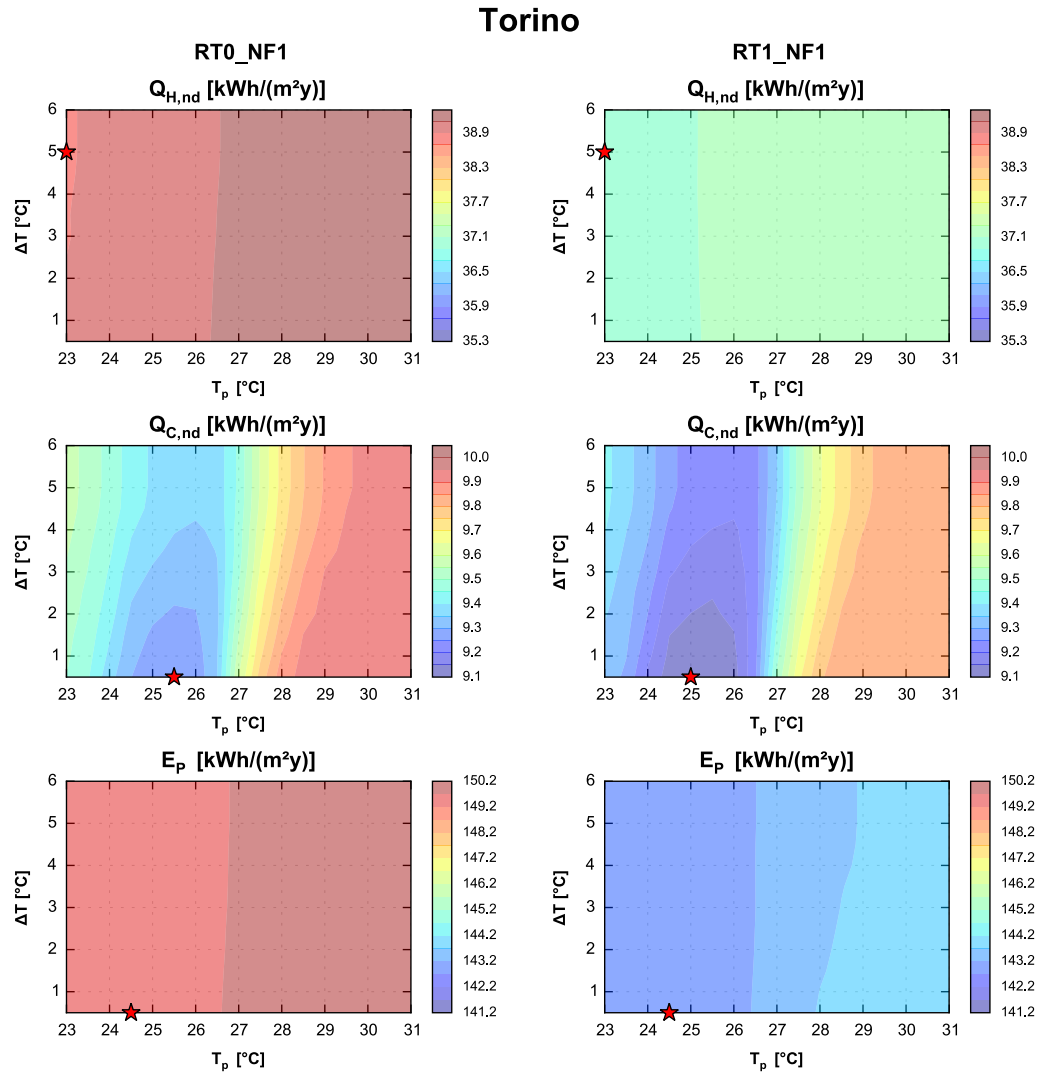
Fig. 6.8 Building energy requirement as a function of peak melting temperature and melting temperature range of PCM (T_p from 23℃ to 31℃).

to the upper bound.

With regard to the energy need for heating, the minimum energy consumption resulted to be ensured with the lowest melting temperature range for peak melting temperatures within the optimal or sub-optimal range. However, as the peak melting temperature distanced from the optimal region, the melting temperature range corresponding to the minimum heating energy need started to increase up to the upper bound. These results are in agreement with the findings from El Mankibi et al. [265].

As it could be already seen in Fig. 6.5 (but more evident in this case), the objective space resulted to be divided in two separate regions with different trends.
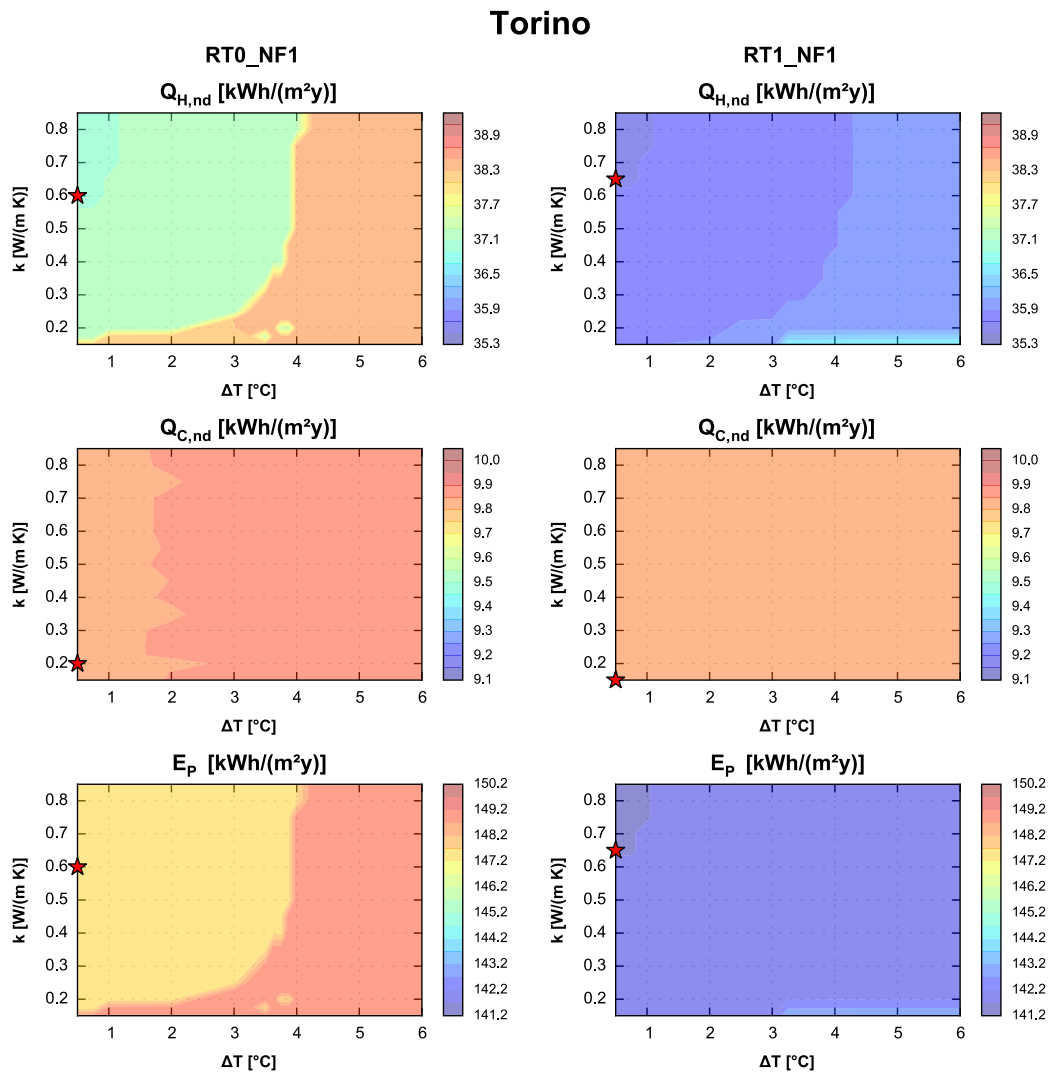
Fig. 6.9 Building energy requirement as a function of melting temperature range and thermal conductivity of PCM.

A local minimum can be observed for peak melting temperatures around 18.5 ℃. This is in line with the literature, for which the optimal peak melting temperature should be approximately one or two degrees lower than the internal set-point temperature [87, 265]. However, the global minimum was found within another region characterised by lower peak melting temperatures. The reason behind the presence of these two regions is likely due to the system operation during daytime only. Therefore, as the internal air temperatures drop at night, a PCM melting temperature that reduces the difference between air and set-point temperatures when the heating system is activated in the morning allows for more significant energy savings than a melting temperature tuned for diurnal energy savings.

For the sake of completeness, the extension of Fig. 6.7 within the domain of PCM2 is additionally reported in Fig. 6.8. The lower bound of the melting temperature range resulted to be optimal also for the peak melting temperature that ensured the lowest cooling energy need.

In general, from these analyses it can be inferred that, given the simultaneous optimality of the peak melting temperature, the best melting temperature range is the lowest possible. However, since the variation in energy performance for different melting temperature ranges in most of the objective space was limited, the lack of a clear trend towards the minimisation of ΔT among the GA solutions could be explained.

The mutual influence of thermal conductivity and melting temperature range on building energy performance is shown in Fig. 6.9. Up to a melting temperature range of 4 ℃, a low thermal conductivity was found to lead to higher heating energy needs. Very low melting temperature ranges were again found to ensure the best energy performance, whereas the thermal conductivity was contrasted among the energy targets.

To conclude, peak melting temperature, melting temperature range and thermal conductivity resulted to be strongly interconnected. Finding the optimal thermal conductivity was proven to be especially difficult when more energy objectives are simultaneously minimised. As it can be confirmed by the box plots of the two-objective optimisation analyses (Fig. A.1 and Fig. A.2), convergence towards an optimal range is easier when only primary energy consumption is addressed.

6.5   Selection of the objective functions

Given the results of the two-objective and three-objective optimisation analyses, some comments on the selection of the objective functions are herewith discussed.

If the aim of the analysis is specific, i.e. there is the need to minimise or maximise one or more functions because the main interest is on the result in terms of objective space, then selecting two functions allows the optimisation algorithm to be more efficient. However, according to the optimisation problem, the Pareto front might be scarcely populated with respect to the initial population, and possible knowledge that can be extracted is found on a small dataset. However, on a bi-dimensional set, finding significant design information is an easier task than on multi-dimensional fronts. On the other hand, if the aim of the analysis is that of understanding the behaviour of a system, performing an optimisation with several objective functions can provide more comprehensive information, such as on the contrast between objectives or on the interaction among variables and fitness functions. Moreover, a high number of optimisation functions generally allows to have a more populated front, so that significant statistical analyses can be performed to retrieve valuable

design information.

With regard to the investigated cases, performing an optimisation search directly on the primary energy consumption implies to fix the efficiency of the systems. Different system efficiencies would therefore result in different Pareto fronts with their own set of design solutions. If an optimisation search is performed by simultaneously minimising each energy term, then the performance of such Pareto solutions could be investigated for various combinations of system efficiencies. In the same way, if the investment cost is also minimised, the global cost could be subsequently evaluated.

This process has been tested for the NF1 case studies in Palermo and Torino. Primary energy consumption values associated to the Pareto fronts of the three-objectives optimisation analyses were parametrically evaluated. Seasonal efficiencies ranging from 0.75 to 0.95 for the heating system and from 2.5 to 4.5 for the cooling system were considered. Obviously, the minimum primary energy consumption was obtained when the system efficiencies for both heating and cooling were simultaneously maximised. However, interesting considerations can be drawn regarding the identification of the best-performing solutions on the Pareto fronts.

In Fig. 6.10 and Fig. 6.11, the projection of the Pareto fronts on the $(Q_{H,nd}, Q_{C,nd})$ plane for the NF1 cases respectively in Palermo and Torino is reported. In the first row, the corresponding overall electricity consumption (due to artificial lighting, equipment and fan operation of the mechanical ventilation system) is also reported in a colour-coded scale. The circled points indicate those individuals which resulted to provide the lowest primary energy consumption. In the second and third rows, the electricity consumption respectively due to artificial lighting and fan operation are additionally reported. The greatest amount was due to the equipment, which was however a constant value. Eventually, in the last row the variation of E_P as a function of the seasonal efficiencies of the heating and cooling systems is plotted for the best performing individual.

In Torino, a single solution for each case was identified as the best solution in terms of E_P regardless of the combination of system efficiencies. For the RT0 case, the lowest E_P was found for the solutions characterised by the lowest heating energy consumption. For the RT1 case, the best performance could instead be guaranteed by a trade-off solution between heating and cooling energy need. For the RT2 case, the best-performing solution was identified in the same region as in the RT0 case; however, this individual did not belong to the bi-dimensional Pareto front between heating and cooling energy need, and it was characterised by a lower electricity consumption compared to the nearby solutions. For the analysed case studies, the electricity use was the major contributor to the primary energy consumption both in Torino and, to an even greater extent, in Palermo. Since in the RT0 case the electricity demand was quite homogeneous, the selection of the best performing individual was driven by the heating energy need. In the RT1 case, however, the best individual in terms of E_P was characterised by the
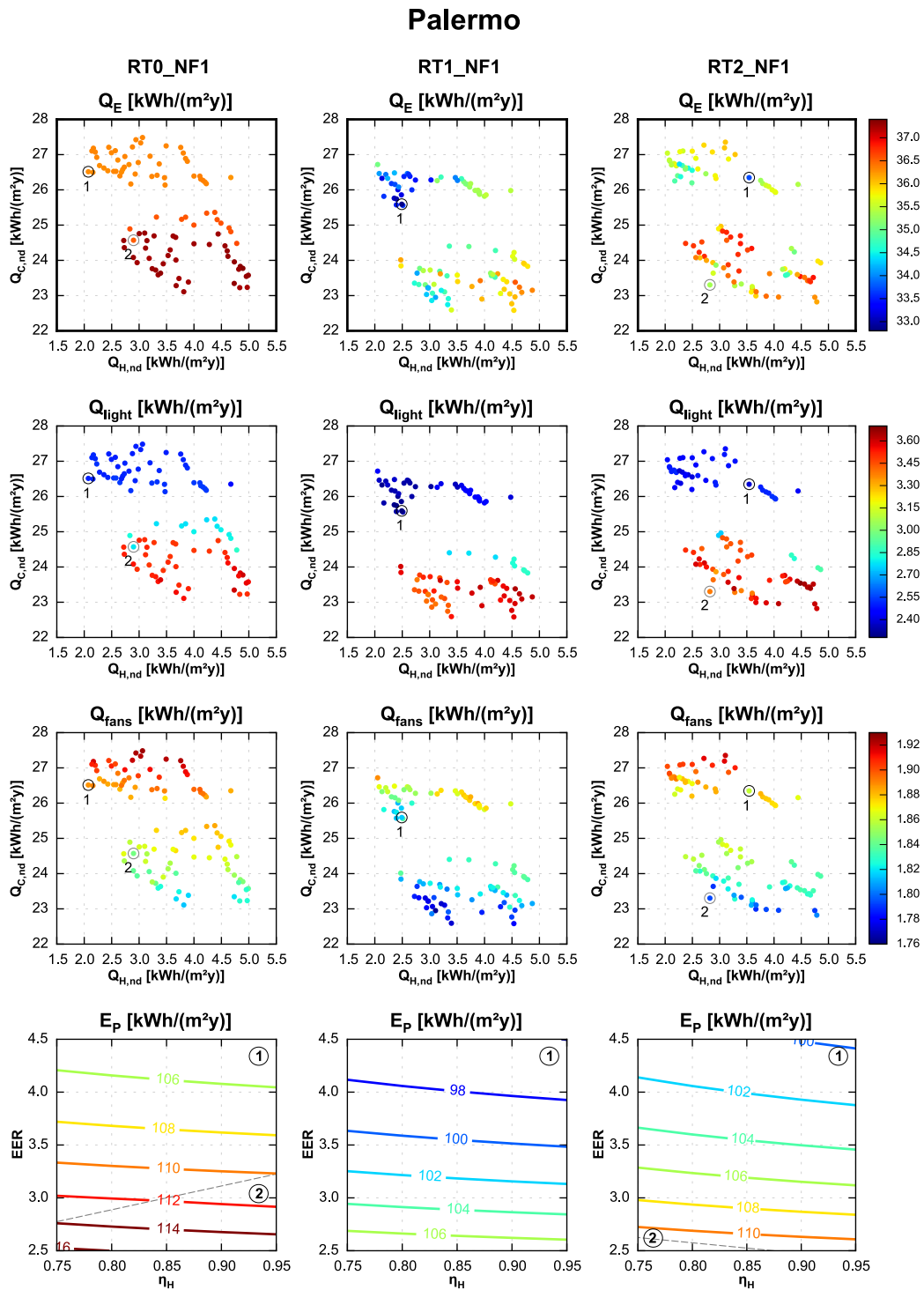
Palermo

Fig. 6.10 Selection of best performing individuals in terms of E_P from the three-objective optimisations in Palermo (units are in kWh/(m^{2}y)).
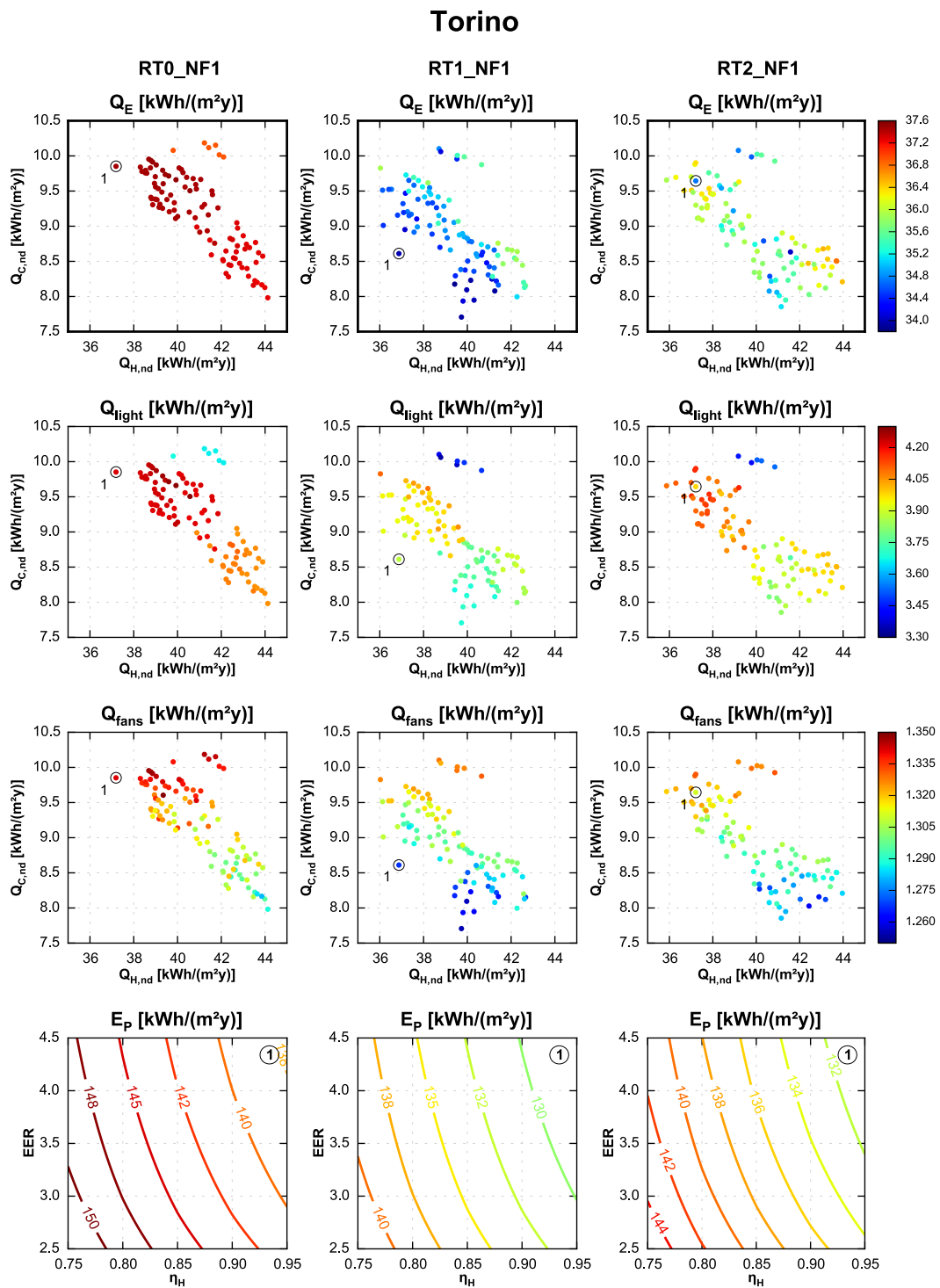
Fig. 6.11 Selection of best performing individuals in terms of E_P from the three-objective optimisations in Torino (units are in kWh/(m²y)).

Palermo

Torino
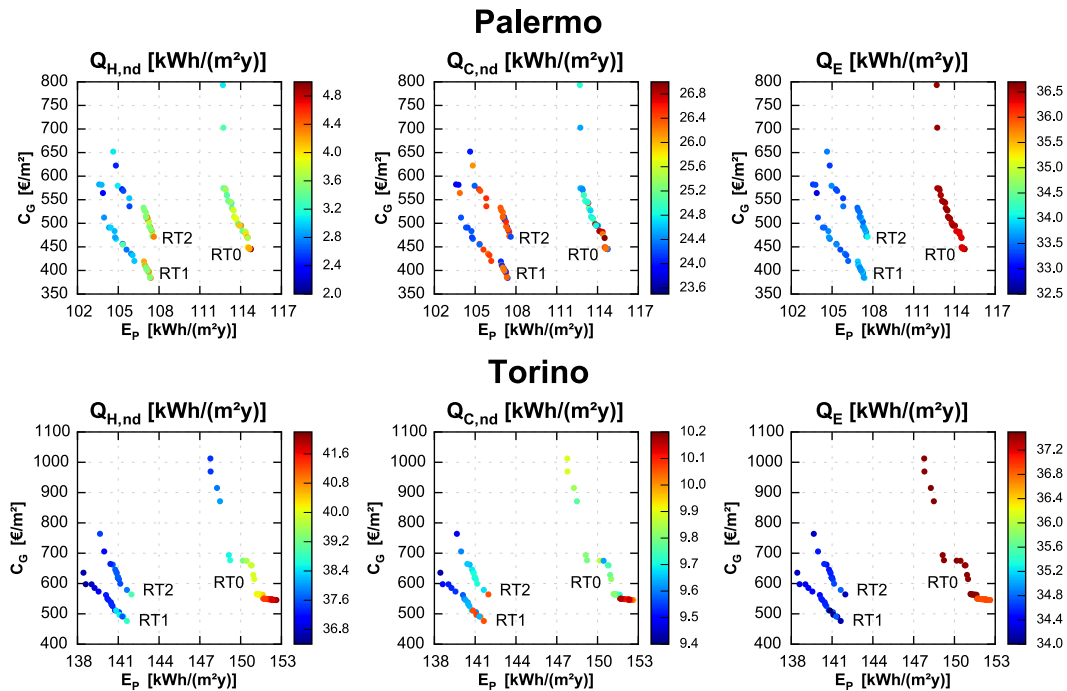
Fig. 6.12 Energy shares of the two-objective Pareto fronts (units are in kWh/(m^{2}y)).

lowest electricity demand among the group of solutions with the lowest heating energy need.

In the case of Palermo, for the RT0 and RT2 retrofit options two solutions were identified as the best performing individuals according to the trade-off between system efficiencies. In the RT0 case, for low EER values a solution with moderately low cooling (and heating) energy need and the lowest electricity demand in the nearby region was found to ensure the lowest primary energy need. For improved system efficiencies, the solution which guaranteed the lowest heating energy need together with a low electricity demand was found to perform better. In the RT2 case, for very low systems efficiencies both for cooling and heating, the solution which ensured the lowest primary energy need was characterised by a trade-off between the simultaneous minimisation of heating and cooling energy need. However, for improved system efficiencies, the best performing solution was characterised by relatively high energy need for heating and cooling but the lowest electricity demand. Eventually, in the RT1 case, a single solution was found. This solution was characterised by low heating energy need and electricity demand.

Some additional comments on the shares of the electricity demand are provided. The energy need for artificial lighting was a function of the visible transmission coefficient of the selected windows. This explains why only window types 1 and 2 were selected in Palermo for the two-objective optimisation analyses; those windows were characterised by the best trade-off between a high visible transmission

coefficient and good thermal properties. With regard to the electricity use for the night ventilation fans, only a small variability was observed within the Pareto fronts, especially in Torino. Reasonably, there was no contrast with the cooling energy need (i.e. a high electricity use for night ventilation fans was associated to a high cooling energy need, and vice versa).

For completeness, the energy shares of the two-objective optimisation analyses are reported in Fig. 6.12. In Torino, the E_P reduction for the RT0 case was mainly obtained by decreasing the heating energy need. The group of solutions with the lowest global cost was simultaneously characterised by a high heating and cooling energy need although by the lowest electricity demand. All the solutions with PCM were characterised by a decreasing trend of the heating energy need, similar cooling energy need and a uniform electricity demand (same window type). In all the other cases in Torino and Palermo, the E_P reduction derived from a trade off between energy shares and was not driven by any of them. The electricity demand was however characterised by the most uniform values among the whole set of solutions.

To conclude, a multi-objective optimisation process as a mean of knowledge extraction would require at least four objective functions, i.e. building energy need for heating and cooling, electricity demand and investment cost. System efficiencies and the corresponding costs could be combined to the results of such an optimisation problem and become a criterion for the selection of the final solution.

Of course, additional functions to investigate other optimisation criteria, such as thermal and visual comfort or environmental impact would also be of interest. However, the greater the number of optimisation objectives, the longer the computational time, the more difficult the convergence to the true Pareto front and the analysis of the results are.

6.6   Comments on the component and building level results

Even though component and building level investigations are not directly comparable, a few comments can nevertheless be discussed. In both cases, the peak melting temperature of the PCM tended to drive the optimisation algorithm towards quite constant values. However, since the component level analyses considered a constant set point temperature which could differ each month, the preference was for the internal set-point temperature which was maintained for the longest time during the year. At the building level, where more variability of internal boundary conditions occurred, finding the optimal melting temperature was much less trivial. In the cases of Palermo and Torino, the choice of the PCM's melting temperature tended to be driven more by the free running conditions at night and during mid

season, in order to supply less energy to the building and therefore allowing for higher energy savings. In Oslo, the choice was mostly driven by a trade-off between diurnal and nocturnal set-point. Moreover, since the set point was on the operative temperature, the aim was of maintaining a high internal surface temperature in order to require less energy to condition the building at a lower air temperature.

With regard to the other PCM's thermo-physical properties, significant differences were observed. A preference towards a high melting temperature range was found from the component-level investigations in order for the PCM to undergo phase change during most of the year. However, at the building level, a low melting temperature range was found to be more beneficial in terms of energy performance. This is in line with the findings of other authors [88, 265]. Moreover, at the building-level a melting temperature range greater than 5 ℃ was indeed found to have no more influence on the results.

With regard to the latent heat of fusion, at the component level L was not clearly maximised due to the constraint which prevented to simultaneously maximise melting temperature range and latent heat of fusion. Since this did not occur at the building level, the latent heat of fusion was often maximised. However, both at the building and component level, a high latent heat of fusion could be seen as an indication that the PCM could effectively undergo melting and solidification cycles [181], even though this was much more clear at the building level.

With regard to the thermal conductivity, due to the variety of positions of the PCM within the wall, clear trends were difficult to be devised. However, at the component level, preferences towards low values were often observed. This is in line with the findings of other authors for PCM layers on the external side of the wall [181]. However, at the building level, the optimal thermal conductivity was found to be dependent on the peak melting temperature. This is in line with the findings in [181], where a careful selection of peak melting temperature and thermal conductivity was found to be desirable for PCM layers on the internal side of the wall. However, this was found to be even more important when the set-point temperature is not constant throughout the day.

Eventually, with regard to distribution of the layers within the wall, a general trend towards an external insulation layer and internal PCM was observed at the component level. In case of retrofit on both sides of the wall (RT2), an external insulation layer and an internal PCM layer were confirmed to be preferred in terms of energy performance, unless minimising investment (and therefore global) cost. However, at the building level, interaction with the windows was found to be fundamental, as thin insulation layers were preferred especially in cold climates to prevent excessive shading. The position of the windows should therefore be carefully selected. In existing buildings, changing the original position of the windows should be taken in serious consideration for improving the energy performance while reducing the retrofit costs, since aerogel insulation is a very expensive option.

In the three-objective optimisations in Torino, where both PCMs were often simultaneously selected, a closer similarity to the component-level results was found, as many solutions presented a wall layout with the following alternation of layers; external insulation, original wall, PCM1, insulation, PCM2.

However, in case of retrofit, just a negligible improvement in terms of heating energy need was found only for the solutions in the group of A's of the RT2 cases compared to retrofit intervention on the internal side of the wall, and the associated costs were significantly higher. Adopting a wall layout with a proper alternation of layers is therefore likely to be more beneficial in new buildings.

6.7   Design guidelines

Given the results of the building-level analyses and the subsequent investigations, a few design guidelines for the application of PCMs to the energy retrofit of office buildings can be provided. However, unless the PCM prices are significantly reduced, their application in the cases under investigation resulted not to be cost-effective. Nevertheless, sub-optimal solutions with a limited amount of PCM were found.

- Whenever possible, retrofit intervention on the internal side of the wall should be preferred, as it resulted to be the most cost-effective option.

- Whether the retrofit is performed on the internal or external side of the walls, the PCM should be placed in the closest position to the internal environment. The innermost position should be however preferred (this is in accordance with the findings from several authors [84, 88, 132, 181, 265]).

- In cooling-dominated climates with mild winters (such as Palermo), PCM can be effective for improving the winter performance of the building. In heating-dominated climates with mild summers (such as Torino), PCM can be effective for improving the summer performance of the building. However, among the investigated cases, a peak melting temperature suitable for winter application was found to be the best option for reducing the overall primary energy consumption regardless of the climate. It should be reminded that this result was found with the adoption of night cooling ventilation.

- When searching for commercial PCMs with thermo-physical properties close to the optimised values, priority should be given to peak melting temperature and latent heat of fusion, as these properties resulted be the most significant in deciding whether a solution belonged to the Pareto front ot not (as they generally assumed constant or almost constant values).

- When the application of PCM can be truly effective in reducing the building energy consumption, a high latent heat of fusion is strongly advisable.

- When the system operation does not imply a constant set-point temperature, peak melting temperature and thermal conductivity should be simultaneously optimised. Otherwise, among the PCM's thermo-physical properties, selecting an appropriate peak melting temperature has the greatest implications on the achievable energy savings.

- When a PCM with optimal or sub-optimal peak melting temperature is chosen, a low melting temperature range is preferable.

- At least within the investigated range of variation, increasing the thickness of PCMs with optimised properties can often imply a linear reduction of primary energy consumption.

Moreover, these strategies for PCM selection and application should be coupled with additional energy-saving measures. A low U-value was found to be especially important in all locations in case of retrofit intervention on the internal side or both sides of the wall to minimise both primary energy consumption and global cost. Window selection should also be accurately performed considering the trade-off between energy need for space heating and cooling, as well as electricity demand for daylighting. The use of aerogel insulation in case of retrofit on the external side of the building resulted to reduce the primary energy consumption due to a reduced shading in winter, but a higher investment cost—and therefore a higher global cost—would be implied in such a choice. Changing the position of the original window should therefore be taken into consideration for reducing both heating energy need and costs while adopting cheaper insulation materials.

Chapter 7

Conclusion

In the present thesis, a methodological approach for the design of opaque building envelope components with phase change materials through the application of optimisation analyses was proposed. Since multi-objective optimisation problems do not generally have a single solution, but result in a series of trade-off solutions called Pareto front, special attention was given to the post-optimisation analyses of the results. Rather than emphasising the objectives' values that could be reached by means of the optimisation procedure, the main focus was to investigate which values assumed by the optimisation variables led to the optimal set of solutions. In this way, the multi-objective optimisation analysis was used as a tool to gain knowledge on specific problems. In particular, three levels of analysis were explored; material level, component level and building level.

7.1 Material-level investigations

At the *material level*, the optimisation approach was applied to estimate the thermo-physical properties of PCMs through best-fit of experimental results. Although the use of phase change materials is promising to improve the energy efficiency of buildings, their application in the building sector is still very limited. One of the obstacles to the diffusion of PCMs is the lack of information regarding their thermo-physical properties. Many manufacturers do not provide data on the enthalpy-temperature curve of their products, or these data are not suitable for application in a building energy simulation tool. An optimisation approach was therefore applied as a method for estimating the enthalpy-temperature curve of PCMs through inverse modelling, in order to provide data that could be directly used in dynamic building energy simulation tools. Starting from heat flux measurements of a PCM sample which was subjected to controlled temperature variations on its surfaces (sinusoidal on one side and constant on the other side), an Evolution Strategy optimisation

algorithm was written and applied to search for the specific heat-temperature curve of the PCM which guaranteed the best fit between measured and simulated heat fluxes on both faces of the sample. The experimental measurements were carried out with a guarded hot plate and heat flow meter apparatus modified by the manufacturer to allow for sinusoidal temperature variations on its plates with a period of 24 hours and a pre-settable amplitude. The numerical simulation of the heat transfer process was carried out with a finite difference model written in Matlab language. The following of optimisation tests were carried out:

- *V1* case. The $c(T)$ curve was described by six variables according to eq. (4.1) (specific heat in solid and liquid phase, peak melting temperature, maximum specific heat and width coefficients of the solidification/melting peak).

- *VR* case. The contact resistances with the plates were added to the problem (eight variables).

- *VR2C* case. In order to consider a more complex shape of the $c(T)$ curve where a double peak could occur, the dependency of the specific heat on temperature was modelled as the sum of two curves; the contact resistances with the plates were also considered (fourteen variables).

The main results are briefly summarised.

- A very good agreement between measured and simulated data was found. The highest MAE and RMSE for the heat flux density, respectively 2.5 W/m^2 and 3.4 W/m^2 on the dynamic plate and 0.20 W/m^2 and 0.25 W/m^2 on the static plate, were obtained for the V1 estimate. Slight improvements were achieved in terms of MAE and RMSE with the VR and VR2C cases, even though they were characterised by increased MBE values.

- For all the estimates, a slight overestimation of the heat flux density was observed on the dynamic plate and underestimation on the static plate.

- Even though modelling the melting and solidification processes with the same $c(T)$ curve may lead to inaccuracies if a certain degree of hysteresis is present, satisfactory results were nevertheless obtained; all fits were characterised by R^2 greater than 0.98.

- The implementation of a model with temperature-dependent thermal conductivity should improve the results by removing a source of error.

The results of the inverse modelling procedure were additionally discussed in comparison with a low-speed (0.05 ℃/min) DSC measurement.

- The estimated value of peak melting temperature (19.0 ℃ on average) was lower than the nominal melting temperature of the PCM (21.7 ℃).

- The estimated peak melting temperature was close to that of the DSC solidification curve, whereas the maximum value of the specific heat was close to

that of the DSC melting curve.

- The specific heat in liquid phase was slightly underestimated. The upper temperature bound of the measurement should have been higher; with more data in full liquid state the model was proven to provide a better fit.

- High discrepancies were observed between the specific heat values in solid phase, but no measurement data was actually available in the full solid state for the model to fit.

- Experimental tests which cover a wider temperature range would allow for a more comprehensive characterisation of the PCM.

Moreover,

- The $c(T)$ curves resulting from the three fits overlapped on the right side of the peak melting temperature, while a higher discrepancy was observed on the left side of the peak and on the maximum value of the specific heat.

- The corresponding $h(T)$ curves resulted to be very similar within the validity range of the fit, while they diverged outside the validity bounds.

- All the enthalpy-temperature curves obtained with the inverse method resulted to be shifted towards lower temperatures than those from DSC. However, due to the narrow measurement range, the latent heat of fusion retrieved by means of the inverse procedure might be underestimated. According to the literature, the discrepancy between DSC and inverse data could be expected to differ mostly in the phase change range.

- No double peak was highlighted in the shape of the $c(T)$ curve despite the presence of multiple peaks on the apparent specific heat curve from the DSC in cooling mode.

- Although the VR2C provided the best fit among the three, adopting an increased number of variables resulted not to be worthy since the greater number of simulation runs did not lead to a significant improvement of the fit.

7.2 Component-level investigations

At the *component level*, to find a possible solution to the thermal characterisation of opaque building envelope components with PCM, a novel approach was proposed by introducing "equivalent" parameters related to the traditional dynamic thermal properties evaluated according to ISO 13786:2007. To consider boundary conditions representative of real building applications, a monthly equivalent periodic thermal transmittance and the corresponding time shift were defined by imposing steady-periodic conditions with monthly average external air temperature and

solar irradiance profiles while keeping a constant air temperature on the internal side. In this way, the monthly equivalent periodic thermal transmittance, Y_{mn}^*, was evaluated as the ratio of the difference between maximum and minimum value of the heat flux density through the surface of the component adjacent to the internal environment on the difference between maximum and minimum value of the sol-air temperature. The corresponding time shift, Δt_{mn}^*, was defined as the time difference between the maximum heat flux density through the surface of the component adjacent to the internal environment and the maximum value of the sol-air temperature. Eventually, the monthly equivalent values can be synthesised in a unique yearly value by means of a simple average. In this way, the characterisation is strictly related to the installation context (not only the specification of the location where the component is mounted is required, but also its orientation and solar absorptance), so the "equivalent" parameters provide information that can be effectively used to compare solutions for a specific application.

The influence of the PCM's thermo-physical properties on these "equivalent" parameters was analysed by means of a parametric analysis. This analysis was carried out on a set of six wall configurations characterised by a different order of the layers (masonry, insulation and PCM) for three locations (Palermo, Torino, and Oslo) and four wall orientations (south, east, north, and west). For each wall configuration, the investigated parametrisation variables were thickness, peak melting temperature and thermal conductivity of the PCM and solar absorption coefficient of the outer surface of the wall. The main results of this analysis are briefly summarised.

- An accurate choice of the PCM allowed to achieve significant improvements in terms of equivalent periodic thermal transmittance.

- Given a constant latent heat, wall configuration and PCM melting temperature had the greatest influence on the dynamic thermal performance.

- The effect of wall configuration on Y_{mn}^* was strong even in absence of phase transition, whereas its effect on the time shift was very limited in absence of phase transition, but it was strongly dependent on PCM melting temperature and boundary conditions during the phase change process.

- In general, higher time shifts were obtained when the PCM was placed on the internal side, whereas the lowest yearly Y_{mn}^* values were obtained for PCM in mid position.

- Decreasing the thermal conductivity of the PCM always resulted in a decrease of the equivalent periodic thermal transmittance and an increase in time shift.

- As the heat transfer is influenced by the thermal resistance of the layers within a wall, the thermal conductivity had a greater influence the thicker the PCM layer.

- The influence of the thermal conductivity on Y_{mn}^* was significant when the PCM was placed towards the outdoor environment and negligible when placed towards the indoor environment. However, when the PCM underwent phase transition, the influence of thermal conductivity on the time shift was significant for every PCM position within the wall.

- The melting temperature which guaranteed the lowest Y_{mn}^* was found to be dependent on the PCM thickness.

- A potential improvement in the yearly equivalent periodic thermal transmittance can be expected by a seasonal change in the PCM melting temperature (adoption of two PCMs with different melting temperatures).

- The effect of the solar absorption coefficient was strongly affected by PCM melting temperature and boundary conditions. According to the month, the same PCM could have been more effective with a low α (high values would have caused the PCM to remain mostly liquid) or with a high α (low values would have caused the PCM to remain mostly solid). Therefore, a direct analysis of the yearly values of Y_{mn}^* and Δt_{mn}^* would be of difficult interpretation.

- The more the PCM is placed towards the outdoor environment, the more the melting temperature of the PCM should be optimised according to the solar absorption coefficient and vice versa.

Once a metric for evaluating the dynamic thermal properties of opaque building envelope components with PCMs was defined, investigations were carried out to identify how to effectively apply PCMs in the building envelope. These analyses focused on the investigation of the best wall configuration (order of the layers) with the adoption of PCMs with at most two melting temperatures (lower or greater than 23 ℃). For this purpose, a parametric model was developed to describe PCM-enhanced multi-layer walls and, given a constant U-value, an optimisation analysis was carried out in the climates of Palermo, Torino and Oslo to find wall layout and PCMs' thermo-physical properties (melting temperature, melting temperature range, latent heat of fusion and thermal conductivity) which minimised yearly equivalent periodic thermal transmittance, overall PCM thickness and overall thickness of the wall. The optimisation analyses were performed through a Python implementation of the NSGA-II algorithm, which was made capable of exchanging information with the same Matlab code used at the material level.

Other than the application of the proposed equivalent periodic thermal transmittance for evaluating the thermal performance of opaque building envelope components with the inclusion of PCM, the novelty of such optimisation approach is that, to the best of the author's knowledge, no investigation on layer distribution and repetition within a wall with the inclusion of phase change materials has been

previously proposed, even less with the simultaneous presence of two PCMs with different thermo-physical properties.

The main results of these optimisation analyses are briefly summarised.

- For all the locations, the non-dominated sets for each orientation were extremely similar. The greatest differences could be observed in Palermo, where the west and east fronts were shifted closer to the zero of Y_{mn}^* than the south and north fronts (in accordance with the results of the parametric analyses).

- A certain degree of contrast was found between Y_{mn}^* and both PCM and wall thickness. No contrast was instead observed between PCM and wall thickness.

- Three points worth of interest were identified in the Pareto fronts. Solution A was characterised by the lowest equivalent periodic thermal transmittance. Due to the contrast between objectives, it was also the solution with highest PCM and wall thickness. Solution B was characterised by the lowest equivalent periodic thermal transmittance achieved with no PCM, whereas solution C was the solution with the lowest wall thickness. It was also characterised by the absence of PCM and the highest equivalent periodic thermal transmittance.

- With regard to the inter-climate differences, the variability of Y_{mn}^* within the Pareto front reasonably increased in warm climates. Moreover, the zone between the solutions in the group of B's and those in the in the group of A's in the Pareto front showed an asymptotic behaviour the colder the climate.

- For each orientation, the edge of the Pareto front between solutions in the group of C's and those in the group of B's was characterised by an increasing mass thickness from the lower to the upper bound, and it spanned the greatest variation in Y_{mn}^*. Given the very low values of Y_{mn}^* already achieved by the solutions in the group of B's, only a small improvement was obtained when adding PCM to such optimised walls.

- The effect of the PCM was far more significant when considering the impact on the overall wall thickness, especially in Palermo. Wall thickness in Torino resulted to have a smaller effect, and it was practically negligible in Oslo.

- The steepness of the Pareto front showed, on one hand, that the more the PCM, the less the influence of the traditional massive layers, as very similar Y_{mn}^* values could be achieved almost regardless of the masonry thickness. On the other hand, a limit on the PCM thickness beyond which no significant improvement could be obtained was highlighted.

- The PCM seemed to show its greatest potential in warm climates, where the same Y_{mn}^* values could be obtained either with a high thickness of mass and a proper alternation of massive and insulating layers, or with a much thinner

wall through the adoption of PCM. This could be especially useful for retrofit applications.

Post-optimisation analyses were eventually performed to investigate which combination of variables lead to the optimal solutions, in order to find design principles and common trends among the various case studies. A series of graphical analyses were carried out. Frequency analyses of the number of layers within the Pareto front solutions, as well as of the number of layers chosen for each material, were performed. The layers' distribution within the walls was also investigated. Box plots and frequency analyses of the variables belonging to the non-dominated sets were represented to find their range of variability and possible constant values. Moreover, the values assumed by each variable were mapped on the Pareto front, in order to explore how the search space variables affected the results in the objective space. The extreme solutions of the Pareto front were also depicted. The main results of the post-optimisation analyses are briefly summarised.

- A clear preference over an external insulation layer and an alternation between several insulating and "massive" (traditional or PCM) layers was found.

- In absence of PCM, a limit thickness beyond which the number of layers was increased (e.g. from two layers of mass and three of insulation to three layers of mass and four of insulation) was found.

- PCM started to be used to a much larger extent when the wall was made of six or more layers.

- In the cooling-dominated climate of Palermo, the "high-temperature" PCM (peak melting temperature greater than 23 ℃, referred to as PCM2) was generally preferred over the "low-temperature" PCM (peak melting temperature lower than 23 ℃, referred to as PCM1), whereas PCM1 was preferred in the heating-dominated climates of Torino and Oslo.

- As innermost layer, PCM2 tended to be preferred in Palermo, insulation in Torino, and PCM1 in Oslo.

- In Palermo, PCM1 was used to a larger extent on the west facing walls, where it was mostly placed in intermediate positions within the wall. Towards east, PCM1 was mostly placed just after the external insulation layer.

- In Torino, PCM1 was placed mostly in the last three layers close to the internal environment. PCM2 was used more scarcely and placed mostly in intermediate positions.

- In Oslo, PCM1 was almost always placed in the innermost position. When eight layers were selected in the south and west orientations, another layer of PCM1 was often added just after the external insulation layer.

- In Palermo, all the solutions shared a uniform peak melting temperature of PCM2 (26.5 ℃ on the north wall and 27 ℃ in the other cases). A preference

for a peak melting temperature of PCM1 of 21 ℃ towards south and east and a milder preference for 19 ℃ in the north and west façades were additionally found.

- In Torino, all the solutions shared a quite uniform peak melting temperature of PCM2 (25.5 ℃ on the north wall, 27 ℃ towards east and slightly more than 26 ℃ in the other cases). A mild preference for a peak melting temperature of PCM1 of 18 ℃ towards south and a clear preference for 19.5/20 ℃ in the north and west façades were additionally found.

- In Oslo, all the solutions shared a uniform peak melting temperature of PCM1 (20 ℃). Towards south and east, the very few solutions with PCM2 were characterised by a peak melting temperature of 23.5 ℃.

- Mild preferences over high values of melting temperature range and latent heat of fusion and over low values of thermal conductivity were mostly observed for both PCMs. However, these trends could respectively be clearly defined or almost negligible whether the PCM (either PCM1 or PCM2) was selected often or seldom according to the climate.

- Apart two exceptions, in all the locations and orientations the solutions in the group of C's (minimum wall thickness) were characterised by an alternation of three layers of insulation and two layers of mass. All the solutions in the group of B's (minimum equivalent periodic thermal transmittance achieved with no PCM) were instead characterised by an alternation of four layers of insulation and three layers of mass.

- In every location, all the solutions in the group pf A's (minimum Y^*_{mn}) were characterised by two layers of masonry on the south façade and a single one on the north-facing walls.

- In Palermo, the solutions in the group of A's were additionally characterised by an external insulation layer immediately followed by PCM1 and mostly by two layers of PCM placed in a sequence close to the indoor environment. The reason for placing PCM1 on the outer side of the wall just after the insulation layer was that it underwent phase transition during mid season and, when the melting temperature range was sufficiently wide, during winter as well.

- In Torino, most of the solutions in the group of A's were characterised by an external insulation layer and by PCM1 as the innermost layer.

- In Oslo, all the solutions in the group of A's were characterised by at least two thin layers of PCM1 on both sides of the wall; one of which was always placed as the innermost layer. According to its position, the outermost PCM1 layer underwent phase transition mostly during mid-season or summer months. Therefore, the same PCM could be used to enhance both winter and summer performance according to its position within the wall.

- The time shift of the solutions in the group of A's showed a great monthly variability, reaching about and even over 24 hours during some months. Generally, such a time shift would not be beneficial as the maximum of the temperature wave would overlap to the maximum of the heat flux wave of the previous day. However, in steady-periodic conditions the entity of the equivalent periodic thermal transmittance was such that the heat flux wave was almost flat, and this potential drawback could hence be ignored.

- Even though the optimisation algorithm was likely not to have found the true Pareto front, the information that can be extracted from the non-dominated set allows to identify improved solutions in a post-processing phase.

Furthermore, the relationship between monthly equivalent periodic thermal transmittance and the corresponding time shift for a variety of mutual positions of mass and insulation layers evenly distributed within the wall was evaluated for the sake of comparison (the overall thickness of mass and insulation was unvaried and no PCM was considered). For these wall configurations, the following results were found:

- On average, the worst performance in terms of Y_{mn}^* was obtained with a single layer of insulation in the middle of the wall and the mass evenly distributed on the sides.

- A correct distribution of the layers (especially placing the insulation in the outermost position) resulted to be more important than having a great amount of thermal mass.

- As the number of layers increased, the absolute value of the time shift always increased, but the equivalent periodic thermal transmittance did not continue to decrease. A minimum value (corresponding in Palermo to the configuration with three layers of mass and four layers of insulation) was found beyond which Y_{mn}^* started to increase again.

7.3   Building-level investigations

At the *building level*, the investigations focused on the application of optimisation analyses for the energy retrofit of office buildings. An archetype office building realised in Italy during the period 1946-1970 was chosen as a case study. The analyses were again carried out in the climates of Palermo, Torino and Oslo. The same building geometry was adopted for all locations, whereas the envelope properties were differentiated by country. Moreover, differences in the building envelope were highlighted in Oslo between buildings pre-1955 and post-1955. Since this difference regarded not only the insulation level of the buildings, but also the wall

typology—i.e. massive or lightweight walls—both cases were considered worth of investigation.

The optimisation analyses were performed considering three retrofit options on the opaque envelope components; intervention either on the external side of the wall, on the internal side of the wall, or on both sides of the wall. A parametric model to explore a variety of retrofit options for each case was developed. Intervention on the external side of the wall (RT0) was considered when interrupting or relocating the office activities during the renovation works was not possible. Intervention on the internal side of the wall (RT1) was considered for buildings subjected to laws on the conservation of historical buildings (in Italy, buildings older than 50 years). Intervention on both sides of the wall (RT2) was considered because, according to the literature for traditional walls, the periodic thermal transmittance is improved with a symmetrical layout and the insulation on the outermost layers, and according to the results from the component-level analyses, the periodic thermal transmittance of the wall is generally improved with an outer insulation layer and an inner PCM layer. Moreover, either the same wall solution for all the walls (NF1) or a different wall solution for each orientation (NF4) were considered. In both cases, a maximum of two PCM materials could be selected by the optimisation algorithm.

Window type, wall configuration, U-value of the wall, insulation and internal lining materials and PCMs' thermo-physical properties (peak melting temperature, melting temperature range, latent heat of fusion and thermal conductivity) were considered as optimisation variables. With regard to the optimisation objectives, the problem was faced under two points of view. On one side, optimisations were run with three objectives to minimise the building energy need for heating and cooling and the investment cost. On the other side, the optimisations were performed with two objectives to minimise primary energy consumption and global cost. Only for the climate of Oslo, where heating is mostly electric and no cooling system was considered, the minimisation objectives were primary energy consumption, global cost and thermal discomfort. The optimisation analyses were performed through a Python implementation of the NSGA-II algorithm, which was made capable of exchanging information with a building energy model developed in EnergyPlus.

To the best of the author's knowledge, no similar investigation on layer distribution within a wall of either new or existing building with the inclusion of phase change materials has been previously proposed, even less with the simultaneous presence of two PCMs with different thermo-physical properties. In the existing literature, investigations of the optimal application of PCMs for new and retrofitted buildings mostly involved simple parametric analyses; when true optimisation processes were adopted, they generally involved either single-objective analyses, or simulations explored only a short time window. Moreover, the comparison between several retrofit strategies and optimisation results according to the selected objective functions introduces an additional novelty to the present work.

As general notes to all the building-level analyses,

- The Pareto fronts in case of same retrofit solution for all the walls (NF1) mostly dominated those with a different wall solution for each orientation (NF4). Considering that the search space for the NF4 cases—and especially the RT2-NF4 case—was much wider than the NF1 case studies, the exploration level achieved by the GA was lower. Nevertheless, with an equal exploration level, broader regions of the NF4 Pareto fronts can be expected to outperform the NF1 cases. The computational time required to perform a deeper investigation would however be significantly higher.

- Even when the GA failed in finding the true optimal solutions for each objective, the information retrieved from the analyses of the Pareto solutions can allow to devise the properties of the true extreme solutions.

- Maximisation of the latent heat of fusion was identified as an indicator of how effectively a PCM undergoes melting and solidification cycles.

- When insulation was placed on the outer side of the wall (either in case of retrofit intervention on the external side or on both sides of the walls), the colder the climate, the more often aerogel was selected as insulation material for minimising the heating energy need. The reason for this choice was that, due to its low thermal conductivity, low U-values could obtained with a small thickness. This has a strong implication on shading; the less the added thickness, the more the available solar gains. The colder the climate, the more preventing excessive shading was found to be important.

- When the retrofit intervention implies acting on the internal side of the wall (RT1 and RT2 cases), a constraint on the overall wall thickness or floor surface reduction resulted to be desirable to avoid an excessively high added thickness; the lowest the net floor area, the lowest the commercial value of the building generally is.

The main results of the two-objective optimisation analyses in Palermo and Torino are reported. Due to the vast amount of results, for the sake of conciseness the information herewith summarised will mostly refer to the NF1 cases. Moreover, results were summarised by dividing them into the following categories:

1. Results shared by all the retrofit types in all the locations;
2. Results shared by all the retrofit types in a specific location;
3. Results shared by the same retrofit type in all the locations;
4. Results specific for a single retrofit type and location.

For each case, solution A refers to the best performing individual with respect to the primary energy consumption (it is therefore also the most expensive), whereas solution B refers to the individual with the lowest global cost but highest primary energy consumption.

The following results shared by all the retrofit types in all the locations were found:

- Retrofit on the internal side allowed to achieve a lower energy consumption with a lower global cost. The retrofit on the external side resulted instead to be the worst option.

- Out of the total population (100 individuals), only few solutions belonged to the non-dominated sets of the two-objective optimisations, whereas almost all the population belonged to the non-dominated sets of the three-objective analyses.

- With regard to the PCM selection, PCM1 was generally preferred over PCM2. In Palermo, being a cooling-dominated climate, choosing the low-temperature PCM may seem unexpected. However, PCM1 was found to have a stabilising effect on the internal temperature for a longer period of time, because the climatic conditions in winter and especially during mid-season are mild. Moreover, high temperatures in summer tended to be too extreme even for PCM2 to work effectively. On the other hand in Torino, since minimising the primary energy consumption in a heating-dominated climate implies mostly reducing the heating energy consumption, this result could be expected.

- The Pareto front was characterised by an increasing PCM thickness in order to decrease the primary energy consumption (hence increasing the global cost). However, the variation in primary energy consumption between best and worst solution within each Pareto front was very small, ranging only from 2 kWh/(m^{2}y) to 5 kWh/(m^{2}y). The difference in terms of global cost was much more significant.

- PCM was never selected for the solutions characterised by minimum global cost unless it could not be avoided (i.e. the only exceptions were the RT2 cases because intervening on both sides of the wall was imposed by the parametric model). The use of PCM resulted therefore not to be cost-optimal.

The following results shared by all the retrofit types within a location were found:

- In Palermo, only window types 2 (air filled DGU with low-emissivity coating on face 2) and window type 1 (air filled DGU with low-emissivity coating on face 3) were selected; since they were characterised by the same cost, choosing one instead of the other had an impact only the primary energy consumption. In particular, those windows were characterised by the best trade-off between good thermal properties and a high visible transmission coefficient in order to reduce the electricity consumption for artificial lighting.

- In Torino, almost only window type 7 (90%Ar filled TGU with low-emissivity coating on faces 3 and 5) and window type 4 (90%Ar filled DGU with low-emissivity coating on face 3) were selected. Window type 4 was the cheapest option but had a worse winter performance, whereas window type 7 was more expensive but the best option to reduce the heating energy consumption.

- In Torino, thermo-plaster was the preferred internal lining material.

The following results shared by the same retrofit type were found:

- In the RT0 and RT1 cases, almost all the solutions with only PCM1 were respectively characterised by wall types *ext1000* (insulation-PCM1-existing wall) and *int1100* (existing wall-insulation-PCM1). In the RT2 cases, wall type *ie100000* (PCM1-existing wall-insulation) was always selected for the solutions with only PCM1, whereas *ie300010* (PCM2-existing wall-PCM1-insulation) and *ie300011* (PCM2-existing wall-insulation-PCM1) were selected for the solutions with both PCMs.

- Very low U-values were selected with the exception of the RT0 case studies. For the RT1 – NF1 and RT2 – NF1, all the solutions shared a U-value equal to 0.15 W/(m^{2}K), i.e. the lower bound. In Palermo, even though the primary energy consumption for heating was lower than that for cooling, its reduction deriving from a lower U-value was greater than the consequent increase in primary energy consumption for cooling and night ventilation fans. In Torino, low U-values were preferred to reduce the heat losses through the opaque envelope in winter. Heating energy consumption was the most important aspect to minimise, and it was indeed effectively reduced.

- In the RT0 cases, the preferred insulation materials were XPS and EPS. The best performing but most expensive solutions adopted aerogel mats. In the RT1 cases, the preferred insulation material was EPS, whereas cork and EPS were mostly selected in the RT2 cases.

- With regard to the PCM properties, in the RT1 – NF1 cases all the solutions shared an almost constant peak melting temperature of PCM1 (20 ℃ in Palermo and 18.5 ℃ in Torino) and were characterised by medium/high thermal conductivity values. Moreover, a very high latent heat of fusion and a medium/low melting temperature range were selected both in the RT1 and RT0 cases. For the few solutions with also PCM2, in the RT1 – NF1 cases, an almost constant peak melting temperature was observed (24.6 ℃ in Palermo and 24.3 ℃ in Torino), together with a medium melting temperature range, medium/low latent heat of fusion and low thermal conductivity.

- In the RT2 cases, all solutions with only PCM1 were characterised by a constant thickness of 0.5 cm. When PCM2 was additionally introduced (with a thickness mostly of 0.5 cm), an increasing thickness of PCM1 could be observed for reducing the primary energy consumption. However, a higher variation for all properties of PCM1 was observed in comparison with RT0 and RT1 cases, likely due to the greater variability of the PCM's position within the wall.

- Solution A (minimum primary energy consumption) in the RT0 cases was characterised by aerogel insulation and 4.0 cm of PCM1 (with a melting

temperature of 20.5 ℃ in Palermo and 16.0 ℃ in Torino), characterised by a low melting temperature range, a high of latent heat of fusion and a high thermal conductivity. In the RT2 cases, solution A was instead characterised by a U-value of 0.15 W/(m²K), thermo-plaster and both PCMs. PCM2 was placed towards the external environment, whereas PCM1 was placed as the innermost layer after the thermo-plaster. Similar thermo-physical properties were selected for both PCMs. Different insulation materials were however selected in Palermo and Torino.

- Solution B (minimum global cost) was characterised by EPS insulation, lime and gypsum plaster (RT1 and RT2 cases) and no PCM. A U-value equal to the upper bound (i.e. the maximum value according to the national standard) was selected for the RT0 case, whereas a U-value equal to the lower bound (i.e. 0.15 W/(m²K)) was chosen for the RT1 and RT2 cases. Only in the RT2 case, 0.5 cm of PCM1 were placed as the outer layer. Since intervening on both sides could not be avoided, the most similar wall configuration to the solutions in the group of B's of the RT1 cases was found.

The following results for a specific retrofit type and location were found:

- When placed on the outer side of the wall (RT0), the peak melting temperature of PCM1 in Palermo tended to increase with the PCM thickness according to a specific relationship. The same occurred in the RT2 case, but a clear relationship could not be identified due to solutions with PCM1 placed on the internal side. On the other hand in Torino, the solutions in the RT0 case shared an almost constant peak melting temperature of PCM1 (16.9 ℃ on average), and its thickness tended to the upper bound (i.e. 4 cm).

- Solution A (minimum primary energy consumption) in the RT1 cases was characterised by a U-value of 0.15 W/(m²K) and EPS insulation. In Palermo, 4.0 cm for both PCMs were selected, and PCM2 was positioned closer to the internal environment. In Torino, only 1.0 cm was selected for PCM2, and the two PCMs' positions were inverted. Different internal lining materials were also selected (clay plaster in Palermo and thermo-plaster in Torino).

The main results of the three-objective optimisation analyses in Palermo and Torino are reported. With regard to the Pareto frontiers, the following characteristics were observed:

- The lowest building energy need for heating was obtained with retrofit intervention on both sides of the wall (RT2), whereas the lowest building energy need for cooling together with the lowest investment cost were achieved with intervention on the internal side (RT1). The only exception was the NF4 case in Torino; this was likely due to the lower exploration level reached by GA in that case. However, the solution characterised by the lowest heating energy need in the RT1 case had only a slightly lower performance but a

significantly lower investment cost.

- For all the cases in Palermo, the lowest investment cost was associated to a high building energy need for heating and cooling, yet not the highest. In Torino the lowest investment cost was instead associated to the highest building energy need for cooling. In both locations, the highest costs were found when simultaneously reducing the building energy need for heating and cooling. However, the greatest impact on investment cost was due to the reduction of building energy need for heating; achieving the lowest building energy need for cooling required only moderate (with respect to the range of variation of the Pareto front) investment costs both in Palermo and Torino.

- The greatest variation between best and worst optimised solution within each Pareto front was observed for the investment cost. Only a limited difference was observed for heating energy need in Palermo and cooling energy need in Torino.

The results from the post-optimisation analyses were summarised by dividing them into the aforementioned categories. For each case, solution A refers to the best performing individual with respect to the heating energy need, solution B was the individual with lowest cooling energy need, and solution C was characterised by the lowest investment cost.

The following results shared by all the retrofit types in all the locations were found:

- The Pareto fronts resulted to be strongly clustered by window type. Unlikely the two-objective analyses, all window types were selected. In the same way, all insulation and internal lining materials were used.

- Solution C was characterised by the cheapest materials; cheapest window type, the maximum allowed U-value, EPS insulation, lime and gypsum plaster (RT1 and RT2 cases), and no PCM except in the RT2 cases, where intervening on both sides could not be avoided. This solution was identical to solution B (minimum global cost) of the two-objective analyses in Torino, whereas a different window type was selected in Palermo.

The following results shared by all the retrofit types within a location were found:

- With regard to the PCM selection, in Palermo PCM1 was generally preferred over PCM2. Even though the Pareto front spanned a greater variation in cooling energy need, the adoption of PCM compared to the solutions without PCM resulted mainly to reduce the heating energy need. However, when reducing the cooling energy need, many solutions were also characterised by the simultaneous presence of both PCMs.

- In Torino, solutions characterised by PCM2 or both PCMs were selected more often than solutions with only PCM1. Even though the Pareto front spanned a greater variation in heating energy need, solutions with both PCMs were

especially able to simultaneously minimise both the energy need for heating and cooling.

- In Palermo, window type 0 (Air filled DGU) was chosen only for the solution with the lowest investment cost (solution C). The group of solutions which mounted window type 1 (air filled DGU with low-emissivity coating on face 3) was characterised by the highest cooling energy need, window type 3 (90%Ar filled DGU with selective coating on face 2) was chosen when reducing the cooling energy need, whereas window type 2 (air filled DGU with low-emissivity coating on face 2) was characterised by an intermediate energy performance. Although individuals with window type 1 were characterised by a better winter performance, the difference compared to window type 3 can be considered negligible.

- In Torino, window type 4 was used only by a small group of solutions characterised by the lowest investment cost and highest cooling energy need. Window type 5 (90%Ar filled DGU with low-emissivity coating on face 2), which was previously almost never selected, was used in the cluster characterised by the lowest cooling energy need and therefore highest heating energy need, and vice versa for window type 7 (90%Ar filled TGU with low-emissivity coating on faces 3 and 5).

- A narrow peak melting temperature of PCM2 around 25 ℃ was found in Torino, especially in the NF1 cases. The melting temperature range tended to assume medium/low values.

- High values of latent heat of fusion were selected for PCM1 in Palermo and for both PCMs in Torino, even though in the latter case the interquartile ranges were not very narrow.

- As for the two-objective cases, thermo-plaster was mostly selected in Torino as internal lining material in the solutions with both PCMs.

The following results shared by the same retrofit type were found:

- Regardless of the type and number of PCM layers, in the NF1 cases the PCM was placed between the existing wall and the external insulation in case of retrofit on the external side (RT0), whereas it was placed close to the internal environment in case of retrofit on the internal side (RT1).

- In case of retrofit either on the external (RT0) or internal side (RT1) and same retrofit solution for all the walls, the peak melting temperature of PCM2 was about 24/25 ℃.

- In case of retrofit on the internal side (RT1), solution A (minimum heating energy need) was characterised by the lowest U-value, aerogel insulation and 4.0 cm of only PCM1. Different internal lining materials, peak melting temperatures of PCM1 and obviously window types were however selected in Palermo and Torino.

- In case of retrofit on the external side (RT0), solution B (minimum cooling energy need) was characterised by the window type having the lowest g-value, the highest U-value allowed for the wall, maximum thickness of both PCM1 and PCM2, with PCM2 placed in the outermost position with respect to PCM1.

The following results for a specific retrofit type and location were found:

- In case of retrofit on the external side (RT0), the U-value in Palermo presented a clear trend within each cluster; high values corresponded to low cooling but high heating energy needs, and vice versa for low U-values. Torino's case was instead very different. Within each cluster, high U-values were mainly associated to a high heating energy need. However, both high and low U-values could lead to low cooling energy need. In case of retrofit on the internal side (RT1), high U-values were associated to a high heating energy need in Palermo, but there seemed to be almost no effect on the cooling energy need. In Torino, low U-values were instead selected for the majority of solutions, and especially by the trade-off solutions which minimised both heating and cooling energy need.

- In the RT0 and RT1 cases in Palermo, the Pareto front was characterised by an increasing PCM1 thickness in order to decrease heating and cooling energy needs (hence increasing the investment cost). In Torino, a high thickness of both PCMs was instead mostly selected in the RT0 case, especially for the solutions placed on the non-dominated set between heating and cooling energy need, whereas in the RT1 case an increasing thickness of PCM2 was observed in each cluster in order to decrease the cooling energy need.

- Similarly to the two-objective case, in case of retrofit on the external side (RT0) in Palermo, the peak melting temperature of PCM1 exhibited a slight tendency to increase with the layer's thickness. However, temperatures around 21.0 ℃ were mostly selected both in the RT0 and RT1 cases. Moreover, the solutions with PCM2 were mostly characterised by a peak melting temperature around 24.5 ℃.

- In the RT0 cases, solution A (minimum heating energy need) in Palermo was characterised by window type 1, a U-value of 0.15 W/(m²K), aerogel insulation and a high thickness of both PCM1 and PCM2. In Torino, solution A was quite similar to that of Palermo; the main differences were the selection of window type 7, the absence of PCM2 and a lower peak melting temperature for PCM1. This solution was almost identical to solution A of the corresponding two-objective optimisation (minimum primary energy consumption).

- In case of retrofit on the internal side (RT1), solution B (minimum cooling energy need) was characterised by the window type having the lowest g-value for each location, the highest U-value allowed for the wall in Palermo

and the lowest one in Torino, thermo-plaster, maximum thickness of both PCM1 and PCM2, with PCM1 placed in the innermost position with respect to PCM2.

The main results of optimisation analyses in Oslo are reported. With regard to the Pareto frontiers, the following characteristics were observed:

- Both in the case of retrofit of the pre-1955 and post-1955 building, intervention on the internal side (RT1) showed an advantage both in terms of energy performance and global cost. Intervention on both sides of the wall (RT2) could instead provide the maximum thermal comfort but to the detriment of the other two objectives.

- The lowest primary energy consumption and LPD could be respectively achieved by the post-1955 and pre-1955 buildings.

- The greatest variation between best and worst optimised solution within each Pareto front was observed for the global cost. The difference in primary energy consumption spanned between 9 kWh/(m^{2}y) and 23 kWh/(m^{2}y), whereas the variation in LPD was almost negligible. However, compared to the pre-retrofit building, thermal comfort was improved in the post-1955 case, whereas it remained almost unvaried in the pre-1955 case and indeed even worsened when global cost was minimised.

Similarly to the previous cases, results were summarised by dividing them into the following categories:

1. Results shared by all the retrofit types and pre-retrofit building (i.e. both pre-1955 and post-1955);

2. Results shared by all the retrofit types for a specific pre-retrofit building;

3. Results shared by the same retrofit type for all the pre-retrofit buildings;

4. Results specific for a single retrofit type and pre-retrofit building.

For each case, solution A refers to the best performing individual with respect to the primary energy consumption, solution B was the individual with lowest global cost, and solution C was characterised by the lowest Long-term Percentage of Dissatisfied.

The following results shared by all the retrofit types and buildings were found:

- PCM1 was clearly preferred over PCM2, and a very narrow peak melting temperature and a high latent heat of fusion were selected. Since the set-point was on the operative temperature, which was set to 21 ℃ with a nocturnal set-back of 19 ℃, the use of PCM could provide the advantage of requiring to maintain a lower air temperature during heating season by guaranteeing higher internal surface temperatures.

- Similarly to the previous three-objective optimisations, the Pareto fronts were clustered by window type. Window type 8, which was characterised by the highest U-value among the options available in Oslo, was almost never selected.

- Window type 10 (95%Kr filled TGU with low-emissivity coating on faces 3 and 5) was chosen for the solutions with the lowest primary energy consumption. Window type 9 (90%Ar filled TGU with low-emissivity coating on faces 3 and 5) was selected for medium energy performance and thermal comfort but lowest global cost, whereas window type 7 (90%Ar filled TGU with low-emissivity coating on faces 3 and 5 and smaller gap size compared to window type 9) characterised the solutions with the worst energy performance but which guaranteed the best thermal comfort.

- A positive effect of PCM1 was found both on primary energy consumption and thermal comfort. However, in the RT0 case for the post-1955 building, the effect on thermal comfort was still present but far less pronounced.

The following results shared by all the retrofit types for a single building were found:

- Medium/low melting temperature ranges were selected for PCM1 in the pre-1955 building, whereas in the post-1955 building medium melting temperature ranges were mostly chosen for the RT0 cases and low values for the RT1 and RT2 cases.

The following results shared by the same retrofit type for both buildings were found:

- A clear preference for aerogel insulation was observed in case of retrofit on the external side of the wall, whereas EPS (i.e. the cheapest insulation material) was mostly preferred for the other cases. In the RT1 cases, clay plaster was preferred as internal lining material.

- In case of retrofit on the external side (RT0), the Pareto front was strongly clustered by insulation material. Two main clusters were present; one cluster grouped the solutions with the lowest primary energy consumption but highest global cost, where only aerogel was selected, and the other cluster grouped all the other insulation materials. Moreover, window type had an additional subclustering effect.

- In the RT1 and RT2 cases, the Pareto front was clustered by PCM use and window type. In particular, solutions with both PCMs were clearly divided by the rest of the front due to their higher global cost. These solutions belonged the non-dominated set between primary energy consumption and LPD.

- In the RT0 and RT1 cases, solutions without PCM were located on the edge of the Pareto front with highest LPD and lowest cost.

- A peak melting temperature of PCM1 of about 19/19.5 ℃ was chosen for the RT1 and RT2 cases, whereas lower values were reasonably selected in case of retrofit intervention on the external side of the walls (RT0).

- In case of retrofit on the external side of the wall (RT0), solution A (minimum primary energy consumption) was characterised by a U-value of 0.15 W/(m^{2}K), aerogel insulation and 4.0 cm of PCM1.

- In case of retrofit on the external side of the wall (RT0), solution B (minimum global cost) was characterised by a U-value of 0.19 W/(m^{2}K), EPS insulation (i.e. the cheapest one) and no PCM. In case of retrofit on the internal side (RT1), a U-value of 0.15 W/(m^{2}K) was chosen (as it occurred also for Palermo and Torino in the two-objectives analyses), and lime and gypsum plaster was selected as internal lining material.

The following results for a specific retrofit type and pre-retrofit building were found:

- In the pre-1955 building, in the RT0 − NF1 and RT1 − NF1 cases the peak melting temperature of the few solutions with PCM2 varied within a narrow range.

- In the RT1 − NF1 case of the post-1955 building, all the solutions shared almost constant properties of both PCMs except for the thermal conductivity. The amount of solutions with PCM2 was however not significant.

- In case of retrofit on the external side of the wall (RT0) in the pre-1955 building, a trend could by identified within each of the two main clusters, for which the lowest U-values corresponded to the lowest primary energy consumption. Very low U-values were instead selected in the post-1955 building for all the solutions except for those simultaneously characterised by the worst energy performance and thermal comfort.

- In case of retrofit on the internal side (RT1), solution A (minimum primary energy consumption) was characterised by a U-value of 0.15 W/(m^{2}K), EPS insulation and 4.0 cm of PCM1 on the inner side of the wall. In the post-1955 building, an additional layer of PCM2 was also placed between the insulation and PCM1.

- In case of retrofit on both sides of the wall (RT2) for the pre-1955 building, solutions A and B were similar to the corresponding solutions of the RT1 case, with the addition of 5 mm of PCM2 on the outer side of the wall, which was selected only because an outer layer was imposed by the parametric model.

- In the pre-1955 building, solution C (minimum Long-term Percentage of Dissatisfied) was characterised by a U-value equal or close to the upper bound for the RT0 case and equal or close to the lower bound in the RT1

and RT2 cases. The opposite occurred in the post-1955 building. For both buildings, in the RT0 case PCM2 was placed as the outermost layer, followed by EPS insulation and PCM1. In the RT1 case, PCM1 was placed close to the internal environment followed by another layer of PCM2 and insulation. In the RT2 case, an external insulation layer and only PCM1 in the innermost layer were chosen.

Among the post-optimisation analyses of the building level investigations, automated innovization runs were performed to find relationships among variables and fitness functions. A summary of the innovization principles and information on their interpretation was presented. Overall, significant relationships were found to a greater extent under the following conditions: same retrofit solution for all the façades (NF1); retrofit intervention on a single side of the wall (i.e. RT0 and RT1); main use of only one PCM.

- When the innovization process involved more than one basis function, the identified parametric relationships were all linear with only one exception. This exception was the only relationship identified between variables and not between a variable and one or more fitness functions, and it was found between thickness and melting temperature of PCM1 in the RT0 – NF1 case of in Palermo (two-objective optimisation).

- Under a design perspective, finding more functional relationships among variables would have been more interesting. It is likely that the combinatorial nature of the problem and the excessive variability of the solutions (i.e. the application of two types of PCMs which could be used in different positions within the wall) reduced this possibility. Moreover, the non-dominated set needed to be sufficiently close to the true Pareto to be able to extract valuable knowledge from it.

- Relationships among variables and fitness functions can also be of interest, answering questions like: "What would the primary energy consumption be if x cm of PCM were installed?". However, relationships are not generally valid—e.g. it is not that "increasing PCM thickness will in any case reduce the primary energy consumption of x kWh/(m²y)"—but they are only valid for the optimised set of variables. If, for example, a constant peak melting temperature was found, the same relationship between E_P and PCM thickness would not apply to a different peak melting temperature.

- For the two-objective optimisation analyses in Palermo and Torino, all the NF1 solutions shared a constant U-value of 0.15 W/(m²K) in the RT1 and RT2 cases, and the same tended to occur for the corresponding NF4 solutions except on the east walls. Other relationships were found between thickness of PCM1 and primary energy consumption or global cost, and obviously between global cost and investment cost.

- For the three-objective optimisation analyses in Palermo and Torino, very few relationships were identified, and they were mainly of constant nature. A uniform peak melting temperature of PCM2 of 25 ℃ was identified for most of the cases in Torino.

- For the three-objective optimisation analyses in Oslo, a uniform peak melting temperature of PCM1 was identified for almost all the cases. Other relationships were found between the objective functions and thickness of PCM1 or U-value of the walls (within some clusters only), and obviously between global cost and investment cost.

To better investigate the effect of thermal conductivity of PCM on the optimality of the results and to analyse the mutual influence between thermal conductivity, peak melting temperature and melting temperature range, a few simple parametric analyses were additionally performed for a few sample cases in Torino.

With respect to the peak melting temperature, the following results were obtained.

- The objective space resulted to be divided in two separate regions with different trends. A local minimum was observed for peak melting temperatures around 18.5 ℃. This is in line with the literature, for which the optimal peak melting temperature should be approximately one or two degrees lower than the internal set-point temperature. However, the global minimum was found within another region characterised by lower peak melting temperatures. The reason behind the presence of these two regions is likely due to the system operation during daytime only. Therefore, as the internal air temperatures drop at night, a PCM melting temperature that reduces the difference between air and set-point temperatures when the heating system is activated in the morning allows for more significant energy savings than a melting temperature tuned for diurnal energy savings.

- Therefore, an optimisation procedure to search for the optimal thermophysical properties of PCMs can be especially useful when the system operation implies a non-trivial solution.

With respect to the melting temperature range, the following results were obtained.

- Beyond a melting temperature range of 5 ℃, energy need for heating and cooling were found not to change. This can explain why the optimisation algorithm almost never selected solutions with melting temperature ranges close to the upper bound.

- The minimum heating energy need resulted to be ensured with the lowest melting temperature range for peak melting temperatures within the optimal or sub-optimal range. However, as the peak melting temperature distanced from the optimal region, the melting temperature range corresponding to the minimum heating energy consumption increased up to the upper bound.

Moreover, the lower bound of the melting temperature range resulted to be optimal also for the peak melting temperature that ensured the lowest cooling energy need.

- Given the simultaneous optimality of the peak melting temperature, the best melting temperature range is the lowest possible. However, since the variation in energy performance for different melting temperature ranges in most of the objective space was limited, the lack of a clear trend towards the minimisation of ΔT among the GA solutions could be explained.

With respect to the thermal conductivity, the following results were obtained.

- Even though the reason behind the general lack of trends in the thermal conductivity of the PCM may be partly ascribed to the variety of positions of the PCM within the wall, the optimum thermal conductivity was found to be dependent on the PCM's melting temperature.

- The thermal conductivity which ensured the minimum energy need for heating was found within the exploration range. Outside the optimal ranges for the peak melting temperature, thermal conductivities equal to the lower bound ensured a slightly better performance. However, since the variation in $Q_{H,nd}$ for such temperatures was very limited, a randomness in the GA solutions could be expected unless the optimal peak melting temperature was found.

- With regard to the energy need for cooling, no region where the influence of thermal conductivity was significant with respect to that of the peak melting temperature was found.

- Given a peak melting temperature, the thermal conductivities which ensured the minimum energy need for heating and cooling were not the same.

- With regard to the primary energy consumption, the optimum was a trade-off between the results for heating and cooling energy need. The optimal thermal conductivity was however closer to the optimum value for the heating energy need due to its higher primary energy share.

- Finding the optimal thermal conductivity resulted not to be a trivial task due both to the complex non-linear shape of the objective space and to the need for a trade-off between heating and cooling.

- Overall, peak melting temperature, melting temperature range and thermal conductivity resulted to be strongly interconnected. Finding the optimal thermal conductivity was proven to be especially difficult when more energy objectives are simultaneously minimised. Convergence towards an optimal range is easier when only primary energy consumption is addressed.

Since performing an optimisation search directly on the primary energy consumption implies to fix the efficiency of the systems, different system efficiencies

would result in different Pareto fronts with their own set of design solutions. If an optimisation search was performed by simultaneously minimising each energy term, then the performance of such Pareto solutions could be investigated for various combinations of system efficiencies. In the same way, if the investment cost was also minimised, the global cost could be subsequently evaluated. This process has been tested for the NF1 case studies in Palermo and Torino. Primary energy consumption values associated to the Pareto fronts of the three-objectives optimisation analyses were parametrically evaluated. The following results were obtained.

- In Torino, a single solution for each case was identified as the best solution in terms of primary energy consumption regardless of the combination of system efficiencies.

- In Palermo, for the RT0 and RT2 retrofit options two solutions were identified as the best performing individuals according to the trade-off between system efficiencies.

- The choice of the best solution was driven by different energy needs according to both location and retrofit type. In Torino, the selection of the best performing individual was mostly driven by the heating energy need or by a trade-off between heating and cooling, whereas in Palermo reducing the electricity demand was especially important.

Eventually, given the results of the building-level analyses and the subsequent investigations, a few design guidelines for the application of PCMs to the energy retrofit of office buildings were provided. However, unless the PCM prices are significantly reduced, their application in the cases under investigation resulted not to be cost-effective. Nevertheless, sub-optimal solutions with a limited amount of PCM were found.

- Whenever possible, retrofit intervention on the internal side of the wall should be preferred, as it resulted to be the most cost-effective option.

- Whether the retrofit is performed on the internal or external side of the walls, the PCM should be placed in the closest position to the internal environment. The innermost position should be however preferred.

- When searching for commercial PCMs with thermo-physical properties close to the optimised values, priority should be given to peak melting temperature and latent heat of fusion.

- When the application of PCM can be truly effective in reducing the building energy consumption, a high latent heat of fusion is strongly advisable.

- When the system operation does not imply a constant set-point temperature, peak melting temperature and thermal conductivity should be simultaneously optimised. Otherwise, among the PCM's thermo-physical properties,

selecting an appropriate peak melting temperature has the greatest implications on the achievable energy savings.

- When a PCM with optimal or sub-optimal peak melting temperature is chosen, a low melting temperature range is preferable.

Moreover, these strategies for PCM selection and application should be coupled with additional energy-saving measures.

- In all the investigated locations, in case of retrofit intervention on the internal side or both sides of the wall a low U-value was found to minimise both primary energy consumption and global cost.

- Window selection should be accurately performed considering the trade-off between energy need for space heating and cooling, as well as electricity demand for daylighting.

- A limited thickness should be added on the outer side of the wall to prevent excessive shading. This can be especially achieved by using aerogel, or else changing the position of the original window should be taken into consideration when using insulation materials characterised by a higher thermal conductivity but lower costs.

7.4 Final remarks and future directions

A comprehensive analysis on PCM application in buildings has been carried out. Material-level investigations were performed to provide a methodology for retrieving the thermo-physical properties of PCMs to be used in building energy simulation tools, with the aim of overcoming the current limitations of measurement procedures such as DSC analyses. Component-level investigations were performed to explore the optimal layout of PCM-enhanced opaque building envelope components, by means of performance indicators which were introduced ad hoc. Eventually, building-level analyses concluded the investigations with the aim of expanding the existing knowledge of the application of PCMs in buildings, especially in case of energy retrofit of office buildings.

The significance of the present work is related to the novelty of both methodology and results. The proposed methodology can be of interest to a scientific audience, as it can be generalised to other optimisation problems. The investigated case studies and the results can be of interest to a scientific audience as well as to designers and practitioners, as they provide novel information on the optimal use of PCMs in energy retrofit applications, which was discovered considering both energy and cost related aspects.

Overall, a robust methodology to drive designers towards an informed choice of the final retrofit solution was provided. Indeed, as valuable and non-trivial information can be discovered through the post-optimisation analyses, exploring the properties of the non-dominated solutions resulting from a multi-objective search process proved to be a promising approach which can be applied to a wide variety of applications. Moreover, additional functions to investigate other optimisation criteria, such as thermal and visual comfort or environmental impact, would also be of interest when performing a multi-objective optimisation as a mean of knowledge extraction. However, the greater the number of optimisation objectives, the longer the computational time, the more difficult the convergence to the true Pareto front and the analysis of the results are.

As future work, at the material level the numerical model to describe PCM-enhanced opaque building envelope components could be improved in order to take variable thermal conductivity into account, and additional experimental measurements on a variety of PCMs could be performed to extensively investigate the performance of the inverse procedure in retrieving sufficiently accurate enthalpy-temperature curves under different conditions (e.g. higher level of hysteresis, etc.). On a higher scale, comparing the results of component and building level analyses performed by adopting the same parametric model of the wall and maintaining a constant set-point temperature within the building could allow to better investigate strengths and limitations of the proposed metrics for evaluating the dynamic thermal performance of PCM-enhanced opaque envelope components. Moreover, optimisation analyses of both opaque and transparent responsive envelope components could be of interest for a comprehensive investigation of the energy-saving potential deriving from the combined use of such technologies. Investigations on additional optimisation objectives, such as the environmental impact, would also be of interest to retrieve information on the overall energy use, which is a critical aspect in the application of PCMs. Furthermore, the post-optimisation process could be deepened by using data mining techniques to explore associations among variables, to extract decision rules, to group solutions according to interesting features, and to build estimation/prediction models. Data analytics supported by the expert knowledge on building physics could represent a powerful tool for making designers more aware of the implications of design choices according to contrasting objectives. Eventually, implementing some of the optimal solutions on real buildings and monitoring their energy performance would provide useful validation data.

References

[1] European Commission, Europe 2020. A European strategy for smart, sustainable and inclusive growth (2010).
URL http://ec.europa.eu/europe2020/

[2] Eurostat, Final energy consumption by sector (2014).
URL http://ec.europa.eu/eurostat/web/main/home

[3] Directive 2010/31/EU. European Parliament and of the Council of 19 May 2010 on the Energy Performance of Buildings (recast), Official Journal of the European Union (2010) 13–35.

[4] IEA-ECBCS, Annex 44 – Integrating Environmentally Responsive Elements in Buildings. Designing with Responsive Building Elements (2009).
URL http://www.ecbcs.org/annexes/annex44.htm

[5] EN ISO 13786:2007, Thermal performance of building components – Dynamic thermal characteristics – Calculation methods, International Organization for Standardization, Geneva, Switzerland, 2007.

[6] K. Deb, A. Srinivasan, Innovization: Innovative design principles through optimization, Kangal report number 2005007, Kanpur Genetic Algorithms Laboratory (KanGAL) – Indian Institute of Technology Kanpur (2005).

[7] S. Bandaru, K. Deb, Towards automating the discovery of certain innovative design principles through a clustering-based optimization technique, Engineering Optimization 43 (9) (2011) 911–941.

[8] S. Bandaru, K. Deb, Higher and lower-level innovizations for knowledge discovery in practical problems, Kangal report number 2011018, Department of Mechanical Engineering, Indian Institute of Technology Kanpur (2011).

[9] S. E. Kalnæs, B. P. Jelle, Phase change materials and products for building applications: A state-of-the-art review and future research opportunities, Energy and Buildings 94 (2015) 150–176.

[10] F. Souayfane, F. Fardoun, P.-H. Biwole, Phase change materials (PCM) for cooling applications in buildings: A review, Energy and Buildings 129 (2016) 396–431.

[11] J. P. Dumas, S. Gibout, P. Cézac, E. Franquet, D. Haillot, Model for the DSC thermograms of the melting of ideal binary solutions, Thermochimica Acta 571 (2013) 64–76.

[12] W. F. Smith, Foundation of Material Science and Engineering, 2nd Edition, McGrow-Hill, 1993.

[13] V. V. Tyagi, D. Buddhi, PCM thermal storage in buildings: A state of art, Renewable and Sustainable Energy Reviews 11 (6) (2007) 1146–1166.

[14] E. Osterman, V. Tyagi, V. Butala, N. Rahim, U. Stritih, Review of PCM based cooling technologies for buildings, Energy and Buildings 49 (2012) 37–49.

[15] J. Schröder, K. Gawron, Latent heat storage, Energy Research 5 (1981) 103–109.

[16] A. Kylili, P. A. Fokaides, Life Cycle Assessment (LCA) of Phase Change Materials (PCMs) for building applications: A review, Journal of Building Engineering 6 (2016) 133–143.

[17] H. Akeiber, P. Nejat, M. Z. A. Majid, M. A. Wahid, F. Jomehzadeh, I. Zeynali Famileh, J. K. Calautit, B. R. Hughes, S. A. Zaki, A review on phase change material (PCM) for sustainable passive cooling in building envelopes, Renewable and Sustainable Energy Reviews 60 (2016) 1470–1497.

[18] M. Kenisarin, Thermophysical properties of some organic phase change materials for latent heat storage. A review, Solar Energy 107 (2014) 553–575.

[19] M. Kenisarin, K. Mahkamov, Salt hydrates as latent heat storage materials: Thermophysical properties and costs, Solar Energy Materials and Solar Cells 145, Part 3 (2016) 255–286.

[20] B. Zalba, J. M. Marín, L. F. Cabeza, H. Mehling, Review on thermal energy storage with phase change: materials, heat transfer analysis and applications, Applied Thermal Engineering 23 (3) (2003) 251–283.

[21] C. Barreneche, A. Solé, L. Miró, I. Martorell, A. I. Fernández, L. F. Cabeza, Study on differential scanning calorimetry analysis with two operation modes and organic and inorganic phase change material (PCM), Thermochimica Acta 553 (2013) 23–26.

[22] F. Kuznik, D. David, K. Johannes, J.-J. Roux, A review on phase change materials integrated in building walls, Renewable and Sustainable Energy Reviews 15 (1) (2011) 379–391.

[23] H. Mehling, L. F. Cabeza, Heat and cold storage with PCM, Springer-Verlag, Berlin, 2008.

[24] Y. Cascone, M. Perino, Estimation of the thermal properties of PCMs through inverse modelling, Energy Procedia 78 (2015) 1714–1719.

[25] G. Buttitta, Y. Cascone, G. Serale, Enthalpy-temperature evaluation of slurry phase change materials with T-history method, Energy Procedia 78 (2015) 1877–1882.

[26] E. Franquet, S. Gibout, J.-P. Bédécarrats, D. Haillot, J.-P. Dumas, Inverse method for the identification of the enthalpy of phase change materials from calorimetry experiments, Thermochimica Acta 546 (2012) 61–80.

[27] T. Kousksou, A. Jamil, K. El Omari, Y. Zeraouli, Y. Le Guer, Effect of heating rate and sample geometry on the apparent specific heat capacity: DSC applications, Thermochimica Acta 519 (1-2) (2010) 59–64.

[28] F. Kuznik, K. Johannes, E. Franquet, L. Zalewski, S. Gibout, P. Tittelein, J. P. Dumas, D. David, J. P. Bédécarrats, S. Lassue, Impact of the enthalpy function on the simulation of a building with phase change material wall, Energy and Buildings 126 (2016) 220–229.

[29] E. Palomo del Barrio, J.-L. Dauvergne, A non-parametric method for estimating enthalpy-temperature functions of shape-stabilized phase change materials, International Journal of Heat and Mass Transfer 54 (5-6) (2011) 1268–1277.

[30] P. Tittelein, S. Gibout, E. Franquet, L. Zalewski, D. Defer, Identification of thermal

properties and thermodynamic model for a cement mortar containing PCM by using inverse method, Energy Procedia 78 (2015) 1696–1701.

[31] L. F. Cabeza, C. Barreneche, I. Martorell, L. Miró, S. Sari-Bey, M. Fois, H. O. Paksoy, N. Sahan, R. Weber, M. Constantinescu, E. M. Anghel, M. Malikova, I. Krupa, M. Delgado, P. Dolado, P. Furmanski, M. Jaworski, T. Haussmann, S. Gschwander, A. I. Fernández, Unconventional experimental technologies available for phase change materials (PCM) characterization. Part 1. Thermophysical properties, Renewable and Sustainable Energy Reviews 43 (2015) 1399–1414.

[32] G. W. H. Höhne, W. Hemminger, H. J. Flammersheim, Differential Scanning Calorimetry, Springer-Verlag, Berlin, 1996.

[33] C. Castellón, E. Günther, H. Mehling, S. Hiebler, L. F. Cabeza, Determination of the enthalpy of PCM as a function of temperature using a heat-flux DSC—A study of different measurement procedures and their accuracy, International Journal of Energy Research 32 (2008) 1258–1265.

[34] E. Günther, S. Hiebler, H. Mehling, R. Redlich, Enthalpy of phase change materials as a function of temperature: required accuracy and suitable measurement methods, International Journal of Thermophysics 30 (2009) 1257–1269.

[35] S. Gschwander, A. Lazaro, L. F. Cabeza, E. Günther, M. Fois, J. Chui, Development of a test-standard for PCM and TCM characterization – Part 1: Characterization of Phase Change Materials, Tech. rep., IEA Report A2.1 part 1. Task 42/Annex 24 (2011).

[36] ECES-IEA, Annex 17 – Implementing Agreement on Energy Conservation through Energy Storage. Advanced thermal energy storage through phase change materials and chemical reactions – Feasibility studies and demonstration projects (2005). URL http://www.ecbcs.org/annexes/annex17.htm

[37] A. Lazaro, C. Peñalosa, A. Solé, G. Diarce, T. Haussmann, M. Fois, B. Zalba, S. Gschwander, L. F. Cabeza, Intercomparative tests on phase change materials characterisation with differential scanning calorimeter, Applied Energy 109 (2013) 415–420.

[38] RAL, RAL-GZ 896 – Phase Change Material, Tech. rep., German Institute for Quality Assurance and Certification, Sankt Augustin (2009).

[39] H. Dong, J. Hunt, A numerical model for a heat flux DSC: Determining heat transfer coefficients within a DSC, Materials Science and Engineering: A 413-414 (2005) 470–473.

[40] Y. P. Zhang, Y. Jiang, J. Y., A simple method, the T-history method, of determining the heat of fusion, specific heat and thermal conductivity of phase-change materials, Measurement Science and Technology 10 (1999) 201–205.

[41] J. M. Marín, B. Zalba, L. F. Cabeza, H. Mehling, Determination of enthalpy-temperature curves of phase change materials with the temperature-history method: improvement to temperature dependent properties, Measurement Science and Technology 14 (2003) 184–189.

[42] B. Sandnes, J. Rekstad, Supercooling salt hydrates: Stored enthalpy as a function of temperature, Solar Energy 80 (2006) 616–625.

[43] E. D. Kravvaritis, K. A. Antonopoulos, C. Tzivanidis, Improvements to the measurement of the thermal properties of phase change materials, Measurement Science and Technology 21 (2010) 5103–5112.

[44] E. D. Kravvaritis, K. A. Antonopoulos, C. Tzivanidis, Experimental determination of the effective thermal capacity function and other thermal properties for various phase change materials using the thermal delay method, Applied Energy 88 (2011) 4459–4469.

[45] S. B. Stanković, P. A. Kyriacou, Improved measurement technique for the characterization of organic and inorganic phase change materials using the T-history method, Applied Energy 109 (2013) 433–440.

[46] A. Solé, L. Miró, C. Barreneche, I. Martorell, L. F. Cabeza, Review of the T-history method to determine thermophysical properties of phase change materials (PCM), Renewable and Sustainable Energy Reviews 26 (2013) 425–436.

[47] L. Gosselin, M. Tye-Gingras, F. Mathieu-Potvin, Review of utilization of genetic algorithms in heat transfer problems, International Journal of Heat and Mass Transfer 52 (2009) 2169–2188.

[48] M. Lachheb, M. Karkri, F. Albouchi, F. Mzali, S. Ben Nasrallah, Thermophysical properties estimation of paraffin/graphite composite phase change material using an inverse method, Energy Conversion and Management 82 (2014) 229–237.

[49] R. Cheng, M. Pomianowski, X. Wang, P. Heiselberg, Y. Zhang, A new method to determine thermophysical properties of PCM-concrete brick, Applied Energy 112 (2013) 988–998.

[50] M. Pomianowski, P. Heiselberg, R. L. Jensen, R. Cheng, Y. Zhang, A new experimental method to determine specific heat capacity of inhomogeneous concrete material with incorporated microencapsulated-PCM, Cement and Concrete Research 55 (2014) 22–34.

[51] M. Cui, X. Gao, J. Zhang, A new approach for the estimation of temperature-dependent thermal properties by solving transient inverse heat conduction problems, International Journal of Thermal Sciences 58 (2012) 113–119.

[52] P. Tittelein, S. Gibout, E. Franquet, K. Johannes, L. Zalewski, F. Kuznik, J.-P. Dumas, S. Lassue, J.-P. Bédécarrats, D. David, Simulation of the thermal and energy behaviour of a composite material containing encapsulated-PCM: Influence of the thermodynamical modelling, Applied Energy 140 (2015) 269–274.

[53] N. Soares, J. J. Costa, A. R. Gaspar, P. Santos, Review of passive PCM latent heat thermal energy storage systems towards buildings' energy efficiency, Energy and Buildings 59 (2013) 82–103.

[54] S. A. Memon, Phase change materials integrated in building walls: A state of the art review, Renewable and Sustainable Energy Reviews 31 (2014) 870–906.

[55] S.-G. Jeong, J. Jeon, J. Cha, J. Kim, S. Kim, Preparation and evaluation of thermal enhanced silica fume by incorporating organic PCM, for application to concrete, Energy and Buildings 62 (2013) 190–195.

[56] H. Cui, W. Liao, X. Mi, T. Y. Lo, D. Chen, Study on functional and mechanical properties of cement mortar with graphite-modified microencapsulated phase-change materials, Energy and Buildings 105 (2015) 273–284.

[57] T. Lecompte, P. Le Bideau, P. Glouannec, D. Nortershauser, S. Le Masson, Mechanical and thermo-physical behaviour of concretes and mortars containing phase change material, Energy and Buildings 94 (2015) 52–60.

[58] D. Zhou, C. Y. Zhao, Y. Tian, Review on thermal energy storage with phase change materials (PCMs) in building applications, Applied Energy 92 (2012) 593–605.

[59] L. F. Cabeza, A. Castell, C. Barreneche, A. de Gracia, A. I. Fernández, Materials used as PCM in thermal energy storage in buildings: A review, Renewable and Sustainable Energy Reviews 15 (3) (2011) 1675–1695.

[60] M. Pomianowski, P. Heiselberg, Y. Zhang, Review of thermal energy storage technologies based on PCM application in buildings, Energy and Buildings 67 (2013) 56–69.

[61] Y. Konuklu, M. Ostry, H. O. Paksoy, P. Charvat, Review on using microencapsulated phase change materials (PCM) in building applications, Energy and Buildings 106 (2015) 134–155, SI: IEA-ECES Annex 31 Special Issue on Thermal Energy Storage.

[62] V. V. Tyagi, S. C. Kaushik, S. K. Tyagi, T. Akiyama, Development of phase change materials based microencapsulated technology for buildings: A review, Renewable and Sustainable Energy Reviews 15 (2) (2011) 1373–1391.

[63] Y. E. Milián, A. Gutiérrez, M. Grágeda, S. Ushak, A review on encapsulation techniques for inorganic phase change materials and the influence on their thermophysical properties, Renewable and Sustainable Energy Reviews 73 (2017) 983–999.

[64] Y. P. Zhang, K. P. Lin, R. Yang, H. F. Di, Y. Jiang, Preparation, thermal performance and application of shape-stabilized PCM in energy efficient buildings, Energy and Buildings 38 (10) (2006) 1262–1269.

[65] G. Fang, F. Tang, L. Cao, Preparation, thermal properties and applications of shape-stabilized thermal energy storage materials, Renewable and Sustainable Energy Reviews 40 (2014) 237–259.

[66] M. Xiao, B. Feng, K. Gong, Thermal performance of a high conductive shape-stabilized thermal storage material, Solar Energy Materials and Solar Cells 69 (3) (2001) 293–296.

[67] Y. Zhang, J. Ding, X. Wang, R. Yang, K. Lin, Influence of additives on thermal conductivity of shape-stabilized phase change material, Solar Energy Materials and Solar Cells 90 (11) (2006) 1692–1702.

[68] S.-G. Jeong, J.-H. Lee, J. Seo, S. Kim, Thermal performance evaluation of bio-based shape stabilized PCM with boron nitride for energy saving, International Journal of Heat and Mass Transfer 71 (2014) 245–250.

[69] Y. Wu, T. Wang, Preparation and characterization of hydrated salts/silica composite as shape-stabilized phase change material via sol-gel process, Thermochimica Acta 591 (2014) 10–15.

[70] M. Xiao, B. Feng, K. Gong, Preparation and performance of shape stabilized phase change thermal storage materials with high thermal conductivity, Energy Conversion and Management 43 (1) (2002) 103–108.

[71] M. M. Kenisarin, K. M. Kenisarina, Form-stable phase change materials for thermal energy storage, Renewable and Sustainable Energy Reviews 16 (4) (2012) 1999–2040.

[72] P. Zhang, X. Xiao, Z. W. Ma, A review of the composite phase change materials: Fabrication, characterization, mathematical modeling and application to performance enhancement, Applied Energy 165 (2016) 472–510.

[73] M. N. Özışık, Heat Conduction, John Wiley & Sons, New York, 1993.

[74] Y. Dutil, D. R. Rousse, N. Ben Salah, S. Lassue, L. Zalewski, A review on phase-change materials: Mathematical modeling and simulations, Renewable and Sustainable Energy Reviews 15 (1) (2011) 112–130.

[75] S. N. Al-Saadi, Z. Zhai, Modeling phase change materials embedded in building enclosure: A review, Renewable and Sustainable Energy Reviews 21 (2013) 659–673.

[76] S. N. Al-Saadi, Z. J. Zhai, Systematic evaluation of mathematical methods and numerical schemes for modeling PCM-enhanced building enclosure, Energy and Buildings 92 (2015) 374–388.

[77] H. Hu, S. A. Argyropoulos, Mathematical modelling of solidification and melting: a review, Modelling and Simulation in Materials Science and Engineering 4 (1996) 371–396.

[78] J. Bony, S. Citherlet, Numerical model and experimental validation of heat storage with phase change materials, Energy and Buildings 39 (10) (2007) 1065–1072.

[79] E. Rodriguez-Ubinas, L. Ruiz-Valero, S. Vega, J. Neila, Applications of phase change material in highly energy-efficient houses, Energy and Buildings 50 (2012) 49–62.

[80] A. Waqas, Z. Ud Din, Phase change material (PCM) storage for free cooling of buildings—A review, Renewable and Sustainable Energy Reviews 18 (2013) 607–625.

[81] E. Rodriguez-Ubinas, B. Arranz Arranz, S. Vega Sánchez, F. J. Neila González, Influence of the use of PCM drywall and the fenestration in building retrofitting, Energy and Buildings 65 (2013) 464–476.

[82] S. Álvarez, L. F. Cabeza, A. Ruiz-Pardo, A. Castell, J. A. Tenorio, Building integration of PCM for natural cooling of buildings, Applied Energy 109 (2013) 514–522.

[83] R. Barzin, J. J. Chen, B. R. Young, M. M. Farid, Application of PCM energy storage in combination with night ventilation for space cooling, Applied Energy 158 (2015) 412–421.

[84] E. Solgi, R. Fayaz, B. M. Kari, Cooling load reduction in office buildings of hot-arid climate, combining phase change materials and night purge ventilation, Renewable Energy 85 (2016) 725–731.

[85] X. Xu, Y. Zhang, K. Lin, H. Di, R. Yang, Modeling and simulation on the thermal performance of shape-stabilized phase change material floor used in passive solar buildings, Energy and Buildings 37 (10) (2005) 1084–1091.

[86] H. Ye, L. Long, H. Zhang, R. Zou, The performance evaluation of shape-stabilized phase change materials in building applications using energy saving index, Applied Energy 113 (2014) 1118–1126.

[87] S. N. Al-Saadi, Z. J. Zhai, A new validated TRNSYS module for simulating latent heat storage walls, Energy and Buildings 109 (2015) 274–290.

[88] J. Lei, J. Yang, E.-H. Yang, Energy performance of building envelopes integrated with phase change materials for cooling load reduction in tropical Singapore, Applied Energy 162 (2016) 207–217.

[89] Y. Sun, S. Wang, F. Xiao, D. Gao, Peak load shifting control using different cold thermal energy storage facilities in commercial buildings: A review, Energy Conversion and Management 71 (2013) 101–114.

[90] K. Lin, Y. Zhang, X. Xu, H. Di, R. Yang, P. Qin, Experimental study of under-floor electric heating system with shape-stabilized PCM plates, Energy and Buildings 37 (3) (2005) 215–220.

[91] R. Barzin, J. J. J. Chen, B. R. Young, M. M. Farid, Application of PCM underfloor heating in combination with PCM wallboards for space heating using price based control system, Applied Energy 148 (2015) 39–48.

[92] P. Devaux, M. M. Farid, Benefits of PCM underfloor heating with PCM wallboards for space heating in winter, Applied Energy 191 (2017) 593–602.

[93] W. Cheng, B. Xie, R. Zhang, Z. Xu, Y. Xia, Effect of thermal conductivities of shape stabilized PCM on under-floor heating system, Applied Energy 144 (2015) 10–18.

[94] W. A. Qureshi, N.-K. C. Nair, M. M. Farid, Impact of energy storage in buildings on electricity demand side management, Energy Conversion and Management 52 (5) (2011) 2110–2120.

[95] R. Barzin, J. J. J. Chen, B. R. Young, M. M. Farid, Peak load shifting with energy storage and price-based control system, Energy 92, Part 3 (2015) 505–514.

[96] R. Barzin, J. J. J. Chen, B. R. Young, M. M. Farid, Application of weather forecast in conjunction with price-based method for PCM solar passive buildings – An experimental study, Applied Energy 163 (2016) 9–18.

[97] F. Kuznik, J. Virgone, K. Johannes, In-situ study of thermal comfort enhancement in a renovated building equipped with phase change material wallboard, Renewable Energy 36 (5) (2011) 1458–1462.

[98] G. Evola, L. Marletta, F. Sicurella, A methodology for investigating the effectiveness of PCM wallboards for summer thermal comfort in buildings, Building and Environment 59 (2013) 517–527.

[99] B. Nghana, F. Tariku, Phase change material's (PCM) impacts on the energy performance and thermal comfort of buildings in a mild climate, Building and Environment 99 (2016) 221–238.

[100] H. Jamil, M. Alam, J. Sanjayan, J. Wilson, Investigation of PCM as retrofitting option to enhance occupant thermal comfort in a modern residential building, Energy and Buildings 133 (2016) 217–229.

[101] F. Goia, M. Perino, V. Serra, Improving thermal comfort conditions by means of PCM glazing systems, Energy and Buildings 60 (2013) 442–452.

[102] J. S. Sage-Lauck, D. J. Sailor, Evaluation of phase change materials for improving thermal comfort in a super-insulated residential building, Energy and Buildings 79 (2014) 32–40.

[103] M. Saffari, A. de Gracia, S. Ushak, L. F. Cabeza, Economic impact of integrating PCM as passive system in buildings using Fanger comfort model, Energy and Buildings 112 (2016) 159–172.

[104] S. M. Sajjadian, J. Lewis, S. Sharples, The potential of phase change materials to reduce domestic cooling energy loads for current and future UK climates, Energy and Buildings 93 (2015) 83–89.

[105] T. Silva, R. Vicente, F. Rodrigue, Literature review on the use of phase change materials in glazing and shading solutions, Renewable and Sustainable Energy Reviews 53 (2016) 515–535.

[106] H. Johra, P. Heiselberg, Influence of internal thermal mass on the indoor thermal dynamics and integration of phase change materials in furniture for building energy storage: A review, Renewable and Sustainable Energy Reviews 69 (2017) 19–32.

[107] M. A. Izquierdo-Barrientos, J. F. Belmonte, D. Rodríguez-Sánchez, A. E. Molina, J. A. Almendros-Ibáñez, A numerical study of external building walls containing phase change materials (PCM), Applied Thermal Engineering 47 (2012) 73–85.

[108] T. Silva, R. Vicente, N. Soares, V. Ferreira, Experimental testing and numerical modelling of masonry wall solution with PCM incorporation: A passive construction solution, Energy and Buildings 49 (2012) 235–245.

[109] R. Vicente, T. Silva, Brick masonry walls with PCM macrocapsules: An experimental approach, Applied Thermal Engineering 67 (1–2) (2014) 24–34.

[110] X. Jin, M. A. Medina, X. Zhang, On the placement of a phase change material thermal shield within the cavity of buildings walls for heat transfer rate reduction, Energy 73 (2014) 780–786.

[111] K. O. Lee, M. A. Medina, E. Raith, X. Sun, Assessing the integration of a thin phase change material (PCM) layer in a residential building wall for heat transfer reduction and management, Applied Energy 137 (2015) 699–706.

[112] P. Schossig, H.-M. Henning, S. Gschwander, T. Haussmann, Micro-encapsulated phase-change materials integrated into construction materials, Solar Energy Materials and Solar Cells 89 (2–3) (2005) 297–306.

[113] Y. Kusama, Y. Ishidoya, Thermal effects of a novel phase change material (PCM) plaster under different insulation and heating scenarios, Energy and Buildings 141 (2017) 226–237.

[114] M. Lachheb, Z. Younsi, H. Naji, M. Karkri, S. Ben Nasrallah, Thermal behavior of a hybrid PCM plaster: A numerical and experimental investigation, Applied Thermal Engineering 111 (2017) 49–59.

[115] A. Oliver, Thermal characterization of gypsum boards with PCM included: Thermal energy storage in buildings through latent heat, Energy and Buildings 48 (2012) 1–7.

[116] A. M. Borreguero, M. L. Sánchez, J. L. Valverde, M. Carmona, J. F. Rodríguez, Thermal testing and numerical simulation of gypsum wallboards incorporated with different PCMs content, Applied Energy 88 (3) (2011) 930–937.

[117] K. Biswas, J. Lu, P. Soroushian, S. Shrestha, Combined experimental and numerical evaluation of a prototype nano-PCM enhanced wallboard, Applied Energy 131 (2014) 517–529.

[118] X. Wang, H. Yu, L. Li, M. Zhao, Experimental assessment on a kind of composite wall incorporated with shape-stabilized phase change materials (SSPCMs), Energy and Buildings 128 (2016) 567–574.

[119] X. Wang, H. Yu, L. Li, M. Zhao, Experimental assessment on the use of phase change materials (PCMs)-bricks in the exterior wall of a full-scale room, Energy Conversion and Management 120 (2016) 81–89.

[120] G. Diarce, A. Campos-Celador, K. Martin, A. Urresti, A. García-Romero, J. Sala, A comparative study of the CFD modeling of a ventilated active façade including phase change materials, Applied Energy 126 (2014) 307–317.

[121] A. de Gracia, L. Navarro, A. Castell, L. F. Cabeza, Energy performance of a ventilated double skin facade with PCM under different climates, Energy and Buildings 91 (2015) 37–42.

[122] J. Kośny, E. Kossecka, A. Brzezinski, A. Tleoubaev, D. Yarbrough, Dynamic thermal performance analysis of fiber insulations containing bio-based phase change materials (PCMs), Energy and Buildings 52 (2012) 122–131.

[123] J. Kośny, A. Fallahi, N. Shukla, E. Kossecka, A. Ramin, Thermal load mitigation and passive cooling in residential attics containing PCM-enhanced insulations, Solar Energy 108 (2014) 164–177.

[124] K. Biswas, R. Abhari, Low-cost phase change material as an energy storage medium in building envelopes: Experimental and numerical analyses, Energy Conversion and Management 88 (2014) 1020–1031.

[125] K. El Omari, Y. Le Guer, P. Bruel, Analysis of micro-dispersed PCM-composite boards behavior in a building's wall for different seasons, Journal of Building Engineering 7 (2016) 361–371.

[126] G. Zhou, Y. Zhang, X. Wang, K. Lin, W. Xiao, An assessment of mixed type PCM-gypsum and shape-stabilized PCM plates in a building for passive solar heating, Solar Energy 81 (11) (2007) 1351–1360.

[127] D. David, F. Kuznik, J.-J. Roux, Numerical study of the influence of the convective heat transfer on the dynamical behaviour of a phase change material wall, Applied Thermal Engineering 31 (16) (2011) 3117–3124.

[128] H. Liu, H. B. Awbi, Performance of phase change material boards under natural convection, Building and Environment 44 (9) (2009) 1788–1793.

[129] G. Evola, L. Marletta, F. Sicurella, Simulation of a ventilated cavity to enhance the effectiveness of PCM wallboards for summer thermal comfort in buildings, Energy and Buildings 70 (2014) 480–489.

[130] B. M. Diaconu, Thermal energy savings in buildings with PCM-enhanced envelope: Influence of occupancy pattern and ventilation, Energy and Buildings 43 (1) (2011) 101–107.

[131] F. Ascione, N. Bianco, R. F. De Masi, F. de' Rossi, G. P. Vanoli, Energy refurbishment of existing buildings through the use of phase change materials: Energy savings and indoor comfort in the cooling season, Applied Energy 113 (2014) 990–1007.

[132] A. Buonomano, G. De Luca, U. Montanaro, A. Palombo, Innovative technologies for NZEBs: An energy and economic analysis tool and a case study of a non-residential building for the Mediterranean climate, Energy and Buildings 121 (2016) 318–343.

[133] A. Pasupathy, R. Velraj, Effect of double layer phase change material in building roof for year round thermal management, Energy and Buildings 40 (3) (2008) 193–203.

[134] N. Zhu, P. Hu, L. Xu, A simplified dynamic model of double layers shape-stabilized phase change materials wallboards, Energy and Buildings 67 (2013) 508–516.

[135] M. Kheradmand, M. Azenha, J. L. B. de Aguiar, J. a. Castro-Gomes, Experimental and numerical studies of hybrid PCM embedded in plastering mortar for enhanced thermal behaviour of buildings, Energy 94 (2016) 250–261.

[136] A. Zastawna-Rumin, K. Nowak, Experimental research of a partition composed of two layers of different types of PCM, Energy Procedia 91 (2016) 259–268, Proceedings of the 4th International Conference on Solar Heating and Cooling for Buildings and Industry (SHC 2015).

[137] F. Ascione, R. F. De Masi, F. de Rossi, S. Ruggiero, G. P. Vanoli, Optimization of building envelope design for nZEBs in Mediterranean climate: Performance analysis of residential case study, Applied Energy 183 (2016) 938–957.

[138] N. Zhu, P. Liu, P. Hu, F. Liu, Z. Jiang, Modeling and simulation on the performance of a novel double shape-stabilized phase change materials wallboard, Energy and Buildings 107 (2015) 181–190.

[139] N. Zhu, P. Liu, F. Liu, P. Hu, M. Wu, Energy performance of double shape-stabilized phase change materials wallboards in office building, Applied Thermal Engineering 105 (2016) 180–188.

[140] A. Jayalath, L. Aye, P. Mendis, T. Ngo, Effects of phase change material roof layers on thermal performance of a residential building in Melbourne and Sydney, Energy and Buildings 121 (2016) 152–158.

[141] E. M. Alawadhi, H. J. Alqallaf, Building roof with conical holes containing PCM to reduce the cooling load: Numerical study, Energy Conversion and Management 52 (8−9) (2011) 2958−2964.

[142] H. J. Alqallaf, E. M. Alawadhi, Concrete roof with cylindrical holes containing PCM to reduce the heat gain, Energy and Buildings 61 (2013) 73−80.

[143] D. Li, Y. Zheng, C. Liu, G. Wu, Numerical analysis on thermal performance of roof contained PCM of a single residential building, Energy Conversion and Management 100 (2015) 147−156.

[144] J. Lei, K. Kumarasamy, K. T. Zingre, J. Yang, M. P. Wan, E.-H. Yang, Cool colored coating and phase change materials as complementary cooling strategies for building cooling load reduction in tropics, Applied Energy 190 (2017) 57−63.

[145] S. Lu, Y. Chen, S. Liu, X. Kong, Experimental research on a novel energy efficiency roof coupled with PCM and cool materials, Energy and Buildings 127 (2016) 159−169.

[146] T. Karlessi, M. Santamouris, A. Synnefa, D. Assimakopoulos, P. Didaskalopoulos, K. Apostolakis, Development and testing of PCM doped cool colored coatings to mitigate urban heat island and cool buildings, Building and Environment 46 (3) (2011) 570−576.

[147] K. K. Roman, T. O'Brien, J. B. Alvey, O. Woo, Simulating the effects of cool roof and PCM (phase change materials) based roof to mitigate UHI (urban heat island) in prominent US cities, Energy 96 (2016) 103−117.

[148] M. H. Chung, J. C. Park, Development of PCM cool roof system to control urban heat island considering temperate climatic conditions, Energy and Buildings 116 (2016) 341−348.

[149] B. L. Gowreesunker, S. B. Stankovic, S. A. Tassou, P. A. Kyriacou, Experimental and numerical investigations of the optical and thermal aspects of a PCM-glazed unit, Energy and Buildings 61 (2013) 239−249.

[150] F. Goia, M. Perino, V. Serra, Experimental analysis of the energy performance of a full-scale PCM glazing prototype, Solar Energy 100 (2014) 217−233.

[151] S. Li, G. Sun, K. Zou, X. Zhang, Experimental research on the dynamic thermal performance of a novel triple-pane building window filled with PCM, Sustainable Cities and Society 27 (2016) 15−22.

[152] K. A. R. Ismail, J. R. Henríquez, Parametric study on composite and PCM glass systems, Energy Conversion and Management 43 (7) (2002) 973−993.

[153] K. A. R. Ismail, C. T. Salinas, J. R. Henríquez, Comparison between PCM filled glass windows and absorbing gas filled windows, Energy and Buildings 40 (5) (2008) 710−719.

[154] F. Goia, Thermo-physical behaviour and energy performance assessment of PCM glazing system configurations: A numerical analysis, Frontiers of Architectural Research 1 (4) (2012) 341−347.

[155] K. Zhong, S. Li, G. Sun, S. Li, X. Zhang, Simulation study on dynamic heat transfer performance of PCM-filled glass window with different thermophysical parameters of phase change material, Energy and Buildings 106 (2015) 87−95, SI: IEA-ECES Annex 31 Special Issue on Thermal Energy Storage.

[156] D. Li, T. Ma, C. Liu, Y. Zheng, Z. Wang, X. Liu, Thermal performance of a PCM-filled double glazing unit with different optical properties of phase change material, Energy and Buildings 119 (2016) 143−152.

[157] D. Li, Z. Li, Y. Zheng, C. Liu, A. Kadhim, X. Liu, Thermal performance of a PCM-filled double-glazing unit with different thermophysical parameters of PCM, Solar Energy 133 (2016) 207–220.

[158] F. Goia, M. Perino, M. Haase, A numerical model to evaluate the thermal behaviour of PCM glazing system configurations, Energy and Buildings 54 (2012) 141–153.

[159] C. Liu, Y. Zheng, D. Li, H. Qi, X. Liu, A model to determine thermal performance of a non-ventilated double glazing unit with PCM and experimental validation, Procedia Engineering 157 (2016) 293–300, selected Papers from IX International Conference on Computational Heat and Mass Transfer (ICCHMT2016).

[160] F. Goia, M. Zinzi, E. Carnielo, V. Serra, Characterization of the optical properties of a PCM glazing system, Energy Procedia 30 (2012) 428–437, 1st International Conference on Solar Heating and Cooling for Buildings and Industry (SHC 2012).

[161] F. Goia, M. Zinzi, E. Carnielo, V. Serra, Spectral and angular solar properties of a PCM-filled double glazing unit, Energy and Buildings 87 (2015) 302–312.

[162] D. Li, Y. Zheng, Z. Li, H. Qi, Optical properties of a liquid paraffin-filled double glazing unit, Energy and Buildings 108 (2015) 381–386.

[163] F. Goia, L. Bianco, Y. Cascone, M. Perino, V. Serra, Experimental analysis of an advanced dynamic glazing prototype integrating pcm and thermotropic layers, Energy Procedia 48 (2014) 1272–1281.

[164] G. Evola, L. Marletta, The effectiveness of PCM wallboards for the energy refurbishment of lightweight buildings, Energy Procedia 62 (2014) 13–21.

[165] X. Sun, Q. Zhang, M. A. Medina, K. O. Lee, Energy and economic analysis of a building enclosure outfitted with a phase change material board (PCMB), Energy Conversion and Management 83 (2014) 73–78.

[166] X. Mi, R. Liu, H. Cui, S. A. Memo, F. Xing, Y. Lo, Energy and economic analysis of building integrated with PCM in different cities of China, Applied Energy 175 (2016) 324–336.

[167] A. Baniassadi, B. Sajadi, M. Amidpour, N. Noori, Economic optimization of PCM and insulation layer thickness in residential buildings, Sustainable Energy Technologies and Assessments 14 (2016) 92–99.

[168] Y. DutiL, D. Rousse, S. Lassue, L. Zalewski, A. Joulin, J. Virgone, F. Kuznik, K. Johannes, J.-P. Dumas, J.-P. Bédécarrats, A. Castell, L. F. Cabeza, Modeling phase change materials behavior in building applications: Comments on material characterization and model validation, Renewable Energy 61 (2014) 132–135.

[169] U.S. Department of Energy, EnergyPlus Engineering Reference – The Reference to EnergyPlus Calculations, Office of Energy Efficiency and Renewable Energy, United States (2013).

[170] P. C. Tabares-Velasco, C. Christensen, M. Bianchi, Verification and validation of EnergyPlus phase change material model for opaque wall assemblies, Building and Environment 54 (2012) 186–196.

[171] University of Strathclyde, ESP-r (2012).
URL http://www.esru.strath.ac.uk/Programs/ESP-r.htm

[172] F. Almeida, D. Zhang, A. S. Fung, W. H. Leong, Comparison of corrective Phase Change Material algorithm with ESP-r simulation, in: Proc. of Building Simulation 2011: 12th Conference of International Building Performance Simulation Association, Sydney, Australia, 14-16 November 2011, pp. 2538–2543.

[173] Solar Energy Laboratory, TRNSYS 17, University of Wisconsin-Madison, Madison (2013).

[174] M. Ibáñez, A. Lázar, B. Zalba, L. F. Cabeza, An approach to the simulation of PCMs in building applications using TRNSYS, Applied Thermal Engineering 25 (11-12) (2005) 1796–1807.

[175] F. Kuznik, J. Virgone, K. Johannes, Development and validation of a new TRNSYS type for the simulation of external building walls containing PCM, Energy and Buildings 42 (7) (2010) 1004–1009.

[176] C. Carbonaro, Y. Cascone, S. Fantucci, V. Serra, M. Perino, M. Dutto, Energy assessment of a PCM-embedded plaster: Embodied energy versus operational energy, Energy Procedia 78 (2015) 3210–3215.

[177] ISO 14040/44:2006, Environmental Management – Life cycle assessment, International Organization for Standardization, Geneva, Switzerland, 2006.

[178] A. de Gracia, L. Rincón, A. Castell, M. Jiménez, D. Boer, M. Medrano, L. F. Cabeza, Life Cycle Assessment of the inclusion of phase change materials (PCM) in experimental buildings, Energy and Buildings 42 (9) (2010) 1517–1523.

[179] K. Menoufi, A. Castell, M. M. Farid, D. Boer, L. F. Cabeza, Life Cycle Assessment of experimental cubicles including PCM manufactured from natural resources (esters): A theoretical study, Renewable Energy 51 (2013) 398–403.

[180] K. Menoufi, A. Castell, L. Navarro, G. Pérez, D. Boer, L. F. Cabeza, Evaluation of the environmental impact of experimental cubicles using Life Cycle Assessment: A highlight on the manufacturing phase, Applied Energy 92 (2012) 534–544.

[181] Y. Zhang, K. Lin, Y. Jiang, G. Zhou, Thermal storage and nonlinear heat-transfer characteristics of PCM wallboard, Energy and Buildings 40 (9) (2008) 1771–1779.

[182] G. Zhou, Y. Yang, X. Wang, J. Cheng, Thermal characteristics of shape-stabilized phase change material wallboard with periodical outside temperature waves, Applied Energy 87 (2010) 2666–2672.

[183] S. Ramakrishnan, X. Wang, M. Alam, J. Sanjayan, J. Wilson, Parametric analysis for performance enhancement of phase change materials in naturally ventilated buildings, Energy and Buildings 124 (2016) 35–45.

[184] L. Royon, L. Karim, A. Bontemps, Optimization of PCM embedded in a floor panel developed for thermal management of the lightweight envelope of buildings, Energy and Buildings 82 (2014) 385–390.

[185] A. Castell, M. M. Farid, Experimental validation of a methodology to assess PCM effectiveness in cooling building envelopes passively, Energy and Buildings 81 (2014) 59–71.

[186] F. Sicurella, G. Evola, E. Wurtz, A statistical approach for the evaluation of thermal and visual comfort in free-running buildings, Energy and Buildings 47 (2012) 402–410.

[187] T. Méndez Echenagucia, A. Capozzoli, Y. Cascone, M. Sassone, The early design stage of a building envelope: Multi-objective search through heating, cooling and lighting energy performance analysis, Applied Energy 154 (2015) 577–591.

[188] K. Deb, Multi-Objective Optimization Using Evolutionary Algorithms, John Wiley & Sons, Chichester, 2001.

[189] V. Pareto, Cours d'economie politique, F. Rouge, Lausanne, 1896.

[190] T. Méndez Echenagucia, Computational search in architectural design, Ph.D. thesis, Politecnico di Torino, Italy (2014).

[191] Y. Zhang, 'Parallel' EnergyPlus and the development of a parametric analysis tool, in: Proceedings of IBPSA BS2009, Glasgow, UK, 27-30 July 2009.

[192] Y. Zhang, I. Korolija, Performing complex parametric simulations with jEPlus, in: Proceedings of SET2010 – 9th International Conference on Sustainable Energy Technologies, Shanghai, China, 24-27 August 2010.

[193] T. Weise, Global Optimization Algorithms – Theory and Application, 2nd Edition, Self-Published, 2009.
URL http://www.it-weise.de/projects/book.pdf

[194] S. Attia, M. Hamdy, W. O'Brien, S. Carlucci, Assessing gaps and needs for integrating building performance optimization tools in net zero energy buildings design, Energy and Buildings 60 (2013) 110–124.

[195] V. Machairas, A. Tsangrassoulis, K. Axarli, Algorithms for optimization of building design: A review, Renewable and Sustainable Energy Reviews 31 (2014) 101–112.

[196] C. A. Coello Coello, Theoretical and numerical constraint-handling techniques used with evolutionary algorithms: a survey of the state of the art, Computer Methods in Applied Mechanics and Engineering 191 (11–12) (2002) 1245–1287.

[197] Z. Michalewicz, A survey of constraint handling techniques in evolutionary computation methods, Evolutionary Programming 4 (1995) 135–155.

[198] K. Deb, An efficient constraint handling method for genetic algorithms, Computer methods in applied mechanics and engineering 186 (2002) 311–338.

[199] J. H. Holland, Adaptation in Natural and Artificial Systems, 1st Edition, The University of Michigan, Ann Arbor, 1975.

[200] D. E. Goldberg, Genetic algorithms in Search, Optimization & Machine Learning, 1st Edition, Addison-Wesley Professional, Boston, 1989.

[201] D. Tuhus-Dubrow, M. Krarti, Genetic-algorithm based approach to optimize building envelope design for residential buildings, Building and Environment 45 (7) (2010) 1574–1581.

[202] Y. Bichiou, M. Krarti, Optimization of envelope and HVAC systems selection for residential buildings, Energy and Buildings 43 (12) (2011) 3373–3382.

[203] H. E. Mechri, A. Capozzoli, V. Corrado, Use of the ANOVA approach for sensitive building energy design, Applied Energy 87 (10) (2010) 3073–3083.

[204] P. Heiselberg, H. Brohus, A. Hesselholt, H. Rasmussen, E. Seinre, S. Thomas, Application of sensitivity analysis in design of sustainable buildings, Renewable Energy 34 (9) (2009) 2030–2036, Special Issue: Building and Urban Sustainability.

[205] Q. Jin, M. Overend, Sensitivity of façade performance on early-stage design variables, Energy and Buildings 77 (2014) 457–466.

[206] M. Adamski, Optimization of the form of a building on an oval base, Building and Environment 42 (2007) 1632–1643.

[207] ESTECO, modeFRONTIER (2014).
URL http://www.esteco.com/modefrontier

[208] MathWorks, MATLAB (2015).
URL http://www.mathworks.com/products/matlab/

[209] MathWorks, Optimization Toolbox (2015).
URL http://www.mathworks.com/products/optimization/

[210] L. B. N. Laboratory, GenOpt (2011).
URL http://www.simulationresearch.lbl.gov/GO/

[211] F. P. Chantrelle, H. Lahmidi, W. Keilholz, M. El Mankibi, P. Michel, Development of a
multicriteria tool for optimizing the renovation of buildings, Applied Energy 88 (4)
(2011) 1386–1394.

[212] M. Turrin, P. von Buelow, R. Stouffs, Design explorations of performance driven
geometry in architectural design using parametric modeling and genetic algorithms,
Advanced Engineering Informatics 25 (4) (2011) 656–675.

[213] National Renewable Energy Laboratory, BEopt (2015).
URL https://beopt.nrel.gov/

[214] A. Nguyen, S. Reiter, P. Rigo, A review on simulation-based optimization methods
applied to building performance analysis, Applied Energy 113 (2014) 1043–1058.

[215] Y. S. Ong, P. B. Nair, A. J. Keane, Evolutionary optimization of computationally
expensive problems via surrogate modeling, AIAA Journal 41 (2003) 687–696.

[216] E. Asadi, M. Gameiro da Silva, C. Henggeler Antunes, L. Dias, L. Glicksman, Multi-
objective optimization for building retrofit: A model using genetic algorithm and
artificial neural network and an application, Energy and Buildings 81 (2014) 444–456.

[217] L. De Boeck, S. Verbeke, A. Audenaert, L. De Mesmaeker, Improving the energy
performance of residential buildings: A literature review, Renewable and Sustainable
Energy Reviews 52 (2015) 960–975.

[218] M. Wette, J. Wright, A comparison of deterministic and probabilistic optimization
algorithms for nonsmooth simulation-based optimization, Building and Environment
39 (2004) 989–999.

[219] R. Evins, A review of computational optimisation methods applied to sustainable
building design, Renewable and Sustainable Energy Reviews 22 (2013) 230–245.

[220] S. Stevanović, Optimization of passive solar design strategies: A review, Renewable
and Sustainable Energy Reviews 25 (2013) 177–196.

[221] Y. Huang, J.-l. Niu, Optimal building envelope design based on simulated performance:
History, current status and new potentials, Energy and Buildings 117 (2015) 387–398.

[222] R. Lollini, G. Barozzi, G. Fasano, I. Meroni, M. Zinzi, Optimisation of opaque compo-
nents of the building envelope. Energy, economic and environmental issues, Building
and Environment 41 (8) (2006) 1001–1013.

[223] A. Ucar, F. Balo, Effect of fuel type on the optimum thickness of selected insulation
materials for the four different climatic regions of Turkey, Applied Energy 86 (5)
(2009) 730–736.

[224] D. B. Özkan, C. Onan, Optimization of insulation thickness for different glazing areas
in buildings for various climatic regions in Turkey, Applied Energy 88 (4) (2011)
1331–1342.

[225] N. Daouas, A study on optimum insulation thickness in walls and energy savings in
Tunisian buildings based on analytical calculation of cooling and heating transmis-
sion loads, Applied Energy 88 (1) (2011) 156–164.

[226] I. Axaopoulos, P. Axaopoulos, J. Gelegenis, Optimum insulation thickness for external

walls on different orientations considering the speed and direction of the wind, Applied Energy 117 (2014) 167–175.

[227] M. Ozel, Effect of insulation location on dynamic heat-transfer characteristics of building external walls and optimization of insulation thickness, Energy and Buildings 72 (2014) 288–295.

[228] D. Gossard, B. Lartigue, F. Thellier, Multi-objective optimization of a building envelope for thermal performance using genetic algorithms and artificial neural network, Energy and Buildings 67 (2013) 253–260.

[229] F. Jiang, X. Wang, Y. Zhang, Analytical optimization of specific heat of building internal envelope, Energy Conversion and Management 63 (2012) 239–244.

[230] J. Wright, M. Mourshed, Geometric optimization of fenestration, in: Proceedings of the Eleventh International IBPSA Conference, Glasgow, Scotland, 27-30 July 2009, pp. 920–927.

[231] F. Goia, M. Haase, M. Perino, Optimizing the configuration of a façade module for office buildings by means of integrated thermal and lighting simulations in a total energy perspective, Applied Energy 108 (2013) 515–527.

[232] N. Harmathy, Z. Magyar, R. Folić, Multi-criterion optimization of building envelope in the function of indoor illumination quality towards overall energy performance improvement, Energy 114 (2016) 302–317.

[233] C. Koo, S. Park, T. Hong, H. S. Park, An estimation model for the heating and cooling demand of a residential building with a different envelope design using the finite element method, Applied Energy 115 (2014) 205–215.

[234] C. Kasinalis, R. C. G. M. Loonen, D. Cóstola, J. L. M. Hensen, Framework for assessing the performance potential of seasonally adaptable facades using multi-objective optimization, Energy and Buildings 79 (2014) 106–113.

[235] P. Ihm, M. Krarti, Design optimization of energy efficient residential buildings in Tunisia, Building and Environment 58 (2012) 81–90.

[236] V. Ž. Leskovar, M. Premrov, An approach in architectural design of energy-efficient timber buildings with a focus on the optimal glazing size in the south-oriented façade, Energy and Buildings 43 (12) (2011) 3410–3418.

[237] Y.-H. Lin, K.-T. Tsai, M.-D. Lin, M.-D. Yang, Design optimization of office building envelope configurations for energy conservation, Applied Energy 171 (2016) 336–346.

[238] A. I. Palmero-Marrero, A. C. Oliveira, Effect of louver shading devices on building energy requirements, Applied Energy 87 (6) (2010) 2040–2049.

[239] M. Manzan, Genetic optimization of external fixed shading devices, Energy and Buildings 72 (2014) 431–440.

[240] R. Shan, Optimization for heating, cooling and lighting load in building façade design, Energy Procedia 57 (2014) 1716–1725.

[241] Y. K. Yi, H. Kim, Agent-based geometry optimization with genetic algorithm (GA) for tall apartment's solar right, Solar Energy 113 (2015) 236–250.

[242] W. Wang, H. Rivard, R. Zmeureanu, Floor shape optimization for green building design, Advanced Engineering Informatics 20 (4) (2006) 363–378.

[243] J.-T. Jin, J.-W. Jeong, Optimization of a free-form building shape to minimize external thermal load using genetic algorithm, Energy and Buildings 85 (2014) 473–482.

[244] G. Rapone, O. Saro, Optimisation of curtain wall façades for office buildings by means of PSO algorithm, Energy and Buildings 45 (2012) 189–196.

[245] J. M. L. Gagne, M. Andersen, A generative façade design method based on daylighting performance goals, Journal of Building Performance Simulation 5 (3) (2012) 141–154.

[246] C. E. Ochoa, M. B. C. Aries, E. J. van Loenen, J. L. M. Hensen, Considerations on design optimization criteria for windows providing low energy consumption and high visual comfort, Applied Energy 95 (2012) 238–245.

[247] S.-G. Yong, J.-H. Kim, Y. Gim, J. Kim, J. Cho, H. Hong, Y.-J. Baik, J. Koo, Impacts of building envelope design factors upon energy loads and their optimization in US standard climate zones using experimental design, Energy and Buildings 141 (2017) 1–15.

[248] R. Pacheco, J. Ordóñez, G. Martínez, Energy efficient design of building: A review, Renewable and Sustainable Energy Reviews 16 (6) (2012) 3559–3573.

[249] S. A. Al-Sanea, M. F. Zedan, Optimized monthly-fixed thermostat-setting scheme for maximum energy-savings and thermal comfort in air-conditioned spaces, Applied Energy 85 (5) (2008) 326–346.

[250] Y. Lu, S. Wang, Y. Sun, C. Yan, Optimal scheduling of buildings with energy generation and thermal energy storage under dynamic electricity pricing using mixed-integer nonlinear programming, Applied Energy 147 (2015) 49–58.

[251] K. J. Kontoleon, E. A. Eumorfopoulou, The influence of wall orientation and exterior surface solar absorptivity on time lag and decrement factor in the Greek region, Renewable Energy 33 (7) (2008) 1652–1664.

[252] S. A. Al-Sanea, M. F. Zedan, Improving thermal performance of building walls by optimizing insulation layer distribution and thickness for same thermal mass, Applied Energy 88 (9) (2011) 3113–3124.

[253] R. Cheng, X. Wang, Y. Zhang, Analytical optimization of the transient thermal performance of building wall by using thermal impedance based on thermal-electric analogy, Energy and Buildings 80 (2014) 598–612.

[254] D. E. M. Bond, W. W. Clark, M. Kimber, Configuring wall layers for improved insulation performance, Applied Energy 112 (2013) 235–245.

[255] C. Baglivo, P. M. Congedo, A. Fazio, D. Laforgia, Multi-objective optimization analysis for high efficiency external walls of zero energy buildings (ZEB) in the Mediterranean climate, Energy and Buildings 84 (2014) 483–492.

[256] C. Baglivo, P. M. Congedo, Design method of high performance precast external walls for warm climate by multi-objective optimization analysis, Energy 90, Part 2 (2015) 1645–1661.

[257] Y. Zhang, K. Lin, Q. Zhang, H. Di, Ideal thermophysical properties for free-cooling (or heating) buildings with constant thermal physical property material, Energy and Buildings 38 (2006) 1164–1170.

[258] Y. Zhang, Q. Chen, Y. Zhang, X. Wang, Exploring buildings' secrets: The ideal thermophysical properties of a building's wall for energy conservation, International Journal of Heat and Mass Transfer 65 (2013) 265–273.

[259] Y. Cui, J. Xie, J. Liu, S. Pan, Review of phase change materials integrated in building walls for energy saving, Procedia Engineering 121 (2015) 763–770, the 9th International Symposium on Heating, Ventilation and Air Conditioning (ISHVAC) joint with

the 3rd International Conference on Building Energy and Environment (COBEE), 12-15 July 2015, Tianjin, China.

[260] X. Jin, M. A. Medina, X. Zhang, On the importance of the location of PCMs in building walls for enhanced thermal performance, Applied Energy 106 (2013) 72–78.

[261] X. Jin, S. Zhang, X. Xu, X. Zhang, Effects of PCM state on its phase change performance and the thermal performance of building walls, Building and Environment 81 (2014) 334–339.

[262] F. Kuznik, J. Virgone, J. Noel, Optimization of a phase change material wallboard for building use, Applied Thermal Engineering 28 (11–12) (2008) 1291–1298.

[263] A. Bastani, F. Haghighat, J. Kozinski, Designing building envelope with PCM wallboards: Design tool development, Renewable and Sustainable Energy Reviews 31 (2014) 554–562.

[264] A. Bastani, F. Haghighat, Expanding Heisler chart to characterize heat transfer phenomena in a building envelope integrated with phase change materials, Energy and Buildings 106 (2015) 164–174.

[265] M. El Mankibi, Z. J. Zhai, S. N. Al-Saadi, A. Zoubir, Numerical modeling of thermal behaviors of active multi-layer living wall, Energy and Buildings 106 (2015) 96–110, SI: IEA-ECES Annex 31 Special Issue on Thermal Energy Storage.

[266] C. Garnier, T. Muneer, L. McCauley, Super insulated aerogel windows: Impact on daylighting and thermal performance, Building and Environment 94, Part 1 (2015) 231–238.

[267] W. J. Hee, M. A. Alghoul, B. Bakhtyar, O. Elayeb, M. A. Shameri, M. S. Alrubaih, K. Sopian, The role of window glazing on daylighting and energy saving in buildings, Renewable and Sustainable Energy Reviews 42 (2015) 323–343.

[268] S. Grynning, A. Gustavsen, B. Time, B. P. Jelle, Windows in the buildings of tomorrow: Energy losers or energy gainers?, Energy and Buildings 61 (2013) 185–192.

[269] M. Thalfeldt, E. Pikas, J. Kurnitski, H. Voll, Facade design principles for nearly zero energy buildings in a cold climate, Energy and Buildings 67 (2013) 309–321.

[270] L. Vanhoutteghem, G. C. J. Skarning, C. A. Hviid, S. Svendsen, Impact of façade window design on energy, daylighting and thermal comfort in nearly zero-energy houses, Energy and Buildings 102 (2015) 149–156.

[271] J. Joe, W. Choi, Y. Kwak, J.-H. Huh, Optimal design of a multi-story double skin facade, Energy and Buildings 76 (2014) 143–150.

[272] J.-M. Dussault, L. Gosselin, T. Galstian, Integration of smart windows into building design for reduction of yearly overall energy consumption and peak loads, Solar Energy 86 (11) (2012) 3405–3416.

[273] F. Favoino, M. Overend, Q. Jin, The optimal thermo-optical properties and energy saving potential of adaptive glazing technologies, Applied Energy 156 (2015) 1–15.

[274] A. Alaidroos, M. Krarti, Optimal design of residential building envelope systems in the Kingdom of Saudi Arabia, Energy and Buildings 86 (2015) 104–117.

[275] M. Karmellos, A. Kiprakis, G. Mavrotas, A multi-objective approach for optimal prioritization of energy efficiency measures in buildings: Model, software and case studies, Applied Energy 139 (2015) 131–150.

[276] S. Carlucci, G. Cattarin, F. Causone, L. Pagliano, Multi-objective optimization of a nearly zero-energy building based on thermal and visual discomfort minimization

using a non-dominated sorting genetic algorithm (NSGA-II), Energy and Buildings 104 (2015) 378–394.

[277] R. Azari, S. Garshasbi, P. Amini, H. Rashed-Ali, Y. Mohammadi, Multi-objective optimization of building envelope design for life cycle environmental performance, Energy and Buildings 126 (2016) 524–534.

[278] M. Hamdy, A. Hasan, K. Siren, Applying a multi-objective optimization approach for design of low-emission cost-effective dwellings, Building and Environment 46 (1) (2011) 109–123.

[279] N. Soares, A. R. Gaspar, P. Santos, J. J. Costa, Multi-dimensional optimization of the incorporation of PCM-drywalls in lightweight steel-framed residential buildings in different climates, Energy and Buildings 70 (2014) 411–421.

[280] F. Kuznik, J. P. Arzamendia Lopez, D. Baillis, K. Johannes, Phase change material wall optimization for heating using metamodeling, Energy and Buildings 106 (2015) 216–224.

[281] S. D. Zwanzig, Y. Lian, E. G. Brehob, Numerical simulation of phase change material composite wallboard in a multi-layered building envelope, Energy Conversion and Management 69 (2013) 27–40.

[282] W. Xiao, X. Wang, Y. Zhang, Analytical optimization of interior PCM for energy storage in a lightweight passive solar room, Applied Energy 86 (10) (2009) 2013–2018.

[283] F. Jiang, X. Wang, Y. Zhang, A new method to estimate optimal phase change material characteristics in a passive solar room, Energy Conversion and Management 52 (2011) 2437–2441.

[284] C. E. Ochoa, I. G. Capeluto, Decision methodology for the development of an expert system applied in an adaptable energy retrofit façade system for residential buildings, Renewable Energy 78 (2015) 498–508.

[285] Z. Ma, P. Cooper, D. Daly, L. Ledo, Existing building retrofits: Methodology and state-of-the-art, Energy and Buildings 55 (2012) 889–902.

[286] J. Huang, H. Lv, T. Gao, W. Feng, Y. Chen, T. Zhou, Thermal properties optimization of envelope in energy-saving renovation of existing public buildings, Energy and Buildings 75 (2014) 504–510.

[287] E. Asadi, M. Gameiro da Silva, C. Henggeler Antunes, L. Dias, A multi-objective optimization model for building retrofit strategies using TRNSYS simulations, GenOpt and MATLAB, Building and Environment 56 (2012) 370–378.

[288] Y. Shao, P. Geyer, W. Lang, Integrating requirement analysis and multi-objective optimization for office building energy retrofit strategies, Energy and Buildings 82 (2014) 356–368.

[289] P. Penna, A. Prada, F. Cappelletti, A. Gasparella, Multi-objectives optimization of energy efficiency measures in existing buildings, Energy and Buildings 95 (2014) 57–69, Special Issue: Historic, historical and existing buildings: designing the retrofit. An overview from energy performances to indoor air quality.

[290] R. Wu, G. Mavromatidis, K. Orehounig, J. Carmeliet, Multiobjective optimisation of energy systems and building envelope retrofit in a residential community, Applied Energy 190 (2017) 634–649.

[291] M. N. Özışık, Finite Difference Methods in Heat Transfer, CRC Press, Boca Raton, 1994.

[292] M. Perino, A. Capozzoli, Y. Cascone, Theoretical and experimental characterization of thermal dynamic wall performance, in: 9th International Masonry Conference, Guimarães, Portugal, 7-9 July 2014.

[293] I. Rechenberg, Evolutionsstrategie: Optimierung technischer systeme und prinzipien der biologischen evolution, Frommann-Holzboog, Stuttgart, 1973.

[294] H. P. Schwefel, Numerical optimization of computer models, Wiley, Chichester, 1981.

[295] H. H. Bock, Automatische Klassifikation, Studia Mathematica, Vandenhoeck & Ruprecht, Göttingen, 1974.

[296] P. G. Alotto, C. Eranda, B. Brandstätter, G. Fürntratt, C. Magele, G. Molinari, M. Nervi, K. Preis, M. Repetto, K. Richter, Stochastic algorithms in electromagnetic optimization, IEEE Transactions on Magnetics 34 (1998) 3674–3684.

[297] H. H. Rosenbrock, An automatic method for finding the greatest or least value of a function, The Computer Journal 3 (1960) 175–184.

[298] K. Deb, A. Pratap, S. Agarwal, T. Meyarivan, A fast and elitist multiobjective genetic algorithm: NSGA-II, IEEE Transactions on Evolutionary Computation 6 (2) (2002) 182–197.

[299] K. Deb, Multi-objective optimization using evolutionary algorithms: An introduction, Kangal report number 2011003, Kanpur Genetic Algorithms Laboratory (KanGAL) – Indian Institute of Technology Kanpur (2011).

[300] J. W. Tukey, Exploratory Data Analysis, Addison-Wesley, Reading, MA, 1977.

[301] P. Berkhin, Survey of clustering data mining techniques, in: K. Jacob, C. Nicholas, M. Teboulle (Eds.), Grouping Multidimensional Data, Springer Berlin Heidelberg, Berlin, 2006, Ch. 2, pp. 25–71.

[302] K. Deb, R. B. Agrawal, Simulated binary crossover for continuous search space, Complex systems 9 (1995) 115–148.

[303] K. Deb, A. Kumar, Real-coded genetic algorithms with simulated binary crossover: studies on multimodal and multiobjective problems, Complex systems 9 (1995) 431–454.

[304] F. Kuznik, J. Virgone, J.-J. Roux, Energy efficiency of room wall containing PCM wallboard: A full scales experimental investigation, Energy and Buildings 40 (2) (2008) 148–156.

[305] F. Kuznik, J. Virgone, Experimental assessment of a phase change material for wall building use, Applied Energy 86 (10) (2009) 2038 – 2046.

[306] LaserComp, Inc., FOX600 and FOX800 Series Instruments Manual.

[307] V. Corrado, S. Paduos, New equivalent parameters for thermal characterization of opaque building envelope components under dynamic conditions, Applied Energy 163 (2016) 313–322.

[308] Ministro dello sviluppo economico, Decreto interministeriale 26 giugno 2015 - Applicazione delle metodologie di calcolo delle prestazioni energetiche e definizione delle prescrizioni e dei requisiti minimi degli edifici (2015).

[309] G. Zhou, Y. Yang, X. Hong, Performance of shape-stabilized phase change material wallboard with periodical outside heat flux waves, Applied Energy 88 (2011) 2113–2121.

[310] EnergyPlus Weather Data – Europe WMO Region 6.
URL https://energyplus.net/weather-region/europe_wmo_region_6

[311] ASHRAE, International Weather for Energy Calculations (IWEC Weather Files) Users Manual and CD-ROM, Atlanta, 2001.

[312] M. C. Peel, B. L. Finlayson, T. A. McMahon, Updated world map of the Köppen-Geiger climate classification, Hydrology and Earth System Sciences 11 (2007) 1633–1644.

[313] ASHRAE, 2009 ASHRAE Handbook – Fundamentals, American Society of Heating, Refrigerating and Air-Conditioning Engineers, Atlanta, GA, 2009.

[314] EN ISO 6946:2007, Building components and building elements - Thermal resistance and thermal transmittance - Calculation method, International Organization for Standardization, Geneva, Switzerland, 2012.

[315] Kommunal- og moderniseringsdepartementet, Forskrift om tekniske krav til bygg-verk (Byggteknisk forskrift), 2010.
URL https://lovdata.no/dokument/SF/forskrift/2010-03-26-489

[316] F. Margiotta, Metodologia per la determinazione delle caratteristiche strutturali ed impiantistiche di "Edifici Tipo" del Parco Edilizio Nazionale ad uso ufficio e Valutazione del Potenziale di Risparmio energetico sulla base della fattibilità degli interventi di riqualificazione energetica, Tech. rep., ENEA, Ricerca di Sistema Elettrico, Report RdS/2010/197 (2010).

[317] L. Rollino, Fabbisogni energetici per edifici caratterizzanti il terziario in Italia: aspetti termici e illuminotecnici, Ph.D. thesis, Politecnico di Torino, Italy (2012).

[318] UNI 10339:1995, Abaco delle strutture costituenti l'involucro opaco degli edifici. Parametri termofisici, 2014.

[319] V. Corrado, I. Ballarini, S. P. Corgnati, Building Typology Brochure – Italy. Fascicolo sulla Tipologia Edilizia Italiana. Nuova edizione, Tech. rep., Politecnico di Torino – Dipartimento Energia – Gruppo di Ricerca TEBE (2014).

[320] UNI/TS 11300-2, Prestazioni energetiche degli edifici Parte 2: Determinazione del fabbisogno di energia primaria e dei rendimenti per la climatizzazione invernale, per la produzione di acqua calda sanitaria, per la ventilazione e per l'illuminazione in edifici non residenziali, 2014.

[321] H. Brattebø, R. O'Born, N. Holck Sandberg, M. I. Vestrum, I. Sartori, Fremtidig utvikling i energiforbruk og CO_2-utslipp for Norges boligmasse, Tech. rep., EPISCOPE National Case Study Report, Norway (2016).

[322] NO_EPISCOPE_EPI-Tables_NationalCaseStudy_NTNU_SINTEF.xls.
URL http://www.episcope.eu/communication/download

[323] FOR-1949-12-15 nr 0000, Byggeforskrifter av 15. desember 1949, bind I, 1949.

[324] H. Brattebø, R. O'Born, I. Sartori, B. Nørstebø, Typologier for norske boligbygg - Eksempler på tiltak for energieffektivisering, Tech. rep., EPISCOPE National Building Typology Brochure, Norway (2016).

[325] I. Sartori, B. J. Wachenfeldt, A. G. Hestnes, Energy demand in the Norwegian building stock: Scenarios on potential reduction, Energy Policy 37 (2009) 1614–1627.

[326] Passive House Institute, Passive House requirements.
URL http://www.passivehouse.com/02_informations/02_passive-house-requirements/02_passive-house-requirements.htm

[327] C. Di Perna, F. Stazi, A. Ursini Casalena, M. D'Orazio, Influence of the internal inertia of the building envelope on summertime comfort in buildings with high internal heat loads, Energy and Buildings 43 (2011) 200–206.

[328] M. Rossi, V. M. Rocco, External walls design: The role of periodic thermal transmittance and internal areal heat capacity, Energy and Buildings 68, Part C (2014) 732–740.

[329] Lawrence Berkeley National Laboratory, WINDOW (2015).
URL https://windows.lbl.gov/software/window/window.html/

[330] UNI/TS 11300-1, Prestazioni energetiche degli edifici Parte 1: Determinazione del fabbisogno di energia termica dell'edificio per la climatizzazione estiva ed invernale, 2014.

[331] NS 3031:2007, Beregning av bygningers energiytelse - Metode og data (Calculation of energy performance of buildings - Method and data), 2007.

[332] D. J. Sailor, H. Fan, Modeling the diurnal variability of effective albedo for cities, Atmospheric Environment 36 (4) (2002) 713–725.

[333] EN ISO 13790:2008, Energy performance of buildings – Calculation of energy use for space heating and cooling, International Organization for Standardization, Geneva, Switzerland, 2008.

[334] UNI 10339:1995, Impianti aeraulici al fini di benessere. Generalità, classificazione e requisiti. Regole per la richiesta d'offerta, l'offerta, l'ordine e la fornitura., 1995.

[335] I. Ballarini, V. Corrado, Analysis of the building energy balance to investigate the effect of thermal insulation in summer conditions, Energy and Buildings 52 (2012) 168–180.

[336] EN 15232:2012, Energy performance of buildings - Impact of Building Automation, Controls and Building Management, 2012.

[337] EN 15603:2008, Energy performance of buildings – Overall energy use and definitions of energy ratings, 2008.

[338] ADAPT Consulting, Conversion factors for electricity in energy policy, Technical report (2013).
URL https://energinorge.no/contentassets/e86a4dc8771845dfb03fee35c1d0f45d/2013-02-15--conversion-factors-for-electricity.pdf

[339] EN 15459:2007, Energy performance of buildings - Economic evaluation procedure for energy systems in buildings, 2007.

[340] Regione Piemonte. Direzione regionale Opere Pubbliche, Difesa del Suolo, Montagna, Foreste, Protezione civile, Trasporti e Logistica. Settore Tecnico Opere Pubbliche, Prezzi di riferimento per opere e lavori pubblici nella Regione Piemonte - edizione dicembre 2014 - valevole per il 2015, 2015.
URL http://www.regione.piemonte.it/oopp/prezzario

[341] J. Kośny, N. Shukla, A. Fallahi, Cost analysis of simple phase change material-enhanced building envelopes in southern U.S. climates, Tech. rep., U.S. Department of Energy, Fraunhofer CSE (2013).
URL http://www.cse.fraunhofer.org/hs-fs/hub/55819/file-20313119-pdf/docs/ba_pcm_enhanced_building_envelopes.pdf

[342] AVANT-GARDE - AdVANced compoNents sysTem for a Green and smARt builDing basEd on nano functionalized materials and coatings, H2020-EeB-02-2014 - Technical Annex - Sessions 1-3 (2014).

[343] N. Chaiyat, Energy and economic analysis of a building air-conditioner with a phase change material (PCM), Energy Conversion and Management 94 (2015) 150–158.

[344] Entropy solutions, http://www.puretemp.com/stories/understanding-pcms, accessed: 06 July 2016.

[345] Autorità per l'energia elettrica il gas e il sistema idrico, Prezzi e tariffe.
URL http://www.autorita.energia.it/it/prezzi.htm

[346] S. Carlucci, Thermal Comfort Assessment of Buildings, Springer, London, 2013.

[347] EN 15251:2008, Indoor environmental input parameters for design and assessment of energy performance of buildings addressing indoor air quality, thermal environment, lighting and acoustics, 2008.

[348] J. F. Nicol, J. Hacker, B. Spires, H. Davies, Suggestion for new approach to overheating diagnostics, Building Research & Information 37 (4) (2009) 348–357.

[349] K. J. Kontoleon, D. K. Bikas, The effect of south wall's outdoor absorption coefficient on time lag, decrement factor and temperature variations, Energy and Buildings 39 (9) (2007) 1011–1018.

[350] A. Gasparella, G. Pernigotto, M. Baratieri, P. Baggio, Thermal dynamic transfer properties of the opaque envelope: Analytical and numerical tools for the assessment of the response to summer outdoor conditions, Energy and Buildings 43 (9) (2011) 2509–2517.

[351] The R Foundation, The R Project for Statistical Computing (2017).
URL http://www.r-project.org

Appendix A

Box plots and frequency analyses

Box plots and frequency analyses of the building-level optimisation analyses in § 4.4.3 are herewith illustrated.

With regard to the box plots, the black plots with red median represent cases with more than 20 points (1/5 of the initial population), the dark grey plots refer to cases with less than 20 point but more than 5, and the light grey boxes indicate cases with less than five points.

The wall codes, as they were concisely reported in the frequency analyses, are reported in Table A.1 (they were numbered in the same sequence as appearing from Fig. 4.19 to Fig. 4.23). Moreover, the codes for window type, insulation and internal lining materials are summarised in Table A.2. The complete set of properties are respectively reported in Table 4.13, Table 4.11 and Table 4.12.

Table A.1 Wall codes as reported in the frequency analyses.

ID	RT0	RT1	RT2	ID	RT2	ID	RT2	ID	RT2
0	ext0000	int0000	ie000000	11	ie210100	22	ie301000	33	ie310101
1	ext1000	int1000	ie100000	12	ie211000	23	ie301001	34	ie310110
2	ext1100	int1100	ie101000	13	ie211100	24	ie301010	35	ie310111
3	ext2000	int2000	ie110000	14	ie300000	25	ie301011	36	ie311000
4	ext2100	int2100	ie111000	15	ie300001	26	ie301100	37	ie311010
5	ext3000	int3000	ie110100	16	ie300010	27	ie301101	38	ie311100
6	ext3010	int3010	ie111000	17	ie300011	28	ie301110	39	ie311101
7	ext3100	int3100	ie111100	18	ie300100	29	ie301111	40	ie311110
8	ext3101	int3101	ie200000	19	ie300101	30	ie310000	41	ie311111
9	ext3110	int3110	ie201000	20	ie300110	31	ie310010		
10	ext3111	int3111	ie210000	21	ie300111	32	ie310100		

Table A.2 Codes for window types, insulation and internal lining materials.

ID	Window type	Insulation material	Internal lining material
0	DGU Air	EPS	Lime and gypsum plaster
1	DGU Air low-e(3)	Rock wool	Clay plaster
2	DGU Air low-e(2)	XPS	Mineralised wooden board
3	DGU 90%Ar selective(2)	Sheep wool	Thermo-plaster
4	DGU 90%Ar low-e(3)	Cork	
5	DGU 90%Ar low-e(2)	Wood-fiber board	
6	TGU Air low-e(3,5)	Cellulose fiber panels	
7	TGU* 90%Ar low-e(3,5)	Aerogel mats	
8	TGU 90%Ar low-e(2,5)		
9	TGU* 90%Ar low-e(3,5)		
10	TGU 95%Kr low-e(3,5)		

* Window types 7 and 9 differed in the gap size.

Palermo_2Obj
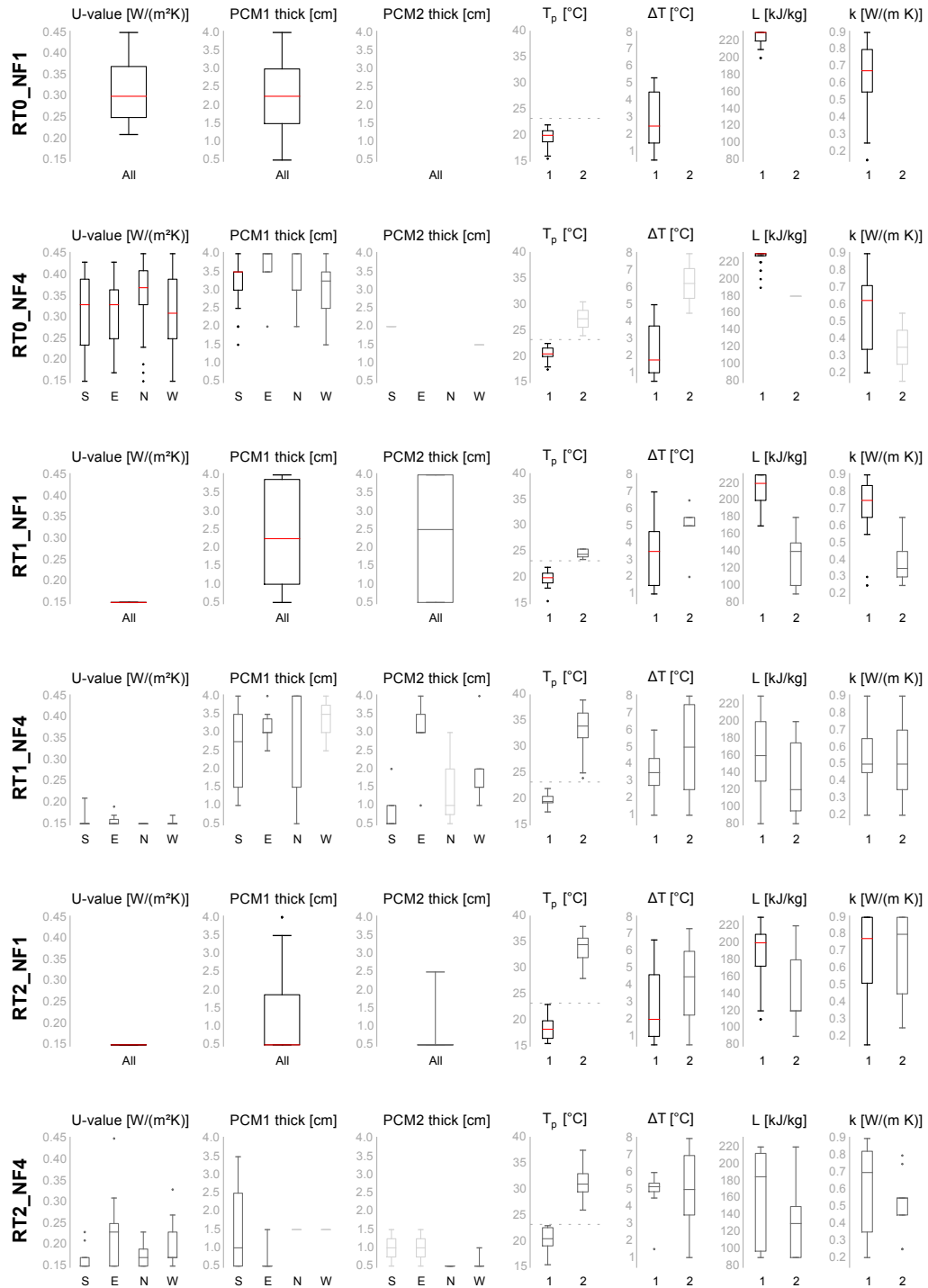
Fig. A.1 Box plots: Palermo, two objectives.

Torino_2Obj
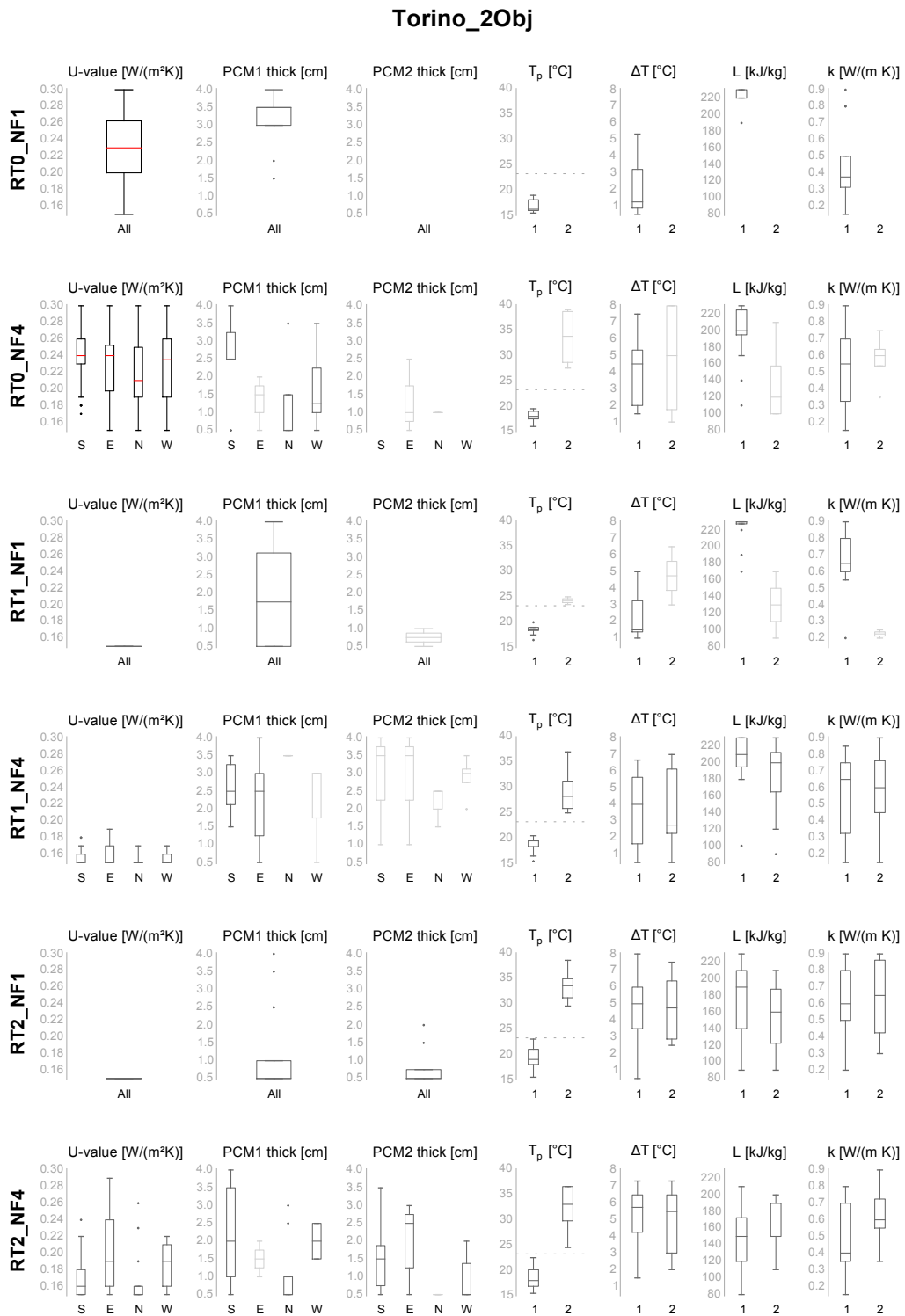
Fig. A.2 Box plots: Torino, two objectives.

Palermo_3Obj
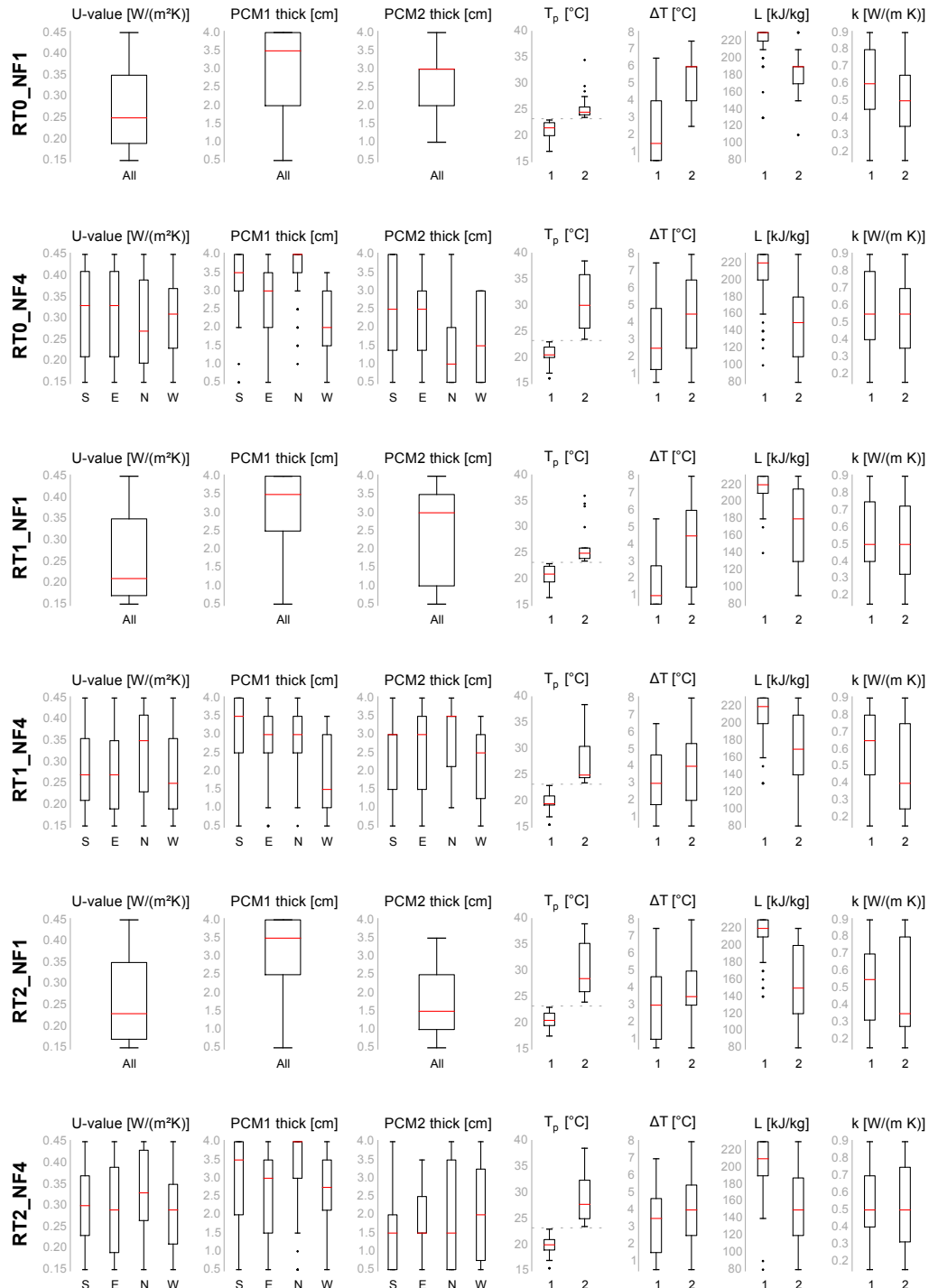
Fig. A.3 Box plots: Palermo, three objectives.
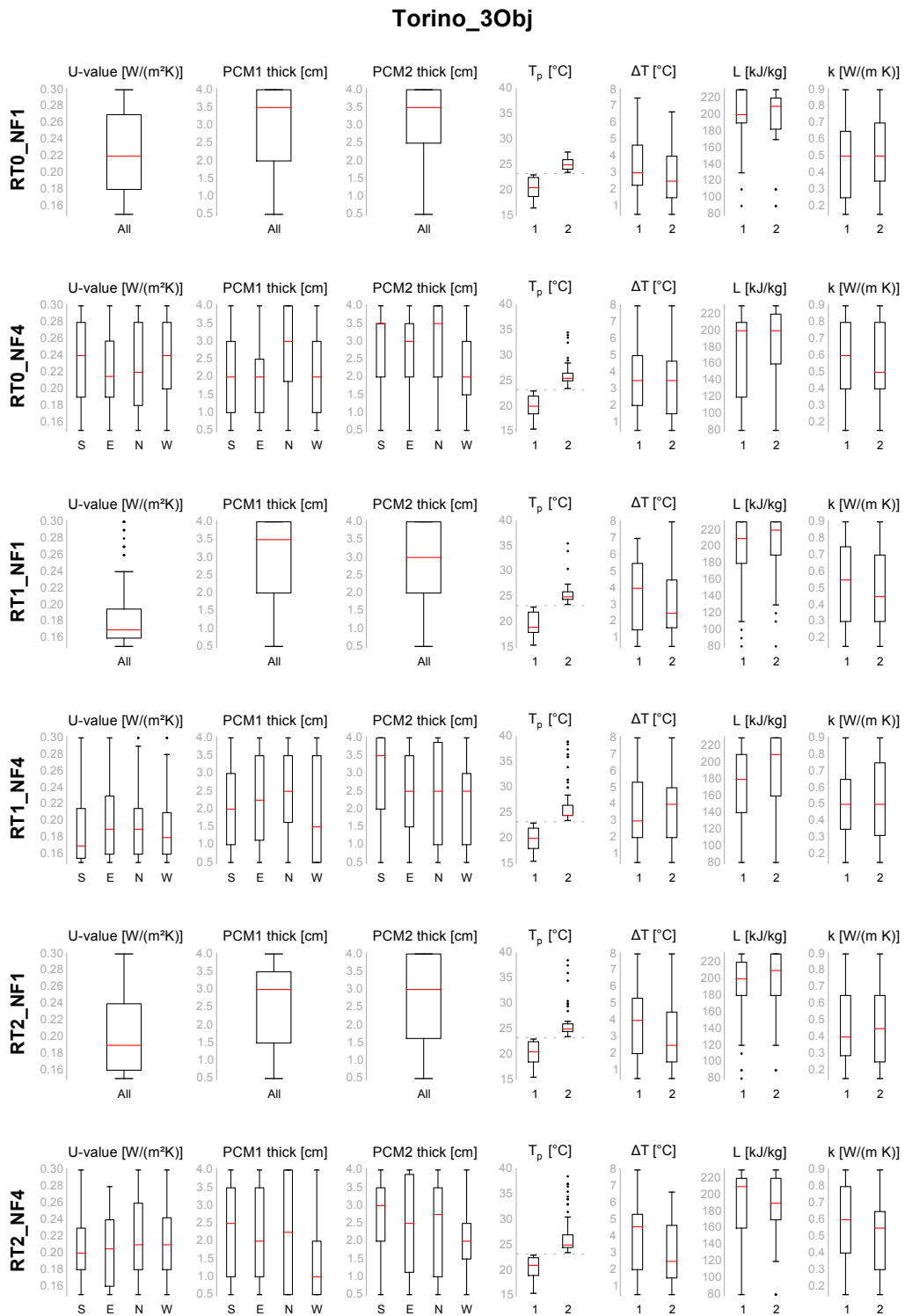
Torino_3Obj

Fig. A.4 Box plots: Torino, three objectives.

Oslo_3Obj_pre-1955
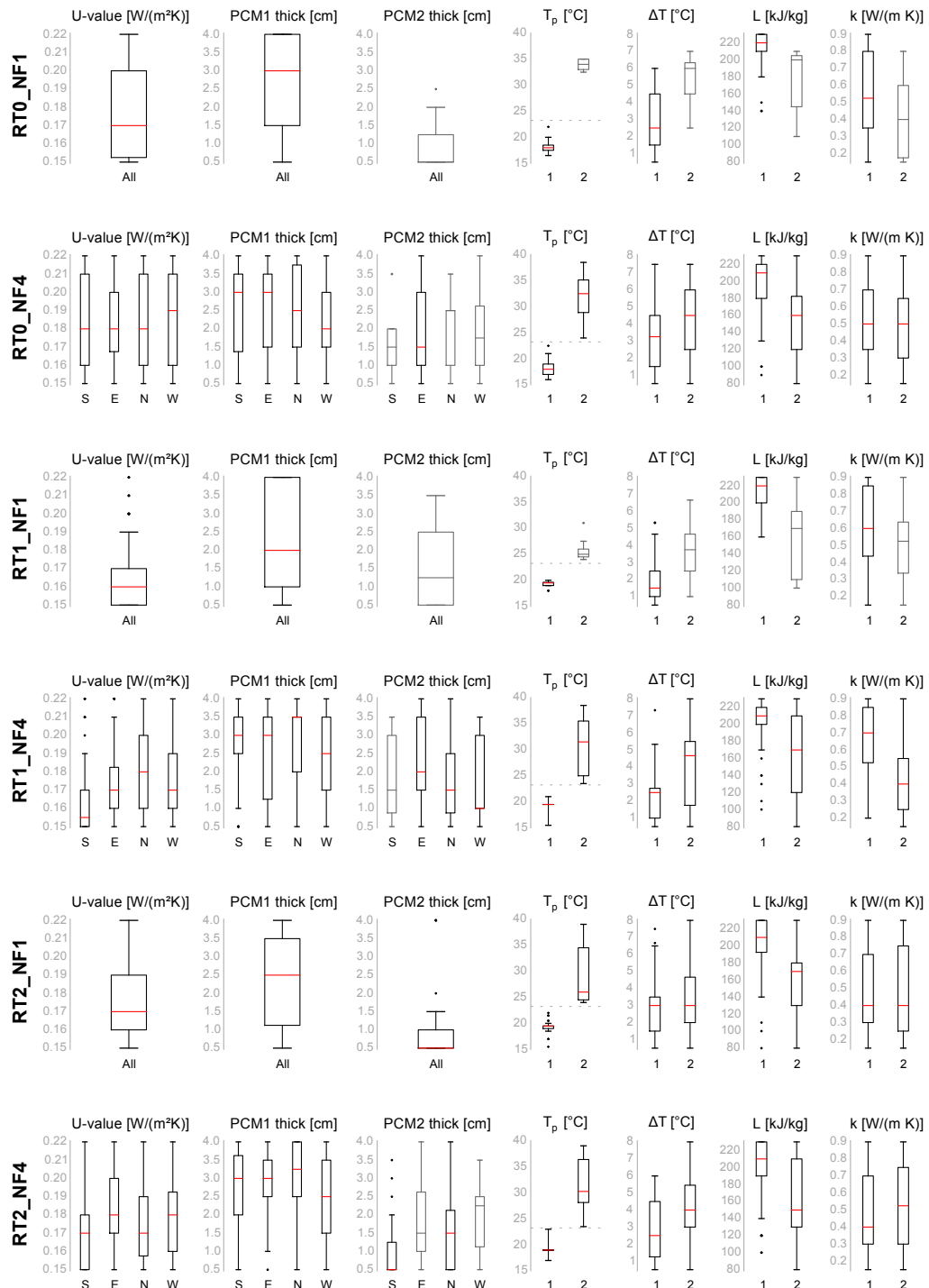
Fig. A.5 Box plots: Oslo, pre-1955.

Oslo_3Obj_post-1955
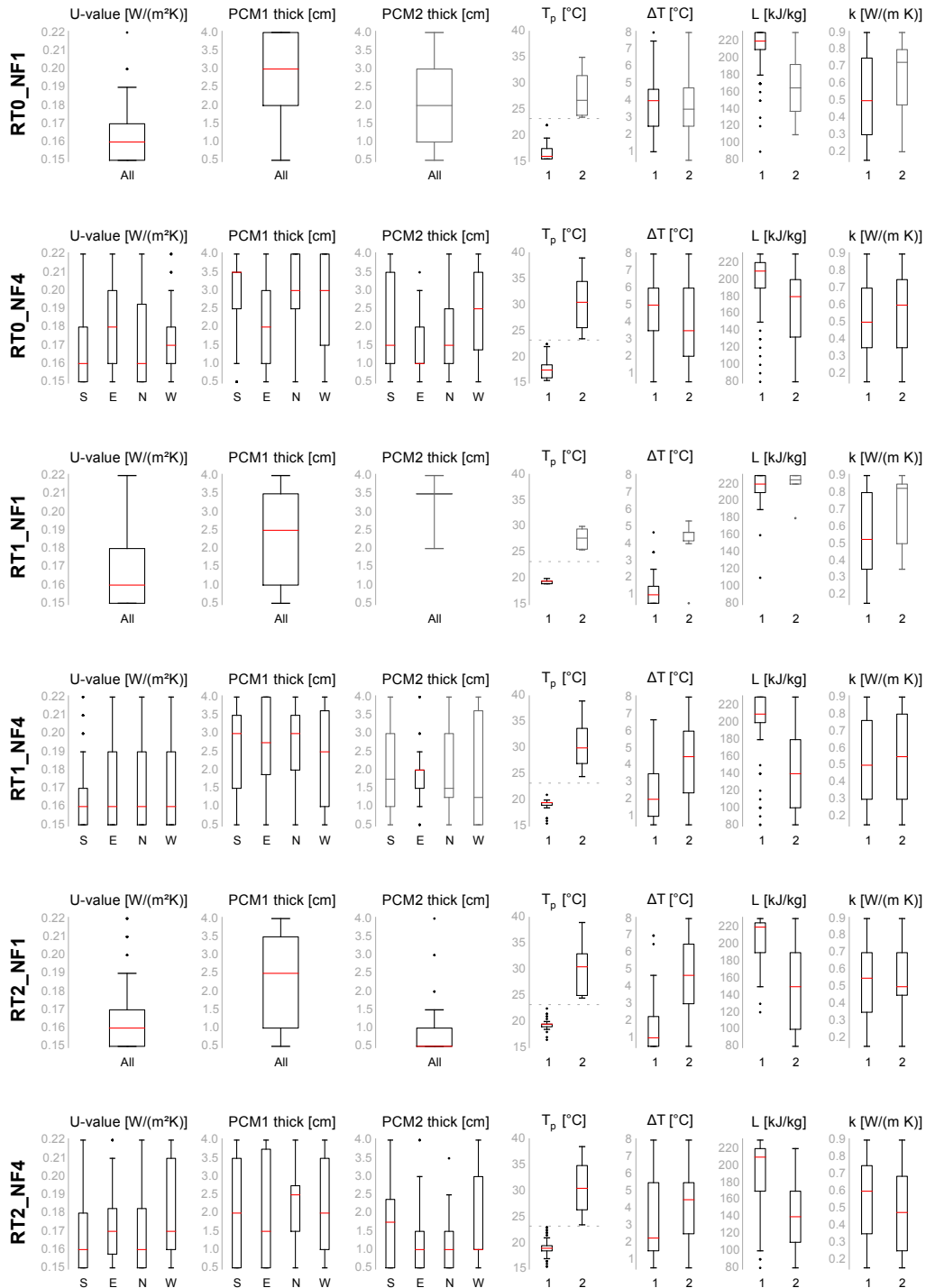
Fig. A.6 Box plots: Oslo, post-1955.
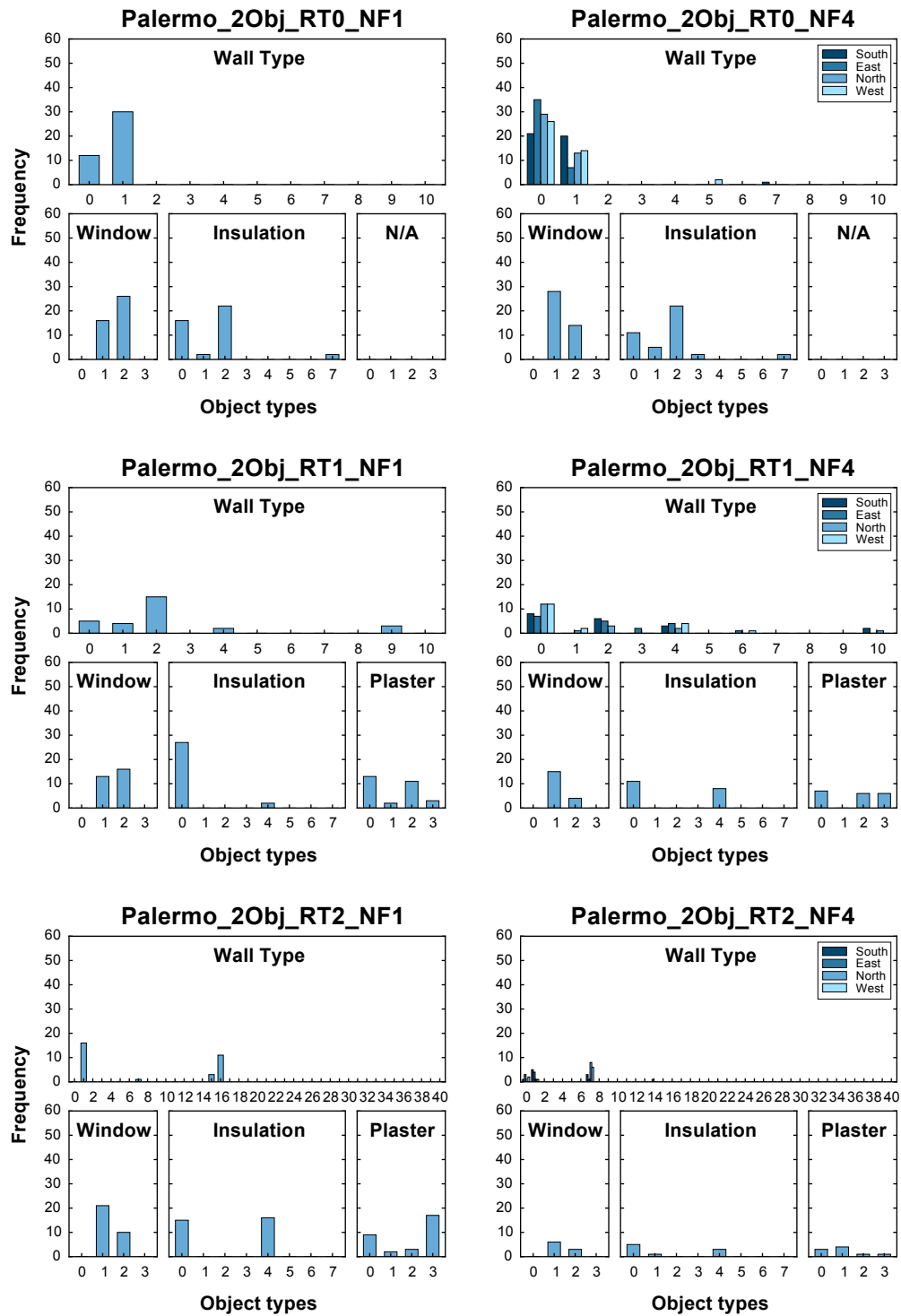
Fig. A.7 Frequency analyses: Palermo_2Obj, discrete variables.
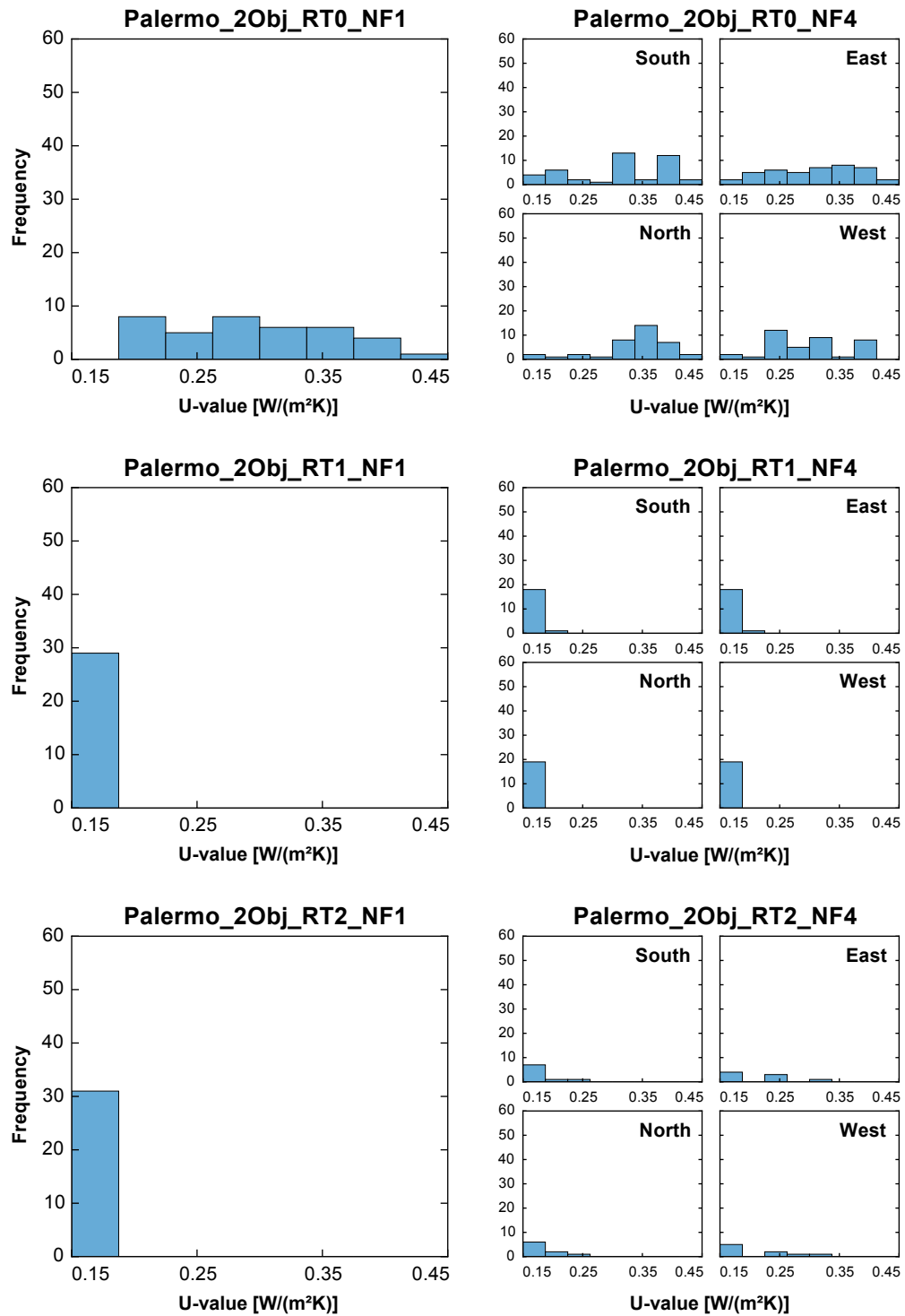
Fig. A.8 Frequency analyses: Palermo_2Obj, U-values.
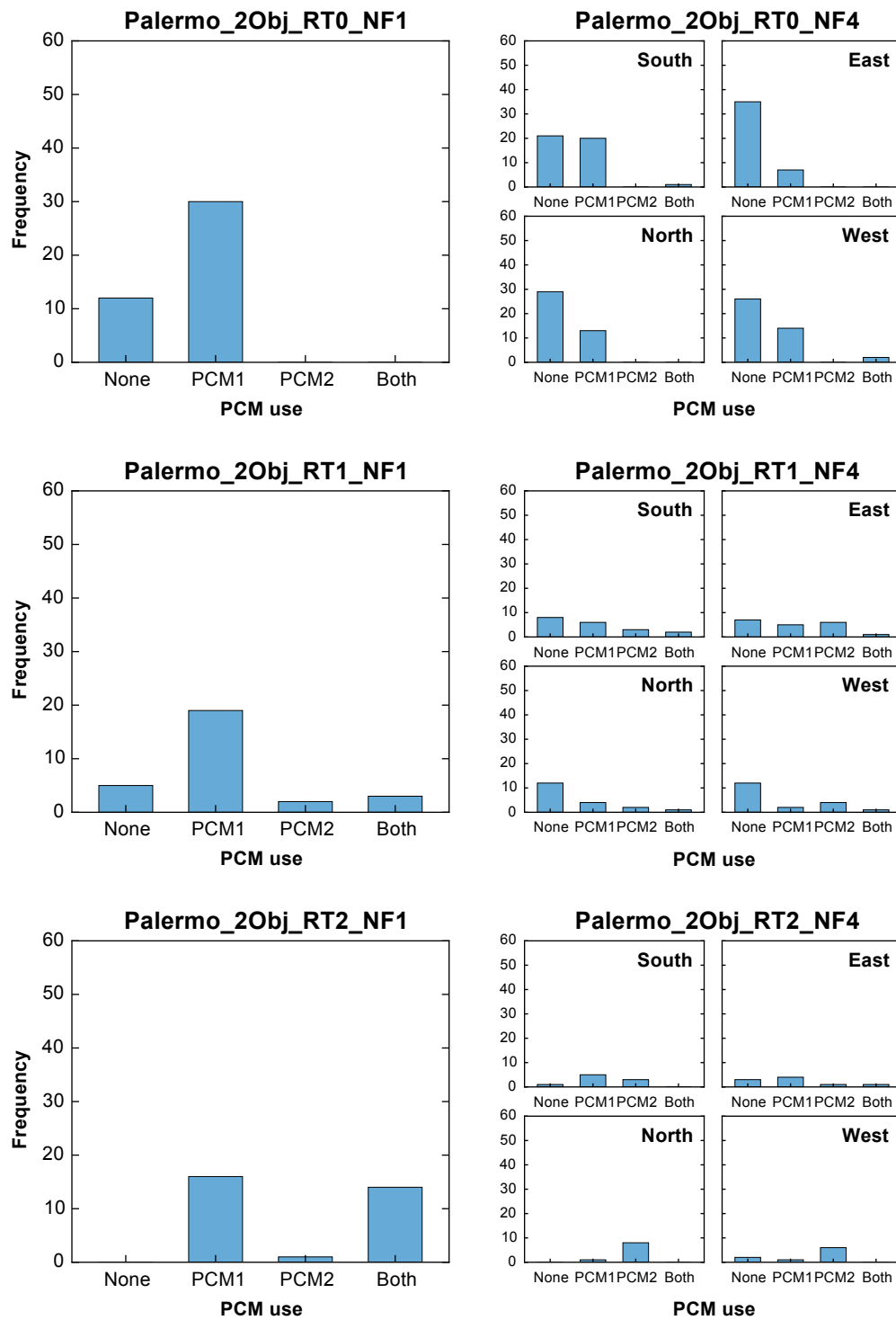
Fig. A.9 Frequency analyses: Palermo_2Obj, PCM use.
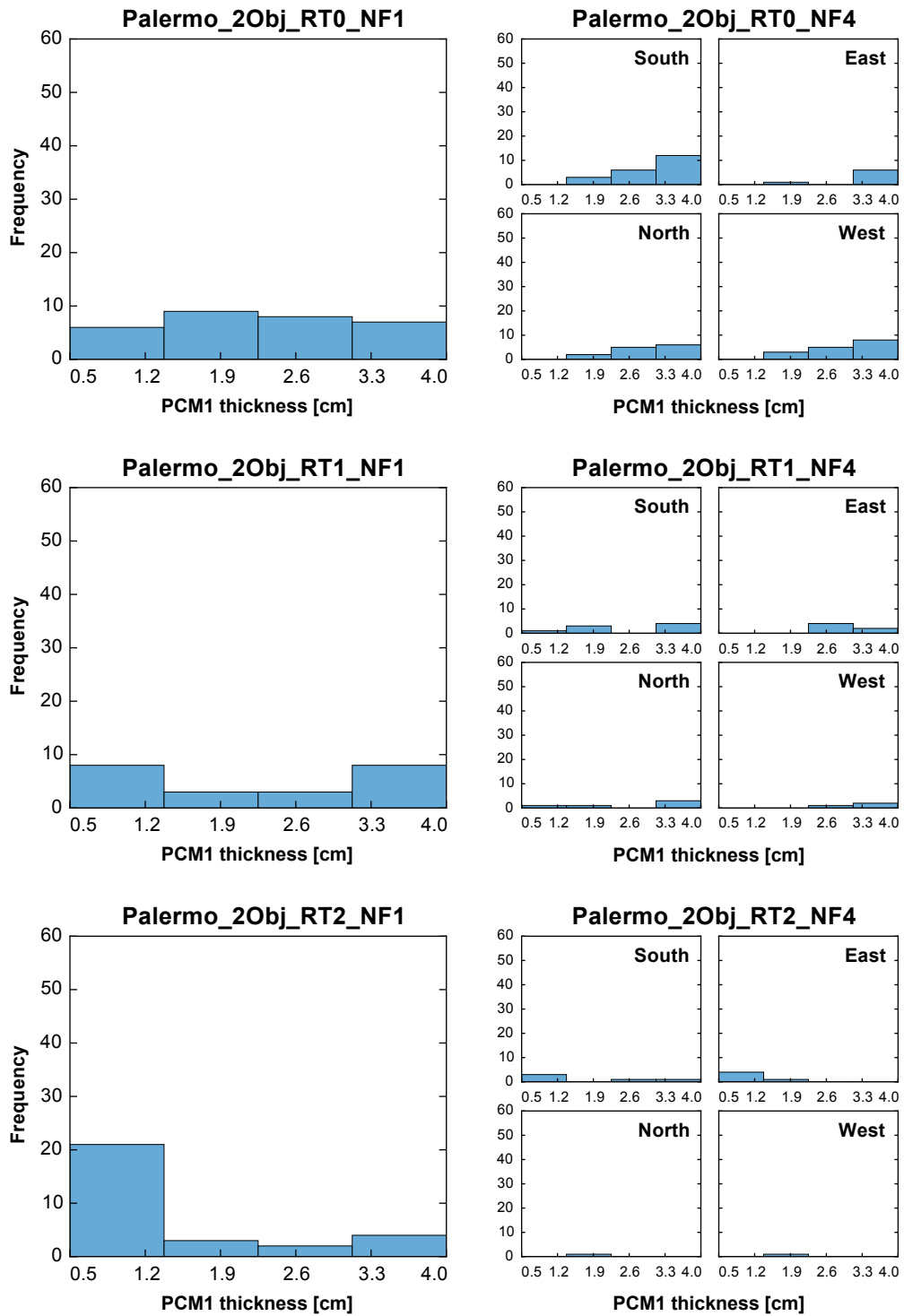
Fig. A.10 Frequency analyses: Palermo_2Obj, PCM1 thickness.
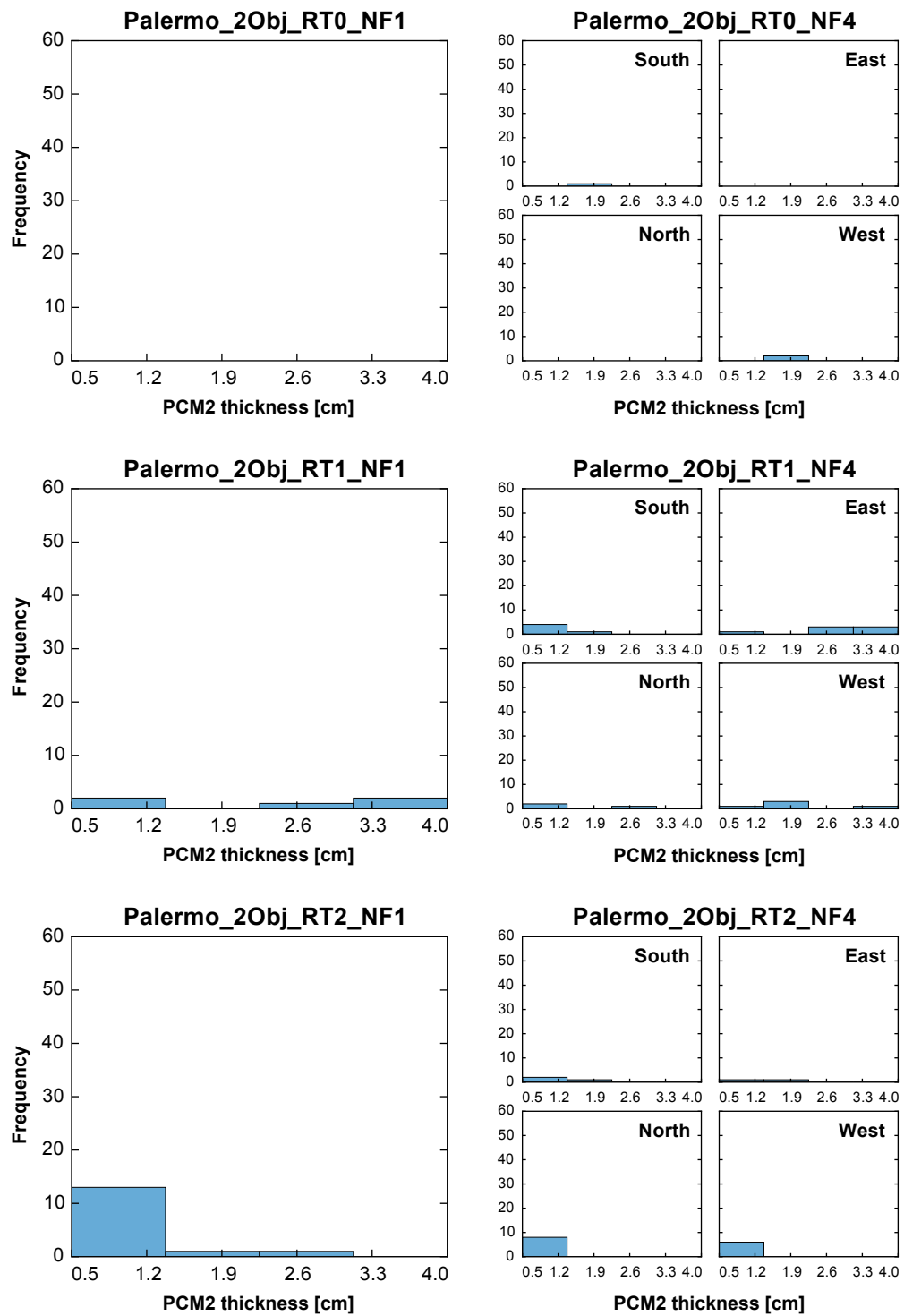
Fig. A.11 Frequency analyses: Palermo_2Obj, PCM2 thickness.
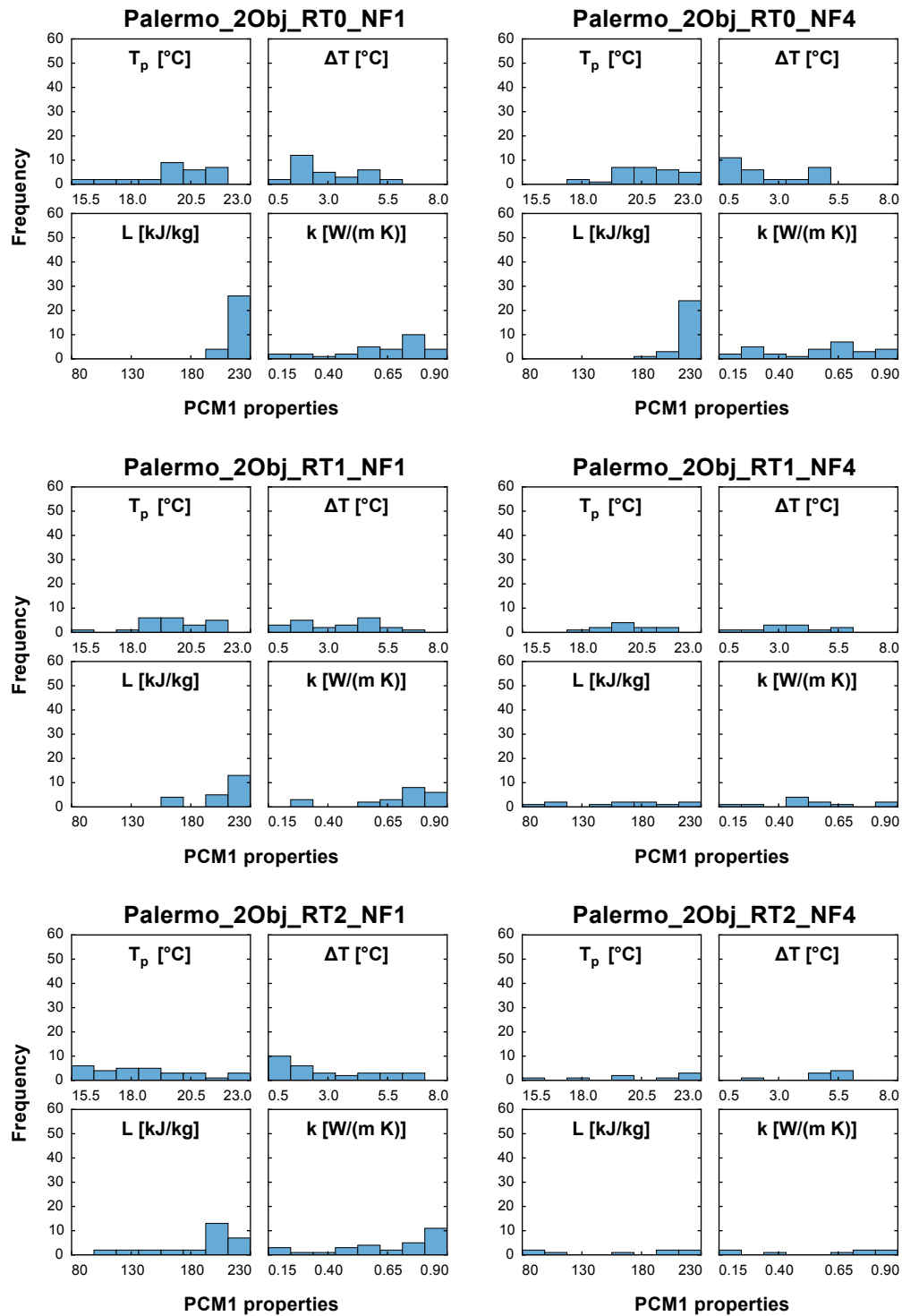
Fig. A.12 Frequency analyses: Palermo_2Obj, PCM1 properties.
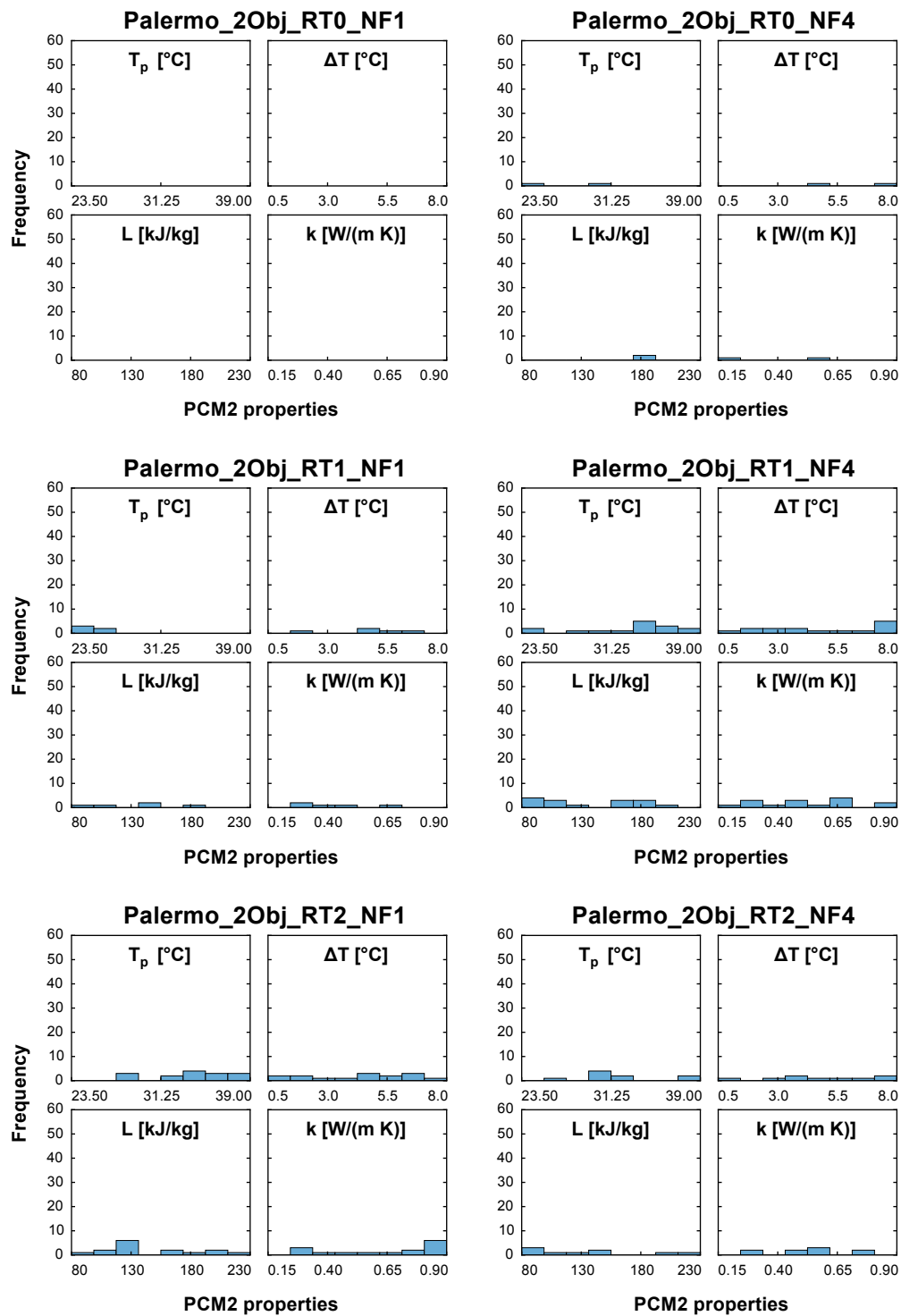
Fig. A.13 Frequency analyses: Palermo_2Obj, PCM2 properties.
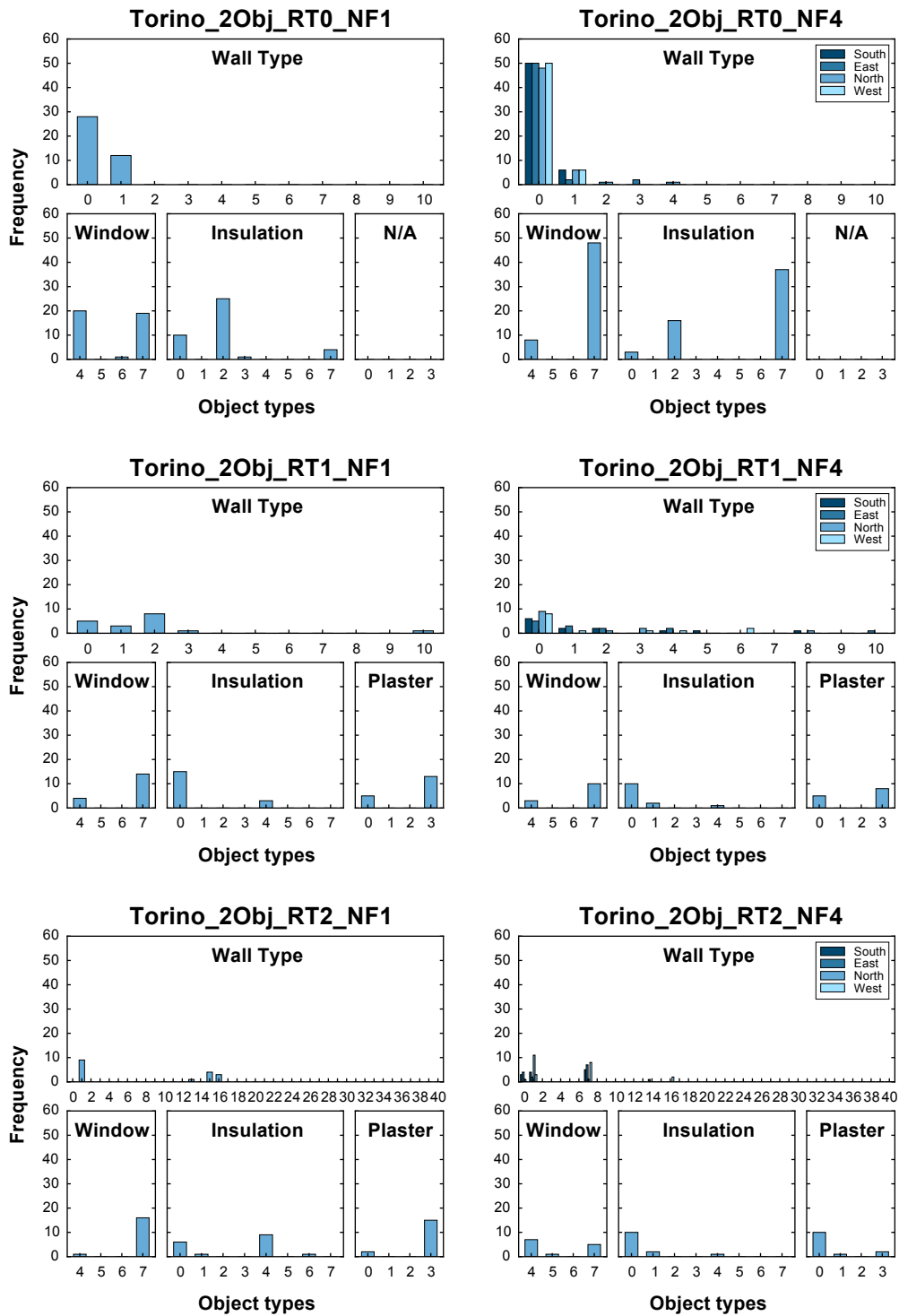
Fig. A.14 Frequency analyses: Torino_2Obj, discrete variables.
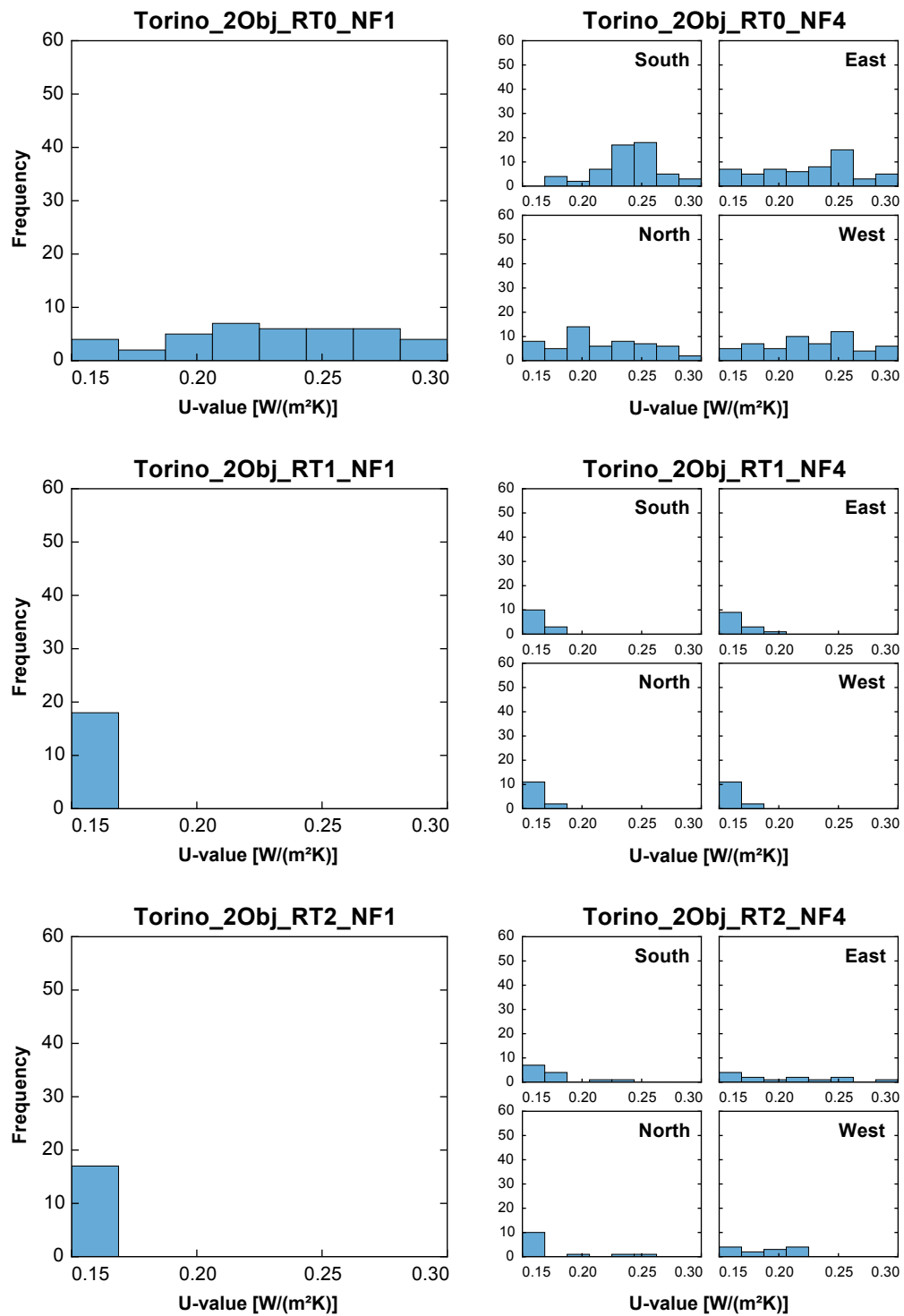
Fig. A.15 Frequency analyses: Torino_2Obj, U-values.
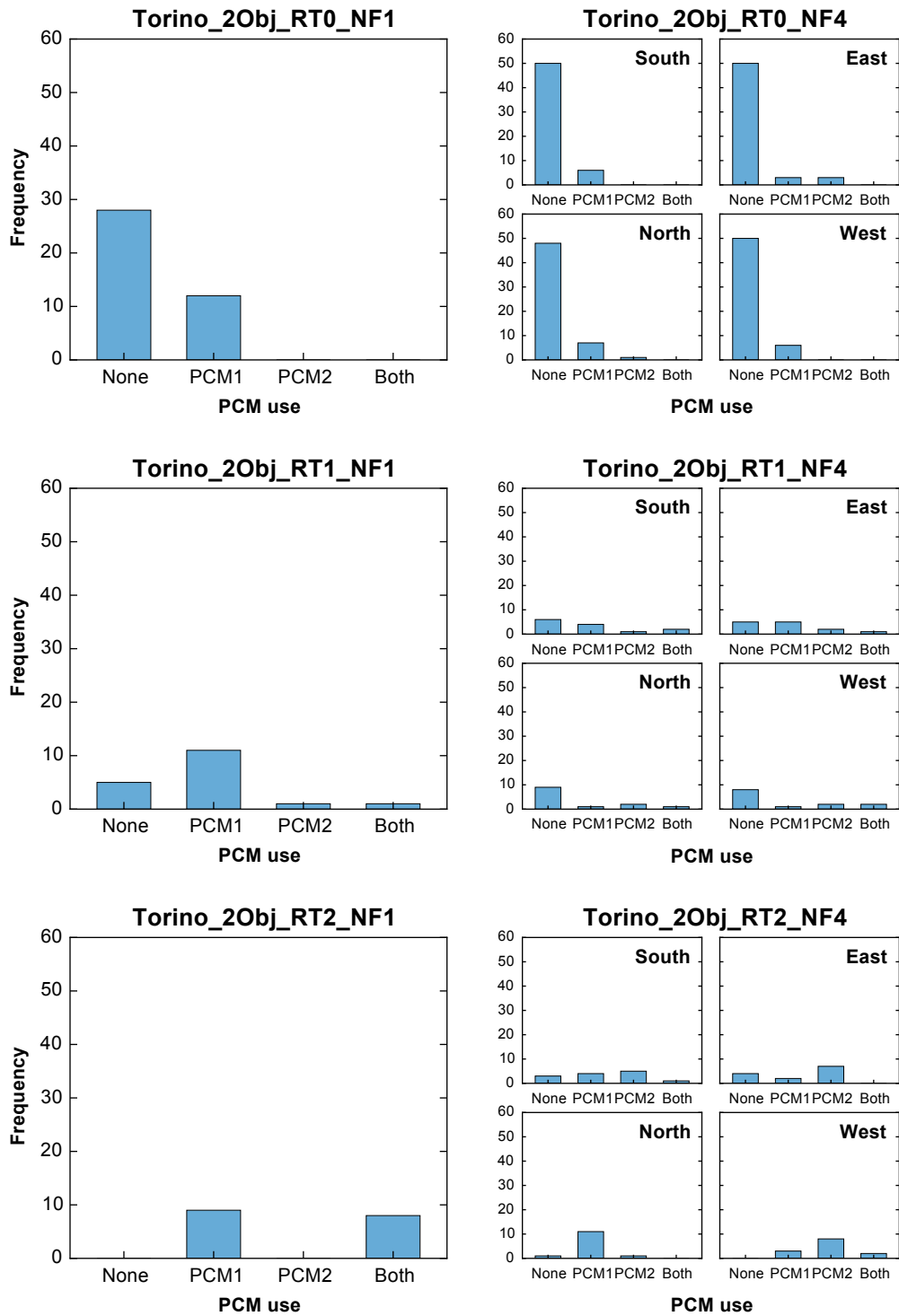
Fig. A.16 Frequency analyses: Torino_2Obj, PCM use.
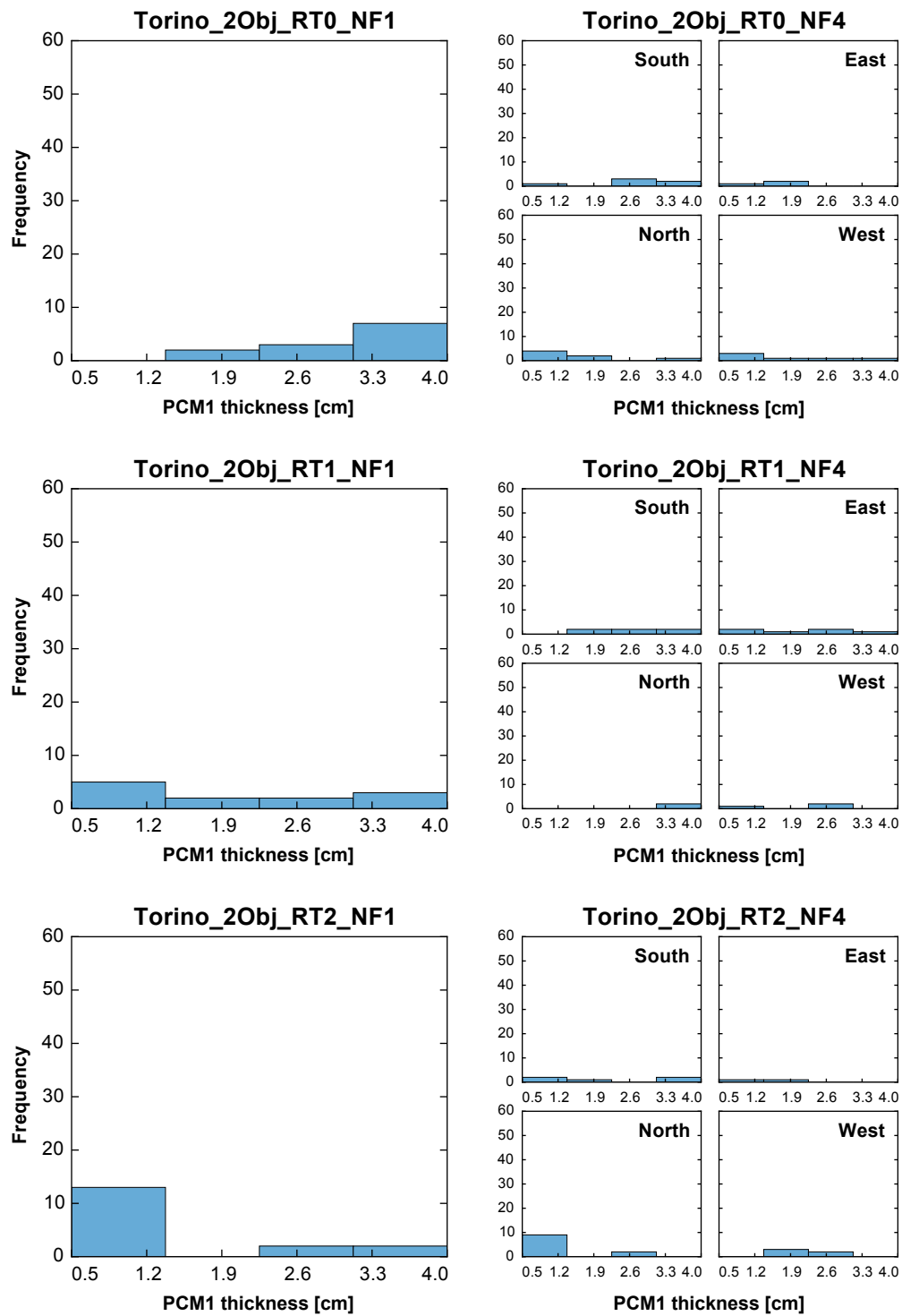
Fig. A.17 Frequency analyses: Torino_2Obj, PCM1 thickness.
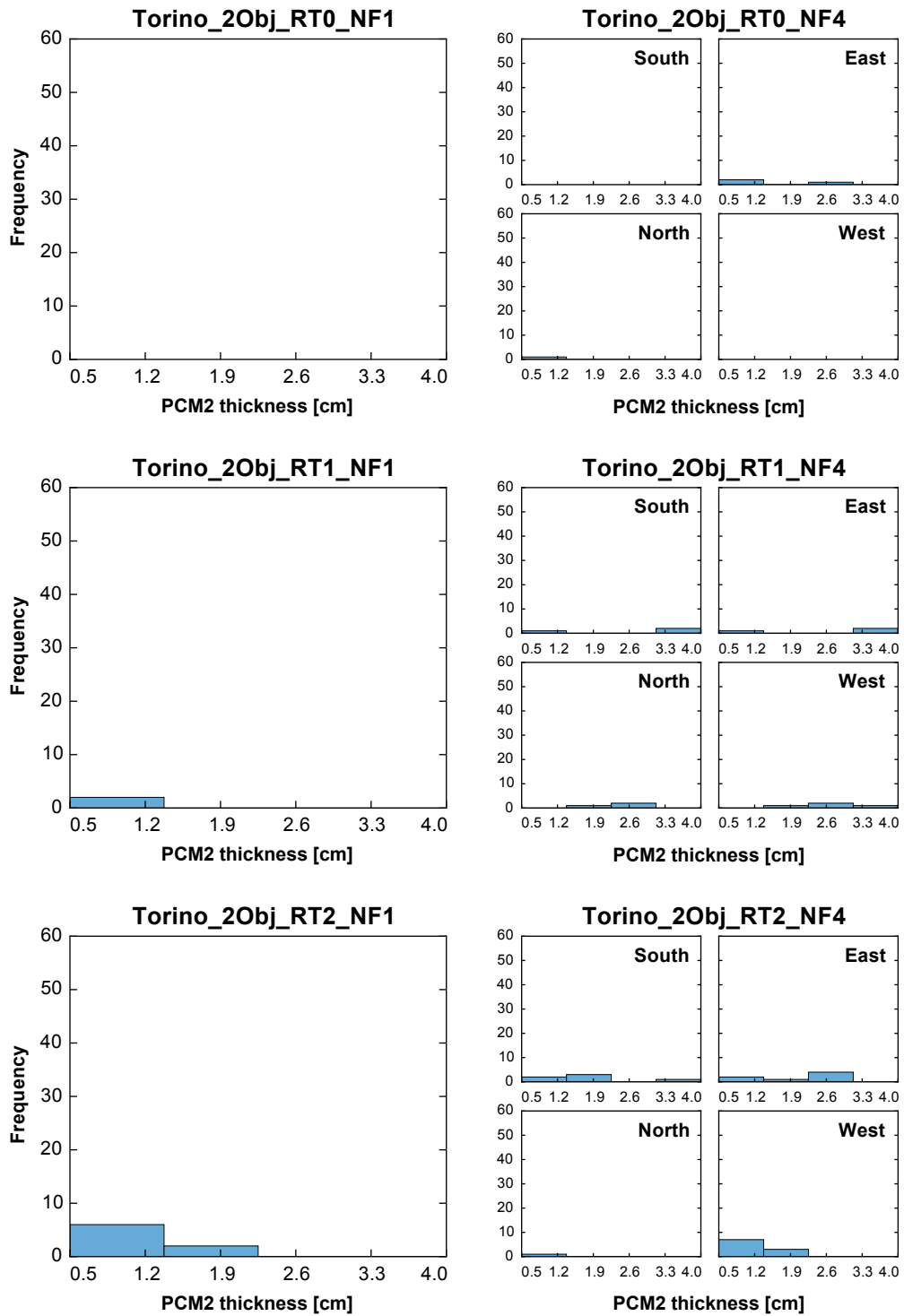
Fig. A.18 Frequency analyses: Torino_2Obj, PCM2 thickness.
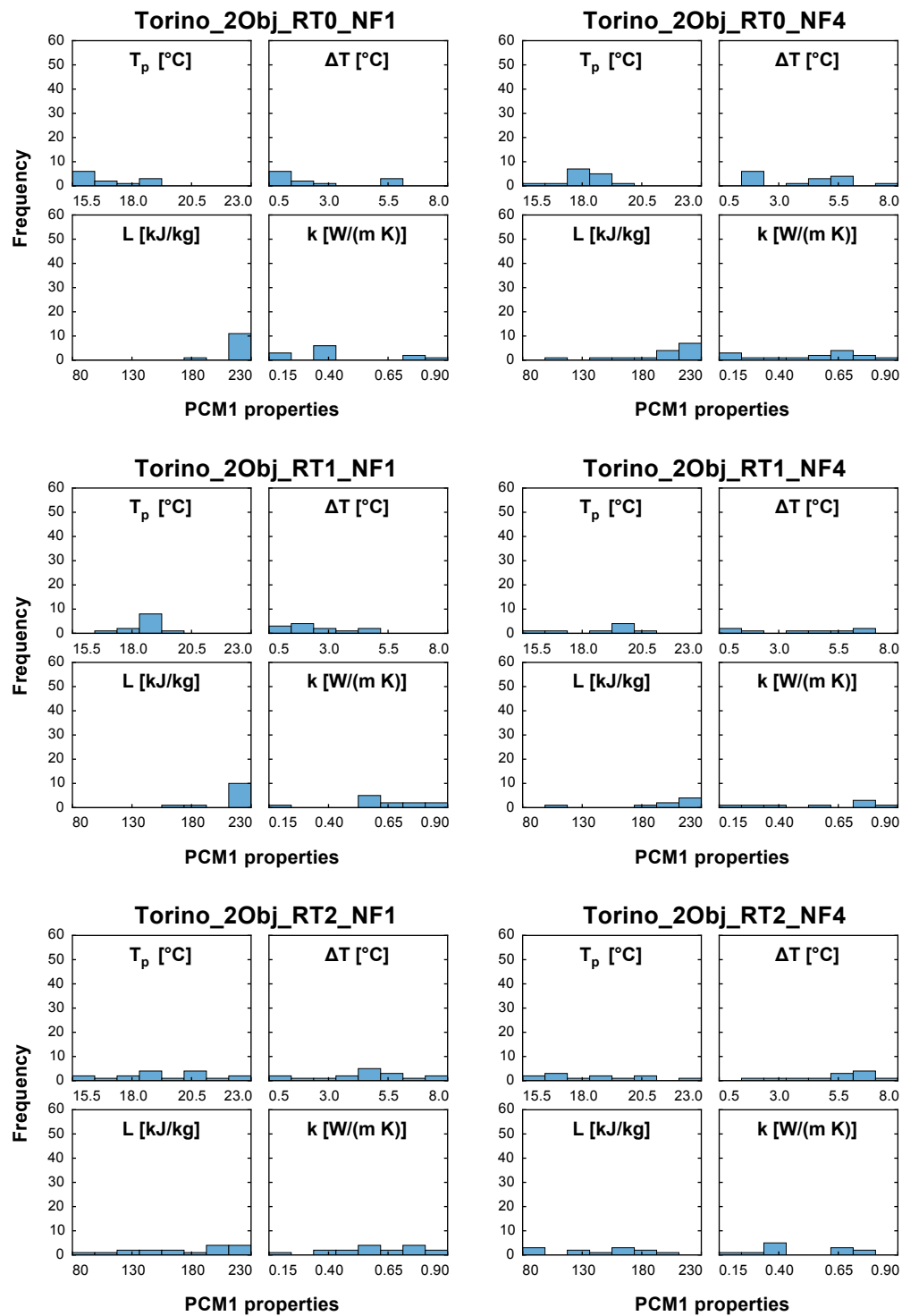
Fig. A.19 Frequency analyses: Torino_2Obj, PCM1 properties.
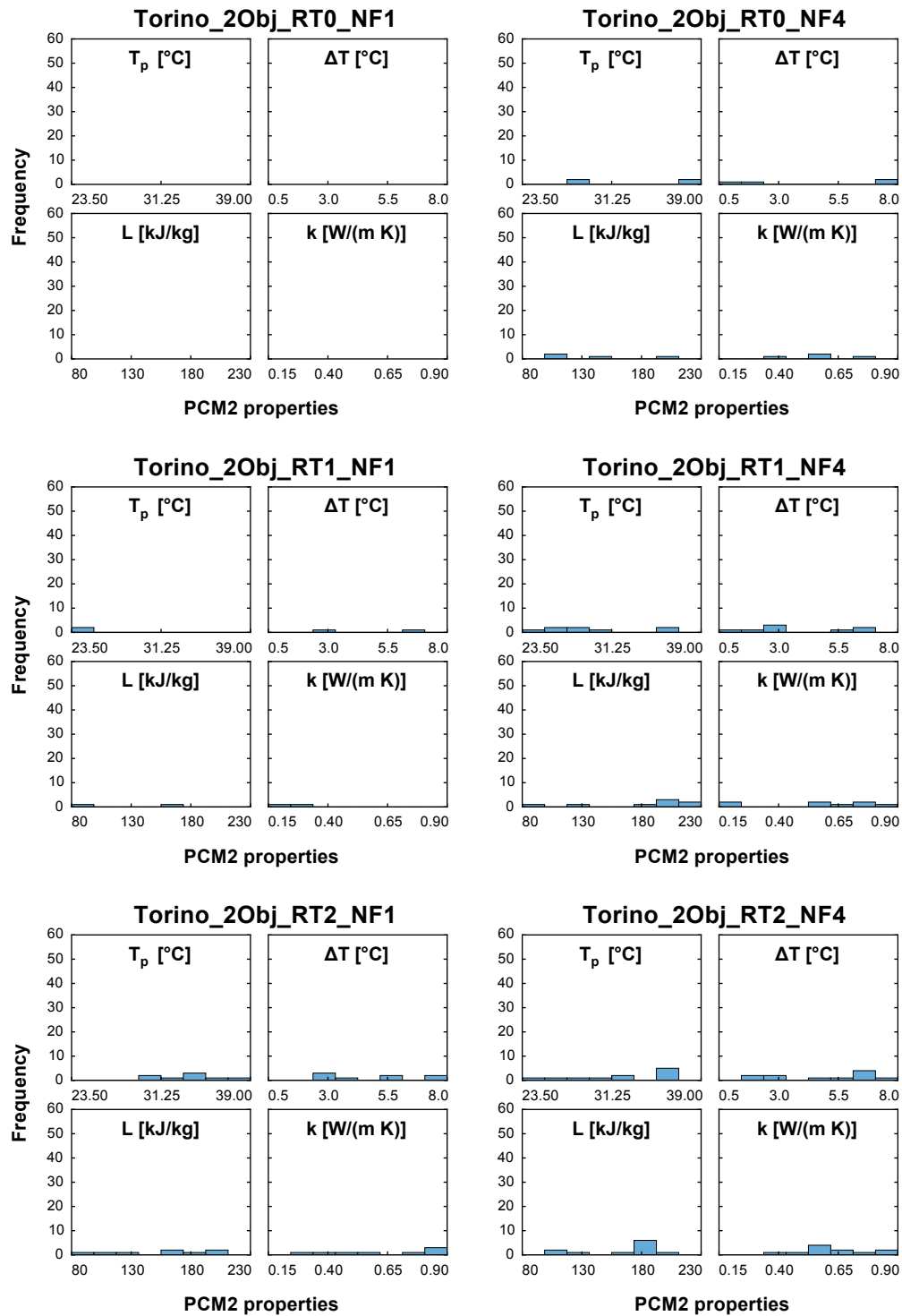
Fig. A.20 Frequency analyses: Torino_2Obj, PCM2 properties.
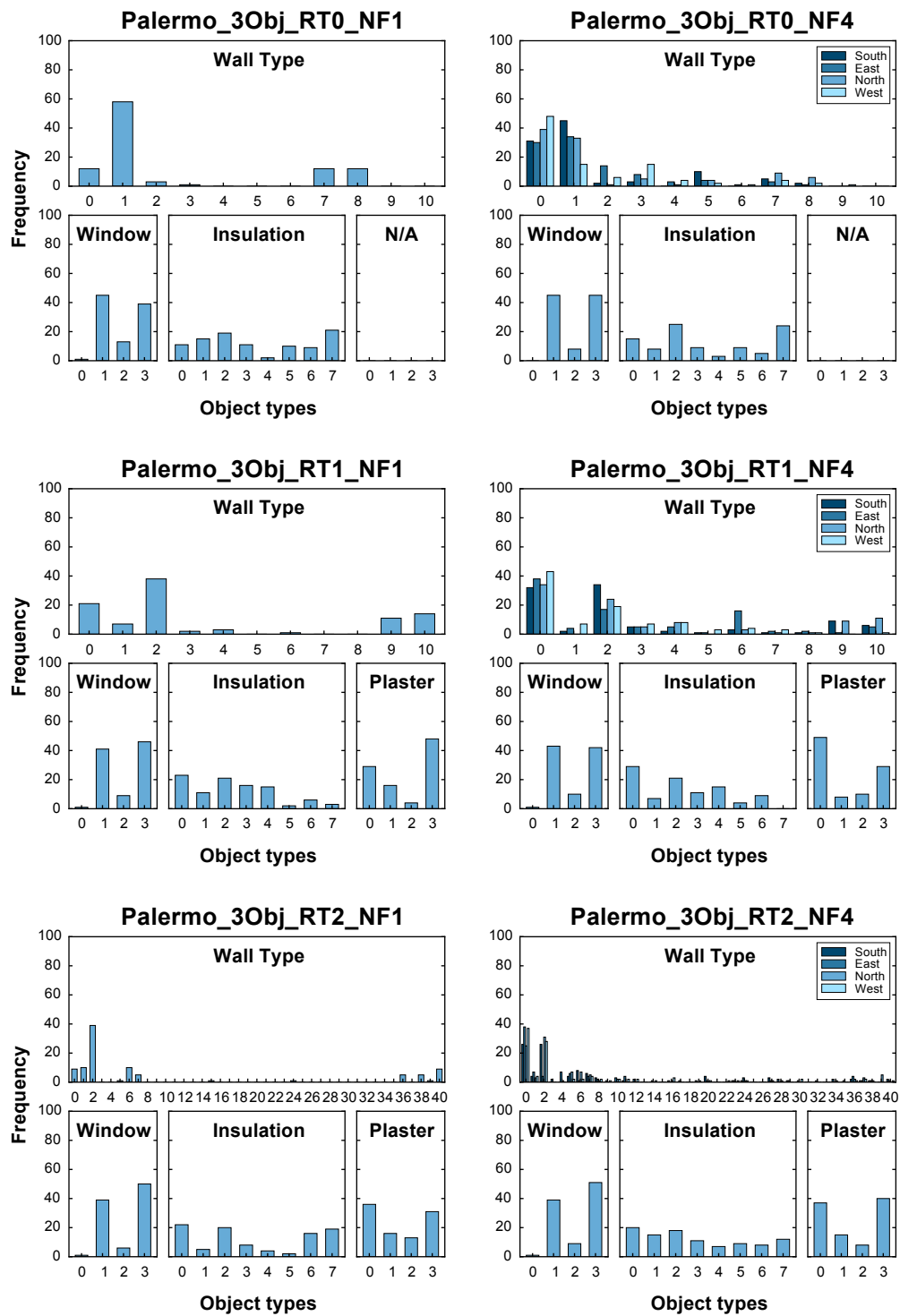
Fig. A.21 Frequency analyses: Palermo_3Obj, discrete variables.
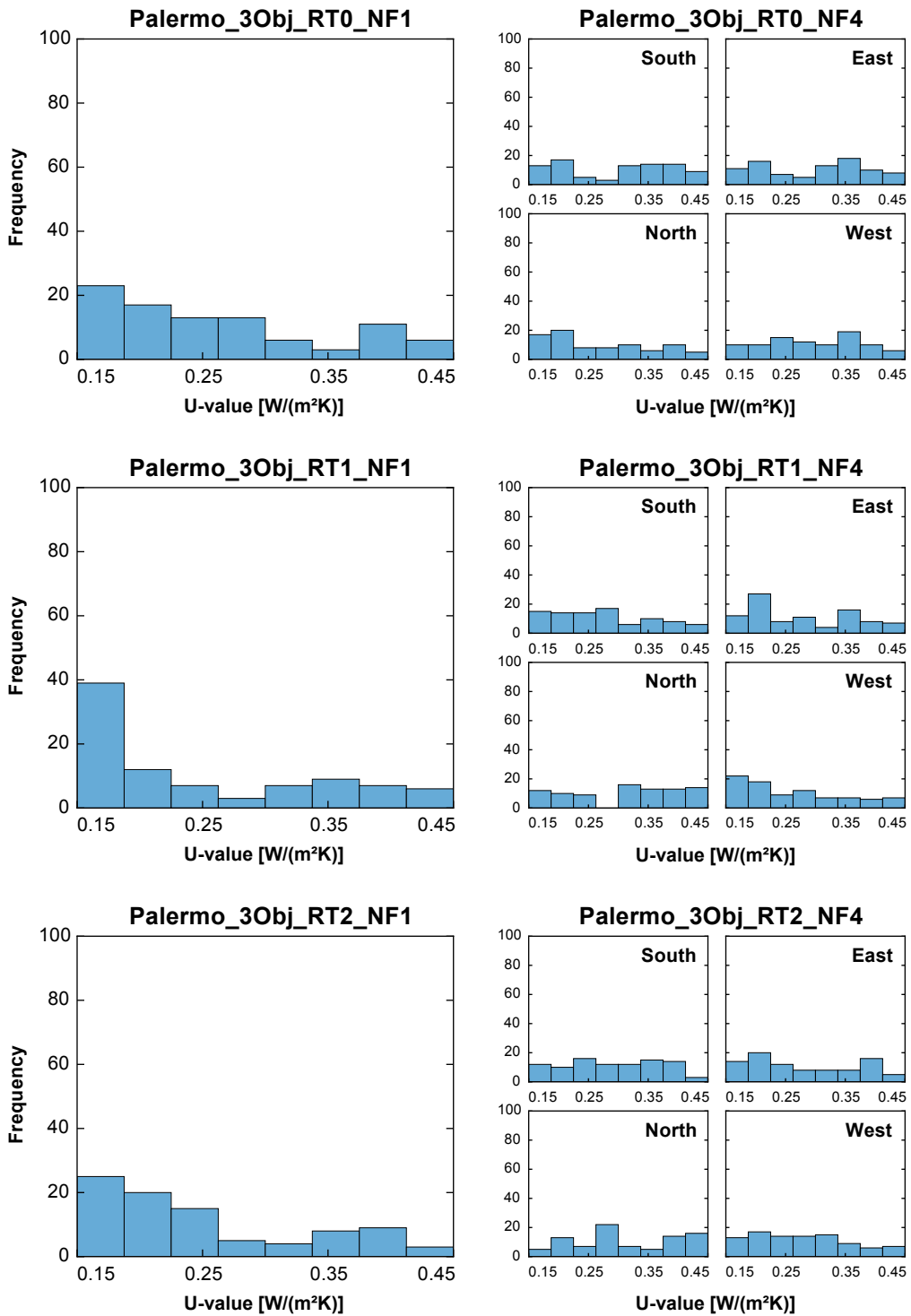
Fig. A.22 Frequency analyses: Palermo_3Obj, U-values.
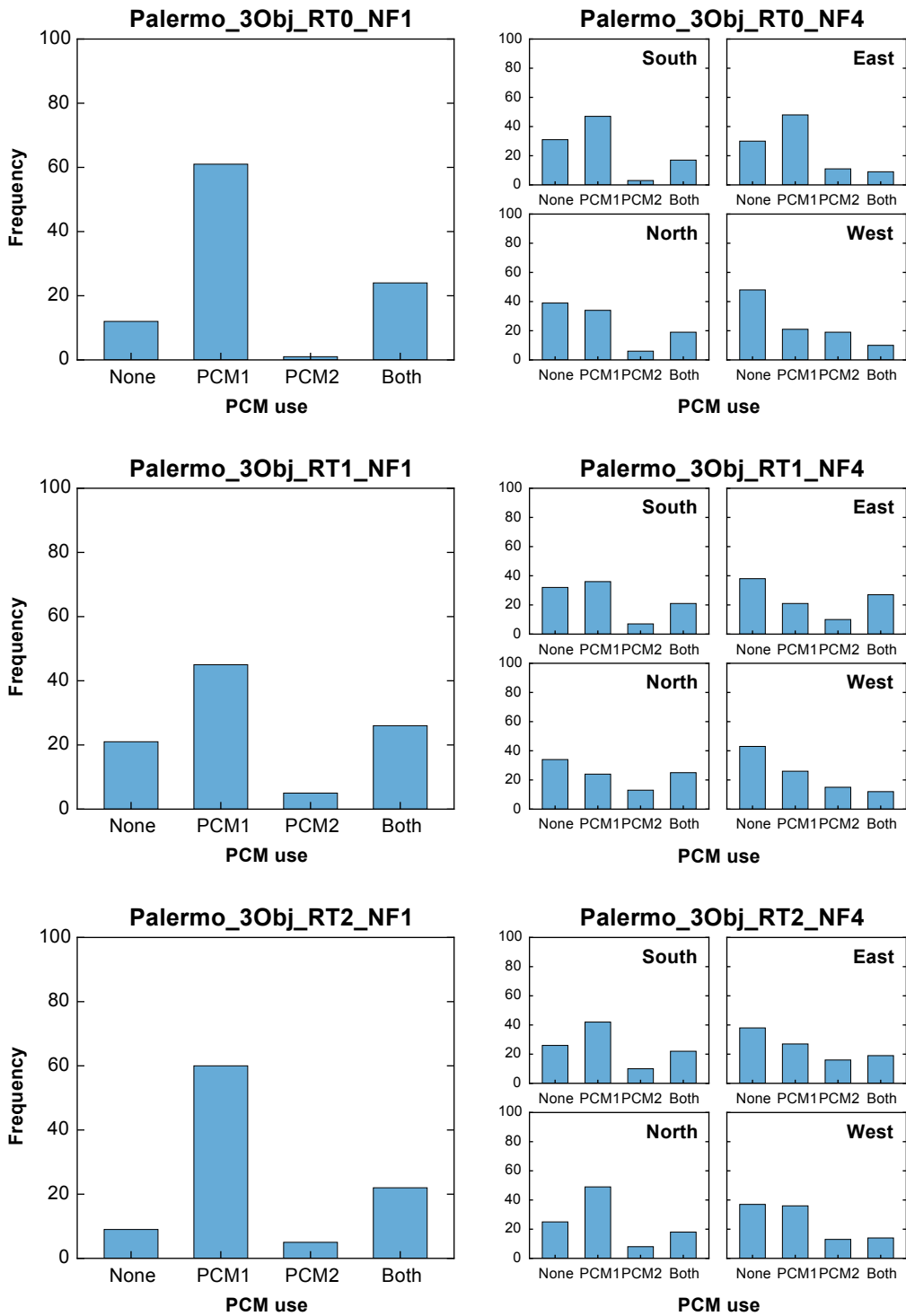
Fig. A.23 Frequency analyses: Palermo_3Obj, PCM use.
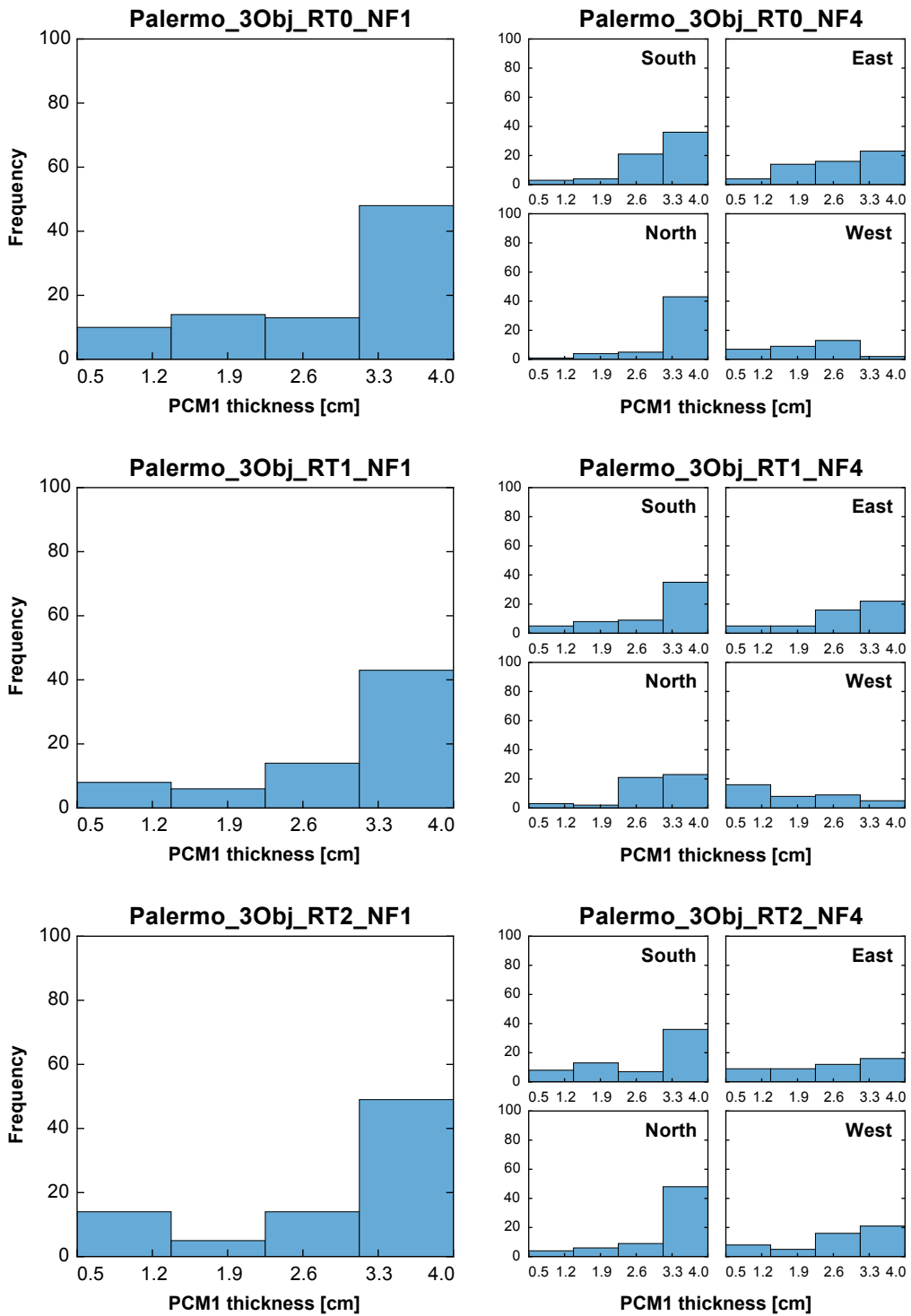
Fig. A.24 Frequency analyses: Palermo_3Obj, PCM1 thickness.
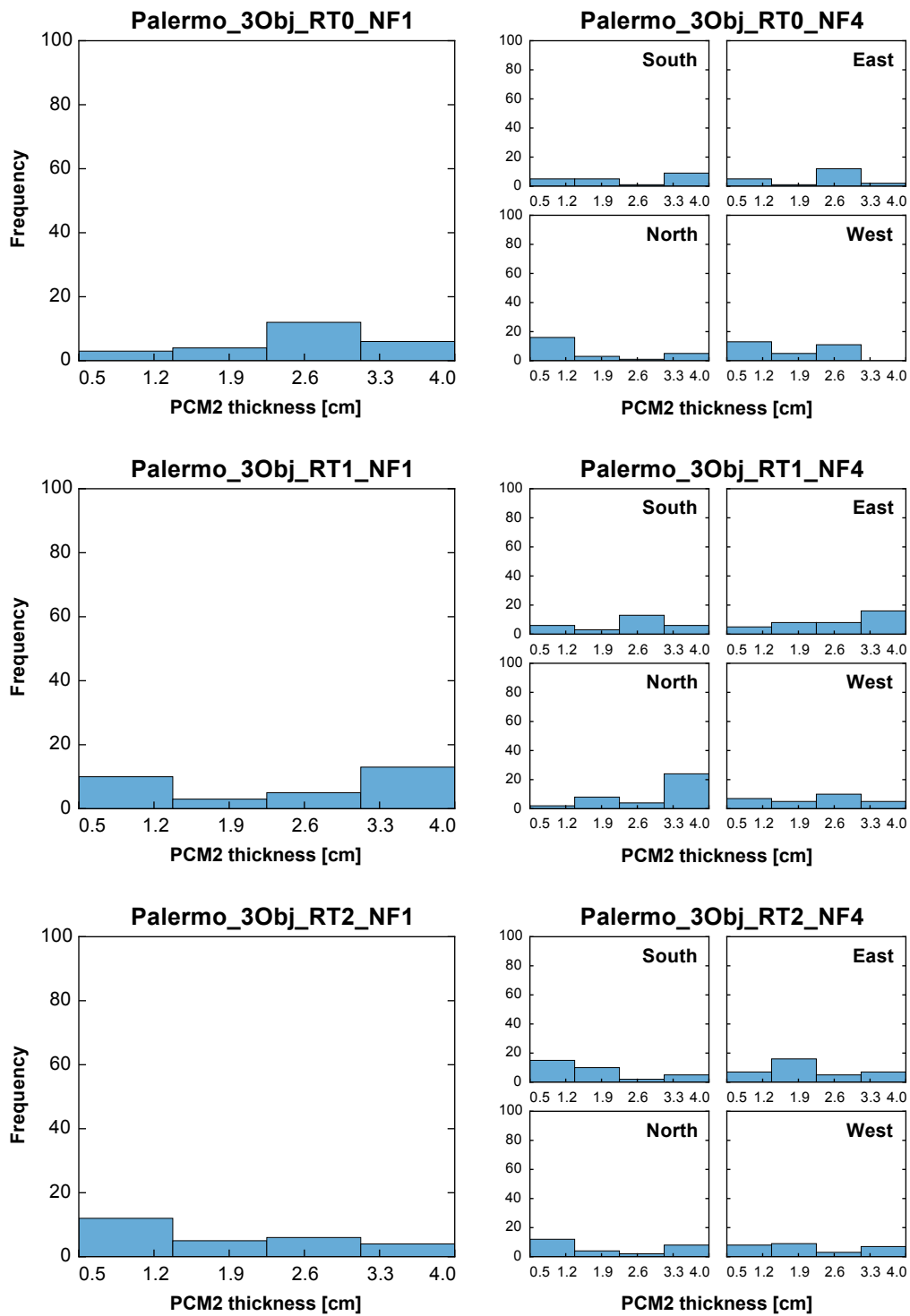
Fig. A.25 Frequency analyses: Palermo_3Obj, PCM2 thickness.
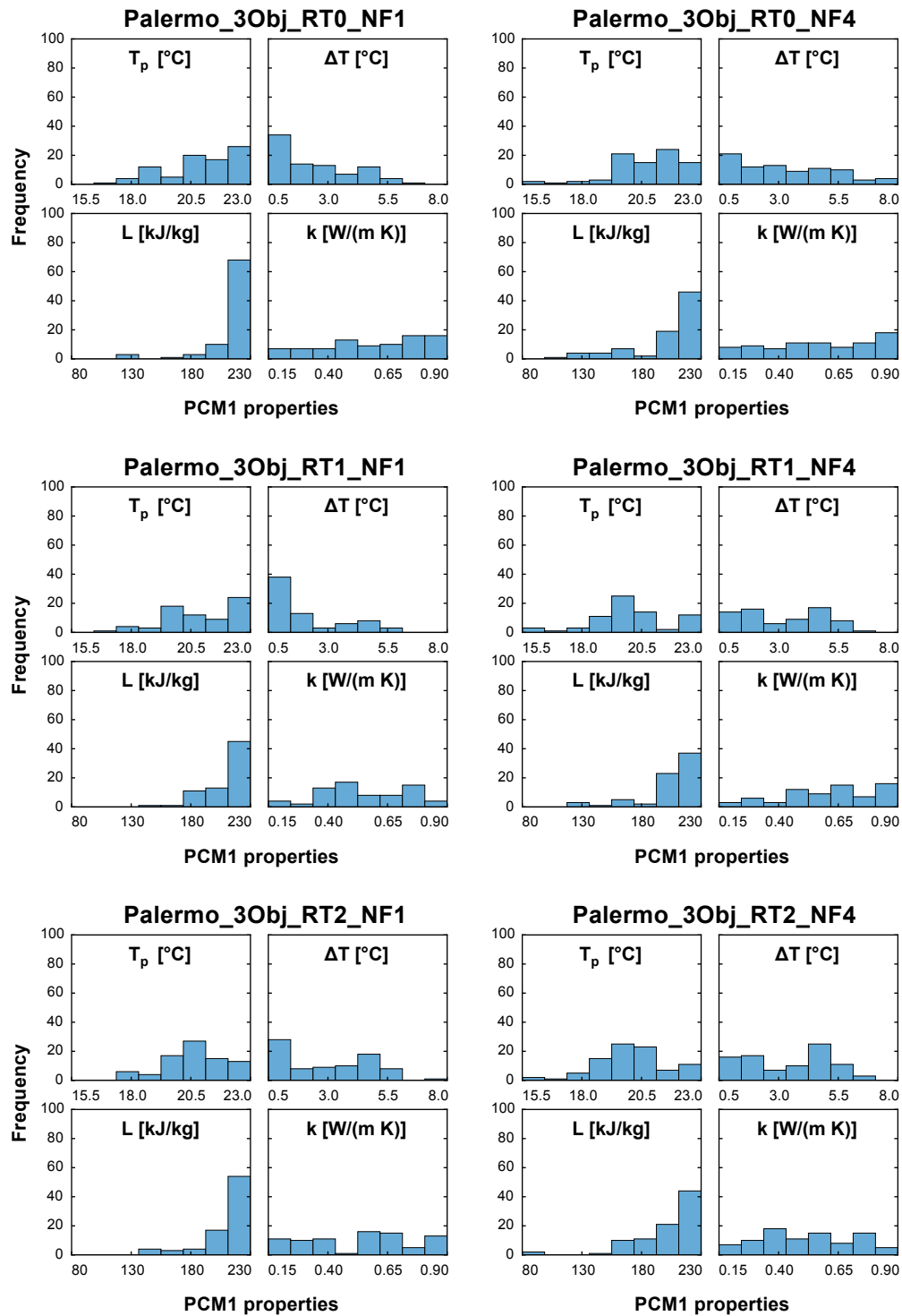
Fig. A.26 Frequency analyses: Palermo_3Obj, PCM1 properties.
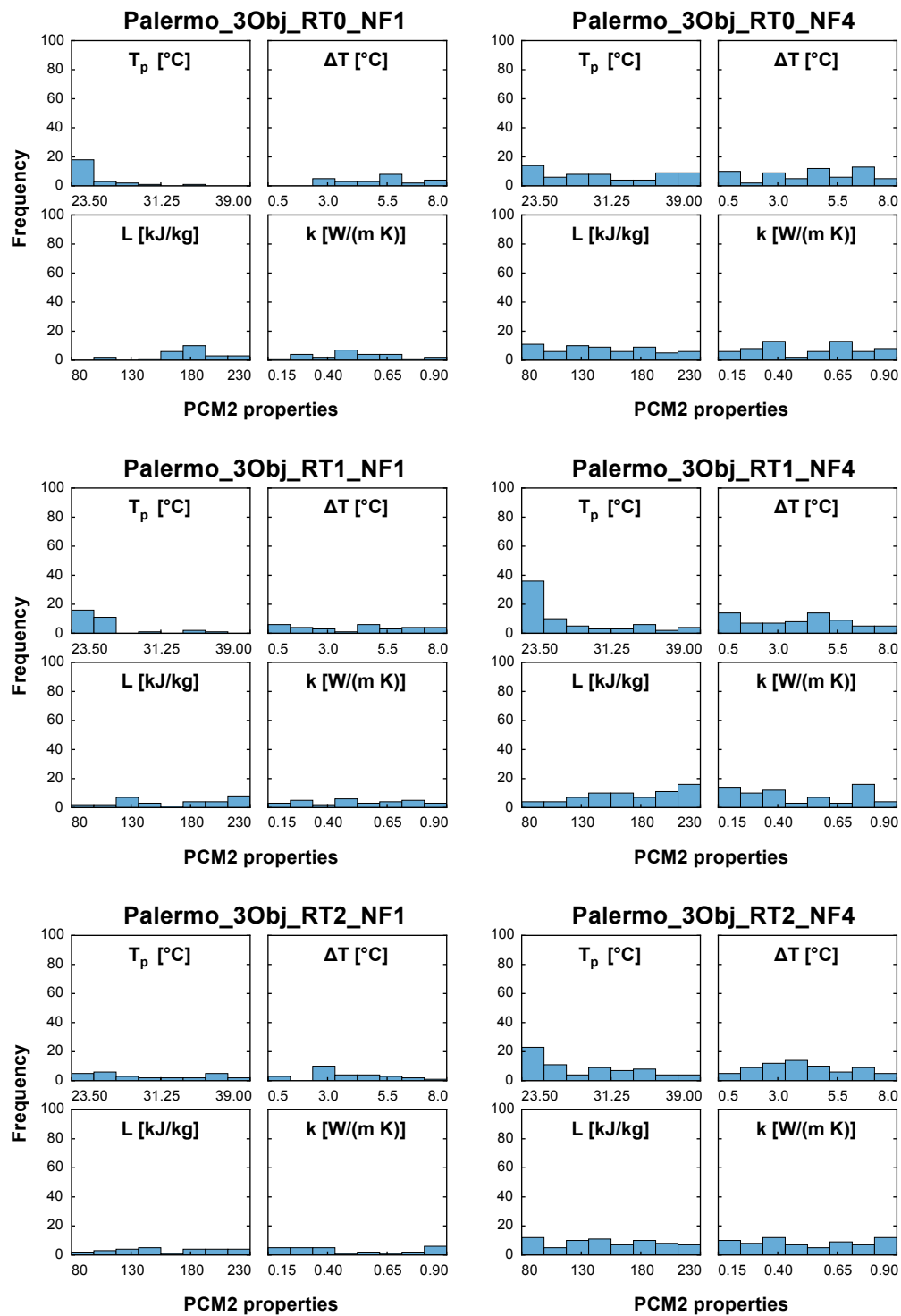
Fig. A.27 Frequency analyses: Palermo_3Obj, PCM2 properties.
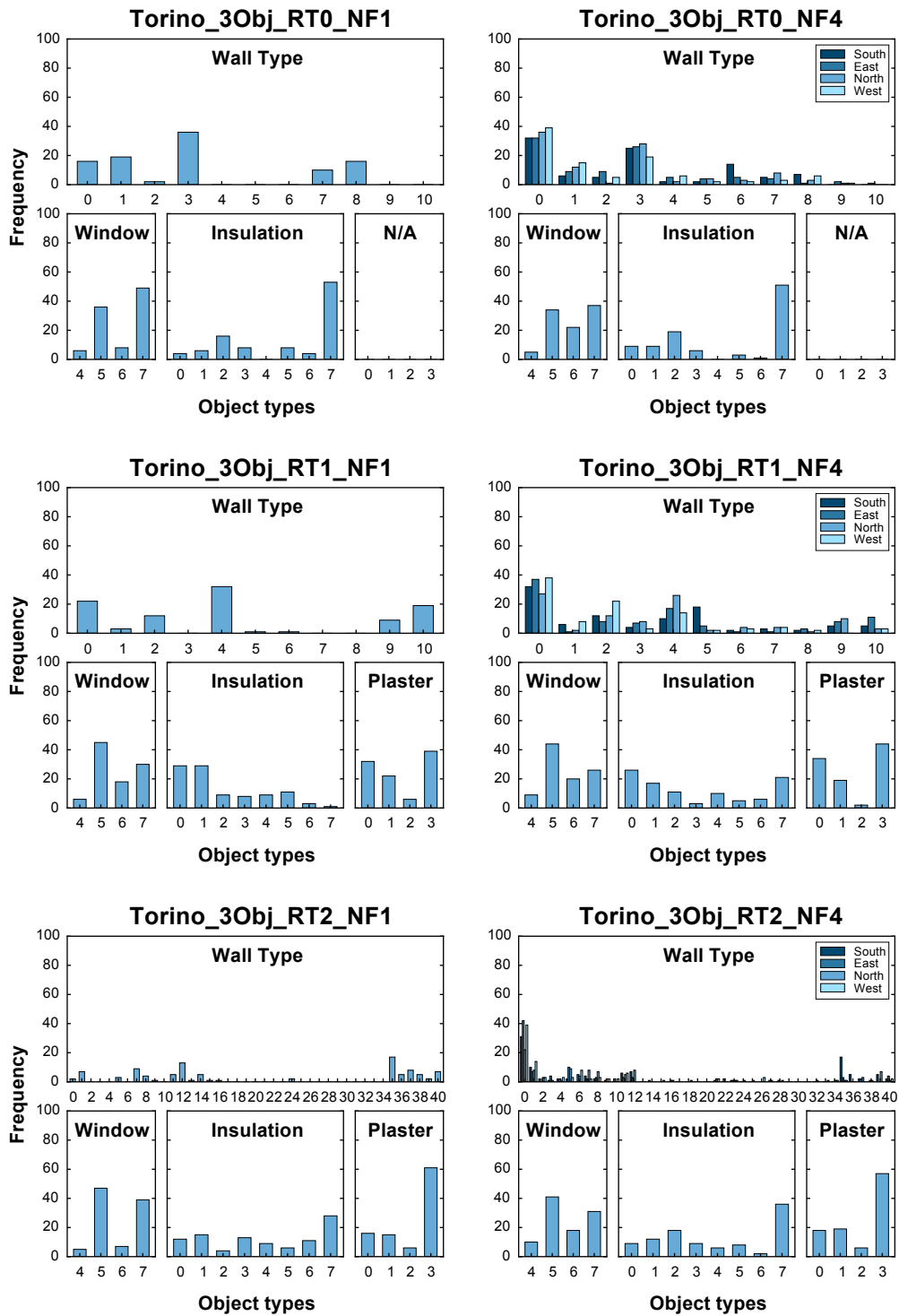
Fig. A.28 Frequency analyses: Torino_3Obj, discrete variables.
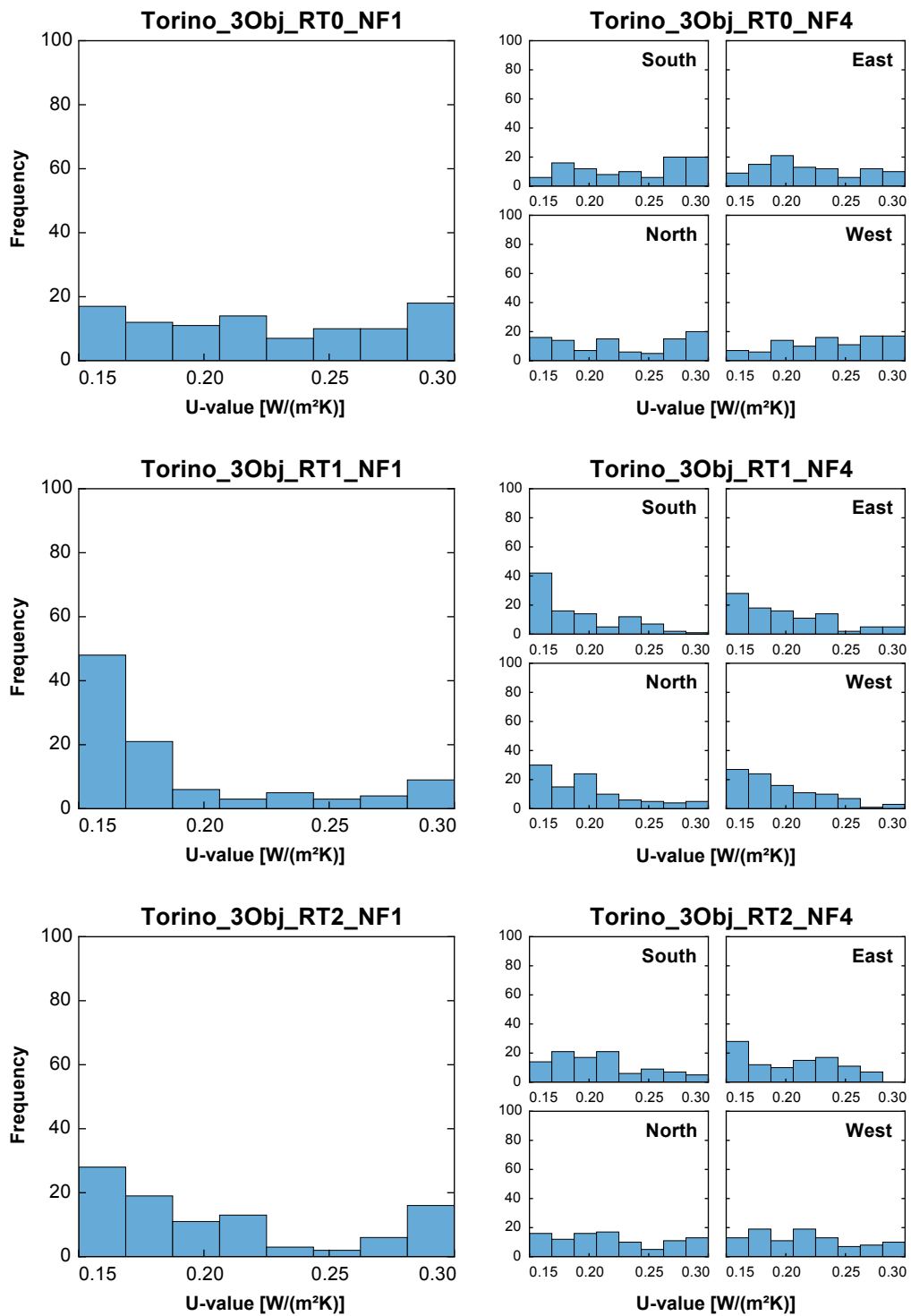
Fig. A.29 Frequency analyses: Torino_3Obj, U-values.
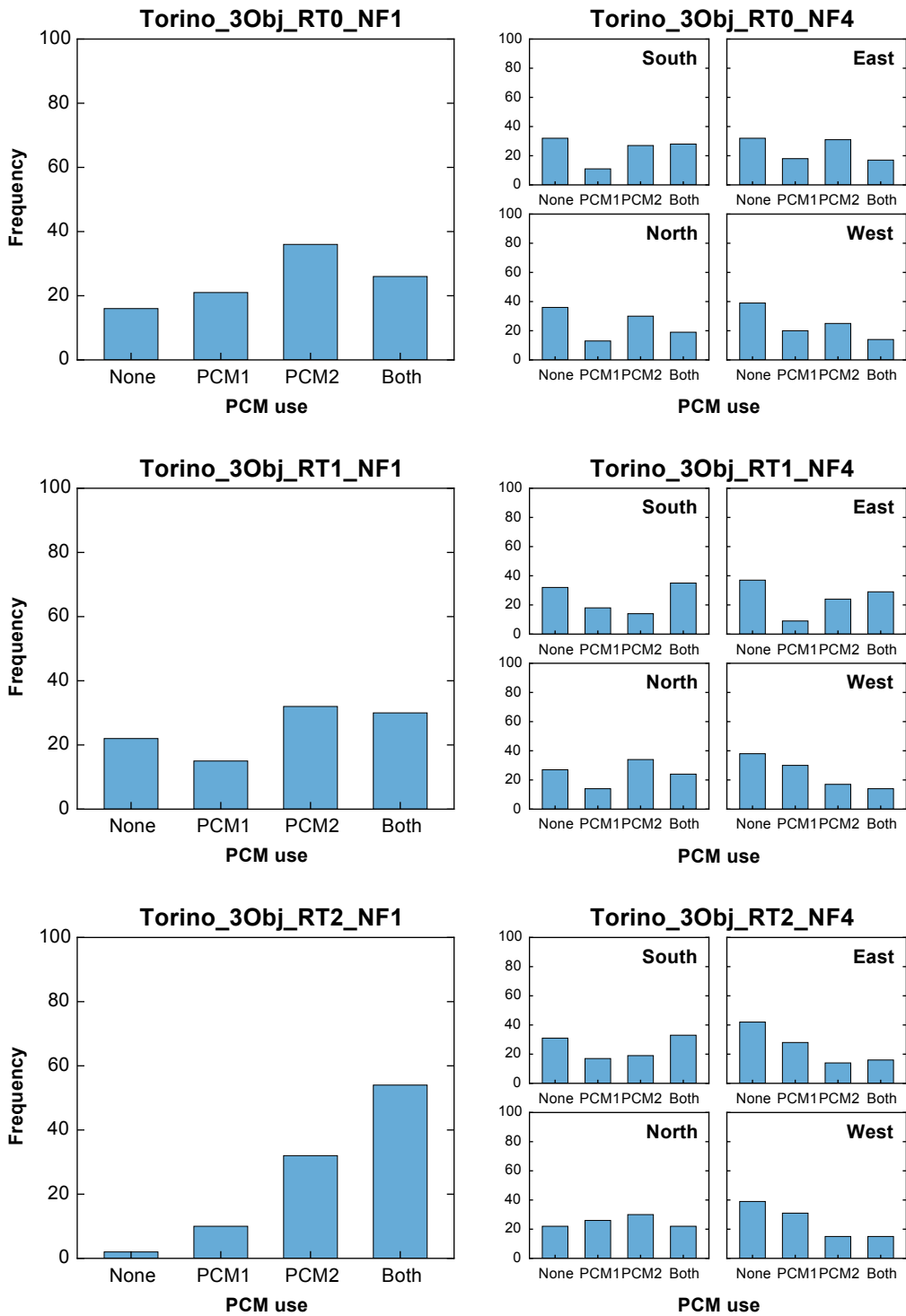
Fig. A.30 Frequency analyses: Torino_3Obj, PCM use.
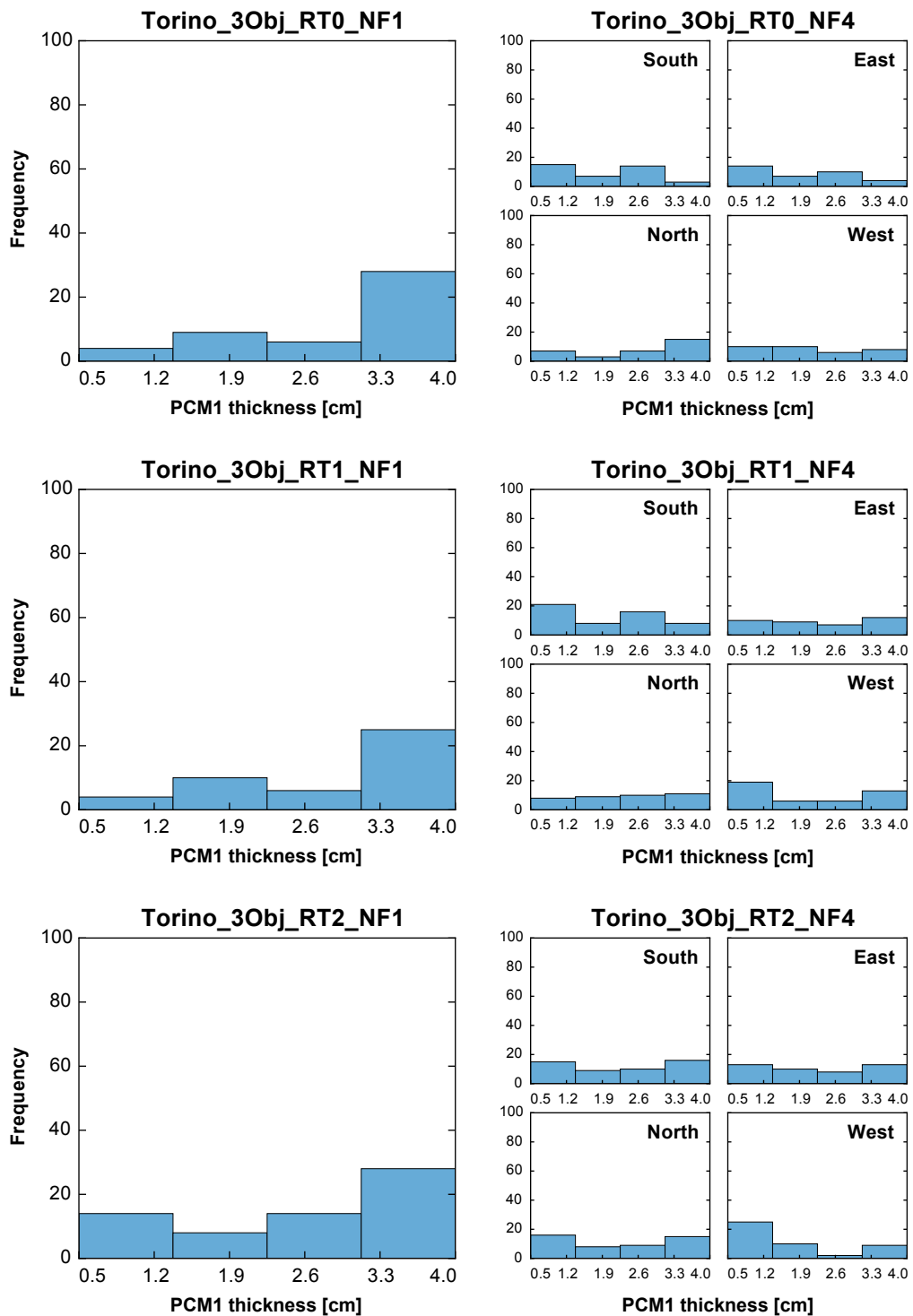
Fig. A.31 Frequency analyses: Torino_3Obj, PCM1 thickness.
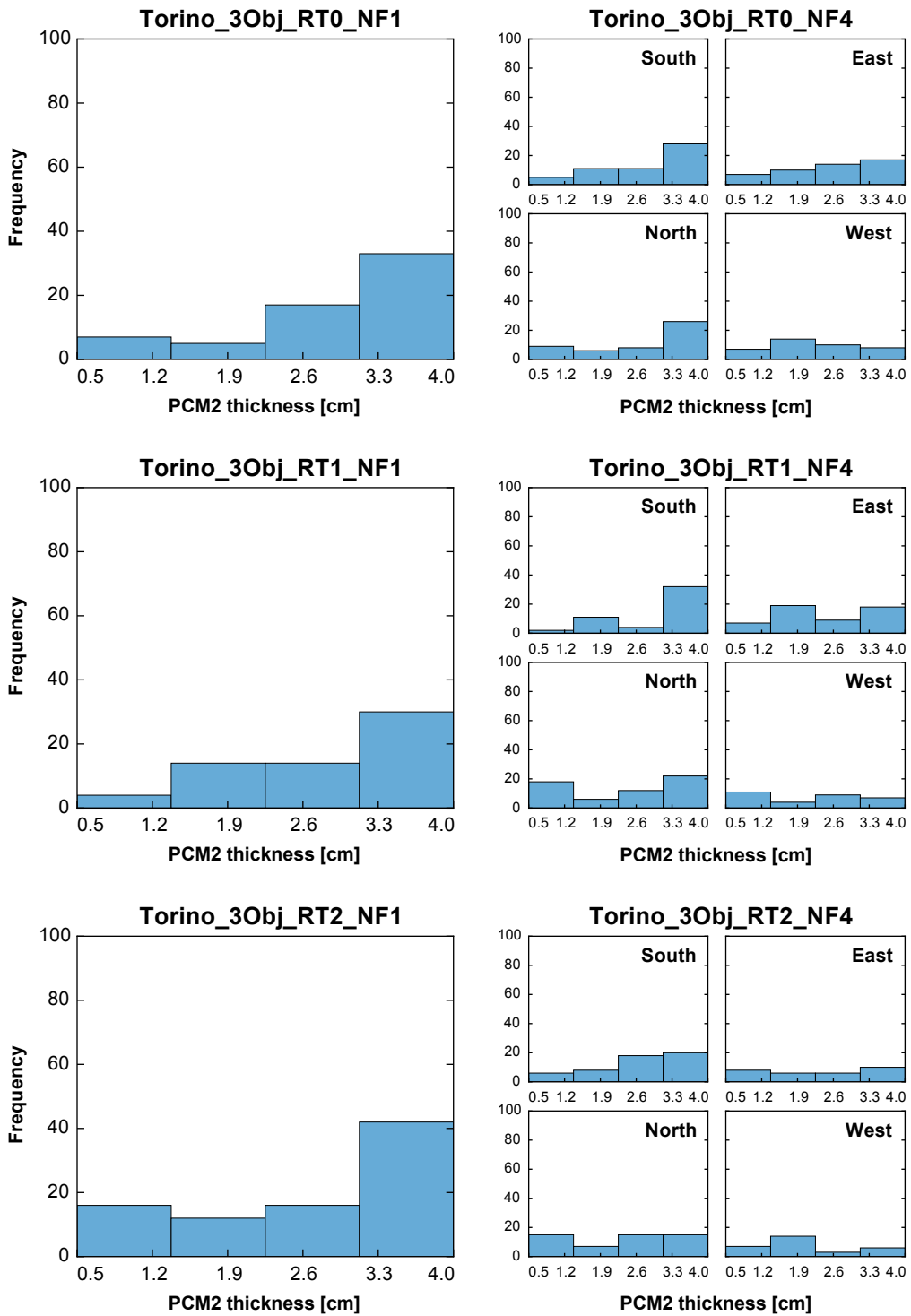
Fig. A.32 Frequency analyses: Torino_3Obj, PCM2 thickness.
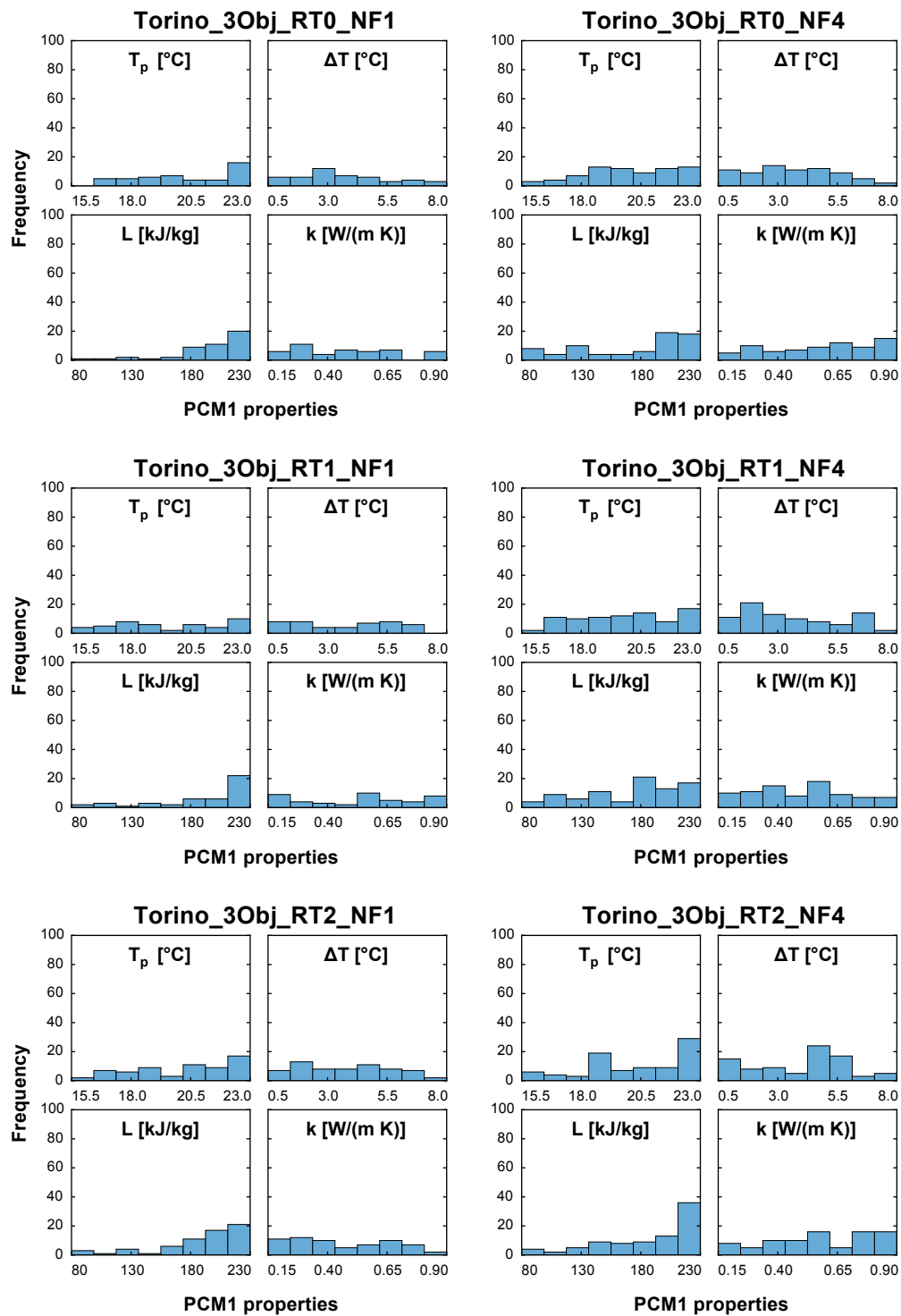
Fig. A.33 Frequency analyses: Torino_3Obj, PCM1 properties.
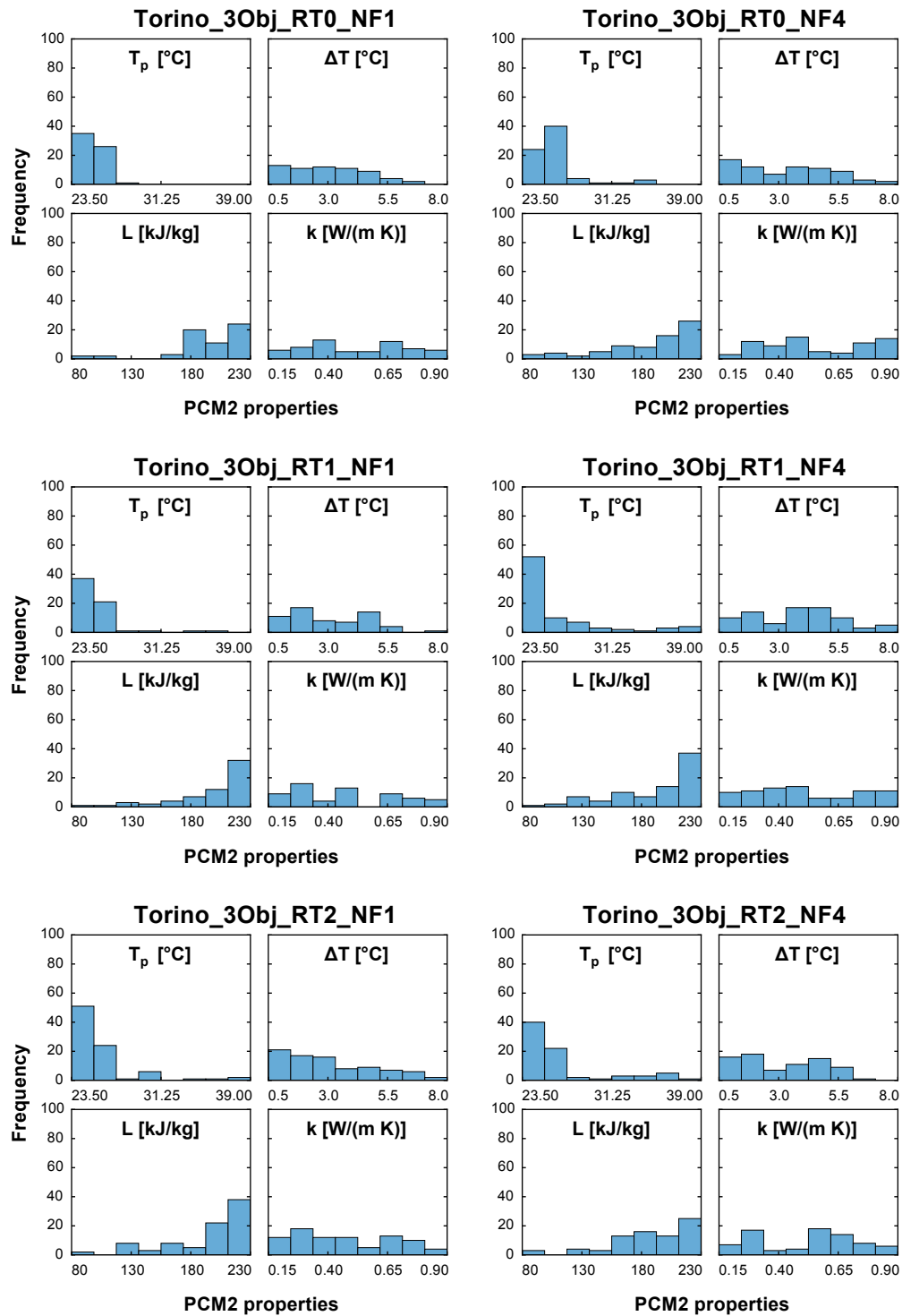
Fig. A.34 Frequency analyses: Torino_3Obj, PCM2 properties.
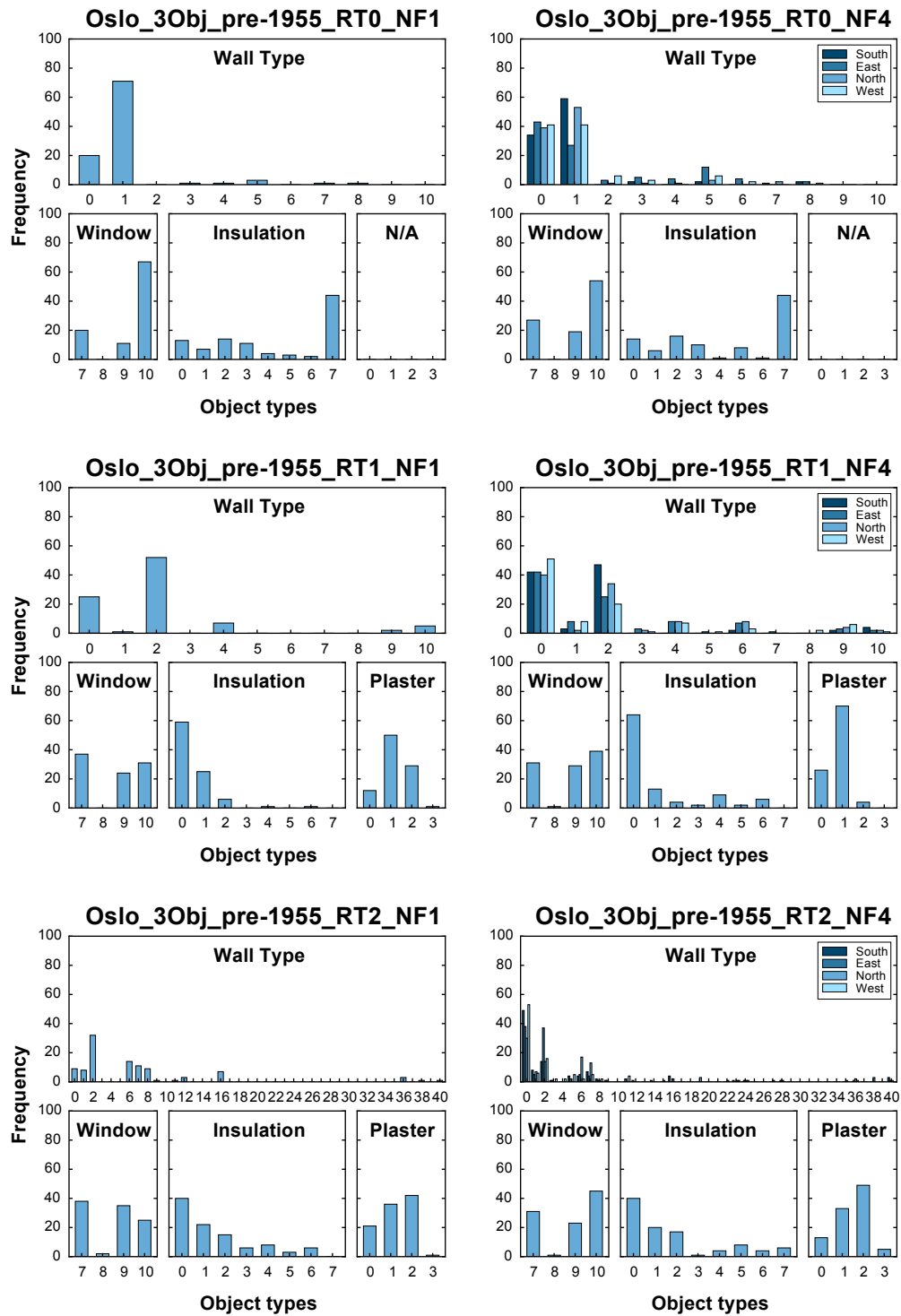
Fig. A.35 Frequency analyses: Oslo_3Obj_pre-1955, discrete variables.
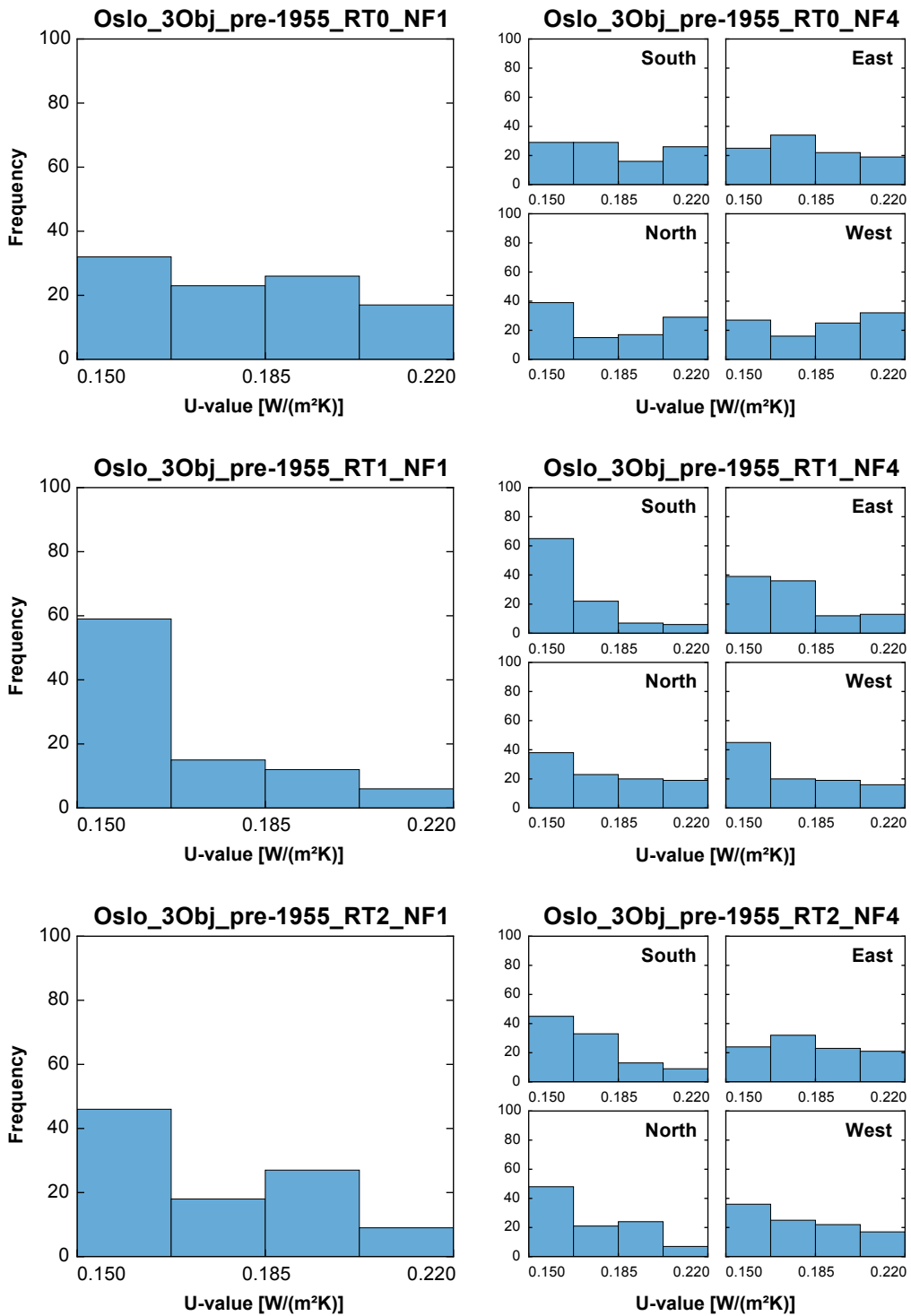
Fig. A.36 Frequency analyses: Oslo_3Obj_pre-1955, U-values.
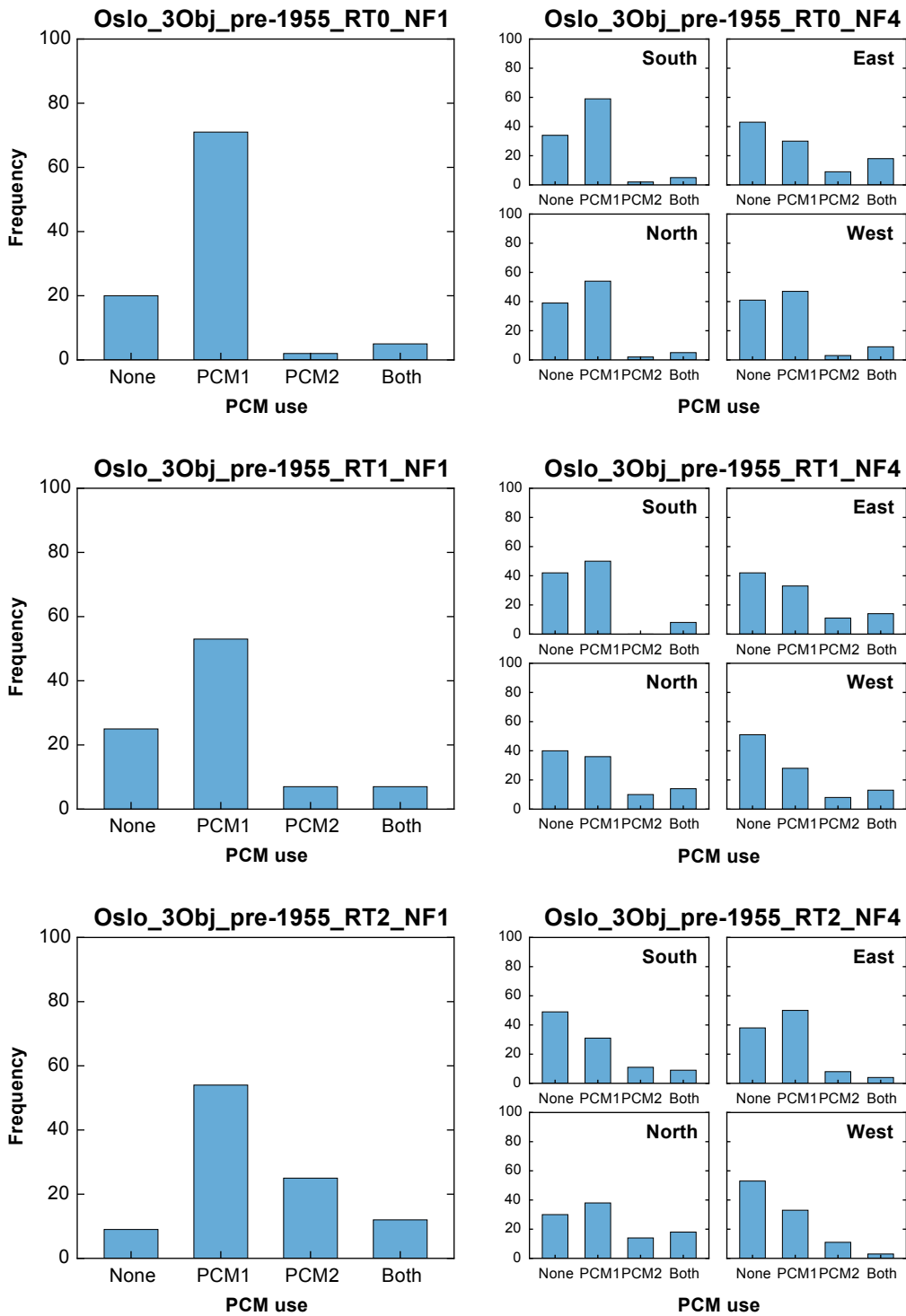
Fig. A.37 Frequency analyses: Oslo_3Obj_pre-1955, PCM use.
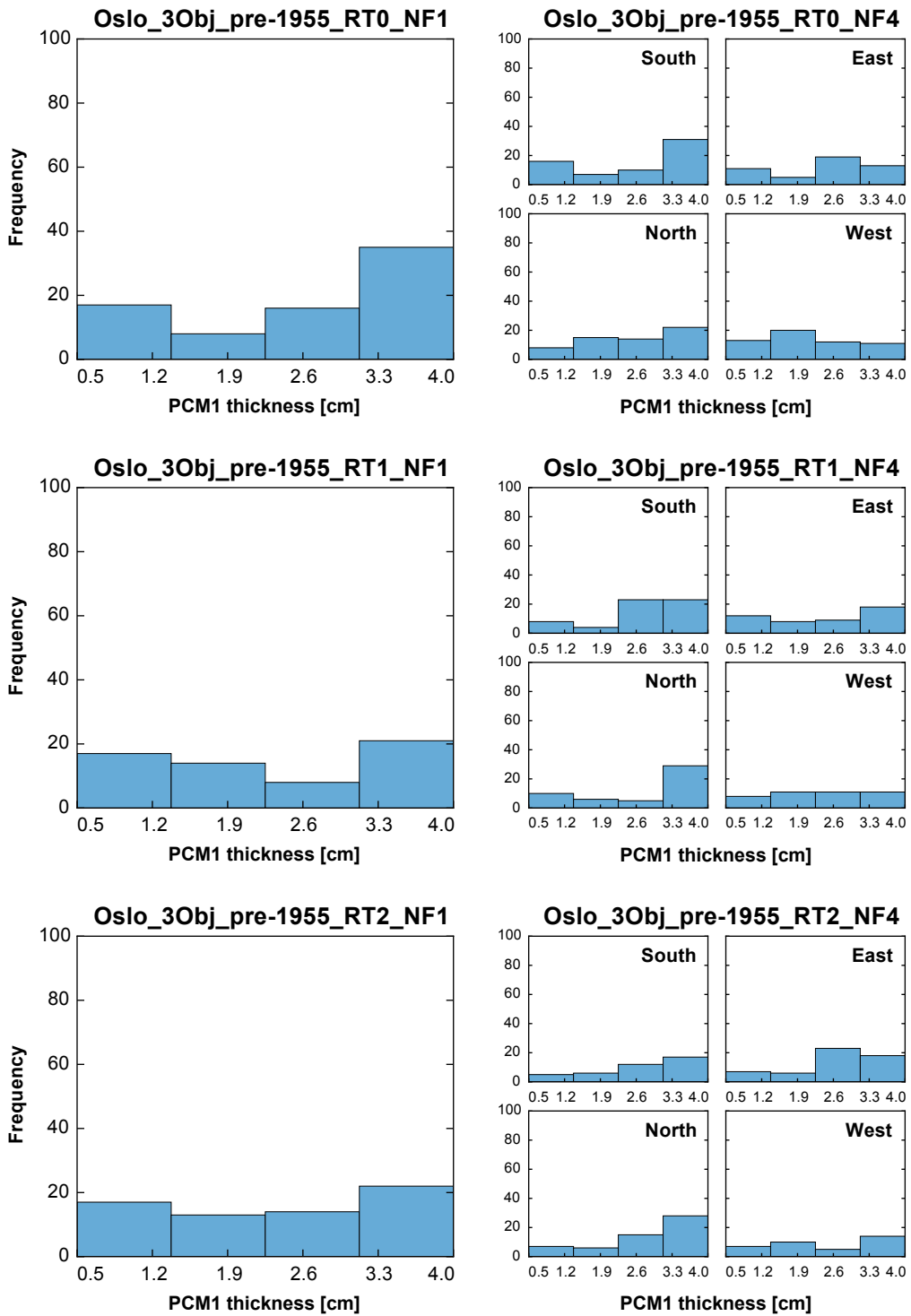
Fig. A.38 Frequency analyses: Oslo_3Obj_pre-1955, PCM1 thickness.
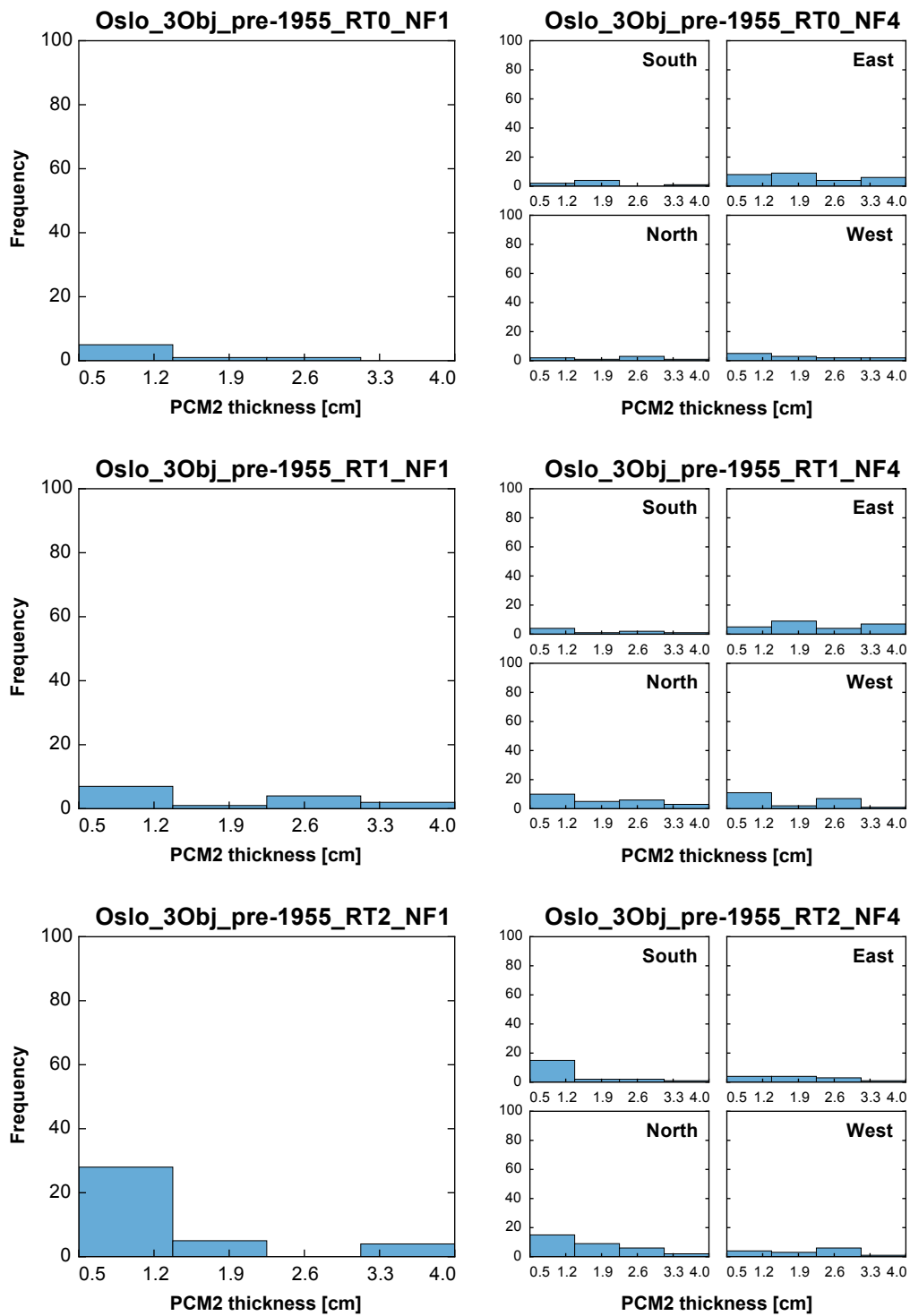
Fig. A.39 Frequency analyses: Oslo_3Obj_pre-1955, PCM2 thickness.
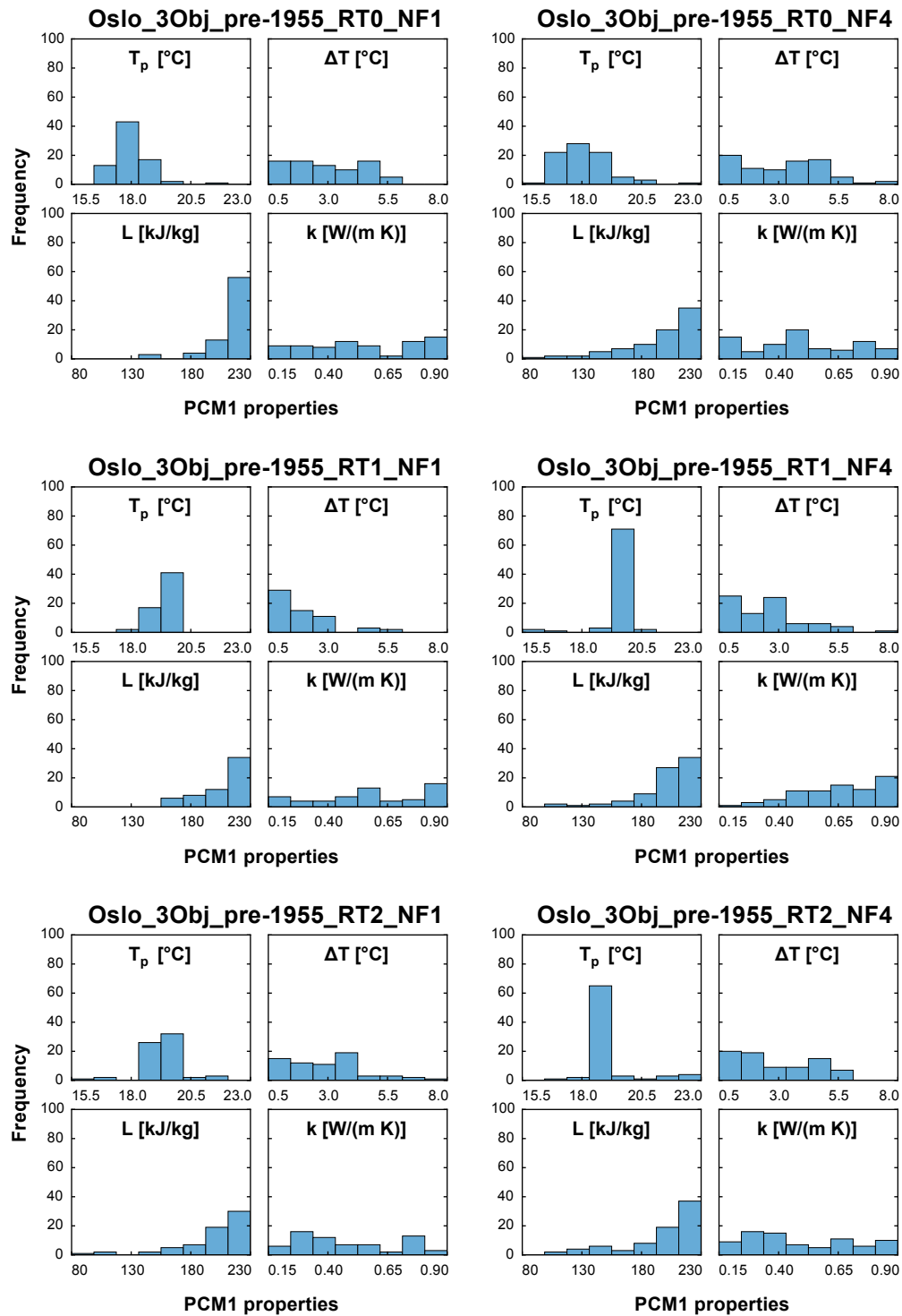
Fig. A.40 Frequency analyses: Oslo_3Obj_pre-1955, PCM1 properties.
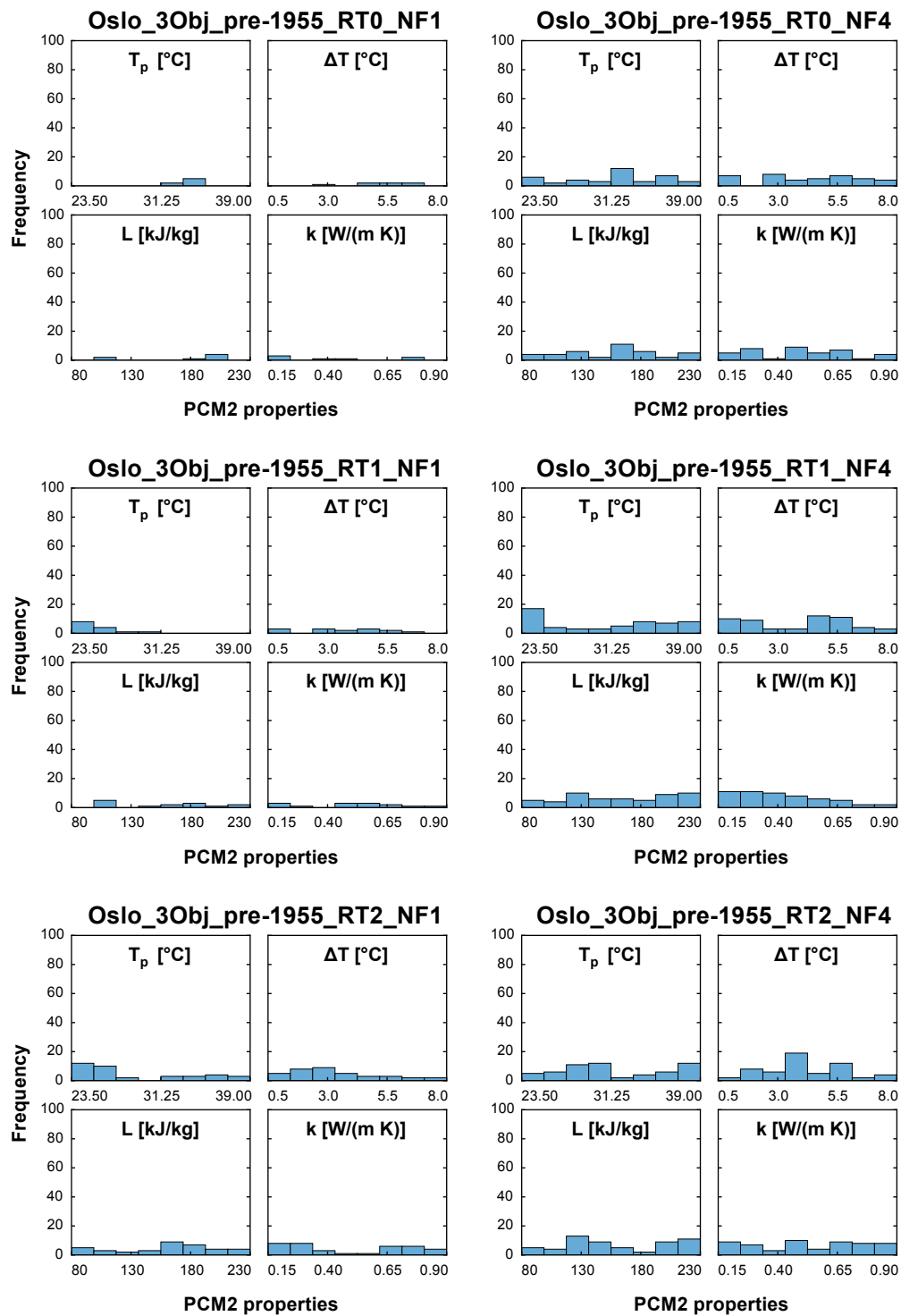
Fig. A.41 Frequency analyses: Oslo_3Obj_pre-1955, PCM2 properties.
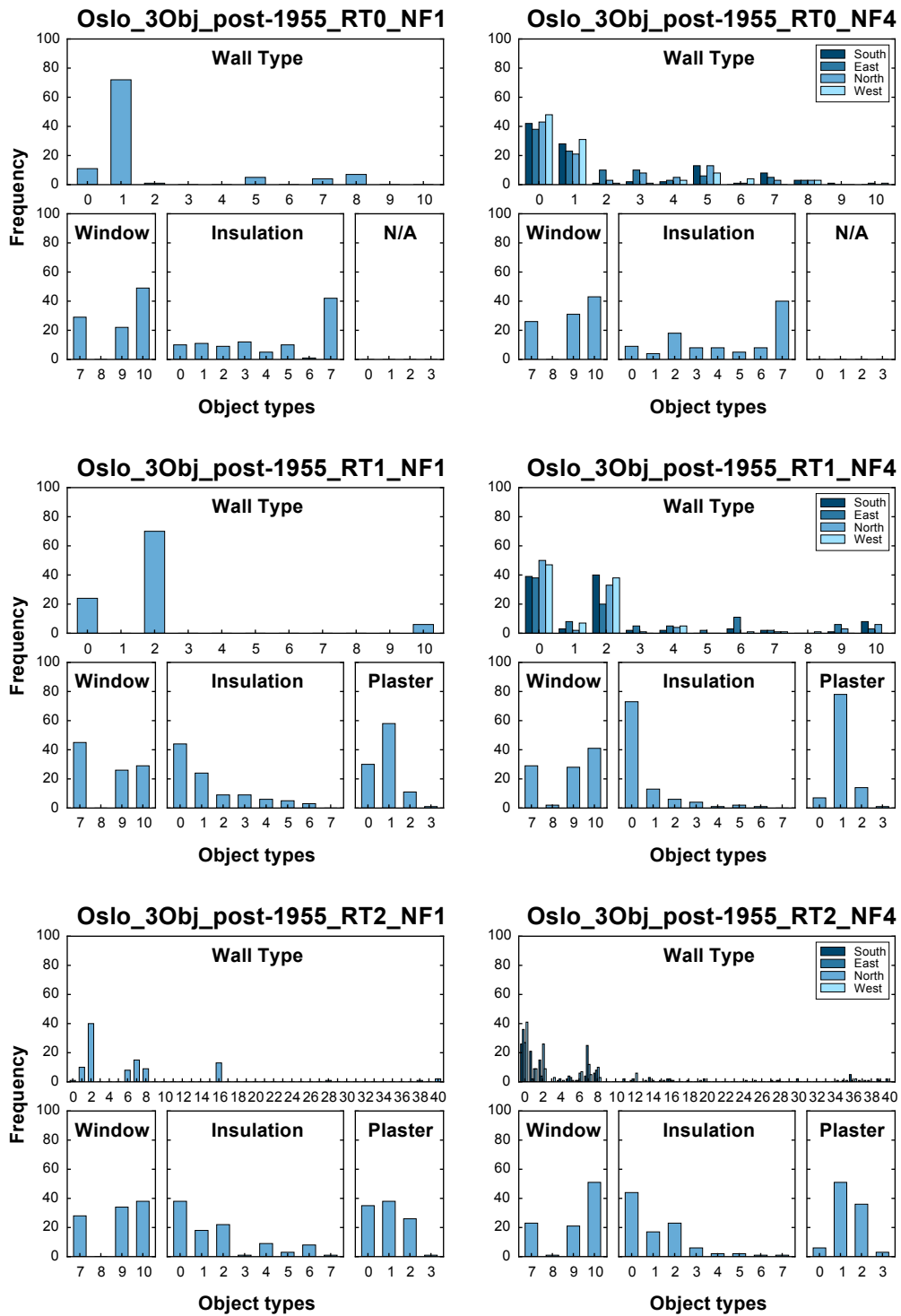
Fig. A.42 Frequency analyses: Oslo_3Obj_post-1955, discrete variables.
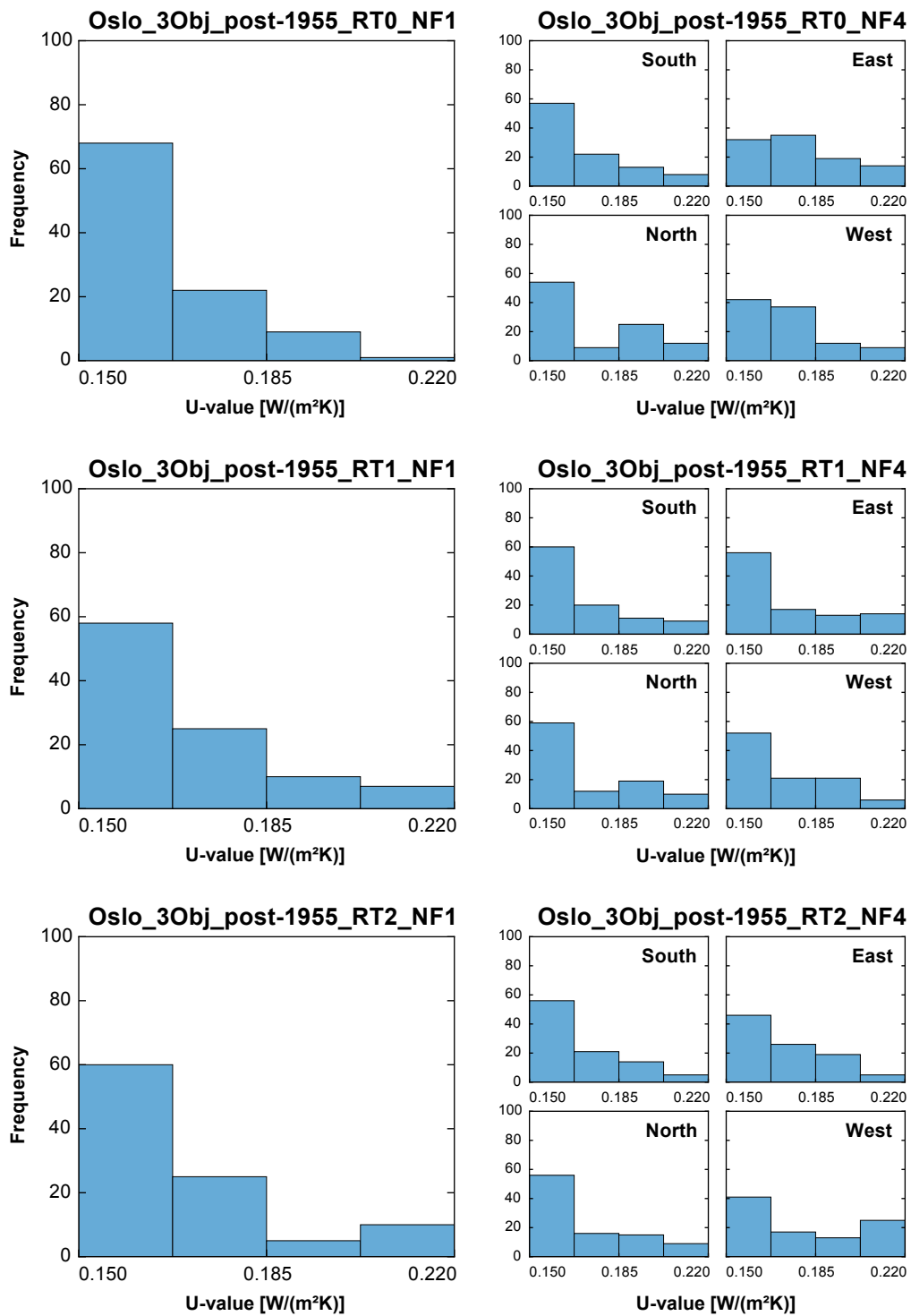
Fig. A.43 Frequency analyses: Oslo_3Obj_post-1955, U-values.
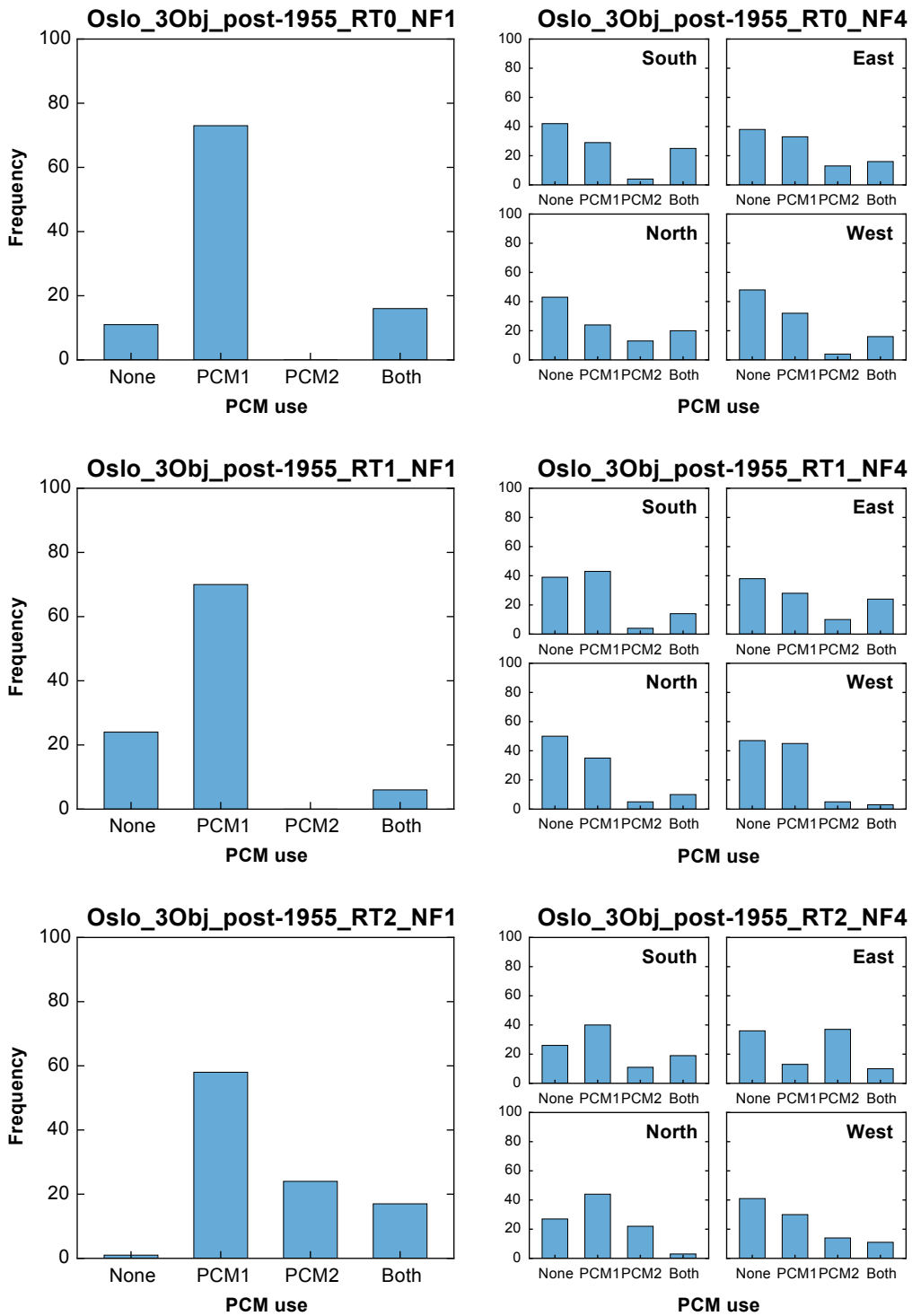
Fig. A.44 Frequency analyses: Oslo_3Obj_post-1955, PCM use.
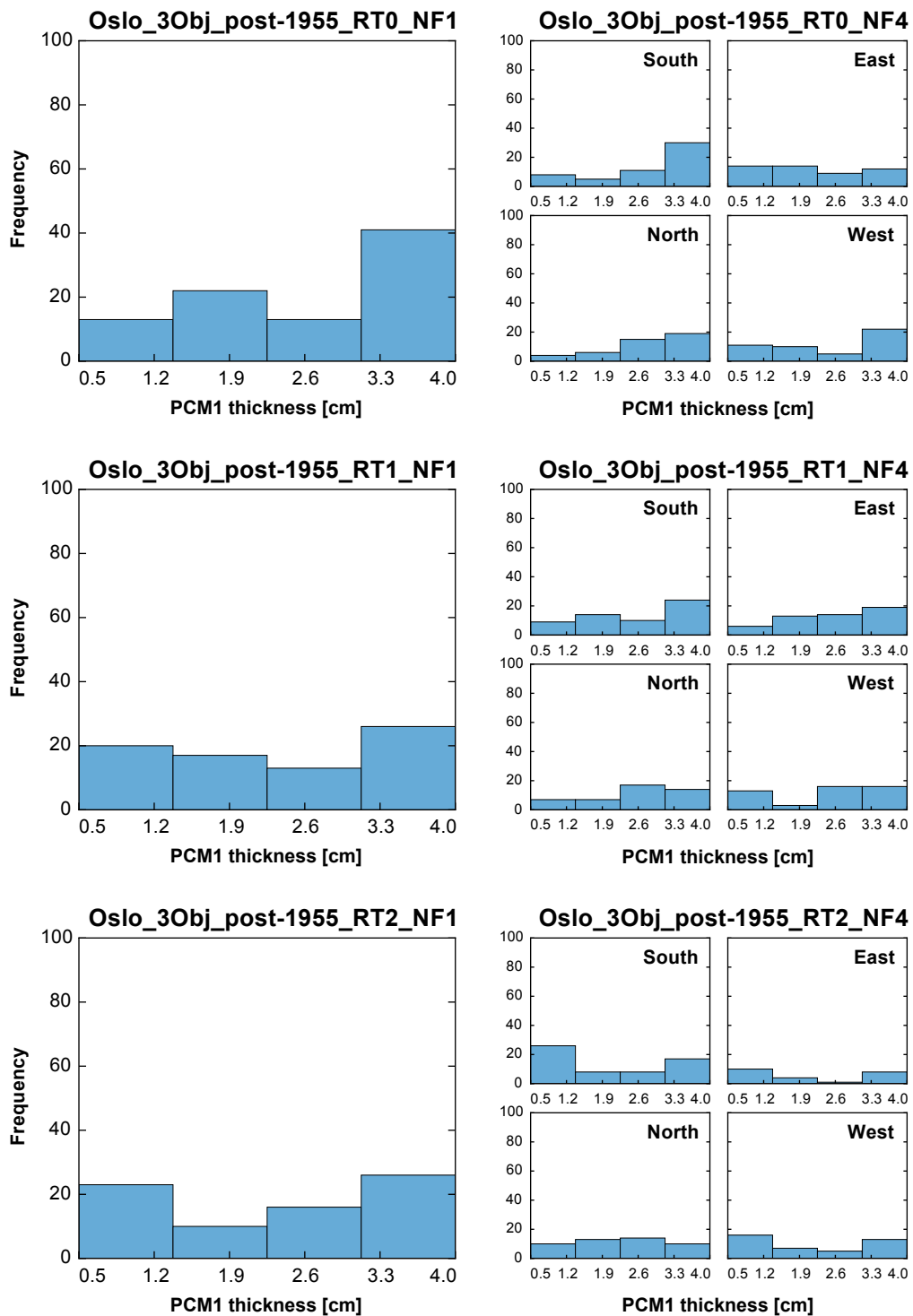
Fig. A.45 Frequency analyses: Oslo_3Obj_post-1955, PCM1 thickness.
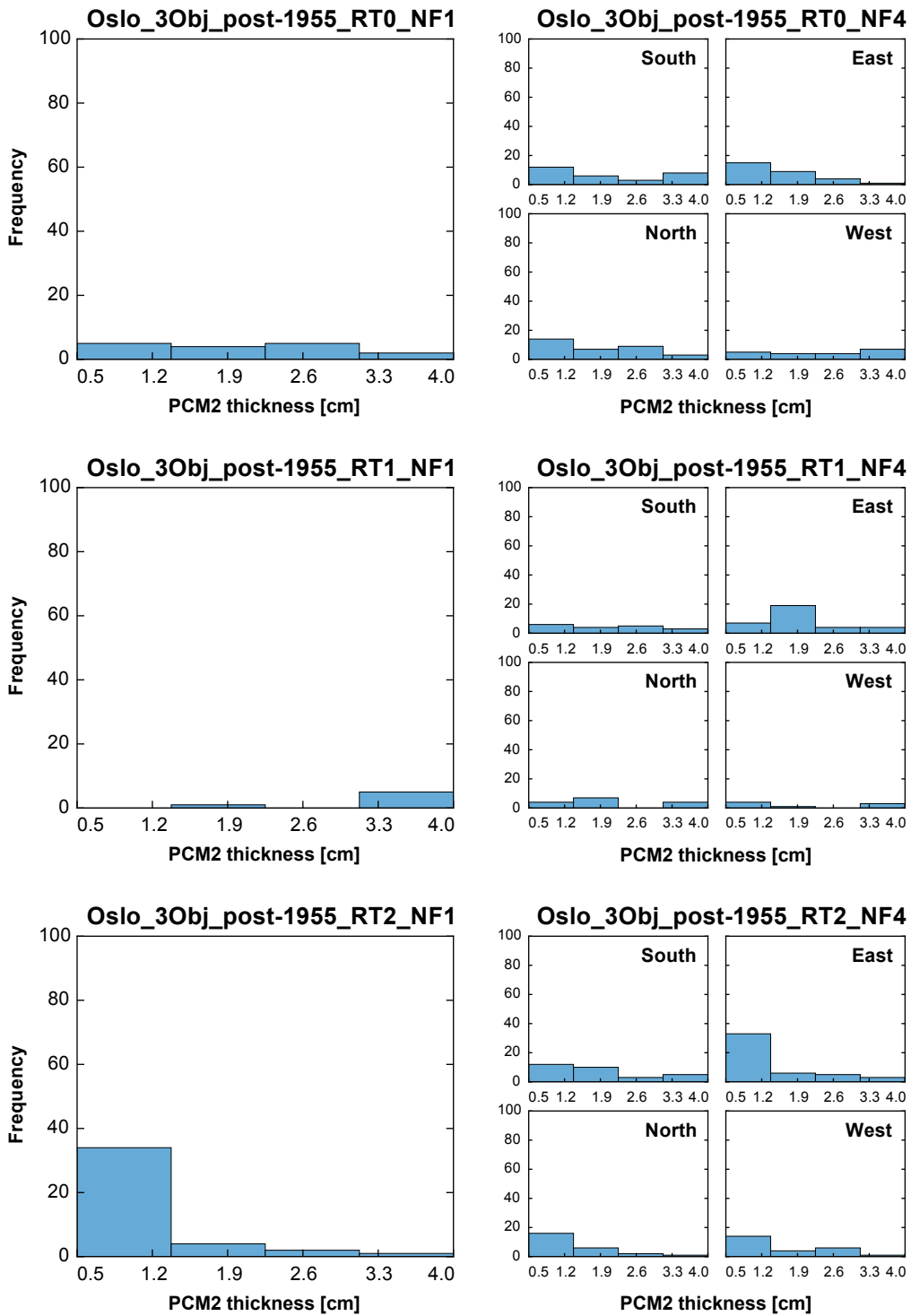
Fig. A.46 Frequency analyses: Oslo_3Obj_post-1955, PCM2 thickness.
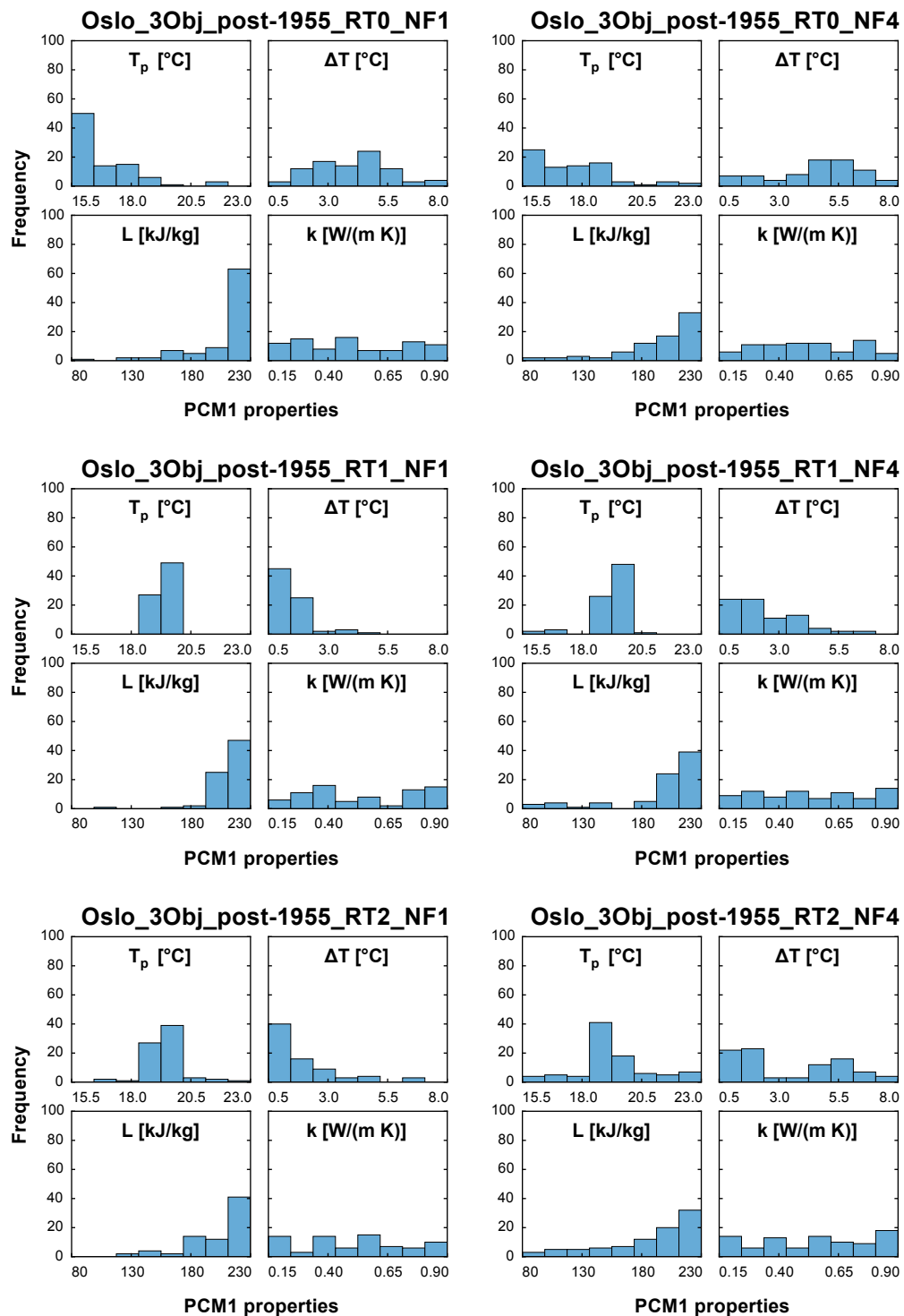
Fig. A.47 Frequency analyses: Oslo_3Obj_post-1955, PCM1 properties.
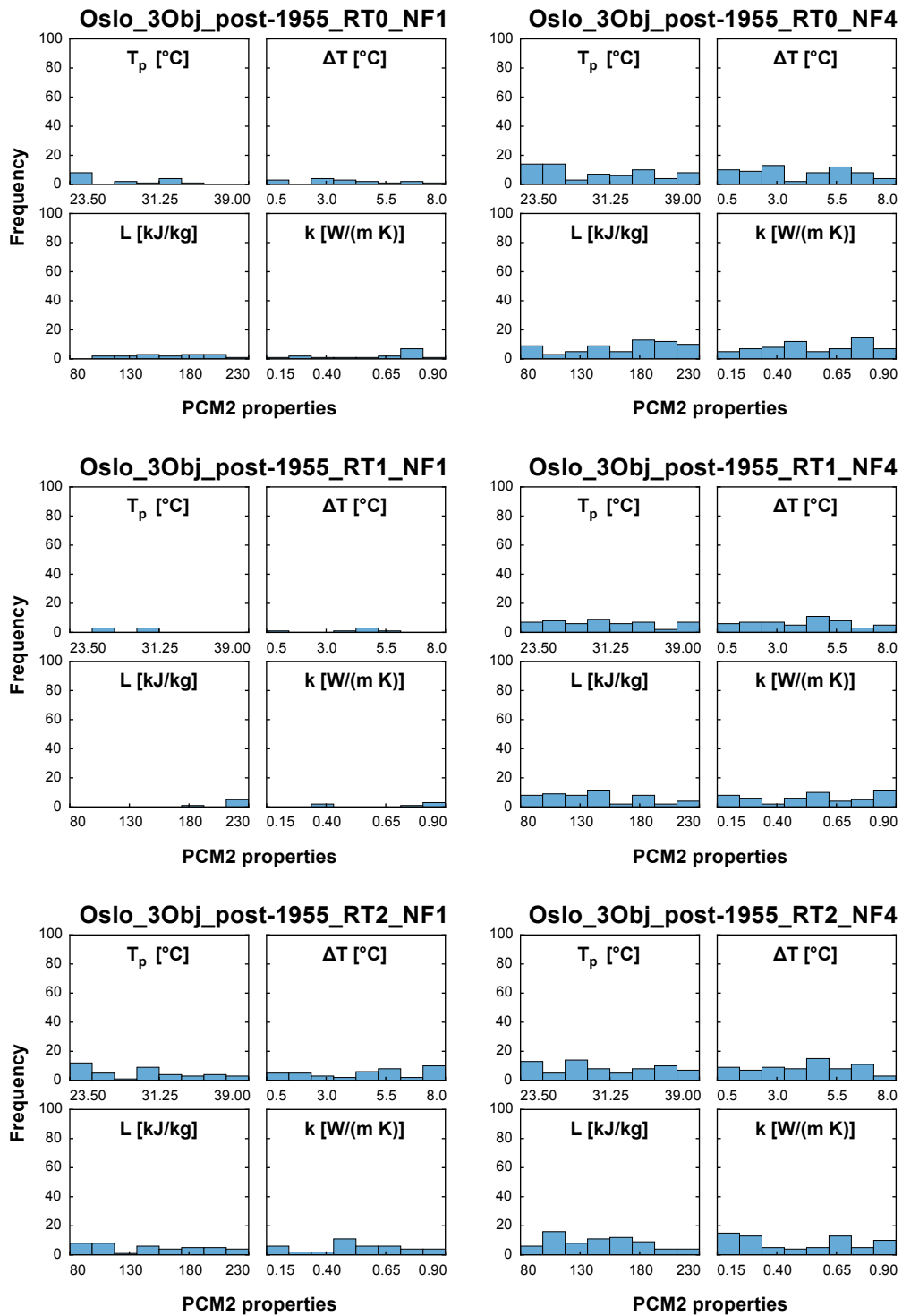
Fig. A.48 Frequency analyses: Oslo_3Obj_post-1955, PCM2 properties.

Appendix B

Variables' mappings on the Pareto fronts

The variables' mappings on the Pareto fronts for the component-level optimisation analyses in § 4.3.4 and the building-level optimisation analyses in § 4.4.3 are herewith illustrated.

With regard to the building-level analyses, the codes for window type, insulation and internal lining materials are summarised in Table A.2. The complete set of properties are respectively reported in Table 4.13, Table 4.11 and Table 4.12.
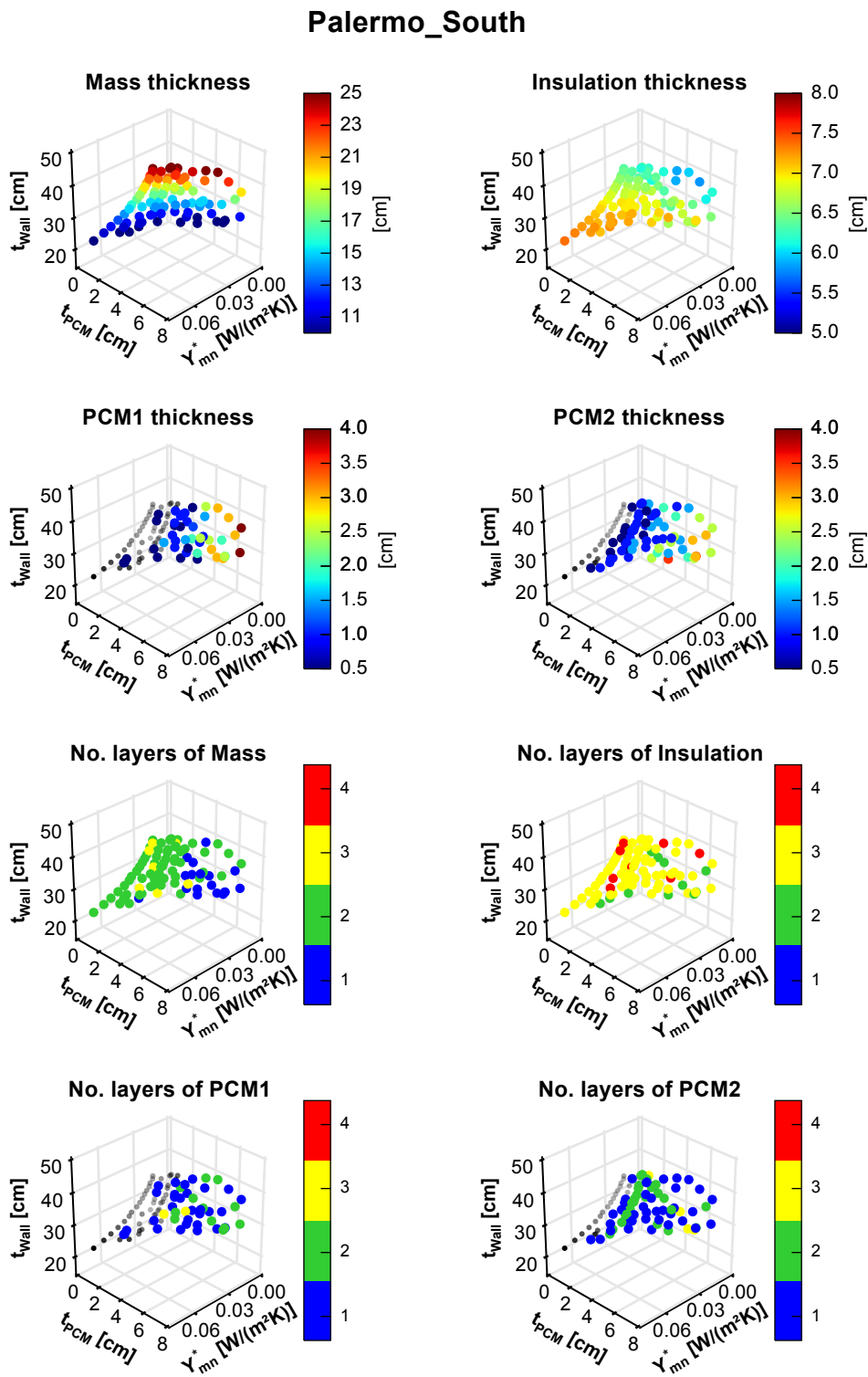
Fig. B.1 Thicknesses and no. of layers within the Pareto front: Palermo, south façade.
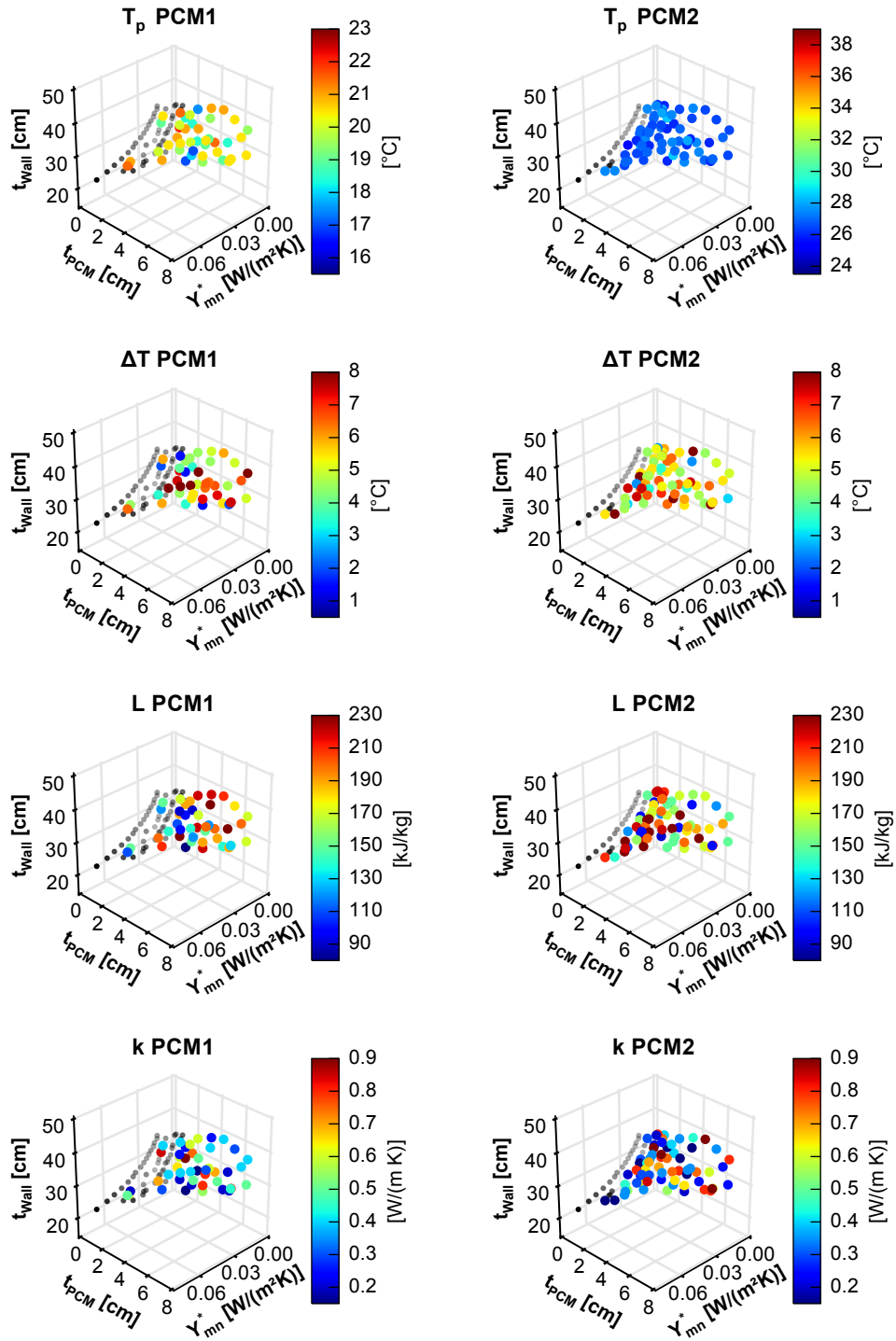
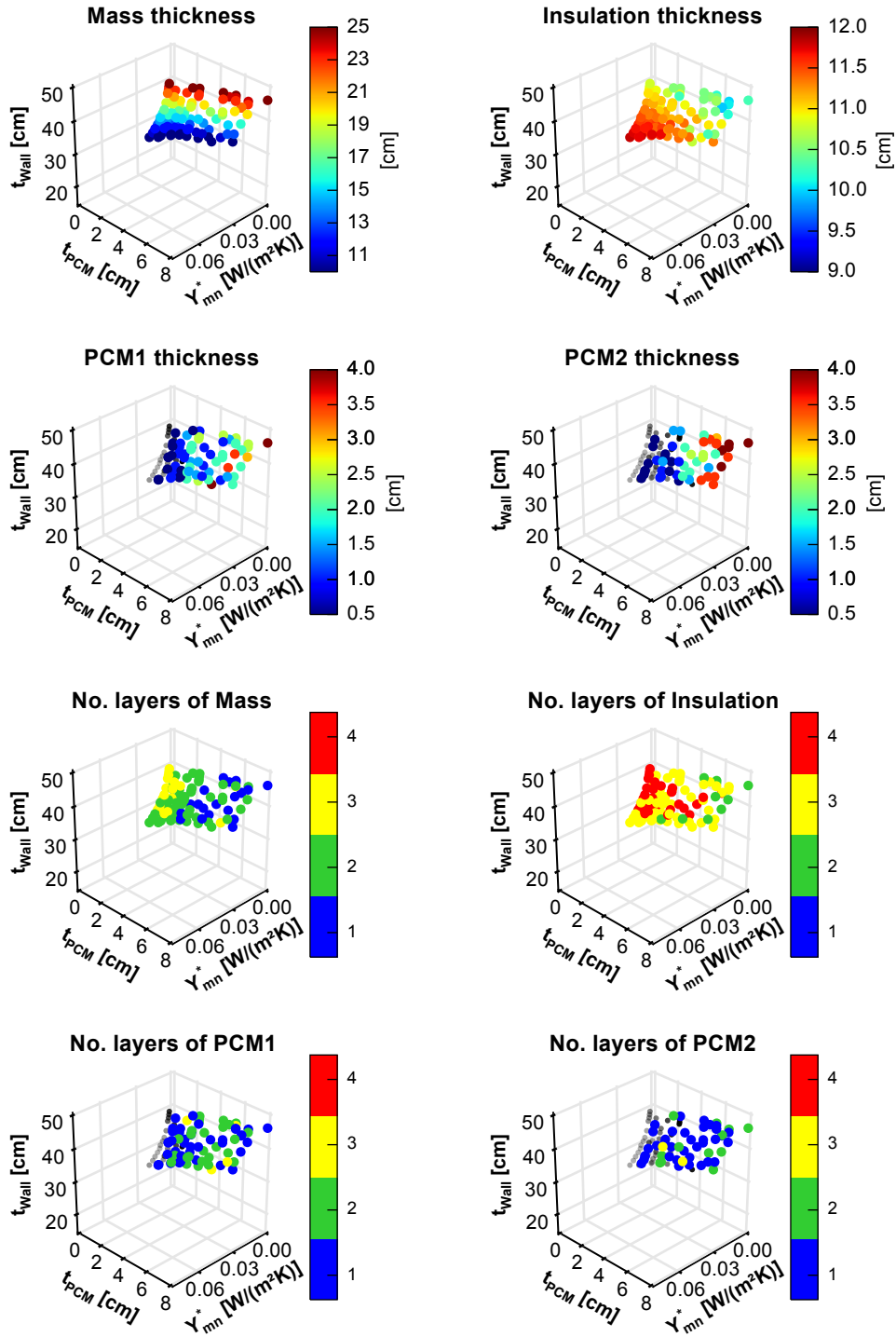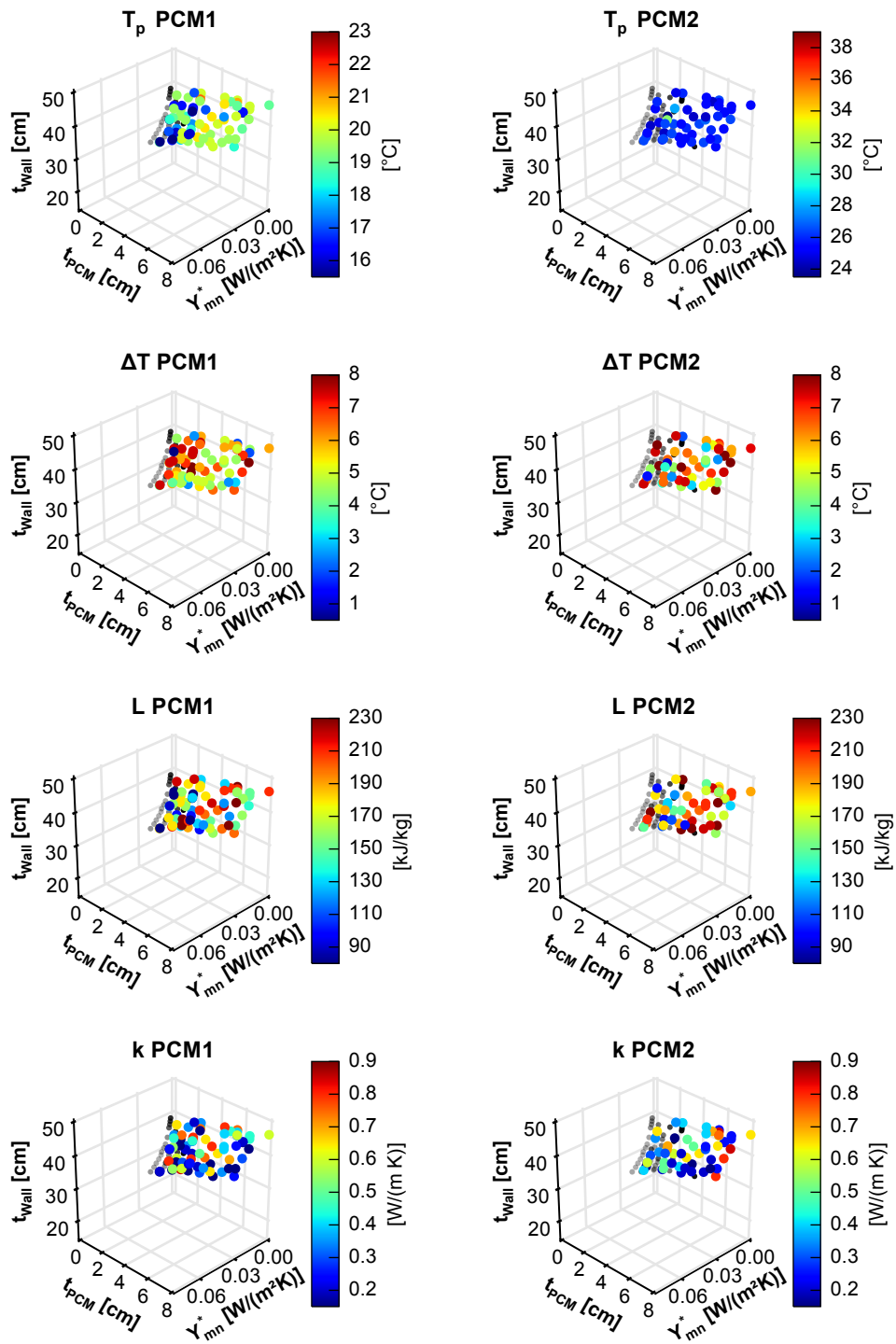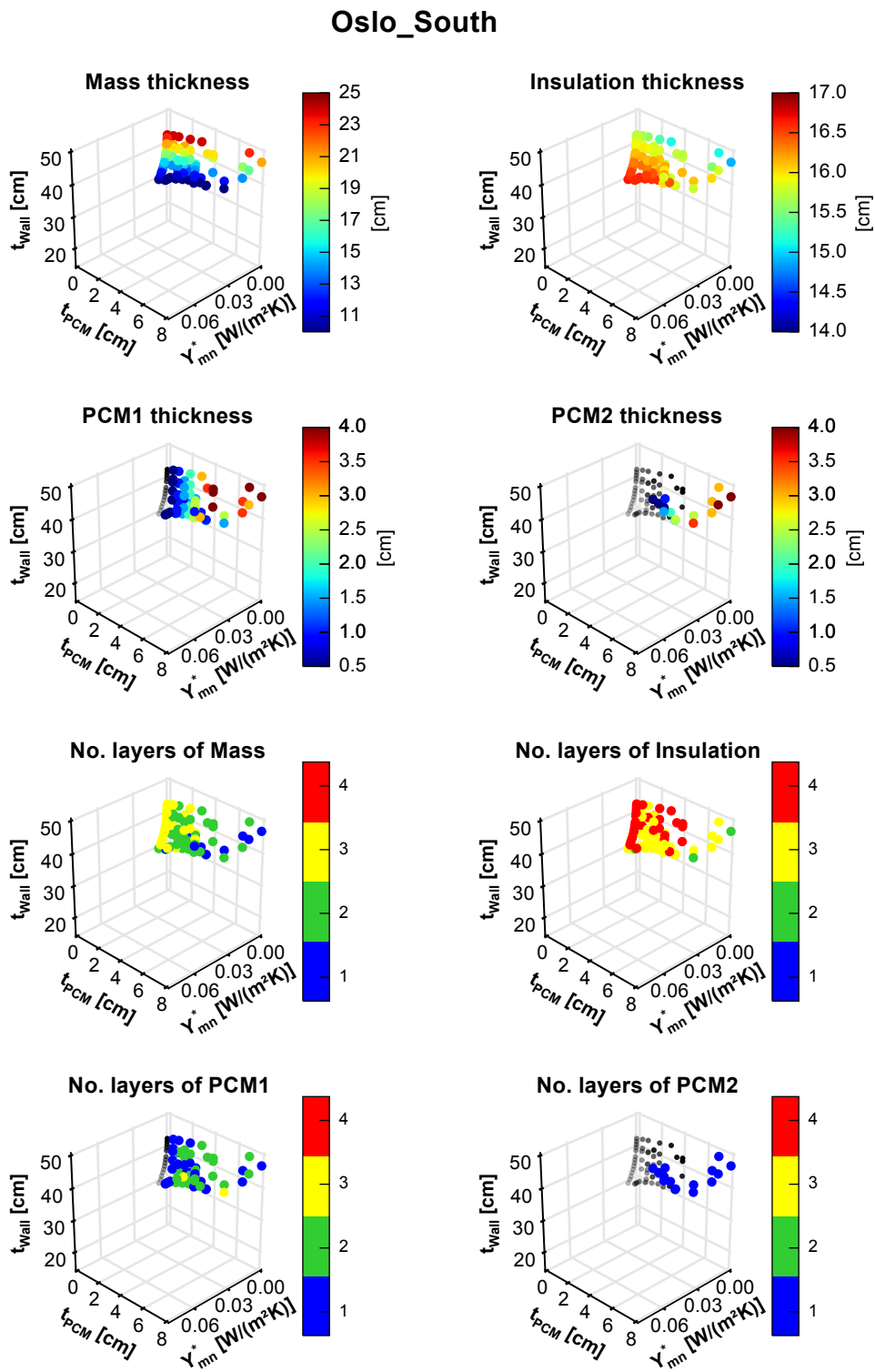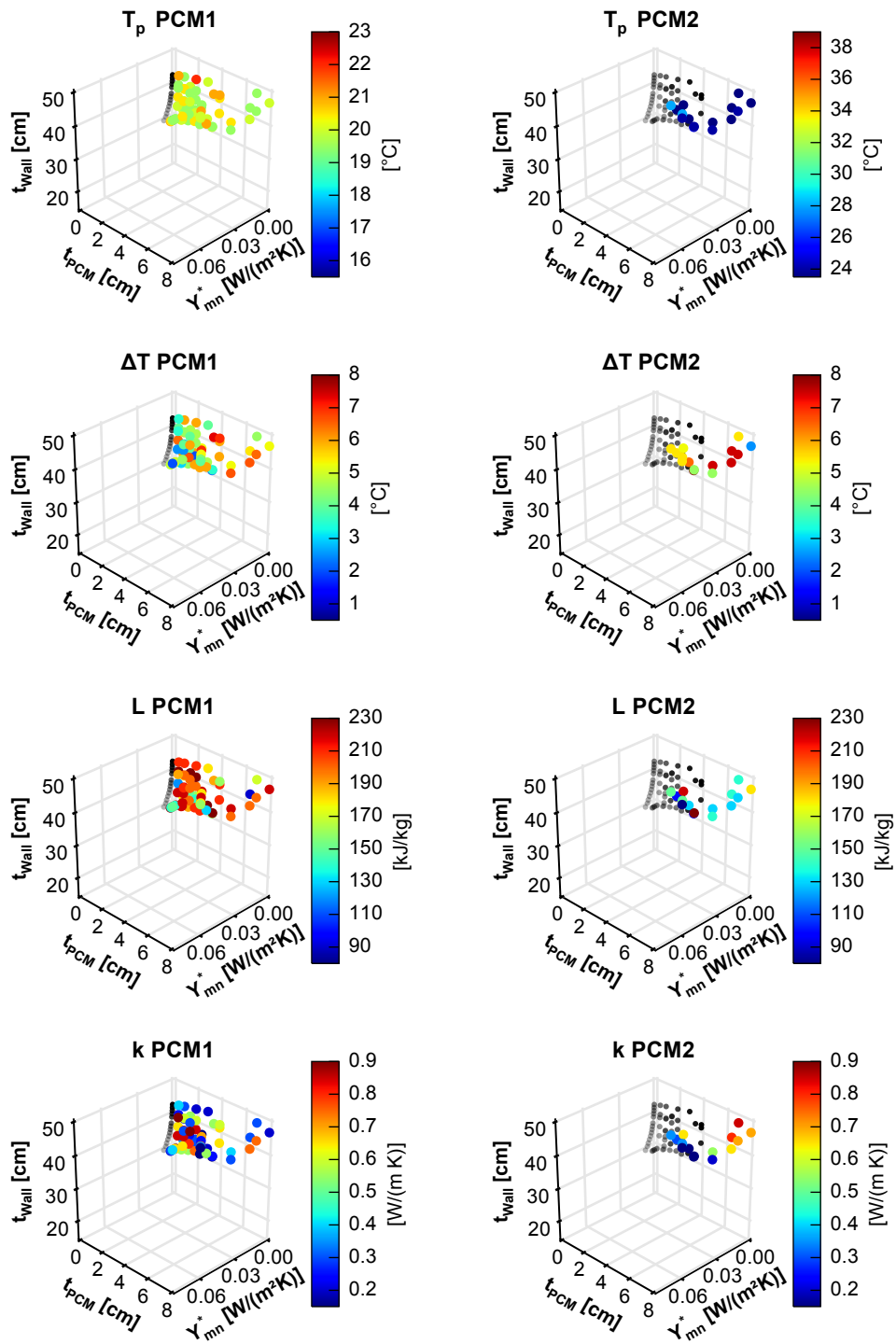Fig. B.2 PCM properties within the Pareto front: Palermo, south façade.
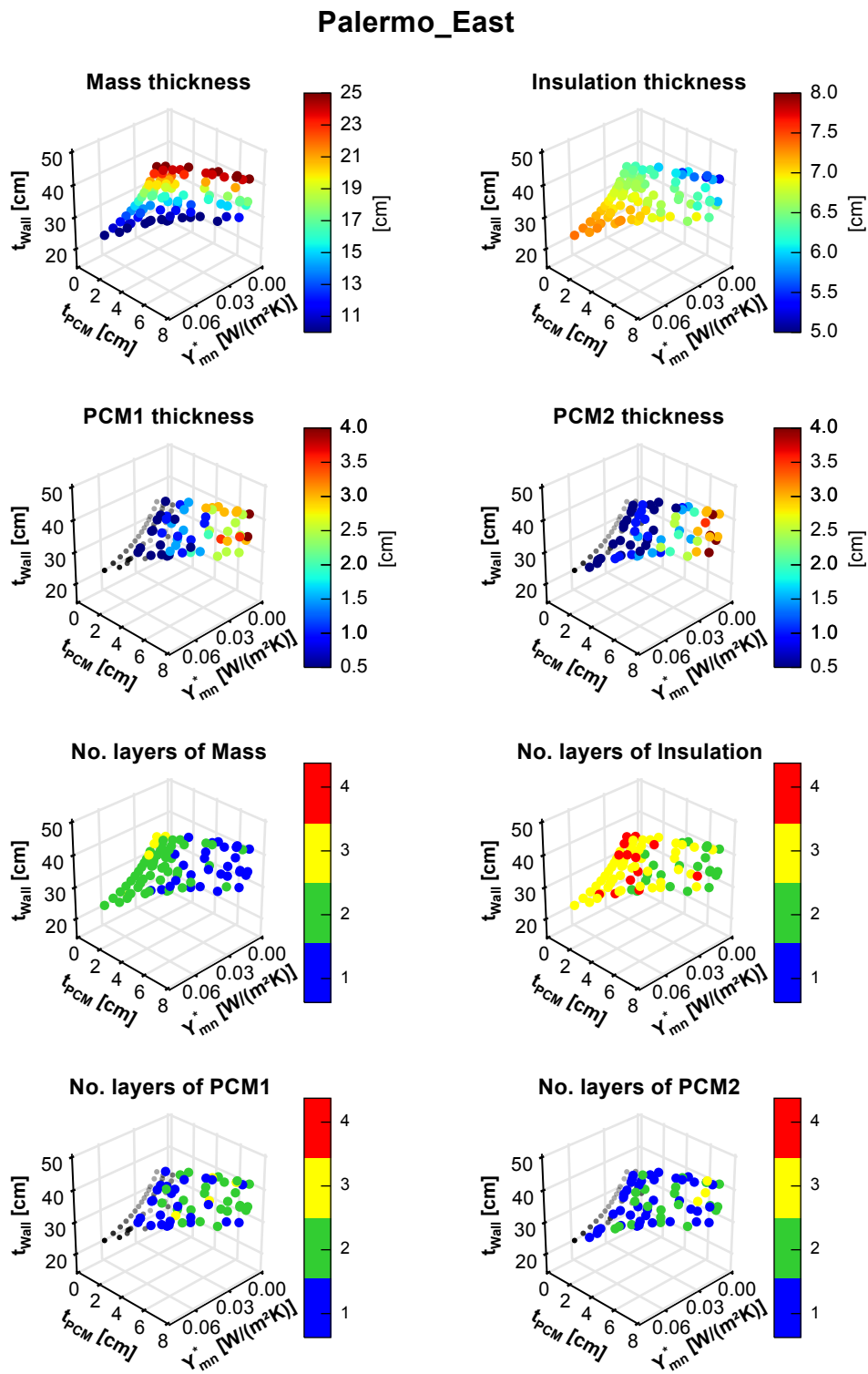
Fig. B.3 Thicknesses and no. of layers within the Pareto front: Palermo, east façade.

Palermo_East
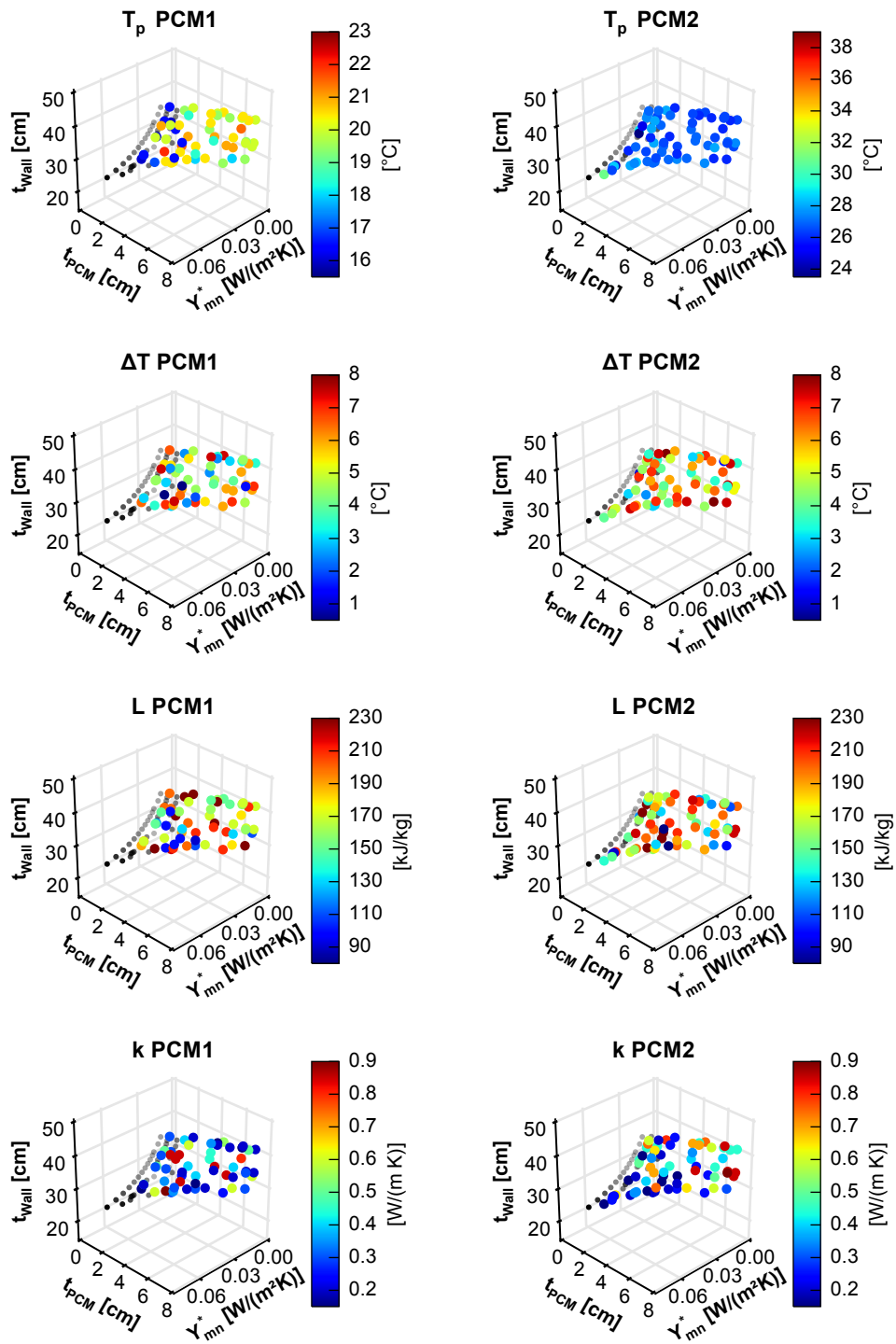
Fig. B.4 PCM properties within the Pareto front: Palermo, east façade.
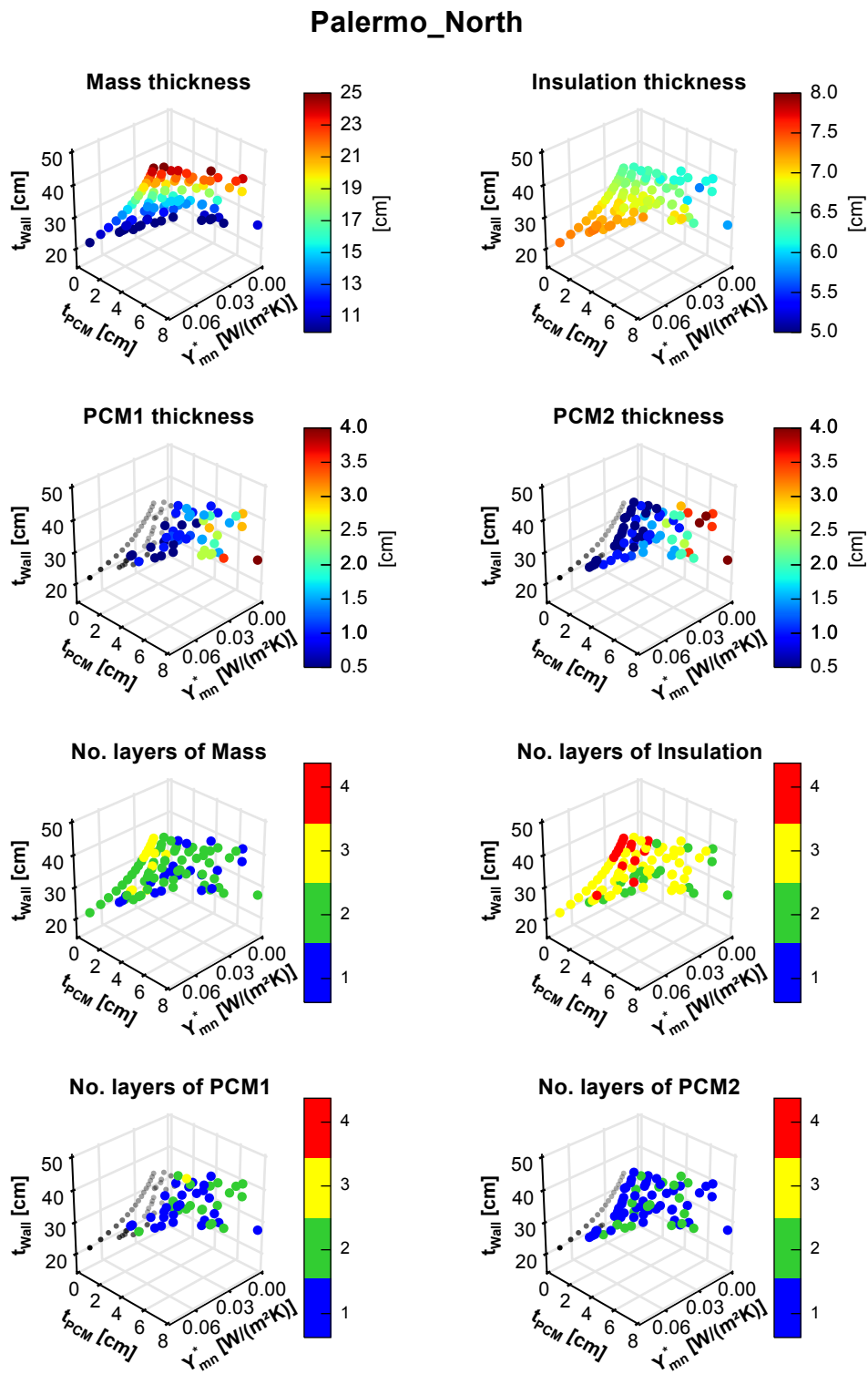
Palermo_North

Fig. B.5 Thicknesses and no. of layers within the Pareto front: Palermo, north façade.

Palermo_North
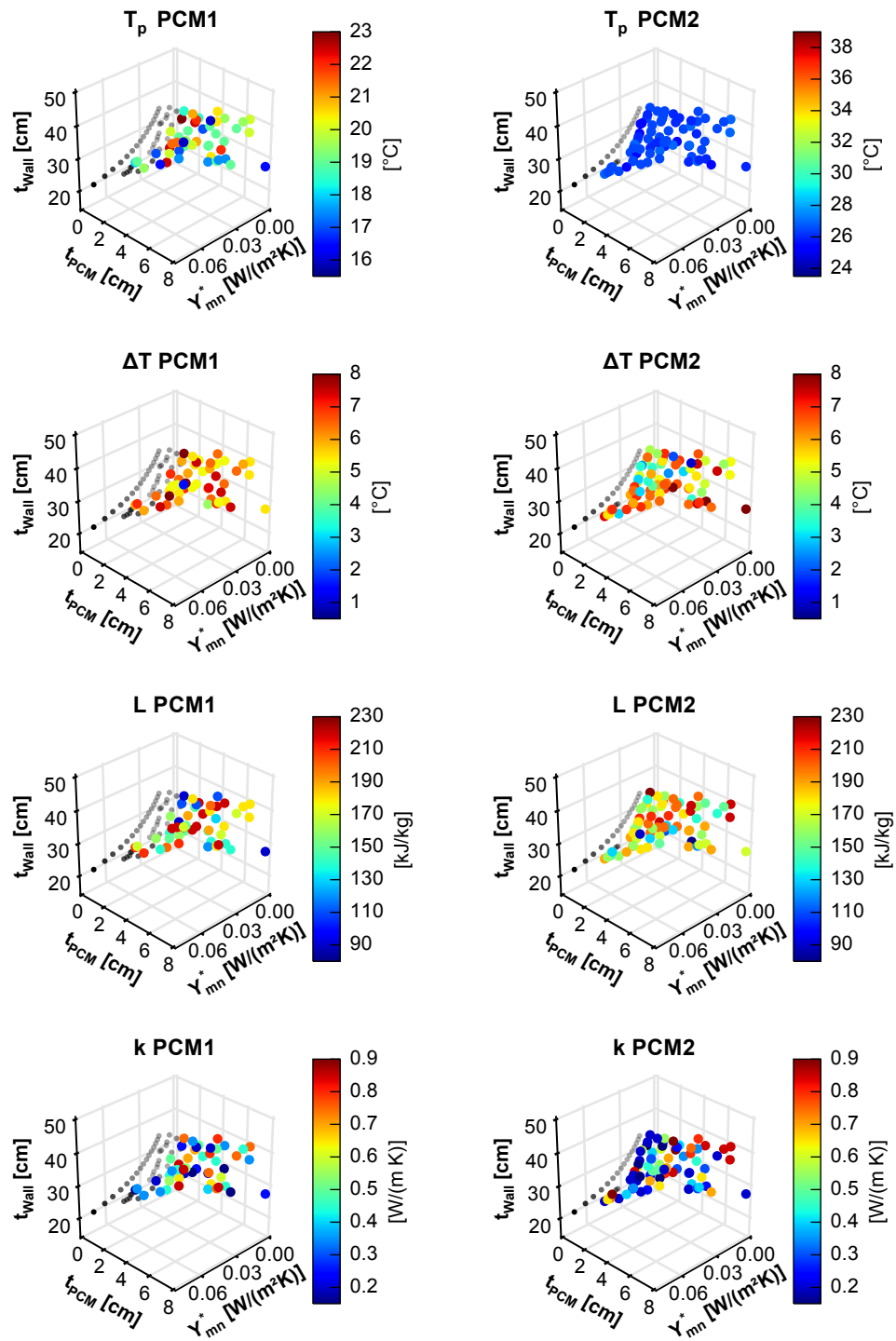
Fig. B.6 PCM properties within the Pareto front: Palermo, north façade.
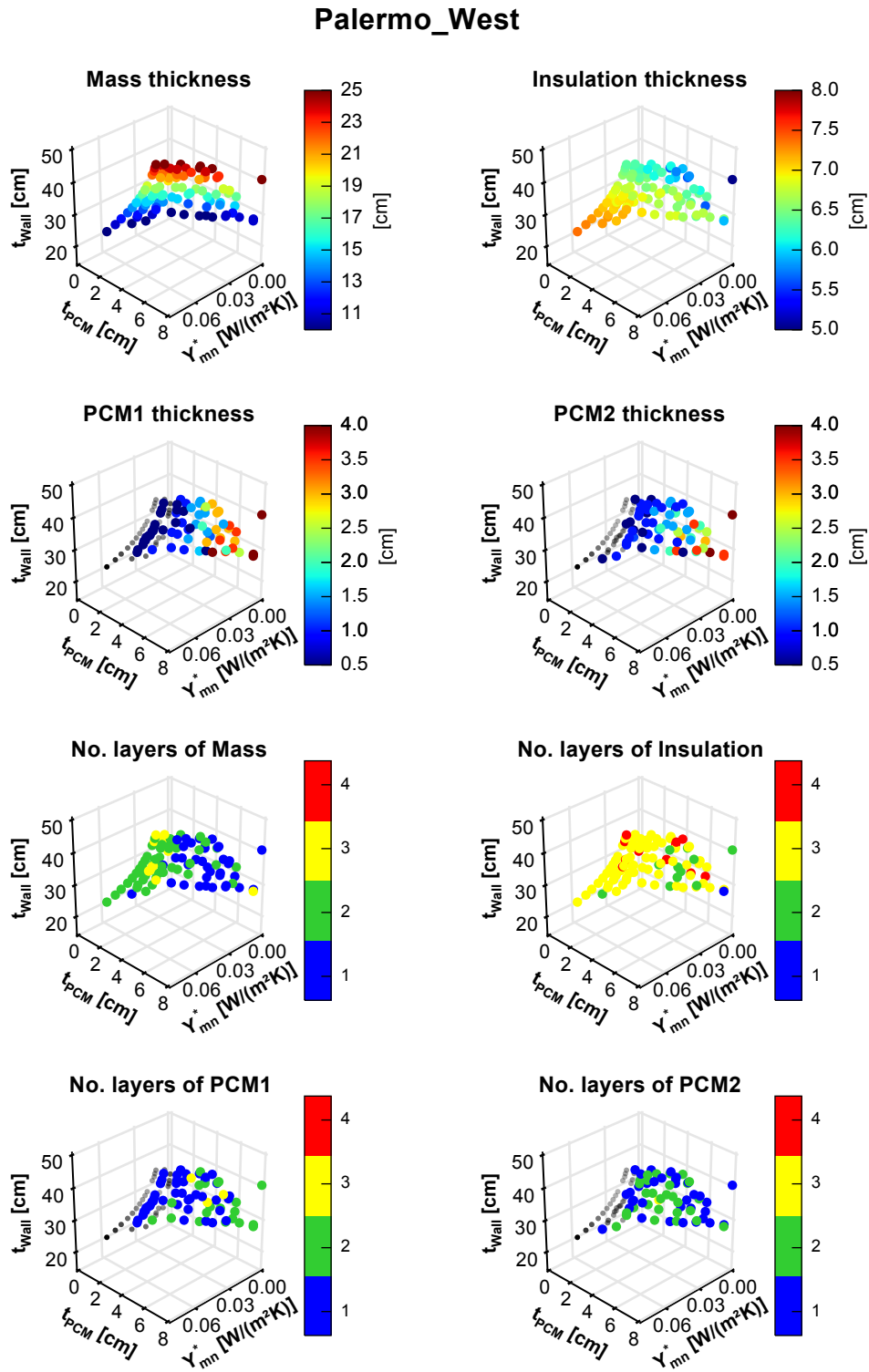
Palermo_West

Fig. B.7 Thicknesses and no. of layers within the Pareto front: Palermo, west façade.
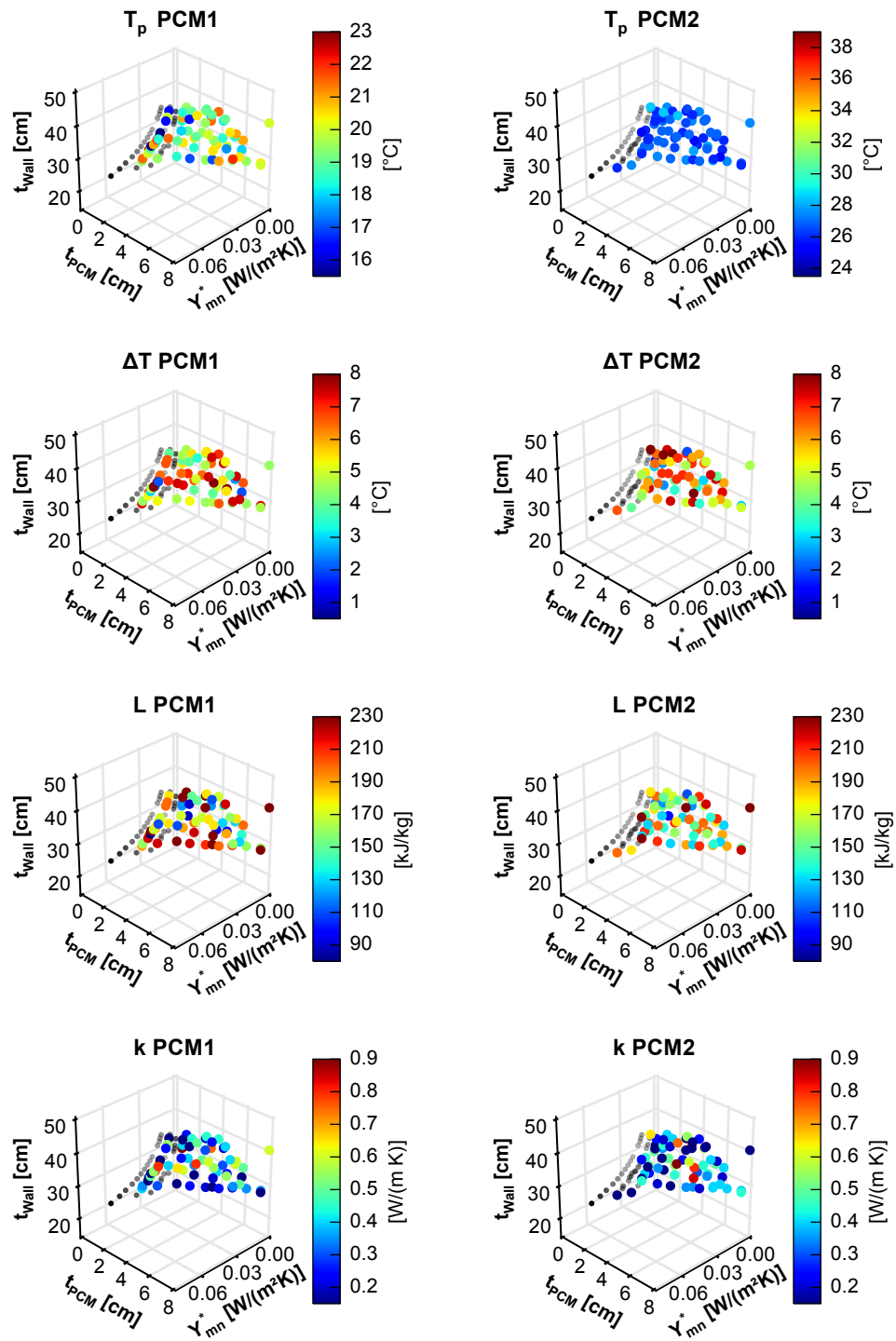
Fig. B.8 PCM properties within the Pareto front: Palermo, west façade.

Torino_South
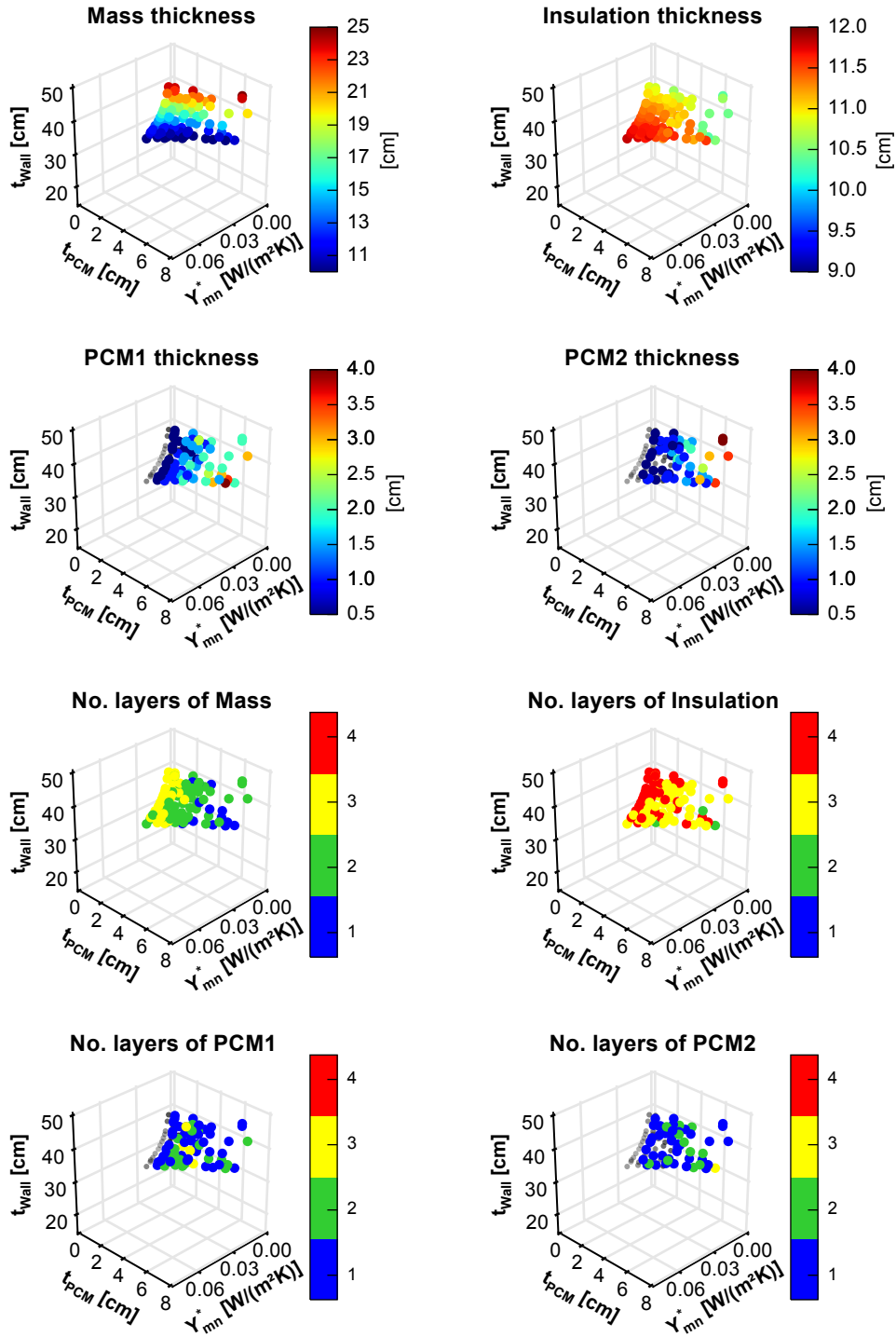
Fig. B.9 Thicknesses and no. of layers within the Pareto front: Torino, south façade.

Torino_South
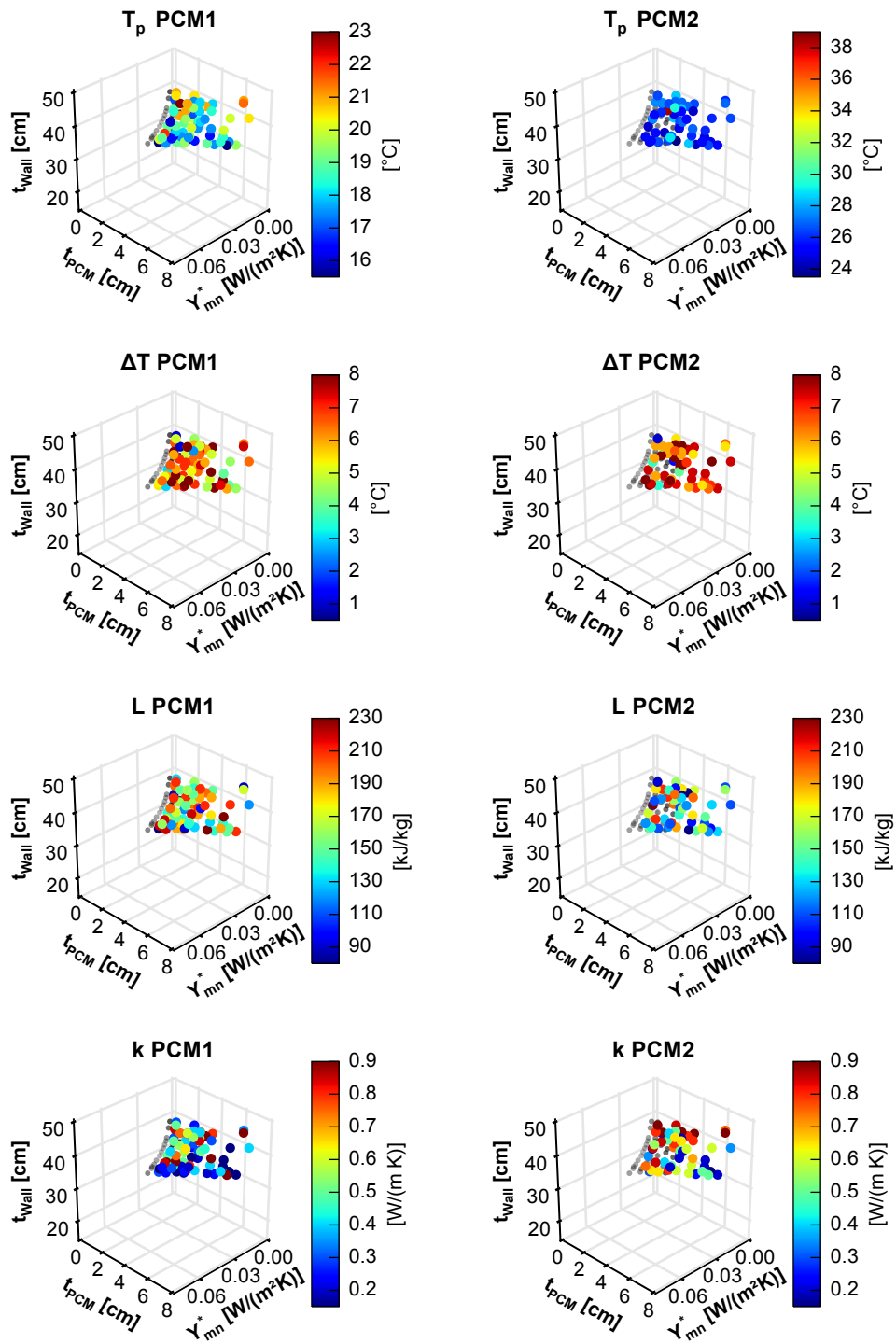
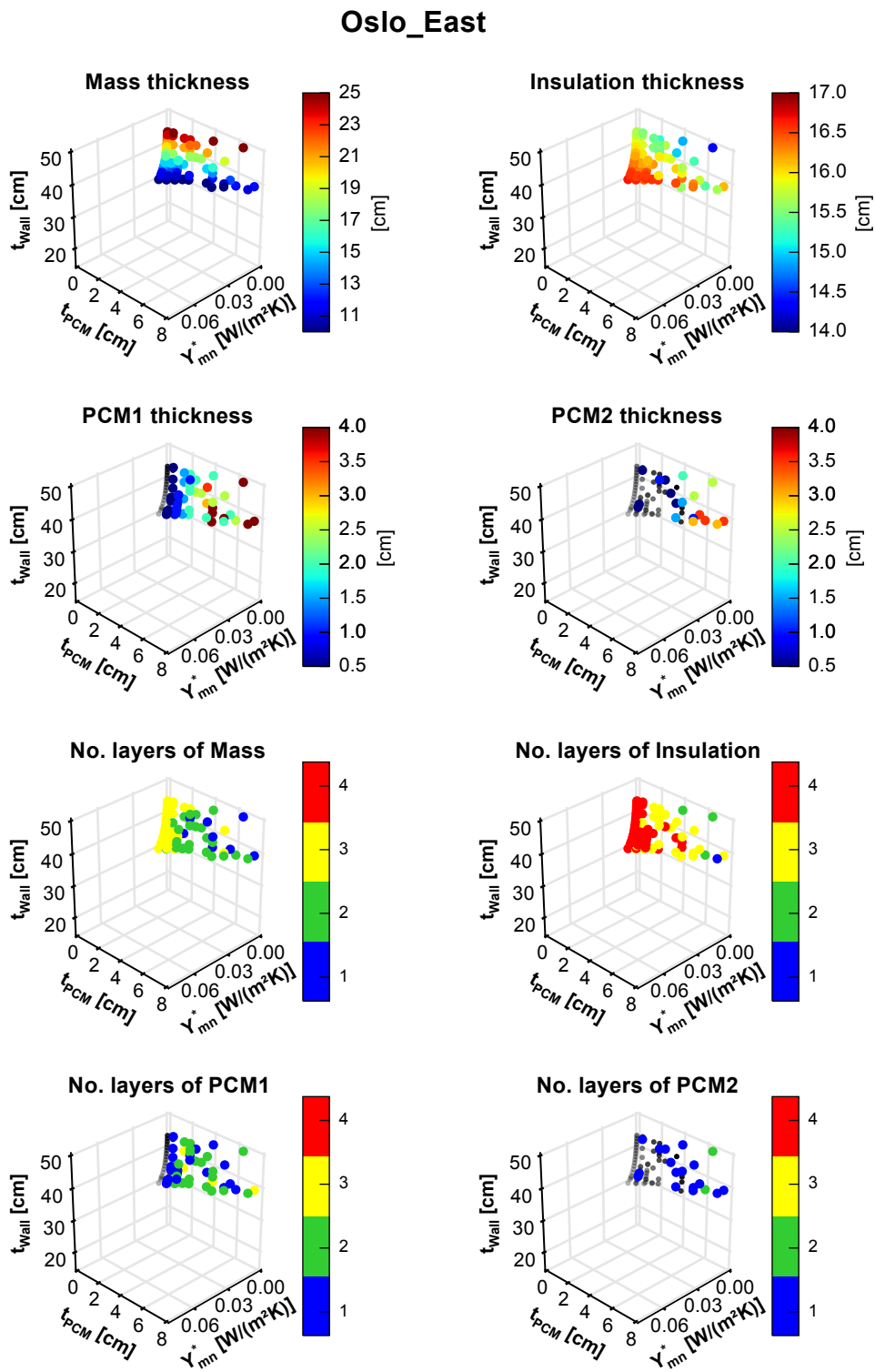Fig. B.10 PCM properties within the Pareto front: Torino, south façade.

Torino_East
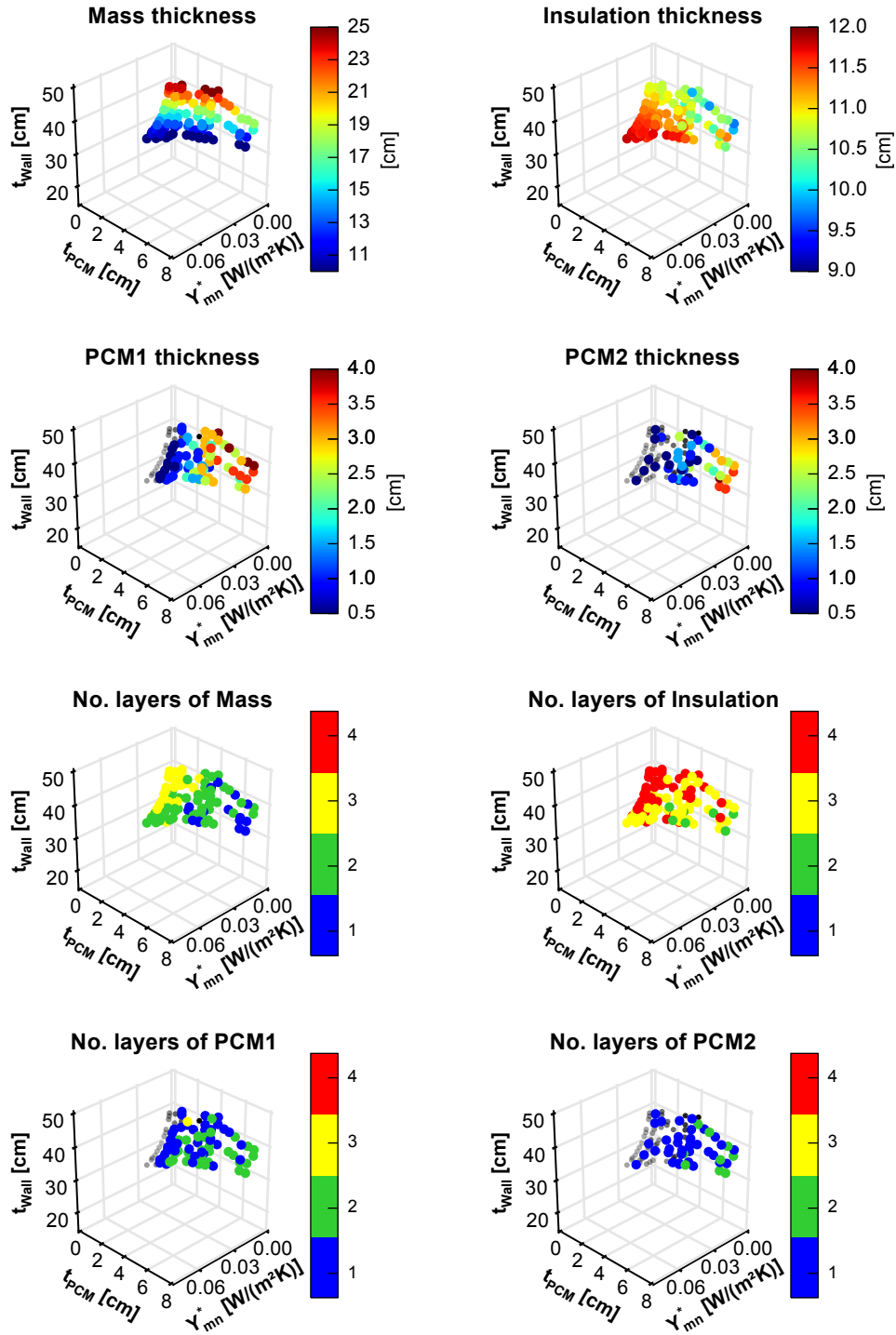
Fig. B.11 Thicknesses and no. of layers within the Pareto front: Torino, east façade.
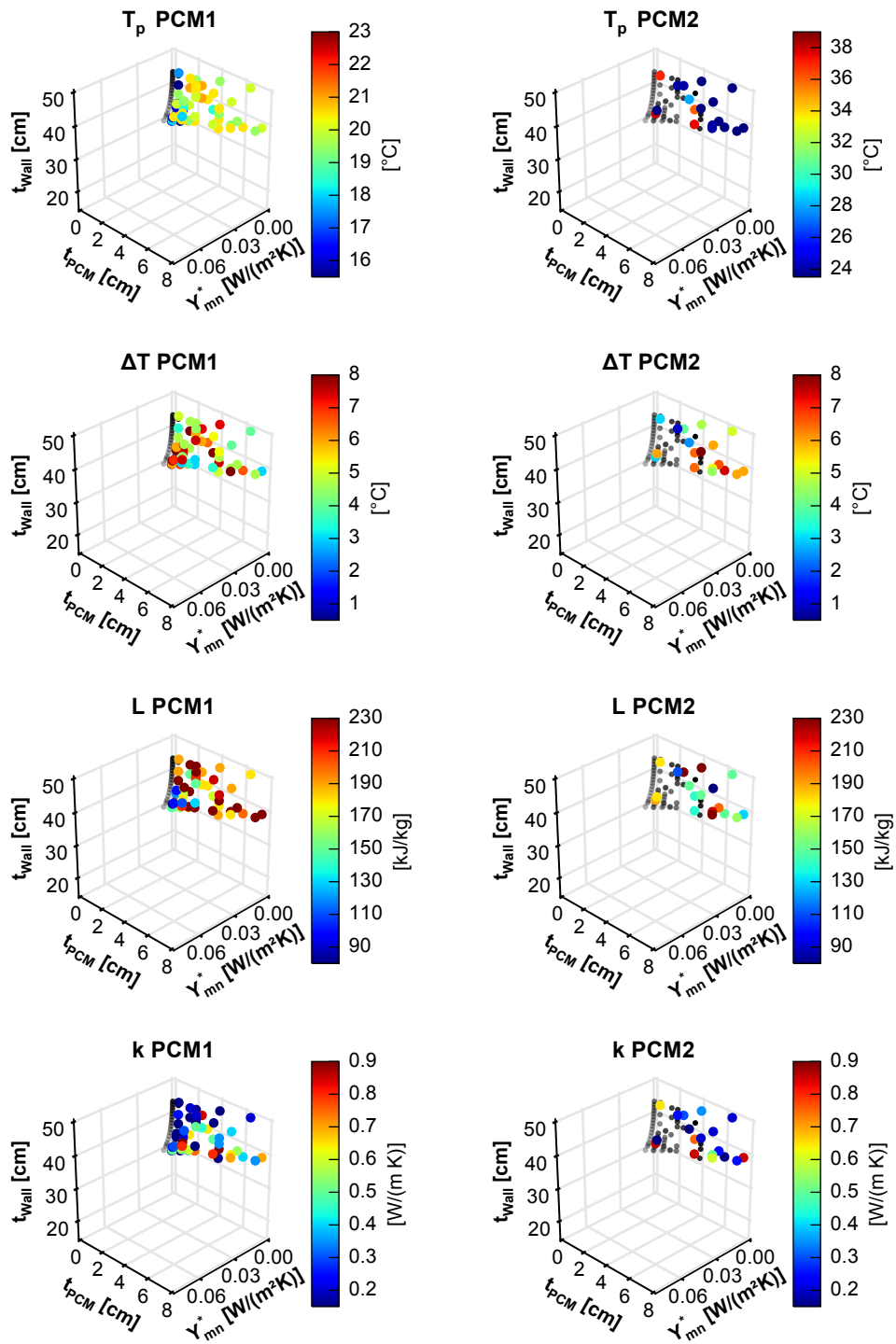
Torino_East
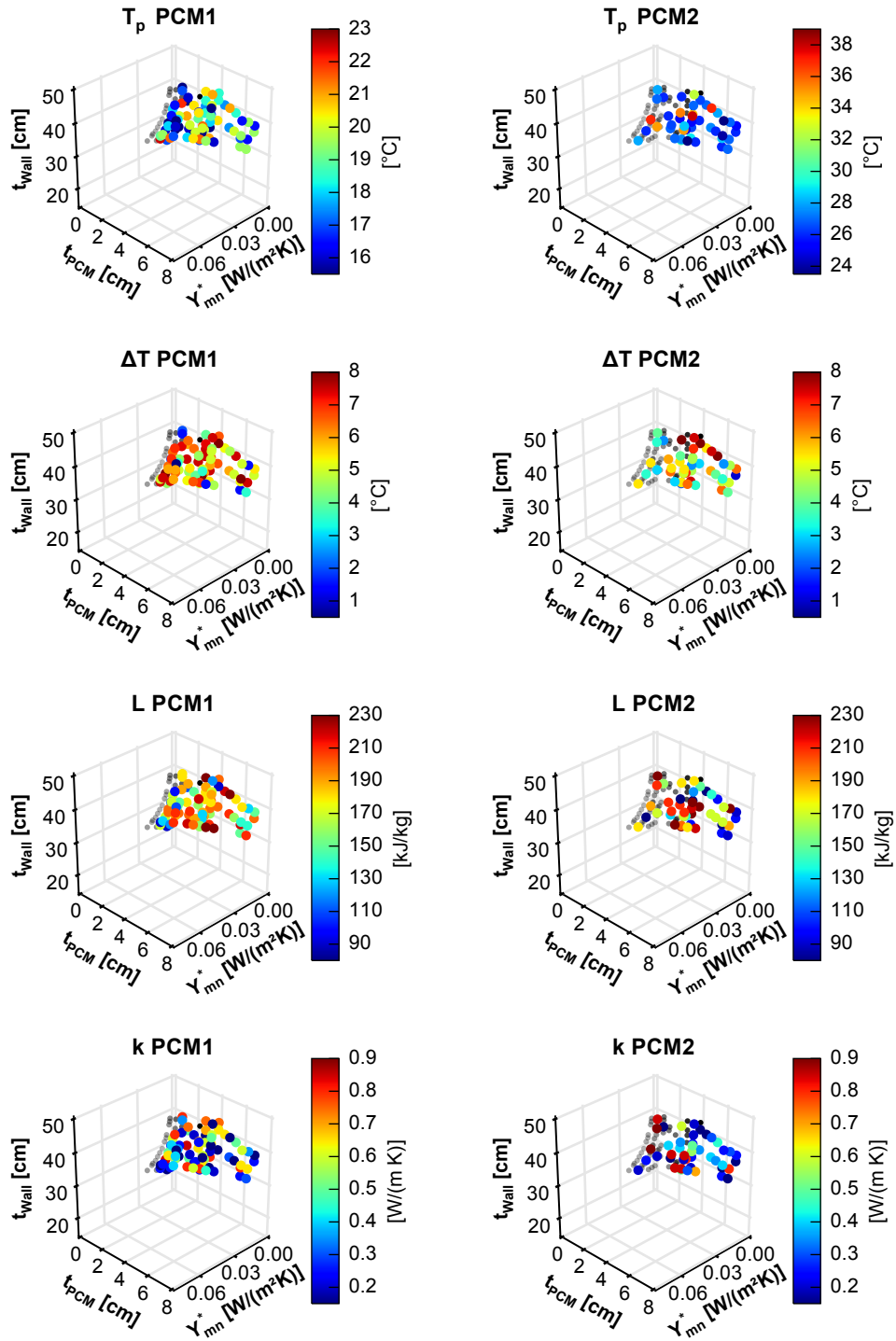
Fig. B.12 PCM properties within the Pareto front: Torino, east façade.
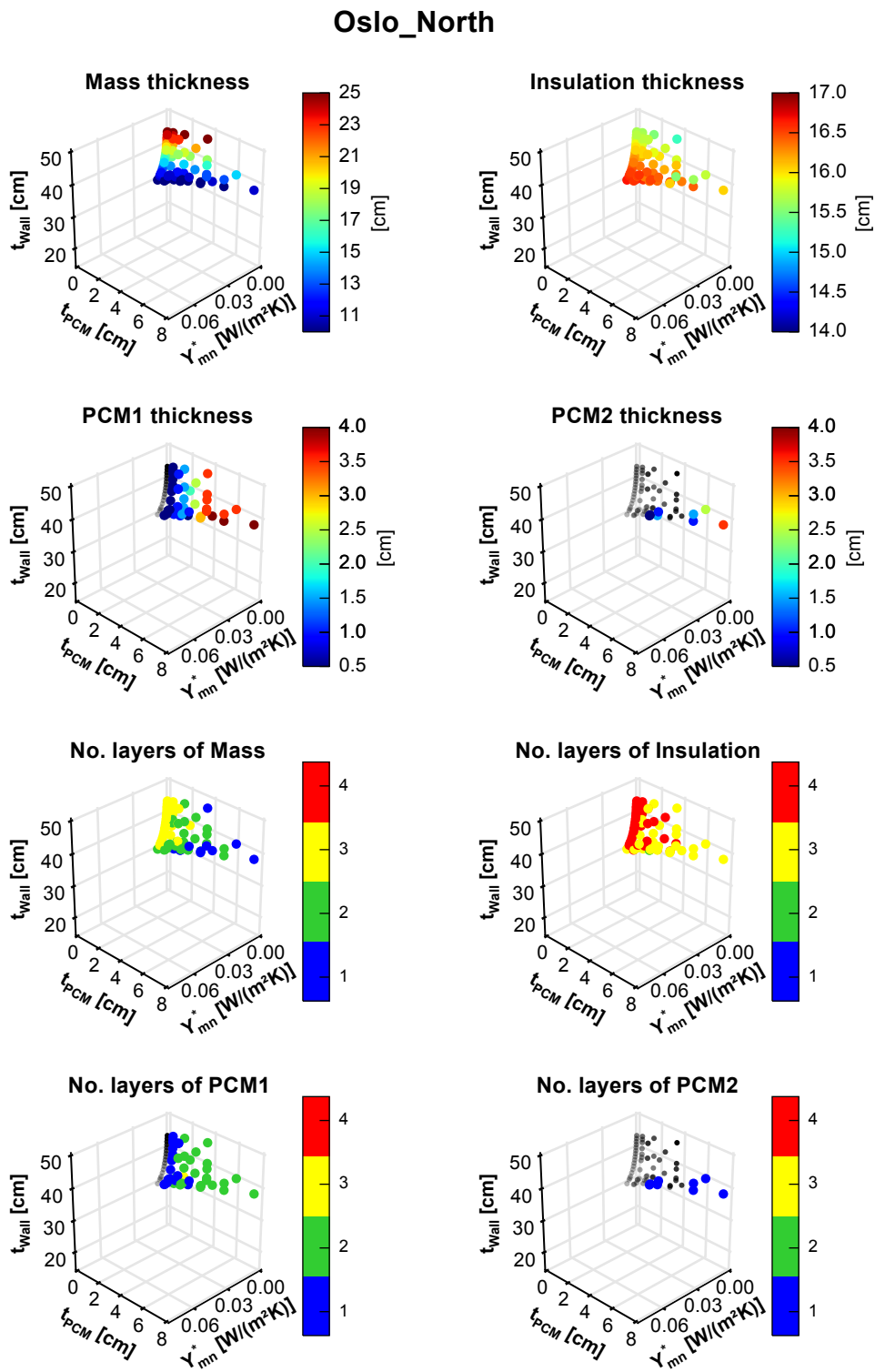
Torino_North
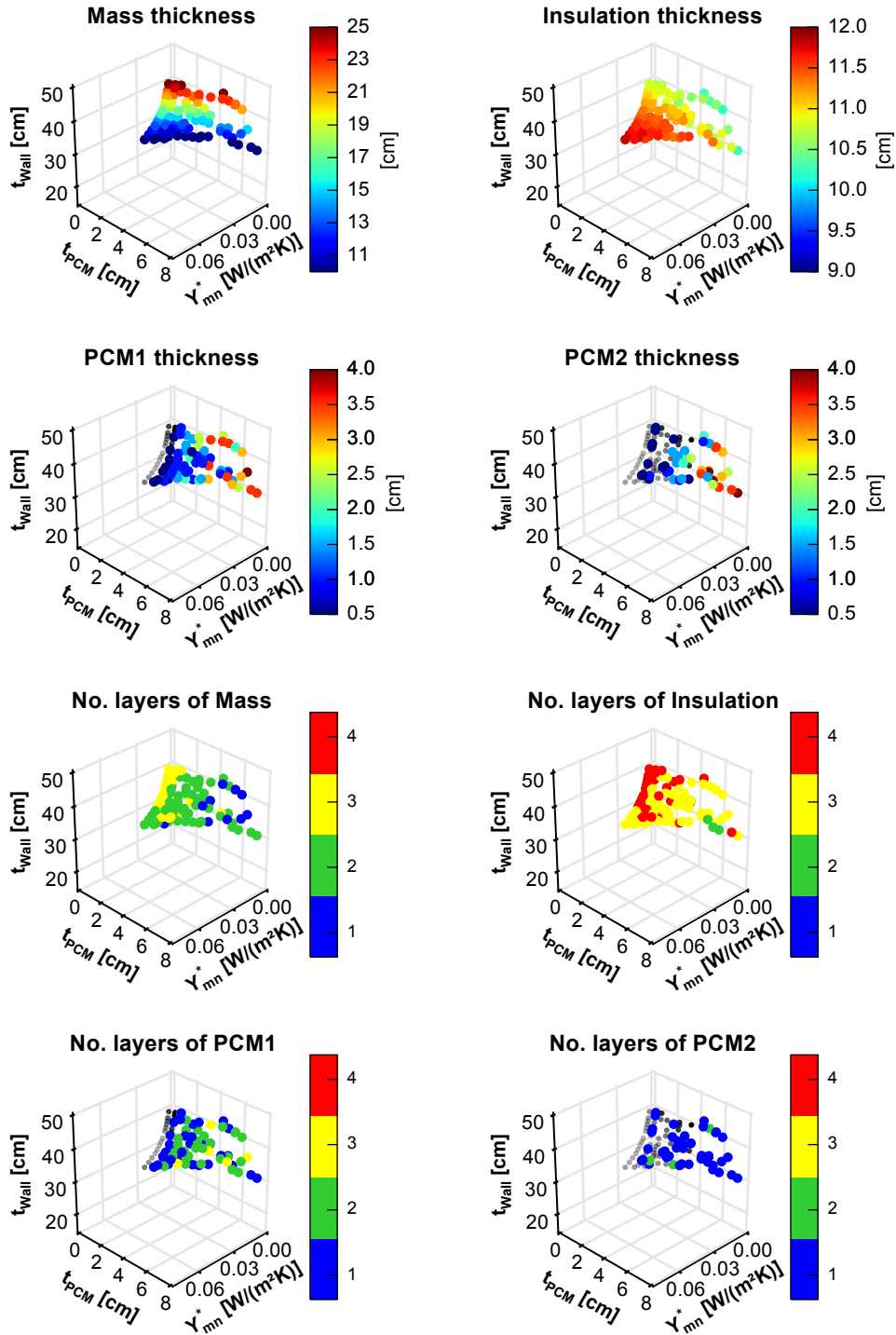
Fig. B.13 Thicknesses and no. of layers within the Pareto front: Torino, north façade.

Torino_North
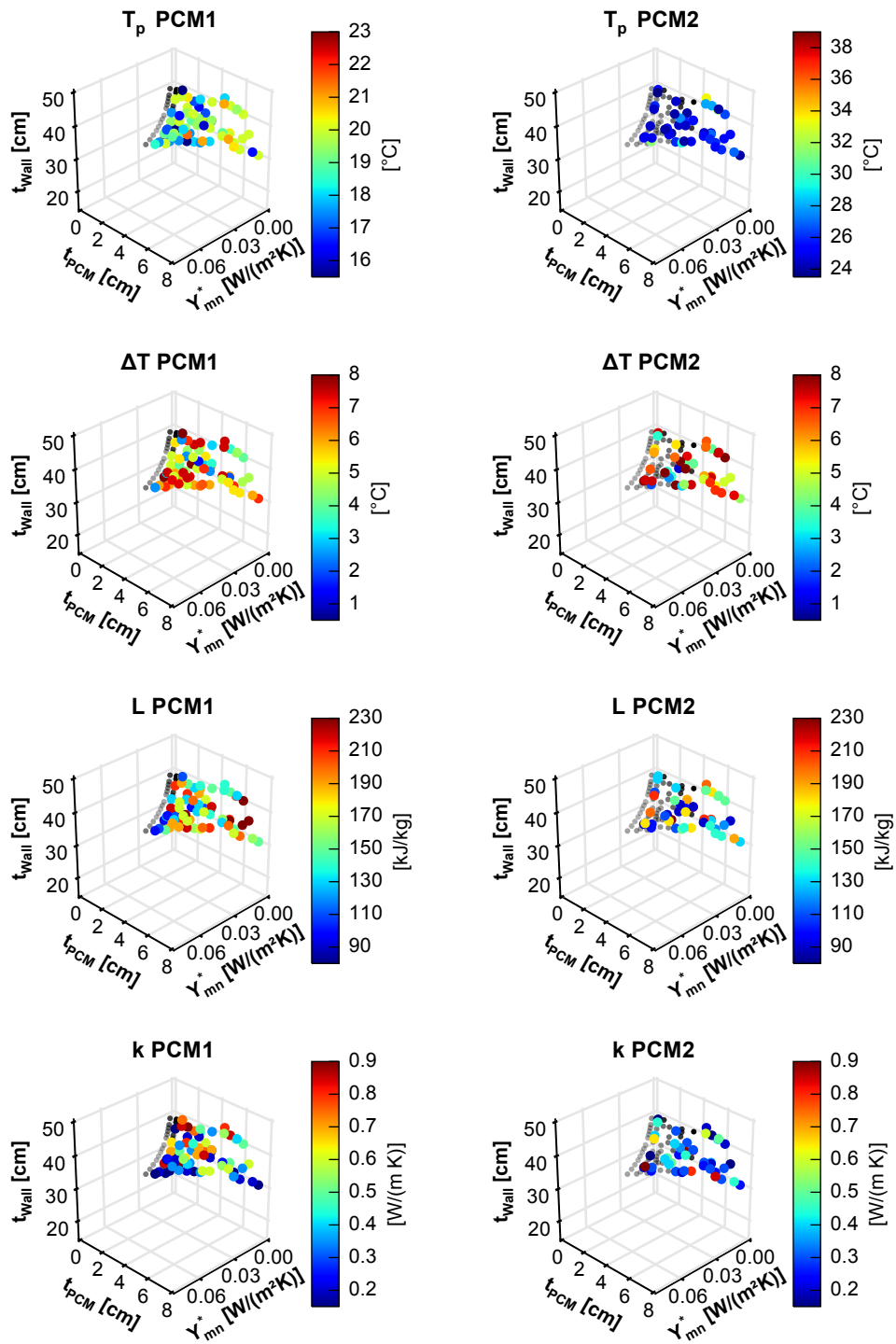
Fig. B.14 PCM properties within the Pareto front: Torino, north façade.

Torino_West

Fig. B.15 Thicknesses and no. of layers within the Pareto front: Torino, west façade.

Torino_West

Fig. B.16 PCM properties within the Pareto front: Torino, west façade.

Fig. B.17 Thicknesses and no. of layers within the Pareto front: Oslo, south façade.
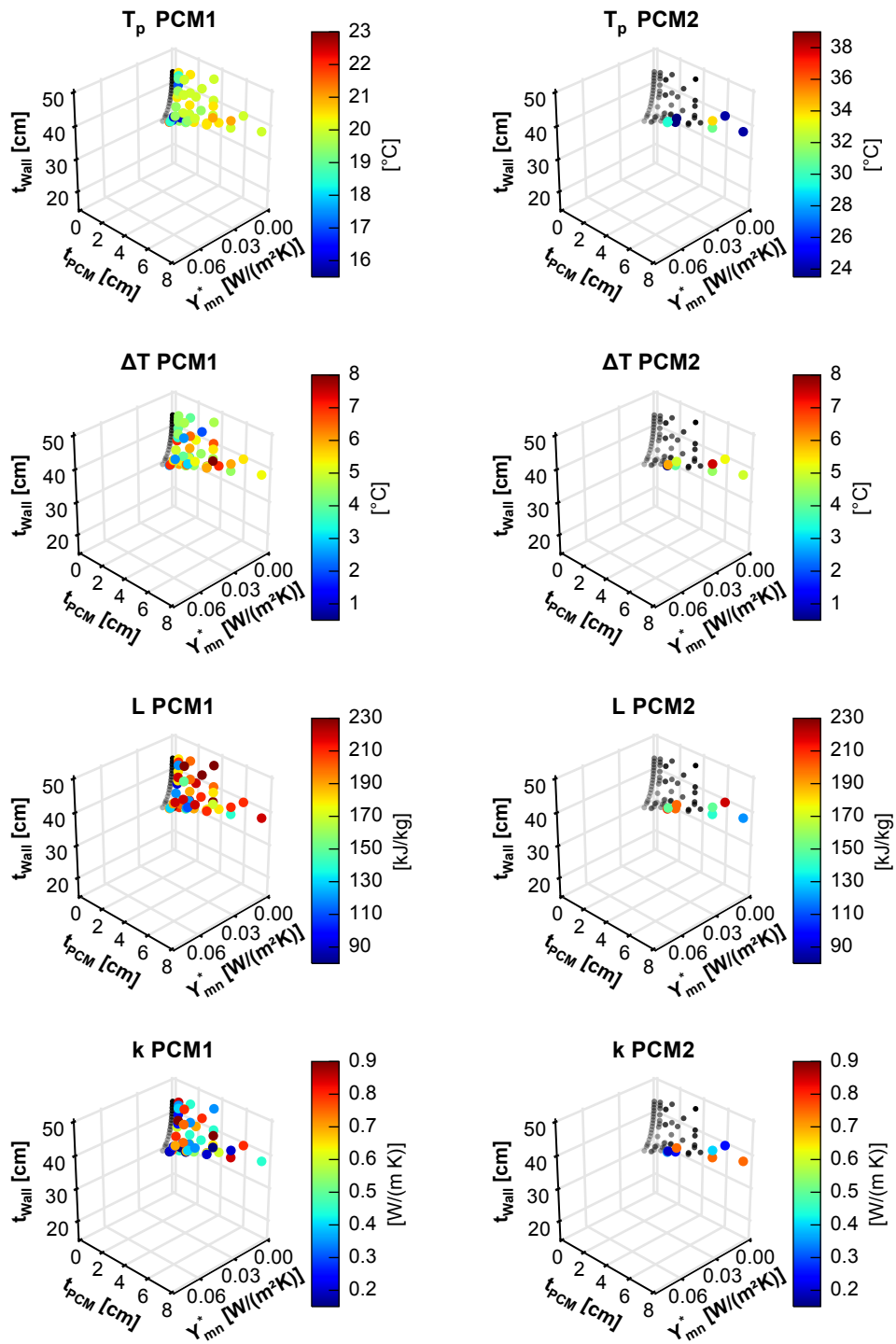
Oslo_South

Fig. B.18 PCM properties within the Pareto front: Oslo, south façade.

Fig. B.19 Thicknesses and no. of layers within the Pareto front: Oslo, east façade.

Oslo_East

T_p PCM1

T_p PCM2

ΔT PCM1

ΔT PCM2

L PCM1

L PCM2

k PCM1

k PCM2

Fig. B.20 PCM properties within the Pareto front: Oslo, east façade.

Fig. B.21 Thicknesses and no. of layers within the Pareto front: Oslo, north façade.

Oslo_North

Fig. B.22 PCM properties within the Pareto front: Oslo, north façade.
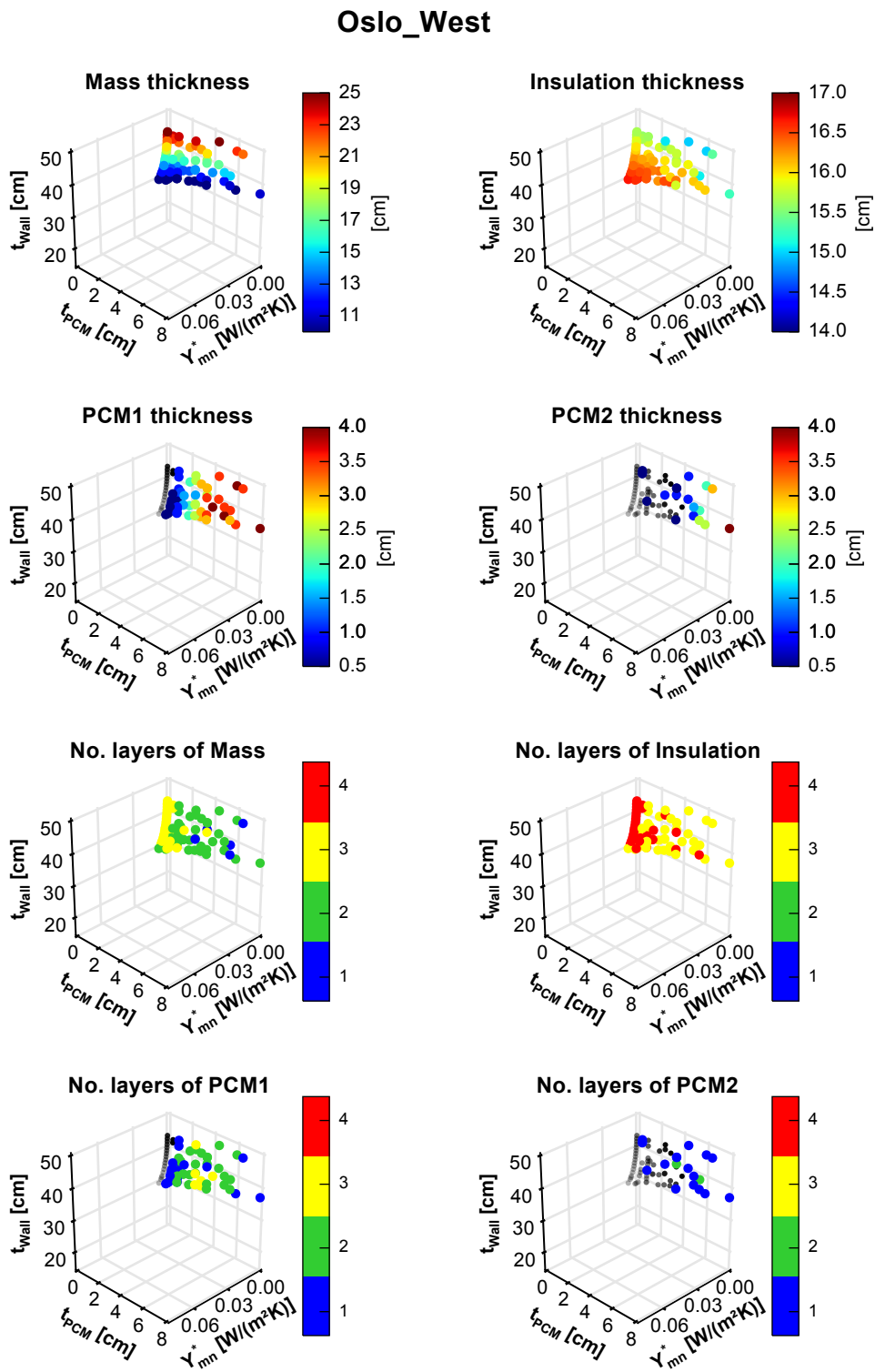
Oslo_West

Fig. B.23 Thicknesses and no. of layers within the Pareto front: Oslo, west façade.
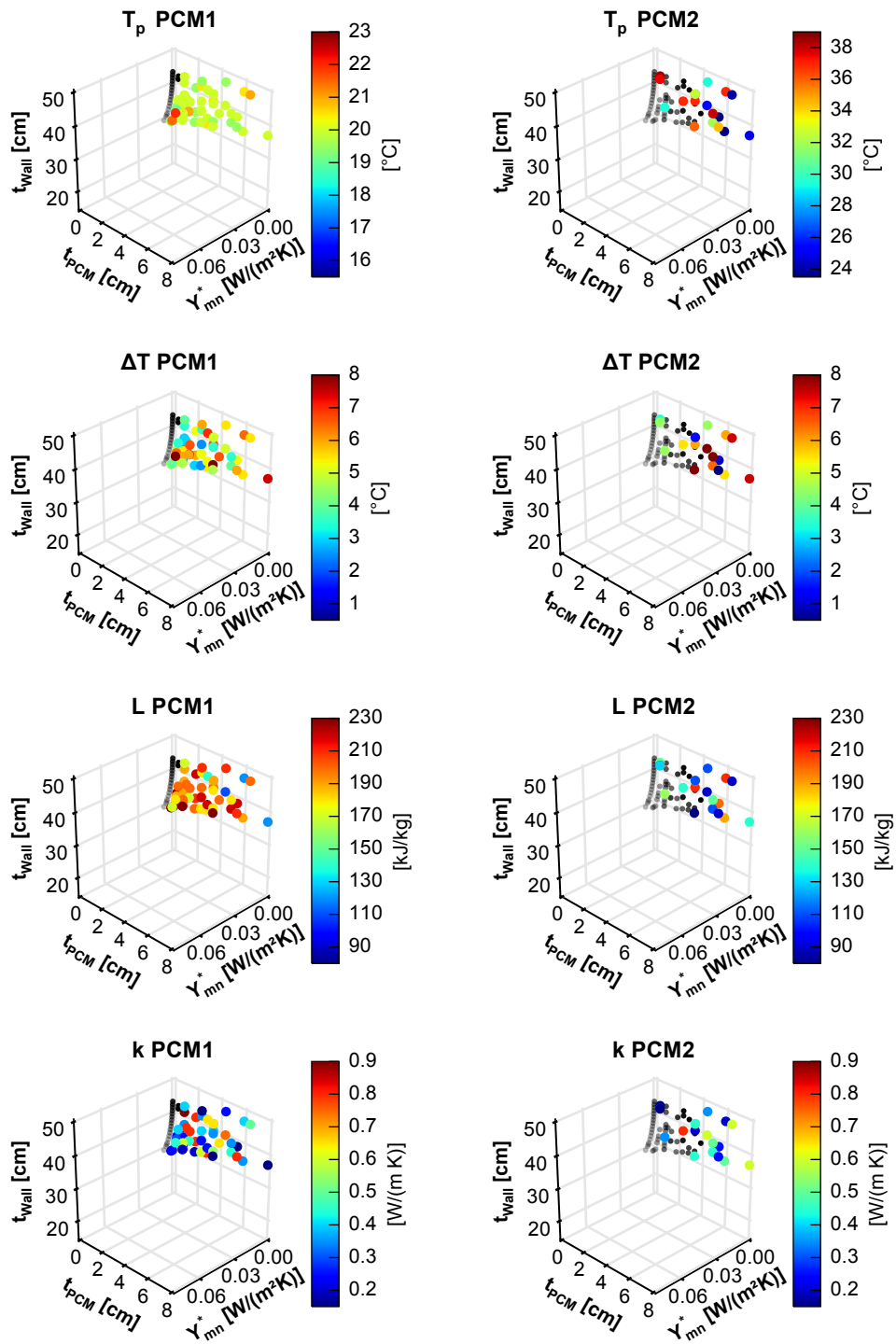
Fig. B.24 PCM properties within the Pareto front: Oslo, west façade.

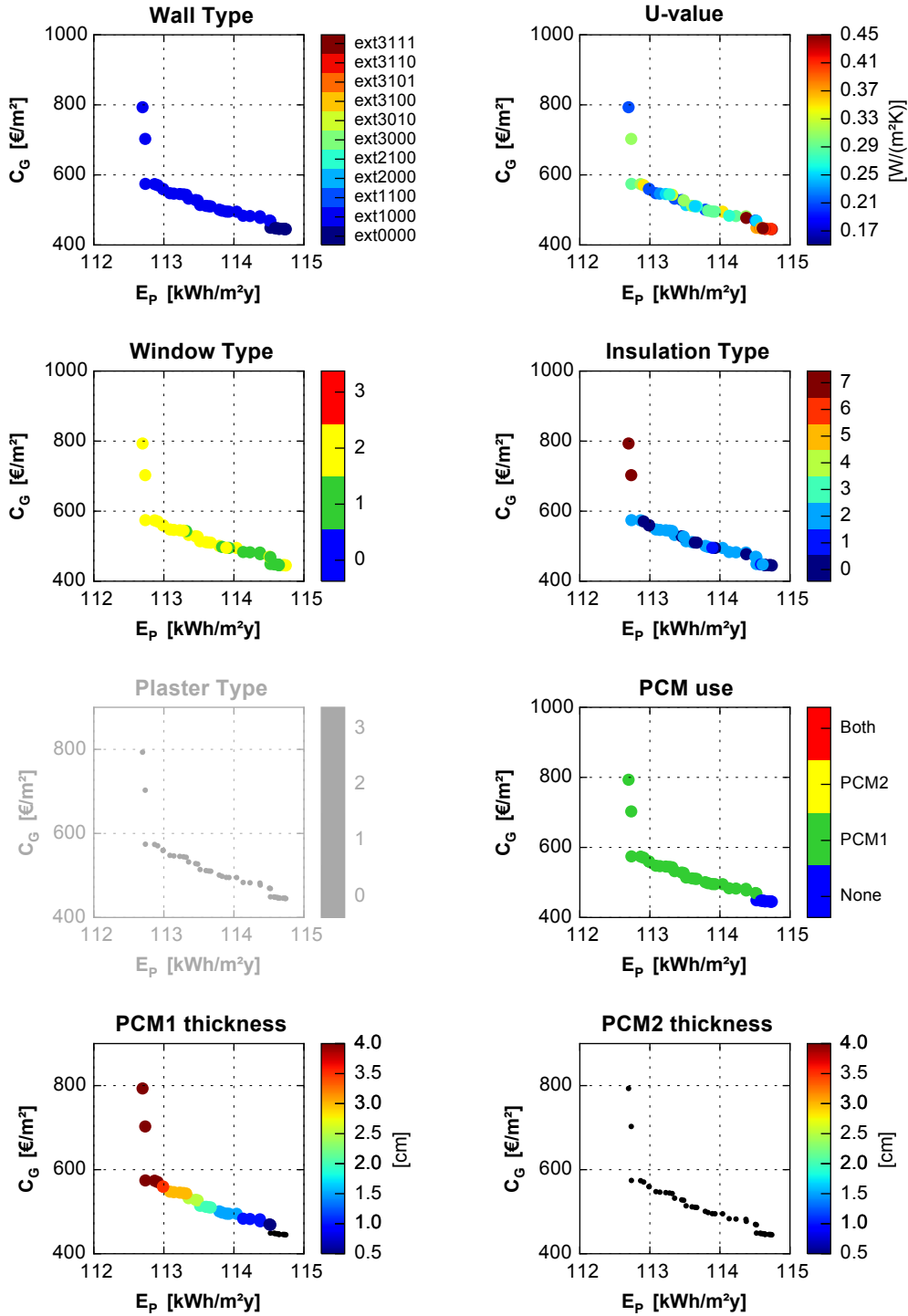# Palermo_2Obj_RT0_NF1

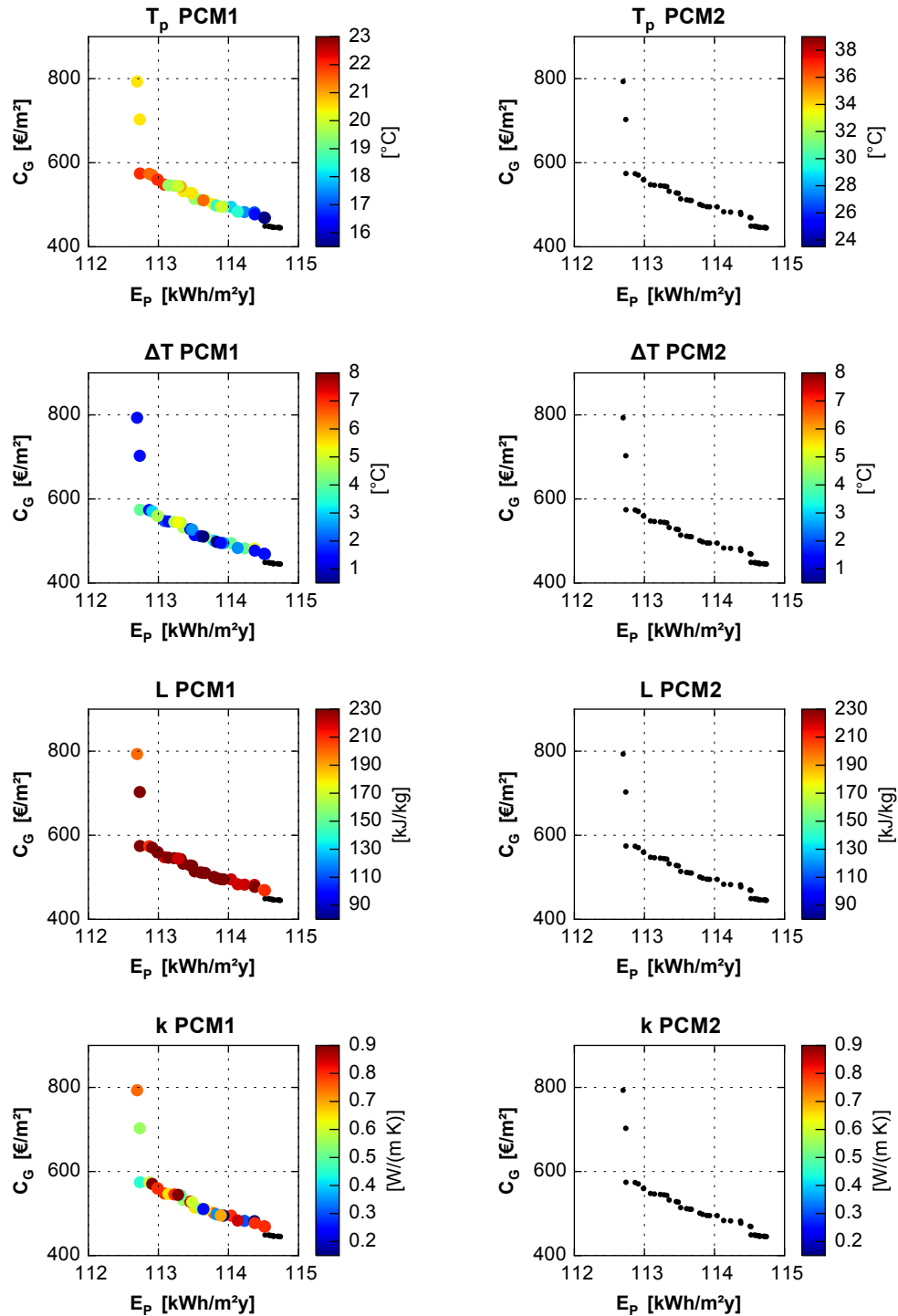Fig. B.25 Pareto mapping: Palermo_2Obj_RT0_NF1.

Palermo_2Obj_RT0_NF1

Fig. B.26 Pareto mapping: PCM properties, Palermo_2Obj_RT0_NF1.
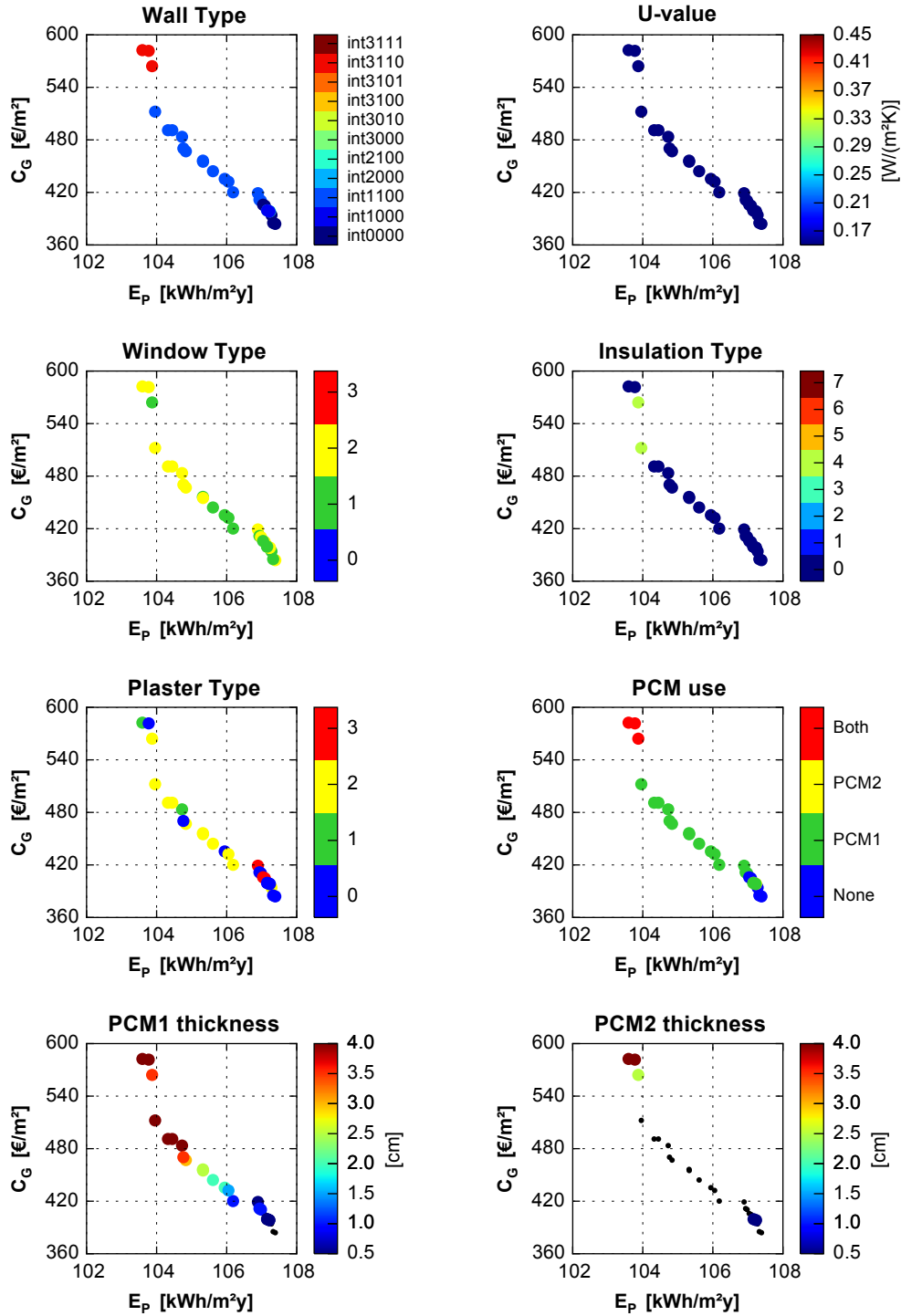
Palermo_2Obj_RT1_NF1

Fig. B.27 Pareto mapping: Palermo_2Obj_RT1_NF1.

Palermo_2Obj_RT1_NF1

Fig. B.28 Pareto mapping: PCM properties, Palermo_2Obj_RT1_NF1.

Palermo_2Obj_RT2_NF1

Fig. B.29 Pareto mapping: Palermo_2Obj_RT2_NF1.

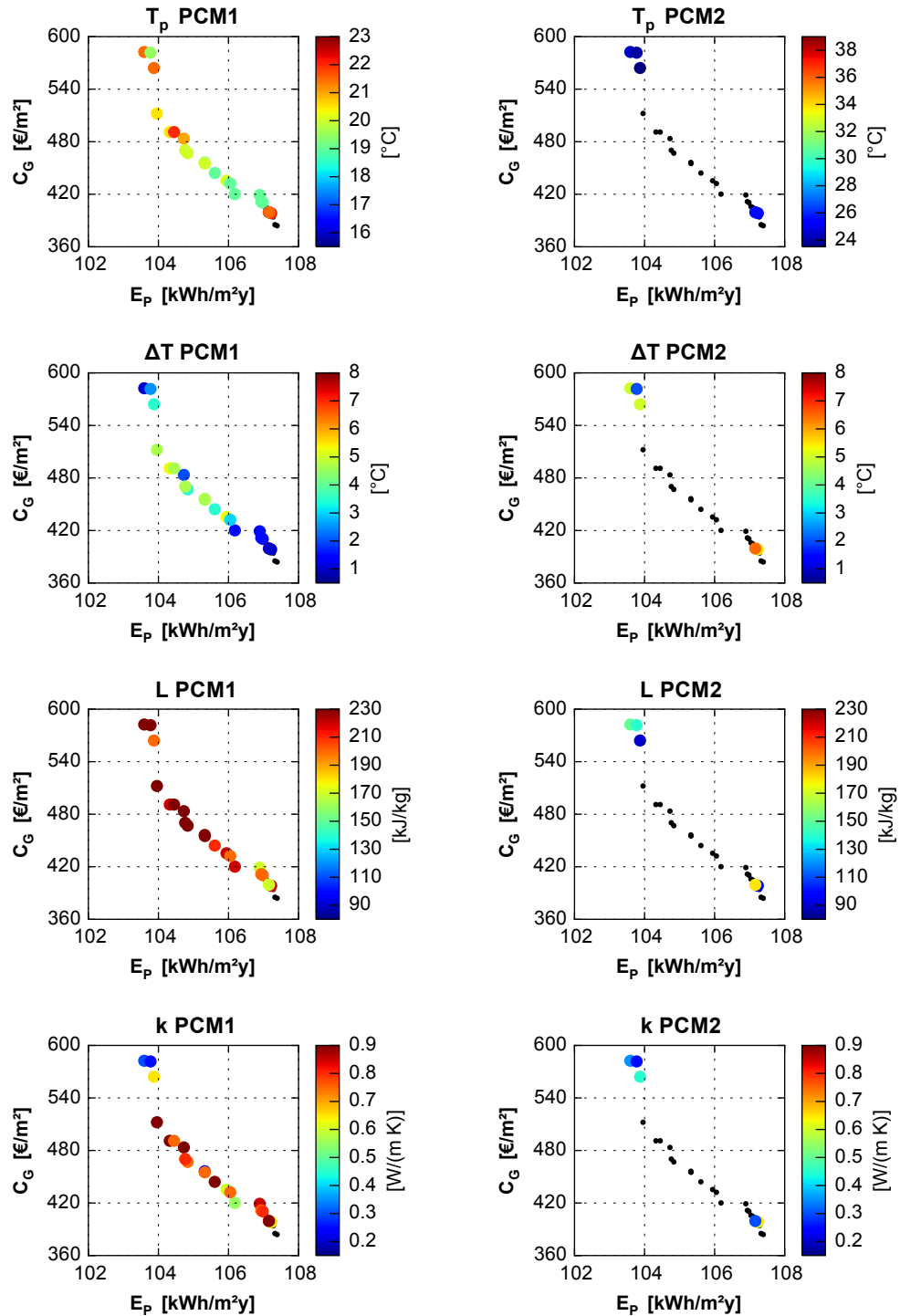Fig. B.30 Pareto mapping: PCM properties, Palermo_2Obj_RT2_NF1.

Fig. B.31 Pareto mapping: Torino_2Obj_RT0_NF1.

Torino_2Obj_RT0_NF1

Fig. B.32 Pareto mapping: PCM properties, Torino_2Obj_RT0_NF1.

Torino_2Obj_RT1_NF1

Fig. B.33 Pareto mapping: Torino_2Obj_RT1_NF1.

Torino_2Obj_RT1_NF1

Fig. B.34 Pareto mapping: PCM properties, Torino_2Obj_RT1_NF1.
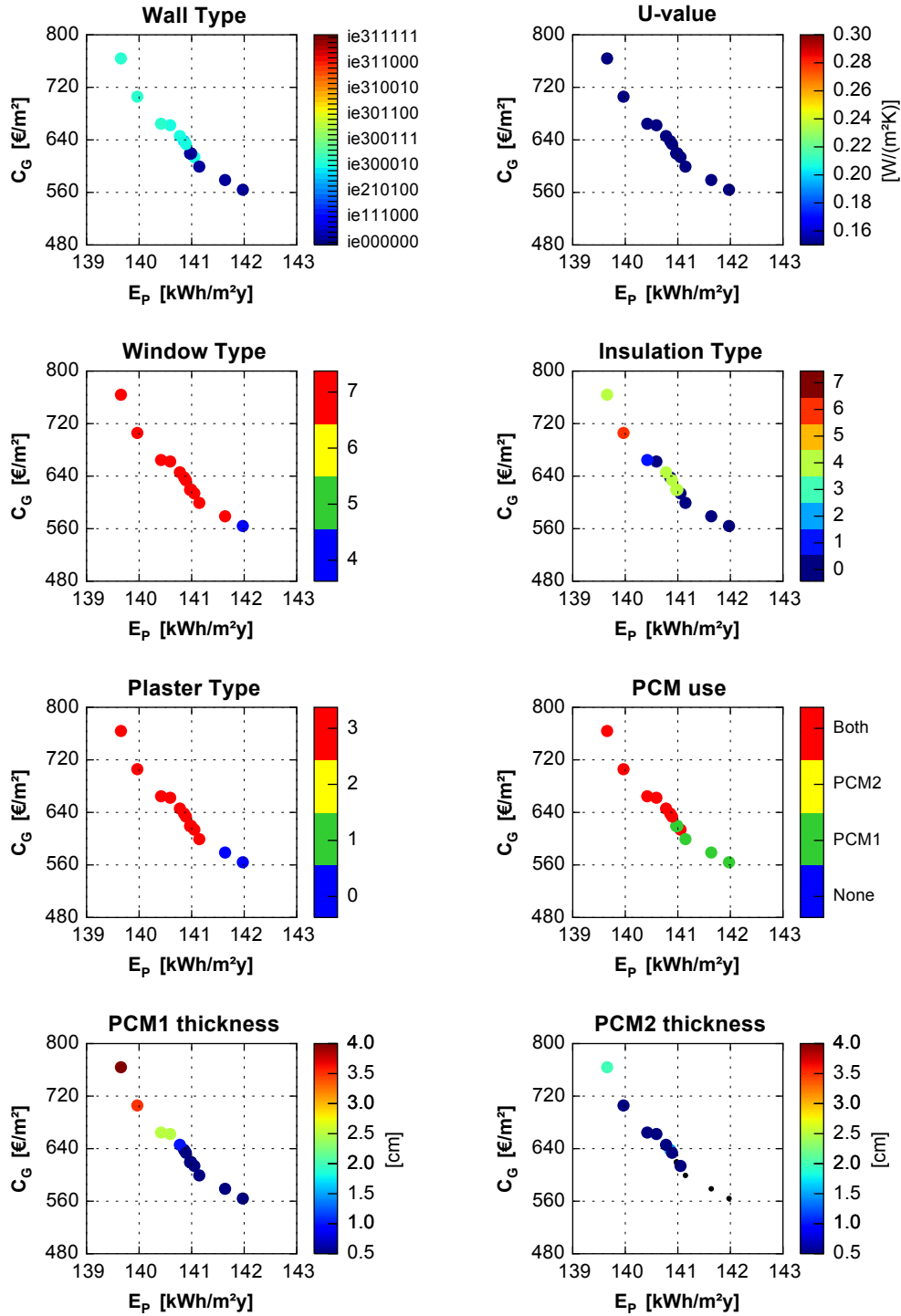
Torino_2Obj_RT2_NF1

Fig. B.35 Pareto mapping: Torino_2Obj_RT2_NF1.

Torino_2Obj_RT2_NF1
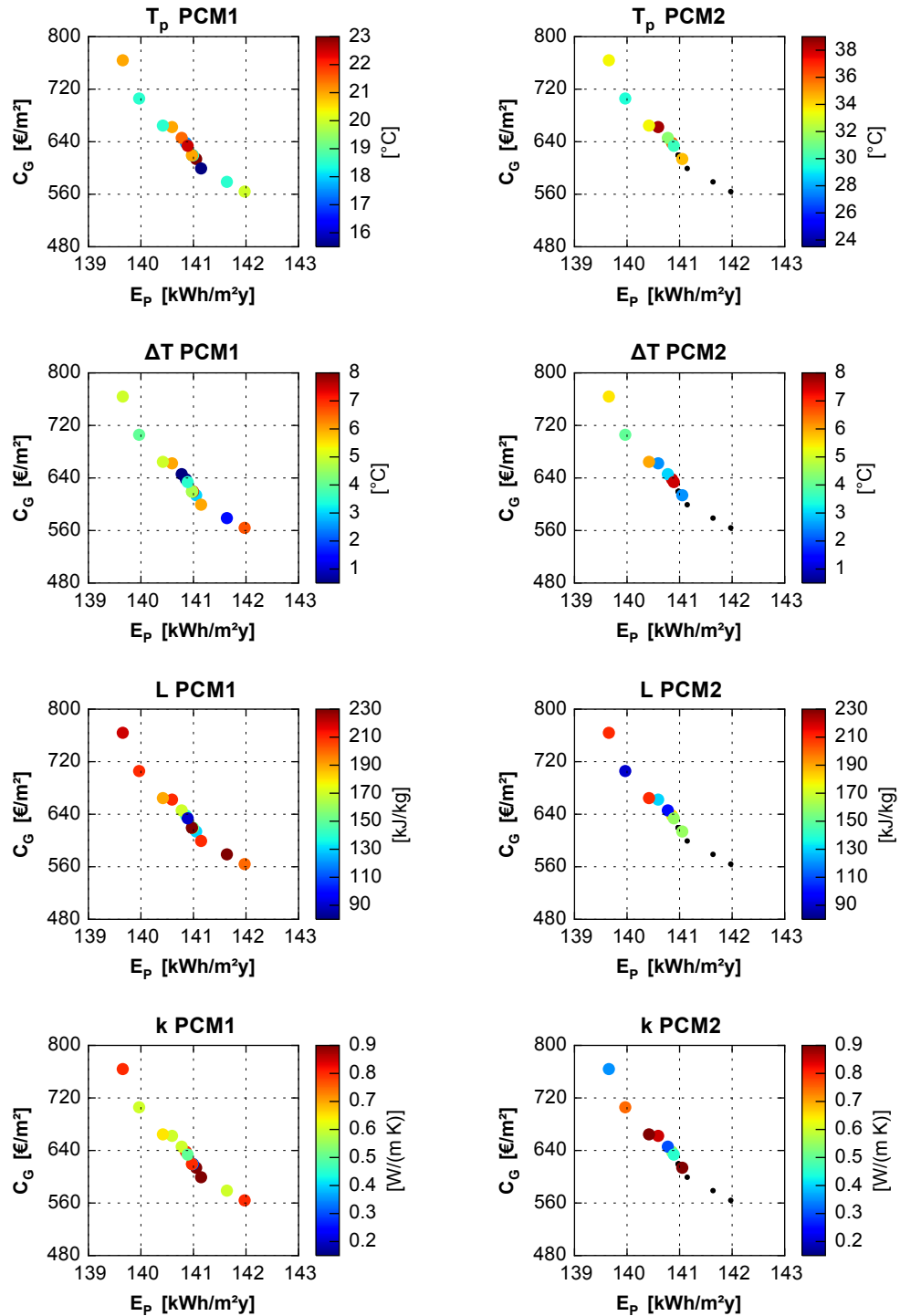
Fig. B.36 Pareto mapping: PCM properties, Torino_2Obj_RT2_NF1.

Palermo_3Obj_RT0_NF1
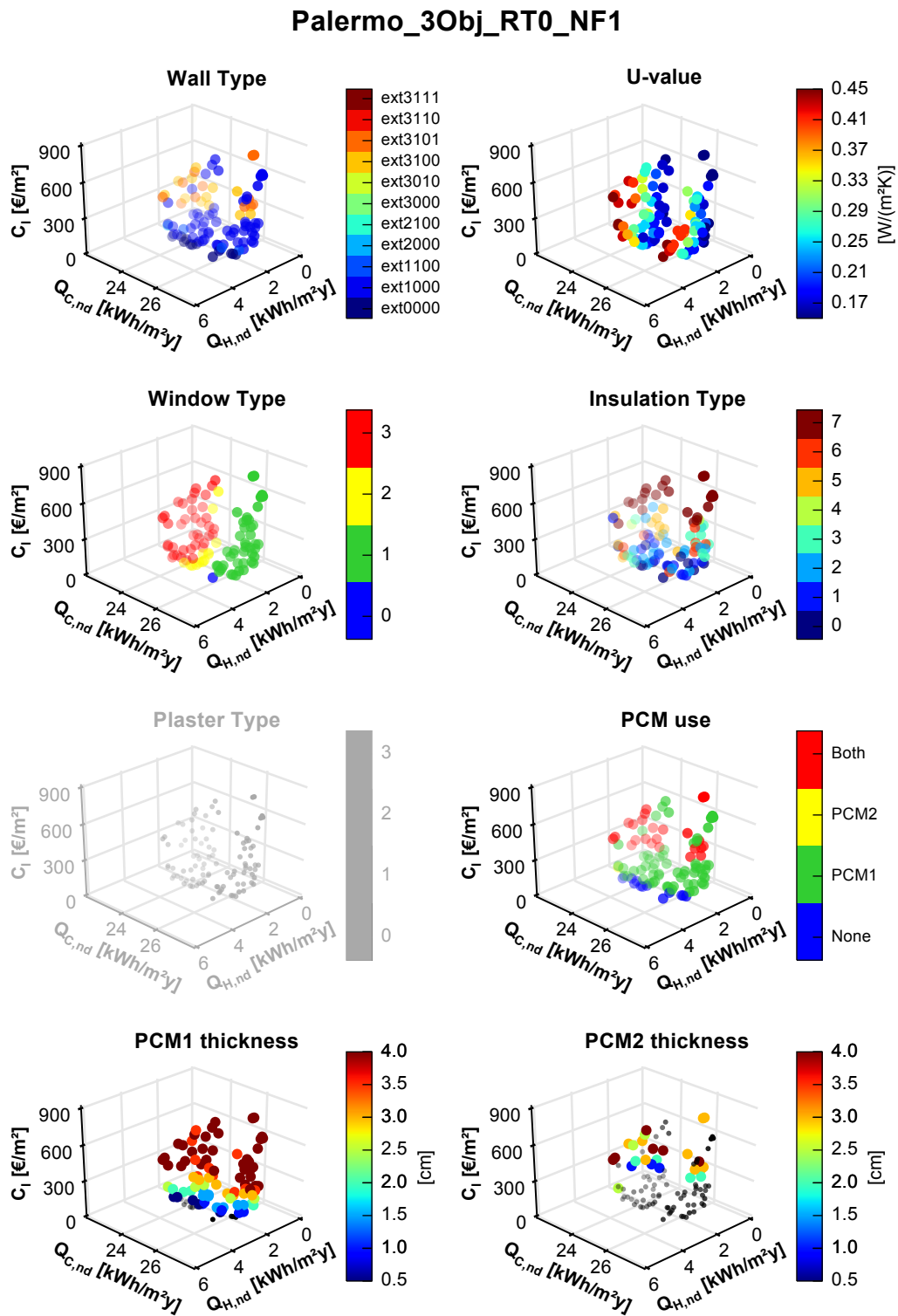
Fig. B.37 Pareto mapping: Palermo_3Obj_RT0_NF1.

Fig. B.38 Pareto mapping: PCM properties, Palermo_3Obj_RT0_NF1.

Palermo_3Obj_RT1_NF1
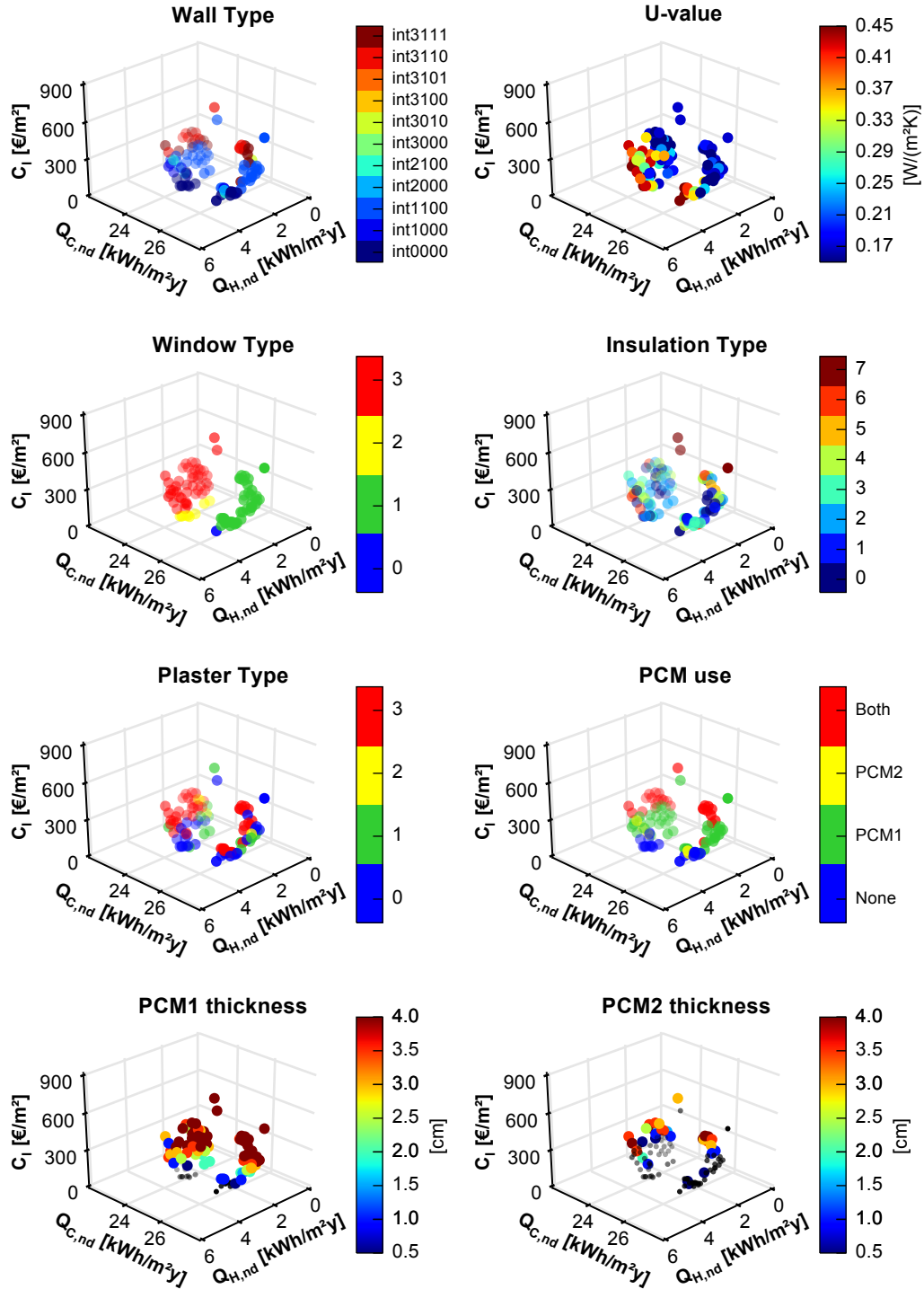
Fig. B.39 Pareto mapping: Palermo_3Obj_RT1_NF1.

Palermo_3Obj_RT1_NF1
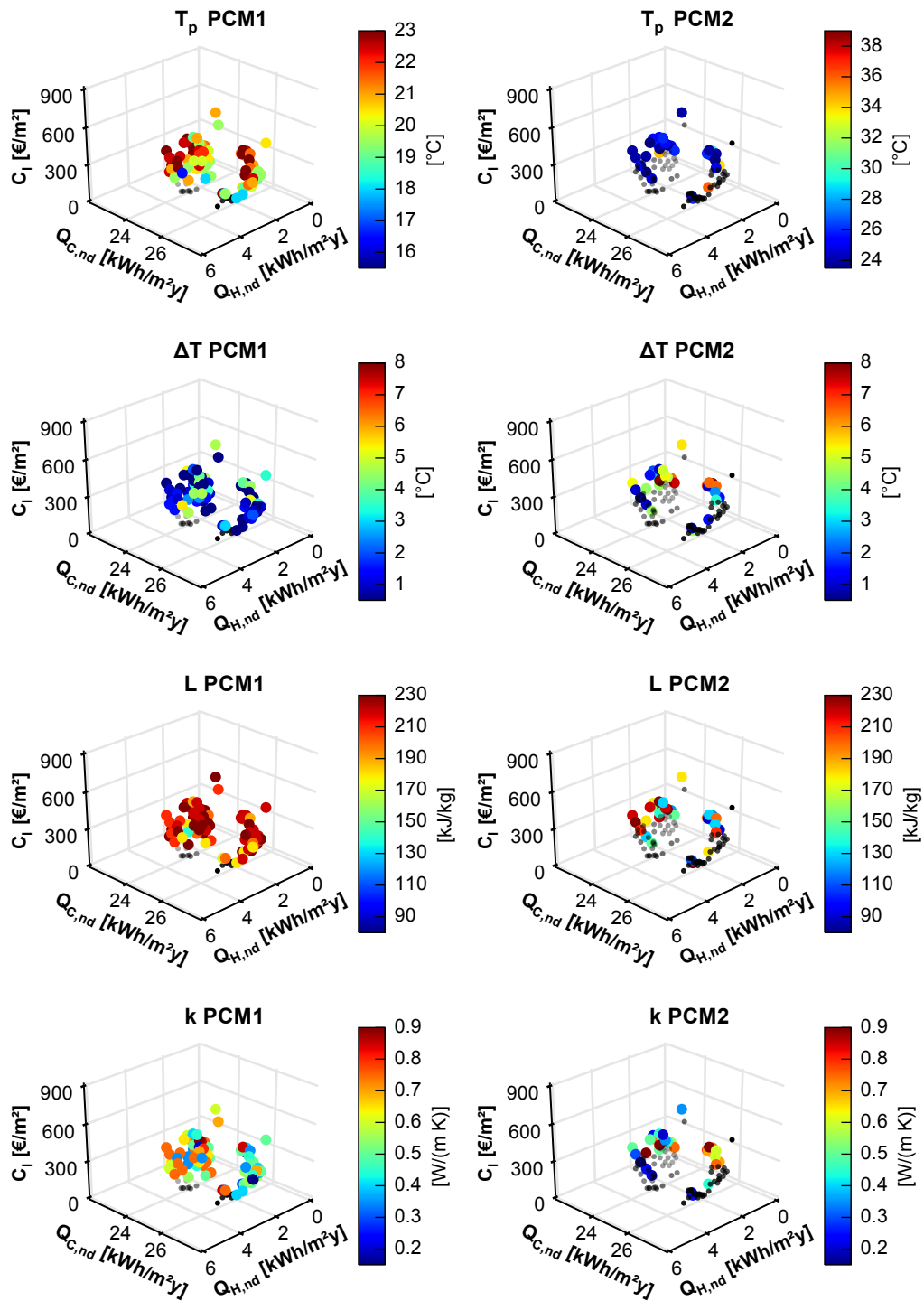
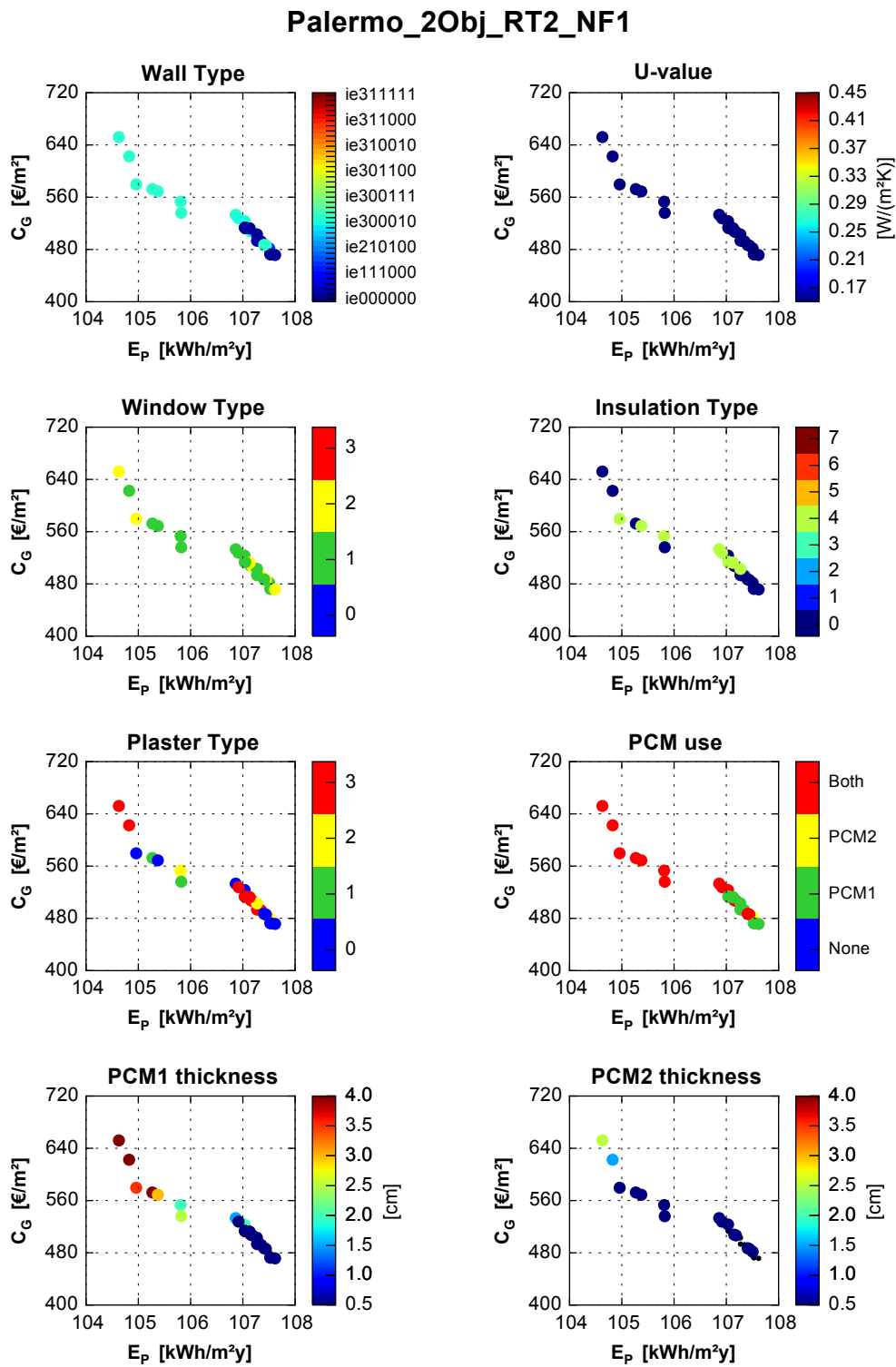Fig. B.40 Pareto mapping: PCM properties, Palermo_3Obj_RT1_NF1.

Palermo_3Obj_RT2_NF1
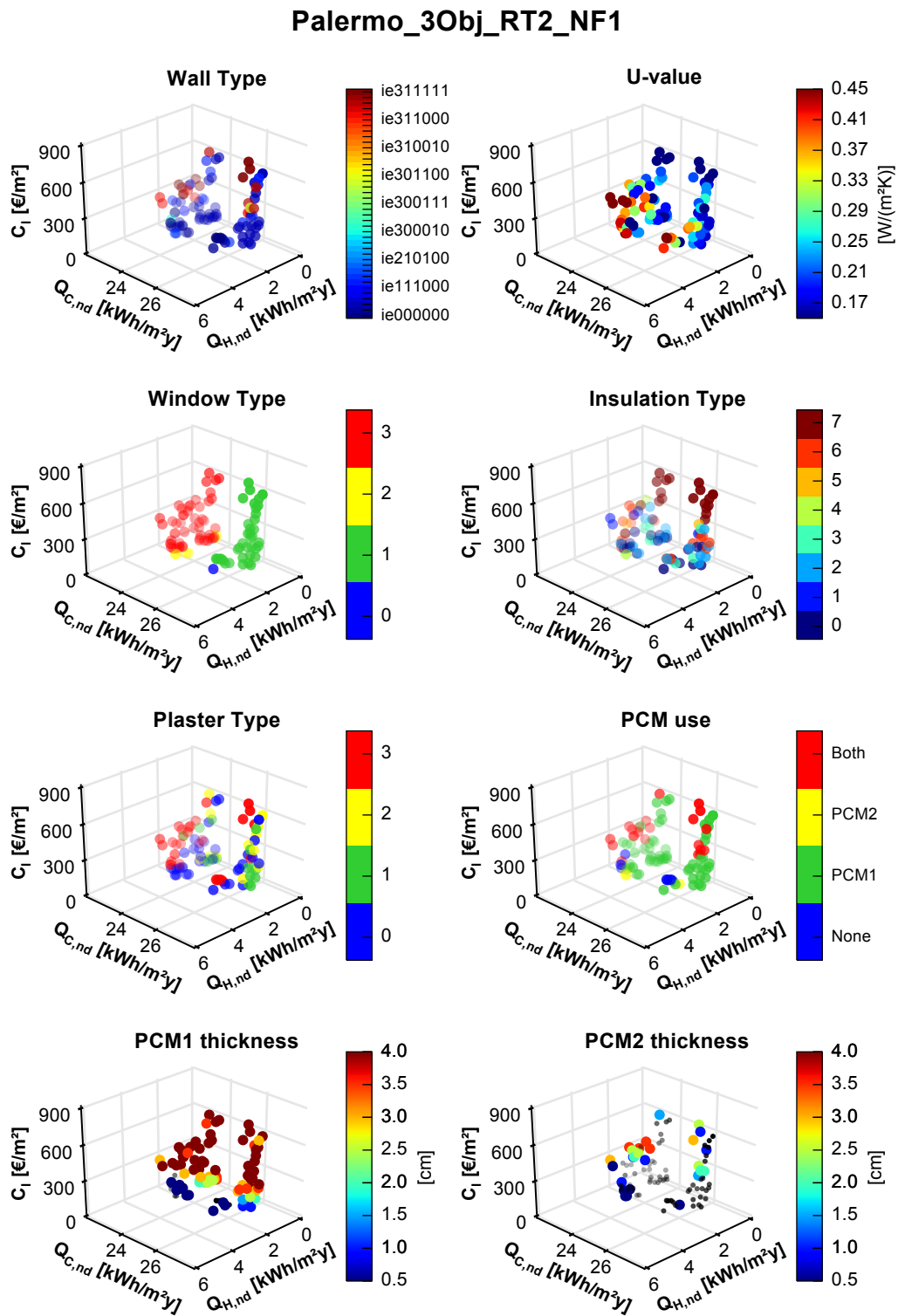
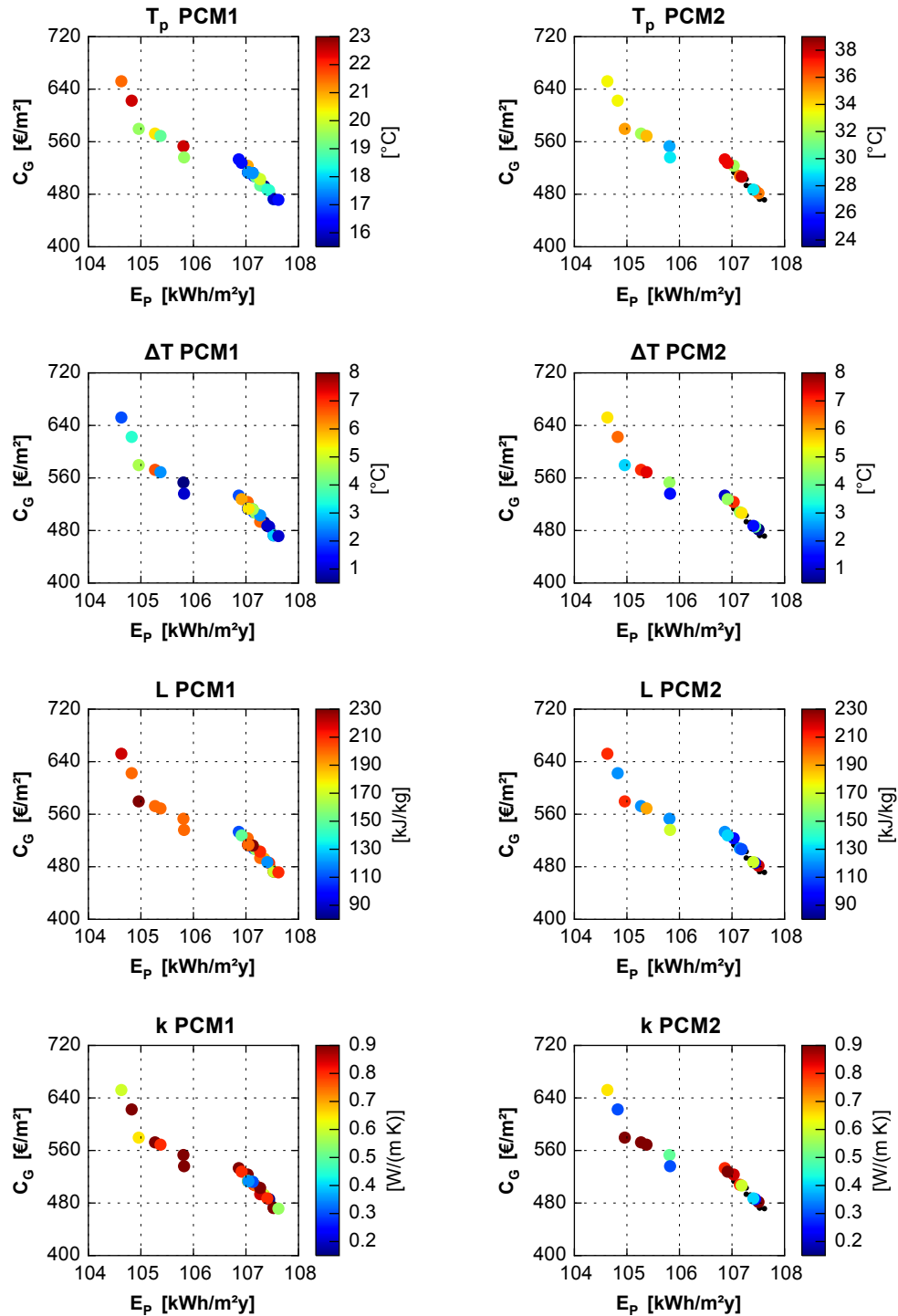Fig. B.41 Pareto mapping: Palermo_3Obj_RT2_NF1.

Palermo_3Obj_RT2_NF1
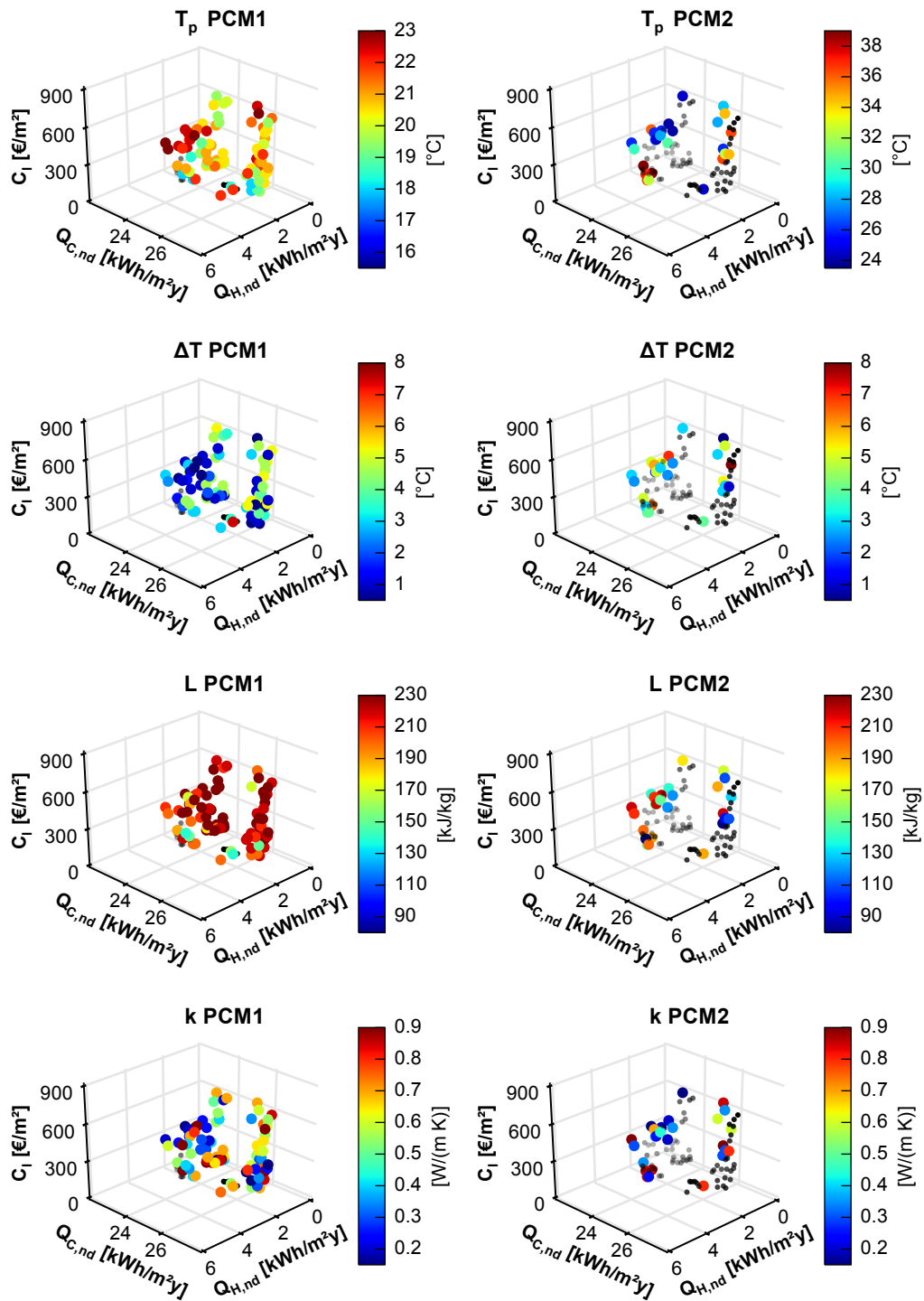
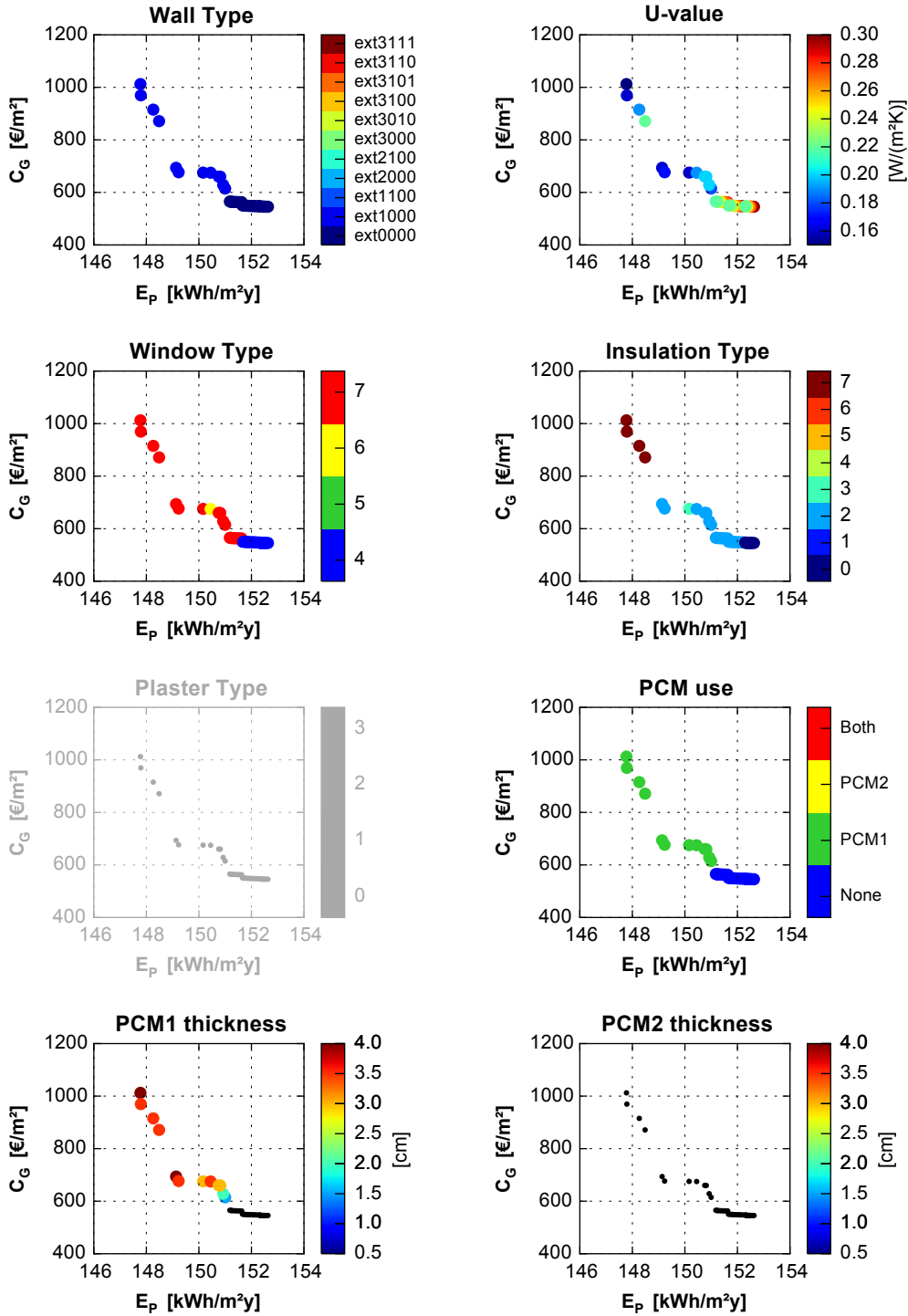Fig. B.42 Pareto mapping: PCM properties, Palermo_3Obj_RT2_NF1.
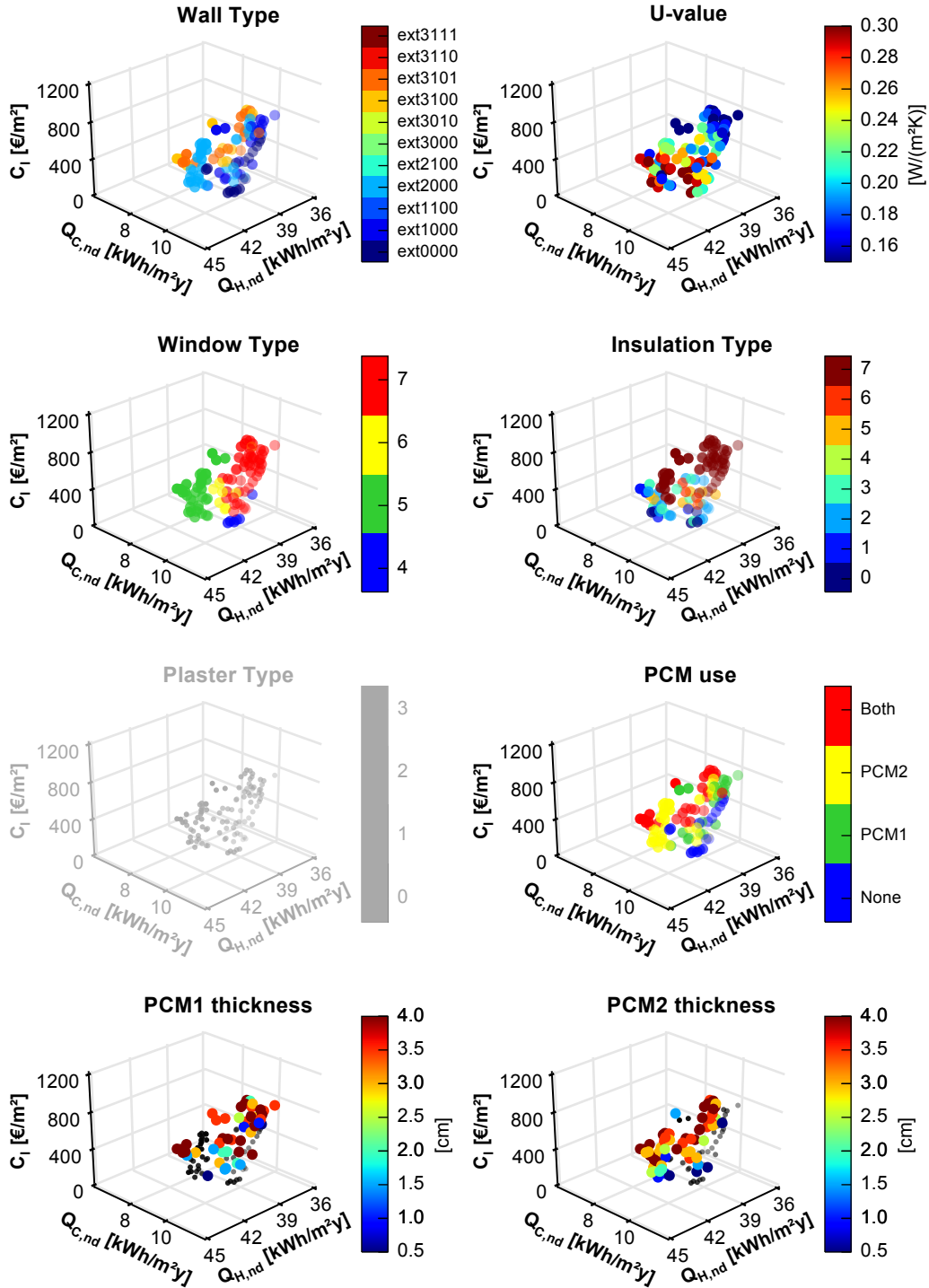
Fig. B.43 Pareto mapping: Torino_3Obj_RT0_NF1.
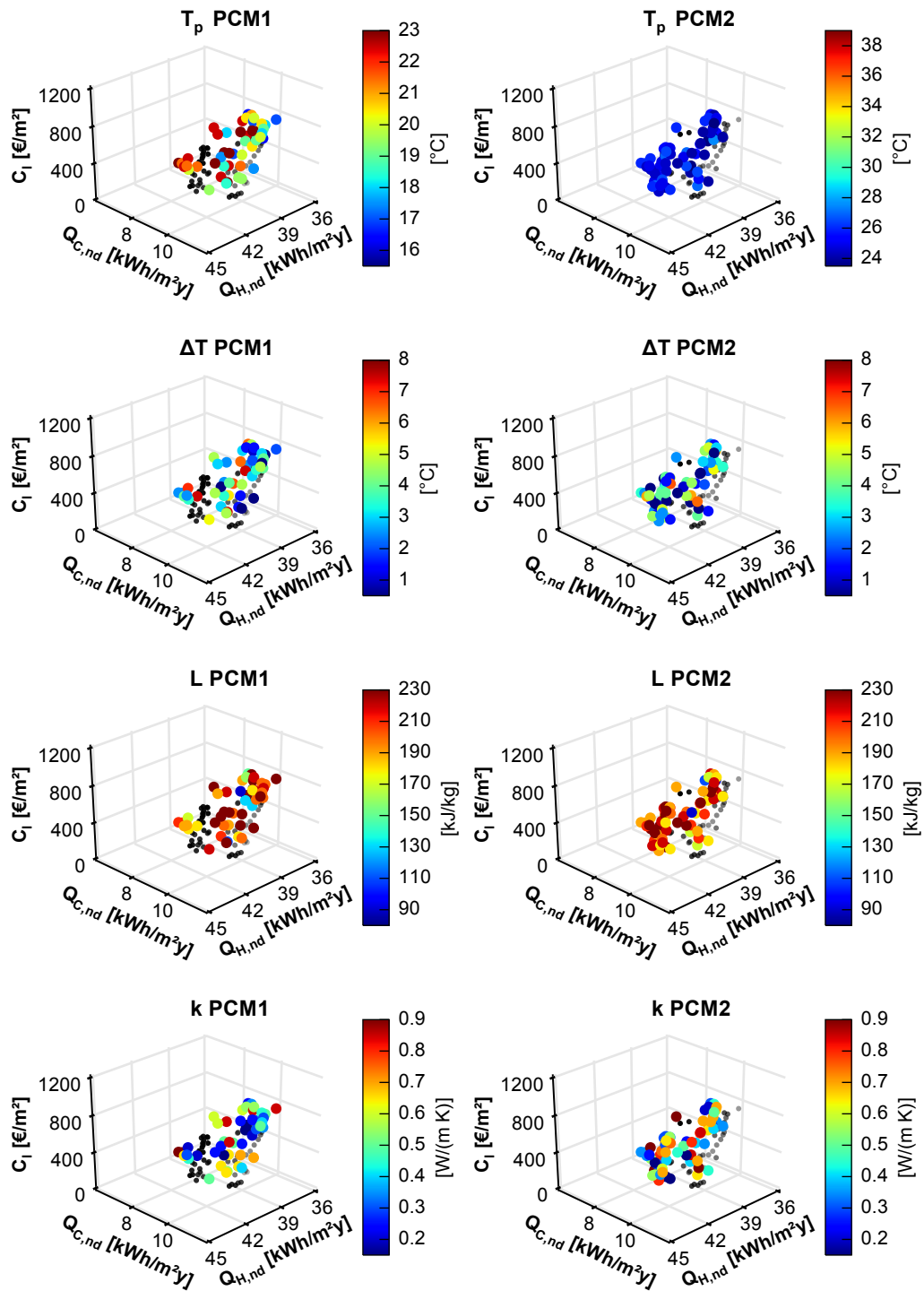
Torino_3Obj_RT0_NF1

Fig. B.44 Pareto mapping: PCM properties, Torino_3Obj_RT0_NF1.
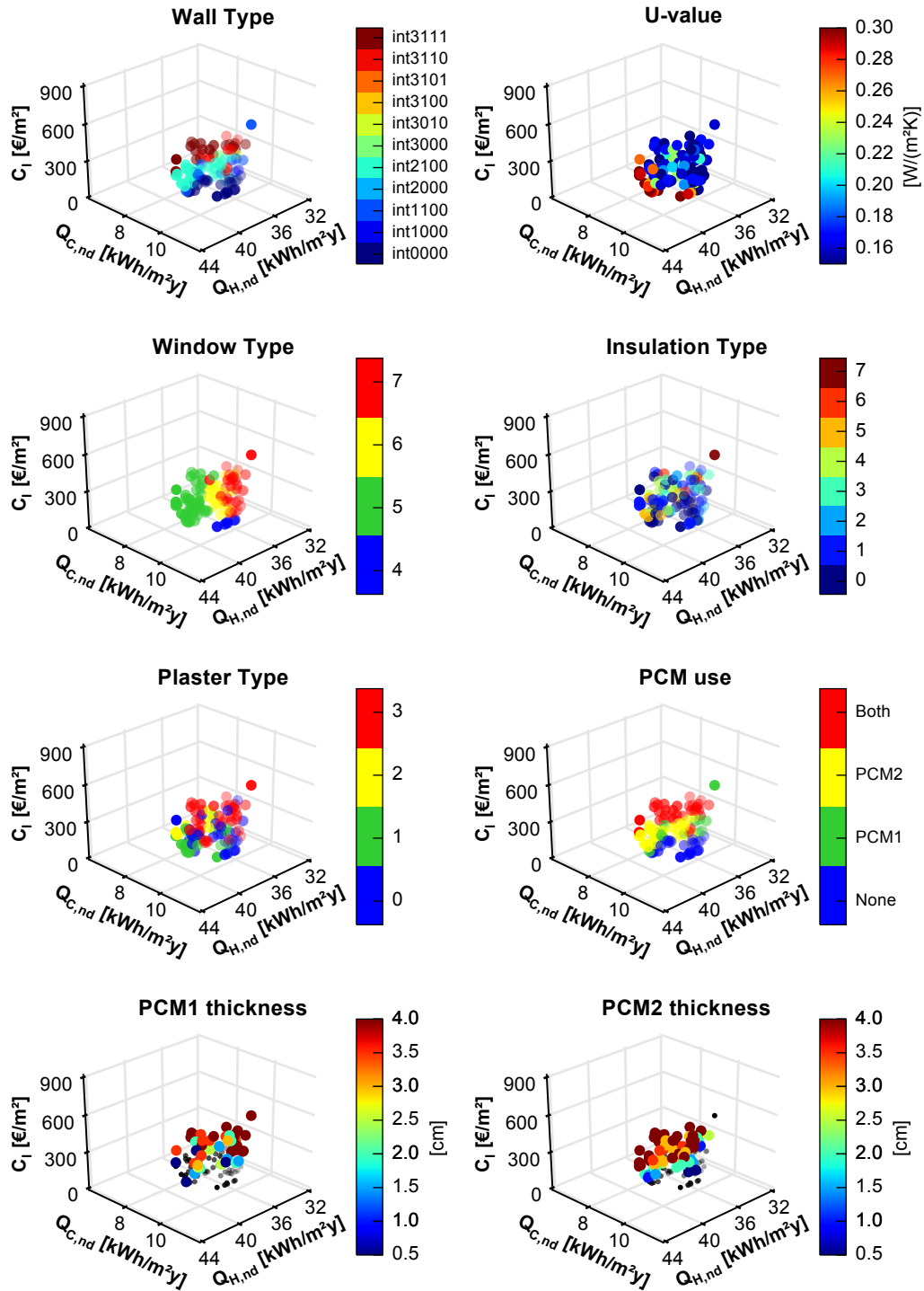
Torino_3Obj_RT1_NF1
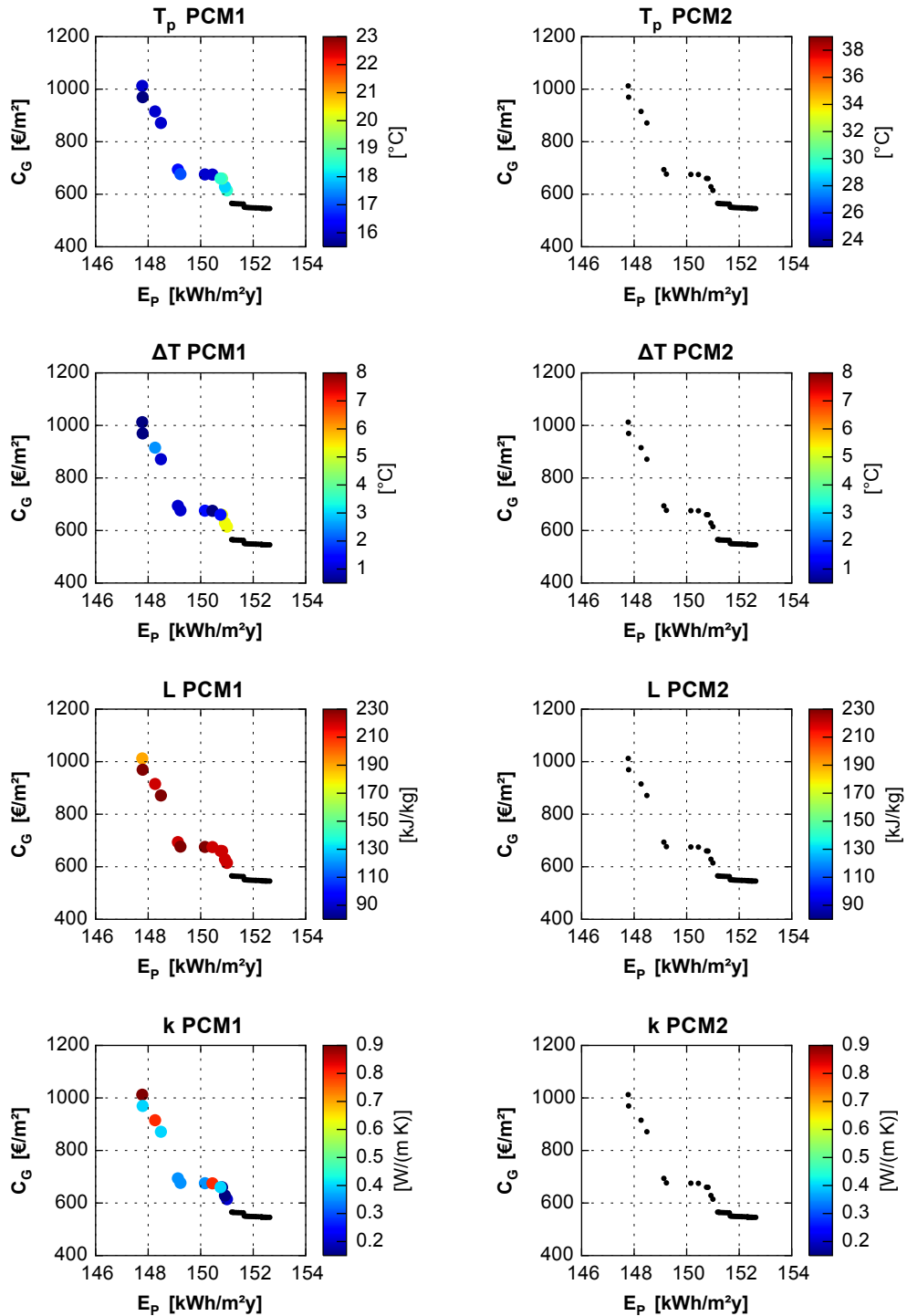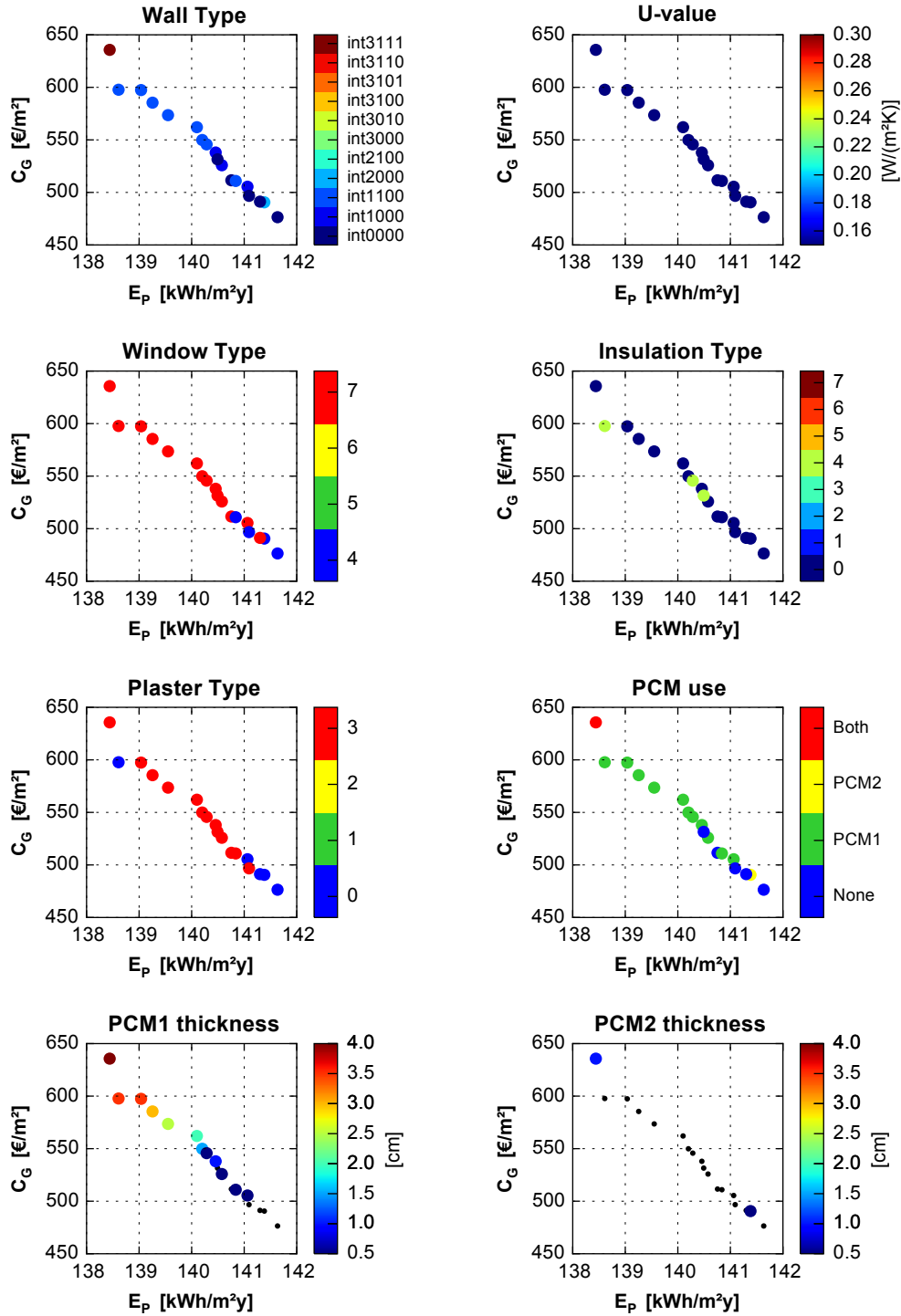

Fig. B.45 Pareto mapping: Torino_3Obj_RT1_NF1.

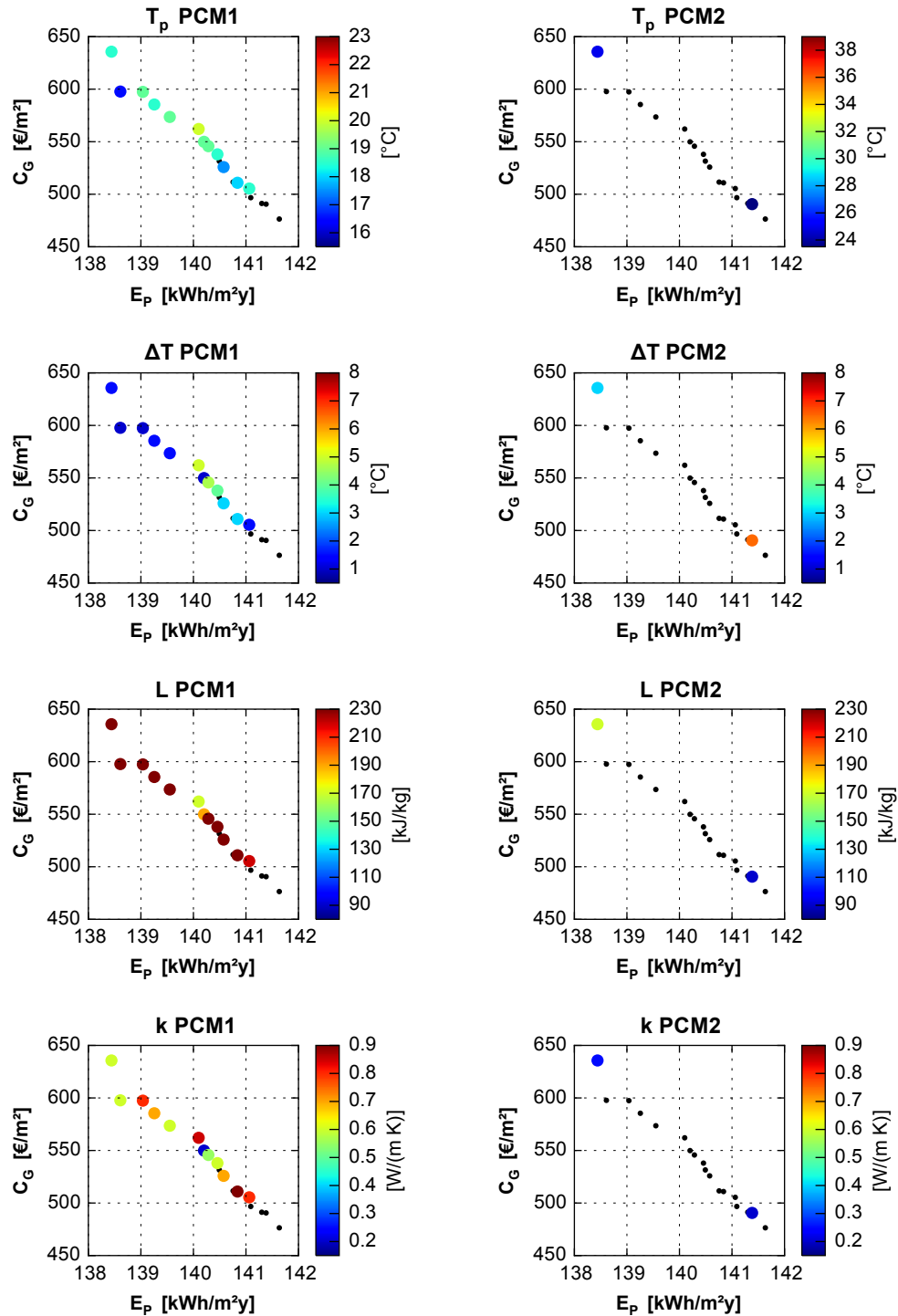Fig. B.46 Pareto mapping: PCM properties, Torino_3Obj_RT1_NF1.

Torino_3Obj_RT2_NF1
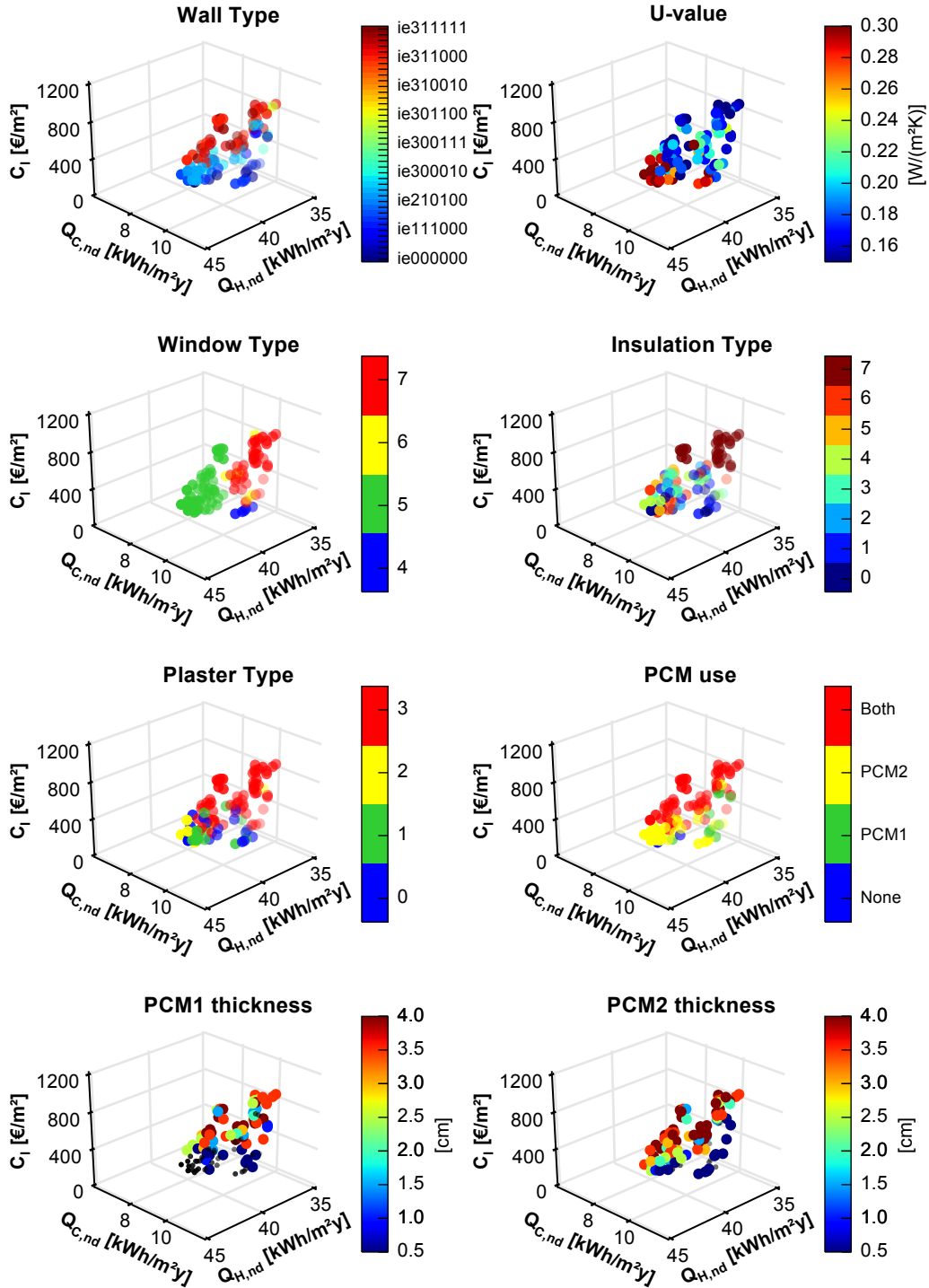
Fig. B.47 Pareto mapping: Torino_3Obj_RT2_NF1.

Torino_3Obj_RT2_NF1
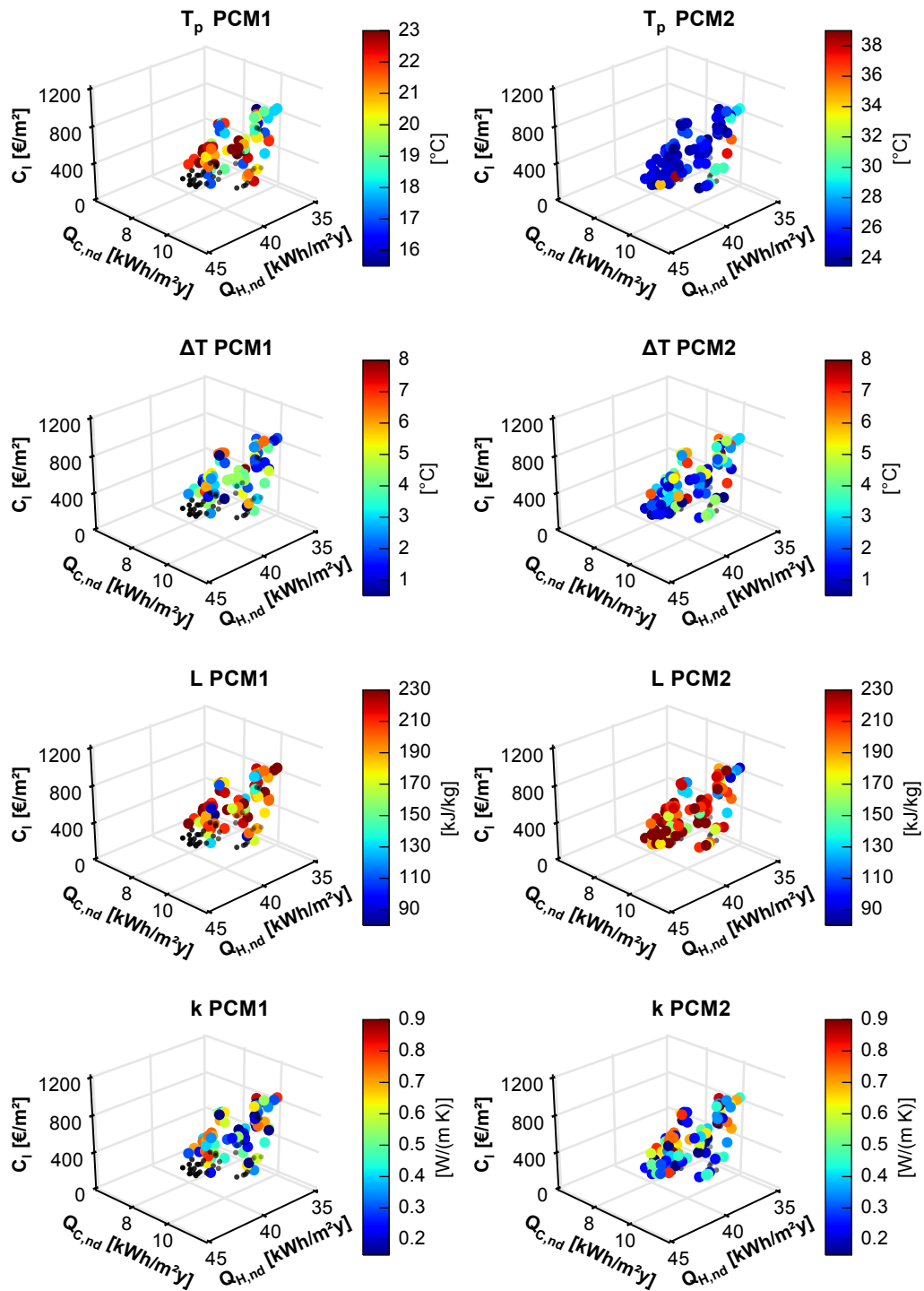
Fig. B.48 Pareto mapping: PCM properties, Torino_3Obj_RT2_NF1.

Oslo_3Obj_pre-1955_RT0_NF1
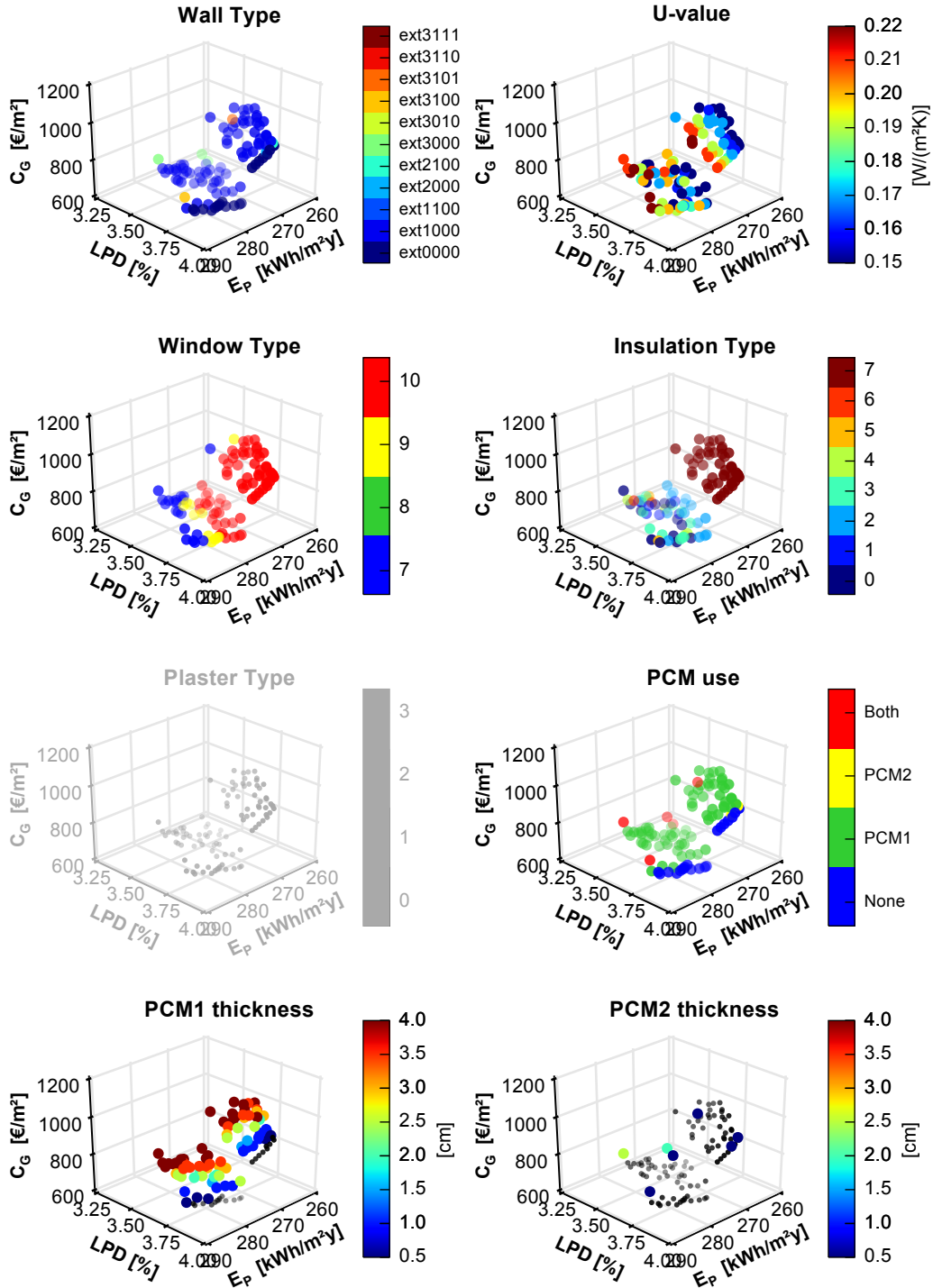
Fig. B.49 Pareto mapping: Oslo_3Obj_pre-1955_RT0_NF1.

Oslo_3Obj_pre-1955_RT0_NF1
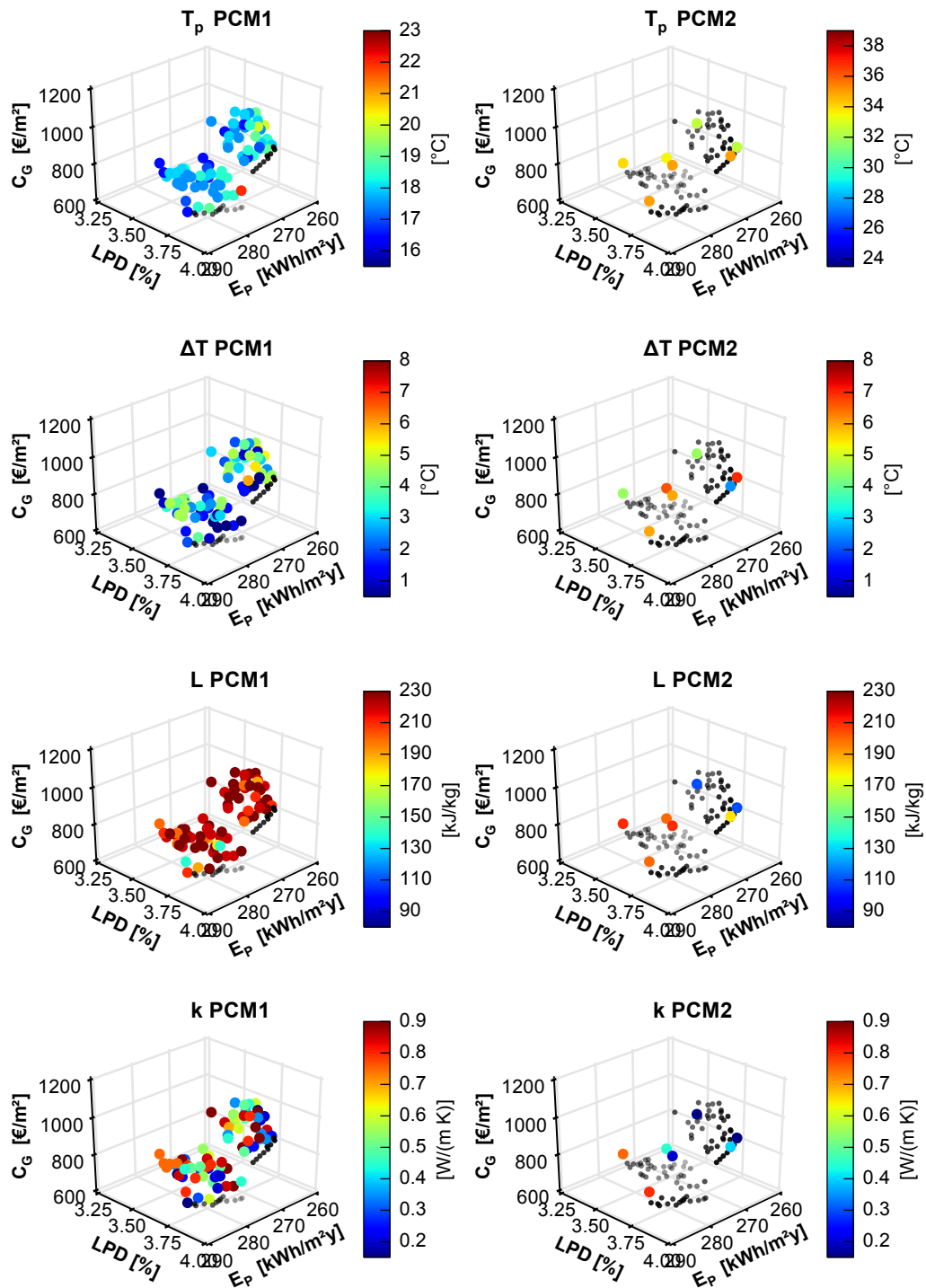
Fig. B.50 Pareto mapping: PCM properties, Oslo_3Obj_pre-1955_RT0_NF1.

Oslo_3Obj_pre-1955_RT1_NF1
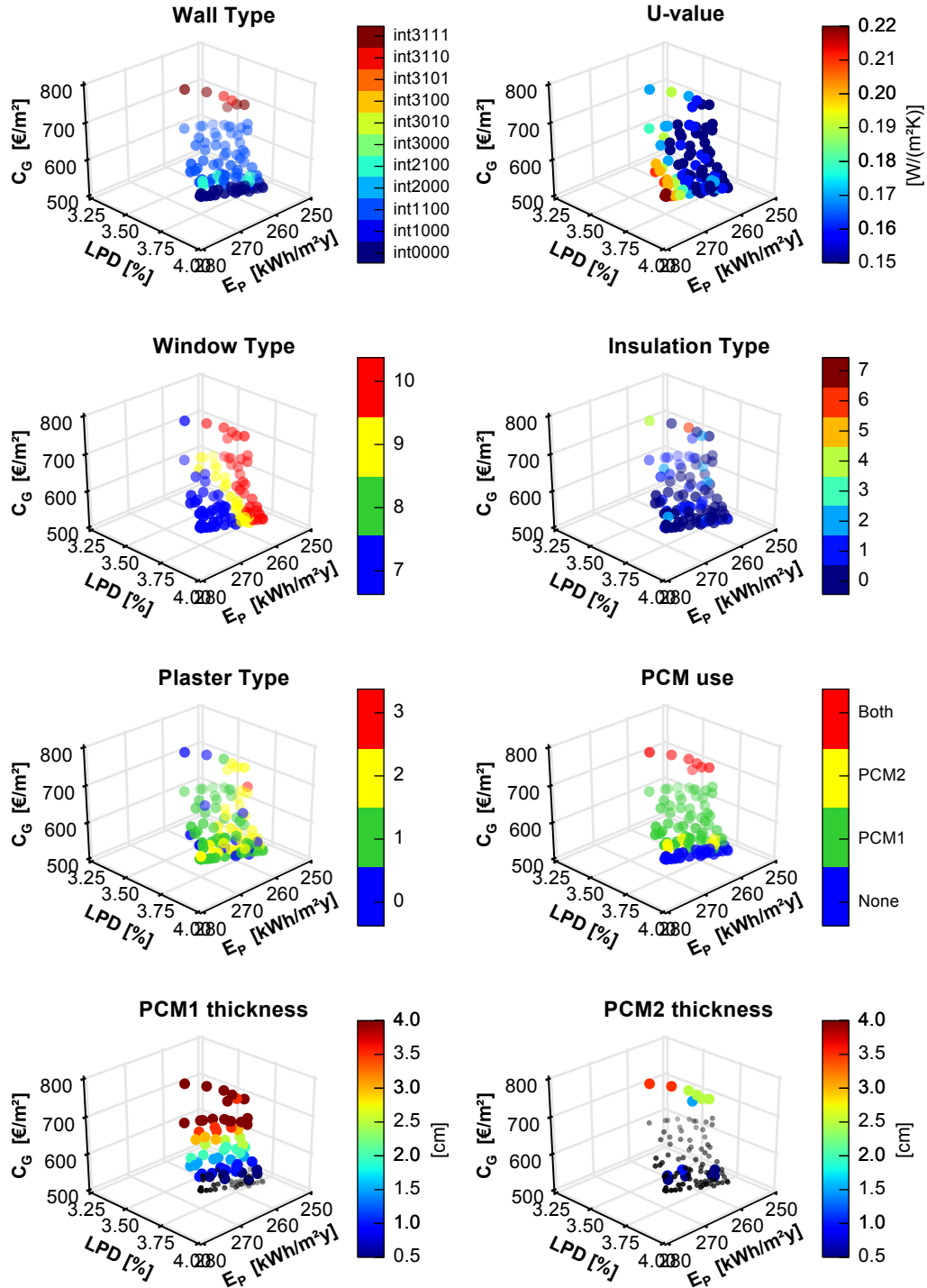
Fig. B.51 Pareto mapping: Oslo_3Obj_pre-1955_RT1_NF1.

Oslo_3Obj_pre-1955_RT1_NF1
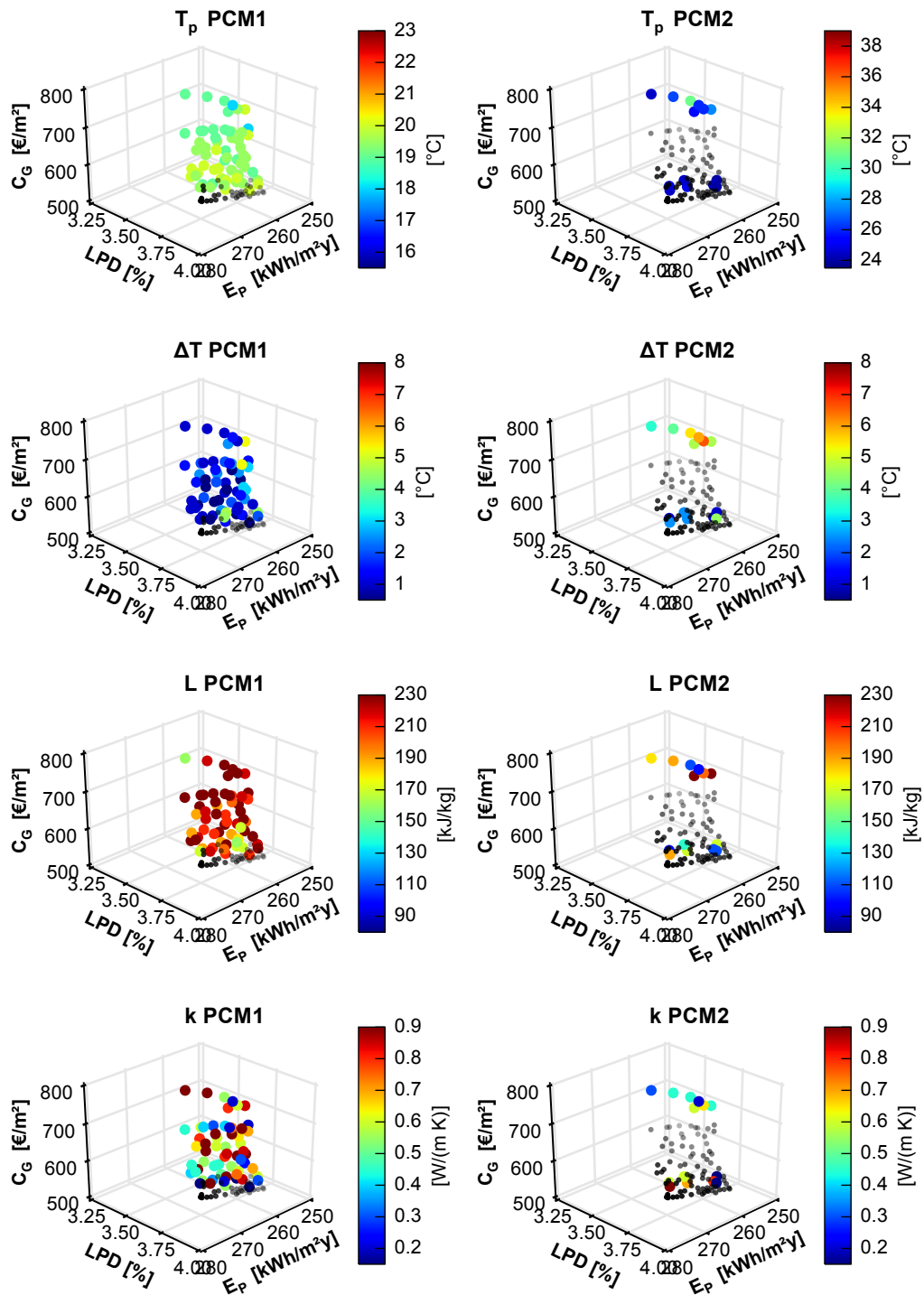
Fig. B.52 Pareto mapping: PCM properties, Oslo_3Obj_pre-1955_RT1_NF1.

Oslo_3Obj_pre-1955_RT2_NF1
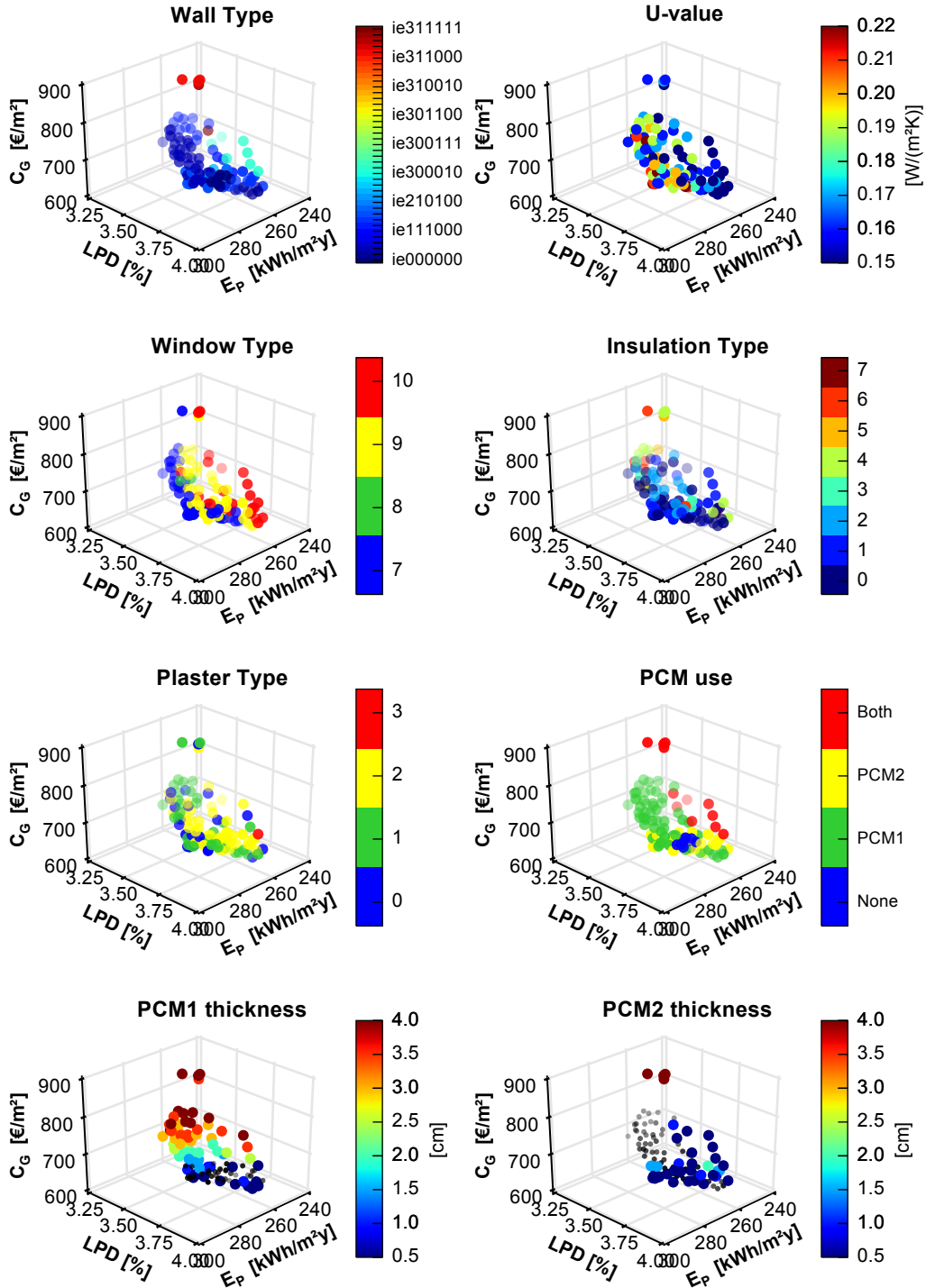
Fig. B.53 Pareto mapping: Oslo_3Obj_pre-1955_RT2_NF1.

Oslo_3Obj_pre-1955_RT2_NF1
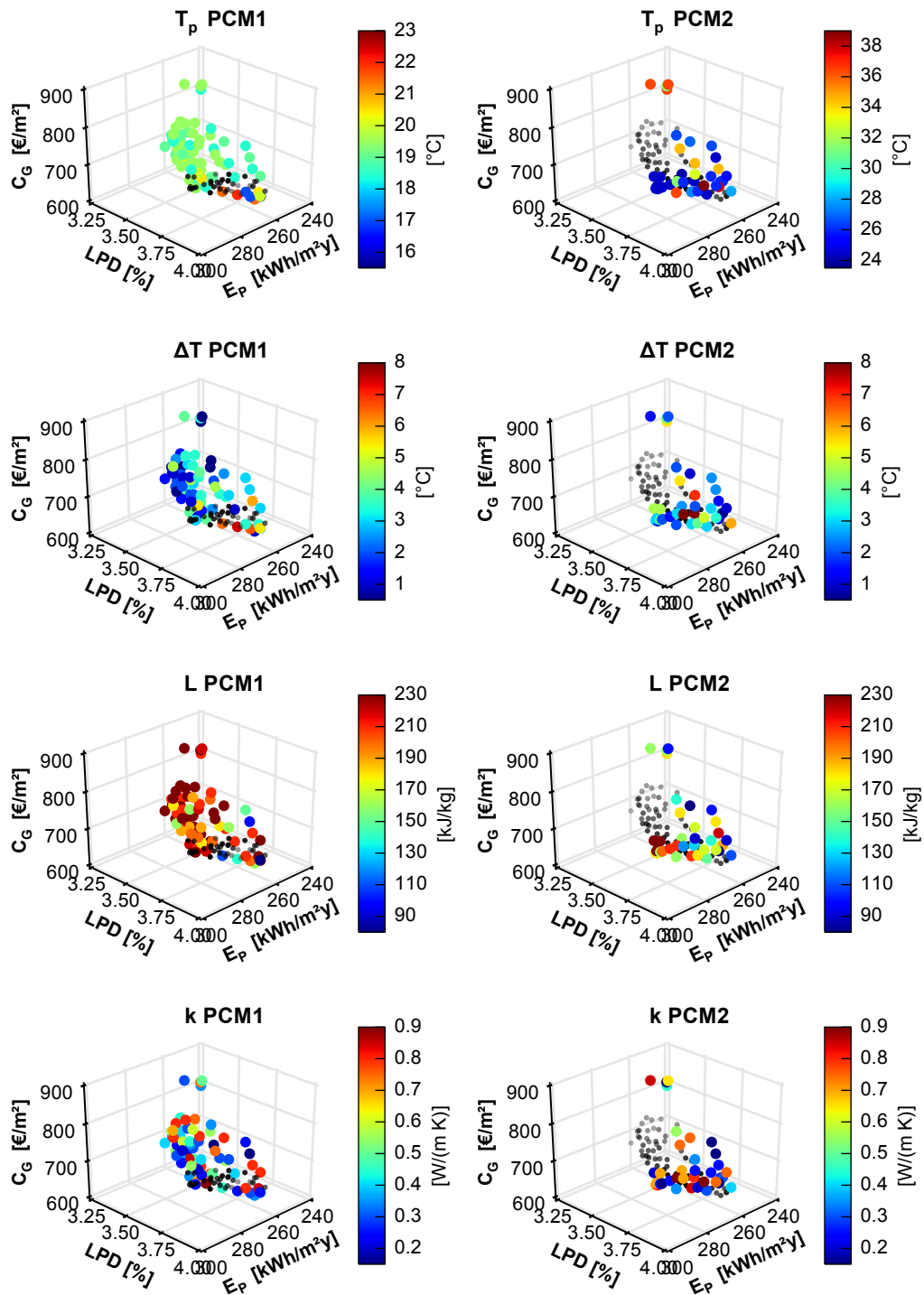
Fig. B.54 Pareto mapping: PCM properties, Oslo_3Obj_pre-1955_RT2_NF1.
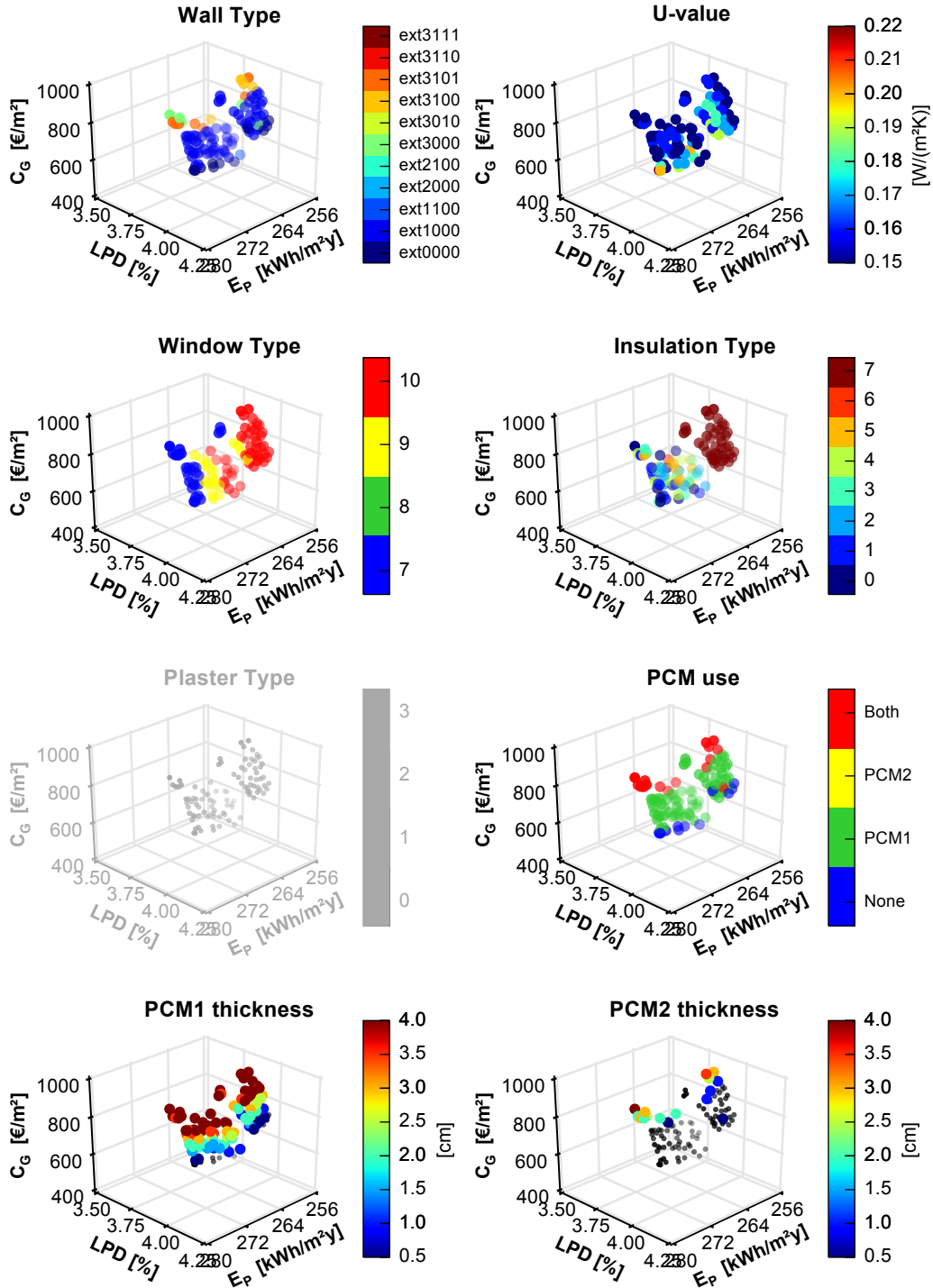
Fig. B.55 Pareto mapping: Oslo_3Obj_post-1955_RT0_NF1.

Oslo_3Obj_post-1955_RT0_NF1

Fig. B.56 Pareto mapping: PCM properties, Oslo_3Obj_post-1955_RT0_NF1.
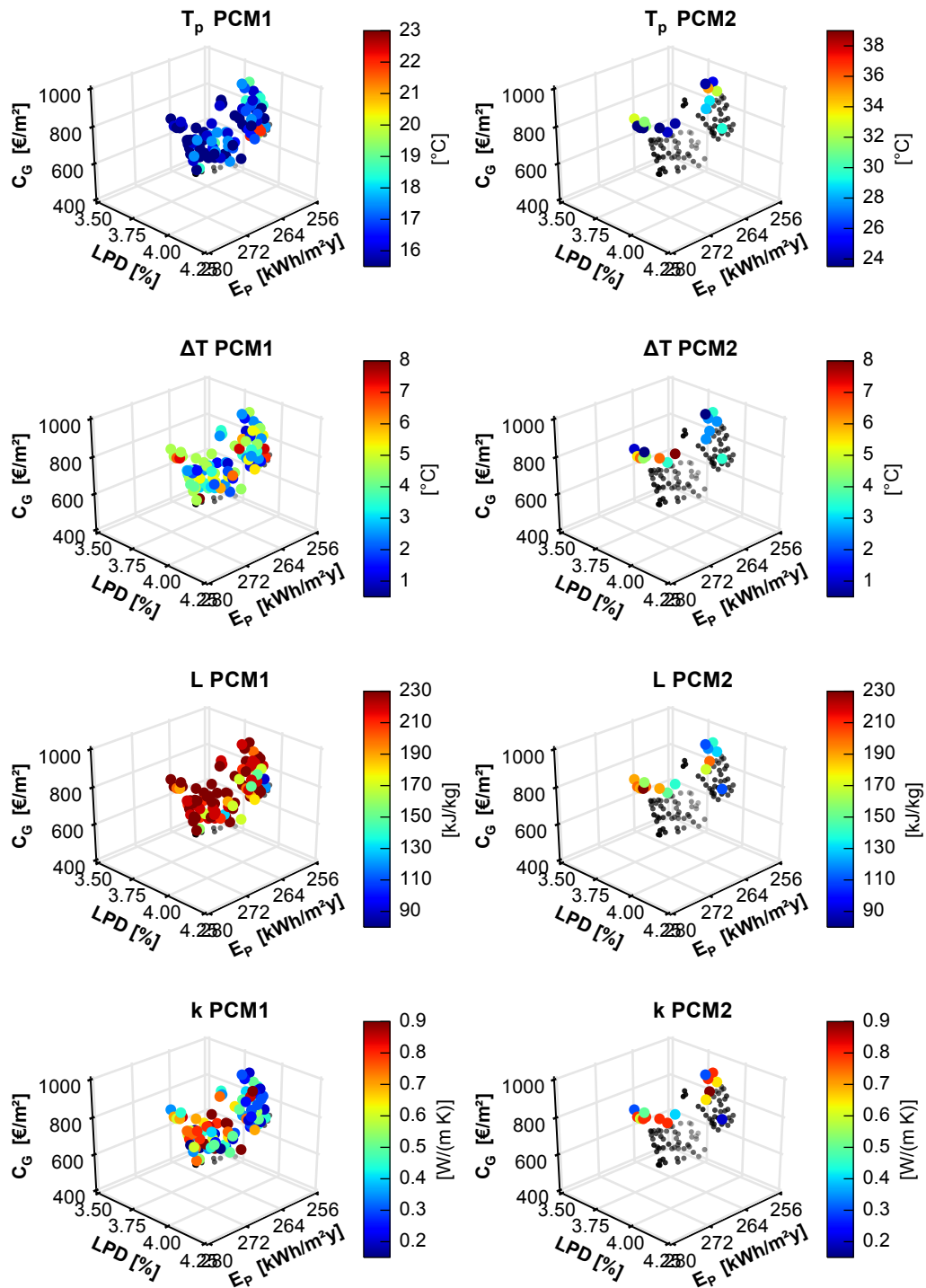
Oslo_3Obj_post-1955_RT1_NF1
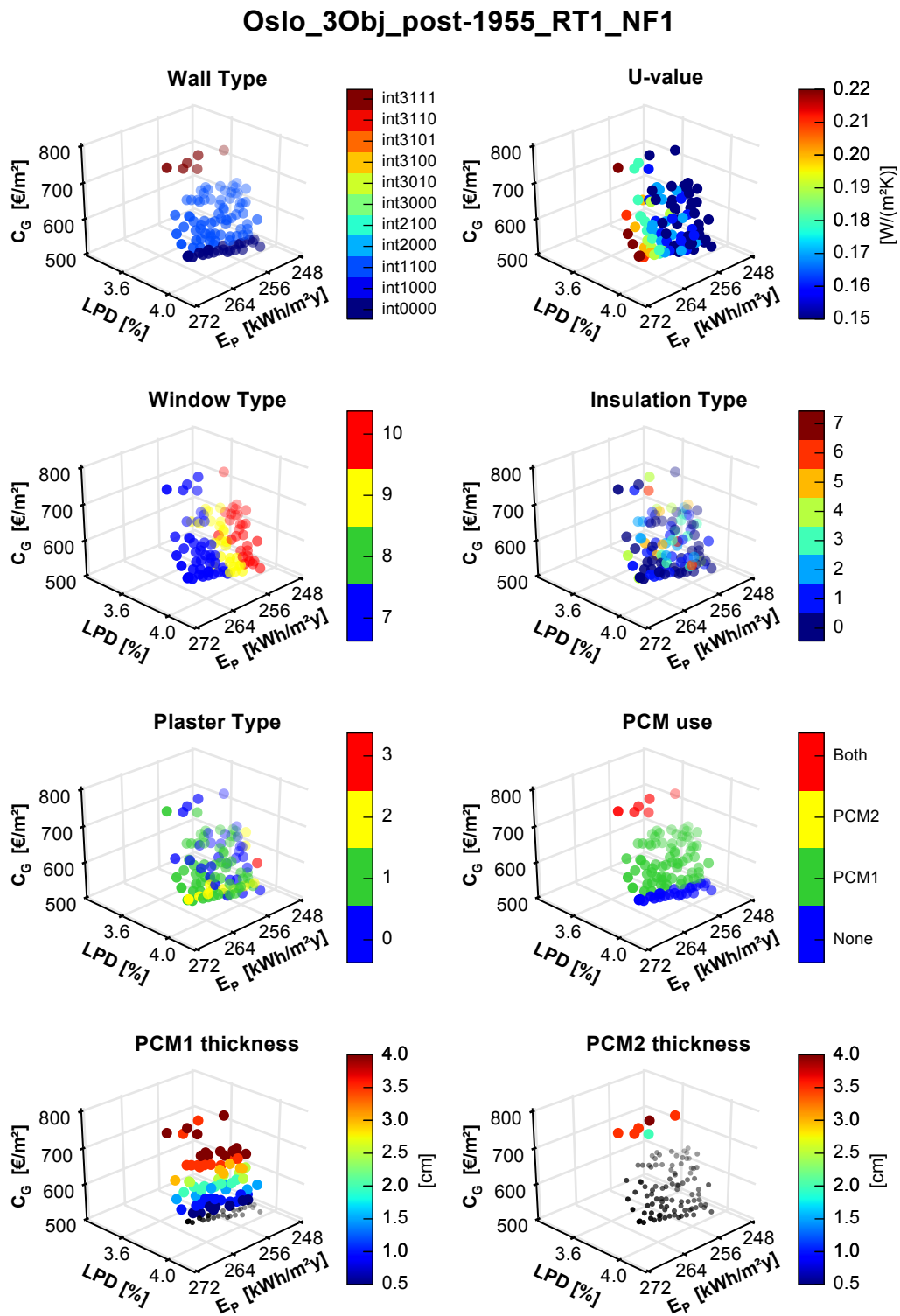
Fig. B.57 Pareto mapping: Oslo_3Obj_post-1955_RT1_NF1.

Oslo_3Obj_post-1955_RT1_NF1
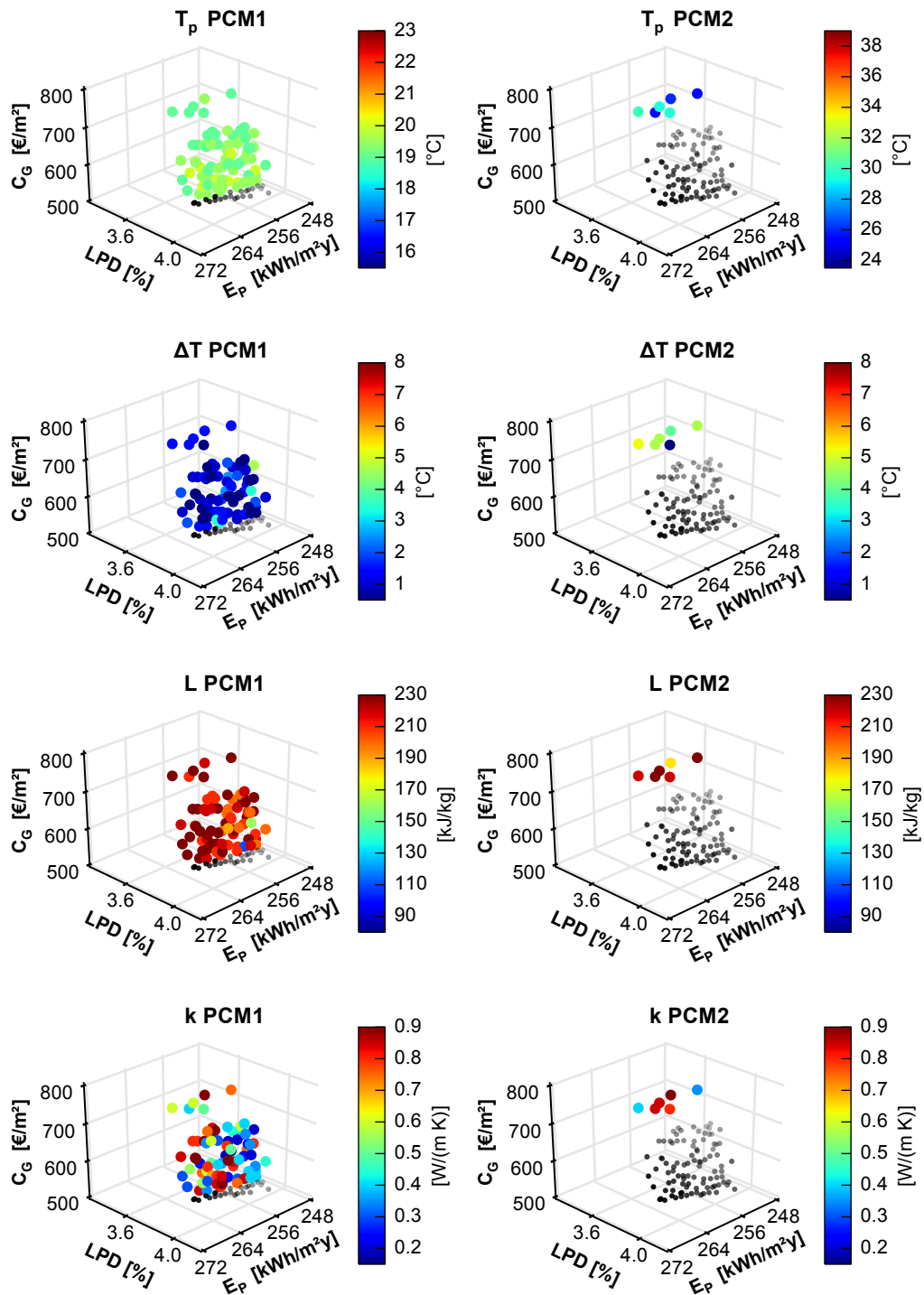
Fig. B.58 Pareto mapping: PCM properties, Oslo_3Obj_post-1955_RT1_NF1.

Oslo_3Obj_post-1955_RT2_NF1
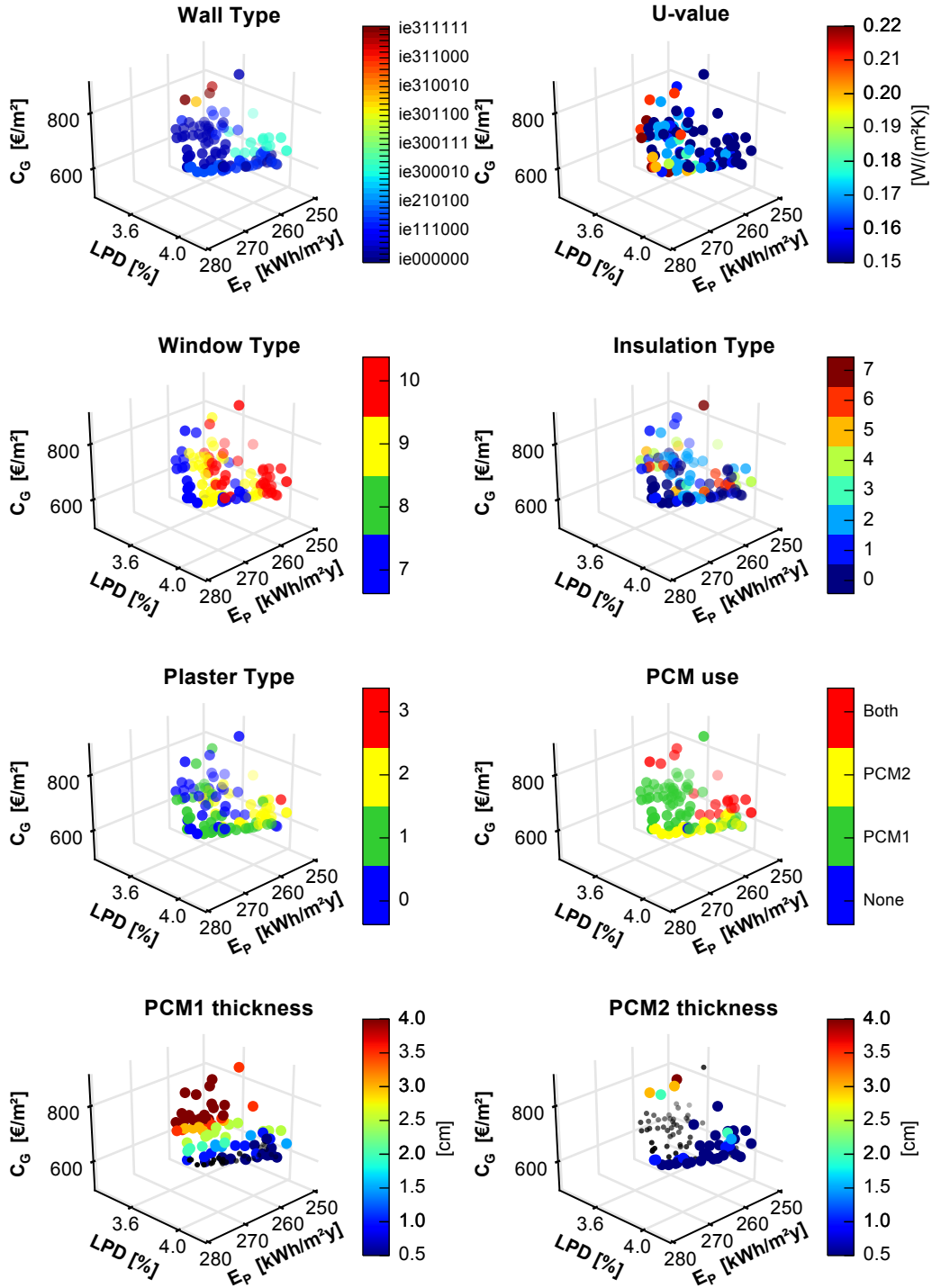
Fig. B.59 Pareto mapping: Oslo_3Obj_post-1955_RT2_NF1.

Oslo_3Obj_post-1955_RT2_NF1
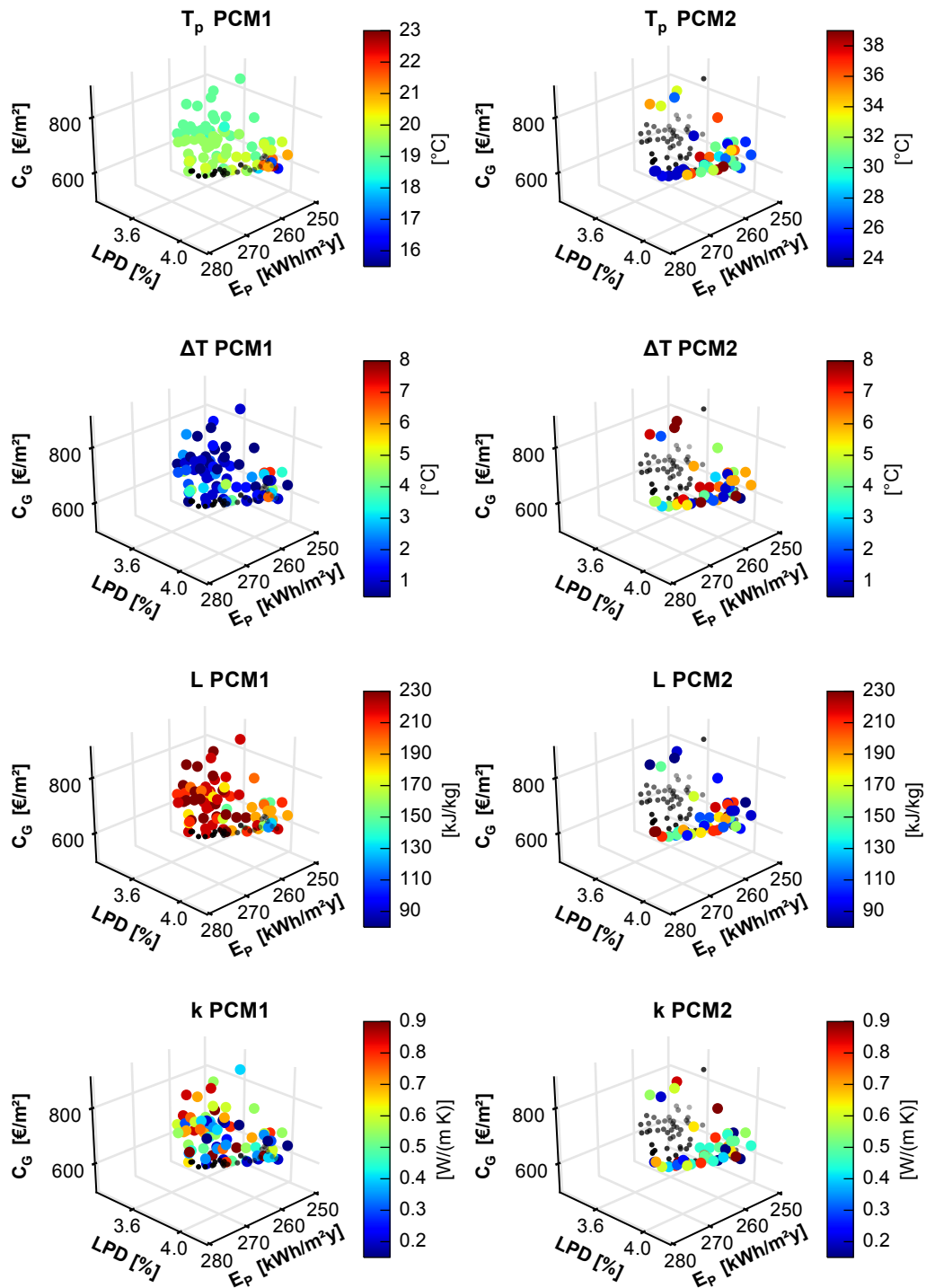
Fig. B.60 Pareto mapping: PCM properties, Oslo_3Obj_post-1955_RT2_NF1.

Appendix C

Extreme solutions

The extreme solutions of the building-level optimisation analyses in § 4.4.3 are herewith illustrated. For the sake of brevity, only the solutions of the NF1 cases (same retrofit type on all the façades) are reported.

The legend to all the graphics in this appendix is reported in Fig. C.1. Wall layouts were represented with the external environment on their left and the internal environment on their right.

Original wall materials

External render
Bricks
Air cavity
Hollow bricks
Internal plaster
Autoclaved aerated concrete
External plasterboard
Internal plasterboard

Insulation materials

EPS
Rock wool
XPS
Sheep wool
Cork
Wood-fiber board
Cellulose fibers panels
Aerogel mats

Plaster materials

Lime and gypsum plaster
Clay plaster
Mineralised wooden board
Thermo-plaster

Phase Change Materials
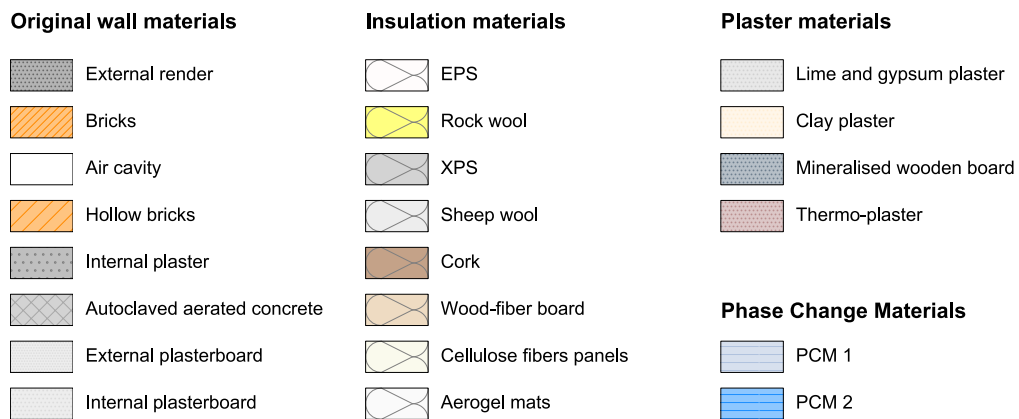
PCM 1
PCM 2

Fig. C.1 Extreme solutions: legend.

Palermo_2Obj_RT0_NF1 - Solution A

U-value: 0.21 W/(m²K)

Window type:	double glazing 4/12/4, Air filled, low-e (2)	
Insulation type:	aerogel mats	
Plaster type:	N/A	

PCM1 properties   **PCM2 properties**

Peak melting temperature:	20.5	°C	N/A
Melting temperature range:	1.5	°C	
Latent heat of fusion:	200	kJ/kg	
Thermal conductivity:	0.75	W/(m K)	

Thickness [cm]

Palermo_2Obj_RT0_NF1 - Solution B

U-value: 0.45 W/(m²K)

Window type:	double glazing 4/12/4, Air filled, low-e (2)	
Insulation type:	EPS	
Plaster type:	N/A	

PCM1 properties   **PCM2 properties**

N/A   N/A

Thickness [cm]
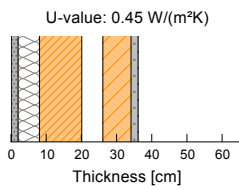
Fig. C.2 Extreme solutions: Palermo_2Obj_RT0_NF1.

Torino_2Obj_RT0_NF1 - Solution A
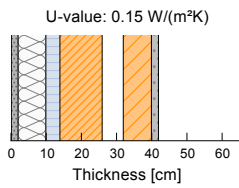
U-value: 0.15 W/(m²K)

Window type:	triple glazing 4/12/4/12/4, 90% Argon filled, low-e (3, 5)	
Insulation type:	aerogel mats	
Plaster type:	N/A	

PCM1 properties   **PCM2 properties**

Peak melting temperature:	16.0	°C	N/A
Melting temperature range:	0.5	°C	
Latent heat of fusion:	190	kJ/kg	
Thermal conductivity:	0.90	W/(m K)	

Thickness [cm]

Torino_2Obj_RT0_NF1 - Solution B

U-value: 0.30 W/(m²K)

Window type:	double glazing 4/12/4, 90% Argon filled, low-e (3)	
Insulation type:	EPS	
Plaster type:	N/A	

PCM1 properties   **PCM2 properties**

N/A   N/A

Thickness [cm]
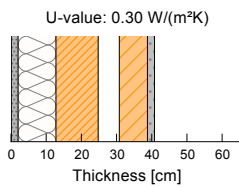
Fig. C.3 Extreme solutions: Torino_2Obj_RT0_NF1.

Palermo_2Obj_RT1_NF1 - Solution A

U-value: 0.15 W/(m²K)

0 10 20 30 40 50 60
Thickness [cm]

Window type:	double glazing 4/12/4, Air filled, low-e (2)
Insulation type:	EPS
Plaster type:	clay plaster

PCM1 properties

Peak melting temperature:	21.5	°C
Melting temperature range:	1.0	°C
Latent heat of fusion:	230	kJ/kg
Thermal conductivity:	0.30	W/(m K)

PCM2 properties

Peak melting temperature:	24.5	°C
Melting temperature range:	5.0	°C
Latent heat of fusion:	150	kJ/kg
Thermal conductivity:	0.35	W/(m K)

Palermo_2Obj_RT1_NF1 - Solution B

U-value: 0.15 W/(m²K)

0 10 20 30 40 50 60
Thickness [cm]

Window type:	double glazing 4/12/4, Air filled, low-e (2)
Insulation type:	EPS
Plaster type:	lime and gypsum plaster

PCM1 properties

N/A

PCM2 properties

N/A

Fig. C.4 Extreme solutions: Palermo_2Obj_RT1_NF1.

Torino_2Obj_RT1_NF1 - Solution A

U-value: 0.15 W/(m²K)

0 10 20 30 40 50 60
Thickness [cm]

Window type:	triple glazing 4/12/4/12/4, 90% Argon filled, low-e (3, 5)
Insulation type:	EPS
Plaster type:	thermo-plaster

PCM1 properties

Peak melting temperature:	18.5	°C
Melting temperature range:	1.5	°C
Latent heat of fusion:	230	kJ/kg
Thermal conductivity:	0.60	W/(m K)

PCM2 properties

Peak melting temperature:	25.0	°C
Melting temperature range:	3.0	°C
Latent heat of fusion:	170	kJ/kg
Thermal conductivity:	0.25	W/(m K)

Torino_2Obj_RT1_NF1 - Solution B

U-value: 0.15 W/(m²K)

0 10 20 30 40 50 60
Thickness [cm]

Window type:	double glazing 4/12/4, 90% Argon filled, low-e (3)
Insulation type:	EPS
Plaster type:	lime and gypsum plaster

PCM1 properties

N/A

PCM2 properties

N/A

Fig. C.5 Extreme solutions: Torino_2Obj_RT1_NF1.

Palermo_2Obj_RT2_NF1 - Solution A
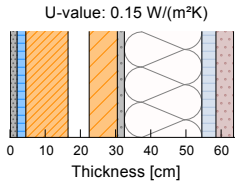
U-value: 0.15 W/(m²K)

0 10 20 30 40 50 60
Thickness [cm]

Window type:	double glazing 4/12/4, Air filled, low-e (2)
Insulation type:	EPS
Plaster type:	thermo-plaster

PCM1 properties

Peak melting temperature:	21.5 °C
Melting temperature range:	2.0 °C
Latent heat of fusion:	220 kJ/kg
Thermal conductivity:	0.60 W/(m K)

PCM2 properties

Peak melting temperature:	33.5 °C
Melting temperature range:	5.5 °C
Latent heat of fusion:	210 kJ/kg
Thermal conductivity:	0.65 W/(m K)

Palermo_2Obj_RT2_NF1 - Solution B
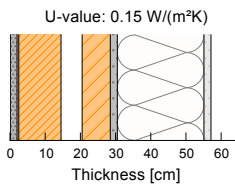
U-value: 0.15 W/(m²K)

0 10 20 30 40 50 60
Thickness [cm]

Window type:	double glazing 4/12/4, Air filled, low-e (2)
Insulation type:	EPS
Plaster type:	lime and gypsum plaster

PCM1 properties

Peak melting temperature:	16.5 °C
Melting temperature range:	1.0 °C
Latent heat of fusion:	210 kJ/kg
Thermal conductivity:	0.55 W/(m K)

PCM2 properties

N/A

Fig. C.6 Extreme solutions: Palermo_2Obj_RT2_NF1.

Torino_2Obj_RT2_NF1 - Solution A
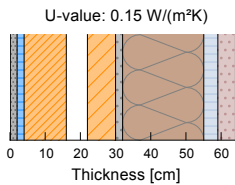
U-value: 0.15 W/(m²K)

0 10 20 30 40 50 60
Thickness [cm]

Window type:	triple glazing 4/12/4/12/4, 90% Argon filled, low-e (3, 5)
Insulation type:	cork
Plaster type:	thermo-plaster

PCM1 properties

Peak melting temperature:	21.0 °C
Melting temperature range:	5.0 °C
Latent heat of fusion:	220 kJ/kg
Thermal conductivity:	0.80 W/(m K)

PCM2 properties

Peak melting temperature:	33.5 °C
Melting temperature range:	5.5 °C
Latent heat of fusion:	210 kJ/kg
Thermal conductivity:	0.35 W/(m K)

Torino_2Obj_RT2_NF1 - Solution B
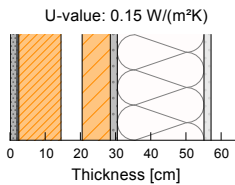
U-value: 0.15 W/(m²K)

0 10 20 30 40 50 60
Thickness [cm]

Window type:	double glazing 4/12/4, 90% Argon filled, low-e (3)
Insulation type:	EPS
Plaster type:	lime and gypsum plaster

PCM1 properties

Peak melting temperature:	20.0 °C
Melting temperature range:	6.7 °C
Latent heat of fusion:	200 kJ/kg
Thermal conductivity:	0.80 W/(m K)

PCM2 properties

N/A

Fig. C.7 Extreme solutions: Torino_2Obj_RT2_NF1.

Palermo_3Obj_RT0_NF1 - Solution A

U-value: 0.15 W/(m²K)

Thickness [cm]

Window type:	double glazing 4/12/4, Air filled, low-e (3)
Insulation type:	aerogel mats
Plaster type:	N/A

PCM1 properties		**PCM2 properties**	
Peak melting temperature:	22.5 °C	Peak melting temperature:	24.0 °C
Melting temperature range:	1.0 °C	Melting temperature range:	6.5 °C
Latent heat of fusion:	220 kJ/kg	Latent heat of fusion:	180 kJ/kg
Thermal conductivity:	0.80 W/(m K)	Thermal conductivity:	0.45 W/(m K)

Palermo_3Obj_RT0_NF1 - Solution B

U-value: 0.43 W/(m²K)

Thickness [cm]

Window type:	double glazing 6/16/4, 90% Argon filled, selective (2)
Insulation type:	aerogel mats
Plaster type:	N/A

PCM1 properties		**PCM2 properties**	
Peak melting temperature:	22.5 °C	Peak melting temperature:	24.0 °C
Melting temperature range:	1.0 °C	Melting temperature range:	2.5 °C
Latent heat of fusion:	220 kJ/kg	Latent heat of fusion:	190 kJ/kg
Thermal conductivity:	0.85 W/(m K)	Thermal conductivity:	0.35 W/(m K)

Palermo_3Obj_RT0_NF1 - Solution C

U-value: 0.45 W/(m²K)

Thickness [cm]

Window type:	double glazing 4/12/4, Air filled
Insulation type:	EPS
Plaster type:	N/A

PCM1 properties	**PCM2 properties**
N/A	N/A

Fig. C.8 Extreme solutions: Palermo_3Obj_RT0_NF1.

Torino_3Obj_RT0_NF1 - Solution A

U-value: 0.15 W/(m²K)

Thickness [cm]

Window type:	triple glazing 4/12/4/12/4, 90% Argon filled, low-e (3, 5)
Insulation type:	aerogel mats
Plaster type:	N/A

PCM1 properties		**PCM2 properties**
Peak melting temperature:	17.0 °C	N/A
Melting temperature range:	2.0 °C	
Latent heat of fusion:	230 kJ/kg	
Thermal conductivity:	0.85 W/(m K)	

Torino_3Obj_RT0_NF1 - Solution B

U-value: 0.29 W/(m²K)

Thickness [cm]

Window type:	double glazing 4/12/4, 90% Argon filled, low-e (2)
Insulation type:	rock wool
Plaster type:	N/A

PCM1 properties		**PCM2 properties**	
Peak melting temperature:	23.0 °C	Peak melting temperature:	26.0 °C
Melting temperature range:	2.5 °C	Melting temperature range:	3.5 °C
Latent heat of fusion:	210 kJ/kg	Latent heat of fusion:	190 kJ/kg
Thermal conductivity:	0.90 W/(m K)	Thermal conductivity:	0.35 W/(m K)

Torino_3Obj_RT0_NF1 - Solution C

U-value: 0.30 W/(m²K)

Thickness [cm]

Window type:	double glazing 4/12/4, 90% Argon filled, low-e (3)
Insulation type:	EPS
Plaster type:	N/A

PCM1 properties	**PCM2 properties**
N/A	N/A

Fig. C.9 Extreme solutions: Torino_3Obj_RT0_NF1.

Palermo_3Obj_RT1_NF1 - Solution A

U-value: 0.17 W/(m²K)

Thickness [cm]

Window type:	double glazing 4/12/4, Air filled, low-e (3)
Insulation type:	aerogel mats
Plaster type:	lime and gypsum plaster

PCM1 properties		**PCM2 properties**	
Peak melting temperature:	20.5 °C	N/A	
Melting temperature range:	3.5 °C		
Latent heat of fusion:	220 kJ/kg		
Thermal conductivity:	0.50 W/(m K)		

Palermo_3Obj_RT1_NF1 - Solution B

U-value: 0.43 W/(m²K)

Thickness [cm]

Window type:	double glazing 6/16/4, 90% Argon filled, selective (2)
Insulation type:	sheep wool
Plaster type:	thermo-plaster

PCM1 properties		**PCM2 properties**	
Peak melting temperature:	23.0 °C	Peak melting temperature:	24.0 °C
Melting temperature range:	0.5 °C	Melting temperature range:	5.3 °C
Latent heat of fusion:	210 kJ/kg	Latent heat of fusion:	220 kJ/kg
Thermal conductivity:	0.75 W/(m K)	Thermal conductivity:	0.50 W/(m K)

Palermo_3Obj_RT1_NF1 - Solution C

U-value: 0.45 W/(m²K)

Thickness [cm]

Window type:	double glazing 4/12/4, Air filled
Insulation type:	EPS
Plaster type:	lime and gypsum plaster

| **PCM1 properties** | **PCM2 properties** |
| N/A | N/A |

Fig. C.10 Extreme solutions: Palermo_3Obj_RT1_NF1.

Torino_3Obj_RT1_NF1 - Solution A

U-value: 0.16 W/(m²K)

Thickness [cm]

Window type:	triple glazing 4/12/4/12/4, 90% Argon filled, low-e (3, 5)
Insulation type:	aerogel mats
Plaster type:	thermo-plaster

PCM1 properties		**PCM2 properties**	
Peak melting temperature:	15.5 °C	N/A	
Melting temperature range:	4.7 °C		
Latent heat of fusion:	230 kJ/kg		
Thermal conductivity:	0.55 W/(m K)		

Torino_3Obj_RT1_NF1 - Solution B

U-value: 0.16 W/(m²K)

Thickness [cm]

Window type:	double glazing 4/12/4, 90% Argon filled, low-e (2)
Insulation type:	rock wool
Plaster type:	thermo-plaster

PCM1 properties		**PCM2 properties**	
Peak melting temperature:	22.5 °C	Peak melting temperature:	25.0 °C
Melting temperature range:	5.3 °C	Melting temperature range:	2.0 °C
Latent heat of fusion:	220 kJ/kg	Latent heat of fusion:	230 kJ/kg
Thermal conductivity:	0.90 W/(m K)	Thermal conductivity:	0.50 W/(m K)

Torino_3Obj_RT1_NF1 - Solution C

U-value: 0.30 W/(m²K)

Thickness [cm]

Window type:	double glazing 4/12/4, 90% Argon filled, low-e (2)
Insulation type:	EPS
Plaster type:	lime and gypsum plaster

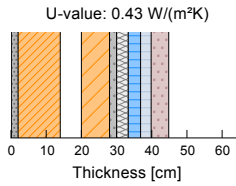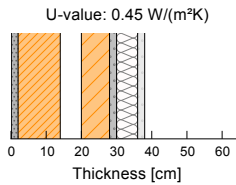| **PCM1 properties** | **PCM2 properties** |
| N/A | N/A |

Fig. C.11 Extreme solutions: Torino_3Obj_RT1_NF1.

Palermo_3Obj_RT2_NF1 - Solution A

U-value: 0.15 W/(m²K)

Window type:	double glazing 4/12/4, Air filled, low-e (3)
Insulation type:	aerogel mats
Plaster type:	mineralised wooden board

PCM1 properties   **PCM2 properties**

Peak melting temperature:	21.5 °C	N/A
Melting temperature range:	5.3 °C	
Latent heat of fusion:	220 kJ/kg	
Thermal conductivity:	0.85 W/(m K)	

Palermo_3Obj_RT2_NF1 - Solution B

U-value: 0.45 W/(m²K)

Window type:	double glazing 6/16/4, 90% Argon filled, selective (2)
Insulation type:	rock wool
Plaster type:	thermo-plaster

PCM1 properties   **PCM2 properties**

Peak melting temperature:	23.0 °C	Peak melting temperature:	26.0 °C
Melting temperature range:	3.0 °C	Melting temperature range:	3.0 °C
Latent heat of fusion:	210 kJ/kg	Latent heat of fusion:	220 kJ/kg
Thermal conductivity:	0.20 W/(m K)	Thermal conductivity:	0.90 W/(m K)

Palermo_3Obj_RT2_NF1 - Solution C

U-value: 0.41 W/(m²K)

Window type:	double glazing 4/12/4, Air filled
Insulation type:	EPS
Plaster type:	lime and gypsum plaster

PCM1 properties   **PCM2 properties**

Peak melting temperature:	22.0 °C	N/A
Melting temperature range:	3.0 °C	
Latent heat of fusion:	200 kJ/kg	
Thermal conductivity:	0.75 W/(m K)	

Fig. C.12 Extreme solutions: Palermo_3Obj_RT2_NF1.

Torino_3Obj_RT2_NF1 - Solution A

U-value: 0.15 W/(m²K)

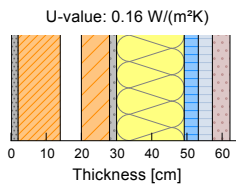| Window type: | triple glazing 4/12/4/12/4, 90% Argon filled, low-e (3, 5) |
| Insulation type: | aerogel mats |
| Plaster type: | thermo-plaster |

PCM1 properties   **PCM2 properties**

Peak melting temperature:	18.0 °C	Peak melting temperature:	29.5 °C
Melting temperature range:	2.0 °C	Melting temperature range:	3.0 °C
Latent heat of fusion:	230 kJ/kg	Latent heat of fusion:	90 kJ/kg
Thermal conductivity:	0.80 W/(m K)	Thermal conductivity:	0.45 W/(m K)

Torino_3Obj_RT2_NF1 - Solution B

U-value: 0.17 W/(m²K)

Window type:	double glazing 4/12/4, 90% Argon filled, low-e (2)
Insulation type:	rock wool
Plaster type:	thermo-plaster

PCM1 properties   **PCM2 properties**

Peak melting temperature:	23.0 °C	Peak melting temperature:	25.5 °C
Melting temperature range:	2.0 °C	Melting temperature range:	4.0 °C
Latent heat of fusion:	230 kJ/kg	Latent heat of fusion:	220 kJ/kg
Thermal conductivity:	0.40 W/(m K)	Thermal conductivity:	0.25 W/(m K)

Torino_3Obj_RT2_NF1 - Solution C

U-value: 0.30 W/(m²K)

Window type:	double glazing 4/12/4, 90% Argon filled, low-e (2)
Insulation type:	EPS
Plaster type:	lime and gypsum plaster

PCM1 properties   **PCM2 properties**

Peak melting temperature:	17.0 °C	N/A
Melting temperature range:	2.5 °C	
Latent heat of fusion:	130 kJ/kg	
Thermal conductivity:	0.25 W/(m K)	

Fig. C.13 Extreme solutions: Torino_3Obj_RT2_NF1.

Oslo_3Obj_pre-1955_RT0_NF1 - Solution A

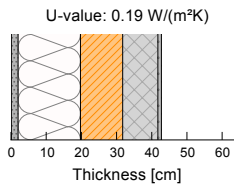U-value: 0.15 W/(m²K)

Thickness [cm]

Window type:	triple glazing 4/12/4/12/4, 95% Kripton filled, low-e (3, 5)
Insulation type:	aerogel mats
Plaster type:	N/A

PCM1 properties   **PCM2 properties**

Peak melting temperature:	19.0 °C	N/A
Melting temperature range:	4.7 °C	
Latent heat of fusion:	230 kJ/kg	
Thermal conductivity:	0.60 W/(m K)	

Oslo_3Obj_pre-1955_RT0_NF1 - Solution B

U-value: 0.19 W/(m²K)

Thickness [cm]

Window type:	triple glazing 4/15/4/15/4, 90% Argon filled, low-e (3, 5)
Insulation type:	EPS
Plaster type:	N/A

PCM1 properties   **PCM2 properties**

N/A   N/A

Oslo_3Obj_pre-1955_RT0_NF1 - Solution C

U-value: 0.21 W/(m²K)

Thickness [cm]

Window type:	triple glazing 4/12/4/12/4, 90% Argon filled, low-e (3, 5)
Insulation type:	EPS
Plaster type:	N/A

PCM1 properties   **PCM2 properties**

Peak melting temperature:	16.5 °C	Peak melting temperature:	34.0 °C
Melting temperature range:	0.5 °C	Melting temperature range:	4.5 °C
Latent heat of fusion:	200 kJ/kg	Latent heat of fusion:	210 kJ/kg
Thermal conductivity:	0.75 W/(m K)	Thermal conductivity:	0.75 W/(m K)

Fig. C.14 Extreme solutions: Oslo_3Obj_pre-1955_RT0_NF1.
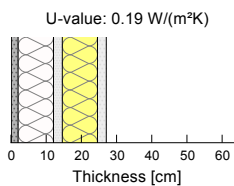
Oslo_3Obj_post-1955_RT0_NF1 - Solution A

U-value: 0.15 W/(m²K)

Thickness [cm]

Window type:	triple glazing 4/12/4/12/4, 95% Kripton filled, low-e (3, 5)
Insulation type:	aerogel mats
Plaster type:	N/A

PCM1 properties   **PCM2 properties**

Peak melting temperature:	17.5 °C	N/A
Melting temperature range:	2.5 °C	
Latent heat of fusion:	230 kJ/kg	
Thermal conductivity:	0.45 W/(m K)	

Oslo_3Obj_post-1955_RT0_NF1 - Solution B

U-value: 0.19 W/(m²K)

Thickness [cm]
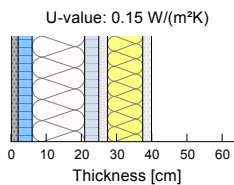
Window type:	triple glazing 4/15/4/15/4, 90% Argon filled, low-e (3, 5)
Insulation type:	EPS
Plaster type:	N/A

PCM1 properties   **PCM2 properties**

N/A   N/A

Oslo_3Obj_post-1955_RT0_NF1 - Solution C

U-value: 0.15 W/(m²K)

Thickness [cm]

Window type:	triple glazing 4/12/4/12/4, 90% Argon filled, low-e (3, 5)
Insulation type:	EPS
Plaster type:	N/A

PCM1 properties   **PCM2 properties**

Peak melting temperature:	15.5 °C	Peak melting temperature:	33.0 °C
Melting temperature range:	4.7 °C	Melting temperature range:	1.0 °C
Latent heat of fusion:	230 kJ/kg	Latent heat of fusion:	190 kJ/kg
Thermal conductivity:	0.35 W/(m K)	Thermal conductivity:	0.30 W/(m K)

Fig. C.15 Extreme solutions: Oslo_3Obj_post-1955_RT0_NF1.
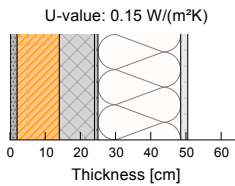
Oslo_3Obj_pre-1955_RT1_NF1 - Solution A

U-value: 0.15 W/(m²K)

Thickness [cm]

Window type:	triple glazing 4/12/4/12/4, 95% Kripton filled, low-e (3, 5)
Insulation type:	EPS
Plaster type:	thermo-plaster

PCM1 properties		**PCM2 properties**	
Peak melting temperature:	18.0 °C	N/A	
Melting temperature range:	1.5 °C		
Latent heat of fusion:	230 kJ/kg		
Thermal conductivity:	0.20 W/(m K)		

Oslo_3Obj_pre-1955_RT1_NF1 - Solution B
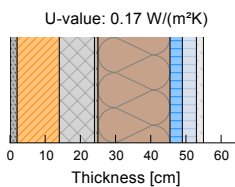
U-value: 0.15 W/(m²K)

Thickness [cm]

Window type:	triple glazing 4/15/4/15/4, 90% Argon filled, low-e (3, 5)
Insulation type:	EPS
Plaster type:	lime and gypsum plaster

| **PCM1 properties** | **PCM2 properties** |
| N/A | N/A |

Oslo_3Obj_pre-1955_RT1_NF1 - Solution C

U-value: 0.17 W/(m²K)

Thickness [cm]

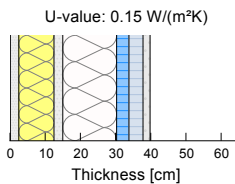| Window type: | triple glazing 4/12/4/12/4, 90% Argon filled, low-e (3, 5) |
| Insulation type: | cork |
| Plaster type: | lime and gypsum plaster |

PCM1 properties		**PCM2 properties**	
Peak melting temperature:	19.0 °C	Peak melting temperature:	24.5 °C
Melting temperature range:	1.0 °C	Melting temperature range:	3.5 °C
Latent heat of fusion:	160 kJ/kg	Latent heat of fusion:	180 kJ/kg
Thermal conductivity:	0.90 W/(m K)	Thermal conductivity:	0.30 W/(m K)

Fig. C.16 Extreme solutions: Oslo_3Obj_pre-1955_RT1_NF1.

Oslo_3Obj_post-1955_RT1_NF1 - Solution A

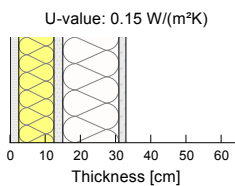U-value: 0.15 W/(m²K)

Thickness [cm]

Window type:	triple glazing 4/12/4/12/4, 95% Kripton filled, low-e (3, 5)
Insulation type:	EPS
Plaster type:	lime and gypsum plaster

PCM1 properties		**PCM2 properties**	
Peak melting temperature:	19.0 °C	Peak melting temperature:	25.5 °C
Melting temperature range:	1.5 °C	Melting temperature range:	4.7 °C
Latent heat of fusion:	230 kJ/kg	Latent heat of fusion:	230 kJ/kg
Thermal conductivity:	0.75 W/(m K)	Thermal conductivity:	0.35 W/(m K)

Oslo_3Obj_post-1955_RT1_NF1 - Solution B
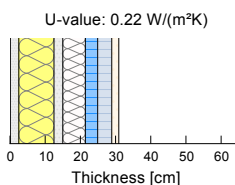
U-value: 0.15 W/(m²K)

Thickness [cm]

Window type:	triple glazing 4/15/4/15/4, 90% Argon filled, low-e (3, 5)
Insulation type:	EPS
Plaster type:	lime and gypsum plaster

| **PCM1 properties** | **PCM2 properties** |
| N/A | N/A |

Oslo_3Obj_post-1955_RT1_NF1 - Solution C

U-value: 0.22 W/(m²K)

Thickness [cm]

Window type:	triple glazing 4/12/4/12/4, 90% Argon filled, low-e (3, 5)
Insulation type:	EPS
Plaster type:	clay plaster

PCM1 properties		**PCM2 properties**	
Peak melting temperature:	19.0 °C	Peak melting temperature:	30.0 °C
Melting temperature range:	1.5 °C	Melting temperature range:	5.3 °C
Latent heat of fusion:	230 kJ/kg	Latent heat of fusion:	220 kJ/kg
Thermal conductivity:	0.60 W/(m K)	Thermal conductivity:	0.40 W/(m K)

Fig. C.17 Extreme solutions: Oslo_3Obj_post-1955_RT1_NF1.

Oslo_3Obj_pre-1955_RT2_NF1 - Solution A

U-value: 0.15 W/(m²K)
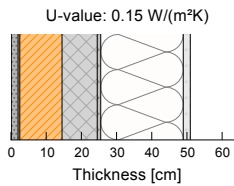

Thickness [cm]
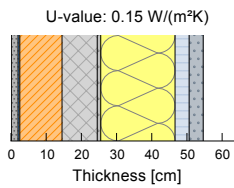
Window type: triple glazing 4/12/4/12/4, 95% Kripton filled, low-e (3, 5)
Insulation type: rock wool
Plaster type: mineralised wooden board

PCM1 properties		**PCM2 properties**	
Peak melting temperature:	18.5 °C	Peak melting temperature:	26.5 °C
Melting temperature range:	3.0 °C	Melting temperature range:	2.5 °C
Latent heat of fusion:	150 kJ/kg	Latent heat of fusion:	100 kJ/kg
Thermal conductivity:	0.25 W/(m K)	Thermal conductivity:	0.15 W/(m K)

Oslo_3Obj_pre-1955_RT2_NF1 - Solution B

U-value: 0.15 W/(m²K)
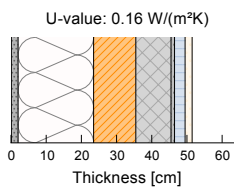

Thickness [cm]

Window type: triple glazing 4/15/4/15/4, 90% Argon filled, low-e (3, 5)
Insulation type: EPS
Plaster type: lime and gypsum plaster

PCM1 properties		**PCM2 properties**
Peak melting temperature:	21.5 °C	N/A
Melting temperature range:	1.0 °C	
Latent heat of fusion:	160 kJ/kg	
Thermal conductivity:	0.35 W/(m K)	

Oslo_3Obj_pre-1955_RT2_NF1 - Solution C

U-value: 0.16 W/(m²K)

Thickness [cm]

Window type: triple glazing 4/12/4/12/4, 90% Argon filled, low-e (3, 5)
Insulation type: EPS
Plaster type: clay plaster

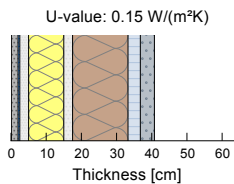| **PCM1 properties**		**PCM2 properties**
Peak melting temperature:	19.0 °C	N/A
Melting temperature range:	1.5 °C	
Latent heat of fusion:	230 kJ/kg	
Thermal conductivity:	0.40 W/(m K)	

Fig. C.18 Extreme solutions: Oslo_3Obj_pre-1955_RT2_NF1.

Oslo_3Obj_post-1955_RT2_NF1 - Solution A

U-value: 0.15 W/(m²K)

Thickness [cm]

Window type: triple glazing 4/12/4/12/4, 95% Kripton filled, low-e (3, 5)
Insulation type: cork
Plaster type: mineralised wooden board

PCM1 properties		**PCM2 properties**	
Peak melting temperature:	19.0 °C	Peak melting temperature:	36.5 °C
Melting temperature range:	0.5 °C	Melting temperature range:	4.5 °C
Latent heat of fusion:	200 kJ/kg	Latent heat of fusion:	100 kJ/kg
Thermal conductivity:	0.55 W/(m K)	Thermal conductivity:	0.90 W/(m K)

Oslo_3Obj_post-1955_RT2_NF1 - Solution B
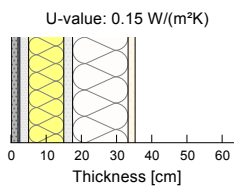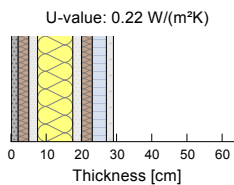
U-value: 0.15 W/(m²K)

Thickness [cm]

Window type: triple glazing 4/15/4/15/4, 90% Argon filled, low-e (3, 5)
Insulation type: EPS
Plaster type: clay plaster

PCM1 properties		**PCM2 properties**
Peak melting temperature:	18.0 °C	N/A
Melting temperature range:	0.5 °C	
Latent heat of fusion:	190 kJ/kg	
Thermal conductivity:	0.20 W/(m K)	

Oslo_3Obj_post-1955_RT2_NF1 - Solution C

U-value: 0.22 W/(m²K)

Thickness [cm]

Window type: triple glazing 4/12/4/12/4, 90% Argon filled, low-e (3, 5)
Insulation type: wood-fiber board
Plaster type: lime and gypsum plaster

PCM1 properties		**PCM2 properties**
Peak melting temperature:	19.0 °C	N/A
Melting temperature range:	2.5 °C	
Latent heat of fusion:	230 kJ/kg	
Thermal conductivity:	0.85 W/(m K)	

Fig. C.19 Extreme solutions: Oslo_3Obj_post-1955_RT2_NF1.